Toni Volkmer

Multivariate Approximation and High-Dimensional Sparse FFT Based on Rank-1 Lattice Sampling

Toni Volkmer

Multivariate Approximation and High-Dimensional Sparse FFT Based on Rank-1 Lattice Sampling

TECHNISCHE UNIVERSITÄT
CHEMNITZ

Universitätsverlag Chemnitz
2017

Impressum

Bibliografische Information der Deutschen Nationalbibliothek

Die Deutsche Nationalbibliothek verzeichnet diese Publikation in der Deutschen Nationalbibliografie; detaillierte bibliografische Angaben sind im Internet über http://dnb.d-nb.de abrufbar.

Titelgrafik: Toni Volkmer
Satz/Layout: Toni Volkmer

Technische Universität Chemnitz/Universitätsbibliothek
Universitätsverlag Chemnitz
09107 Chemnitz
http://www.tu-chemnitz.de/ub/univerlag

readbox unipress
in der readbox publishing GmbH
Am Hawerkamp 31
48155 Münster
http://unipress.readbox.net

ISBN 978-3-96100-020-3

http://nbn-resolving.de/urn:nbn:de:bsz:ch1-qucosa-222820

Multivariate Approximation and High-Dimensional Sparse FFT Based on Rank-1 Lattice Sampling

von der Fakultät für Mathematik
der Technischen Universität Chemnitz
genehmigte

Dissertation

zur Erlangung des akademischen Grades

doctor rerum naturalium
(Dr. rer. nat.)

vorgelegt

von Dipl.-Math. Toni Volkmer

Tag der Einreichung: 02. Januar 2017

Betreuer: Prof. Dr. Daniel Potts, Technische Universität Chemnitz

Gutachter: Prof. Dr. Daniel Potts, Technische Universität Chemnitz
Prof. Dr. Gerlind Plonka-Hoch, Universität Göttingen
JProf. Dr. Dirk Pflüger, Universität Stuttgart

Tag der öffentlichen Prüfung: 28. März 2017

Contents

Chapter 1

Introduction

The approximation of multivariate functions is an important problem in numerical analysis. The discretization of multivariate problems often leads to a dramatic growth of the degrees of freedom for increasing refinements even for moderate dimensions, like four or five, since the degrees of freedom may grow exponentially in the dimension when the approximation error shall be decreased by a factor. This issue is known as the curse of dimensionality [Bel61]. In two or three dimensions, approaches using tensor products of univariate methods are frequently used. However, for higher dimensions, such a straightforward approach is usually impracticable. Methods for attenuating this problem are generally based on assuming additional structure like smoothness or sparsity. Then, we also have a chance to deal with high-dimensional problems. In order to be able to apply such a method in practice for larger problem sizes, this property may not be enough. For that reason, we may need fast algorithms for the numerical computations.

For high-dimensional periodic functions, multivariate trigonometric polynomials are very well-suited as approximants, see e.g. [Tem85, Tem89, Tem93, DuU13, KSU14, KSU15, DTU16]. One possibility to obtain such a multivariate trigonometric polynomial is to use a truncated Fourier series of a function, and a comprehensive analysis of the associated approximation errors exists. Often, the error analysis is performed for functions from function spaces characterized by the decay or summability of their Fourier coefficients with respect to certain weights. Since the Fourier coefficients are unknown in general, common methods for the construction of approximants are based on samples of a function. For this, one typically assumes that the function, which we want to approximate, is given as a black box and that the evaluation of function values is possible at arbitrary nodes or at least at certain nodes. Then, a fast Fourier transform (FFT) can be applied to function values and this yields approximated Fourier coefficients. Now, we can use the corresponding approximated Fourier partial sum, which is a multivariate trigonometric polynomial, as approximant of the function.

For moderately high-dimensional problems, e.g. up to ~ 20 dimensions, sparse grids are frequently used as spatial discretization, which are sampling sets belonging to Smolyak's algorithm [Smo63], see also [Tem85, Tem93, Ull08, DTU16], and approximants with frequencies supported on hyperbolic cross index sets yield a huge reduction in the degrees of freedom from $\mathcal{O}(N^d)$ to $\mathcal{O}(N \log^{d-1} N)$, where d denotes the dimension and the number of nodes in one coordinate direction is $\mathcal{O}(N)$. If the underlying function is sufficiently smooth, for instance has bounded mixed derivatives, this reduction only slightly affects the approximation error.

Even higher dimensions are possible using spatially adaptive versions of sparse grids for function approximation, see e.g. [Pfl10]. Moreover, there exist fast versions of the FFT adapted to sparse grids called hyperbolic cross FFT (HCFFT), see e.g. [BD89, Hal92, Gra07, GH14], which allow switching between sparse grids in spatial domain and hyperbolic crosses in frequency domain in only $\mathcal{O}(N \log^d N)$ arithmetic operations. However, for growing refinements N and dimensions d, the condition number of the Fourier matrix corresponding to the hyperbolic cross discrete Fourier transform grows distinctly [KK11]. Moreover, the efficient implementation of the HCFFT may be effortful due to the hierarchical scheme, e.g. see the implementation considerations in [Hal92] and [Gra07].

An alternative approach for obtaining approximants of multivariate periodic functions is based on using lattices as spatial discretization. Lattice rules are well known in numerical integration, see e.g. [Kor59, SK87, Tem86, SJ94] as well as the surveys [CN08, DKS13], they have already been used by Korobov [Kor59, Kor63] and Hlawka [Hla62] at the end of the 1950ies and the beginning of the 1960ies. In recent years, the utilization of lattice rules for multivariate integration was considered again starting with [SW01] and was followed by many contributions, see e.g. [SR02, SKJ02b, SKJ02a, Kuo03, Nuy07, CN08, CKN10]. Numerical integration and function approximation are closely related, since the computation of (approximated) Fourier coefficients from samples of a function may be regarded as (approximately) computing Fourier coefficients, defined by multivariate integrals of the function, with the help of cubature formulas. Therefore, lattice rules have also been used for multivariate function approximation for a long time, see e.g. [Kor63, Tem86, Tem89, Tem93] and the surveys [DKS13, DTU16], and were considered again in recent times, see e.g. [LH03, ZLH06, KSW06, KSW08, KWW09].

Rank-1 lattice rules or the "method of good lattice points" are preferably used due to their simple structure, the existence of fast and easy construction methods, explicit error formulas as well as extensive tractability results, see e.g. the survey [DKS13] and the references therein. A rank-1 lattice $\Lambda(\boldsymbol{z}, M)$ is completely characterized by two parameters, the generating vector $\boldsymbol{z} \in \mathbb{Z}^d$ and the size $M \in \mathbb{N}$. The corresponding rank-1 lattice rule is the cubature formula with rank-1 lattice nodes $\boldsymbol{x}_j := \frac{j}{M}\boldsymbol{z} \bmod 1$, $j = 0, \ldots, M-1$, and equal weights $1/M$. We remark that a rank-1 lattice rule is a quasi-Monte Carlo rule, see e.g. [Nie78, DKS13].

Despite the relatively simple structure of rank-1 lattices $\Lambda(\boldsymbol{z}, M)$, an exhaustive search of its parameters may be too costly. Even for given rank-1 lattice size M, the generating vector $\boldsymbol{z} \in \{0, 1, \ldots, M-1\}^d$ may have $\mathcal{O}(M^d)$ possible values. For the efficient construction of rank-1 lattices $\Lambda(\boldsymbol{z}, M)$ for integration and approximation, construction methods were developed which work in a component-by-component (CBC) way, considering one component of the generating vector $\boldsymbol{z}$ at a time and yielding a reduction of the search space to $\mathcal{O}(d\,M)$. Within the search method, the component of the generating vector $\boldsymbol{z}$ is typically chosen to minimize a certain error criterion. We remark that CBC construction methods were first considered in [Kor59, Kor63] and we refer to the survey [DKS13] for more historical details. More recently, important results for CBC construction methods and integration error analysis were obtained in [SR02] and many contributions followed afterwards, see e.g. [SKJ02b, SKJ02a, Kuo03] for weighted Sobolev spaces and Korobov spaces in different settings. Moreover, fast CBC construction methods based on FFTs were developed for functions in reproducing kernel Hilbert spaces, cf. [Nuy07, CN08], which reduce the number of required arithmetic operations for the CBC search distinctly. In recent years, the approximate computation of the Fourier coefficients of a function by lattice rules was considered in [LH03, ZLH06] and CBC construction methods as well as tractability results were discussed in [KSW06, KSW08, KWW09]. Again, fast construction methods based on FFTs

may be used to accelerate the CBC approach, see e.g. [CKN10, DKS13]. Moreover, the computation of the approximated Fourier coefficients can be performed by a FFT, see [LH03], in $\mathcal{O}(M \log M)$ arithmetic operations.

More recently, another CBC construction approach was developed which ensures that multivariate trigonometric polynomials can be exactly reconstructed from samples taken at the nodes $\boldsymbol{x}_j$ of a rank-1 lattice $\Lambda(\boldsymbol{z}, M)$, which fulfills a special reconstruction property, by applying a rank-1 lattice rule, see [KKP12, Käm13, Käm14a, Käm14b]. For a multivariate trigonometric polynomial p_I with frequencies supported on an arbitrary index set $I \subset \mathbb{Z}^d$ of finite cardinality, $|I| < \infty$, such a rank-1 lattice $\Lambda(\boldsymbol{z}, M)$ is called *reconstructing rank-1 lattice* [Käm14a] for the frequency index set I and is denoted by $\Lambda(\boldsymbol{z}, M, I)$. From samples at the corresponding nodes, the exact computation of the Fourier coefficients is very simple, using only a single one-dimensional FFT followed by a simple index transform, and requires only $\mathcal{O}(M \log M)$ arithmetic operations (under mild assumptions). Moreover, the corresponding Fourier matrix has always condition number 1 and the reconstruction method is perfectly stable.

In this work, we consider the approximation of multivariate periodic functions $f\colon \mathbb{T}^d \to \mathbb{C}$ by multivariate trigonometric polynomials p_I based on samples of f taken along reconstructing rank-1 lattices $\Lambda(\boldsymbol{z}, M, I)$, see also [KPV15a, KPV15b, BKUV16]. In doing so, we assume that we know the frequency index sets I which contain the non-zero Fourier coefficients $\hat{p}_{\boldsymbol{k}} \neq 0$ of multivariate trigonometric polynomials p_I or the approximately largest Fourier coefficients of multivariate periodic functions f due to the function classes they belong to. We show error estimates for rank-1 lattice sampling of multivariate periodic functions f from weighted subspaces $\mathcal{A}^{\alpha,\beta,\gamma}(\mathbb{T}^d)$ of the Wiener algebra $\mathcal{A}(\mathbb{T}^d)$ and for functions f from periodic Sobolev spaces of generalized mixed smoothness $\mathcal{H}^{\alpha,\beta,\gamma}(\mathbb{T}^d)$. Moreover, we develop a Taylor expansion based method for the fast evaluation along perturbed rank-1 lattices, see also [Vol13], as well as for the fast reconstruction, see also [KPV15a]. We obtain sampling error estimates which yield similar results as in the unperturbed case. Numerical tests for function approximation in up to 25 dimensions confirm the high performance and theoretical error estimates of the proposed methods.

A main contribution of this work is that we transfer the approach from the periodic case to the non-periodic case, where we develop a fast evaluation and reconstruction framework as well as an approximation method. Here, we use multivariate algebraic polynomials in Chebyshev form a_I, which are linear combinations of tensor product Chebyshev polynomials of the first kind $T_{\boldsymbol{k}}$, with frequencies $\boldsymbol{k}$ supported on an arbitrary known index set $I \subset \mathbb{N}_0^d$ of finite cardinality, $|I| < \infty$. As spatial discretization, we employ rank-1 Chebyshev lattices $\mathrm{CL}(\boldsymbol{z}, M)$ [CP11]. For the special case of ℓ_1-ball frequency index sets $I = I_{\mathrm{a},n}^{d,-\infty}$, the reconstruction has already been considered in [CP11, BDMV16, BDMV15]. In this work, we discuss methods for the fast evaluation of arbitrary multivariate algebraic polynomials in Chebyshev form a_I at the nodes $\boldsymbol{x}_j := \cos(\frac{j}{M}\pi\boldsymbol{z})$, $j = 0, \ldots, M$, of an arbitrary rank-1 Chebyshev lattice $\mathrm{CL}(\boldsymbol{z}, M)$. We develop methods for the fast and exact reconstruction of arbitrary multivariate algebraic polynomials in Chebyshev form a_I with frequencies supported on arbitrary known index sets $I \subset \mathbb{N}_0^d$, $|I| < \infty$, from samples, see also [PV15]. For this, we establish reconstruction properties for this non-periodic setting and define reconstructing rank-1 Chebyshev lattices $\mathrm{CL}(\boldsymbol{z}, M, I)$ analogously to the periodic case. Interestingly, we can use the generating vector $\boldsymbol{z}$ of certain reconstructing rank-1 lattices $\Lambda(\boldsymbol{z}, M, \hat{I})$ from the periodic case for the non-periodic case, which has already been considered for so-called tent transformed rank-1 lattices in [SNC16] for a different non-periodic setting than ours. We describe CBC construction algorithms for generating reconstructing rank-1 Chebyshev

lattices $\mathrm{CL}(\boldsymbol{z}, M, I)$ for arbitrary frequency index sets $I \in \mathbb{N}_0^d$, $|I| < \infty$. As in the periodic case, we show sampling error estimates for the approximation of multivariate non-periodic functions $f\colon [-1,1]^d \to \mathbb{R}$ from subspaces $\mathcal{A}^{\alpha,\beta}([-1,1]^d)$ of the analogon of the Wiener algebra $\mathcal{A}([-1,1]^d)$ and for functions f from corresponding Sobolev-type spaces of generalized mixed smoothness $\mathcal{H}^{\alpha,\beta}([-1,1]^d)$. Numerical tests in up to 25 dimensions confirm the effectiveness of the proposed reconstruction methods for multivariate algebraic polynomials in Chebyshev form a_I and for multivariate non-periodic functions f.

Until now, we assumed that we know frequency index sets I, which contain the locations of the non-zero Fourier or Chebyshev coefficients of a multivariate trigonometric polynomial p_I or multivariate algebraic polynomial a_I, respectively. However, these frequency locations are unknown in many cases. In general, it is a very challenging task to obtain such frequency index sets I, especially in higher dimensions.

A further main contribution of this work is the development of sparse FFT methods, which determine these unknown frequency locations in a dimension-incremental way based on a CBC approach, see also [PV16] for the periodic case. Especially notable are the simple structure, the general and easy applicability as well as the numerically observed high robustness of the proposed methods. We discuss a framework based on dimension-incremental projections parallel to the coordinate axes. Starting with the first component, we determine the unknown frequency locations $\tilde{I}$ belonging to the approximately largest Fourier or Chebyshev coefficients one component at a time and then proceed with the next component. As sampling sets, we employ the nodes of reconstructing rank-1 lattices $\Lambda(\boldsymbol{z}, M, \tilde{I})$ or reconstructing rank-1 Chebyshev lattices $\mathrm{CL}(\boldsymbol{z}, M, \tilde{I})$, and we make use of fast reconstruction algorithms. We develop methods for the reconstruction of high-dimensional trigonometric polynomials p_I as well as for the approximation of multivariate periodic functions f with infinitely many non-zero Fourier coefficients, using rank-1 lattice sampling. For high-dimensional algebraic polynomials in Chebyshev form a_I as well as for multivariate non-periodic functions f with infinitely many non-zero Chebyshev coefficients, we discuss modifications using rank-1 Chebyshev lattice sampling. We only require that a very large superset Γ of possible frequency locations, the search domain, is known and that we are able to obtain sampling values from the function under consideration. The proposed methods are successfully applied in numerical tests for the reconstruction of high-dimensional trigonometric polynomials p_I in up to 30 dimensions and high-dimensional algebraic polynomials in Chebyshev form a_I in up to 15 dimensions as well as for the approximation of a 10-dimensional periodic test function and a 9-dimensional non-periodic test function.

Parts of this work have already been published in [Vol13, KPV15a, KPV15b, KKM$^+$14, PV16, PV15, PTV16, BKUV16].

Outline of the Thesis

In the following, we give a short overview of the remaining chapters of this thesis. For a detailed overview, we refer to the introduction of each chapter.

Chapter 2: Multivariate Trigonometric Polynomials

We introduce necessary notations for multivariate trigonometric polynomials p_I. Our main focus is on the fast evaluation and fast reconstruction of multivariate trigonometric polynomials p_I with frequencies supported on arbitrary known index sets $I \subset \mathbb{Z}^d$, $|I| < \infty$, as well as the fast approximation of multivariate periodic functions $f\colon \mathbb{T}^d \to \mathbb{C}$ by multivariate

trigonometric polynomials p_I. We give a short overview of results for sparse grid sampling. In the main part of this chapter, we develop results for rank-1 lattice sampling and perturbed rank-1 lattice sampling based on reconstructing rank-1 lattices $\Lambda(\boldsymbol{z}, M, I)$. We collect the obtained error estimates for rank-1 lattice sampling in Table 2.1, 2.2 and 2.4.

In Section 2.1, we deal with the fast evaluation at rank-1 lattice nodes and perturbed rank-1 lattice nodes. We review the fast evaluation of arbitrary multivariate trigonometric polynomials p_I at the nodes $\boldsymbol{x}_j$ of an arbitrary rank-1 lattice $\Lambda(\boldsymbol{z}, M)$ using a simple index transform and a single one-dimensional FFT of length M. In Section 2.1.2, we develop a Taylor expansion based method for the fast evaluation at perturbed rank-1 lattice nodes and we show error estimates in Lemma 2.1 and Theorem 2.3. The evaluation error is small if the perturbations are not too large or if the Fourier coefficients $\hat{p}_{\boldsymbol{k}}$ have a certain decay.

In Section 2.2, we deal with the fast reconstruction using samples at rank-1 lattice nodes or perturbed rank-1 lattice nodes. We review results for the fast and exact reconstruction of arbitrary multivariate trigonometric polynomials p_I at the nodes $\boldsymbol{x}_j$ of a reconstructing rank-1 lattice $\Lambda(\boldsymbol{z}, M, I)$ as well as methods for the CBC construction of such lattices. Moreover, we show bounds on the cardinalities $|I_N^{d,T,\mathbf{1}}|$ of frequency index sets $I_N^{d,T,\mathbf{1}}$, cf. (2.14), in Lemma 2.5 and we collect bounds on the sizes M of reconstructing rank-1 lattices $\Lambda(\boldsymbol{z}, M, I_N^{d,T,\mathbf{1}})$ for $I_N^{d,T,\mathbf{1}}$ in Table 2.3. Depending on the choice of the shape parameter $T \in [-\infty, 1)$, the considered frequency index sets $I_N^{d,T,\mathbf{1}}$ include ℓ_1-balls $I_N^{d,-\infty,\mathbf{1}}$ and hyperbolic crosses $I_N^{d,0,\mathbf{1}}$ as well as energy-norm based hyperbolic crosses $I_N^{d,T,\mathbf{1}}$ for $0 < T < 1$. In general, we have an oversampling, i.e., we may require significantly more rank-1 lattice nodes $\boldsymbol{x}_j$ than there are frequencies $\boldsymbol{k} \in I$, $|I| \leq M \lesssim |I|^2$. In Section 2.2.2, we consider the reconstruction from samples taken at perturbed nodes originating from a reconstructing rank-1 lattice $\Lambda(\boldsymbol{z}, M, I)$ and we obtain error estimates in Theorem 2.10. The reconstruction is stable if the perturbations are not too large.

In Section 2.3, we consider the approximation of multivariate periodic functions $f\colon \mathbb{T}^d \to \mathbb{C}$ from weighted subspaces $\mathcal{A}^{\alpha,\beta,\gamma}(\mathbb{T}^d)$ of the Wiener algebra $\mathcal{A}(\mathbb{T}^d) = \mathcal{A}^{0,0,\mathbf{1}}(\mathbb{T}^d)$ and from periodic Sobolev spaces of generalized mixed smoothness $\mathcal{H}^{\alpha,\beta,\gamma}(\mathbb{T}^d) \hookrightarrow L_2(\mathbb{T}^d) = \mathcal{H}^{0,0,\mathbf{1}}(\mathbb{T}^d)$ by multivariate trigonometric polynomials p_I with focus on rank-1 lattice sampling and perturbed rank-1 lattice sampling. In Section 2.3.1, we consider norm inequalities and embeddings for the used function spaces in Lemma 2.11, 2.12 and 2.14. In Section 2.3.2, we show error estimates for truncation errors in Theorem 2.17 and 2.20 as well as Corollary 2.21 and 2.22, i.e., for the approximation of a multivariate periodic function $f\colon \mathbb{T}^d \to \mathbb{C}$ by a truncated Fourier series, which is a multivariate trigonometric polynomial p_I. In Section 2.3.3, we consider rank-1 lattice sampling and require only $\mathcal{O}(M \log M + d\,|I|)$ arithmetic operations for the computation of approximated Fourier coefficients from samples along reconstructing rank-1 lattices $\Lambda(\boldsymbol{z}, M, I)$ using Algorithm 2.4. Moreover, we show error estimates for rank-1 lattice sampling of multivariate periodic functions $f \in \mathcal{A}(\mathbb{T}^d)$ using reconstructing rank-1 lattices $\Lambda(\boldsymbol{z}, M, I)$. We obtain theoretical results, where the error rates asymptotically correspond to the ones of the truncation errors in Section 2.3.2 (up to logarithmic factors in some cases), see Table 2.1 and 2.2. In Section 2.3.4, we show error estimates for the case of perturbed rank-1 lattice sampling in Theorem 2.46 using the method from Section 2.2.2. In Section 2.3.5, we discuss various numerical examples for the approximation of multivariate periodic functions f by multivariate trigonometric polynomials p_I based on rank-1 lattice sampling for up to 25 dimensions and based on perturbed rank-1 lattice sampling for up to 10 dimensions. Moreover, we compare the obtained numerical results with the theoretical estimates. The observed decay rates of the sampling errors correspond approximately to the theoretical estimates.

Chapter 3: Multivariate Algebraic Polynomials in Chebyshev Form

We transfer the results from the periodic case of Chapter 2 to the non-periodic case. As basis functions, we use tensor products of Chebyshev polynomials of the first kind and we consider multivariate algebraic polynomials in Chebyshev form a_I which are a linear combination of these. As spatial discretization, we use rank-1 Chebyshev lattices $\mathrm{CL}(\boldsymbol{z}, M)$. Our main focus is on the fast evaluation and fast reconstruction of multivariate algebraic polynomials in Chebyshev form a_I with frequencies supported on arbitrary known index sets $I \subset \mathbb{N}_0^d$, $|I| < \infty$, as well as the fast approximation of multivariate non-periodic functions $f\colon [-1,1]^d \to \mathbb{R}$ by multivariate algebraic polynomials in Chebyshev form a_I. We mention results for sparse grid sampling and develop results for rank-1 Chebyshev lattice sampling.

In Section 3.1, we deal with the fast evaluation of arbitrary multivariate algebraic polynomials in Chebyshev form a_I at the nodes of an arbitrary rank-1 Chebyshev lattice $\mathrm{CL}(\boldsymbol{z}, M)$. We present a method indicated in Algorithm 3.1 which only uses easy-to-compute index transforms and a single one-dimensional discrete cosine transform (DCT), requiring $\mathcal{O}(M \log M + d\, 2^d |I|)$ arithmetic operations in total.

In Section 3.2, we consider the fast and exact reconstruction of arbitrary multivariate algebraic polynomials in Chebyshev form a_I with frequencies supported on arbitrary known index sets $I \subset \mathbb{N}_0^d$, $|I| < \infty$, from samples at the nodes of special rank-1 Chebyshev lattices $\mathrm{CL}(\boldsymbol{z}, M)$. In Section 3.2.1, we develop a method for the reconstruction indicated in Algorithm 3.2 which is based on using a single one-dimensional DCT and easy-to-compute index transforms, requiring $\mathcal{O}(M \log M + d\, 2^d |I|)$ arithmetic operations in total. Using the extended symmetric index set $\mathcal{M}(I)$, a modified version of Algorithm 3.2 for the fast and exact reconstruction has an arithmetic complexity of $\mathcal{O}(M \log M + d\, |\mathcal{M}(I)|)$, which may be distinctly less if only some components of the frequency index set I are coupled. We derive conditions which allow for the exact reconstruction, i.e., we establish reconstruction properties (3.22), (3.23) and (3.25), and we define reconstructing rank-1 Chebyshev lattices $\mathrm{CL}(\boldsymbol{z}, M, I)$ based on these. In Section 3.2.2, we develop two CBC construction approaches for reconstructing rank-1 Chebyshev lattices $\mathrm{CL}(\boldsymbol{z}, M, I)$. One method is based on building a reconstructing rank-1 lattice $\Lambda(\boldsymbol{z}, M, \mathcal{M}(I))$ from the periodic case for the extended symmetric index set $\mathcal{M}(I)$, see Theorem 3.4, and the second method directly uses the obtained reconstruction property (3.25) of the non-periodic case, see Algorithm 3.3.

In Section 3.3, we mention relations to other non-periodic approaches. In Section 3.3.1, we explain relations of reconstructing rank-1 Chebyshev lattices $\mathrm{CL}(\boldsymbol{z}, M, I)$ to Padua point sets and Lissajous curves. In Section 3.3.2, we discuss a related non-periodic approach based on tent transformed rank-1 lattices which uses different basis functions than Chebyshev polynomials.

In Section 3.4, we consider rank-1 Chebyshev lattice sampling for the approximation of multivariate non-periodic functions f. We consider norm inequalities and embeddings for the used function spaces in Lemma 3.9 analogously to the considerations in Section 2.3.1. Moreover, we develop an aliasing formula for rank-1 Chebyshev lattice sampling in Lemma 3.11. Analogously to the periodic case, we use reconstructing rank-1 Chebyshev lattices $\mathrm{CL}(\boldsymbol{z}, M, I)$ as sampling sets for function approximation and we obtain Algorithm 3.4, which requires $\mathcal{O}(M \log M + d\, 2^d\, |I|)$ arithmetic operations for the computation of approximated Chebyshev coefficients from the samples. We discuss a modified version of Algorithm 3.4 which requires $\mathcal{O}(M \log M + d\, |\mathcal{M}(I)|)$ arithmetic operations. We show error estimates for rank-1 Chebyshev lattice sampling in Theorem 3.16 and 3.17 as well as Corollary 3.18 and 3.19 similar to the results from the periodic case.

In Section 3.5, we give numerical results for the fast reconstruction of multivariate alge-

braic polynomials in Chebyshev form a_I. Additionally, we apply rank-1 Chebyshev lattice sampling for test functions in up to 25 dimensions. Moreover, we compare the numerical results with the error estimates and approximately observe the theoretical upper bounds.

Chapter 4: High-Dimensional Sparse FFT

For unknown frequency index sets I, we introduce a dimension-incremental method for determining the location of the non-zero Fourier coefficients of a multivariate trigonometric polynomial p_I based on rank-1 lattice sampling from Chapter 2. In doing so, we assume that the unknown frequency locations are a subset of a search domain $\Gamma \subset \mathbb{Z}^d$ which may be very, very large, e.g., a d-dimensional full grid. We apply this method for determining the (roughly) largest approximated Fourier coefficients of multivariate periodic functions f with infinitely many non-zero Fourier coefficients. Moreover, we transfer this idea to the non-periodic case and we obtain an analog method using the results from Chapter 3.

In Section 4.1, we deal with the periodic case. In Section 4.1.1, we introduce the general idea of a CBC based dimension-incremental projection method as Algorithm 4.1 and explain this on the reconstruction of a three-dimensional trigonometric polynomial using rank-1 lattice sampling in Figure 4.1. In Section 4.1.2, we develop two randomized algorithms indicated in Algorithm 4.2 and 4.3 for the general approach from Section 4.1.1. Both algorithms only differ in one computation step when building a reconstructing rank-1 lattice $\Lambda(\boldsymbol{z}, M, \tilde{I})$. Algorithm 4.2 performs a search in step 2b using a method similar to Algorithm 2.2, whereas Algorithm 4.3 directly uses Theorem 2.7. Consequently, the obtained rank-1 lattice sizes M and numbers of required samples of Algorithm 4.2 may be smaller but Algorithm 4.3 may be faster. In Section 4.1.3, we discuss situations when the successful detection may fail. In Section 4.1.4, we discuss the number of required samples and the arithmetic complexity of the proposed methods. Assuming $\sqrt{N} \lesssim s \lesssim N^d$ for sparsity parameter $s \in \mathbb{N}$, which is an input parameter of Algorithm 4.2 and 4.3, we require $\mathcal{O}(d\, s^2 N)$ many samples for both algorithms as well as $\mathcal{O}(d\, s^3 N^2)$ and $\mathcal{O}(d\, s^3 + d\, s^2 N \log(s\, N))$ arithmetic operations for Algorithm 4.2 and 4.3, respectively. If all detections succeed, we can replace s by the sparsity $|\operatorname{supp} \hat{p}|$, i.e., the number of non-zero Fourier coefficients $\hat{p}_{\boldsymbol{k}} \neq 0$ of a multivariate trigonometric polynomial p_I, in the sampling and arithmetic complexities. In Section 4.1.5, we give purely deterministic versions of the randomized algorithms from Section 4.1.2, which can be applied if the Fourier coefficients $\hat{p}_{\boldsymbol{k}}$ of the multivariate trigonometric polynomials p_I fulfill certain properties. For instance, this is the case when all Fourier coefficients $\hat{p}_{\boldsymbol{k}}$ are non-negative or non-positive. In Section 4.1.6, we present numerical results for up to 30 dimensions which confirm the effectiveness and high performance of the presented methods. Especially, we consider a numerical example where we successfully reconstruct the frequency locations of sparse 10-dimensional trigonometric polynomials p_I when the samples are perturbed by heavy noise. Moreover, we apply (a modified version of) Algorithm 4.2 and 4.3 for the approximate reconstruction of the (roughly) largest Fourier coefficients of a 10-dimensional test function with infinitely many non-zero Fourier coefficients. We successfully determine approximated Fourier coefficients and the corresponding frequency locations yielding small approximation errors.

In Section 4.2, we transfer the results from the periodic case to the non-periodic case. In Section 4.2.1, we describe the required modifications of the methods from Section 4.1.2 for the non-periodic case. For this, we replace all computations in Algorithm 4.2 related to rank-1 lattice sampling and reconstructing rank-1 lattices $\Lambda(\boldsymbol{z}, M, \tilde{I})$ by their non-periodic counterparts from Chapter 3, i.e., by rank-1 Chebyshev lattice sampling and reconstructing rank-1

Chebyshev lattices $\mathrm{CL}(\boldsymbol{z}, M, \tilde{I})$. We obtain Algorithm 4.4, which uses the first CBC construction method from Section 3.2.2 by searching for reconstructing rank-1 lattices $\Lambda(\boldsymbol{z}, M, \mathcal{M}(\tilde{I}))$ from the periodic case for the extended symmetric index set $\mathcal{M}(\tilde{I})$, and Algorithm 4.5, which uses the second CBC construction method, i.e., the reconstructing rank-1 Chebyshev lattices $\mathrm{CL}(\boldsymbol{z}, M, \tilde{I})$ are directly searched for. In Section 4.2.2, we present numerical examples which again show very promising results. We successfully reconstruct the frequency locations and non-zero Chebyshev coefficients $\hat{a}_{\boldsymbol{k}} \neq 0$ of high-dimensional sparse algebraic polynomials in Chebyshev form a_I in up to 15 dimensions. Moreover, we apply (a modified version of) Algorithm 4.4 and 4.5 for the approximate reconstruction of the (roughly) largest Chebyshev coefficients of a 9-dimensional test function with infinitely many non-zero Chebyshev coefficients. We successfully determine approximated Chebyshev coefficients and the corresponding frequency locations yielding small approximation errors.

Chapter 5: Conclusion

We briefly summarize the topics discussed in this work and recapitulate main contributions.

Acknowledgments

First and foremost, I would like to express my deepest appreciation and gratitude to my advisor Prof. Dr. Daniel Potts for his great and constant encouragement, his patient guidance, and his valuable advices. Additionally, I appreciate the excellent cooperations and valuable discussions with Dr. Lutz Kämmerer, Dr. Tino Ullrich, Glenn Byrenheid, and Prof. Dr. Manfred Tasche. Especially, I thank Prof. Dr. Vladimir Temlyakov for pointing out existing results on rank-1 lattice sampling. I thank my colleagues Dr. Manuel Gräf, Dr. Ralf Hielscher, Franziska Nestler, Dr. Michael Pippig, Michael Quellmalz, Prof. Dr. Karla Rost, and the above mentioned for the excellent working climate.

Chapter 2

Multivariate Trigonometric Polynomials

We consider multivariate trigonometric polynomials

$$p_I \in \Pi_I := \operatorname{span}\{\mathrm{e}^{2\pi\mathrm{i}\boldsymbol{k}\cdot\circ} \colon \boldsymbol{k} \in I\}, \tag{2.1}$$

$$p_I(\boldsymbol{x}) := \sum_{\boldsymbol{k}\in I} \hat{p}_{\boldsymbol{k}}\, \mathrm{e}^{2\pi\mathrm{i}\boldsymbol{k}\cdot\boldsymbol{x}}, \tag{2.2}$$

with frequencies $\boldsymbol{k} \in \mathbb{Z}^d$ supported on arbitrary index sets $I \subset \mathbb{Z}^d$, $|I| < \infty$, and corresponding Fourier coefficients $\hat{p}_{\boldsymbol{k}} \in \mathbb{C}$. Throughout this chapter, we assume that the frequency index set I is arbitrarily chosen but known and of finite cardinality, $|I| < \infty$. We are interested in methods for the *fast evaluation* of such a multivariate trigonometric polynomial (2.2) at certain nodes as well as the *fast reconstruction* of the Fourier coefficients $\hat{p}_{\boldsymbol{k}}$, $\boldsymbol{k} \in I$, from samples. Moreover, we apply these methods for the *fast approximation* of multivariate periodic signals $f \colon \mathbb{T}^d \to \mathbb{C}$ by trigonometric polynomials p_I based on samples of f. Then, the index set I contains the frequencies $\boldsymbol{k}$ belonging to the roughly largest Fourier coefficients of f and those Fourier coefficients are approximately obtained using a reconstruction method based on function values of f taken at certain nodes.

Various fast evaluation and reconstruction methods are already known for special cases. For instance, if the frequency index I is a d-dimensional full grid, e.g. $I := [-N, N)^d \cap \mathbb{Z}^d$ with refinement $N \in \mathbb{N}$, then one may use nodes $\boldsymbol{y}_j \in \mathbb{T}^d \simeq [0,1)^d$ on the d-dimensional full grid $\mathcal{Y} := \{0, 1, \ldots, 2N-1\}^d/(2N)$ in spatial domain. Here, a d-dimensional fast Fourier transform (FFT) of length $2N$ in each coordinate direction allows for the easy and fast computation of the function values $p_I(\boldsymbol{y}_j)$ from the Fourier coefficients $\hat{p}_{\boldsymbol{k}}$ and vice versa, see Figure 2.1 for an illustration. However, since the cardinalities $|I|$ of the frequency index set I and $|\mathcal{Y}|$ of the spatial grid $\mathcal{Y}$ are both $(2N)^d$, this approach suffers heavily from the curse of dimensionality [Bel61] even for moderate dimensions d, like e.g. $d = 4, 5, 6$.

This problem can be attenuated by using thinner frequency index sets I, like hyperbolic crosses, see e.g. the survey [DTU16] and the references therein. In case of the approximation of a periodic signal f, its Fourier coefficients should decrease accordingly to such frequency index sets I in order to obtain a reasonable approximation error. If we consider a hyperbolic cross confined in a cube $[-N, N]^d \cap \mathbb{Z}^d$, $N \in \mathbb{N}$, the cardinality $|I|$ is $\mathcal{O}(N \log^{d-1} N)$, see e.g. [Tem93], and the constant may be exponential in the dimension d. As spatial node set $\mathcal{Y} \subset \mathbb{T}^d$, one may use the nodes $\boldsymbol{y}_j$ of a sparse grid, which is a sampling set belonging to Smolyak's algorithm [Smo63], see also [Tem85, Tem93, Ull08, DTU16]. In this case, there exist fast algorithms for the evaluation and reconstruction called HCFFT (hyperbolic cross

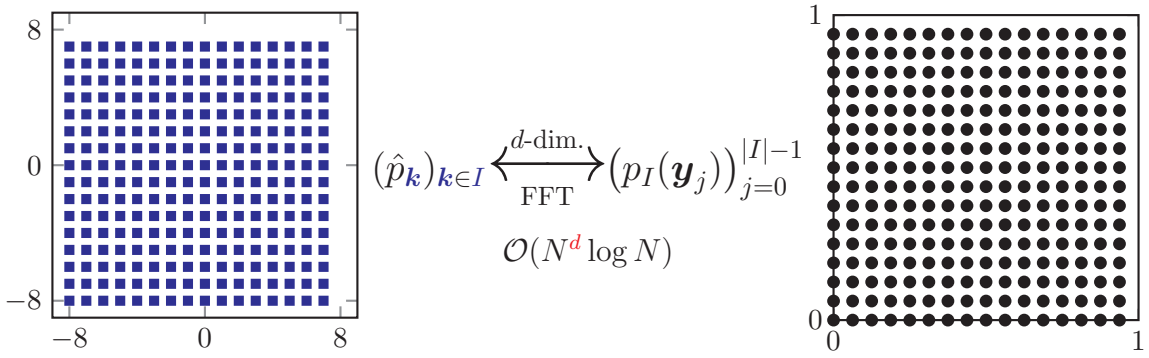

Figure 2.1: d-dimensional FFT between full grids.

fast Fourier transform), cf. [BD89, Hal92, Gra07, GH14]. In Figure 2.2, a two-dimensional hyperbolic cross and sparse grid are depicted.

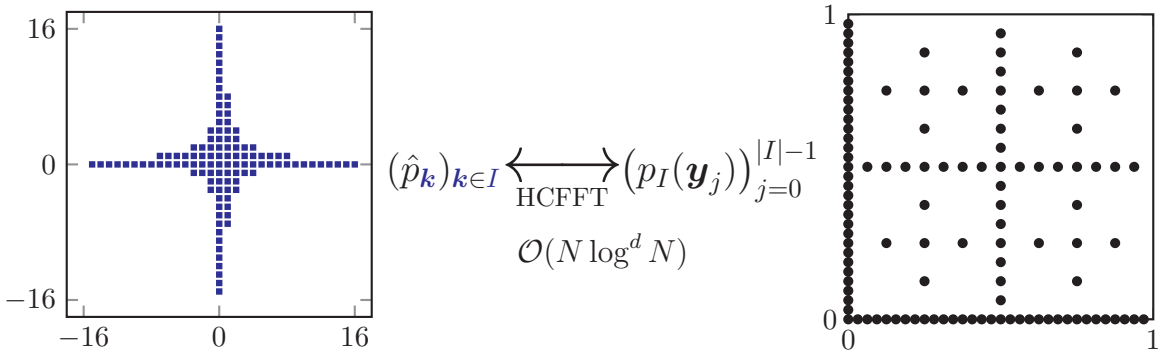

Figure 2.2: d-dimensional FFT between hyperbolic cross index set I and sparse grid $\{\boldsymbol{y}\}_{j=0}^{|I|-1}$, see e.g. [BD89, Hal92, Gra07, GH14].

However, as proven in [KK11], the condition number of the Fourier matrix corresponding to the hyperbolic cross discrete Fourier transform grows for increasing refinement N and dimension d. For fixed refinement N, the condition number scales approximately like $|I|^2$ and for fixed dimension d approximately like $\sqrt{|I|}$. Moreover, the implementation of a fast efficient version of such a HCFFT may be effortful due to the hierarchical scheme, e.g. see the implementation considerations in [Hal92] and [Gra07].

A generalization of hyperbolic cross index sets allows for even thinner frequency index sets, cf. [BG99, BG04, Kna00, GH14], where the cardinality $|I|$ is only $\mathcal{O}(N)$ for so-called energy-norm based hyperbolic crosses. Correspondingly, one may use generalized sparse grids as spatial discretization and there exists a version of the HCFFT which allows for the fast conversion between function values $p_I(\boldsymbol{y}_j)$ and Fourier coefficients $\hat{p}_{\boldsymbol{k}}$ in $\mathcal{O}(N \log N)$ arithmetic operations, see e.g. [GH14].

Still, the issue with the growing condition numbers for increasing hyperbolic cross index sets and the implementation effort for the HCFFT motivate to consider alternative approaches, where the corresponding Fourier matrix is better conditioned and the computation is very easy to implement.

Such an approach, which is suitable for arbitrary frequency index sets $I \subset \mathbb{Z}^d$ of finite cardinality, $|I| < \infty$, is going to be considered in this chapter. As spatial discretization,

so-called rank-1 lattices

$$\Lambda(\boldsymbol{z}, M) := \left\{ \boldsymbol{x}_j := \frac{j}{M}\boldsymbol{z} \bmod 1 \colon j = 0, \ldots, M-1 \right\} \subset \mathbb{T}^d \tag{2.3}$$

are used, which are characterized by the generating vector $\boldsymbol{z} \in \mathbb{Z}^d$ and the rank-1 lattice size $M \in \mathbb{N}$, see e.g. [SJ94, DKS13] and the references therein as well as Figure 2.3 for illustration. The number $|\Lambda(\boldsymbol{z}, M)|$ of distinct nodes $\boldsymbol{x}_j$ of the rank-1 lattice $\Lambda(\boldsymbol{z}, M)$ is a positive integer $\leq M$. We emphasize that the frequency index set I of finite cardinality $|I|$ may be arbitrarily chosen from $\mathbb{Z}^d$ and we do not have an admissibility condition, which may be required for sparse grids, cf. [GG03]. The striking advantage of using rank-1 lattices $\Lambda(\boldsymbol{z}, M)$ as spatial discretization is that for an arbitrary multivariate trigonometric polynomial p_I, $I \subset \mathbb{Z}^d$, $|I| < \infty$, all the function values $p_I(\boldsymbol{x}_j)$ at the nodes $\boldsymbol{x}_j$, $j = 0, \ldots, M-1$, of an arbitrary rank-1 lattice $\Lambda(\boldsymbol{z}, M) \subset \mathbb{T}^d$ can be computed using a simple index transform and a single one-dimensional FFT of length M with total computational costs of $\mathcal{O}(M \log M + d\,|I|)$, see e.g. [Käm14a]. In order to be able to reconstruct the Fourier coefficients $\hat{p}_{\boldsymbol{k}}$, $\boldsymbol{k} \in I$, from samples of p_I taken at the rank-1 lattice nodes $\boldsymbol{x}_j$, $j = 0, \ldots, M-1$, a certain *reconstruction property* needs to be fulfilled for the rank-1 lattice $\Lambda(\boldsymbol{z}, M)$ with respect to the frequency index set I, i.e., the equivalent conditions (2.25), (2.26), (2.27), (2.28) and (2.30), cf. [KKP12, Käm13, Käm14a]. Then, the condition number of the Fourier matrix is 1 and the reconstruction is perfectly stable. Such a rank-1 lattice will be called *reconstructing rank-1 lattice* $\Lambda(\boldsymbol{z}, M, I)$ for a given frequency index set I, see [Käm14a] where this name was used for the first time, and it can be easily constructed using a component-by-component (CBC) approach, see e.g. the survey [DKS13] for CBC constructions for integration lattices. The Fourier coefficients $\hat{p}_{\boldsymbol{k}}$, $\boldsymbol{k} \in I$, may be computed from samples along a reconstructing rank-1 lattice $\Lambda(\boldsymbol{z}, M, I)$ using a single one-dimensional FFT and a simple index transform, cf. [Käm14a] and see Figure 2.4 for illustration. We remark that for special frequency index sets I like hyperbolic crosses, the concept of reconstructing rank-1 lattices $\Lambda(\boldsymbol{z}, M, I)$ has already been used earlier, see e.g. [Tem86]. Moreover, CBC based construction methods for lattices also have a long history dating back at least to Korobov in 1959, see e.g. the surveys [CN08, DKS13] and the references therein.

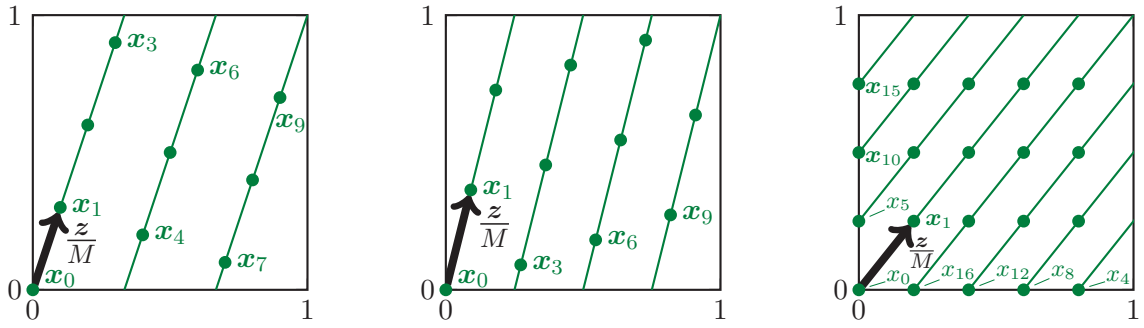

(a) $\boldsymbol{z} := (1,3)^\top$, $M := 10$ (b) $\boldsymbol{z} := (1,4)^\top$, $M := 11$ (c) $\boldsymbol{z} := (4,5)^\top$, $M := 20$

Figure 2.3: Examples of two-dimensional rank-1 lattices $\Lambda(\boldsymbol{z}, M)$.

Based on these results, we consider the usage of trigonometric polynomials p_I for the

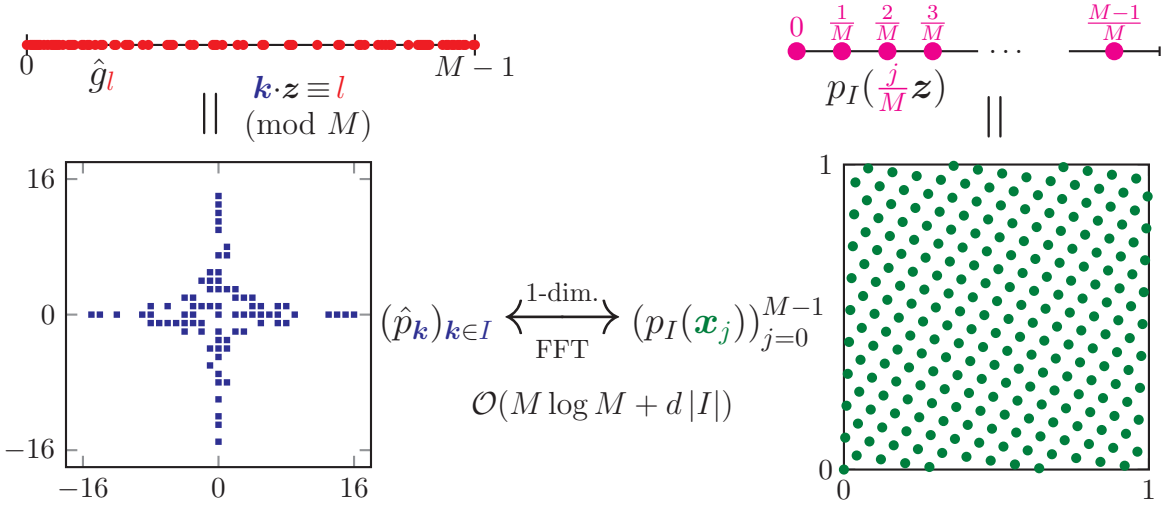

Figure 2.4: FFT between arbitrary index set I and suitable rank-1 lattice $\Lambda(\boldsymbol{z}, M)$.

approximation of periodic signals f from weighted subspaces of the Wiener algebra

$$\mathcal{A}(\mathbb{T}^d) := \left\{ f \in L_1(\mathbb{T}^d) \colon \|f|\mathcal{A}(\mathbb{T}^d)\| := \sum_{\boldsymbol{k}\in\mathbb{Z}^d} |\hat{f}_{\boldsymbol{k}}| < \infty \right\}, \tag{2.4}$$

where $L_1(\mathbb{T}^d)$ is the space of all absolutely (Lebesgue) integrable functions defined on the d-dimensional torus $\mathbb{T}^d$ and the Fourier coefficients of f are (formally) given by

$$\hat{f}_{\boldsymbol{k}} := \int_{\mathbb{T}^d} f(\boldsymbol{x})\, \mathrm{e}^{-2\pi \mathrm{i}\boldsymbol{k}\cdot\boldsymbol{x}}\, \mathrm{d}\boldsymbol{x}, \quad \boldsymbol{k} \in \mathbb{Z}^d. \tag{2.5}$$

Using the Fourier coefficients $\hat{f}_{\boldsymbol{k}}$, a function $f \in \mathcal{A}(\mathbb{T}^d)$ can be approximated by the Fourier partial sum

$$S_I f := \sum_{\boldsymbol{k}\in I} \hat{f}_{\boldsymbol{k}}\, \mathrm{e}^{2\pi \mathrm{i}\boldsymbol{k}\cdot\circ}, \tag{2.6}$$

i.e., by a truncated Fourier series which is a trigonometric polynomial p_I from (2.1). We call the error $f - S_I f$ of this approximation *truncation error*. We remark that multivariate trigonometric polynomials p_I are very well-suited for the approximation of high-dimensional periodic functions, see e.g. the survey [DTU16] and the references therein as well as [Tem85, Tem89, Tem93, DuU13, KSU14, KSU15].

Since the Fourier coefficients $\hat{f}_{\boldsymbol{k}}$, $\boldsymbol{k} \in \mathbb{Z}^d$, of a function $f \in \mathcal{A}(\mathbb{T}^d)$ are usually neither known nor easy to obtain analytically, one computes approximations of the Fourier coefficients $\hat{f}_{\boldsymbol{k}}$, e.g. based on samples of the function f. Motivated by the easy construction of a reconstructing rank-1 lattice $\Lambda(\boldsymbol{z}, M, I)$ and by the fast computation of Fourier coefficients $\hat{p}_{\boldsymbol{k}}$, $\boldsymbol{k} \in I$, from function samples $p_I(\boldsymbol{x}_j)$ taken along a reconstructing rank-1 lattice $\Lambda(\boldsymbol{z}, M, I)$, we consider the approximation of the integrals (2.5) by a lattice rule in this work. For this, we sample the function f at the nodes $\boldsymbol{x}_j := \frac{j}{M}\boldsymbol{z} \bmod \mathbf{1}$, $j = 0, \ldots, M-1$, of a reconstructing rank-1 lattice $\Lambda(\boldsymbol{z}, M, I)$. Here, we assume that the function $f \in \mathcal{A}(\mathbb{T}^d)$ is continuous or identify f by its continuous representative, cf. Remark 2.15. We compute all the approximated Fourier

coefficients $\hat{f}_{\boldsymbol{k}}^{\Lambda}$, $\boldsymbol{k} \in I$, by applying the same rank-1 lattice rule to the integrand in (2.5),

$$\hat{f}_{\boldsymbol{k}}^{\Lambda} := \frac{1}{M} \sum_{j=0}^{M-1} f\left(\frac{j}{M}\boldsymbol{z} \bmod \mathbf{1}\right) \mathrm{e}^{-2\pi \mathrm{i} j \boldsymbol{k}\cdot\boldsymbol{z}/M}, \qquad \boldsymbol{k} \in I. \tag{2.7}$$

This computation can be performed in $\mathcal{O}(M \log M + d\,|I|)$ arithmetic operations using a single one-dimensional FFT of length M and a simple index transform, see e.g. [Käm14a]. Based on (2.7), we define an approximation of the function f by the approximated Fourier partial sum

$$S_I^{\Lambda} f := \sum_{\boldsymbol{k}\in I} \hat{f}_{\boldsymbol{k}}^{\Lambda} \mathrm{e}^{2\pi \mathrm{i} \boldsymbol{k}\cdot\circ}, \tag{2.8}$$

which itself is a trigonometric polynomial $p_I \in \Pi_I$ of the form (2.2). We will call the corresponding error $f - S_I^{\Lambda} f$ *sampling error*. We remark that in [KPV15a, KPV15b], this error was called "approximation error". Moreover, the described approach of rank-1 lattice sampling has already been used for a long time for certain function classes, see e.g. [Kor63, Tem86, Tem93] and the references therein. Later, rank-1 lattice sampling was considered again in [LH03, ZLH06, KSW06, KSW08, KWW09]. As an alternative to using reconstructing rank-1 lattices $\Lambda(\boldsymbol{z}, M, I)$ as sampling sets, rank-1 lattices $\Lambda(\boldsymbol{z}, M)$ may be constructed by a CBC method minimizing certain error criteria, see e.g. [KSW06, KSW08, KWW09]. Moreover, there exist fast CBC construction methods based on FFTs for rank-1 lattices, which are constructed for the approximate integration and reconstruction of functions in reproducing kernel Hilbert spaces, cf. [Nuy07] as well as [CN08, CKN10].

In general, the approximated Fourier coefficients $\hat{f}_{\boldsymbol{k}}^{\Lambda}$ and the Fourier coefficients $\hat{f}_{\boldsymbol{k}}$ do not coincide and using the approximated Fourier partial sum $S_I^{\Lambda} f$ instead of the Fourier partial sum $S_I f$ causes an additional error, which will be called *aliasing error* $S_I f - S_I^{\Lambda} f$ in the following. When we estimate the sampling error $f - S_I^{\Lambda} f$ in this chapter for various norms, we usually split this error into the truncation error and aliasing error,

$$f - S_I^{\Lambda} f = (f - S_I f) + (S_I f - S_I^{\Lambda} f), \tag{2.9}$$

and using the triangle inequality yields

$$\|f - S_I^{\Lambda} f\| \le \|f - S_I f\| + \|S_I f - S_I^{\Lambda} f\|, \tag{2.10}$$

where $\|\circ\|$ is a given norm. As a consequence of this approximation approach, we are going to characterize the considered functions $f \in \mathcal{A}(\mathbb{T}^d)$ by the decay behavior of their Fourier coefficients $\hat{f}_{\boldsymbol{k}}$, $\boldsymbol{k} \in \mathbb{Z}^d$. We remark that function spaces, where the Fourier coefficients $\hat{f}_{\boldsymbol{k}}$ decay like hyperbolic crosses already occurred in [Kor59], see e.g. the survey [DTU16], and error estimates for rank-1 lattice sampling in such spaces were already presented in [Kor63]. Moreover, function spaces for various weighted $\ell_p(\mathbb{Z}^d)$ norms, $1 \le p \le \infty$, of the Fourier coefficients $\hat{f}_{\boldsymbol{k}}$ were discussed in [Spr97a]. Using the notation from [KPV15a], we consider the periodic Sobolev spaces of generalized mixed smoothness

$$\mathcal{H}^{\alpha,\beta,\boldsymbol{\gamma}}(\mathbb{T}^d) := \left\{ f \in L_1(\mathbb{T}^d) \colon \|f|\mathcal{H}^{\alpha,\beta,\boldsymbol{\gamma}}(\mathbb{T}^d)\| := \sqrt{\sum_{\boldsymbol{k}\in\mathbb{Z}^d} \omega^{\alpha,\beta,\boldsymbol{\gamma}}(\boldsymbol{k})^2 |\hat{f}_{\boldsymbol{k}}|^2} < \infty \right\} \subset L_2(\mathbb{T}^d) \tag{2.11}$$

with smoothness parameters $\beta \ge 0$ and $\alpha \ge -\beta$, where the weights $\omega^{\alpha,\beta,\boldsymbol{\gamma}}$ are defined by

$$\omega^{\alpha,\beta,\boldsymbol{\gamma}}(\boldsymbol{k}) := \max(1, \|\boldsymbol{k}\|_1)^{\alpha} \prod_{s=1}^{d} \max(1, \gamma_s^{-1}|k_s|)^{\beta}, \quad \boldsymbol{k} := \begin{pmatrix} k_1 \\ \vdots \\ k_d \end{pmatrix}, \quad \boldsymbol{\gamma} := \begin{pmatrix} \gamma_1 \\ \vdots \\ \gamma_d \end{pmatrix} \in (0,1]^d, \tag{2.12}$$

which are Hilbert spaces, and we have $\mathcal{H}^{0,0,\mathbf{1}}(\mathbb{T}^d) = L_2(\mathbb{T}^d)$. The parameter α characterizes the isotropic smoothness and the parameter β the so-called dominating mixed smoothness. Moreover, the weight parameter $\boldsymbol{\gamma}$ moderates the dependencies and importances of the different variables, cf. [SW98, KSW06]. A large value $\gamma_s \in (0,1]$, $s \in \{1,\ldots,d\}$, close to one means high importance and a small value close to zero a low importance of the s-th component. As discussed in [NSW04, p. 125], the weighted norm $\|f|\mathcal{H}^{\alpha,\beta,\boldsymbol{\gamma}}(\mathbb{T}^d)\|$ with weight parameter $\boldsymbol{\gamma} \in (0,1]^d$ and the unweighted norm $\|f|\mathcal{H}^{\alpha,\beta,\mathbf{1}}(\mathbb{T}^d)\|$ with $\boldsymbol{\gamma} := \mathbf{1}$ only differ by a constant, which may be exponential in the dimension d. Equivalent function spaces

$$\mathcal{H}^{\beta,\alpha}_{\mathrm{mix}}(\mathbb{T}^d) := \mathcal{H}^{\beta\mathbf{1}+\alpha\boldsymbol{e}_1}_{\mathrm{mix}}(\mathbb{T}^d) \cap \cdots \cap \mathcal{H}^{\beta\mathbf{1}+\alpha\boldsymbol{e}_d}_{\mathrm{mix}}(\mathbb{T}^d),$$

where $\mathcal{H}^{\boldsymbol{s}}_{\mathrm{mix}}(\mathbb{T}^d) := \mathcal{H}^{s_1}(\mathbb{T}) \otimes \cdots \otimes \mathcal{H}^{s_d}(\mathbb{T})$ and $\boldsymbol{e}_j$ denotes the j-th unit vector in $\mathbb{R}^d$, were introduced in [GK00, GH07] as a mixture of functions from the periodic isotropic Sobolev spaces $\mathcal{H}^{\alpha}(\mathbb{T}^d) = \mathcal{H}^{0,\alpha}_{\mathrm{mix}}(\mathbb{T}^d) = \mathcal{H}^{\alpha,0}(\mathbb{T}^d)$ and the periodic Sobolev spaces of dominating mixed smoothness $\mathcal{H}^{\beta}_{\mathrm{mix}}(\mathbb{T}^d) = \mathcal{H}^{\beta,0}_{\mathrm{mix}}(\mathbb{T}^d) = \mathcal{H}^{0,\beta}(\mathbb{T}^d)$. Please note that there are various names and characterizations with equivalent norms for these spaces. For instance, the periodic isotropic Sobolev spaces $\mathcal{H}^{\alpha}(\mathbb{T}^d) = \mathcal{H}^{0,\alpha}_{\mathrm{mix}}(\mathbb{T}^d) = \mathcal{H}^{\alpha,0}(\mathbb{T}^d)$ are also named periodic Bessel-Potential or Lebesgue or Liouville spaces, cf. [ST87, 3.5.4 (11)], the periodic Sobolev spaces of dominating mixed smoothness $\mathcal{H}^{\beta}_{\mathrm{mix}}(\mathbb{T}^d) = \mathcal{H}^{\beta,0}_{\mathrm{mix}}(\mathbb{T}^d) = \mathcal{H}^{0,\beta}(\mathbb{T}^d)$ are also named classes of functions of dominating mixed derivatives [GK00] or classes of functions with bounded mixed derivatives [Tem89] or weighted Korobov spaces [KSW06]. Instead of using the 1-norm for the isotropic smoothness in (2.12), other authors also commonly use a modified version with ∞-norm [GH14] or 2-norm [GH07, BDuSU16]. Moreover, Littlewood-Paley type dyadic decompositions are also used, see e.g. [BDuSU16, DTU16]. There exist various equivalent weights which have different approximation properties for large dimensions d, especially if one also considers the constants with respect to the dimension d, cf. [KSU14, KSU15]. Moreover, we remark that for smoothness parameters $\alpha, \beta \in \mathbb{N}_0$, we also have the equivalent characterization

$$\mathcal{H}^{\alpha,\beta,\mathbf{1}}(\mathbb{T}^d) = \left\{ f \in L_1(\mathbb{T}^d) \colon \|f|\tilde{\mathcal{H}}^{\alpha,\beta}(\mathbb{T}^d)\| := \sqrt{\sum_{\|\boldsymbol{m}\|_1 \le \alpha} \sum_{\|\boldsymbol{n}\|_\infty \le \beta} \|D^{\boldsymbol{m}+\boldsymbol{n}} f\|_2^2} < \infty \right\},$$

see e.g. [BKUV16]. In addition to the Hilbert spaces $\mathcal{H}^{\alpha,\beta,\boldsymbol{\gamma}}(\mathbb{T}^d)$, we consider the subspaces

$$\mathcal{A}^{\alpha,\beta,\boldsymbol{\gamma}}(\mathbb{T}^d) := \left\{ f \in L_1(\mathbb{T}^d) \colon \|f|\mathcal{A}^{\alpha,\beta,\boldsymbol{\gamma}}(\mathbb{T}^d)\| := \sum_{\boldsymbol{k} \in \mathbb{Z}^d} \omega^{\alpha,\beta,\boldsymbol{\gamma}}(\boldsymbol{k}) |\hat{f}_{\boldsymbol{k}}| < \infty \right\} \tag{2.13}$$

of the Wiener algebra $\mathcal{A}(\mathbb{T}^d) = \mathcal{A}^{0,0,\mathbf{1}}(\mathbb{T}^d)$ with dominating mixed smoothness $\beta \ge 0$, isotropic smoothness $\alpha \ge -\beta$ and weight parameter $\boldsymbol{\gamma} \in (0,1]^d$. These spaces are a mixture and extension of the spaces $A^{\alpha}_1(\mathbb{T}^d)$ of order α and of the spaces $S^{\beta,\beta}_{1,1}(\mathbb{T}^2)$ of bivariate periodic functions with dominating mixed smoothness of order β from [Spr97a].

As frequency index sets I, we use the weighted frequency index sets

$$I_N^{d,T,\boldsymbol{\gamma}} := \left\{ \boldsymbol{k} \in \mathbb{Z}^d \colon \omega^{-T,1,\boldsymbol{\gamma}}(\boldsymbol{k}) = \max(1, \|\boldsymbol{k}\|_1)^{-T} \prod_{s=1}^{d} \max(1, \gamma_s^{-1}|k_s|) \le N^{1-T} \right\}, \tag{2.14}$$

where $N \ge 1$ is the refinement, $T \in (-\infty, 1)$ is the shape parameter, $\boldsymbol{\gamma}$ is the weight parameter as specified in (2.12) and the weights $\omega^{\alpha,\beta,\boldsymbol{\gamma}}(\boldsymbol{k})$ are defined as in (2.12). As a natural extension

for $T = -\infty$, we define the weighted frequency index set $I_N^{d,-\infty,\boldsymbol{\gamma}}$ as the d-dimensional ℓ_1-ball of size N,

$$I_N^{d,-\infty,\boldsymbol{\gamma}} := \left\{ \boldsymbol{k} \in \mathbb{Z}^d \colon \max(1, \|\boldsymbol{k}\|_1) \leq N \right\}. \tag{2.15}$$

Good choices of the shape parameter $T \in [-\infty, 1)$ depend on the function spaces and the norms where the truncation, aliasing and sampling errors are measured. In Figure 2.5, two-dimensional examples of frequency index sets $I_N^{d,T,\boldsymbol{\gamma}}$ are shown for refinement $N := 32$, weight parameter $\boldsymbol{\gamma} := \mathbf{1}$ and different choices of the shape parameter $T \in [\infty, 1)$.

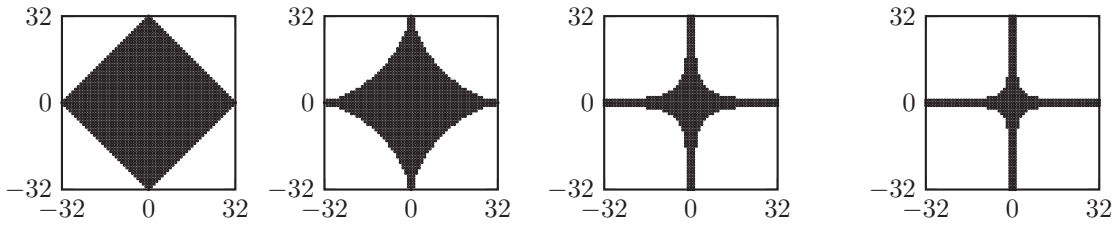

l_1-ball $I_{32}^{2,-\infty,\mathbf{1}}$ | index set $I_{32}^{2,-5,\mathbf{1}}$ | symmetric hyperbolic cross $I_{32}^{2,0,\mathbf{1}}$ | energy-norm based hyperbolic cross $I_{32}^{2,1/2,\mathbf{1}}$

Figure 2.5: ([KPV15b, Figure 1.1]). Frequency index sets $I_{32}^{2,T,\mathbf{1}}$ for $T \in \{-\infty, -5, 0, \frac{1}{2}\}$.

In this chapter, we show error estimates for rank-1 lattice sampling errors $f - S_I^\Lambda f$ with respect to the refinement N and cardinality $|I|$ for functions f from periodic Sobolev spaces of generalized mixed smoothness $\mathcal{H}^{\alpha,\beta,\boldsymbol{\gamma}}(\mathbb{T}^d)$, when using reconstructing rank-1 lattices $\Lambda(\boldsymbol{z}, M, I)$. We obtain results which correspond to those from (generalized) sparse grid sampling [SU07, BDuSU16, DTU16]. For functions f from subspaces $\mathcal{A}^{\alpha,\beta,\boldsymbol{\gamma}}(\mathbb{T}^d)$ of the Wiener algebra $\mathcal{A}(\mathbb{T}^d)$, we obtain comparable error bounds for the rank-1 lattice sampling error $f - S_I^\Lambda f$ with respect to the refinement N or cardinality $|I|$. Additionally, we discuss the rank-1 lattice sampling error $f - S_I^\Lambda f$ with respect to the number of samples M. The obtained error estimates are asymptotically best possible in several cases, since the upper bounds correspond to the lower bounds, see also [BKUV16]. However, the obtained sampling rate with respect to the number of samples M has only half the main rate compared to (generalized) sparse grid sampling, see also [BKUV16, DTU16]. Nevertheless, rank-1 lattice sampling is a very efficient and an easy-to-use method for the approximation of high-dimensional periodic functions f.

The remaining parts of this chapter are structured as follows.

In Section 2.1, we review the fast evaluation of a trigonometric polynomial p_I from (2.2) with frequencies supported on an arbitrary index set $I \subset \mathbb{Z}^d$, $|I| < \infty$, at the nodes $\boldsymbol{x}_j$, $j = 0, \ldots, M-1$, of an arbitrary rank-1 lattice $\Lambda(\boldsymbol{z}, M) \subset \mathbb{T}^d$ and we discuss the case of perturbed rank-1 lattice nodes. In Section 2.1.1, we deal with (exact) rank-1 lattice nodes $\boldsymbol{x}_j$ and give a method for the fast evaluation, see e.g. [LH03, KKP12], which uses a simple index transform and a single one-dimensional FFT. In this work, we extend these considerations to the case where the rank-1 lattice nodes $\boldsymbol{x}_j$ are perturbed. In Section 2.1.2, a Taylor expansion based method for the fast evaluation is presented as well as error estimates, see also [Vol13].

In Section 2.2, we deal with the fast reconstruction of the Fourier coefficients $\hat{p}_{\boldsymbol{k}}$, $\boldsymbol{k} \in I$, from samples of a trigonometric polynomial p_I taken at rank-1 lattice nodes $\boldsymbol{x}_j$, $j = 0, \ldots, M-1$, or perturbed rank-1 lattice nodes. Here we can not use arbitrarily chosen rank-1 lattices $\Lambda(\boldsymbol{z}, M)$. Instead, we have to use a *reconstructing rank-1 lattice* $\Lambda(\boldsymbol{z}, M, I)$. In Section 2.2.1, we review important properties and construction strategies for such lattices,

see also [KKP12, Käm13, Käm14a]. The condition number of the Fourier matrix for the unperturbed case is 1 and consequently, the reconstruction is perfectly stable. However, there is a price to pay for this nice property. In general, the number M of samples for the reconstruction is distinctly higher than the number $|I|$ of Fourier coefficients $\hat{p}_{\boldsymbol{k}}$, cf. [Käm14b], it may scale like up to $|I|^2$, e.g. for energy-norm based hyperbolic crosses $I = I_N^{d,T,\boldsymbol{\gamma}}$, $0 < T < 1$. In such cases, we may observe an oversampling factor $M/|I|$ of up to about $|I|$, i.e., we may have approximately $|I|$ times more sampling nodes $\boldsymbol{x}_j$ than frequencies $\boldsymbol{k} \in I$. Consequently, if we use this method for the approximation of a periodic signal from samples, then we generally do not have an interpolation but so-called hyperinterpolation, see [Slo95]. On the other hand, under mild assumptions, there exists a constructive method for obtaining such a reconstructing rank-1 lattice $\Lambda(\boldsymbol{z}, M, I)$ of size $M \leq |I|^2$ with no further dependence on the dimension d, cf. Theorem 2.4. Especially, if the frequency index set I does not have an exponential dependence on the dimension d, then we are able to construct these special rank-1 lattices, allowing for the reconstruction of any multivariate trigonometric polynomial p_I with frequencies supported on I, where the rank-1 lattice size M has the same property. Additionally, the Fourier coefficients $\hat{p}_{\boldsymbol{k}}$, $\boldsymbol{k} \in I$, may be computed from samples along a reconstructing rank-1 lattice $\Lambda(\boldsymbol{z}, M, I)$ using a single one-dimensional FFT and a simple index transform, cf. [Käm14a] and see Figure 2.4 for illustration. In this work, we extend these considerations to the case of perturbed reconstructing rank-1 lattices analogously to the considerations from Section 2.1.2, see also [KPV15a]. In Section 2.2.2, we obtain a method for the approximation of the Fourier coefficients $\hat{p}_{\boldsymbol{k}}$, $\boldsymbol{k} \in I$, which uses multivariate Taylor expansion and one-dimensional FFTs. Moreover, we give error estimates.

In Section 2.3, we consider the approximation of periodic functions $f\colon \mathbb{T}^d \to \mathbb{C}$ from Banach spaces $\mathcal{A}^{\alpha,\beta,\boldsymbol{\gamma}}(\mathbb{T}^d)$ and from periodic Sobolev spaces of generalized mixed smoothness $\mathcal{H}^{\alpha,\beta,\boldsymbol{\gamma}}(\mathbb{T}^d)$ for suitable choices of the isotropic smoothness α, the dominating mixed smoothness β and the weight parameter $\boldsymbol{\gamma}$ using rank-1 lattice sampling, see also [KPV15a, KPV15b].

In Section 2.3.1, we discuss various embeddings between different periodic function spaces, which yield admissible values for the smoothness parameters α, β and which are required in the following sections. In Figure 2.6, we present an overview of the admissible values of the statements in Section 2.3.2 and 2.3.3. The allowed parameter choices in Figure 2.6a and 2.6b guarantee the existence of a continuous representative of a function $f \in \mathcal{A}^{\alpha,\beta,\boldsymbol{\gamma}}(\mathbb{T}^d)$ and $f \in \mathcal{H}^{\alpha,\beta,\boldsymbol{\gamma}}(\mathbb{T}^d)$, respectively, cf. Remark 2.15 as well as Lemma 2.12 and 2.14.

In Section 2.3.2, we discuss the error estimates for the truncation error $f - S_I f$, since we estimate the sampling error $f - S_I^\Lambda f$ using inequality (2.10). This means, we consider the approximation of the function f by the truncated Fourier series $S_I f$ and we show error estimates which are optimal up to constants for the considered function classes for suitable choices of the frequency index set I and of the involved norms. For dominating mixed smoothness $\beta \geq 0$ and isotropic smoothness $\alpha > -\beta$, we use weighted frequency index sets $I := I_N^{d,T,\boldsymbol{\gamma}}$ with shape parameter $T := -\alpha/\beta \in [-\infty, 1)$ and we obtain for the truncation error $f - S_I f$ of a function $f \in \mathcal{A}^{\alpha,\beta,\boldsymbol{\gamma}}(\mathbb{T}^d) \hookrightarrow \mathcal{A}(\mathbb{T}^d)$ the with respect to the refinement N asymptotically sharp bounds

$$\|\boldsymbol{\gamma}\|_\infty^\beta \, (N+1)^{-(\alpha+\beta)} \leq \| \operatorname{Id} - S_{I_N^{d,T,\boldsymbol{\gamma}}} | \mathcal{A}^{\alpha,\beta,\boldsymbol{\gamma}}(\mathbb{T}^d) \to L_\infty(\mathbb{T}^d) \| \leq N^{-(\alpha+\beta)}$$

from Theorem 2.17, see the first entry in Table 2.1. Similarly in the Hilbert space cases, for dominating mixed smoothness $\beta \geq t \geq 0$ and isotropic smoothness $r, \alpha \in \mathbb{R}$ with $\alpha + \beta > r + t \geq 0$, we set the shape parameter $T := -\frac{\alpha - r}{\beta - t} \in [-\infty, 1)$ and we obtain for the truncation error $f - S_I f$ of a function $f \in \mathcal{H}^{\alpha,\beta,\boldsymbol{\gamma}}(\mathbb{T}^d) \hookrightarrow L_2(\mathbb{T}^d)$ the with respect to the refinement N

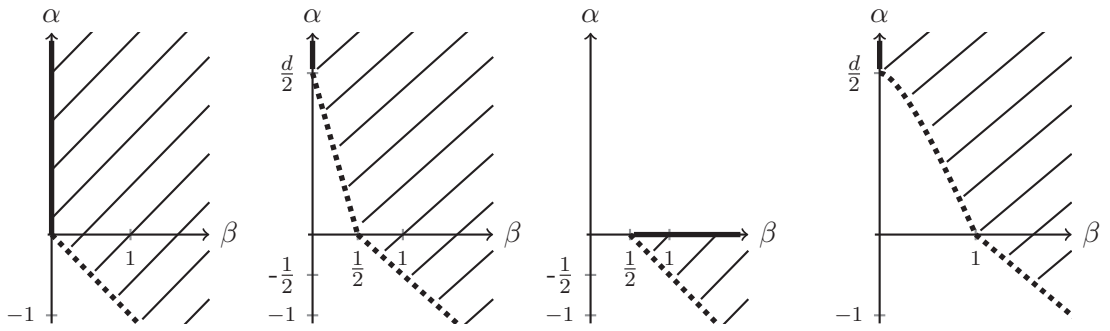

(a) Theorem 2.17, 2.24, 2.26; Corollary 2.40; $\mathcal{A}^{\alpha,\beta,\gamma}(\mathbb{T}^d) \hookrightarrow \mathcal{A}(\mathbb{T}^d) \hookrightarrow \mathcal{C}(\mathbb{T}^d)$. Theorem 2.20; $\mathcal{H}^{\alpha,\beta,\gamma}(\mathbb{T}^d) \hookrightarrow L_2(\mathbb{T}^d)$.

(b) Lemma 2.12 for $\alpha \geq 0$, Lemma 2.14 for $\alpha < 0$; $\mathcal{H}^{\alpha,\beta,\gamma}(\mathbb{T}^d) \hookrightarrow \mathcal{A}(\mathbb{T}^d) \hookrightarrow \mathcal{C}(\mathbb{T}^d)$.

(c) Theorem 2.30, 2.42; Corollary 2.44; $\mathcal{H}^{\alpha,\beta,\gamma}(\mathbb{T}^d) \hookrightarrow \mathcal{A}(\mathbb{T}^d) \hookrightarrow \mathcal{C}(\mathbb{T}^d)$.

(d) Theorem 2.36 for $\alpha \geq 0$, Theorem 2.39 for $\alpha < 0$; Corollary 2.41 for $\alpha > 0$, Corollary 2.45 for $\alpha \leq 0$; $\mathcal{H}^{\alpha,\beta,\gamma}(\mathbb{T}^d) \hookrightarrow \mathcal{A}(\mathbb{T}^d) \hookrightarrow \mathcal{C}(\mathbb{T}^d)$.

Figure 2.6: Visualization of admissible values from Table 2.1, 2.2 and 2.4 as well as from Lemma 2.12 and 2.14 for isotropic smoothness $\alpha \in \mathbb{R}$ and dominating mixed smoothness $\beta \geq 0$ setting $r = t = 0$.

asymptotically sharp bounds

$$\|\boldsymbol{\gamma}\|_\infty^{\beta-t}\,(N+1)^{-(\alpha-r+\beta-t)} \leq \|\operatorname{Id} - S_{I_N^{d,T,\boldsymbol{\gamma}}} | \mathcal{H}^{\alpha,\beta,\boldsymbol{\gamma}}(\mathbb{T}^d) \to \mathcal{H}^{r,t,\boldsymbol{\gamma}}(\mathbb{T}^d)\| \leq N^{-(\alpha-r+\beta-t)}$$

from Theorem 2.20, see the first entry in Table 2.2. We depict the admissible values of the smoothness parameters α and β in Figure 2.6a. Alternatively, the error bounds may be expressed with respect to the degrees of freedom $|I_N^{d,T,\boldsymbol{\gamma}}|$, which also gives sharp asymptotic bounds for increasing refinement N due to the sharp asymptotic bounds on the cardinalities $|I_N^{d,T,\boldsymbol{\gamma}}|$ in Table 2.3, see Corollary 2.21 and 2.22.

setting	error estimates
truncation error	$\|\operatorname{Id} - S_{I_N^{d,T,\boldsymbol{\gamma}}} \| \mathcal{A}^{\alpha,\beta,\boldsymbol{\gamma}}(\mathbb{T}^d) \to L_\infty(\mathbb{T}^d)\| \asymp N^{-(\alpha+\beta)}$
$T := -\alpha/\beta \in [-\infty, 1)$	Theorem 2.17, $\beta \geq 0$, $\alpha > -\beta$
sampling error	$\|f - S^\Lambda_{I_N^{d,T,\boldsymbol{\gamma}}} f \| L_\infty(\mathbb{T}^d)\| \leq \|f - S^\Lambda_{I_N^{d,T,\boldsymbol{\gamma}}} f \| \mathcal{A}(\mathbb{T}^d)\|$
arbitrary $\Lambda(\boldsymbol{z}, M, I_N^{d,T,\boldsymbol{\gamma}})$	$\leq 2\, N^{-(\alpha+\beta)} \|f \| \mathcal{A}^{\alpha,\beta,\boldsymbol{\gamma}}(\mathbb{T}^d)\|$
$T := -\alpha/\beta \in [-\infty, 1)$	Theorem 2.24, $\beta \geq 0$, $\alpha > -\beta$

Table 2.1: Overview of truncation error estimates and rank-1 lattice sampling error estimates from Section 2.3.2 and 2.3.3 for functions $f \in \mathcal{A}^{\alpha,\beta,\boldsymbol{\gamma}}(\mathbb{T}^d)$ with respect to refinement N of frequency index sets $I_N^{d,T,\boldsymbol{\gamma}}$.

In Section 2.3.3, we investigate the utilization of rank-1 lattice sampling for function approximation by trigonometric polynomials, see also [KPV15a, KPV15b]. In doing so, we always use reconstructing rank-1 lattices $\Lambda(\boldsymbol{z}, M, I)$, which may be arbitrarily chosen in many

truncation error	$\|\operatorname{Id} - S_{I_N^{d,T,\boldsymbol{\gamma}}} \| \mathcal{H}^{\alpha,\beta,\boldsymbol{\gamma}}(\mathbb{T}^d) \to \mathcal{H}^{r,t,\boldsymbol{\gamma}}(\mathbb{T}^d)\| \asymp N^{-(\alpha-r+\beta-t)}$
$T := -\frac{\alpha-r}{\beta-t} \in [-\infty, 1)$	Theorem 2.20, $r, \alpha \in \mathbb{R}$, $\beta \geq t \geq 0$, $\alpha + \beta > r + t \geq 0$
sampling error	$\|f - S^{\Lambda}_{I_N^{d,T,\boldsymbol{\gamma}}} f \| \mathcal{H}^{r,t,\boldsymbol{\gamma}}(\mathbb{T}^d)\| \leq 2\, N^{-(\alpha-r+\beta-t)} \|f \| \mathcal{A}^{\alpha,\beta,\boldsymbol{\gamma}}(\mathbb{T}^d)\|$
arbitrary $\Lambda(\boldsymbol{z}, M, I_N^{d,T,\boldsymbol{\gamma}})$	$\lesssim N^{-(\alpha-r+\beta-t)} \|f \| \mathcal{H}^{\alpha,\beta+\lambda,\boldsymbol{\gamma}}(\mathbb{T}^d)\|$
$T := -\frac{\alpha-r}{\beta-t} \in [-\infty, 1)$	Theorem 2.26, $r, \alpha \in \mathbb{R}$, $\beta \geq t \geq 0$, $\alpha + \beta > r + t \geq 0$, $T \in [-\frac{r}{t}, -\frac{\alpha}{\beta}]$
sampling error	$\|f - S^{\Lambda}_{I_N^{d,0,\mathbf{1}}} f \| \mathcal{H}^{0,t,\mathbf{1}}(\mathbb{T}^d)\| \lesssim \|f \| \mathcal{H}^{\alpha,\beta,\mathbf{1}}(\mathbb{T}^d)\|\, N^{-(\alpha+\beta-t)}$
arbitrary $\Lambda(\boldsymbol{z}, M, I_N^{d,0,\mathbf{1}})$	$\cdot \begin{cases} (\log N)^{(d-1)/2} & \text{for } \alpha = 0, \\ 1 & \text{for } \alpha < 0, \end{cases}$
$T := 0$	Theorem 2.30, $\beta > \frac{1}{2}$, $\alpha \leq 0$, $t \geq 0$, $\alpha + \beta > \max\{t, \frac{1}{2}\}$
sampling error	$\|f - S^{\Lambda}_{I_N^{d,T,\mathbf{1}}} f \| L_2(\mathbb{T}^d)\| \lesssim N^{-(\alpha+\beta)}\, \|f \| \mathcal{H}^{\alpha,\beta,\mathbf{1}}(\mathbb{T}^d)\|$
special Korobov lattice	
$T := -\alpha/\beta \in [-\infty, 0]$	Theorem 2.36, $\alpha, \beta \geq 0$, $\alpha + \beta > \frac{d}{2} \frac{2d\beta+\alpha}{d\beta+\alpha} \frac{\beta+\alpha}{d\beta+\alpha} > 0$
sampling error	$\|f - S^{\Lambda}_{I_N^{d,T,\mathbf{1}}} f \| L_2(\mathbb{T}^d)\| \lesssim N^{-(\alpha+\beta)}\, \|f \| \mathcal{H}^{\alpha,\beta,\mathbf{1}}(\mathbb{T}^d)\|$
special Korobov lattice	
$T := -\alpha/\beta \in (0, 1)$	Theorem 2.39, $\alpha < 0$, $\beta > 1 - \alpha$

Table 2.2: Overview of truncation and rank-1 lattice sampling error estimates from Section 2.3.2 and 2.3.3 for functions $f \in \mathcal{H}^{\alpha,\beta,\boldsymbol{\gamma}}(\mathbb{T}^d)$ and $f \in \mathcal{H}^{\alpha,\beta+\lambda,\boldsymbol{\gamma}}(\mathbb{T}^d)$, $\lambda > \frac{1}{2}$, with respect to the refinement N of frequency index sets $I_N^{d,T,\boldsymbol{\gamma}}$.

cases as long as the reconstruction property (2.25) is fulfilled. For dominating mixed smoothness $\beta \geq 0$, isotropic smoothness $\alpha > -\beta$ and shape parameter $T := -\alpha/\beta \in [-\infty, 1)$, we show in the proof of Theorem 2.24 that the aliasing error fulfills $\|S_{I_N^{d,T,\boldsymbol{\gamma}}} - S^{\Lambda}_{I_N^{d,T,\boldsymbol{\gamma}}} f | L_\infty(\mathbb{T}^d)\| \leq \|f - S_{I_N^{d,T,\boldsymbol{\gamma}}} f | \mathcal{A}(\mathbb{T}^d)\| \leq N^{-(\alpha+\beta)}\, \|f | \mathcal{A}^{\alpha,\beta,\boldsymbol{\gamma}}(\mathbb{T}^d)\|$ and consequently, we obtain for the sampling error

$$\|f - S^{\Lambda}_{I_N^{d,T,\boldsymbol{\gamma}}} f | L_\infty(\mathbb{T}^d)\| \leq 2\, N^{-(\alpha+\beta)}\, \|f | \mathcal{A}^{\alpha,\beta,\boldsymbol{\gamma}}(\mathbb{T}^d)\|,$$

see the second entry in Table 2.1. In the Hilbert space case, we show in this work in the proof of Theorem 2.26 for the aliasing error of a function $f \in \mathcal{H}^{\alpha,\beta+\lambda,\boldsymbol{\gamma}}(\mathbb{T}^d)$ the estimate

$$\|S_{I_N^{d,T,\boldsymbol{\gamma}}} f - S^{\Lambda}_{I_N^{d,T,\boldsymbol{\gamma}}} f | \mathcal{H}^{r,t,\boldsymbol{\gamma}}(\mathbb{T}^d)\| \leq (1 + 2\zeta(2\lambda))^{\frac{d}{2}}\, N^{-(\alpha-r+\beta-t)} \|f | \mathcal{H}^{\alpha,\beta+\lambda,\boldsymbol{\gamma}}(\mathbb{T}^d)\|,$$

where the dominating mixed smoothness $\beta \geq t \geq 0$, an additive factor $\lambda > \frac{1}{2}$, the isotropic smoothness $r, \alpha \in \mathbb{R}$ with $\alpha + \beta > r + t \geq 0$ and the shape parameter $T := -\frac{\alpha-r}{\beta-t}$ with the additional constraint $T \in [-\frac{r}{t}, -\frac{\alpha}{\beta}]$, see the second entry in Table 2.2. Since the norm on the right hand side is stronger by the additive factor $\lambda > 1/2$, this estimate and the resulting upper bound for the sampling error $\|f - S^{\Lambda}_{I_N^{d,T,\boldsymbol{\gamma}}} f | \mathcal{H}^{r,t,\boldsymbol{\gamma}}(\mathbb{T}^d)\| \lesssim N^{-(\alpha-r+\beta-t)} \|f | \mathcal{H}^{\alpha,\beta+\lambda,\boldsymbol{\gamma}}(\mathbb{T}^d)\|$ are not asymptotically optimal. By using a different proof technique and restricting the

considered parameter combinations further to hyperbolic cross frequency index sets $I_N^{d,0,\mathbf{1}}$ with shape parameter $T := 0$, isotropic smoothness $r := 0$ and $\alpha \leq 0$, dominating mixed smoothness $t \geq 0$ and $\beta > 1/2$ with $\alpha + \beta > \max\{t, 1/2\}$, we obtain from Theorem 2.30 that the sampling error is bounded by

$$\|f - S^{\Lambda}_{I_N^{d,T,\boldsymbol{\gamma}}} f | \mathcal{H}^{0,t,\boldsymbol{\gamma}}(\mathbb{T}^d)\| \lesssim \|f|\mathcal{H}^{\alpha,\beta,\mathbf{1}}(\mathbb{T}^d)\| \, N^{-(\alpha+\beta-t)} \begin{cases} (\log N)^{(d-1)/2} & \text{for } \alpha = 0, \\ 1 & \text{for } \alpha < 0, \end{cases}$$

which is asymptotically best possible up to the logarithmic factor $(\log N)^{(d-1)/2}$ in the case of isotropic smoothness $\alpha = 0$ and asymptotically best possible for $\alpha < 0$, see the third entry in Table 2.2 and compare with the truncation error in the first entry. We remark that for sparse grids, similar results can be obtained, see e.g. [BDuSU16, DTU16]. We denote the approximated Fourier partial sum where the corresponding approximated Fourier coefficients are computed using a suitable sparse grid by S_I^{SG} with $I := I_N^{d,0,\mathbf{1}}$. Then for isotropic smoothness $r := 0$, $\alpha \leq 0$ and dominating mixed smoothness $t := 0$, $\beta > 1/2 - \alpha$, the sparse grid sampling error is bounded by

$$\|f - S_I^{\mathrm{SG}} f | L_2(\mathbb{T}^d)\| \lesssim \|f|\mathcal{H}^{\alpha,\beta,\mathbf{1}}(\mathbb{T}^d)\| \, N^{-(\alpha+\beta)} \begin{cases} (\log N)^{(d-1)/2} & \text{for } \alpha = 0, \\ 1 & \text{for } \alpha < 0, \end{cases}$$

due to [SU07, Theorem 8] and [BDuSU16, Theorem 6.10]. In the case of dominating mixed smoothness $t > 0$ and $\beta > \max\{t, 1/2\} - \alpha$, the sparse grid sampling error is bounded by

$$\|f - S_I^{\mathrm{SG}} f | \mathcal{H}^{0,t,\mathbf{1}}(\mathbb{T}^d)\| \lesssim N^{-(\alpha+\beta-t)} \|f|\mathcal{H}^{\alpha,\beta,\mathbf{1}}(\mathbb{T}^d)\|$$

due to [BDuSU16, Theorem 6.10]. For rank-1 lattice sampling in the hyperbolic cross case $T := 0$ with isotropic smoothness $r = \alpha = 0$ and dominating mixed smoothness $t := 0$, $\beta > 1$, the logarithmic factor $(\log N)^{(d-1)/2}$ in the sampling error $\|f - S_I^{\Lambda} f | L_2(\mathbb{T}^d)\|$ can be removed when using special reconstructing rank-1 lattices $\Lambda(\boldsymbol{z}, M, I_N^{d,0,\mathbf{1}})$ with generating vector $\boldsymbol{z} := (1, a, a^2, \ldots, a^{d-1})$ of Korobov form [Kor60], which fulfill certain additional properties, cf. [Tem86], and one obtains $\|f - S^{\Lambda}_{I_N^{d,0,\mathbf{1}}} f | L_2(\mathbb{T}^d)\| \lesssim N^{-\beta} \, \|f|\mathcal{H}^{0,\beta,\mathbf{1}}(\mathbb{T}^d)\|$ in this case. We remark that (parts of) the used proof ideas and the employed rank-1 lattices are non-constructive. In this work, we extend these results for the special rank-1 lattices of Korobov form using proof techniques from [Tem86] to the sampling error estimates

$$\|f - S^{\Lambda}_{I_N^{d,T,\mathbf{1}}} f | L_2(\mathbb{T}^d)\| \lesssim N^{-(\alpha+\beta)} \, \|f|\mathcal{H}^{\alpha,\beta,\mathbf{1}}(\mathbb{T}^d)\|$$

for shape parameters $T := -\alpha/\beta \in [-\infty, 0]$ with $\alpha, \beta \geq 0$, $\alpha + \beta > \frac{d}{2} \frac{2d\beta+\alpha}{d\beta+\alpha} \frac{\beta+\alpha}{d\beta+\alpha} > 0$ in Theorem 2.36 as well as for shape parameters $T := -\alpha/\beta \in (0, 1)$ with $\alpha < 0$, $\beta > 1 - \alpha$ in Theorem 2.39, see the last two entries in Table 2.2 and see also [KPV15b].

Please note that since the used rank-1 lattice sampling method employs reconstructing rank-1 lattices $\Lambda(\boldsymbol{z}, M, I)$ and we do not have an interpolation in general, the results for the error estimates in Table 2.1 and 2.2 look slightly different if we consider the sampling errors $f - S_I^{\Lambda} f$ with respect to the number of samples M instead of the refinement N or cardinality $|I|$, cf. Table 2.4. In case of (standard or energy-norm based) hyperbolic cross frequency index sets $I := I_N^{d,T,\boldsymbol{\gamma}}$, $0 \leq T < 1$, the numbers of samples M for rank-1 lattice sampling behave approximately like $|I|^2$ and consequently the errors only decay with half of the rate in the main order with respect to the number of samples M compared to the

results with respect to the refinement N, cf. [BKUV16], or compared to the case of sparse grid sampling, cf. [BDuSU16, DTU16] and the references therein.

In Section 2.3.4, we extend the idea of sampling along reconstructing rank-1 lattices $\Lambda(\boldsymbol{z}, M, I)$ to the case of perturbed rank-1 lattices using the results from Section 2.2.2 and we obtain estimates for the corresponding sampling errors similar to the results from Section 2.3.3.

Finally, in Section 2.3.5, we give several numerical examples in up to 25 dimensions for the theoretical results of Section 2.3.2, 2.3.3 and 2.3.4.

2.1 Fast evaluation

In this section, the fast evaluation of trigonometric polynomials p_I, as defined in (2.2), at the nodes of a rank-1 lattice $\Lambda(\boldsymbol{z}, M)$ is reviewed, see also [KPV15a] and the references therein. The fast evaluation can be realized using a simple index transform and a single one-dimensional FFT of length M with total computational costs of $\mathcal{O}(M \log M + d\,|I|)$. We extend these considerations to the case of perturbed rank-1 lattice nodes and obtain a fast Taylor expansion based method, which uses several one-dimensional FFTs of length M. Moreover, we give error estimates for our approximate method, see also [Vol13].

2.1.1 Rank-1 lattices

Given an arbitrary trigonometric polynomial (2.2), we are going to evaluate p_I at the nodes $\boldsymbol{x}_j := \frac{j}{M}\boldsymbol{z} \bmod 1$, $j = 0, \ldots, M-1$, of an arbitrary rank-1 lattice $\Lambda(\boldsymbol{z}, M) \subset \mathbb{T}^d$. For this, we obtain from the definition by appropriate grouping of the summands

$$\begin{aligned} p_I(\boldsymbol{x}_j) &= \sum_{\boldsymbol{k}\in I} \hat{p}_{\boldsymbol{k}}\, \mathrm{e}^{2\pi \mathrm{i} \boldsymbol{k}\cdot\boldsymbol{x}_j} = \sum_{\boldsymbol{k}\in I} \hat{p}_{\boldsymbol{k}}\, \mathrm{e}^{2\pi \mathrm{i} j \boldsymbol{k}\cdot\boldsymbol{z}/M} \\ &= \sum_{l=0}^{M-1} \underbrace{\left(\sum_{\substack{\boldsymbol{k}\in I \\ \boldsymbol{k}\cdot\boldsymbol{z} \equiv l \pmod M}} \hat{p}_{\boldsymbol{k}} \right)}_{=:\,\hat{g}_l} \mathrm{e}^{2\pi \mathrm{i} j l/M} = \sum_{l=0}^{M-1} \hat{g}_l\, \mathrm{e}^{2\pi \mathrm{i} j l/M}, \quad j = 0, \ldots, M-1, \end{aligned} \tag{2.16}$$

see e.g. [LH03, KKP12]. The term on the right-hand side is simply a one-dimensional discrete Fourier transform (DFT) of length M. This means we can evaluate the trigonometric polynomial p_I at all rank-1 lattice nodes $\boldsymbol{x}_j$, $j = 0, \ldots, M-1$, by computing the inner sums $\hat{g}_l$ followed by a single one-dimensional FFT of length M. In total, the computational costs are $\mathcal{O}(M \log M + d\,|I|)$, where the constants do not depend on d. The implementation is very easy, for instance one line of Octave / MATLAB code suffices,

$$(p_I(\boldsymbol{x}_j))_{j=0}^{M-1} \texttt{ = } M\texttt{*ifft(accumarray(mod(}I\texttt{*}\boldsymbol{z}\texttt{,}M\texttt{)+1,(}\hat{p}_{\boldsymbol{k}}\texttt{)}_{\boldsymbol{k}\in I}\texttt{,[}M\texttt{,1],@sum));}$$

cf. [Käm14c].

2.1.2 Perturbed rank-1 lattices

In Section 2.1.1, the fast and exact evaluation of an arbitrary trigonometric polynomial p_I at the nodes of an arbitrary rank-1 lattice $\Lambda(\boldsymbol{z}, M)$ has already been discussed. Based on this,

we consider the case where the evaluation nodes $\boldsymbol{y}_\ell \in \mathbb{T}^d$ are perturbed versions of rank-1 lattice nodes $\boldsymbol{x}_j$.

As presented in [Vol13, KPV15a] and based on the ideas in [AD96, Kun08], we evaluate a trigonometric polynomial p_I from (2.2) at nodes $\boldsymbol{y}_\ell \in \mathbb{T}^d$, $\ell = 0, \ldots, L-1$, using a Taylor expansion s_m of degree $m-1$, $m \in \mathbb{N}$, at a closest rank-1 lattice node $\boldsymbol{x}_{j'} \in \Lambda(\boldsymbol{z}, M)$ for each node $\boldsymbol{y}_\ell$,

$$p_I(\boldsymbol{x}) \approx s_m(\boldsymbol{x}) := \sum_{0 \le |\boldsymbol{\nu}| < m} \frac{D^{\boldsymbol{\nu}} p(\boldsymbol{x}_{j'})}{\boldsymbol{\nu}!} (\boldsymbol{x} - \boldsymbol{x}_{j'})^{\boldsymbol{\nu}},$$

where $D^{\mathbf{0}} p_I := p_I$, $D^{\boldsymbol{\nu}} p_I := \frac{\partial^{\nu_1}}{\partial {x_1}^{\nu_1}} \ldots \frac{\partial^{\nu_d}}{\partial {x_d}^{\nu_d}} p_I$, $\boldsymbol{x} := (x_1, \ldots, x_d)^\top \in \mathbb{T}^d$, $\boldsymbol{\nu} := (\nu_1, \ldots, \nu_d) \in \mathbb{N}_0^d$, $|\boldsymbol{\nu}| := |\nu_1| + \ldots + |\nu_d|$, $\boldsymbol{\nu}! := \nu_1! \cdot \ldots \cdot \nu_d!$, $\boldsymbol{x}^{\boldsymbol{\nu}} := {x_1}^{\nu_1} \cdot \ldots \cdot {x_d}^{\nu_d}$. Since the $\boldsymbol{\nu}$-th derivative

$$D^{\boldsymbol{\nu}} p_I(\boldsymbol{x}) := \frac{\partial^{\nu_1}}{\partial {x_1}^{\nu_1}} \ldots \frac{\partial^{\nu_d}}{\partial {x_d}^{\nu_d}} p_I(\boldsymbol{x}) = \sum_{\boldsymbol{k} \in I} (2\pi \mathrm{i} \boldsymbol{k})^{\boldsymbol{\nu}} \, \hat{p}_{\boldsymbol{k}} \, \mathrm{e}^{2\pi \mathrm{i} \boldsymbol{k} \cdot \boldsymbol{x}}, \quad \boldsymbol{x} \in \mathbb{T}^d,$$

of p_I is again a trigonometric polynomial in Π_I and

$$D^{\boldsymbol{\nu}} p_I(\boldsymbol{x}_j) = \sum_{l=0}^{M-1} \left(\sum_{\substack{\boldsymbol{k} \in I \\ \boldsymbol{k} \cdot \boldsymbol{z} \equiv l \pmod M}} (2\pi \mathrm{i} \boldsymbol{k})^{\boldsymbol{\nu}} \, \hat{p}_{\boldsymbol{k}} \right) \mathrm{e}^{2\pi \mathrm{i} j l / M},$$

we can also perform the fast evaluation of the $\boldsymbol{\nu}$-th derivative $D^{\boldsymbol{\nu}} p_I$ at all rank-1 lattice nodes $\boldsymbol{x}_j$, $j = 0, \ldots, M-1$, by a one-dimensional FFT of length M in $\mathcal{O}(M \log M + d\,|I|)$ arithmetic operations. We obtain

$$s_m(\boldsymbol{x}) = \sum_{0 \le |\boldsymbol{\nu}| < m} \frac{(\boldsymbol{x} - \boldsymbol{x}_{j'})^{\boldsymbol{\nu}}}{\boldsymbol{\nu}!} \sum_{\boldsymbol{k} \in I} (2\pi \mathrm{i} \boldsymbol{k})^{\boldsymbol{\nu}} \, \hat{p}_{\boldsymbol{k}} \, \mathrm{e}^{2\pi \mathrm{i} \boldsymbol{k} \cdot \boldsymbol{x}_{j'}}. \tag{2.17}$$

In order to present error estimates for the approximate evaluation of the trigonometric polynomial p_I by the Taylor expansion s_m of degree $m-1$, we first introduce additional notation. We define the metric $\rho(\boldsymbol{y}, \boldsymbol{x}) := \min_{\boldsymbol{h} \in \mathbb{Z}^d} \|\boldsymbol{x} - \boldsymbol{y} + \boldsymbol{h}\|_\infty$ for $\boldsymbol{y}, \boldsymbol{x} \in \mathbb{T}^d$. For a given point $\boldsymbol{y} \in \mathbb{T}^d$, the corresponding expansion point $\boldsymbol{x}_{j'} \in \mathbb{T}^d$ in (2.17) is chosen as a closest rank-1 lattice point $\boldsymbol{x}_{j'} \in \Lambda(\boldsymbol{z}, M)$ where $\rho(\boldsymbol{y}, \boldsymbol{x}_{j'}) = \min_{\boldsymbol{x}_j \in \Lambda(\boldsymbol{z}, M)} \rho(\boldsymbol{y}, \boldsymbol{x}_j)$.

Assuming that the index $\mu_\ell \in \{0, \ldots, M-1\}$ of a closest rank-1 lattice node $\boldsymbol{x}_{\mu_\ell} \in \Lambda(\boldsymbol{z}, M)$, $\rho(\boldsymbol{y}_\ell, \boldsymbol{x}_{\mu_\ell}) = \min_{\boldsymbol{x}_j \in \Lambda(\boldsymbol{z}, M)} \rho(\boldsymbol{y}_\ell, \boldsymbol{x}_j)$, is known for each evaluation node $\boldsymbol{y}_\ell$, $\ell = 0, \ldots, L-1$, the approximate evaluation of the trigonometric polynomial p_I using the Taylor expansion s_m of degree $m-1$ can be realized in $\mathcal{O}\left(m^d (L + M \log M + d\,|I|)\right)$ arithmetic operations for L evaluation nodes $\boldsymbol{y}_\ell$. We write the evaluation of the Taylor expansion s_m at evaluation nodes $\boldsymbol{y}_\ell$, $\ell = 0, \ldots, L-1$, in matrix-vector notation as

$$(s_m(\boldsymbol{y}_\ell))_{\ell=0}^{L-1} = \boldsymbol{A}_{m-1} \hat{\boldsymbol{p}} = \sum_{0 \le |\boldsymbol{\nu}| \le m-1} \boldsymbol{B}_{\boldsymbol{\nu}} \boldsymbol{F} \boldsymbol{D}_{\boldsymbol{\nu}} \hat{\boldsymbol{p}}, \tag{2.18}$$

where $\hat{\boldsymbol{p}} := (\hat{p}_{\boldsymbol{k}})_{\boldsymbol{k} \in I} \in \mathbb{C}^{|I|}$ is the vector of the Fourier coefficients, $\boldsymbol{D}_{\boldsymbol{\nu}} := \operatorname{diag}\left(((2\pi \mathrm{i} \boldsymbol{k})^{\boldsymbol{\nu}})_{\boldsymbol{k} \in I}\right) \in \mathbb{C}^{|I| \times |I|}$ is a diagonal matrix, $\boldsymbol{F} := \left(\mathrm{e}^{2\pi \mathrm{i} j \boldsymbol{k} \cdot \boldsymbol{z} / M}\right)_{j=0;\, \boldsymbol{k} \in I}^{M-1} \in \mathbb{C}^{M \times |I|}$ is the Fourier matrix for the rank-1 lattice $\Lambda(\boldsymbol{z}, M)$ and frequency index set I, $\boldsymbol{B}_{\boldsymbol{\nu}} \in \mathbb{R}^{L \times M}$ is a sparse matrix with at most one non-zero entry $(\boldsymbol{y}_\ell - \boldsymbol{x}_{\mu_\ell})^{\boldsymbol{\nu}} / \boldsymbol{\nu}!$ at column μ_ℓ in each row $\ell = 0, \ldots, L-1$.

Next, we establish error bounds for the approximate evaluation of a trigonometric polynomial $p_I \in \Pi_I$ by a Taylor expansion s_m of degree $m-1$ from (2.17) for nodes $\boldsymbol{y} \in \mathcal{Y}_\varepsilon$ from the set of admissible evaluation nodes

$$\mathcal{Y}_\varepsilon := \{\boldsymbol{x} \in \mathbb{T}^d \colon \exists \boldsymbol{x}_{j'} \in \Lambda(\boldsymbol{z}, M) \text{ such that } \rho(\boldsymbol{x}, \boldsymbol{x}_{j'}) \le \varepsilon\} \tag{2.19}$$

with perturbation parameter $\varepsilon \in [0, \frac{1}{2}]$, see Figure 2.7 for an illustration. The results for the error bounds in Theorem 2.3 are similar to the ones in [Vol13, Theorem III.1]. However, in the latter one, we allowed arbitrary evaluation nodes $\boldsymbol{x} \in \mathbb{T}^d$ and used the so-called mesh norm δ, whereas we restrict the evaluation nodes $\boldsymbol{y}$ here to the set $\mathcal{Y}_\varepsilon$, i.e., to those nodes from $\mathbb{T}^d$ which are close to the rank-1 lattice $\Lambda(\boldsymbol{z}, M)$ with respect to the perturbation parameter ε.

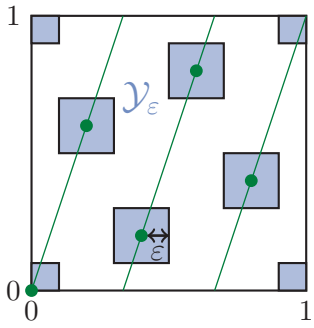

Figure 2.7: Illustration of set $\mathcal{Y}_\varepsilon$ of admissible evaluation nodes.

First, we give a general error estimate for trigonometric polynomials p_I with frequencies supported on arbitrary index sets $I \subset \mathbb{Z}^d$ of finite cardinality, $|I| < \infty$.

Lemma 2.1. *Let a trigonometric polynomial $p_I \in \Pi_I$ with frequencies supported on an arbitrary index set $I \subset \mathbb{Z}^d$ of finite cardinality, $|I| < \infty$, be given. Furthermore, let $\Lambda(\boldsymbol{z}, M)$ be a rank-1 lattice and $\mathcal{Y}_\varepsilon$ be a special set of admissible evaluation nodes for a parameter $\varepsilon \in [0, \frac{1}{2}]$ from (2.19). For the approximate evaluation of the trigonometric polynomial p_I by a truncated Taylor series*

$$s_m(\boldsymbol{y}) := \sum_{|\boldsymbol{\nu}|=0}^{m-1} \frac{D^{\boldsymbol{\nu}} p_I(\boldsymbol{x}_{j'})}{\boldsymbol{\nu}!} (\boldsymbol{y} - \boldsymbol{x}_{j'})^{\boldsymbol{\nu}}$$

of degree $m-1$ at nodes $\boldsymbol{y} \in \mathcal{Y}_\varepsilon$ with expansion point $\boldsymbol{x}_{j'} \in \Lambda(\boldsymbol{z}, M)$, $\rho(\boldsymbol{y}, \boldsymbol{x}_{j'}) = \min_{\boldsymbol{x}_j \in \Lambda(\boldsymbol{z}, M)} \rho(\boldsymbol{y}, \boldsymbol{x}_j)$, we obtain that the remainder $R_m(\boldsymbol{y}) := p_I(\boldsymbol{y}) - s_m(\boldsymbol{y})$ is bounded by

$$|R_m(\boldsymbol{y})| \le \frac{(2\pi)^m}{m!}\, \varepsilon^m \sum_{\boldsymbol{k} \in I} |\hat{p}_{\boldsymbol{k}}|\, \|\boldsymbol{k}\|_1^m, \qquad \boldsymbol{y} \in \mathcal{Y}_\varepsilon.$$

Proof. This proof follows the major steps of the proof of [Vol13, Theorem III.1]. Let $\boldsymbol{\xi}(t) := \boldsymbol{x}_{j'} + t(\boldsymbol{y} - \boldsymbol{x}_{j'})$, $t \in [0,1]$. We use a one-dimensional Taylor expansion on the function $g(t) := p_I(\boldsymbol{\xi}(t))$ at the point $t = 0$, where $g(0) = p_I(\boldsymbol{x}_{j'})$ and $g(1) = p_I(\boldsymbol{y})$, and this yields $p_I(\boldsymbol{y}) = \sum_{\ell=0}^{m-1} g^{(\ell)}(0)/\ell! + \int_0^1 (1-t)^{m-1} g^{(m)}(0)/m!\, \mathrm{d}t$, cf. e.g. [Hör90, Ch. 1]. Due to the multivariate chain rule, we have

$$g^{(\ell)}(t) = \frac{\mathrm{d}^\ell}{\mathrm{d}t^\ell}\, p_I\left(\boldsymbol{x}_{j'} + t(\boldsymbol{y} - \boldsymbol{x}_{j'})\right) = \sum_{|\boldsymbol{\nu}|=\ell} \frac{\ell!}{\boldsymbol{\nu}!} (D^{\boldsymbol{\nu}} p_I)\left(\boldsymbol{x}_{j'} + t(\boldsymbol{y} - \boldsymbol{x}_{j'})\right) (\boldsymbol{y} - \boldsymbol{x}_{j'})^{\boldsymbol{\nu}}$$

and the remainder $R_m(\boldsymbol{y}) = \int_0^1 (1-t)^{m-1} g^{(m)}(0)/m!\,\mathrm{d}t$ can be written in the form

$$R_m(\boldsymbol{y}) = m \int_0^1 (1-t)^{m-1} \sum_{|\boldsymbol{\nu}|=m} D^{\boldsymbol{\nu}} p_I(\boldsymbol{\xi}(t)) \frac{(\boldsymbol{y}-\boldsymbol{x}_{j'})^{\boldsymbol{\nu}}}{\boldsymbol{\nu}!}\,\mathrm{d}t.$$

Then, the remainder $R_m(\boldsymbol{y})$ is bounded by

$$\begin{aligned} |R_m(\boldsymbol{y})| &\leq m \int_0^1 (1-t)^{m-1} \sum_{|\boldsymbol{\nu}|=m} |D^{\boldsymbol{\nu}} p_I(\boldsymbol{\xi}(t))| \frac{\left|(\boldsymbol{y}-\boldsymbol{x}_{j'})^{\boldsymbol{\nu}}\right|}{\boldsymbol{\nu}!}\,\mathrm{d}t \\ &\leq \max_{t\in[0,1]} \sum_{|\boldsymbol{\nu}|=m} \left| \sum_{\boldsymbol{k}\in I} (2\pi \mathrm{i}\boldsymbol{k})^{\boldsymbol{\nu}} \hat{p}_{\boldsymbol{k}}\, \mathrm{e}^{2\pi \mathrm{i}\boldsymbol{k}\cdot\boldsymbol{\xi}(t)} \right| \frac{\left|(\boldsymbol{y}-\boldsymbol{x}_{j'})^{\boldsymbol{\nu}}\right|}{\boldsymbol{\nu}!}. \end{aligned}$$

Since we have $\rho(\boldsymbol{y}, \boldsymbol{x}_{j'}) \leq \varepsilon$ and by applying the multinomial theorem, we get

$$\begin{aligned} |R_m(\boldsymbol{y})| &\leq \max_{t\in[0,1]} \sum_{|\boldsymbol{\nu}|=m} \frac{\varepsilon^{|\boldsymbol{\nu}|}}{\boldsymbol{\nu}!} \sum_{\boldsymbol{k}\in I} |(2\pi \mathrm{i}\boldsymbol{k})^{\boldsymbol{\nu}}|\, |\hat{p}_{\boldsymbol{k}}|\, |\mathrm{e}^{2\pi \mathrm{i}\boldsymbol{k}\cdot\boldsymbol{\xi}(t)}| \\ &\leq 2^m \pi^m \varepsilon^m \sum_{\boldsymbol{k}\in I} |\hat{p}_{\boldsymbol{k}}| \sum_{|\boldsymbol{\nu}|=m} \frac{|k_1|^{\nu_1} \cdot \ldots \cdot |k_d|^{\nu_d}}{\boldsymbol{\nu}!} = \frac{2^m \pi^m}{m!}\, \varepsilon^m \sum_{\boldsymbol{k}\in I} |\hat{p}_{\boldsymbol{k}}|\, \|\boldsymbol{k}\|_1^m \end{aligned}$$

for arbitrary $\boldsymbol{y} \in \mathcal{Y}_\varepsilon$. ∎

Next, we consider results for special cases of weighted frequency index sets $I = I_N^{d,T,\boldsymbol{\gamma}}$ as defined in (2.14) and (2.15).

Lemma 2.2. *([KPV15a, Lemma 2.3]). Let a refinement $N \in \mathbb{R}$, $N \geq 1$, a shape parameter $T \in [-\infty, 1)$ and a weight parameter $\boldsymbol{\gamma} \in (0,1]^d$ be given. The following inclusions hold*

$$I_N^{d,T,\boldsymbol{\gamma}} \subset \begin{cases} \mathbb{Z}^d \cap [-N, N]^d & \text{for } T \leq 0, \\ \mathbb{Z}^d \cap [-d^{\frac{T}{1-T}} N, d^{\frac{T}{1-T}} N]^d & \text{for } 0 < T < 1. \end{cases} \tag{2.20}$$

Proof. In order to prove the inclusions, we use

$$\max(1, \|\boldsymbol{k}\|_\infty) \leq \prod_{s=1}^d \max(1, \gamma_s^{-1} |k_s|) \tag{2.21}$$

$$\text{and} \qquad \max(1, \|\boldsymbol{k}\|_\infty) \leq \max(1, \|\boldsymbol{k}\|_1) \leq d \max(1, \|\boldsymbol{k}\|_\infty). \tag{2.22}$$

For $\boldsymbol{k} \in I_N^{d,T,\boldsymbol{\gamma}}$ and $T \in (-\infty, 1)$, we infer

$$\begin{aligned} N &\geq \left(\prod_{s=1}^d \max(1, \gamma_s^{-1} |k_s|) \right)^{\frac{1}{1-T}} \max(1, \|\boldsymbol{k}\|_1)^{-\frac{T}{1-T}} \\ &\geq \max(1, \|\boldsymbol{k}\|_\infty)^{\frac{1}{1-T}} \begin{cases} \max(1, \|\boldsymbol{k}\|_\infty)^{-\frac{T}{1-T}} & \text{for } -\frac{T}{1-T} \geq 0, \\ d^{-\frac{T}{1-T}} \max(1, \|\boldsymbol{k}\|_\infty)^{-\frac{T}{1-T}} & \text{for } -\frac{T}{1-T} < 0. \end{cases} \end{aligned}$$

Similarly, we estimate $N \geq \max(1, \|\boldsymbol{k}\|_1) \geq \max(1, \|\boldsymbol{k}\|_\infty)$ for $\boldsymbol{k} \in I_N^{d,-\infty,\boldsymbol{\gamma}}$. Thus, we have $\max(1, \|\boldsymbol{k}\|_\infty) \leq \left\{ \begin{array}{ll} N & \text{for } T \leq 0 \\ d^{\frac{T}{1-T}} N & \text{for } 0 < T < 1 \end{array} \right\}$ and this yields the assertion. ∎

Estimating parts of the isotropic smoothness in Lemma 2.1 in terms of dominating mixed smoothness leads to

Theorem 2.3. *([KPV15a, Theorem 4.1]). Let a weighted frequency index set $I = I_N^{d,T,\boldsymbol{\gamma}}$ and a trigonometric polynomial (2.2) be given by its Fourier coefficients $\hat{p}_{\boldsymbol{k}} \in \mathbb{C}$, where the refinement $N \geq 1$, the shape parameter $T \in [-\infty, 1)$ and the weight parameter $\boldsymbol{\gamma} \in (0,1]^d$. Furthermore, let $\Lambda(\boldsymbol{z}, M)$ be a rank-1 lattice and $\mathcal{Y}_\varepsilon$ be a special set of admissible evaluation nodes for a perturbation parameter $\varepsilon \geq 0$. Additionally, let a Taylor expansion parameter $m \in \mathbb{N}$, the dominating mixed smoothness $\beta \geq 0$ and the isotropic smoothness $\alpha \in \mathbb{R}$ be given, where $0 \leq \alpha + \beta \leq m$. We approximately evaluate the trigonometric polynomial p_I by a truncated Taylor series $s_m(\boldsymbol{y}) := \sum_{|\boldsymbol{\nu}|=0}^{m-1} D^{\boldsymbol{\nu}} p_I(\boldsymbol{x}_{j'}) \, (\boldsymbol{y} - \boldsymbol{x}_{j'})^{\boldsymbol{\nu}} / \boldsymbol{\nu}!$ of degree $m-1$ at nodes $\boldsymbol{y} \in \mathcal{Y}_\varepsilon$, where the expansion point $\boldsymbol{x}_{j'} \in \Lambda(\boldsymbol{z}, M)$, $\rho(\boldsymbol{y}, \boldsymbol{x}_{j'}) = \min_{\boldsymbol{x}_j \in \Lambda(\boldsymbol{z}, M)} \rho(\boldsymbol{y}, \boldsymbol{x}_j)$. Then, the remainder $R_m := p_I - s_m$ is bounded by*

$$|R_m(\boldsymbol{y})| \quad \leq \quad \frac{(2\pi)^m}{m!} d^{\frac{m-\alpha-T\beta}{1-T}} \varepsilon^m N^{m-\alpha-\beta} \sum_{\boldsymbol{k} \in I_N^{d,T,\boldsymbol{\gamma}}} |\hat{p}_{\boldsymbol{k}}| \, \omega^{\alpha,\beta,\boldsymbol{\gamma}}(\boldsymbol{k}).$$

Proof. Applying Lemma 2.1 and using the simple inequality $\|\boldsymbol{k}\|_1^m \leq \max(1, \|\boldsymbol{k}\|_1)^m = \omega^{m,0,\boldsymbol{\gamma}}(\boldsymbol{k})$, $m > 0$, we obtain

$$|R_m(\boldsymbol{y})| \leq \frac{2^m \pi^m}{m!} \, \varepsilon^m \sum_{\boldsymbol{k} \in I_N^{d,T,\boldsymbol{\gamma}}} \omega^{m,0,\boldsymbol{\gamma}}(\boldsymbol{k}) \, |\hat{p}_{\boldsymbol{k}}|.$$

Furthermore, we estimate parts of the isotropic smoothness in terms of the dominating mixed smoothness, $\omega^{\frac{m-\alpha-T\beta}{1-T},0,\boldsymbol{\gamma}}(\boldsymbol{k}) \leq d^{\frac{m-\alpha-T\beta}{1-T}} \, \omega^{0,\frac{m-\alpha-T\beta}{1-T},\boldsymbol{\gamma}}(\boldsymbol{k})$ for all $\boldsymbol{k} \in \mathbb{Z}^d$, using the inequalities (2.21) and (2.22). Therefore, we have

$$\begin{aligned}
\omega^{m,0,\boldsymbol{\gamma}}(\boldsymbol{k}) &= \omega^{m-\alpha-\frac{m-\alpha-T\beta}{1-T},-\beta,\boldsymbol{\gamma}}(\boldsymbol{k}) \, \omega^{\frac{m-\alpha-T\beta}{1-T},0,\boldsymbol{\gamma}}(\boldsymbol{k}) \, \omega^{\alpha,\beta,\boldsymbol{\gamma}}(\boldsymbol{k}) \\
&\leq \omega^{m-\alpha-\frac{m-\alpha-T\beta}{1-T},-\beta,\boldsymbol{\gamma}}(\boldsymbol{k}) \, d^{\frac{m-\alpha-T\beta}{1-T}} \, \omega^{0,\frac{m-\alpha-T\beta}{1-T},\boldsymbol{\gamma}}(\boldsymbol{k}) \, \omega^{\alpha,\beta,\boldsymbol{\gamma}}(\boldsymbol{k}) \\
&= d^{\frac{m-\alpha-T\beta}{1-T}} \, \omega^{-\frac{T}{1-T}(m-\alpha-\beta),\frac{1}{1-T}(m-\alpha-\beta),\boldsymbol{\gamma}}(\boldsymbol{k}) \quad \omega^{\alpha,\beta,\boldsymbol{\gamma}}(\boldsymbol{k})
\end{aligned}$$

for $\boldsymbol{k} \in \mathbb{Z}$. Consequently, we infer

$$|R_m(\boldsymbol{y})| \leq \frac{(2\pi)^m}{m!} \, d^{\frac{m-\alpha-T\beta}{1-T}} \, \varepsilon^m \max_{\boldsymbol{k} \in I_N^{d,T,\boldsymbol{\gamma}}} \left(\omega^{-\frac{T}{1-T},\frac{1}{1-T},\boldsymbol{\gamma}}(\boldsymbol{k})\right)^{m-\alpha-\beta} \sum_{\boldsymbol{k} \in I_N^{d,T,\boldsymbol{\gamma}}} \omega^{\alpha,\beta,\boldsymbol{\gamma}}(\boldsymbol{k}) \, |\hat{p}_{\boldsymbol{k}}|.$$

We observe by (2.14) that

$$I_N^{d,T,\boldsymbol{\gamma}} = \left\{ \boldsymbol{k} \in \mathbb{Z}^d \colon \max(1, \|\boldsymbol{k}\|_1)^{-\frac{T}{1-T}} \prod_{s=1}^{d} \max(1, \gamma_s^{-1} |k_s|)^{\frac{1}{1-T}} \leq N \right\}. \tag{2.23}$$

and we obtain $\max_{\boldsymbol{k} \in I_N^{d,T,\boldsymbol{\gamma}}} \left(\omega^{-\frac{T}{1-T},\frac{1}{1-T},\boldsymbol{\gamma}}(\boldsymbol{k})\right)^{m-\alpha-\beta} \leq N^{m-\alpha-\beta}$. This yields the assertion. ∎

The results of Theorem 2.3 will be used later in the proof of Theorem 2.10 in Section 2.2.2 for the fast reconstruction of trigonometric polynomials p_I from samples at perturbed rank-1 lattice nodes as well as in the proof of Theorem 2.46 in Section 2.3.4 for the fast approximation of periodic signals $f \colon \mathbb{T}^d \to \mathbb{C}$.

As a consequence of Theorem 2.3, we have several possibilities to ensure a small (relative) approximation error R_m for fixed Taylor expansion parameter m and increasing refinement N.

1. Choose the perturbation parameter ε like $\sim d^{-\frac{m-\alpha-T\beta}{(1-T)m}} N^{-\frac{m-\alpha-\beta}{m}}$ or smaller and restrict evaluation nodes to the set $\mathcal{Y}_\varepsilon$, i.e., permit only relatively small perturbations to the nodes $\boldsymbol{x}_j$ of the rank-1 lattice.

2. Allow arbitrarily chosen evaluation nodes $\boldsymbol{x} \in \mathbb{T}^d$ and use trigonometric polynomials p_I with a certain decay of the Fourier coefficients $\hat{p}_{\boldsymbol{k}}$. For instance, choose $\alpha + \beta = m$ and ensure that the Fourier coefficients $\hat{p}_{\boldsymbol{k}}$ decay at least like $\sim 1/\omega^{\alpha,\beta,\gamma}(\boldsymbol{k})$ or faster.

2.2 Fast reconstruction for known frequency index sets

In this section, we discuss the reconstruction of the Fourier coefficients $\hat{p}_{\boldsymbol{k}}$, $\boldsymbol{k} \in I$, of a trigonometric polynomial (2.2) from samples using fast and (relatively) simple algorithms. As sampling nodes, we review the usage of the nodes $\boldsymbol{x}_j := \frac{j}{M}\boldsymbol{z} \bmod 1$ of a reconstructing rank-1 lattice $\Lambda(\boldsymbol{z}, M, I)$ in Section 2.2.1. We extend these considerations to the case of perturbed versions of such a reconstructing rank-1 lattice $\Lambda(\boldsymbol{z}, M, I)$ in Section 2.2.2, see also [KPV15a].

2.2.1 Rank-1 lattices

In this subsection, we summarize various results from [Käm14a, Käm14b, KPV15a, KPV15b, PV16] for the reconstruction of trigonometric polynomials p_I from samples along reconstructing rank-1 lattices $\Lambda(\boldsymbol{z}, M, I)$. We are going to compute the Fourier coefficients $\hat{p}_{\boldsymbol{k}}$, $\boldsymbol{k} \in I$, of a trigonometric polynomial p_I, which are formally given by

$$\hat{p}_{\boldsymbol{k}} = \int_{\mathbb{T}^d} p_I(\boldsymbol{x})\, \mathrm{e}^{-2\pi \mathrm{i} \boldsymbol{k}\cdot\boldsymbol{x}}\, \mathrm{d}\boldsymbol{x}, \quad \boldsymbol{k} \in I,$$

using the rank-1 lattice rule

$$\hat{p}^{\Lambda}_{\boldsymbol{k}} := \frac{1}{M} \sum_{j=0}^{M-1} p_I(\boldsymbol{x}_j)\, \mathrm{e}^{-2\pi \mathrm{i} \boldsymbol{k}\cdot\boldsymbol{x}_j} = \frac{1}{M} \sum_{j=0}^{M-1} p_I\left(\frac{j}{M}\boldsymbol{z}\right)\, \mathrm{e}^{-2\pi \mathrm{i} j \boldsymbol{k}\cdot\boldsymbol{z}}, \quad \boldsymbol{k} \in I. \tag{2.24}$$

This means we compute all Fourier coefficients $\hat{p}_{\boldsymbol{k}}$, $\boldsymbol{k} \in I$, of p_I using a cubature formula with equal weights $1/M$ and identical samples $p_I(\boldsymbol{x}_j)$ taken at the rank-1 lattice nodes $\boldsymbol{x}_j := \frac{j}{M}\boldsymbol{z} \bmod 1$, $j = 0, \ldots, M-1$, for all frequencies $\boldsymbol{k} \in I$. We remark that the cubature formula (2.24) is a quasi-Monte Carlo rule, see e.g. [Nie78] as well as the survey [DKS13] and the references therein.

Now, we ask for the exactness of this cubature formula, i.e., under which condition is $\hat{p}_{\boldsymbol{k}} = \hat{p}^{\Lambda}_{\boldsymbol{k}}$ for all frequencies $\boldsymbol{k} \in I$. As discussed in [Käm13, KPV15a, KPV15b], the condition

$$\frac{1}{M} \sum_{j=0}^{M-1} \mathrm{e}^{2\pi \mathrm{i} j (\boldsymbol{k}'-\boldsymbol{k})\cdot\boldsymbol{z}/M} = \begin{cases} 1 & \text{for } \boldsymbol{k} = \boldsymbol{k}' \\ 0 & \text{for } \boldsymbol{k} \neq \boldsymbol{k}', \boldsymbol{k}, \boldsymbol{k}' \in I, \end{cases} \tag{2.25}$$

has to be fulfilled since we have

$$\hat{p}^{\Lambda}_{\boldsymbol{k}} = \frac{1}{M} \sum_{j=0}^{M-1} \sum_{\boldsymbol{k}' \in I} \hat{p}_{\boldsymbol{k}'}\, \mathrm{e}^{2\pi \mathrm{i} j \boldsymbol{k}'\cdot\boldsymbol{z}/M} \mathrm{e}^{-2\pi \mathrm{i} j \boldsymbol{k}\cdot\boldsymbol{z}/M} = \sum_{\boldsymbol{k}' \in I} \hat{p}_{\boldsymbol{k}'} \frac{1}{M} \sum_{j=0}^{M-1} \mathrm{e}^{2\pi \mathrm{i} j (\boldsymbol{k}'-\boldsymbol{k})\cdot\boldsymbol{z}/M}.$$

In matrix-vector notation, this means $\boldsymbol{F}^{\mathrm{H}}\boldsymbol{F} = M\boldsymbol{I}$, where

$$\boldsymbol{F} := \left(\mathrm{e}^{2\pi \mathrm{i} j \boldsymbol{k}\cdot\boldsymbol{z}/M}\right)_{j=0;\, \boldsymbol{k}\in I}^{M-1} \in \mathbb{C}^{M \times |I|}$$

is the Fourier matrix and $\boldsymbol{I}$ the identity matrix. This is the case if and only if

$$(\boldsymbol{k}' - \boldsymbol{k}) \cdot \boldsymbol{z} \not\equiv 0 \pmod{M} \; \forall \boldsymbol{k}, \boldsymbol{k}' \in I, \boldsymbol{k} \neq \boldsymbol{k}', \tag{2.26}$$

$$\iff \boldsymbol{k} \cdot \boldsymbol{z} \not\equiv \boldsymbol{k}' \cdot \boldsymbol{z} \pmod{M} \; \forall \boldsymbol{k}, \boldsymbol{k}' \in I, \boldsymbol{k} \neq \boldsymbol{k}', \tag{2.27}$$

see also [Käm14a, Section 2]. Using the notion of the difference set

$$\mathcal{D}(I) := \{\boldsymbol{h} := \boldsymbol{k} - \boldsymbol{k}' \colon \boldsymbol{k}, \boldsymbol{k}' \in I\}$$

for the frequency index set I, we can rewrite the above conditions to

$$\boldsymbol{h} \cdot \boldsymbol{z} \not\equiv 0 \pmod{M} \; \forall \boldsymbol{h} \in \mathcal{D}(I) \setminus \{\boldsymbol{0}\}. \tag{2.28}$$

Introducing the notion of the integer dual lattice

$$\Lambda^{\perp}(\boldsymbol{z}, M) := \{\boldsymbol{h} \in \mathbb{Z}^d \colon \boldsymbol{h} \cdot \boldsymbol{z} \equiv 0 \pmod{M}\} \tag{2.29}$$

of a rank-1 lattice $\Lambda(\boldsymbol{z}, M)$, which contains all integer frequencies which alias to the origin, we obtain

$$\hat{p}_{\boldsymbol{k}}^{\Lambda} = \frac{1}{M} \sum_{j=0}^{M-1} \sum_{\boldsymbol{h} \in \mathbb{Z}^d} \hat{p}_{\boldsymbol{h}} \, \mathrm{e}^{-2\pi \mathrm{i} j (\boldsymbol{k}-\boldsymbol{h}) \cdot \boldsymbol{z}/M} = \sum_{\boldsymbol{h} \in \mathbb{Z}^d} \hat{p}_{\boldsymbol{h}} \frac{1}{M} \sum_{j=0}^{M-1} \mathrm{e}^{-2\pi \mathrm{i} j (\boldsymbol{k}-\boldsymbol{h}) \cdot \boldsymbol{z}/M} = \sum_{\boldsymbol{h} \in \Lambda^{\perp}(\boldsymbol{z}, M)} \hat{p}_{\boldsymbol{k}+\boldsymbol{h}}.$$

Consequently, condition (2.28) may be rewritten as

$$\Lambda^{\perp}(\boldsymbol{z}, M) \cap \mathcal{D}(I) = \{\boldsymbol{0}\}. \tag{2.30}$$

We will use this notation later in Section 2.3 for characterizing the aliasing and obtaining estimates for the sampling error.

A rank-1 lattice $\Lambda(\boldsymbol{z}, M)$ which fulfills the equivalent conditions (2.25), (2.26), (2.27), (2.28), (2.30) for a given frequency index set I will be called *reconstructing rank-1 lattice* $\Lambda(\boldsymbol{z}, M, I)$ for I and is suitable for the reconstruction of multivariate trigonometric polynomials (2.2). Each of the equivalent conditions (2.25), (2.26), (2.27), (2.28), (2.30) will be called *reconstruction property*. Later, we will typically use the condition which is most convenient in terms of notation for the specific task.

Using samples of a trigonometric polynomial p_I along such a reconstruction rank-1 lattice $\Lambda(\boldsymbol{z}, M, I)$, we easily obtain all the Fourier coefficients $\hat{p}_{\boldsymbol{k}} = \hat{p}_{\boldsymbol{k}}^{\Lambda}$, $\boldsymbol{k} \in I$, in a fast and exact way by means of Algorithm 2.1. As in the case of the fast evaluation, the implementation is very easy and can be done with two lines of Octave / MATLAB code,

$$\texttt{g\_hat = fft(} \, (p_I(\boldsymbol{x}_j))_{j=0}^{M-1} \, \texttt{);}$$

$$(\hat{p}_{\boldsymbol{k}})_{\boldsymbol{k} \in I} \texttt{ = g\_hat(mod(}I\texttt{*}\boldsymbol{z}\texttt{,}M\texttt{)+1) / }M\texttt{;}$$

cf. [Käm14c].

Algorithm 2.2 describes an approach for searching for a reconstructing rank-1 lattice $\Lambda(\boldsymbol{z}, M, I)$ for a given (arbitrary) frequency index set $I_{\text{input}} := I$, $|I| < \infty$. Please note that we do not assume any structure for the frequency index set I.

The next theorem gives general bounds on the rank-1 lattice size M of reconstructing rank-1 lattices $\Lambda(\boldsymbol{z}, M, I)$.

Algorithm 2.1 ([Käm14b, Algorithm 3.2]). Fast and exact reconstruction of a multivariate trigonometric polynomial $p_I \in \Pi_I$ from sampling values on a reconstructing rank-1 lattice $\Lambda(\boldsymbol{z}, M, I)$.

Input:	$I \subset \mathbb{Z}^d$	frequency index set of finite cardinality
	$\Lambda(\boldsymbol{z}, M, I)$	reconstructing rank-1 lattice for I of size M with generating vector $\boldsymbol{z} \in \mathbb{Z}^d$
	$\boldsymbol{p} = \left(p_I\left(\frac{j}{M}\boldsymbol{z} \bmod \mathbf{1}\right)\right)_{j=0}^{M-1}$	sampling values of p_I

Compute $\hat{\boldsymbol{g}} := \texttt{FFT\_1D}(\boldsymbol{p})$, i.e. $\hat{g}_l := \sum_{j=0}^{M-1} p_I(\frac{j}{M}\boldsymbol{z} \bmod \mathbf{1})\, \mathrm{e}^{-2\pi \mathrm{i} l j/M}$ for $l = 0, \ldots, M-1$.
for each $\boldsymbol{k} \in I$ **do**
  $\hat{p}_{\boldsymbol{k}} = \hat{p}^{\Lambda}_{\boldsymbol{k}} := \frac{1}{M}\, \hat{g}_{\boldsymbol{k}\cdot\boldsymbol{z} \bmod M}$
end for

Output:	$\hat{\boldsymbol{p}} := \left(\hat{p}^{\Lambda}_{\boldsymbol{k}}\right)_{\boldsymbol{k}\in I}$	Fourier coefficients of p_I
Complexity:	$\mathcal{O}\left(M \log M + d\,\lvert I\rvert\right)$	

Theorem 2.4. *([PV16, Theorem 2.1] as a consequence of [Käm14a, Käm14b]). For a given frequency index set $I \subset \mathbb{Z}^d$, $1 \le |I| < \infty$, and any prime rank-1 lattice size*

$$M \ge \max\left\{\frac{|\mathcal{D}(I)|+3}{2},\, \max_{\boldsymbol{k}\in I} 2\|\boldsymbol{k}\|_\infty + 1\right\}, \tag{2.31}$$

there always exists a generating vector $\boldsymbol{z} \in \mathbb{Z}^d$ such that $\Lambda(\boldsymbol{z}, M)$ is a reconstructing rank-1 lattice $\Lambda(\boldsymbol{z}, M, I)$. Moreover, there always exists a prime rank-1 lattice size M,

$$\begin{aligned} |I| \le M &\le \max\left\{\frac{2}{3}(|\mathcal{D}(I)|+7),\, \max_{\boldsymbol{k}\in I} 3\|\boldsymbol{k}\|_\infty\right\} \\ &\le \max\left\{\frac{2}{3}(|I|^2-|I|+8),\, \max_{\boldsymbol{k}\in I} 3\|\boldsymbol{k}\|_\infty\right\}, \end{aligned} \tag{2.32}$$

and a generating vector $\boldsymbol{z} \in \mathbb{Z}^d$ such that $\Lambda(\boldsymbol{z}, M)$ is a reconstructing rank-1 lattice $\Lambda(\boldsymbol{z}, M, I)$. For such a suitable rank-1 lattice size M, the generating vector $\boldsymbol{z} \in \mathbb{Z}^d$ can be constructed using the component-by-component (CBC) approach in Algorithm 2.2, see [Käm14a], and the construction requires no more than $3\,d\,|I|M$ arithmetic operations.

Proof. The inequality (2.32) is a consequence of [Käm14a, Corollary 1] and [Käm14b, inequality (3.8)]. The lower bound for the rank-1 lattice size M is a consequence from [Käm14a, Theorem 1 and Lemma 2].
When searching for the component z_t, $t \in \{1, \ldots, d\}$, of the generating vector $\boldsymbol{z} := (z_1, \ldots, z_d)^\top$ in the component-by-component step t, the tests for the reconstruction property (2.28) for a given component z_t take no more than $|I|$ multiplications, $|I|$ additions as well as $|I|$ modulo operations, and this yields $3\,|I|$ many arithmetic operations. Due to this and since each component z_t, $t \in \{1, \ldots, d\}$, of the generating vector $\boldsymbol{z}$ can only have M different values modulo M, we obtain that the construction requires no more than $3\,d\,|I|M$ arithmetic operations in total. ∎

We refer to [Käm14b] for detailed considerations for specific frequency index sets I and on how to efficiently determine the cardinality $|\mathcal{D}(I)|$ of the difference set $\mathcal{D}(I)$. Next, we give cardinalities for frequency index sets $I_N^{d,T,\mathbf{1}}$, $N \ge 1$, $T \in [-\infty, 1)$, from (2.14), which result

Algorithm 2.2 Combined Algorithm 1 and 2 from [Käm14a] for obtaining a reconstructing rank-1 lattice $\Lambda(\boldsymbol{z}, M, I_{\text{input}})$, which is suitable for the reconstruction of multivariate trigonometric polynomials (2.2) with frequencies supported on the index set $I := I_{\text{input}}$.

Input: index set $I_{\text{input}} \subset \mathbb{Z}^d$, $|I_{\text{input}}| < \infty$.
Determine suitable initial rank-1 lattice size M_{start}, see e.g. Theorem 2.4.
for $t := 1, \ldots, d$ **do**
  for $z_t := 0, \ldots, M_{\text{start}}$ **do**
    if condition (2.27) is valid for $I := \{(k_1, \ldots, k_t)^\top : \boldsymbol{k} \in I_{\text{input}}\}$, $\boldsymbol{z} := (z_1, \ldots, z_t)^\top$, $M := M_{\text{start}}$, i.e. if $|\{\boldsymbol{k} \cdot \boldsymbol{z} \bmod M\}| = |I|$, **then**
      break
    end if
  end for
end for
for $M := |I_{\text{input}}|, \ldots, M_{\text{start}}$ **do**
  if condition (2.27) is valid for $I := I_{\text{input}}$, $\boldsymbol{z} := (z_1, \ldots, z_d)^\top$, M **then**
    break
  end if
end for
Output: generating vector $\boldsymbol{z} \in \mathbb{N}_0^d$ and rank-1 lattice size $M \in \mathbb{N}_0$ fulfilling the equivalent conditions (2.25), (2.26), (2.27), (2.28), (2.30) for index set $I := I_{\text{input}}$.

in bounds on the size M of the existence of constructively built reconstructing rank-1 lattices $\Lambda(\boldsymbol{z}, M, I_N^{d,T,\mathbf{1}})$ due to Theorem 2.4. For the case of weighted frequency index sets $I_N^{d,T,\boldsymbol{\gamma}}$, $\boldsymbol{\gamma} \in (0,1]^d$, we refer to [Käm14b].

Lemma 2.5. *([KPV15b, Lemma 4.1]). Let the dimension $d \in \mathbb{N}$, and a shape parameter $T \in [-\infty, 1)$ be given. Then, the cardinalities of the frequency index sets $I_N^{d,T,\mathbf{1}}$ are*

$$|I_N^{d,T,\mathbf{1}}| \asymp \begin{cases} N^d & \text{for } T = -\infty, \\ N^{\frac{T-1}{T/d-1}} & \text{for } -\infty < T < 0, \\ N \log^{d-1} N & \text{for } T = 0, \\ N & \text{for } 0 < T < 1, \end{cases} \tag{2.33}$$

for fixed parameters d and T, where the constants only depend on d and T.

Proof. We show the cardinalities for the different cases.

- Case $T = -\infty$. Since we have the inclusions $\{-\lfloor \frac{N}{d} \rfloor, \ldots, \lfloor \frac{N}{d} \rfloor\}^d \subset I_N^{d,-\infty,\mathbf{1}} \subset \{-N, \ldots, N\}^d$, we infer $c_1(d) N^d \leq |I_N^{d,-\infty,\mathbf{1}}| \leq C_1(d) N^d$, where $c_1(d) = d^{-d}$ and $C_1(d) = 3^d$.

- Case $-\infty < T < 0$. First, we consider the lower bound and for this, we show $I_{N^{(1-T)/(d-T)}}^{d,-\infty,\mathbf{1}} \subset I_N^{d,T,\mathbf{1}}$. For arbitrary $\boldsymbol{k} \in I_{N^{(1-T)/(d-T)}}^{d,-\infty,\mathbf{1}}$, we have

$$N^{\frac{1-T}{d-T}} \geq \max(1, \|\boldsymbol{k}\|_1) = \max(1, \|\boldsymbol{k}\|_1)^{-\frac{T}{d-T}} \max(1, \|\boldsymbol{k}\|_1)^{1+\frac{T}{d-T}}.$$

Since $\max(1,\|\boldsymbol{k}\|_1)^d \geq \max(1,\|\boldsymbol{k}\|_\infty)^d \geq \prod_{s=1}^d \max(1,|k_s|)$, we infer

$$\begin{aligned} N^{\frac{1-T}{d-T}} &\geq \max(1,\|\boldsymbol{k}\|_1)^{-\frac{T}{d-T}} \prod_{s=1}^d \max(1,|k_s|)^{\frac{1}{d}(1+\frac{T}{d-T})} \\ &= \max(1,\|\boldsymbol{k}\|_1)^{-\frac{T}{1-T}\,\frac{1-T}{d-T}} \prod_{s=1}^d \max(1,|k_s|)^{\frac{1}{1-T}\,\frac{1-T}{d-T}} \end{aligned}$$

and consequently $\max(1,\|\boldsymbol{k}\|_1)^{-\frac{T}{1-T}} \prod_{s=1}^d \max(1,|k_s|)^{\frac{1}{1-T}} \leq N$. This means, we have $\boldsymbol{k} \in I_N^{d,T,\mathbf{1}}$ and therefore we obtain $I_{N^{(1-T)/(d-T)}}^{d,-\infty,\mathbf{1}} \subset I_N^{d,T,\mathbf{1}}$. Since we have $|I_{N^{(1-T)/(d-T)}}^{d,-\infty,\mathbf{1}}| \geq c_1(d) N^{\frac{1-T}{d-T}\,d}$, we obtain $|I_N^{d,T,\mathbf{1}}| \geq |I_{N^{(1-T)/(d-T)}}^{d,-\infty,\mathbf{1}}| \geq c_1(d) N^{\frac{1-T}{d-T}\,d} = c_1(d) N^{\frac{T-1}{T/d-1}}$.

Due to [GK00, Lemma 1], we obtain $|I_N^{d,T,\mathbf{1}}| \leq C_2(d,T) N^{\frac{T-1}{T/d-1}}$, where $C_2(d,T) > 0$ is a constant depending only on d and T.

- Case $T = 0$. We apply the inclusions of [KKP12, Lemma 2.1] and use the results from [Hal92, Section 5.3]. This yields $c_3(d) N \log_2^{d-1} N \leq |I_N^{d,0}| \leq C_3(d) N \max(1,\log_2 N)^{d-1}$, where $c_3(d) = (8d-8)^{-d+1}$ and $C_3(d) = \frac{8}{3}\frac{(d+1)^{d-1}}{(d-1)!} 12^d$.

- Case $0 < T < 1$. Since the frequencies on the coordinate axis from $-\lfloor N \rfloor$ to $\lfloor N \rfloor$ are elements of $I_N^{d,T,\mathbf{1}}$, we obtain $|I_N^{d,T,\mathbf{1}}| \geq 2d\lfloor N \rfloor + 1 \geq 2d(N-1)+1 \geq c_4(d) N$ for $N \geq 2$, where $c_4(d) = d$.
  Due to [GK09, Lemma 4.2], we obtain $|I_N^{d,T,\mathbf{1}}| \leq C_4(d,T) N$, where $C_4(d,T) > 0$ is a constant depending only on d and T.

These estimates yield the assertion. ∎

Next, we show for shape parameters $T \in [-\infty, 0]$ that we can cover the difference set $\mathcal{D}(I_N^{d,T,\mathbf{1}})$ with the index set $I_L^{d,T,\mathbf{1}}$ of larger refinement $L = 2^{\frac{d-T}{1-T}} N^{1+\frac{d}{d-T}}$. This yields smaller upper bounds for the existence of reconstructing rank-1 lattices $\Lambda(\boldsymbol{z}, M, I_N^{d,T,\mathbf{1}})$ for shape parameters $T \in [-\infty, 0)$.

Lemma 2.6. *([KPV15b, Lemma 4.2]). Let the dimension $d \in \mathbb{N}$ and a shape parameter $T \in [-\infty, 0]$ be given. We consider the difference set $\mathcal{D}(I_N^{d,T,\mathbf{1}}) := \left\{ \boldsymbol{k}' - \boldsymbol{k} \colon \boldsymbol{k}, \boldsymbol{k}' \in I_N^{d,T,\mathbf{1}} \right\}$. Then, we have the inclusion*

$$\mathcal{D}(I_N^{d,T,\mathbf{1}}) \subset I^{d,T,\mathbf{1}}_{2^{\frac{d-T}{1-T}}\, N^{1+\frac{d}{d-T}}}. \tag{2.34}$$

Proof. For $\boldsymbol{k} \in I_N^{d,T,\mathbf{1}}$, we have $\max(1,\|\boldsymbol{k}\|_1)^{-\frac{T}{1-T}} \prod_{s=1}^d \max(1,|k_s|)^{\frac{1}{1-T}} \leq N$ by definition. Consequently, for $\boldsymbol{k}, \boldsymbol{k}' \in I_N^{d,T,\mathbf{1}}$ and $-\infty \leq T < 0$, we infer

$$\begin{aligned} &\max(1,\|\boldsymbol{k}-\boldsymbol{k}'\|_1) \prod_{s=1}^d \max(1,|k_s - k_s'|)^{-\frac{1}{T}} \\ \leq\ & \big(\max(1,\|\boldsymbol{k}\|_1) + \max(1,\|\boldsymbol{k}'\|_1)\big) \prod_{s=1}^d \big(\max(1,|k_s|) + \max(1,|k_s'|)\big)^{-\frac{1}{T}} \\ \leq\ & \big(\max(1,\|\boldsymbol{k}\|_1) + \max(1,\|\boldsymbol{k}'\|_1)\big)\ 2^{-\frac{d}{T}} \prod_{s=1}^d \max(1,|k_s|)^{-\frac{1}{T}} \max(1,|k_s'|)^{-\frac{1}{T}} \\ \leq\ & 2^{-\frac{d}{T}} N^{-\frac{1-T}{T}} \left(\prod_{s=1}^d \max(1,|k_s'|)^{-\frac{1}{T}} + \prod_{s=1}^d \max(1,|k_s|)^{-\frac{1}{T}} \right). \end{aligned}$$

Next, we estimate dominating mixed smoothness by isotropic smoothness. Since we have $\prod_{s=1}^{d} \max(1,|k_s|) \leq \max(1,\|\boldsymbol{k}\|_\infty)^d \leq \max(1,\|\boldsymbol{k}\|_1)^d$ for $\boldsymbol{k} \in \mathbb{Z}^d$, we obtain

$$\begin{aligned}
\prod_{s=1}^{d} \max(1,|k_s|)^{-\frac{1}{T}} &= \prod_{s=1}^{d} \max(1,|k_s|)^{\frac{1}{d-T}} \prod_{s=1}^{d} \max(1,|k_s|)^{-\frac{1}{T}-\frac{1}{d-T}} \\
&\leq \max(1,\|\boldsymbol{k}\|_1)^{\frac{d}{d-T}} \prod_{s=1}^{d} \max(1,|k_s|)^{-\frac{d}{T(d-T)}} \\
&= \left(\max(1,\|\boldsymbol{k}\|_1)^{-\frac{T}{1-T}} \prod_{s=1}^{d} \max(1,|k_s|)^{\frac{1}{1-T}} \right)^{-\frac{1-T}{T}\frac{d}{d-T}} \\
&\leq N^{-\frac{1-T}{T}\frac{d}{d-T}}
\end{aligned}$$

and analogously $\prod_{s=1}^{d} \max(1,|k'_s|)^{-\frac{1}{T}} \leq N^{-\frac{1-T}{T}\frac{d}{d-T}}$. For $T = 0$, we have

$$\prod_{s=1}^{d} \max(1,|k_s - k'_s|) \leq 2^d \prod_{s=1}^{d} \max(1,|k_s|) \prod_{s=1}^{d} \max(1,|k'_s|) \leq 2^d N^2.$$

These results yield

$$\max(1,\|\boldsymbol{k}-\boldsymbol{k}'\|_1)^{-\frac{T}{1-T}} \prod_{s=1}^{d} \max(1,|k_s-k'_s|)^{\frac{1}{1-T}} \leq 2^{\frac{d-T}{1-T}} N^{1+\frac{d}{d-T}} \text{ for all } \boldsymbol{k},\boldsymbol{k}' \in I_N^{d,T,\mathbf{1}}$$

and inclusion (2.34) follows. ∎

In Table 2.3, we give the cardinalities and bounds on sizes of reconstructing rank-1 lattices for ℓ_∞-balls $I = \hat{G}_N^d := [-N,N]^d \cap \mathbb{Z}^d$, ℓ_1-balls $I = I_N^{d,-\infty,\mathbf{1}}$, hyperbolic crosses $I = I_N^{d,0,\mathbf{1}}$, and energy-norm based hyperbolic crosses $I = I_N^{d,T,\mathbf{1}}$, $0 < T < 1$, depending on the refinement $N \in \mathbb{R}$, $N \geq 1$, as well as for generic unstructured index sets $I \subset \mathbb{Z}^d$ of finite cardinality, $|I| < \infty$, fulfilling a mild assumption. The upper bound on the rank-1 lattice size M for hyperbolic cross index sets $I = I_N^{d,0,\mathbf{1}}$ is discussed in [Käm13]. The lower bounds for the structured index sets in Table 2.3 are a consequence of (2.32) and (2.33) as well as [BKUV16, Lemma 4]. The latter states that the size M of a reconstructing rank-1 lattice for an index set I which contains the coordinate axes in two dimensions from $-N$ to N, e.g. $I \supset (\{-N,\dots,N\} \times \{0\}^{d-1}) \cup (\{0\} \times \{-N,\dots,N\} \times \{0\}^{d-2})$, must be greater than N^2.

In preparation for the rank-1 lattice based sparse FFT in Chapter 4, we additionally repeat some statements from [Käm14a] and [PV16]. The next theorem and corollary will play an important role. They give a straightforward answer to the problem of obtaining a reconstructing rank-1 lattice (for an index set of higher dimension), if one already has a reconstructing rank-1 lattice of a (lower dimensional) frequency index set and an additional dimension should be added (by Cartesian product).

Theorem 2.7. *(see [Käm14a]). Let a dimension $d \in \mathbb{N}$, $d \geq 2$, and a frequency index set $I \subset \mathbb{Z}^d$ of finite cardinality $|I| \geq 2$ be given. We assume that $\Lambda(\boldsymbol{z},M)$ with generating vector $\boldsymbol{z} := (z_1,\dots,z_{d-1})^\top$ is a reconstructing rank-1 lattice $\Lambda(\boldsymbol{z},M,I^{(1,\dots,d-1)})$ for the frequency index set $I^{(1,\dots,d-1)} := \{(k_s)_{s=1}^{d-1} \colon \boldsymbol{k} \in I\}$. Then, the rank-1 lattice $\Lambda((z_1,\dots,z_{d-1},M)^\top, MS)$ with*

$$S := \min\{m \in \mathbb{N} \colon |\{k_d \bmod m \colon \boldsymbol{k} \in I\}| = |\{k_d \colon \boldsymbol{k} \in I\}|\}$$

is a reconstructing rank-1 lattice $\Lambda((z_1,\dots,z_{d-1},M)^\top, MS, I)$.

index set I	cardinality $\lvert I\rvert$	guarantee of existence of reconstructing rank-1 lattice, size M lower bound	upper bound
ℓ_∞-ball $\hat{G}_N^d := [-N, N]^d \cap \mathbb{Z}^d$ ℓ_1-ball $I_N^{d,-\infty,\mathbf{1}}$	$\Theta(N^d)$	$\Theta(N^d)$	
frequency index set $I_N^{d,T,\mathbf{1}}$, $-\infty < T < 0$	$\Theta\left(N^{\frac{1-T}{1-T/d}}\right)$	$\Omega\left(N^{\max\left\{2,\frac{1-T}{1-T/d}\right\}}\right)$	$\mathcal{O}\left(N^{\frac{1-T}{1-T/d}\frac{2-T/d}{1-T/d}}\right)$
hyperbolic cross $I_N^{d,0,\mathbf{1}}$	$\Theta(N \log^{d-1} N)$	$\Omega(N^2)$	$\mathcal{O}(N^2 \log^{d-2} N)$
energy-norm based hyperbolic cross $I_N^{d,T,\mathbf{1}}$, $T \in (0,1)$	$\Theta(N)$	$\Theta(N^2)$	
generic unstructured index set $I \subset \mathbb{Z}^d \cap [-N, N]^d$, $\lvert I\rvert \geq N \geq 4$		$\lvert I\rvert$	$\lvert I\rvert^2$

Table 2.3: Bounds (for fixed dimension $d \geq 2$ and shape parameter $T \in [-\infty, 1)$) on cardinalities $|I|$ of selected frequency index sets I from Lemma 2.5 and on rank-1 lattice sizes M which guarantee the existence of a generating vector $\boldsymbol{z}$ such that $\Lambda(\boldsymbol{z}, M)$ is a reconstructing rank-1 lattice $\Lambda(\boldsymbol{z}, M, I)$. The bounds on M follow from Theorem 2.4, Lemma 2.5, Lemma 2.6 and [Käm13].

Corollary 2.8. *([PV16, Corollary 2.3]). Let a frequency set $I' \subset \hat{G}_N^d$, $|I'| = s \geq 2$, be given. Furthermore, let $I'' \subset \hat{G}_N^1$ be another non-empty frequency index set. Then, there exists a reconstructing rank-1 lattice $\Lambda(\boldsymbol{z}, M, I' \times I'')$ for $I' \times I''$ of size $M \leq \max\{2s^2, 3N\}\, 2(N+1)$.*

Proof. Due to (2.32) in Theorem 2.4, there exists a reconstructing rank-1 lattice $\Lambda(\boldsymbol{z}, M', I')$ for I' with generating vector $\boldsymbol{z} := (z_1, \ldots, z_{d-1})^\top$ and size

$$M' \leq \max\left\{\frac{2}{3}(s^2 - s + 8), 3N\right\} \leq \max\{2s^2, 3N\}.$$

We apply Theorem 2.7 with $I := I' \times I''$. Consequently, $I^{(1,\ldots,d-1)} := \{(k_s)_{s=1}^{d-1} \colon \boldsymbol{k} \in I\} = I'$ and $\{k_d \colon \boldsymbol{k} \in I\} = I''$ in Theorem 2.7. Since we have $S \leq \max(I') - \min(I') + 1 \leq 2(N+1)$, the rank-1 lattice $\Lambda((z_1, \ldots, z_{d-1}, M')^\top, M'S)$ is a reconstructing rank-1 lattice for $I = I' \times I''$ of size $M := M'S \leq \max\{2s^2, 3N\}\, 2(N+1)$. ∎

Based on Theorem 2.7, an alternative component-by-component construction algorithm of a reconstructing rank-1 lattice $\Lambda(\boldsymbol{z}, M, I)$ can be obtained for unknown rank-1 lattice size M, see Algorithm 2.3. This approach determines the rank-1 lattice size M in a dimension incremental way and does not (explicitly) search for the components of the generating vector $\boldsymbol{z}$. Instead, it uses the rank-1 lattice size M_{t-1} from the previous dimension increment step $t \in \{1, \ldots, d\}$ as component z_t of the generating vector $\boldsymbol{z}$. Due to this, using Algorithm 2.3 instead of Algorithm 2.2 should improve the runtime required for building a reconstructing rank-1 lattice $\Lambda(\boldsymbol{z}, M, I)$ but may increase the lattice size M.

Algorithm 2.3 ([Käm14b, Algorithm 3.7]). Alternative approach for building reconstructing rank-1 lattice $\Lambda(\boldsymbol{z}, M, I_{\text{input}})$ suitable for reconstruction of multivariate trigonometric polynomials (2.2) with frequencies supported on the index set $I := I_{\text{input}}$.

Input: frequency index set $I_{\text{input}} \subset \mathbb{Z}^d$, $|I_{\text{input}}| < \infty$.

1: $M_1 := \min\{m \in \mathbb{N} \colon |\{k_1 \bmod m \colon \boldsymbol{k} \in I_{\text{input}}\}| = |\{k_1 \colon \boldsymbol{k} \in I_{\text{input}}\}|\}$
2: $z_1 := 1$
3: **for** $t := 2, \ldots, d$ **do**
4: $\quad S := \min\{m \in \mathbb{N} \colon |\{k_t \bmod m \colon \boldsymbol{k} \in I_{\text{input}}\}| = |\{k_t \colon \boldsymbol{k} \in I_{\text{input}}\}|\}$
5: $\quad z_t := M_{t-1}$
6: $\quad I := \{(k_1, \ldots, k_t)^\top \colon \boldsymbol{k} \in I_{\text{input}}\}$
7: $\quad M_t := \min\{m \in \mathbb{N} \colon |\{\boldsymbol{h} \cdot (z_1, \ldots, z_t) \bmod m \colon \boldsymbol{h} \in I\}| = |I|\} \leq S M_{t-1}$
8: **end for**

Output: generating vector $\boldsymbol{z} := (z_1, \ldots, z_d) \in \mathbb{N}_0^d$ and rank-1 lattice size $M := M_d \in \mathbb{N}_0$ fulfilling the equivalent conditions (2.25), (2.26), (2.27), (2.28), (2.30) for the frequency index set $I := I_{\text{input}}$.

2.2.2 Perturbed rank-1 lattices

This section has already been presented in [KPV15a].

Let a frequency index set $I \subset \hat{G}_N^d := ([-N, N]^d \cap \mathbb{Z}^d)$, $N \geq 1$, be given. In addition, let a reconstructing rank-1 lattice $\Lambda(\boldsymbol{z}, M, I)$ be given that allows for the exact reconstruction of the Fourier coefficients $\hat{p}_{\boldsymbol{k}} \in \mathbb{C}$, $\boldsymbol{k} \in I$, of a trigonometric polynomial (2.2). Our aim is now to approximately reconstruct the Fourier coefficients $\hat{p}_{\boldsymbol{k}}$, $\boldsymbol{k} \in I$, from sampling values $p_I(\boldsymbol{y}_\ell)$, $\ell = 0, \ldots, L-1$, using the approach from Section 2.1.2. In matrix-vector notation this problem reads as follows: Solve the linear system of equations $\boldsymbol{A}_{m-1}\, \tilde{\hat{\boldsymbol{p}}} = \boldsymbol{p}$ in the least-squares sense,

$$\tilde{\hat{\boldsymbol{p}}} := \operatorname*{arg\,min}_{\hat{\boldsymbol{g}} \in \mathbb{C}^{|I|}} \|\boldsymbol{A}_{m-1}\, \hat{\boldsymbol{g}} - \boldsymbol{p}\|_2, \tag{2.35}$$

where $\boldsymbol{A}_{m-1} := \sum_{|\boldsymbol{\nu}| \leq m-1} \boldsymbol{B}_{\boldsymbol{\nu}} \boldsymbol{F} \boldsymbol{D}_{\boldsymbol{\nu}} \in \mathbb{C}^{M \times |I|}$ is the approximated Fourier matrix, see (2.18), $\tilde{\hat{\boldsymbol{p}}} := (\tilde{\hat{p}}_{\boldsymbol{k}})_{\boldsymbol{k} \in I_N^{d,T,\boldsymbol{\gamma}}}$ is the vector of approximated Fourier coefficients and $\boldsymbol{p} := (p(\boldsymbol{y}_\ell))_{\ell=0,\ldots,L-1}$ is the vector of sampling values. Assuming that the approximated Fourier matrix $\boldsymbol{A}_{m-1}$ has full column rank, we expect a unique solution of (2.35) solving the normal equation of the first kind, $\boldsymbol{A}_{m-1}^{\mathrm{H}} \boldsymbol{A}_{m-1}\, \tilde{\hat{\boldsymbol{p}}} = \boldsymbol{A}_{m-1}^{\mathrm{H}}\, \boldsymbol{p}$.

This normal equation may be solved fast using an iterative method like the LSQR algorithm [PS82] in combination with (2.18) and its adjoint version for the fast matrix vector multiplication of the matrix $\boldsymbol{A}_{m-1}$ with a vector $\hat{\boldsymbol{g}} \in \mathbb{C}^{|I|}$ and of the matrix $\boldsymbol{A}_{m-1}^{\mathrm{H}}$ with a vector $\boldsymbol{g} \in \mathbb{C}^L$, respectively.

In the following, we assume that the number L of sampling nodes $\boldsymbol{y}_\ell$ is equal to the rank-1 lattice size M and that each rank-1 lattice node $\boldsymbol{x}_j$ is a closest one for the sampling node $\boldsymbol{y}_j$, $j = 0, \ldots, M-1$. Then, the sparse matrix $\boldsymbol{B}_{\boldsymbol{\nu}}$ from (2.18) is a diagonal matrix,

$$\boldsymbol{B}_{\boldsymbol{\nu}} = \operatorname{diag}\left(\left[\frac{(\boldsymbol{y}_j - \boldsymbol{x}_j)^{\boldsymbol{\nu}}}{\boldsymbol{\nu}!}\right]_{j=0,\ldots,M-1}\right) \in \mathbb{R}^{M \times M}, \quad \boldsymbol{\nu} \in \mathbb{N}_0^d. \tag{2.36}$$

Moreover, we have computational costs of $\mathcal{O}\left(K\, m^d (M \log M + d\,|I|)\right)$ for numerically computing (2.35), where K is the maximal number of iterations of the LSQR algorithm. Choosing $K = \left\lceil \frac{\log(2\,\kappa(\boldsymbol{A}_{m-1})) - \log \delta}{\log(\kappa(\boldsymbol{A}_{m-1})+1) - \log(\kappa(\boldsymbol{A}_{m-1})-1)} \right\rceil$ guarantees a relative error of $\|\tilde{\hat{\boldsymbol{h}}} - \tilde{\hat{\boldsymbol{p}}}\|_2 / \|\tilde{\hat{\boldsymbol{p}}}\|_2 \leq \delta$,

cf. [Bjö96, Section 7.4.4], where $\tilde{\tilde{\boldsymbol{h}}}$ is the approximation of $\tilde{\tilde{\boldsymbol{p}}}$ obtained by the LSQR algorithm, $\kappa(\boldsymbol{A}_{m-1}) := \sigma_1(\boldsymbol{A}_{m-1})/\sigma_{|I|}(\boldsymbol{A}_{m-1})$ denotes the condition number of the approximated Fourier matrix $\boldsymbol{A}_{m-1}$ as well as $\sigma_1(\boldsymbol{A}_{m-1})$ and $\sigma_{|I|}(\boldsymbol{A}_{m-1})$ are the largest and smallest singular values of $\boldsymbol{A}_{m-1}$, respectively.

Theorem 2.9. *([KPV15a, Theorem 4.2]). Let a frequency index set $I \subset \hat{G}_N^d$, $N \geq 1$, and a reconstructing rank-1 lattice $\Lambda(\boldsymbol{z}, M, I)$ be given as well as a Taylor expansion parameter $m \in \mathbb{N}$. Let the sparse matrix $\boldsymbol{B}_{\boldsymbol{\nu}}$ from (2.18) be a diagonal matrix of form (2.36) and $\|\boldsymbol{y}_j - \boldsymbol{x}_j\|_\infty \leq \varepsilon$, $j = 0, \ldots, M-1$, for fixed perturbation parameter ε, $0 \leq \varepsilon < \ln 2/(2\pi dN)$. Then, the condition number $\kappa(\boldsymbol{A}_{m-1})$ can be estimated by*

$$\kappa(\boldsymbol{A}_{m-1}) \leq \frac{1 + \sum_{r=1}^{m-1} (2\pi dN\varepsilon)^r / r!}{1 - \sum_{r=1}^{m-1} (2\pi dN\varepsilon)^r / r!} \leq \frac{\mathrm{e}^{2\pi dN\varepsilon}}{2 - \mathrm{e}^{2\pi dN\varepsilon}}.$$

Proof. For the case $m = 1$, we obtain $\boldsymbol{A}_0^{\mathrm{H}} \boldsymbol{A}_0 = \boldsymbol{D}_{\boldsymbol{0}}^{\mathrm{H}} \boldsymbol{F}^{\mathrm{H}} \boldsymbol{B}_{\boldsymbol{0}}^{\mathrm{H}} \boldsymbol{B}_{\boldsymbol{0}} \boldsymbol{F} \boldsymbol{D}_{\boldsymbol{0}}$. Since $\boldsymbol{D}_{\boldsymbol{0}} = \boldsymbol{I}_{|I|}$ and $\boldsymbol{B}_{\boldsymbol{0}} = \boldsymbol{I}_M$ are identity matrices, it follows from condition (2.25) that $\boldsymbol{A}_0^{\mathrm{H}} \boldsymbol{A}_0 = \boldsymbol{F}^{\mathrm{H}} \boldsymbol{F} = M \boldsymbol{I}_M$ and thus, all singular values $\sigma_1(\boldsymbol{A}_0) = \ldots = \sigma_{|I|}(\boldsymbol{A}_0) = \sqrt{M}$. Therefore, the condition number $\kappa(\boldsymbol{A}_0) = \sigma_1(\boldsymbol{A}_0)/\sigma_{|I|}(\boldsymbol{A}_0) = 1$. In the following, we consider the case $m > 1$. For the largest singular value $\sigma_1(\boldsymbol{A}_{m-1})$, we have

$$\sigma_1(\boldsymbol{A}_{m-1}) \leq \|\boldsymbol{B}_{\boldsymbol{0}} \boldsymbol{F} \boldsymbol{D}_{\boldsymbol{0}}\|_2 + \left\| \sum_{1 \leq |\boldsymbol{\nu}| \leq m-1} \boldsymbol{B}_{\boldsymbol{\nu}} \boldsymbol{F} \boldsymbol{D}_{\boldsymbol{\nu}} \right\|_2 = \sqrt{M} + \sigma_1 \left(\sum_{1 \leq |\boldsymbol{\nu}| \leq m-1} \boldsymbol{B}_{\boldsymbol{\nu}} \boldsymbol{F} \boldsymbol{D}_{\boldsymbol{\nu}} \right). \tag{2.37}$$

Next, we show an upper bound for $\sigma_1 \left(\sum_{1 \leq |\boldsymbol{\nu}| \leq m-1} \boldsymbol{B}_{\boldsymbol{\nu}} \boldsymbol{F} \boldsymbol{D}_{\boldsymbol{\nu}} \right)$. We have

$$\begin{aligned} \sigma_1 \left(\sum_{1 \leq |\boldsymbol{\nu}| \leq m-1} \boldsymbol{B}_{\boldsymbol{\nu}} \boldsymbol{F} \boldsymbol{D}_{\boldsymbol{\nu}} \right) &\leq \sum_{1 \leq |\boldsymbol{\nu}| \leq m-1} \|\boldsymbol{B}_{\boldsymbol{\nu}} \boldsymbol{F} \boldsymbol{D}_{\boldsymbol{\nu}}\|_2 \leq \sum_{1 \leq |\boldsymbol{\nu}| \leq m-1} \|\boldsymbol{B}_{\boldsymbol{\nu}}\|_2 \|\boldsymbol{F}\|_2 \|\boldsymbol{D}_{\boldsymbol{\nu}}\|_2 \\ &= \sum_{1 \leq |\boldsymbol{\nu}| \leq m-1} \sigma_1(\boldsymbol{B}_{\boldsymbol{\nu}})\, \sigma_1(\boldsymbol{F})\, \sigma_1(\boldsymbol{D}_{\boldsymbol{\nu}}). \end{aligned} \tag{2.38}$$

Since $\boldsymbol{B}_{\boldsymbol{\nu}} = \operatorname{diag}\left(\left[(\boldsymbol{y}_j - \boldsymbol{x}_j)^{\boldsymbol{\nu}} / \boldsymbol{\nu}! \right]_{j=0,\ldots,M-1} \right) \in \mathbb{R}^{M \times M}$, $\boldsymbol{F} \in \mathbb{C}^{M \times |I|}$ has orthogonal columns and $\boldsymbol{D}_{\boldsymbol{\nu}} = \operatorname{diag}\left([(2\pi \mathrm{i} \boldsymbol{k})^{\boldsymbol{\nu}}]_{\boldsymbol{k} \in I} \right) \in \mathbb{C}^{|I| \times |I|}$, we obtain $\sigma_1(\boldsymbol{B}_{\boldsymbol{\nu}}) \leq \varepsilon^{|\boldsymbol{\nu}|}/\boldsymbol{\nu}!$, $\sigma_1(\boldsymbol{F}) = \sqrt{M}$ and $\sigma_1(\boldsymbol{D}_{\boldsymbol{\nu}}) \leq (2\pi N)^{|\boldsymbol{\nu}|}$. Due to this fact and by applying the multinomial theorem

$$(\xi_1 + \ldots + \xi_d)^r = \sum_{|\boldsymbol{\nu}| = r} \frac{r!}{\boldsymbol{\nu}!} \boldsymbol{\xi}^{\boldsymbol{\nu}}, \qquad \boldsymbol{\xi} := (\xi_1, \ldots, \xi_d)^\top,$$

on $\sum_{|\boldsymbol{\nu}|=r} 1^{|\boldsymbol{\nu}|}/\boldsymbol{\nu}! = \sum_{|\boldsymbol{\nu}|=r} (1, \ldots, 1)^{\boldsymbol{\nu}}/\boldsymbol{\nu}! = d^r/r!$, we infer

$$\begin{aligned} \sigma_1 \left(\sum_{1 \leq |\boldsymbol{\nu}| \leq m-1} \boldsymbol{B}_{\boldsymbol{\nu}} \boldsymbol{F} \boldsymbol{D}_{\boldsymbol{\nu}} \right) &\overset{(2.38)}{\leq} \sum_{1 \leq |\boldsymbol{\nu}| \leq m-1} \frac{(2\pi N\varepsilon)^{|\boldsymbol{\nu}|}}{\boldsymbol{\nu}!} \sqrt{M} = \sqrt{M} \sum_{r=1}^{m-1} (2\pi N\varepsilon)^r \sum_{|\boldsymbol{\nu}|=r} \frac{1^{|\boldsymbol{\nu}|}}{\boldsymbol{\nu}!} \\ &= \sqrt{M} \sum_{r=1}^{m-1} \frac{(2\pi dN\varepsilon)^r}{r!} \leq \sqrt{M}\, (\mathrm{e}^{2\pi dN\varepsilon} - 1). \end{aligned}$$

With (2.37), we obtain $\sigma_1(\boldsymbol{A}_{m-1}) \le \sqrt{M} + \sqrt{M}\sum_{r=1}^{m-1}(2\pi dN\varepsilon)^r/r! \le \sqrt{M}\mathrm{e}^{2\pi dN\varepsilon}$.
Next, we estimate the smallest singular values $\sigma_{|I|}(\boldsymbol{A}_{m-1})$. Therefor, we use the well-known inequality for the singular values (cf. [HJ91, Theorem 3.3.16]) for arbitrary matrices $\boldsymbol{E}, \boldsymbol{G} \in \mathbb{C}^{r\times s}$,

$$\sigma_{p+q-1}(\boldsymbol{E}+\boldsymbol{G}) \le \sigma_p(\boldsymbol{E}) + \sigma_q(\boldsymbol{G}) \quad \text{if} \quad p+q-1 \le \min(r,s).$$

Setting $\boldsymbol{E} := \boldsymbol{A}_{m-1} = \sum_{|\boldsymbol{\nu}|\le m-1} \boldsymbol{B}_{\boldsymbol{\nu}}\boldsymbol{F}\boldsymbol{D}_{\boldsymbol{\nu}}$, $\boldsymbol{G} := -\sum_{1\le|\boldsymbol{\nu}|\le m-1} \boldsymbol{B}_{\boldsymbol{\nu}}\boldsymbol{F}\boldsymbol{D}_{\boldsymbol{\nu}}$, $p = |I|$ and $q = 1$, this yields

$$\begin{aligned}\sigma_{|I|}\left(\boldsymbol{A}_{m-1}\right) &\ge \sigma_{|I|}\left(\boldsymbol{B}_{\boldsymbol{0}}\boldsymbol{F}\boldsymbol{D}_{\boldsymbol{0}}\right) - \sigma_1\left(-\sum_{1\le|\boldsymbol{\nu}|\le m-1}\boldsymbol{B}_{\boldsymbol{\nu}}\boldsymbol{F}\boldsymbol{D}_{\boldsymbol{\nu}}\right)\\ &\ge \sqrt{M} - \sqrt{M}\sum_{r=1}^{m-1}\frac{(2\pi dN\varepsilon)^r}{r!} \ge \sqrt{M}\left(2-\mathrm{e}^{2\pi dN\varepsilon}\right). \qquad (2.39)\end{aligned}$$

The condition $\varepsilon < \ln 2/(2\pi dN)$ guarantees $\sigma_1\left(\sum_{1\le|\boldsymbol{\nu}|\le m-1}\boldsymbol{B}_{\boldsymbol{\nu}}\boldsymbol{F}\boldsymbol{D}_{\boldsymbol{\nu}}\right) < \sqrt{M}$ for all $m > 1$ and thus, we have $\sigma_{|I|}(\boldsymbol{A}_{m-1}) > 0$. Altogether, this yields the assertion. ■

Similar statements can be found in [Grö92, FG93, PT08] with the same maximal and minimal singular values. However, in these publications, the approximated Fourier coefficients $\tilde{\tilde{\boldsymbol{p}}}$ are not the solution of the (unweighted) optimization problem (2.35) but of a weighted problem. Furthermore, they assume that the so-called mesh-norm of the sampling set $\{\boldsymbol{y}_\ell\}_{\ell=0}^{L-1}$ has the upper bound $\ln 2/(2\pi dN)$, while we assume in Theorem 2.9 that the perturbation parameter ε has this upper bound.

Based on the evaluation error of (2.18) and based on the stability results from Theorem 2.9, we consider the error for the fast and approximate reconstruction of trigonometric polynomials $p_{I_N^{d,T,\boldsymbol{\gamma}}} \in \Pi_{I_N^{d,T,\boldsymbol{\gamma}}}$ by sampling at perturbed nodes $\boldsymbol{y}_j$, $j = 0,\dots,M-1$, of a reconstructing rank-1 lattice $\Lambda(\boldsymbol{z}, M, I_N^{d,T,\boldsymbol{\gamma}})$.

Theorem 2.10. *([KPV15a, Theorem 4.3]). Let a weighted frequency index set $I = I_N^{d,T,\boldsymbol{\gamma}}$ and a trigonometric polynomial (2.2) be given by its Fourier coefficients $\hat{p}_{\boldsymbol{k}} \in \mathbb{C}$, where the refinement $N \ge 1$, the shape parameter $T \in [-\infty, 1)$ and the weight parameter $\boldsymbol{\gamma} \in (0,1]^d$. Furthermore, let a Taylor expansion parameter $m \in \mathbb{N}$, a reconstructing rank-1 lattice $\Lambda(\boldsymbol{z}, M, I_N^{d,T,\boldsymbol{\gamma}})$ and a set of sampling nodes $\mathcal{Y} = \{\boldsymbol{y}_j\}_{j=0}^{M-1}$ be given, where $\|\boldsymbol{y}_j - \boldsymbol{x}_j\|_\infty \le \varepsilon$, $j = 0,\dots,M-1$, for fixed perturbation parameter ε, $0 \le \varepsilon < \left(2\pi\left(d^{1+\max\left(0,\frac{T}{1-T}\right)}\right)N\right)^{-1}\ln 2$. Then, the error of the approximation $\tilde{S}_I\, p_I(\boldsymbol{x}) = \sum_{\boldsymbol{k}\in I}\tilde{\hat{p}}_{\boldsymbol{k}}\mathrm{e}^{2\pi\mathrm{i}\boldsymbol{k}\cdot\boldsymbol{x}}$ of the trigonometric polynomial p_I with $\left(\tilde{\hat{p}}_{\boldsymbol{k}}\right)_{\boldsymbol{k}\in I} := \operatorname*{arg\,min}_{\hat{\boldsymbol{g}}\in\mathbb{C}^{|I|}}\|\boldsymbol{A}_{m-1}\,\hat{\boldsymbol{g}} - \boldsymbol{p}\|_2$ and $\boldsymbol{p} := p_I(\boldsymbol{y}_j)_{j=0}^{M-1}$ is bounded by*

$$\|p_I - \tilde{S}_I\, p_I | L_2(\mathbb{T}^d)\| \le \frac{C(d,T,\alpha,\beta,m)}{2-\mathrm{e}^{2\pi\left(d^{1+\max\left(0,\frac{T}{1-T}\right)}\right)N\varepsilon}}\, N^{-(\alpha+\beta)}\sum_{\boldsymbol{k}\in I}\omega^{\alpha,\beta,\boldsymbol{\gamma}}(\boldsymbol{k})\,|\hat{p}_{\boldsymbol{k}}|,$$

where the constant $C(d,T,\alpha,\beta,m) := d^{\frac{\min(0,Tm)-\alpha-T\beta}{1-T}}\frac{(\ln 2)^m}{m!}$ and the smoothness parameters $\alpha,\beta \in \mathbb{R}$, $\beta \ge 0$, $0 < \alpha+\beta \le m$.

Proof. By Parseval's identity, we have $\|p_I - \tilde{S}_I\, p_I | L_2(\mathbb{T}^d)\| = \left\|(\hat{p}_{\boldsymbol{k}} - \tilde{\hat{p}}_{\boldsymbol{k}})_{\boldsymbol{k}\in I}\right\|_2$. Based on the normal equation $\boldsymbol{A}_{m-1}^{\mathrm{H}}\boldsymbol{A}_{m-1}\left(\tilde{\hat{p}}_{\boldsymbol{k}}\right)_{\boldsymbol{k}\in I} = \boldsymbol{A}_{m-1}^{\mathrm{H}}\boldsymbol{p}$, we obtain

$$\boldsymbol{A}_{m-1}^{\mathrm{H}}\boldsymbol{A}_{m-1}\left(\tilde{\hat{p}}_{\boldsymbol{k}} - \hat{p}_{\boldsymbol{k}}\right)_{\boldsymbol{k}\in I} = \boldsymbol{A}_{m-1}^{\mathrm{H}}\left(\boldsymbol{p} - \boldsymbol{A}_{m-1}\left(\hat{p}_{\boldsymbol{k}}\right)_{\boldsymbol{k}\in I}\right).$$

Since we have (2.20) by Lemma 2.2 and $\varepsilon < \left(2\pi\left(d^{1+\max\left(0,\frac{T}{1-T}\right)}\right)N\right)^{-1}\ln 2$, the smallest singular value $\sigma_{|I|}\left(\boldsymbol{A}_{m-1}^{\mathrm{H}}\boldsymbol{A}_{m-1}\right) = \sigma_{|I|}\left(\boldsymbol{A}_{m-1}\right)^2 > 0$ by (2.39) in the proof of Theorem 2.9 Consequently, the matrix $\boldsymbol{A}_{m-1}^{\mathrm{H}}\boldsymbol{A}_{m-1}$ is invertible. Therefore, we obtain

$$\left(\tilde{\hat{p}}_{\boldsymbol{k}} - \hat{p}_{\boldsymbol{k}}\right)_{\boldsymbol{k}\in I} = \left(\boldsymbol{A}_{m-1}^{\mathrm{H}}\boldsymbol{A}_{m-1}\right)^{-1}\boldsymbol{A}_{m-1}^{\mathrm{H}}\left(\boldsymbol{p} - \boldsymbol{A}_{m-1}\left(\hat{p}_{\boldsymbol{k}}\right)_{\boldsymbol{k}\in I}\right).$$

This yields the estimate

$$\left\|(\hat{p}_{\boldsymbol{k}} - \tilde{\hat{p}}_{\boldsymbol{k}})_{\boldsymbol{k}\in I}\right\|_2 \le \left\|(\boldsymbol{A}_{m-1}^{\mathrm{H}}\boldsymbol{A}_{m-1})^{-1}\boldsymbol{A}_{m-1}^{\mathrm{H}}\right\|_2 \left\|\boldsymbol{p} - \boldsymbol{A}_{m-1}\left(\hat{p}_{\boldsymbol{k}}\right)_{\boldsymbol{k}\in I}\right\|_2. \tag{2.40}$$

According to [Bjö96, Subsection 1.4.3], we have $\left\|(\boldsymbol{A}_{m-1}^{\mathrm{H}}\boldsymbol{A}_{m-1})^{-1}\boldsymbol{A}_{m-1}^{\mathrm{H}}\right\|_2 = 1/\sigma_{|I|}(\boldsymbol{A}_{m-1})$. Thus, we obtain $\left\|(\boldsymbol{A}_{m-1}^{\mathrm{H}}\boldsymbol{A}_{m-1})^{-1}\boldsymbol{A}_{m-1}^{\mathrm{H}}\right\|_2 \le \dfrac{1}{\sqrt{M}\left(2-\mathrm{e}^{2\pi\left(d^{1+\max\left(0,\frac{T}{1-T}\right)}\right)N\varepsilon}\right)}$ by (2.39) in the proof of Theorem 2.9. Furthermore, we have

$$\left\|\boldsymbol{p} - \boldsymbol{A}_{m-1}\left(\hat{p}_{\boldsymbol{k}}\right)_{\boldsymbol{k}\in I}\right\|_2 \le \sqrt{M}\ \left\|\boldsymbol{p} - \boldsymbol{A}_{m-1}\left(\hat{p}_{\boldsymbol{k}}\right)_{\boldsymbol{k}\in I}\right\|_\infty = \sqrt{M}\left\|\left(R_m(\boldsymbol{y}_j)\right)_{j=0}^{M-1}\right\|_\infty,$$

where R_m is the remainder from Theorem 2.3. We apply Theorem 2.3 and infer

$$\begin{aligned}\left\|\left(R_m(\boldsymbol{y}_j)\right)_{j=0}^{M-1}\right\|_\infty &\le \frac{(2\pi)^m}{m!}\, d^{\frac{m-\alpha-T\beta}{1-T}}\varepsilon^m\, N^{m-\alpha-\beta}\sum_{\boldsymbol{k}\in I}|\hat{p}_{\boldsymbol{k}}|\,\omega^{\alpha,\beta,\gamma}(\boldsymbol{k})\\ &\le \frac{(\ln 2)^m}{m!}\,\underbrace{d^{\frac{m-\alpha-T\beta}{1-T}}\left(d^{1+\max\left(0,\frac{T}{1-T}\right)}\right)^{-m}}_{=d^{\frac{\min(0,Tm)-\alpha-T\beta}{1-T}}}\, N^{-\alpha-\beta}\sum_{\boldsymbol{k}\in I}|\hat{p}_{\boldsymbol{k}}|\,\omega^{\alpha,\beta,\gamma}(\boldsymbol{k}).\end{aligned}$$

Altogether, this yields the assertion. ∎

The steps of the proof of Theorem 2.10 will be also used in the proof of Theorem 2.46 to show an error bound for sampling functions from subspaces of the Wiener algebra $\mathcal{A}(\mathbb{T}^d)$ at nodes of perturbed rank-1 lattices. If the perturbation parameter ε is not too large, the order of the sampling error does not deteriorate compared to the results of Theorem 2.26 for rank-1 lattice sampling.

2.3 Approximation of multivariate periodic signals

In this section, we consider the approximation of multivariate periodic signals $f\colon \mathbb{T}^d \to \mathbb{C}$ from certain weighted function spaces by trigonometric polynomials p_I. In doing so, we assume that we (approximately) know the corresponding function space of a function f and we choose the frequency index set $I \subset \mathbb{Z}^d$ accordingly. As mentioned in the introduction of this chapter, we consider the subspaces $\mathcal{A}^{\alpha,\beta,\gamma}(\mathbb{T}^d)$ as defined in (2.13) of the Wiener algebra $\mathcal{A}(\mathbb{T}^d) = \mathcal{A}^{0,0,\mathbf{1}}(\mathbb{T}^d)$ and the periodic Sobolev spaces of generalized mixed smoothness $\mathcal{H}^{\alpha,\beta,\gamma}(\mathbb{T}^d)$ as

defined in (2.11) for dominating mixed smoothness $\beta \geq 0$ and isotropic smoothness $\alpha > -\beta$, where the weights $\omega^{\alpha,\beta,\gamma}(\boldsymbol{k})$ are defined as in (2.12) and the Fourier coefficients $\hat{f}_{\boldsymbol{k}}$ of a function f are (formally) given by (2.5).

We proceed in this section as follows. First, we discuss various norm inequalities and give several function space embeddings in Section 2.3.1, which will be used afterwards.

In Section 2.3.2, we consider the approximation of a function $f \in \mathcal{A}(\mathbb{T}^d)$ by the Fourier partial sum $S_I f$ using the Fourier coefficients $\hat{f}_{\boldsymbol{k}}$, $\boldsymbol{k} \in I$, as defined in (2.6), and $S_I f$ is a trigonometric polynomial p_I from (2.1). The main results are shown as "truncation error" in Table 2.1 and 2.2 in the introduction of this chapter.

In Section 2.3.3, we apply the results from Section 2.2.1 and use a rank-1 lattice rule for the computation of the approximated Fourier coefficients $\hat{f}_{\boldsymbol{k}}^{\Lambda} \approx \hat{f}_{\boldsymbol{k}}$, $\boldsymbol{k} \in I$, as defined in (2.7) based on samples along a reconstructing rank-1 lattice $\Lambda(\boldsymbol{z}, M, I)$. Since we sample the function $f \in \mathcal{A}(\mathbb{T}^d)$, we additionally demand that f is continuous or identify f by its continuous representative as discussed in Remark 2.15. In Table 2.1 and Table 2.2, we present an overview of error estimates when approximating a function $f \in \mathcal{A}(\mathbb{T}^d) \cap \mathcal{C}(\mathbb{T}^d)$ by the approximated Fourier partial sum $S_I^{\Lambda} f$ as defined in (2.8), where the corresponding approximated Fourier coefficients $\hat{f}_{\boldsymbol{k}}^{\Lambda}$ were defined in (2.7). For the parameter choices of isotropic smoothness α and dominating mixed smoothness β in both tables, the condition $f \in \mathcal{A}(\mathbb{T}^d)$ is fulfilled, cf. Lemma 2.11, 2.12 and 2.14. We remark that the admissible values of the smoothness parameters α and β are also illustrated in Figure 2.6. In Table 2.4, we summarize the error estimates with respect to the number of samples M from Section 2.3.3. We observe for shape parameters $T \in [0, 1)$ that we have about half of the main rate compared to sampling along sparse grids, cf. [BKUV16]. The reason for this is that for reconstructing rank-1 lattices $\Lambda(\boldsymbol{z}, M, I)$, in general, the rank-1 lattice size M is larger than the cardinality $|I|$ of the frequency index set I, i.e., we require more samples than we have degrees of freedom. As we see from the lower bounds in Theorem 2.42 and the third entry in Table 2.4 for the sampling errors $f - S_I^{\Lambda} f$ when using an arbitrary rank-1 lattice $\Lambda(\boldsymbol{z}, M)$, the corresponding upper bounds in Table 2.4 when using reconstructing rank-1 lattices $\Lambda(\boldsymbol{z}, M, I)$ are asymptotically best possible (up to logarithmic factors) for shape parameters $T \in [0, 1)$ and functions $f \in \mathcal{H}^{\alpha,\beta,\mathbf{1}}(\mathbb{T}^d)$.

In Section 2.3.4, we consider the case where we do not obtain the samples of the function f exactly at rank-1 lattice nodes $\boldsymbol{x}_j$. Instead, we assume that the sampling nodes are perturbed versions of these. If the perturbation is sufficiently small, we obtain similar results as in Section 2.3.3.

In Section 2.3.5, we give various numerical examples for rank-1 lattice sampling and compare the observed behavior with the theoretical results of this section. Moreover, we present examples for sampling along perturbed rank-1 lattices.

2.3.1 Norm inequalities and embeddings of function spaces

Later in this chapter, we repeatedly use embeddings between subspaces $\mathcal{A}^{\alpha,\beta,\gamma}(\mathbb{T}^d)$ of the Wiener algebra $\mathcal{A}(\mathbb{T}^d)$ and periodic Sobolev spaces of generalized mixed smoothness $\mathcal{H}^{\alpha,\beta,\gamma}(\mathbb{T}^d)$.

Lemma 2.11. *([KPV15a, Lemma 2.2]). Let a function $f \in \mathcal{A}^{\alpha,\beta,\gamma}(\mathbb{T}^d)$ be given, where the smoothness parameters $\alpha, \beta \in \mathbb{R}$, $\beta \geq 0$, $\alpha > -\beta$, and the weight parameter $\boldsymbol{\gamma} \in (0, 1]^d$. Then, we have $\|f|\mathcal{H}^{\alpha,\beta,\gamma}(\mathbb{T}^d)\| \leq \|f|\mathcal{A}^{\alpha,\beta,\gamma}(\mathbb{T}^d)\|$. For $f \in \mathcal{H}^{\alpha,\beta+\lambda,\gamma}(\mathbb{T}^d)$ with $\lambda > 1/2$, we have*

$$\|f|\mathcal{A}^{\alpha,\beta,\gamma}(\mathbb{T}^d)\| \leq (1 + 2\zeta(2\lambda))^{\frac{d}{2}} \, \|f|\mathcal{H}^{\alpha,\beta+\lambda,\gamma}(\mathbb{T}^d)\|, \tag{2.41}$$

setting	error estimates
CBC $\Lambda(\boldsymbol{z}, M, I_N^{d,T,\mathbf{1}})$	$\|f - S^{\Lambda}_{I_N^{d,T,\mathbf{1}}} f \| L_\infty(\mathbb{T}^d)\| \leq \|f - S^{\Lambda}_{I_N^{d,T,\mathbf{1}}} f \| \mathcal{A}(\mathbb{T}^d)\|$
using [Käm14b, Tab. 3.1]	$\lesssim \|f\|\mathcal{A}^{\alpha,\beta,\mathbf{1}}(\mathbb{T}^d)\| \begin{cases} M^{-\left(\frac{\alpha}{d}+\beta\right)\left(1-\frac{\beta}{2\beta+\alpha/d}\right)} & \text{for } \alpha > \beta \geq 0, \\ M^{-\frac{\beta}{2}} (\log M)^{\frac{d-2}{2}\beta} & \text{for } \beta > \alpha = 0, \\ M^{-\frac{\alpha+\beta}{2}} & \text{for } -\beta < \alpha < 0, \end{cases}$
$T := -\alpha/\beta \in [-\infty, 1)$	Corollary 2.40, $\beta \geq 0$, $\alpha > -\beta$
special Korobov lattice	$\|f - S^{\Lambda}_{I_N^{d,T,\mathbf{1}}} f \| L_2(\mathbb{T}^d)\| \lesssim \|f\|\mathcal{H}^{\alpha,\beta,\mathbf{1}}(\mathbb{T}^d)\| \, M^{-\left(\frac{\alpha}{d}+\beta\right)\left(1-\frac{\beta}{2\beta+\alpha/d}\right)}$
$T := -\alpha/\beta \in [-\infty, 0)$	Corollary 2.41, $\beta \geq 0$, $\alpha > \max\left(d\,(\frac{1}{4} + \frac{1}{4}\sqrt{8\beta+1} - \beta), 0\right)$
arbitrary $\Lambda(\boldsymbol{z}, M)$	$\|\operatorname{Id} - S^{\Lambda}_{I_N^{d,T,\mathbf{1}}} \| \mathcal{H}^{\alpha,\beta,\mathbf{1}}(\mathbb{T}^d) \to \mathcal{H}^{0,t,\mathbf{1}}(\mathbb{T}^d)\| \gtrsim M^{-\frac{\alpha+\beta-t}{2}}$
$T \in [0, 1)$	Theorem 2.42, $\beta > \frac{1}{2}$, $t \geq 0$, $\alpha \leq 0$, $\alpha + \beta > \max\{t, \frac{1}{2}\}$
CBC $\Lambda(\boldsymbol{z}, M, I_N^{d,0,\mathbf{1}})$	$\|f - S^{\Lambda}_{I_N^{d,0,\mathbf{1}}} f \| \mathcal{H}^{0,t,\mathbf{1}}(\mathbb{T}^d)\| \lesssim \|f\|\mathcal{H}^{\alpha,\beta,\mathbf{1}}(\mathbb{T}^d)\| \, \dfrac{(\log M)^{\frac{d-2}{2}(\alpha+\beta-t)}}{M^{\frac{\alpha+\beta-t}{2}}}$
using [Käm14b, Tab. 3.1]	$\cdot \begin{cases} (\log M)^{(d-1)/2} & \text{for } \alpha = 0, \\ 1 & \text{for } \alpha < 0, \end{cases}$
$T := 0$	Corollary 2.44, $\beta > \frac{1}{2}$, $t \geq 0$, $\alpha \leq 0$, $\alpha + \beta > \max\{t, \frac{1}{2}\}$
special Korobov lattice	$\|f - S^{\Lambda}_{I_N^{d,T,\mathbf{1}}} f \| L_2(\mathbb{T}^d)\| \lesssim \|f\|\mathcal{H}^{\alpha,\beta,\mathbf{1}}(\mathbb{T}^d)\| \, M^{-\frac{\alpha+\beta}{2}}$ $\cdot \begin{cases} (\log M)^{(d-1)\frac{\alpha+\beta}{2}} & \text{for } \alpha = 0, \\ 1 & \text{for } \alpha < 0, \end{cases}$
$T := -\alpha/\beta \in [0, 1)$	Corollary 2.45, $\alpha \leq 0$, $\beta > 1 - \alpha$

Table 2.4: Overview of rank-1 lattice sampling error estimates from Section 2.3.3 with respect to rank-1 lattice size M for functions $f \in \mathcal{A}^{\alpha,\beta,\mathbf{1}}(\mathbb{T}^d)$ and $f \in \mathcal{H}^{\alpha,\beta,\mathbf{1}}(\mathbb{T}^d)$ for certain choices of the isotropic smoothness α and the dominating mixed smoothness β.

where ζ denotes the Riemann zeta function. Therefore, we have the continuous embeddings

$$\mathcal{H}^{\alpha,\beta+\lambda,\gamma}(\mathbb{T}^d) \hookrightarrow \mathcal{A}^{\alpha,\beta,\gamma}(\mathbb{T}^d) \hookrightarrow \mathcal{A}(\mathbb{T}^d) \hookrightarrow L_2(\mathbb{T}^d) \hookrightarrow L_1(\mathbb{T}^d).$$

Proof. Using the Cauchy-Schwarz inequality, one obtains the inequalities, see e.g. the proof of [KPV15a, Lemma 2.2].
The first embedding is due to (2.41) and the second one follows since the weights $\omega^{\alpha,\beta,\gamma}(\boldsymbol{k})$ are bounded from below. The third embedding is due to Parseval's identity, since we have $\|f|L_2(\mathbb{T}^d)\| = \sqrt{\sum_{\boldsymbol{k}\in\mathbb{Z}^d} |\hat{f}_{\boldsymbol{k}}|^2} \leq \sum_{\boldsymbol{k}\in\mathbb{Z}^d} |\hat{f}_{\boldsymbol{k}}| =: \|f|\mathcal{A}(\mathbb{T}^d)\|$ for $f \in \mathcal{A}(\mathbb{T}^d)$. ∎

As the embeddings in Lemma 2.11 suggest, periodic Sobolev spaces of generalized mixed smoothness $\mathcal{H}^{\alpha,\beta,\gamma}(\mathbb{T}^d)$ are subspaces of the Wiener algebra $\mathcal{A}(\mathbb{T}^d)$ for certain parameter choices.

Lemma 2.12. *([KPV15b, Lemma 4.6]). Let the dimension $d \in \mathbb{N}$, $d \geq 2$, and a function $f \in \mathcal{H}^{\alpha,\beta,\boldsymbol{\gamma}}(\mathbb{T}^d)$ be given, where the smoothness parameters $\alpha, \beta \geq 0$ with $\alpha > d(\frac{1}{2} - \beta)$ and the weight parameter $\boldsymbol{\gamma} \in (0,1]^d$. Then, the function f has an absolutely converging Fourier series, $\sum_{\boldsymbol{k}\in\mathbb{Z}^d} |\hat{f}_{\boldsymbol{k}}| < \infty$, and we have the continuous embedding $\mathcal{H}^{\alpha,\beta,\boldsymbol{\gamma}}(\mathbb{T}^d) \hookrightarrow \mathcal{A}(\mathbb{T}^d)$.*

Proof. For $f \in \mathcal{H}^{\alpha,\beta,\boldsymbol{\gamma}}(\mathbb{T}^d)$, we apply the Cauchy-Schwarz inequality and obtain

$$\begin{aligned}\sum_{\boldsymbol{k}\in\mathbb{Z}^d} |\hat{f}_{\boldsymbol{k}}| &\leq \sqrt{\sum_{\boldsymbol{k}\in\mathbb{Z}^d} \frac{1}{\omega^{\alpha,\beta,\boldsymbol{\gamma}}(\boldsymbol{k})^2}} \sqrt{\sum_{\boldsymbol{k}\in\mathbb{Z}^d} \omega^{\alpha,\beta,\boldsymbol{\gamma}}(\boldsymbol{k})^2 |\hat{f}_{\boldsymbol{k}}|^2} \\ &= \sqrt{\sum_{\boldsymbol{k}\in\mathbb{Z}^d} \frac{1}{\max(1,\|\boldsymbol{k}\|_1)^{2\alpha} \prod_{s=1}^d \max(1,\gamma_s^{-1}|k_s|)^{2\beta}}} \, \|f|\mathcal{H}^{\alpha,\beta,\boldsymbol{\gamma}}(\mathbb{T}^d)\|.\end{aligned}$$

Due to $\prod_{s=1}^d \max(1,\gamma_s^{-1}|k_s|) \leq \max(1,\|\boldsymbol{k}\|_1)^d \prod_{s=1}^d \gamma_s^{-1}$ for $\boldsymbol{k} \in \mathbb{Z}^d$, we infer

$$\begin{aligned}\sum_{\boldsymbol{k}\in\mathbb{Z}^d} |\hat{f}_{\boldsymbol{k}}| &\leq \left(\prod_{s=1}^d \gamma_s\right)^{-\frac{\alpha}{d}} \sqrt{\sum_{\boldsymbol{k}\in\mathbb{Z}^d} \prod_{s=1}^d \frac{1}{\max(1,|k_s|)^{2(\beta+\frac{\alpha}{d})}}} \, \|f|\mathcal{H}^{\alpha,\beta,\boldsymbol{\gamma}}(\mathbb{T}^d)\| \\ &= \left(\prod_{s=1}^d \gamma_s\right)^{-\frac{\alpha}{d}} \left(1 + 2\,\zeta\left(2\left(\beta + \frac{\alpha}{d}\right)\right)\right)^{\frac{d}{2}} \, \|f|\mathcal{H}^{\alpha,\beta,\boldsymbol{\gamma}}(\mathbb{T}^d)\|,\end{aligned}$$

where ζ is the Riemann zeta function. Since $\beta \geq 0$ and $\alpha > d(\frac{1}{2} - \beta)$, we obtain $2\left(\beta + \frac{\alpha}{d}\right) > 2\left(\beta + \frac{1}{2} - \beta\right) = 1$ and consequently $\zeta\left(2\left(\beta + \frac{\alpha}{d}\right)\right) < \infty$. Due to this and since $f \in \mathcal{H}^{\alpha,\beta,\boldsymbol{\gamma}}(\mathbb{T}^d)$, we infer $\sum_{\boldsymbol{k}\in\mathbb{Z}^d} |\hat{f}_{\boldsymbol{k}}| < \infty$. ∎

Remark 2.13. For non-negative integers α and β, we can give an alternative characterization of periodic Sobolev spaces of generalized mixed smoothness $\mathcal{H}^{\alpha,\beta,\mathbf{1}}(\mathbb{T}^d)$, which is equivalent with respect to the norms and which uses partial derivatives $D^{\boldsymbol{m}} f$, $\boldsymbol{m} \in \mathbb{N}_0^d$,

$$\tilde{\mathcal{H}}^{\alpha,\beta}(\mathbb{T}^d) := \left\{ f \in L_2(\mathbb{T}^d) \colon \|f|\tilde{\mathcal{H}}^{\alpha,\beta}(\mathbb{T}^d)\|^2 := \sum_{\|\boldsymbol{m}\|_1 \leq \alpha} \sum_{\|\boldsymbol{n}\|_\infty \leq \beta} \|D^{\boldsymbol{m}+\boldsymbol{n}} f\|_2^2 < \infty \right\}, \quad (2.42)$$

see e.g. [BKUV16] and the references therein. □

Lemma 2.14. *([KPV15b, Lemma 4.9]). Let the dimension $d \in \mathbb{N}$, $d \geq 2$ and a function $f \in \mathcal{H}^{\alpha,\beta,\boldsymbol{\gamma}}(\mathbb{T}^d)$ be given, where $0 > \alpha > \frac{1}{2} - \beta$ and the weight parameter $\boldsymbol{\gamma} \in (0,1]^d$. Then, the function f has an absolutely converging Fourier series, $\sum_{\boldsymbol{k}\in\mathbb{Z}^d} |\hat{f}_{\boldsymbol{k}}| < \infty$, and we have the continuous embedding $\mathcal{H}^{\alpha,\beta,\boldsymbol{\gamma}}(\mathbb{T}^d) \hookrightarrow \mathcal{A}(\mathbb{T}^d)$.*

Proof. As in the proof of Lemma 2.12, we apply the Cauchy-Schwarz inequality and obtain

$$\sum_{\boldsymbol{k}\in\mathbb{Z}^d} |\hat{f}_{\boldsymbol{k}}| \leq \sqrt{\sum_{\boldsymbol{k}\in\mathbb{Z}^d} \frac{1}{\max(1,\|\boldsymbol{k}\|_1)^{2\alpha} \prod_{s=1}^d \max(1,\gamma_s^{-1}|k_s|)^{2\beta}}} \, \|f|\mathcal{H}^{\alpha,\beta,\boldsymbol{\gamma}}(\mathbb{T}^d)\|.$$

Due to (2.21) and (2.22), we have $\max(1,\|\boldsymbol{k}\|_1) \leq d \prod_{s=1}^d \max(1,\gamma_s^{-1}|k_s|)$ for $\boldsymbol{k} \in \mathbb{Z}^d$ and since $\alpha < 0$, we infer

$$\begin{aligned}\sum_{\boldsymbol{k}\in\mathbb{Z}^d} |\hat{f}_{\boldsymbol{k}}| &\leq \sqrt{\sum_{\boldsymbol{k}\in\mathbb{Z}^d} d^{-\alpha} \prod_{s=1}^d \frac{1}{\max(1,\gamma_s^{-1}|k_s|)^{2(\beta+\alpha)}}} \, \|f|\mathcal{H}^{\alpha,\beta,\boldsymbol{\gamma}}(\mathbb{T}^d)\| \\ &= d^{-\frac{\alpha}{2}} \left(1 + 2\,\zeta\left(2(\alpha+\beta)\right)\right)^{\frac{d}{2}} \, \|f|\mathcal{H}^{\alpha,\beta,\boldsymbol{\gamma}}(\mathbb{T}^d)\|.\end{aligned}$$

Since we have $2(\alpha + \beta) > 1$ and $f \in \mathcal{H}^{\alpha,\beta,\boldsymbol{\gamma}}(\mathbb{T}^d)$, we obtain $\sum_{\boldsymbol{k}\in\mathbb{Z}^d} |\hat{f}_{\boldsymbol{k}}| < \infty$. ∎

Furthermore, the considered parameter choices yield the existence of a continuous representative for a function from those spaces.

Remark 2.15. Since the Fourier coefficients of functions f from the Wiener algebra $\mathcal{A}(\mathbb{T}^d)$ are absolutely summable, they have continuous representatives in $L_1(\mathbb{T}^d)$, $\mathcal{A}(\mathbb{T}^d) \hookrightarrow \mathcal{C}(\mathbb{T}^d)$. As we are going to construct the approximant based on function values of the original function, we usually identify a function $f \in \mathcal{A}(\mathbb{T}^d)$ by its continuous representative given by its Fourier series $\sum_{\boldsymbol{k}\in\mathbb{Z}^d} \hat{f}_{\boldsymbol{k}}\, \mathrm{e}^{2\pi\mathrm{i}\boldsymbol{k}\cdot\circ}$, see e.g. [Käm14b, equation (2.6)], and we denote this by $f \in \mathcal{A}(\mathbb{T}^d) \cap \mathcal{C}(\mathbb{T}^d)$. □

2.3.2 Truncation error

For functions $f \in \mathcal{A}(\mathbb{T}^d)$, we formally approximate f by the Fourier partial sum $S_I f$ as defined in (2.6), where $I \subset \mathbb{Z}^d$ is a frequency index set of finite cardinality, $|I| < \infty$. We remark that the Fourier partial sum $S_I f$ is a trigonometric polynomial (2.2). In particular, $S_I f$ is an orthogonal projection of the function f with respect to the $L_2(\mathbb{T}^d)$ scalar product. The error $f - S_I f$ of this approximation will be called *truncation error* in this work and may be measured in various norms. For estimating the error, we give upper bounds on the maximum of the weight function $\omega^{\alpha,\beta,\boldsymbol{\gamma}}$ of frequency index sets $I_N^{d,T,\boldsymbol{\gamma}}$ as defined in (2.12) and in (2.14).

Lemma 2.16. *([KPV15a, Lemma 3.2]). Let a dominating mixed smoothness $\tilde{\beta} \geq 0$, an isotropic smoothness $\tilde{\alpha} > -\tilde{\beta}$, a shape parameter $T \in [-\infty, 1)$ and a weighted frequency index set $I_N^{d,T,\boldsymbol{\gamma}}$ be given, where the refinement $N \geq 1$ and the weight parameter $\boldsymbol{\gamma} \in (0,1]^d$. Then, we have*

$$\max_{\boldsymbol{k}\in\mathbb{Z}^d\setminus I_N^{d,T,\boldsymbol{\gamma}}} \omega^{-\tilde{\alpha},-\tilde{\beta},\boldsymbol{\gamma}}(\boldsymbol{k}) \leq N^{-(\tilde{\alpha}+\tilde{\beta})} \begin{cases} \left(N^{d-1}\prod_{s=1}^d \gamma_s^{-1}\right)^{\frac{T\tilde{\beta}+\tilde{\alpha}}{d-T}} & \text{for } T > -\frac{\tilde{\alpha}}{\tilde{\beta}}, \\ 1 & \text{for } T = -\frac{\tilde{\alpha}}{\tilde{\beta}}, \\ d^{-\frac{T\tilde{\beta}+\tilde{\alpha}}{1-T}} & \text{for } T < -\frac{\tilde{\alpha}}{\tilde{\beta}}, \end{cases}$$

where $-\frac{\tilde{\alpha}}{\tilde{\beta}} := -\infty$ for $\tilde{\beta} = 0$.

Proof. In the case of shape parameter $T := -\tilde{\alpha}/\tilde{\beta}$, we observe due to the definition of the frequency index sets $I_N^{d,T,\boldsymbol{\gamma}}$ in (2.14) that

$$\begin{aligned} \mathbb{Z}^d \setminus I_N^{d,T,\boldsymbol{\gamma}} &= \left\{\boldsymbol{k}\in\mathbb{Z}^d\colon \max(1,\|\boldsymbol{k}\|_1)^{\frac{T}{1-T}} \prod_{s=1}^d \max(1,\gamma_s^{-1}|k_s|)^{-\frac{1}{1-T}} < N^{-1}\right\} \\ &= \left\{\boldsymbol{k}\in\mathbb{Z}^d\colon \max(1,\|\boldsymbol{k}\|_1)^{-\frac{\tilde{\alpha}}{\tilde{\alpha}+\tilde{\beta}}} \prod_{s=1}^d \max(1,\gamma_s^{-1}|k_s|)^{-\frac{\tilde{\beta}}{\tilde{\alpha}+\tilde{\beta}}} < N^{-1}\right\}. \end{aligned}$$

This yields $\omega^{-\tilde{\alpha},-\tilde{\beta},\boldsymbol{\gamma}}(\boldsymbol{k}) = \left(\max(1,\|\boldsymbol{k}\|_1)^{-\frac{\tilde{\alpha}}{\tilde{\alpha}+\tilde{\beta}}} \prod_{s=1}^d \max(1,\gamma_s^{-1}|k_s|)^{-\frac{\tilde{\beta}}{\tilde{\alpha}+\tilde{\beta}}}\right)^{\tilde{\alpha}+\tilde{\beta}} \leq N^{-(\tilde{\alpha}+\tilde{\beta})}$ for all $\boldsymbol{k} \in \mathbb{Z}^d \setminus I_N^{d,T,\boldsymbol{\gamma}}$ and the assertion follows. For the other cases, we refer to the proof of [KPV15a, Lemma 3.2]. ■

First, we estimate the truncation error $f - S_I f$ in the $L_\infty(\mathbb{T}^d)$ norm for functions f from subspaces $\mathcal{A}^{\alpha,\beta,\boldsymbol{\gamma}}(\mathbb{T}^d)$ of the Wiener algebra $\mathcal{A}(\mathbb{T}^d)$.

Theorem 2.17. *([KPV15a, Theorem 3.3]). Let a function $f \in \mathcal{A}^{\alpha,\beta,\boldsymbol{\gamma}}(\mathbb{T}^d)$ and a weighted frequency index set $I_N^{d,T,\boldsymbol{\gamma}}$ be given, where the refinement $N \geq 1$, the dominating mixed smoothness $\beta \geq 0$, the isotropic smoothness $\alpha > -\beta$, $-\frac{\alpha}{\beta} := -\infty$ for $\beta = 0$, and the weight parameter $\boldsymbol{\gamma} \in (0,1]^d$. Then, the truncation error $f - S_{I_N^{d,T,\boldsymbol{\gamma}}} f$ is bounded by*

$$\begin{aligned}\|f - S_{I_N^{d,T,\boldsymbol{\gamma}}} f | L_\infty(\mathbb{T}^d)\| &\leq \|f - S_{I_N^{d,T,\boldsymbol{\gamma}}} f | \mathcal{A}(\mathbb{T}^d)\| \\ &\leq N^{-(\alpha+\beta)} \, \|f|\mathcal{A}^{\alpha,\beta,\boldsymbol{\gamma}}(\mathbb{T}^d)\| \begin{cases} \left(N^{d-1} \prod_{s=1}^d \gamma_s^{-1}\right)^{\frac{T\beta+\alpha}{d-T}} & \text{for } T > -\frac{\alpha}{\beta}, \\ 1 & \text{for } T = -\frac{\alpha}{\beta}, \\ d^{-\frac{T\beta+\alpha}{1-T}} & \text{for } T < -\frac{\alpha}{\beta}. \end{cases}\end{aligned}$$

More specifically for $T := -\alpha/\beta$, the operator norm of $\mathrm{Id} - S_{I_N^{d,T,\boldsymbol{\gamma}}}$ is bounded by

$$\|\boldsymbol{\gamma}\|_\infty^\beta \, (N+1)^{-(\alpha+\beta)} \leq \|\mathrm{Id} - S_{I_N^{d,T,\boldsymbol{\gamma}}} | \mathcal{A}^{\alpha,\beta,\boldsymbol{\gamma}}(\mathbb{T}^d) \to L_\infty(\mathbb{T}^d)\| \leq N^{-(\alpha+\beta)} \tag{2.43}$$

where Id *denotes the embedding operator from $\mathcal{A}^{\alpha,\beta,\boldsymbol{\gamma}}(\mathbb{T}^d)$ into $L_\infty(\mathbb{T}^d)$.*

Proof. We have $f - S_{I_N^{d,T,\boldsymbol{\gamma}}} f = \sum_{\boldsymbol{k} \in \mathbb{Z}^d \setminus I_N^{d,T,\boldsymbol{\gamma}}} \hat{f}_{\boldsymbol{k}} \, \mathrm{e}^{2\pi \mathrm{i} \boldsymbol{k} \cdot \circ}$. Using the weights $\omega^{\alpha,\beta,\boldsymbol{\gamma}}(\boldsymbol{k})$, we obtain

$$\begin{aligned}\|f - S_{I_N^{d,T,\boldsymbol{\gamma}}} f | L_\infty(\mathbb{T}^d)\| &\leq \sum_{\boldsymbol{k} \in \mathbb{Z}^d \setminus I_N^{d,T,\boldsymbol{\gamma}}} |\hat{f}_{\boldsymbol{k}}| = \|f - S_{I_N^{d,T,\boldsymbol{\gamma}}} f | \mathcal{A}(\mathbb{T}^d)\| \\ &= \sum_{\boldsymbol{k} \in \mathbb{Z}^d \setminus I_N^{d,T,\boldsymbol{\gamma}}} \max(1, \|\boldsymbol{k}\|_1)^{-\alpha} \prod_{s=1}^d \max(1, \gamma_s^{-1} |k_s|)^{-\beta} \, \omega^{\alpha,\beta,\boldsymbol{\gamma}}(\boldsymbol{k}) \, |\hat{f}_{\boldsymbol{k}}| \\ &\leq \max_{\boldsymbol{k} \in \mathbb{Z}^d \setminus I_N^{d,T,\boldsymbol{\gamma}}} \left(\max(1, \|\boldsymbol{k}\|_1)^{-\alpha} \prod_{s=1}^d \max(1, \gamma_s^{-1} |k_s|)^{-\beta} \right) \sum_{\boldsymbol{k} \in \mathbb{Z}^d \setminus I_N^{d,T,\boldsymbol{\gamma}}} \omega^{\alpha,\beta,\boldsymbol{\gamma}}(\boldsymbol{k}) \, |\hat{f}_{\boldsymbol{k}}|.\end{aligned}$$

Applying Lemma 2.16 yields

$$\begin{aligned}\|f - S_{I_N^{d,T,\boldsymbol{\gamma}}} f | L_\infty(\mathbb{T}^d)\| &\leq \|f - S_{I_N^{d,T,\boldsymbol{\gamma}}} f | \mathcal{A}(\mathbb{T}^d)\| \\ &\leq N^{-(\alpha+\beta)} \sum_{\boldsymbol{k} \in \mathbb{Z}^d \setminus I_N^{d,T,\boldsymbol{\gamma}}} \omega^{\alpha,\beta,\boldsymbol{\gamma}}(\boldsymbol{k}) \, |\hat{f}_{\boldsymbol{k}}| \begin{cases} \left(N^{d-1} \prod_{s=1}^d \gamma_s^{-1}\right)^{\frac{T\beta+\alpha}{d-T}} & \text{for } T > -\frac{\alpha}{\beta}, \\ 1 & \text{for } T = -\frac{\alpha}{\beta}, \\ d^{-\frac{T\beta+\alpha}{1-T}} & \text{for } T < -\frac{\alpha}{\beta}. \end{cases}\end{aligned} \tag{2.44}$$

and the upper bound follows. For the lower bound, we modify the explicit example from [KPV15b, Lemma 4.4]. Let $s' \in \{1, \ldots, d\}$ be an index where $\gamma_{s'} = \|\boldsymbol{\gamma}\|_\infty$ and let the trigonometric polynomial $g(\boldsymbol{x}) = \mathrm{e}^{2\pi \mathrm{i} \boldsymbol{k'} \cdot \boldsymbol{x}}$ be given, where $\boldsymbol{k'} := (k'_1, \ldots, k'_d)^\top$ with $k'_s := N+1$ for $s = s'$ and $k'_s := 0$ otherwise. We have $\boldsymbol{k'} \notin I_N^{d,T,\boldsymbol{\gamma}}$ and we calculate

$$\begin{aligned}\|g - S_{I_N^{d,T,\boldsymbol{\gamma}}} g | L_\infty(\mathbb{T}^d)\| &= \|g | L_\infty(\mathbb{T}^d)\| = \operatorname{ess\,sup}_{\boldsymbol{x} \in \mathbb{T}^d} |\mathrm{e}^{2\pi \mathrm{i} \boldsymbol{k'} \cdot \boldsymbol{x}}| = 1 = \|g | \mathcal{A}(\mathbb{T}^d)\| \\ &= \omega^{-\alpha,-\beta,\boldsymbol{\gamma}}(\boldsymbol{k'}) \, \omega^{\alpha,\beta,\boldsymbol{\gamma}}(\boldsymbol{k'}) \, |\hat{f}_{\boldsymbol{k'}}| \\ &= (N+1)^{-\alpha} \left(\gamma_{s'}^{-1} \, (N+1)\right)^{-\beta} \, \|g | \mathcal{A}^{\alpha,\beta,\boldsymbol{\gamma}}(\mathbb{T}^d)\|\end{aligned}$$

and we conclude that the norm of $\mathrm{Id} - S_{I_N^{d,T,\boldsymbol{\gamma}}}$ is bounded from below by (2.43). ∎

Remark 2.18. If we had used the ∞-norm for the isotropic smoothness α in the definition of the weights $\omega^{\alpha,\beta,\boldsymbol{\gamma}}(\boldsymbol{k})$, then the third case in (2.44) would have the constant 1 instead of $d^{-\frac{T\beta+\alpha}{1-T}}$. □

One can derive three cases for the relationship between the parameter T of a weighted frequency index set $I_N^{d,T,\boldsymbol{\gamma}}$ and the smoothness parameters α, β, see also [KPV15a, Section 3.1].

1. The weighted frequency index set $I_N^{d,T,\boldsymbol{\gamma}}$ is "thinner" than required by the isotropic smoothness α and dominating mixed smoothness β, i.e., the shape parameter $T > -\alpha/\beta$. Consequently, the approximation order with respect to N worsens as T increases, see the first case in (2.44).

2. The weighted frequency index set $I_N^{d,T,\boldsymbol{\gamma}}$ fits the isotropic smoothness α and dominating mixed smoothness β, i.e., the shape parameter $T = -\alpha/\beta$, see the second case in (2.44).

3. The weighted frequency index set $I_N^{d,T,\boldsymbol{\gamma}}$ is "thicker" than required by the isotropic smoothness α and dominating mixed smoothness β, i.e., the shape parameter $T < -\alpha/\beta$. Choosing the parameter T smaller than $-\alpha/\beta$ does not improve the estimate for the truncation error compared to the case $T = -\alpha/\beta$, see the third case in (2.44).

In this work, we concentrate on the second case, i.e., the weighted frequency index set $I_N^{d,T,\boldsymbol{\gamma}}$ is chosen in an "optimal" way.

Remark 2.19. Instead of the Banach spaces $\mathcal{A}^{\alpha,\beta,\boldsymbol{\gamma}} \hookrightarrow \mathcal{A}(\mathbb{T}^d)$, one may consider (more general) spaces $\mathcal{A}^{\omega}(\mathbb{T}^d) := \{f \in L_1(\mathbb{T}^d) \colon \|f|\mathcal{A}^{\omega}(\mathbb{T}^d)\| := \sum_{\boldsymbol{k}\in\mathbb{Z}^d} \omega(\boldsymbol{k})|\hat{f}_{\boldsymbol{k}}| < \infty\} \hookrightarrow \mathcal{A}(\mathbb{T}^d)$ with general weight function $\omega \colon \mathbb{Z}^d \to [c, \infty]$, $c > 0$, see e.g. [Käm14b, (2.9)]. Then, using the index set $I_N^{\omega} := \{\boldsymbol{k} \in \mathbb{Z}^d \colon \omega(\boldsymbol{k}) \leq N\}$, $|I_N^{\omega}| < \infty$, the truncation error can be estimated by

$$\|f - S_{I_N} f|L_\infty(\mathbb{T}^d)\| \leq \|f - S_{I_N} f|\mathcal{A}(\mathbb{T}^d)\| \leq N^{-1}\|f|\mathcal{A}^{\omega}(\mathbb{T}^d)\|,$$

cf. [Käm14b, Lemma 2.2] and [KPV15b, Lemma 3.3]. In this setting, higher smoothness leads to smaller frequency index sets I_N^{ω} in contrast to a higher decay rate with respect to the refinement N in Theorem 2.17. □

For estimates in the Hilbert space norm, one may again consider different choices for the shape parameter $T \in [-\infty, 1)$. Here we concentrate on the case where the shape parameter is again chosen in an "optimal" way to match the norms on the left and right hand side. For the other cases, we refer to [KPV15a, Theorem 3.4].

Theorem 2.20. *Let smoothness parameters $r, \alpha \in \mathbb{R}$, $\beta \geq t \geq 0$, $\alpha + \beta > r + t \geq 0$, the shape parameter $T := -\frac{\alpha - r}{\beta - t}$ with $T := -\infty$ for $\beta = t$, a function $f \in \mathcal{H}^{\alpha,\beta,\boldsymbol{\gamma}}(\mathbb{T}^d)$ and a weighted frequency index set $I_N^{d,T,\boldsymbol{\gamma}}$ be given, where the refinement $N \geq 1$ and the weight parameter $\boldsymbol{\gamma} \in (0, 1]^d$. Then, the truncation error $f - S_{I_N^{d,T,\boldsymbol{\gamma}}} f$ is bounded by*

$$\|f - S_{I_N^{d,T,\boldsymbol{\gamma}}} f|\mathcal{H}^{r,t,\boldsymbol{\gamma}}(\mathbb{T}^d)\| \leq N^{-(\alpha-r+\beta-t)} \, \|f|\mathcal{H}^{\alpha,\beta,\boldsymbol{\gamma}}(\mathbb{T}^d)\|. \tag{2.45}$$

More specifically, the operator norm of $\mathrm{Id} - S_{I_N^{d,T,\boldsymbol{\gamma}}}$ *is bounded by*

$$\|\boldsymbol{\gamma}\|_\infty^{\beta-t} \, (N+1)^{-(\alpha-r+\beta-t)} \leq \|\mathrm{Id} - S_{I_N^{d,T,\boldsymbol{\gamma}}}|\mathcal{H}^{\alpha,\beta,\boldsymbol{\gamma}}(\mathbb{T}^d) \to \mathcal{H}^{r,t,\boldsymbol{\gamma}}(\mathbb{T}^d)\| \leq N^{-(\alpha-r+\beta-t)} \tag{2.46}$$

where Id *denotes the embedding operator from $\mathcal{H}^{\alpha,\beta,\boldsymbol{\gamma}}(\mathbb{T}^d)$ into $\mathcal{H}^{r,t,\boldsymbol{\gamma}}(\mathbb{T}^d)$.*

Proof. We proceed as in the proof of [KPV15a, Theorem 3.4] and [KPV15b, Lemma 4.4]. For a function $f \in \mathcal{H}^{\alpha,\beta,\boldsymbol{\gamma}}(\mathbb{T}^d)$, we have

$$f - S_{I_N^{d,T,\boldsymbol{\gamma}}} f = \sum_{\boldsymbol{k} \in \mathbb{Z}^d \setminus I_N^{d,T,\boldsymbol{\gamma}}} \hat{f}_{\boldsymbol{k}} \, \mathrm{e}^{2\pi \mathrm{i} \boldsymbol{k} \cdot \circ}.$$

Using the weights $\omega^{\alpha,\beta,\boldsymbol{\gamma}}(\boldsymbol{k})$, we obtain

$$\begin{aligned} \|f - S_{I_N^{d,T,\boldsymbol{\gamma}}} f | \mathcal{H}^{r,t,\boldsymbol{\gamma}}(\mathbb{T}^d)\|^2 &= \sum_{\boldsymbol{k} \in \mathbb{Z}^d \setminus I_N^{d,T,\boldsymbol{\gamma}}} \omega^{r,t,\boldsymbol{\gamma}}(\boldsymbol{k})^2 \, \frac{\omega^{\alpha,\beta,\boldsymbol{\gamma}}(\boldsymbol{k})^2}{\omega^{\alpha,\beta,\boldsymbol{\gamma}}(\boldsymbol{k})^2} \, |\hat{f}_{\boldsymbol{k}}|^2 \\ &\leq \max_{\boldsymbol{k} \in \mathbb{Z}^d \setminus I_N^{d,T,\boldsymbol{\gamma}}} \omega^{-(\alpha-r),-(\beta-t),\boldsymbol{\gamma}}(\boldsymbol{k})^2 \sum_{\boldsymbol{k} \in \mathbb{Z}^d \setminus I_N^{d,T,\boldsymbol{\gamma}}} \omega^{\alpha,\beta,\boldsymbol{\gamma}}(\boldsymbol{k})^2 \, |\hat{f}_{\boldsymbol{k}}|^2. \end{aligned}$$

Applying Lemma 2.16 with $\tilde{\alpha} := \alpha - r$ and $\tilde{\beta} := \beta - t$ yields (2.45) which is also the upper bound in (2.46). For the lower bound, we modify the explicit example from [KPV15b, Lemma 4.4]. Let $s' \in \{1, \ldots, d\}$ be an index where $\gamma_{s'} = \|\boldsymbol{\gamma}\|_\infty$ and let the trigonometric polynomial $g(\boldsymbol{x}) = \mathrm{e}^{2\pi \mathrm{i} \boldsymbol{k'} \cdot \boldsymbol{x}}$ be given, where $\boldsymbol{k'} := (k'_1, \ldots, k'_d)^\top$ with $k'_s = \begin{cases} N+1 & \text{for } s = s', \\ 0 & \text{otherwise.} \end{cases}$ We have $\boldsymbol{k'} \notin I_N^{d,T,\boldsymbol{\gamma}}$ and we calculate

$$\begin{aligned} \|g - S_{I_N^{d,T,\boldsymbol{\gamma}}} g | \mathcal{H}^{r,t,\boldsymbol{\gamma}}(\mathbb{T}^d)\| = \|g | \mathcal{H}^{r,t,\boldsymbol{\gamma}}(\mathbb{T}^d)\| &= \sqrt{\omega^{r-\alpha,t-\beta,\boldsymbol{\gamma}}(\boldsymbol{k'})^2 \, \omega^{\alpha,\beta,\boldsymbol{\gamma}}(\boldsymbol{k'})^2 \, |\hat{f}_{\boldsymbol{k'}}|^2} \\ &= (N+1)^{r-\alpha} \left(\gamma_{s'}^{-1} \, (N+1)\right)^{t-\beta} \, \|g | \mathcal{H}^{\alpha,\beta,\boldsymbol{\gamma}}(\mathbb{T}^d)\| \end{aligned}$$

and we conclude that the norm of $\mathrm{Id} - S_{I_N^{d,T,\boldsymbol{\gamma}}}$ is bounded from below by (2.46). ∎

One can also formulate bounds on the truncation error with respect to the cardinality of the weighted frequency index sets $I_N^{d,T,\boldsymbol{\gamma}}$. Here we concentrate on the unweighted case $\boldsymbol{\gamma} := \mathbf{1}$.

Corollary 2.21. *Let the dimension $d \in \mathbb{N}$, $d \geq 2$, the dominating mixed smoothness $\beta \geq 0$, the isotropic smoothness $\alpha > -\beta$, the shape parameter $T := -\alpha/\beta$ with $T := -\infty$ for $\beta = 0$, and frequency index sets $I_N^{d,T,\mathbf{1}}$ be given, where the refinements $N \geq 1$. Then, the operator norm of $\mathrm{Id} - S_{I_N^{d,T,\mathbf{1}}}$ is bounded by*

$$\begin{aligned} &\|\mathrm{Id} - S_{I_N^{d,T,\mathbf{1}}} | \mathcal{A}^{\alpha,\beta,\mathbf{1}}(\mathbb{T}^d) \to L_\infty(\mathbb{T}^d)\| \asymp \|\mathrm{Id}_1 - S_{I_N^{d,T,\mathbf{1}}} | \mathcal{A}^{\alpha,\beta,\mathbf{1}}(\mathbb{T}^d) \to \mathcal{A}(\mathbb{T}^d)\| \\ &\asymp \begin{cases} |I_N^{d,T,\mathbf{1}}|^{-(\beta+\alpha/d)} & \text{for } T \in [-\infty, 0), \\ |I_N^{d,0,\mathbf{1}}|^{-\beta} (\log |I_N^{d,0,\mathbf{1}}|)^{(d-1)\beta} & \text{for } T = 0, \\ |I_N^{d,T,\mathbf{1}}|^{-(\alpha+\beta)} & \text{for } T \in (0, 1). \end{cases} \end{aligned} \tag{2.47}$$

where Id *and* Id_1 *denote the embedding operators from* $\mathcal{A}^{\alpha,\beta,\mathbf{1}}(\mathbb{T}^d)$ *into* $L_\infty(\mathbb{T}^d)$ *and* $\mathcal{A}^{\alpha,\beta,\mathbf{1}}(\mathbb{T}^d)$ *into* $\mathcal{A}(\mathbb{T}^d)$*, respectively.*

Proof. From (the proof of) Theorem 2.17, we obtain $\|\mathrm{Id} - S_{I_N^{d,T,\boldsymbol{\gamma}}} | \mathcal{A}^{\alpha,\beta,\boldsymbol{\gamma}}(\mathbb{T}^d) \to L_\infty(\mathbb{T}^d)\| \asymp \|\mathrm{Id}_1 - S_{I_N^{d,T,\boldsymbol{\gamma}}} | \mathcal{A}^{\alpha,\beta,\boldsymbol{\gamma}}(\mathbb{T}^d) \to \mathcal{A}(\mathbb{T}^d)\| \asymp N^{-(\alpha+\beta)}$. We have $N \asymp |I_N^{d,T,\mathbf{1}}|^{\frac{1-T/d}{1-T}} = |I_N^{d,T,\mathbf{1}}|^{\frac{\beta+\alpha/d}{\beta+\alpha}}$ for $T := -\alpha/\beta \in [-\infty, 0)$ and $N \asymp |I_N^{d,T,\mathbf{1}}|$ for $T := -\alpha/\beta \in (0, 1)$ due to (2.33) in Lemma 2.5. This yields the lower and upper bounds for $T \in [-\infty, 1) \setminus \{0\}$.

For the upper bound in the case $T = \alpha = 0$, we have $N^{-1} \asymp |I_N^{d,0,\mathbf{1}}| \log^{d-1} N \leq |I_N^{d,0,\mathbf{1}}|(\log |I_N^{d,0,\mathbf{1}}|)^{d-1}$ which results in the upper bound. For the corresponding lower bound, we have $N^{-1} \asymp |I_N^{d,0,\mathbf{1}}| \log^{d-1} N = |I_N^{d,0,\mathbf{1}}| 2^{1-d} \log^{d-1} N^2 \gtrsim |I_N^{d,0,\mathbf{1}}| \log^{d-1} |I_N^{d,0,\mathbf{1}}|$ and the assertion follows. ■

Corollary 2.22. *Let the dimension $d \in \mathbb{N}$, $d \geq 2$, smoothness parameters $r, \alpha \in \mathbb{R}$, $\beta \geq t \geq 0$, $\alpha + \beta > r + t \geq 0$, the shape parameter $T := -\frac{\alpha - r}{\beta - t}$ with $T := -\infty$ for $\beta = t$ and frequency index sets $I_N^{d,T,\mathbf{1}}$ be given, where the refinements $N \geq 1$. Then, the operator norm of $\mathrm{Id} - S_{I_N^{d,T,\mathbf{1}}}$ is bounded by*

$$\begin{aligned} &\| \mathrm{Id} - S_{I_N^{d,T,\mathbf{1}}} | \mathcal{H}^{\alpha,\beta,\mathbf{1}}(\mathbb{T}^d) \to \mathcal{H}^{r,t,\mathbf{1}}(\mathbb{T}^d) \| \\ &\asymp \begin{cases} |I_N^{d,T,\mathbf{1}}|^{-(\beta - t + \frac{\alpha - r}{d})} & \text{for } T \in [-\infty, 0), \\ |I_N^{d,0,\mathbf{1}}|^{-(\beta - t)} (\log |I_N^{d,0,\mathbf{1}}|)^{(d-1)(\beta - t)} & \text{for } T = 0, \\ |I_N^{d,T,\mathbf{1}}|^{-(\alpha - r + \beta - t)} & \text{for } T \in (0, 1). \end{cases} \end{aligned} \tag{2.48}$$

where Id *denotes the embedding operator from $\mathcal{H}^{\alpha,\beta,\mathbf{1}}(\mathbb{T}^d)$ into $\mathcal{H}^{r,t,\mathbf{1}}(\mathbb{T}^d)$.*

Proof. From Theorem 2.20, we obtain $\|\mathrm{Id} - S_{I_N^{d,T,\boldsymbol{\gamma}}} | \mathcal{H}^{\alpha,\beta,\boldsymbol{\gamma}}(\mathbb{T}^d) \to \mathcal{H}^{r,t,\boldsymbol{\gamma}}(\mathbb{T}^d)\| \asymp N^{-(\alpha - r + \beta - t)}$. We proceed as in the proof of Corollary 2.21 and obtain the assertion. ■

2.3.3 Rank-1 lattice sampling and error estimates

Since the Fourier coefficients $\hat{f}_{\boldsymbol{k}}$, $\boldsymbol{k} \in \mathbb{Z}^d$, of functions $f \in \mathcal{A}(\mathbb{T}^d)$ are usually neither known nor easy to compute analytically, one computes approximations of the Fourier coefficients $\hat{f}_{\boldsymbol{k}}$, e.g. based on samples of the function f. Here, we consider the approximation by a lattice rule. For this, we sample the function f at nodes $\boldsymbol{x}_j := \frac{j}{M} \boldsymbol{z} \bmod \mathbf{1}$, $j = 0, \ldots, M-1$, of a rank-1 lattice $\Lambda(\boldsymbol{z}, M)$. In doing so, we assume that f is continuous or identify f by its continuous representative, cf. Remark 2.15. We compute all the approximated Fourier coefficients $\hat{f}_{\boldsymbol{k}}^{\Lambda}$, $\boldsymbol{k} \in I$, by (2.7), i.e., by applying the same rank-1 lattice rule to the integrand in (2.5). This computation can be performed in $\mathcal{O}(M \log M + d\,|I|)$ arithmetic operations using a single one-dimensional FFT of length M and a simple index transform. We approximate the function f by the approximated Fourier partial sum $S_I^{\Lambda} f$ as defined in (2.8), which itself is a trigonometric polynomial $p_I \in \Pi_I$ of the form (2.2). In general, the approximated Fourier coefficients $\hat{f}_{\boldsymbol{k}}^{\Lambda}$ and the Fourier coefficients $\hat{f}_{\boldsymbol{k}}$ do not coincide. When we use the approximated Fourier partial sum $S_I^{\Lambda} f$ instead of the Fourier partial sum $S_I f$ for approximating the function f, we additionally obtain the aliasing error $S_I f - S_I^{\Lambda} f$, see equation (2.9).

In this section, we give a formula for the aliasing error $S_I f - S_I^{\Lambda} f$ in the general case and we present an algorithm for rank-1 lattice sampling. In Subsection 2.3.3.1, we use these results and we show error estimates for the sampling error $f - S_I^{\Lambda} f$ measured in the $L_\infty(\mathbb{T}^d)$ norm with respect to the refinement N of weighted frequency index sets $I := I_N^{d,T,\boldsymbol{\gamma}}$ and the norm of functions $f \in \mathcal{A}^{\alpha,\beta,\boldsymbol{\gamma}}(\mathbb{T}^d)$ when sampling along arbitrary reconstructing rank-1 lattices $\Lambda(\boldsymbol{z}, M, I)$. Based on these estimates and inequality (2.41) from Lemma 2.11 of Section 2.3.1, we give corresponding results measured in norms of periodic Sobolev spaces of generalized mixed smoothness $\mathcal{H}^{\alpha,\beta,\boldsymbol{\gamma}}(\mathbb{T}^d)$ in Subsection 2.3.3.2, where the obtained results are not asymptotically optimal. In Subsection 2.3.3.3, we improve these results using a different proof technique, see also [BKUV16], for special choices of the involved norms. The obtained results are asymptotically best possible in the main term with respect to the refinement N and may additionally

contain logarithmic factors. In Subsection 2.3.3.4, the logarithmic factors are removed and different choices of the involved norms are possible, but non-constructively obtained reconstructing rank-1 lattices $\Lambda(\boldsymbol{z}, M, I)$ with generating vector $\boldsymbol{z} := (1, a, \ldots, a^{d-1})^\top$ of Korobov form fulfilling additional properties have to be used. Finally, in Subsection 2.3.3.5, we consider the sampling errors with respect to the number of samples M, which yields different results in many cases compared to the estimates with respect to the refinement N from the previous subsections, since reconstructing rank-1 lattices $\Lambda(\boldsymbol{z}, M, I)$ generally require more samples M than degrees of freedom $|I_N^{d,T,\gamma}|$, cf. Table 2.3.

We start with a characterization of the aliasing error $S_I f - S_I^\Lambda f$ for arbitrary frequency index sets $I \subset \mathbb{Z}^d$, $|I| < \infty$, and arbitrary rank-1 lattices $\Lambda(\boldsymbol{z}, M) \subset \mathbb{T}^d$. This means we do not assume any (reconstruction) property for the used rank-1 lattice $\Lambda(\boldsymbol{z}, M)$ or any structure on the frequency index set $I \subset \mathbb{Z}^d$ in the next lemma.

Lemma 2.23. *([KPV15a, Lemma 3.1]). Let a function $f \in \mathcal{A}(\mathbb{T}^d) \cap \mathcal{C}(\mathbb{T}^d)$, a frequency index set $I \subset \mathbb{Z}^d$, $|I| < \infty$, and an arbitrary rank-1 lattice $\Lambda(\boldsymbol{z}, M) \subset \mathbb{T}^d$ with nodes $\boldsymbol{x}_j := \frac{j}{M}\boldsymbol{z} \bmod \mathbf{1}$, $j = 0, \ldots, M-1$, be given. The approximated Fourier coefficients $\hat{f}_{\boldsymbol{k}}^\Lambda$, $\boldsymbol{k} \in I$, computed by applying the lattice rule* (2.7)*, are aliased versions of the Fourier coefficients $\hat{f}_{\boldsymbol{k}}$ of the function f,*

$$\hat{f}_{\boldsymbol{k}}^\Lambda = \sum_{\substack{\boldsymbol{h} \in \mathbb{Z}^d \\ \boldsymbol{h}\cdot\boldsymbol{z} \equiv 0 \pmod{M}}} \hat{f}_{\boldsymbol{k}+\boldsymbol{h}} = \sum_{\boldsymbol{h} \in \Lambda^\perp(\boldsymbol{z}, M)} \hat{f}_{\boldsymbol{k}+\boldsymbol{h}},$$

where the dual lattice $\Lambda^\perp(\boldsymbol{z}, M)$ is defined in (2.29)*. The aliasing error is given by*

$$S_I f - S_I^\Lambda f = -\sum_{\boldsymbol{k} \in I} \sum_{\boldsymbol{h} \in \Lambda^\perp(\boldsymbol{z}, M) \setminus \{\mathbf{0}\}} \hat{f}_{\boldsymbol{k}+\boldsymbol{h}}\, \mathrm{e}^{2\pi \mathrm{i} \boldsymbol{k} \cdot \circ}. \tag{2.49}$$

Proof. Since we have $f(\frac{j}{M}\boldsymbol{z} \bmod \mathbf{1}) = \sum_{\boldsymbol{h} \in \mathbb{Z}^d} \hat{f}_{\boldsymbol{h}}\, \mathrm{e}^{2\pi \mathrm{i} j \boldsymbol{h}\cdot\boldsymbol{z}/M}$, we obtain

$$\hat{f}_{\boldsymbol{k}}^\Lambda = \frac{1}{M} \sum_{j=0}^{M-1} \sum_{\boldsymbol{h} \in \mathbb{Z}^d} \hat{f}_{\boldsymbol{h}}\, \mathrm{e}^{-2\pi \mathrm{i} j (\boldsymbol{k}-\boldsymbol{h})\cdot\boldsymbol{z}/M} = \sum_{\boldsymbol{h} \in \mathbb{Z}^d} \hat{f}_{\boldsymbol{h}} \frac{1}{M} \sum_{j=0}^{M-1} \mathrm{e}^{-2\pi \mathrm{i} j (\boldsymbol{k}-\boldsymbol{h})\cdot\boldsymbol{z}/M} = \sum_{\boldsymbol{h} \in \Lambda^\perp(\boldsymbol{z}, M)} \hat{f}_{\boldsymbol{k}+\boldsymbol{h}}$$

and the assertion follows. ∎

Since we do not want aliasing within the frequency index set I, we use a reconstructing rank-1 lattice $\Lambda(\boldsymbol{z}, M, I)$ for I, cf. reconstruction property (2.30). Therefore, we only have aliasing from Fourier coefficients $\hat{f}_{\boldsymbol{k}}$ with frequencies $\boldsymbol{k} \in \mathbb{Z}^d \setminus I$. The method for computing the approximated Fourier coefficients $\hat{f}_{\boldsymbol{k}}^\Lambda$, $\boldsymbol{k} \in I$, is presented as Algorithm 2.4 and can be realized using two lines of Octave / MATLAB code,

```
g_hat = fft( (f(x_j))_{j=0}^{M-1} );
(f̂_k^Λ)_{k∈I} = g_hat(mod(I*z,M)+1) / M;
```

cf. [Käm14c].

We consider the sampling error $f - S^\Lambda_{I_N^{d,T,\gamma}} f$ in different norms in the remaining part of this section. In doing so, we will also deal with the question on how good our approximation $S^\Lambda_{I_N^{d,T,\gamma}} f$ is. The answer to this question substantially depends on the used reference value and the employed norms. Here, we are going to consider the refinement N of the frequency index sets $I_N^{d,T,\gamma}$ and the number of samples M as reference values as well as the $L_\infty(\mathbb{T}^d)$ norm and Hilbert space norms $\mathcal{H}^{\alpha,\beta,\gamma}(\mathbb{T}^d)$. Typically, we will use inequality (2.10).

Algorithm 2.4 ([KPV15a, Algorithm 1]). Approximate reconstruction of a function $f \in \mathcal{A}(\mathbb{T}^d) \cap \mathcal{C}(\mathbb{T}^d)$ from sampling values on a reconstructing rank-1 lattice $\Lambda(\boldsymbol{z}, M, I)$ for I, i.e., application of Algorithm 2.1 on a function $f \in \mathcal{A}(\mathbb{T}^d) \cap \mathcal{C}(\mathbb{T}^d)$.

Input:	$I \subset \mathbb{Z}^d$	frequency index set of finite cardinality
	$\Lambda(\boldsymbol{z}, M, I)$	reconstructing rank-1 lattice for I of size M with generating vector $\boldsymbol{z} \in \mathbb{Z}^d$
	$\boldsymbol{f} = \left(f\left(\frac{j}{M}\boldsymbol{z} \bmod \mathbf{1}\right)\right)_{j=0}^{M-1}$	function values $f(\boldsymbol{x}_j)$, $\boldsymbol{x}_j := \frac{j}{M}\boldsymbol{z} \bmod \mathbf{1}$, of $f \in \mathcal{A}(\mathbb{T}^d) \cap \mathcal{C}(\mathbb{T}^d)$
$\hat{\boldsymbol{g}} := \texttt{FFT\_1D}(\boldsymbol{f})$		
for each $\boldsymbol{k} \in I$ **do**		
$\hat{f}_{\boldsymbol{k}}^{\Lambda} := \frac{1}{M}\,\hat{g}_{\boldsymbol{k}\cdot\boldsymbol{z} \bmod M}$		
end for		
Output:	$\hat{\boldsymbol{f}}^{\Lambda} = \left(\hat{f}_{\boldsymbol{k}}^{\Lambda}\right)_{\boldsymbol{k}\in I}$	approximated Fourier coefficients of $f \in \mathcal{A}(\mathbb{T}^d) \cap \mathcal{C}(\mathbb{T}^d)$
Complexity:	$\mathcal{O}\left(M \log M + d\,\lvert I\rvert\right)$	

We have already given upper bounds on the truncation error $f - S_{I_N^{d,T,\boldsymbol{\gamma}}} f$ in Theorem 2.17 and 2.20. Now, it remains to obtain bounds for the aliasing error $S_{I_N^{d,T,\boldsymbol{\gamma}}} f - S^{\Lambda}_{I_N^{d,T,\boldsymbol{\gamma}}} f$. The corresponding estimates use the aliasing formula (2.49) in Lemma 2.23 as starting point and rely on the equivalent reconstruction properties (2.25), (2.26), (2.27), (2.28) and (2.30) of reconstructing rank-1 lattices $\Lambda(\boldsymbol{z}, M, I_N^{d,T,\boldsymbol{\gamma}})$. In many cases, we make use of the Minkowski inequality for obtaining upper bounds.

Please note that the smoothness parameters $\alpha, \beta \in \mathbb{R}$ in the remaining theorems and corollaries of this section are chosen such that $\mathcal{A}^{\alpha,\beta,\boldsymbol{\gamma}} \hookrightarrow \mathcal{A}(\mathbb{T}^d) \hookrightarrow \mathcal{C}(\mathbb{T}^d)$ or $\mathcal{H}^{\alpha,\beta,\boldsymbol{\gamma}} \hookrightarrow \mathcal{A}(\mathbb{T}^d) \hookrightarrow \mathcal{C}(\mathbb{T}^d)$. Nevertheless, we demand for the sampled function $f \in \mathcal{A}^{\alpha,\beta,\boldsymbol{\gamma}} \cap \mathcal{C}(\mathbb{T}^d)$ or $f \in \mathcal{H}^{\alpha,\beta,\boldsymbol{\gamma}} \cap \mathcal{C}(\mathbb{T}^d)$ to express that we sample the continuous representative of f given by its Fourier series, cf. Remark 2.15.

2.3.3.1 Sampling error measured in $L_\infty(\mathbb{T}^d)$ norm

First, we estimate the sampling error $\|f - S^{\Lambda}_{I_N^{d,T,\boldsymbol{\gamma}}} f | L_\infty(\mathbb{T}^d)\|$ with the refinement N as reference value for functions f from subspaces $\mathcal{A}^{\alpha,\beta,\boldsymbol{\gamma}}(\mathbb{T}^d)$ of the Wiener algebra $\mathcal{A}(\mathbb{T}^d)$. For simplicity, we concentrate on the special case where the shape parameter T and weight parameter $\boldsymbol{\gamma}$ matches the smoothness and weight parameters of the function spaces $\mathcal{A}^{\alpha,\beta,\boldsymbol{\gamma}}(\mathbb{T}^d)$. The remaining cases, cf. [KPV15a, Theorem 3.3], are not more difficult but rather technical as can be observed at the estimation of the truncation error $f - S_{I_N^{d,T,\boldsymbol{\gamma}}} f$ in the proof of Theorem 2.17.

Theorem 2.24. *([KPV15a, Theorem 3.3]). Let a function $f \in \mathcal{A}^{\alpha,\beta,\boldsymbol{\gamma}}(\mathbb{T}^d) \cap \mathcal{C}(\mathbb{T}^d)$, a weighted frequency index set $I = I_N^{d,T,\boldsymbol{\gamma}}$ and a reconstructing rank-1 lattice $\Lambda(\boldsymbol{z}, M, I_N^{d,T,\boldsymbol{\gamma}})$ be given, where the refinement $N \geq 1$, the dominating mixed smoothness $\beta \geq 0$, the isotropic smoothness $\alpha > -\beta$, the shape parameter $T := -\frac{\alpha}{\beta}$ with $T := -\infty$ for $\beta = 0$ and the weight parameter $\boldsymbol{\gamma} \in (0,1]^d$. Then, the sampling error is bounded by*

$$\|f - S^{\Lambda}_{I_N^{d,T,\boldsymbol{\gamma}}} f | L_\infty(\mathbb{T}^d)\| \leq \|f - S^{\Lambda}_{I_N^{d,T,\boldsymbol{\gamma}}} f | \mathcal{A}(\mathbb{T}^d)\| \leq 2\, N^{-(\alpha+\beta)}\, \|f | \mathcal{A}^{\alpha,\beta,\boldsymbol{\gamma}}(\mathbb{T}^d)\|. \tag{2.50}$$

Proof. Applying inequality (2.10) in the $L_\infty(\mathbb{T}^d)$ norm, we estimate the sampling error by $\|f - S^{\Lambda}_{I_N^{d,T,\boldsymbol{\gamma}},\boldsymbol{\gamma}} f | L_\infty(\mathbb{T}^d)\| \le \|f - S_{I_N^{d,T,\boldsymbol{\gamma}}} f | L_\infty(\mathbb{T}^d)\| + \|S_{I_N^{d,T,\boldsymbol{\gamma}}} f - S^{\Lambda}_{I_N^{d,T,\boldsymbol{\gamma}},\boldsymbol{\gamma}} f | L_\infty(\mathbb{T}^d)\|$. For the truncation error, we obtain

$$\|f - S_{I_N^{d,T,\boldsymbol{\gamma}}} f | L_\infty(\mathbb{T}^d)\| \le \|f - S_{I_N^{d,T,\boldsymbol{\gamma}}} f | \mathcal{A}(\mathbb{T}^d)\| \le N^{-(\alpha+\beta)} \, \|f | \mathcal{A}^{\alpha,\beta,\boldsymbol{\gamma}}(\mathbb{T}^d)\|$$

from Theorem 2.17. Last, we estimate the aliasing error. Due to (2.49), we infer

$$\|S_{I_N^{d,T,\boldsymbol{\gamma}}} f - S^{\Lambda}_{I_N^{d,T,\boldsymbol{\gamma}},\boldsymbol{\gamma}} f | L_\infty(\mathbb{T}^d)\| \le \sum_{\boldsymbol{k} \in I_N^{d,T,\boldsymbol{\gamma}}} \sum_{\boldsymbol{h} \in \Lambda^\perp(\boldsymbol{z},M) \setminus \{\boldsymbol{0}\}} |\hat{f}_{\boldsymbol{k}+\boldsymbol{h}}|. \tag{2.51}$$

As discussed in the proof of [BKUV16, Lemma 6], reconstruction property (2.30) yields

$$\boldsymbol{k} + \boldsymbol{h} \neq \boldsymbol{k'} + \boldsymbol{h'} \text{ for all } \boldsymbol{h}, \boldsymbol{h'} \in \Lambda^\perp(\boldsymbol{z}, M) \text{ and } \boldsymbol{k}, \boldsymbol{k'} \in I \text{ with } \boldsymbol{k} \neq \boldsymbol{k'} \tag{2.52}$$

since otherwise $\boldsymbol{0} \neq \boldsymbol{k} - \boldsymbol{k'} = \boldsymbol{h'} - \boldsymbol{h} \in \Lambda^\perp(\boldsymbol{z}, M)$ which is in contradiction to (2.30). By considering the case $\boldsymbol{h'} := \boldsymbol{0}$, one obtains that

$$\boldsymbol{k} + \boldsymbol{h} \notin I \text{ for all } \boldsymbol{k} \in I \text{ and } \boldsymbol{h} \in \Lambda^\perp(\boldsymbol{z}, M) \setminus \{\boldsymbol{0}\}. \tag{2.53}$$

This means each Fourier coefficient $\hat{f}_{\boldsymbol{k'}}$, $\boldsymbol{k'} \in \mathbb{Z}^d \setminus I_N^{d,T,\boldsymbol{\gamma}}$ occurs at most once on the right hand side in the estimate (2.51) and the Fourier coefficients $\hat{f}_{\boldsymbol{k}}$, $\boldsymbol{k} \in I_N^{d,T,\boldsymbol{\gamma}}$, do not occur. Consequently, we obtain $\|S_{I_N^{d,T,\boldsymbol{\gamma}}} f - S^{\Lambda}_{I_N^{d,T,\boldsymbol{\gamma}},\boldsymbol{\gamma}} f | L_\infty(\mathbb{T}^d)\| \le \sum_{\boldsymbol{k} \in \mathbb{Z}^d \setminus I_N^{d,T,\boldsymbol{\gamma}}} |\hat{f}_{\boldsymbol{k}}|$ and proceed as in the estimate of the truncation error in the proof of Theorem 2.17. This yields the assertion. ∎

From the previous theorem, we obtain upper bounds for the sampling error measured in the $L_\infty(\mathbb{T}^d)$ norm identical to the upper bounds for the truncation error in (2.43) of Theorem 2.17 up to a constant factor of two for functions f from the weighted Banach spaces $\mathcal{A}^{\alpha,\beta,\boldsymbol{\gamma}}(\mathbb{T}^d)$ and suitable frequency index sets $I_N^{d,T,\boldsymbol{\gamma}}$.

2.3.3.2 Sampling error measured in Hilbert space norm

Next, we estimate sampling errors $f - S_I^\Lambda f$ in the norm of periodic Sobolev spaces of generalized mixed smoothness $\mathcal{H}^{r,t,\boldsymbol{\gamma}}(\mathbb{T}^d)$ of a continuous function $f \in \mathcal{A}^{\alpha,\beta,\boldsymbol{\gamma}}(\mathbb{T}^d) \subset \mathcal{H}^{\alpha,\beta,\boldsymbol{\gamma}}(\mathbb{T}^d)$ for suitable frequency index sets $I = I_N^{d,T,\boldsymbol{\gamma}}$.

Before we continue, we need to show embeddings into "thicker" weighted frequency index sets $I_N^{d,\tilde{T},\boldsymbol{\gamma}}$, i.e., for parameters $\tilde{T} \le T$. These statements are going to be used in Theorem 2.26, where we estimate the sampling error in the norm of periodic Sobolev spaces of generalized mixed smoothness $\mathcal{H}^{\alpha,\beta,\boldsymbol{\gamma}}(\mathbb{T}^d)$.

Lemma 2.25. *([KPV15a, Lemma 2.4]). Let a refinement $N \in \mathbb{R}$, $N \ge 1$, a weight parameter $\boldsymbol{\gamma} \in (0,1]^d$ and shape parameters $T, \tilde{T} \in [-\infty, 1)$, $-\infty \le \tilde{T} \le T < 1$, be given. Then, the following upper bound holds*

$$\max_{\boldsymbol{k} \in I_N^{d,T,\boldsymbol{\gamma}}} \omega^{-\frac{\tilde{T}}{1-\tilde{T}}, \frac{1}{1-\tilde{T}}, \boldsymbol{\gamma}}(\boldsymbol{k}) \le \begin{cases} d^{\frac{T-\tilde{T}}{(1-T)(1-\tilde{T})}} N & \text{for } \tilde{T} > -\infty, \\ d^{\frac{1}{1-T}} N & \text{for } \tilde{T} = -\infty, \end{cases}$$

where we define $\frac{\infty}{1+\infty} := 1$ and $\frac{1}{1+\infty} := 0$. This implies the following inclusion

$$I_N^{d,T,\boldsymbol{\gamma}} \subset \begin{cases} I^{d,\tilde{T},\boldsymbol{\gamma}}_{d^{(T-\tilde{T})/(1-T)/(1-\tilde{T})} N} & \text{for } \tilde{T} > -\infty, \\ I^{d,-\infty,\boldsymbol{\gamma}}_{d^{1/(1-T)} N} & \text{for } \tilde{T} = -\infty. \end{cases}$$

Proof. We observe by (2.14) that

$$I_N^{d,T,\boldsymbol{\gamma}} = \left\{ \boldsymbol{k} \in \mathbb{Z}^d \colon \max(1, \|\boldsymbol{k}\|_1)^{-\frac{T}{1-T}} \prod_{s=1}^{d} \max(1, \gamma_s^{-1}|k_s|)^{\frac{1}{1-T}} \leq N \right\}.$$

Let $\tilde{T} > -\infty$ and $\boldsymbol{k} \in I_N^{d,T,\boldsymbol{\gamma}}$. We estimate

$$\begin{aligned} N &\geq \omega^{-\frac{T}{1-T},\frac{1}{1-T},\boldsymbol{\gamma}}(\boldsymbol{k}) = \omega^{-\frac{T}{1-T}+\frac{T-\tilde{T}}{(1-T)(1-\tilde{T})},\frac{1}{1-T}-\frac{T-\tilde{T}}{(1-T)(1-\tilde{T})},\boldsymbol{\gamma}}(\boldsymbol{k}) \omega^{-\frac{T-\tilde{T}}{(1-T)(1-\tilde{T})},\frac{T-\tilde{T}}{(1-T)(1-\tilde{T})},\boldsymbol{\gamma}}(\boldsymbol{k}) \\ &= \omega^{-\frac{\tilde{T}}{1-\tilde{T}},\frac{1}{1-\tilde{T}},\boldsymbol{\gamma}}(\boldsymbol{k}) \left(\frac{\prod_{s=1}^{d} \max(1, \gamma_s^{-1}|k_s|)}{\max(1, \|\boldsymbol{k}\|_1)} \right)^{\frac{T-\tilde{T}}{(1-T)(1-\tilde{T})}}. \end{aligned}$$

Due to $\frac{T-\tilde{T}}{(1-T)(1-\tilde{T})} \geq 0$ and using the inequalities (2.21) and (2.22), we continue

$$N \geq \omega^{-\frac{\tilde{T}}{1-\tilde{T}},\frac{1}{1-\tilde{T}},\boldsymbol{\gamma}}(\boldsymbol{k}) \left(\frac{\prod_{s=1}^{d} \max(1, \gamma_s^{-1}|k_s|)}{d \prod_{s=1}^{d} \max(1, \gamma_s^{-1}|k_s|)} \right)^{\frac{T-\tilde{T}}{(1-T)(1-\tilde{T})}}$$

and obtain $d^{\frac{T-\tilde{T}}{(1-T)(1-\tilde{T})}} N \geq \omega^{-\frac{\tilde{T}}{1-\tilde{T}},\frac{1}{1-\tilde{T}},\boldsymbol{\gamma}}(\boldsymbol{k})$. This yields $\boldsymbol{k} \in I^{d,\tilde{T},\boldsymbol{\gamma}}_{d^{(T-\tilde{T})/(1-T)/(1-\tilde{T})}N}$.
In order to prove all inclusions from the assertion above, we have to deal separately with $\tilde{T} = -\infty$. Obviously, for $T = \tilde{T} = -\infty$, the inclusion from above holds. So, let us assume $-\infty = \tilde{T} < T < 1$. Due to the inequalities (2.21) and (2.22), we estimate for $\boldsymbol{k} \in I_N^{d,T,\boldsymbol{\gamma}}$ and $T \in (-\infty, 1)$

$$\begin{aligned} N &\geq \left(\prod_{s=1}^{d} \max(1, \gamma_s^{-1}|k_s|) \right)^{\frac{1}{1-T}} \max(1, \|\boldsymbol{k}\|_1)^{-\frac{T}{1-T}} \\ &\geq \left(d^{-1} \max(1, \|\boldsymbol{k}\|_1) \right)^{\frac{1}{1-T}} \max(1, \|\boldsymbol{k}\|_1)^{-\frac{T}{1-T}} = d^{-\frac{1}{1-T}} \max(1, \|\boldsymbol{k}\|_1) \end{aligned}$$

and obtain $\boldsymbol{k} \in I^{d,-\infty,\boldsymbol{\gamma}}_{d^{\frac{1}{1-T}}N}$. The upper bound in the Lemma then follows. ∎

The following theorem is a special case and a consequence of [KPV15a, Theorem 3.4].

Theorem 2.26. *(special case of [KPV15a, Theorem 3.4]). Let smoothness parameters $r, t, \alpha, \beta \in \mathbb{R}$, $\beta \geq t \geq 0$, $\alpha + \beta > r + t \geq 0$, and the shape parameter $T := -\frac{\alpha - r}{\beta - t} \in [-\frac{r}{t}, -\frac{\alpha}{\beta}]$ be given with $T := -\infty$ for $\beta = t$, $-\frac{r}{t} := -\infty$ for $t = 0$ and $-\frac{\alpha}{\beta} := -\infty$ for $\beta = 0$. Furthermore, let a function $f \in \mathcal{A}^{\alpha,\beta,\boldsymbol{\gamma}}(\mathbb{T}^d) \cap \mathcal{C}(\mathbb{T}^d)$, a weighted frequency index set $I_N^{d,T,\boldsymbol{\gamma}}$ and a reconstructing rank-1 lattice $\Lambda(\boldsymbol{z}, M, I_N^{d,T,\boldsymbol{\gamma}})$ be given, where the refinement $N \geq 1$ and the weight parameter $\boldsymbol{\gamma} \in (0,1]^d$. Then, the sampling error is bounded by*

$$\|f - S^{\Lambda}_{I_N^{d,T,\boldsymbol{\gamma}}} f | \mathcal{H}^{r,t,\boldsymbol{\gamma}}(\mathbb{T}^d)\| \leq N^{-(\alpha - r + \beta - t)} \left(\|f | \mathcal{H}^{\alpha,\beta,\boldsymbol{\gamma}}(\mathbb{T}^d)\| + \|f | \mathcal{A}^{\alpha,\beta,\boldsymbol{\gamma}}(\mathbb{T}^d)\| \right) \tag{2.54}$$

and for functions $f \in \left(\mathcal{H}^{\alpha,\beta+\lambda,\boldsymbol{\gamma}}(\mathbb{T}^d) \cap \mathcal{C}(\mathbb{T}^d) \right) \subset \mathcal{A}^{\alpha,\beta,\boldsymbol{\gamma}}(\mathbb{T}^d)$, $\lambda > 1/2$, this can be estimated by

$$\leq \left(1 + (1 + 2\zeta(2\lambda))^{\frac{d}{2}} \right) N^{-(\alpha - r + \beta - t)} \|f | \mathcal{H}^{\alpha,\beta+\lambda,\boldsymbol{\gamma}}(\mathbb{T}^d)\|. \tag{2.55}$$

Proof. For a function $f \in \mathcal{A}^{\alpha,\beta,\boldsymbol{\gamma}}(\mathbb{T}^d) \subset \mathcal{H}^{\alpha,\beta,\boldsymbol{\gamma}}(\mathbb{T}^d)$, we have

$$f - S_{I_N^{d,T,\boldsymbol{\gamma}}} f = \sum_{\boldsymbol{k} \in \mathbb{Z}^d \setminus I_N^{d,T,\boldsymbol{\gamma}}} \hat{f}_{\boldsymbol{k}}\, \mathrm{e}^{2\pi \mathrm{i} \boldsymbol{k} \cdot \circ}.$$

From Theorem 2.20, the first summand in (2.54) follows.
For the aliasing error of a function $f \in \mathcal{A}^{\alpha,\beta,\boldsymbol{\gamma}}(\mathbb{T}^d) \cap \mathcal{C}(\mathbb{T}^d)$, we have (2.49) and, in consequence of the concaveness of the square root function, we conclude

$$\begin{aligned}
\|S_{I_N^{d,T,\boldsymbol{\gamma}}} f - S^{\Lambda}_{I_N^{d,T,\boldsymbol{\gamma}}} f | \mathcal{H}^{r,t,\boldsymbol{\gamma}}(\mathbb{T}^d)\| &\le \left(\sum_{\boldsymbol{k} \in I_N^{d,T,\boldsymbol{\gamma}}} \omega^{r,t,\boldsymbol{\gamma}}(\boldsymbol{k})^2 \left| \sum_{\boldsymbol{h} \in \Lambda^\perp(\boldsymbol{z},M)\setminus\{\boldsymbol{0}\}} \hat{f}_{\boldsymbol{k}+\boldsymbol{h}} \right|^2 \right)^{\frac{1}{2}} && (2.56)\\
&\le \sum_{\boldsymbol{k} \in I_N^{d,T,\boldsymbol{\gamma}}} \left| \sum_{\boldsymbol{h} \in \Lambda^\perp(\boldsymbol{z},M)\setminus\{\boldsymbol{0}\}} \omega^{r,t,\boldsymbol{\gamma}}(\boldsymbol{k})\, \hat{f}_{\boldsymbol{k}+\boldsymbol{h}} \right| && (2.57)\\
&\le \max_{\boldsymbol{k} \in I_N^{d,T,\boldsymbol{\gamma}}} \omega^{r,t,\boldsymbol{\gamma}}(\boldsymbol{k}) \sum_{\boldsymbol{k} \in I_N^{d,T,\boldsymbol{\gamma}}} \sum_{\boldsymbol{h} \in \Lambda^\perp(\boldsymbol{z},M)\setminus\{\boldsymbol{0}\}} \left| \hat{f}_{\boldsymbol{k}+\boldsymbol{h}} \right|. && (2.58)
\end{aligned}$$

Since we have $\max\limits_{\boldsymbol{k} \in I_N^{d,T,\boldsymbol{\gamma}}} \left\{ \omega^{r,t,\boldsymbol{\gamma}}(\boldsymbol{k}) \right\} = \left\{ \begin{array}{ll} \max_{\boldsymbol{k} \in I_N^{d,T,\boldsymbol{\gamma}}} \left\{ \omega^{\frac{r/t}{1+r/t}, \frac{1}{1+r/t}, \boldsymbol{\gamma}}(\boldsymbol{k}) \right\}^{(1+r/t)t} & \text{for } t > 0 \\ \max_{\boldsymbol{k} \in I_N^{d,T,\boldsymbol{\gamma}}} \left\{ \omega^{1,0,\boldsymbol{\gamma}}(\boldsymbol{k}) \right\}^r & \text{for } t = 0 \end{array} \right\}$
and by applying Lemma 2.25 with $\tilde{T} = -\frac{r}{t}$, we estimate

$$\max_{\boldsymbol{k} \in I_N^{d,T,\boldsymbol{\gamma}}} \left\{ \omega^{r,t,\boldsymbol{\gamma}}(\boldsymbol{k}) \right\} \le \left\{ \begin{array}{ll} (d^{(T+\frac{r}{t})/(1-T)/(1+\frac{r}{t})} N)^{t+r} & \text{for } t > 0 \\ (d^{1/(1-T)} N)^r & \text{for } t = 0 \end{array} \right\} = d^{(Tt+r)/(1-T)} N^{r+t}. \tag{2.59}$$

Due to the reconstruction property (2.28), the representation property (2.52) follows and we have (2.53). Thus, we infer

$$\begin{aligned}
\|S_{I_N^{d,T,\boldsymbol{\gamma}}} f - S^{\Lambda}_{I_N^{d,T,\boldsymbol{\gamma}}} f | \mathcal{H}^{r,t,\boldsymbol{\gamma}}(\mathbb{T}^d)\| &\le d^{\frac{Tt+r}{1-T}} N^{r+t} \sum_{\boldsymbol{k} \in \mathbb{Z}^d \setminus I_N^{d,T,\boldsymbol{\gamma}}} \frac{\omega^{\alpha,\beta,\boldsymbol{\gamma}}(\boldsymbol{k})}{\omega^{\alpha,\beta,\boldsymbol{\gamma}}(\boldsymbol{k})} \left| \hat{f}_{\boldsymbol{k}} \right| \\
&\le d^{\frac{Tt+r}{1-T}} N^{r+t} \max_{\boldsymbol{k} \in \mathbb{Z}^d \setminus I_N^{d,T,\boldsymbol{\gamma}}} \frac{1}{\omega^{\alpha,\beta,\boldsymbol{\gamma}}(\boldsymbol{k})} \|f | \mathcal{A}^{\alpha,\beta,\boldsymbol{\gamma}}(\mathbb{T}^d)\|.
\end{aligned}$$

Applying Lemma 2.16 with $\tilde{\alpha} := \alpha$ and $\tilde{\beta} := \beta$ yields the second summand in (2.54).
Using inequality (2.41) we obtain the statement of Theorem 2.55 with the $\mathcal{H}^{\alpha,\beta+\lambda,\boldsymbol{\gamma}}(\mathbb{T}^d)$ norm on the right hand side for functions $f \in \left(\mathcal{H}^{\alpha,\beta+\lambda,\boldsymbol{\gamma}}(\mathbb{T}^d) \cap \mathcal{C}(\mathbb{T}^d) \right) \subset \mathcal{A}^{\alpha,\beta,\boldsymbol{\gamma}}(\mathbb{T}^d)$, $\lambda > 1/2$. ∎

Alternatively, one obtains a different version of the upper bound (2.55) in Theorem 2.26 in the case $\beta \ge \lambda > 1/2$ by substituting $\tilde{\beta} := \beta + \lambda$.

Corollary 2.27. *Let smoothness parameters $\beta \ge \lambda > 1/2$, $r, t, \alpha \in \mathbb{R}$, $\beta - \lambda \ge t \ge 0$, $\alpha + \beta - \lambda > r + t \ge 0$, the shape parameter $T := -\frac{\alpha - r}{\beta - t - \lambda} \in [-\frac{r}{t}, -\frac{\alpha}{\beta - \lambda}]$ with $T := -\infty$ for $\beta - \lambda = t$, a function $f \in \mathcal{H}^{\alpha,\beta,\boldsymbol{\gamma}}(\mathbb{T}^d) \cap \mathcal{C}(\mathbb{T}^d)$, a weighted frequency index set $I_N^{d,T,\boldsymbol{\gamma}}$ and a reconstructing rank-1 lattice $\Lambda(\boldsymbol{z}, M, I_N^{d,T,\boldsymbol{\gamma}})$ be given, where the refinement $N \ge 1$ and the weight parameter $\boldsymbol{\gamma} \in (0,1]^d$. Then, the sampling error is bounded by*

$$\|f - S^{\Lambda}_{I_N^{d,T,\boldsymbol{\gamma}}} f | \mathcal{H}^{r,t,\boldsymbol{\gamma}}(\mathbb{T}^d)\| \le C(d, r, t, \alpha, \beta, \lambda)\; N^{-(\alpha - r + \beta - t - \lambda)} \|f | \mathcal{H}^{\alpha,\beta,\boldsymbol{\gamma}}(\mathbb{T}^d)\|, \tag{2.60}$$

where the constant $C(d, r, t, \alpha, \beta, \lambda) \ge 1$ depends on the parameters $d, r, t, \alpha, \beta, \lambda$.

Remark 2.28. As we observe from Theorem 2.26, the dominating mixed smoothness β on the right hand side is increased by an additional additive factor $\lambda > 1/2$. Alternatively, see Corollary 2.27, this may be seen as losing an additive factor $\lambda > 1/2$ in the approximation order with respect to the refinement N of the generalized hyperbolic cross $I_N^{d,T,\boldsymbol{\gamma}}$. The reason for this is inequality (2.57) in combination with (2.58), where we switch between discrete two-norms and one-norms, which themselves consist of inner sums of weighted Fourier coefficients, and use a "uniform" estimate. Subsequently, we introduce two alternative approaches which solve this issue when measuring the sampling error $f - S_I^\Lambda f$ in the $L_2(\mathbb{T}^d)$ norm and the function f in the $\mathcal{H}^{\alpha,\beta,\boldsymbol{\gamma}}(\mathbb{T}^d)$ norm of the periodic Sobolev space of generalized mixed smoothness. □

2.3.3.3 Improved sampling error measured in norm of Sobolev space of dominating mixed smoothness when using reconstructing rank-1 lattices

In [BKUV16], it is shown that one can also obtain results similar to the ones from Theorem 2.26 and Corollary 2.27 without the additive factor $\lambda > 1/2$ in the main order of approximation using a reconstructing rank-1 lattice $\Lambda(\boldsymbol{z}, M, I_N^{d,T,\boldsymbol{\gamma}})$. A key ingredient to loose the additive factor $\lambda > 1/2$ is to partition the frequencies $\boldsymbol{k} + \boldsymbol{h}$, $\boldsymbol{k} \in I_N^{d,T,\boldsymbol{\gamma}}$ and $\boldsymbol{h} \in \Lambda^\perp(\boldsymbol{z}, M) \setminus \{\boldsymbol{0}\}$, in (2.56) into dyadic blocks, see e.g. [DTU16] and the references therein, and to have control over the number of frequencies in each partition.

First we introduce additional notation from [BKUV16]. As frequency index sets, so-called generalized dyadic hyperbolic crosses $I = H_R^{d,T} := \bigcup_{\boldsymbol{j} \in J_R^{d,T}} Q_{\boldsymbol{j}}$, are used, where $R \in \mathbb{R}$, $R \geq \frac{1-d}{1-T}$, denotes the refinement, $T \in [0,1)$ is an additional parameter,

$$J_R^{d,T} := \{\boldsymbol{j} \in \mathbb{N}_0^d \colon \|\boldsymbol{j}\|_1 - T\|\boldsymbol{j}\|_\infty \leq (1-T)R + d - 1\},$$

and $Q_{\boldsymbol{j}} := \times_{s=1}^d Q_{j_s}$ are sets of tensorized dyadic intervals

$$Q_j := \begin{cases} \{-1, 0, 1\} & \text{for } j = 0, \\ ([-2^j, -2^{j-1} - 1] \cup [2^{j-1} + 1, 2^j]) \cap \mathbb{Z} & \text{for } j > 0, \end{cases} \tag{2.61}$$

cf. [Kna00]. Then, for $R \geq 1$, the cardinalities

$$|H_R^{d,T}| \asymp \begin{cases} 2^R R^{d-1} & \text{for } T = 0, \\ 2^R & \text{for } 0 < T < 1, \end{cases}$$

for fixed dimension d and shape parameter T, see e.g. [BKUV16, Lemma 2] or the survey [DTU16].

Next, we state a relation between dyadic hyperbolic crosses $H_R^{d,0}$ and hyperbolic cross index sets $I_N^{d,0,\boldsymbol{\gamma}}$, see also [DTU16], which is required for estimating the sampling error.

Lemma 2.29. *Let the dimension $d \in \mathbb{N}$ and the refinement $N \in \mathbb{R}$, $N \geq 2$, be given. Then, we have $H_{\lceil \log_2 N \rceil}^{d,0} \subset I_{2^d N}^{d,0,\mathbf{1}}$.*

Proof. For each $\boldsymbol{k} \in H_{\lceil \log_2 N \rceil}^{d,0}$, there exists exactly one $\boldsymbol{j} \in J_{\lceil \log_2 N \rceil}^{d,0}$ with $\boldsymbol{k} \in Q_{\boldsymbol{j}}$. Due to the definition of the tensorized dyadic interval $Q_{\boldsymbol{j}}$, we have $\prod_{s=1}^d \max(1, |k_s|) \leq \prod_{s=1}^d 2^{j_s} = 2^{\|\boldsymbol{j}\|_1}$. Since $\boldsymbol{j} \in J_{\lceil \log_2 N \rceil}^{d,0}$, we have $\|\boldsymbol{j}\|_1 \leq \lceil \log_2 N \rceil + d - 1 \leq \log_2 N + d$ and $\prod_{s=1}^d \max(1, |k_s|) \leq 2^d N$ follows which yields $\boldsymbol{k} \in I_{2^d N}^{d,0,\mathbf{1}}$. ■

The previous lemma and the method in [BKUV16] give an improved upper bound for the sampling error of a function from periodic Sobolev spaces $\mathcal{H}^{\alpha,\beta,\mathbf{1}}(\mathbb{T}^d)$ of generalized mixed smoothness measured in the $\mathcal{H}^{0,t,\mathbf{1}}(\mathbb{T}^d)$ norm of periodic Sobolev spaces of dominating mixed smoothness for isotropic smoothness $\alpha \leq 0$.

Theorem 2.30. *Let the smoothness parameters $\beta > \frac{1}{2}$, $\alpha \leq 0$, $t \geq 0$ with $\alpha+\beta > \max\{t, \frac{1}{2}\}$, the dimension $d \in \mathbb{N}$, $d \geq 2$, a function $f \in \mathcal{H}^{\alpha,\beta,\mathbf{1}}(\mathbb{T}^d) \cap \mathcal{C}(\mathbb{T}^d)$, a hyperbolic cross index set $I_N^{d,0,\mathbf{1}}$ with refinement $N \geq 2^{d+1}$, and a reconstructing rank-1 lattice $\Lambda(\boldsymbol{z}, M, I_N^{d,0,\mathbf{1}})$ for $I_N^{d,0,\mathbf{1}}$ be given. Then, we obtain*

$$\|f - S^{\Lambda}_{I_N^{d,0,\mathbf{1}}} f | \mathcal{H}^{0,t,\mathbf{1}}(\mathbb{T}^d)\| \lesssim \|f|\mathcal{H}^{\alpha,\beta,\mathbf{1}}(\mathbb{T}^d)\|\, N^{-(\alpha+\beta-t)} \begin{cases} (\log N)^{(d-1)/2} & \text{for } \alpha = 0, \\ 1 & \text{for } \alpha < 0, \end{cases}$$

where the constants may depend on the dimension d and smoothness parameters α, β, t.

Proof. As usually, we apply the triangle inequality (2.10),

$$\|f - S^{\Lambda}_{I_N^{d,0,\mathbf{1}}} f | \mathcal{H}^{0,t,\mathbf{1}}(\mathbb{T}^d)\| \leq \|f - S_{I_N^{d,0,\mathbf{1}}} f | \mathcal{H}^{0,t,\mathbf{1}}(\mathbb{T}^d)\| + \|S_{I_N^{d,0,\mathbf{1}}} f - S^{\Lambda}_{I_N^{d,0,\mathbf{1}}} f | \mathcal{H}^{0,t,\mathbf{1}}(\mathbb{T}^d)\|,$$

and we obtain for the first summand on the right hand side

$$\|f - S_{I_N^{d,0,\mathbf{1}}} f | \mathcal{H}^{0,t,\mathbf{1}}(\mathbb{T}^d)\| \leq N^{-(\alpha+\beta-t)} \|f|\mathcal{H}^{\alpha,\beta,\mathbf{1}}(\mathbb{T}^d)\|$$

as in the proof of Theorem 2.26.
For the second summand, we have

$$\|S_{I_N^{d,0,\mathbf{1}}} f - S^{\Lambda}_{I_N^{d,0,\mathbf{1}}} f | \mathcal{H}^{0,t,\mathbf{1}}(\mathbb{T}^d)\|^2 \leq \sum_{\boldsymbol{k} \in I_N^{d,0,\mathbf{1}}} \omega^{0,t,\mathbf{1}}(\boldsymbol{k})^2 \left| \sum_{\boldsymbol{h} \in \Lambda^{\perp}(\boldsymbol{z},M)\setminus\{\mathbf{0}\}} \hat{f}_{\boldsymbol{k}+\boldsymbol{h}} \right|^2$$

due to (2.56). Following the proof of [BKUV16, Theorem 2], we apply the Cauchy-Schwarz inequality followed by the Hölder inequality and we continue

$$\leq \sum_{\boldsymbol{k} \in I_N^{d,0,\mathbf{1}}} \omega^{0,t,\mathbf{1}}(\boldsymbol{k})^2 \left(\sum_{\boldsymbol{h} \in \Lambda^{\perp}(\boldsymbol{z},M)\setminus\{\mathbf{0}\}} \omega^{-\alpha,-\beta,\mathbf{1}}(\boldsymbol{k}+\boldsymbol{h})^2 \right) \left(\sum_{\boldsymbol{h} \in \Lambda^{\perp}(\boldsymbol{z},M)\setminus\{\mathbf{0}\}} \omega^{\alpha,\beta,\mathbf{1}}(\boldsymbol{k}+\boldsymbol{h})^2 |\hat{f}_{\boldsymbol{k}+\boldsymbol{h}}|^2 \right)$$

$$\leq \left(\max_{\boldsymbol{k} \in I_N^{d,0,\mathbf{1}}} \omega^{0,t,\mathbf{1}}(\boldsymbol{k})^2 \right) \left(\max_{\boldsymbol{k} \in I_N^{d,0,\mathbf{1}}} \sum_{\boldsymbol{h} \in \Lambda^{\perp}(\boldsymbol{z},M)\setminus\{\mathbf{0}\}} \omega^{-\alpha,-\beta,\mathbf{1}}(\boldsymbol{k}+\boldsymbol{h})^2 \right)$$
$$\cdot \left(\sum_{\boldsymbol{k} \in I_N^{d,0,\mathbf{1}}} \sum_{\boldsymbol{h} \in \Lambda^{\perp}(\boldsymbol{z},M)\setminus\{\mathbf{0}\}} \omega^{\alpha,\beta,\mathbf{1}}(\boldsymbol{k}+\boldsymbol{h})^2 |\hat{f}_{\boldsymbol{k}+\boldsymbol{h}}|^2 \right).$$

For the last part, we obtain

$$\sum_{\boldsymbol{k} \in I_N^{d,0,\mathbf{1}}} \sum_{\boldsymbol{h} \in \Lambda^{\perp}(\boldsymbol{z},M)\setminus\{\mathbf{0}\}} \omega^{\alpha,\beta,\mathbf{1}}(\boldsymbol{k}+\boldsymbol{h})^2 |\hat{f}_{\boldsymbol{k}+\boldsymbol{h}}|^2 \leq \|f|\mathcal{H}^{\alpha,\beta,\gamma}(\mathbb{T}^d)\|^2,$$

see the proof of Theorem 2.26.
We define $\tilde{\theta}^2_{\beta,\alpha}(\boldsymbol{k},\boldsymbol{z},M) := \sum_{\boldsymbol{h}\in\Lambda^\perp(\boldsymbol{z},M)\setminus\{\boldsymbol{0}\}} \omega^{-\alpha,-\beta,\mathbf{1}}(\boldsymbol{k}+\boldsymbol{h})^2$ and we proceed analogously to the proof of [BKUV16, Lemma 6]. This means we define the indicator function

$$\varphi_{\boldsymbol{j}}(\boldsymbol{k}) := \begin{cases} 0 & \text{for } \boldsymbol{k} \notin Q_{\boldsymbol{j}}, \\ 1 & \text{for } \boldsymbol{k} \in Q_{\boldsymbol{j}}, \end{cases} \qquad \boldsymbol{k} \in \mathbb{Z}^d, \boldsymbol{j} \in \mathbb{N}_0^d,$$

and we achieve

$$\tilde{\theta}^2_{\beta,\alpha}(\boldsymbol{k},\boldsymbol{z},M) = \sum_{\boldsymbol{h}\in\Lambda^\perp(\boldsymbol{z},M)\setminus\{\boldsymbol{0}\}} \sum_{\boldsymbol{j}\in\mathbb{N}_0^d} \varphi_{\boldsymbol{j}}(\boldsymbol{k}+\boldsymbol{h})\, \omega^{-\alpha,-\beta,\mathbf{1}}(\boldsymbol{k}+\boldsymbol{h})^2$$

for fixed $\boldsymbol{k} \in I_N^{d,0,\mathbf{1}}$. Due to the reconstruction property (2.28), the representation property (2.52) follows for $I = I_N^{d,0,\mathbf{1}}$ and we have (2.53). Since we have $H^{d,0}_{-d+\log_2 N} \subset I_N^{d,0,\mathbf{1}}$ for $N \geq 2^{d+1}$ due to Lemma 2.29 and since the summands are only non-zero for $\boldsymbol{k}+\boldsymbol{h} \in Q_{\boldsymbol{j}}$ due to the definition of the indicator function $\varphi_{\boldsymbol{j}}$, we infer

$$\begin{aligned}
\tilde{\theta}^2_{\beta,\alpha}(\boldsymbol{k},\boldsymbol{z},M) &= \sum_{\boldsymbol{j}\in\mathbb{N}_0^d\setminus J^{d,0}_{-d+\log_2 N}} \sum_{\boldsymbol{h}\in\Lambda^\perp(\boldsymbol{z},M)\setminus\{\boldsymbol{0}\}} \varphi_{\boldsymbol{j}}(\boldsymbol{k}+\boldsymbol{h})\, \omega^{-\alpha,-\beta,\mathbf{1}}(\boldsymbol{k}+\boldsymbol{h})^2 \\
&\leq \sum_{\boldsymbol{j}\in\mathbb{N}_0^d\setminus J^{d,0}_{-d+\log_2 N}} \left(\max_{\boldsymbol{k'}\in Q_{\boldsymbol{j}}} \omega^{-\alpha,-\beta,\mathbf{1}}(\boldsymbol{k'})^2 \right) \sum_{\boldsymbol{h}\in\Lambda^\perp(\boldsymbol{z},M)\setminus\{\boldsymbol{0}\}} \varphi_{\boldsymbol{j}}(\boldsymbol{k}+\boldsymbol{h})
\end{aligned}$$

for fixed $\boldsymbol{k} \in I_N^{d,0,\mathbf{1}}$. Using the definition of the weights $\omega^{-\alpha,-\beta,\mathbf{1}}$ and of the tensorized dyadic intervals $Q_{\boldsymbol{j}}$, we obtain

$$\begin{aligned}
\max_{\boldsymbol{k'}\in Q_{\boldsymbol{j}}} \omega^{-\alpha,-\beta,\mathbf{1}}(\boldsymbol{k'})^2 &= \max_{\boldsymbol{k'}\in Q_{\boldsymbol{j}}} \max(1,\|\boldsymbol{k'}\|_1)^{-2\alpha} \prod_{s=1}^d \max(1,|k'_s|)^{-2\beta} \\
&\leq \max_{\boldsymbol{k'}\in Q_{\boldsymbol{j}}} d^{-2\alpha} \max(1,\|\boldsymbol{k'}\|_\infty)^{-2\alpha} \prod_{s=1}^d (2^{j_s-2})^{-2\beta} \\
&\leq d^{-2\alpha}\, 2^{4d\beta}\, 2^{-2\alpha\|\boldsymbol{j}\|_\infty}\, 2^{-2\beta\|\boldsymbol{j}\|_1}.
\end{aligned}$$

This yields

$$\tilde{\theta}^2_{\beta,\alpha}(\boldsymbol{k},\boldsymbol{z},M) \lesssim \sum_{\boldsymbol{j}\in\mathbb{N}_0^d\setminus J^{d,0}_{-d+\log_2 N}} 2^{-(2\alpha\|\boldsymbol{j}\|_\infty+2\beta\|\boldsymbol{j}\|_1)} \sum_{\boldsymbol{h}\in\Lambda^\perp(\boldsymbol{z},M)\setminus\{\boldsymbol{0}\}} \varphi_{\boldsymbol{j}}(\boldsymbol{k}+\boldsymbol{h})$$

for $\boldsymbol{k} \in I_N^{d,0,\mathbf{1}}$. We apply [BKUV16, Lemma 5] with $R := -d + \log_2 N$ and consequently, for $\boldsymbol{k} \in I_N^{d,0,\mathbf{1}}$, we have

$$\tilde{\theta}^2_{\beta,\alpha}(\boldsymbol{k},\boldsymbol{z},M) \lesssim N^{-1} \sum_{\boldsymbol{j}\in\mathbb{N}_0^d\setminus J^{d,0}_{-d+\log_2 N}} 2^{-(2\alpha\|\boldsymbol{j}\|_\infty+(2\beta-1)\|\boldsymbol{j}\|_1)}.$$

Using [BKUV16, Lemma 7] with $R := -d + \log_2 N$, we obtain

$$\max_{\boldsymbol{k}\in I_N^{d,0,\mathbf{1}}} \tilde{\theta}^2_{\beta,\alpha}(\boldsymbol{k},\boldsymbol{z},M) \lesssim N^{-1} \begin{cases} N^{-(2\beta-1+2\alpha)} & \text{for } \alpha < 0, \\ N^{-(2\beta-1)} (\log N)^{d-1} & \text{for } \alpha = 0, \end{cases}$$

and the assertion follows. ∎

Remark 2.31. Theorem 2.30 does not give results for the case where the isotropic smoothness $\alpha > 0$. This issue will be dealt with later in Theorem 2.36 using a different approach. □

2.3.3.4 Optimal sampling error in $L_2(\mathbb{T}^d)$ norm with respect to refinement N for special rank-1 lattices with generating vector of Korobov form

In the following, we discuss another approach for improving the results of Theorem 2.26 and Corollary 2.27 by removing the additional additive factor $\lambda > 1/2$ in the order of approximation, see [KPV15b] for more detailed explanations and proofs. This is done using and extending ideas and techniques from [Tem86], where the case $\alpha = 0$ was considered. For simplicity, we concentrate on the unweighted case $\boldsymbol{\gamma} := \mathbf{1}$. We remark that we only obtain existence results here, i.e., that there exist special reconstructing rank-1 lattices $\Lambda(\boldsymbol{z}, M, I_N^{d,T,\mathbf{1}})$ such that the optimal approximation order with respect to the refinement $N \in \mathbb{R}$, $N \geq 1$, of the frequency index set $I_N^{d,T,\mathbf{1}}$, $T \in [-\infty, 1)$, is achieved. This means we do not have a constructive method or conditions testable on a computer for obtaining such a special reconstructing rank-1 lattice $\Lambda(\boldsymbol{z}, M, I_N^{d,T,\mathbf{1}})$.

The following lemma states that there exists a reconstructing rank-1 lattice $\Lambda(\boldsymbol{z}, M, I_N^{d,T,\mathbf{1}})$ with generating vector $\boldsymbol{z} := (1, a, \ldots, a^{d-1}) \in \mathbb{N}^d$ of Korobov form where the number of points in the dual lattice $\Lambda(\boldsymbol{z}, M)^\perp := \{\boldsymbol{h} \in \mathbb{Z}^d \colon \boldsymbol{h} \cdot \boldsymbol{z} \equiv 0 \pmod{M}\}$ is bounded in a certain way.

Lemma 2.32. *We define the frequency index sets*

$$\mathcal{I}_N := \begin{cases} I^{d,T,\mathbf{1}}_{2^{\frac{d-T}{1-T}} N^{1+\frac{d}{d-T}}} \supset \mathcal{D}\left(I_N^{d,T,\mathbf{1}}\right) & \text{for } -\infty \leq T \leq 0, \\ \mathcal{D}\left(I_N^{d,T,\mathbf{1}}\right) & \text{for } 0 < T < 1, \end{cases}$$

where the refinement $N \in \mathbb{R}$, $N \geq 1$, and the shape parameter $T \in [-\infty, 1)$. For fixed N and T, let the rank-1 lattice size $M \in \mathbb{N}$ be a prime number such that

$$M > \frac{d\,|\mathcal{I}_N|}{1 - 2^{-\kappa}} + 1 \tag{2.62}$$

for arbitrarily chosen parameter $\kappa \in \mathbb{R}$, $\kappa > 0$. We define the shells $F_l(N) := \mathcal{I}_{N2^l} \setminus \mathcal{I}_{N2^{l-1}}$, $l \in \mathbb{N}$, and for each generating vector $\boldsymbol{z} := (1, a, \ldots, a^{d-1}) \in \mathbb{N}^d$ of Korobov form with parameter $a \in \{1, \ldots, M-1\}$ the sets

$$M_a^l := \{\boldsymbol{h} \in F_l(N) \colon \boldsymbol{h} \cdot \boldsymbol{z} = h_1 + h_2\, a + \ldots + h_d\, a^{d-1} \equiv 0 \pmod{M} \text{ and } \boldsymbol{h} \neq M\boldsymbol{i} \ \ \forall \boldsymbol{i} \in \mathbb{Z}^d\}$$

of non-trivially aliasing frequencies within these shells. Then, there exists a number $a \in \{1, \ldots, M-1\}$, such that $\Lambda(\boldsymbol{z}, M, I_N^{d,T,\mathbf{1}})$ is a reconstructing rank-1 lattice for $I_N^{d,T,\mathbf{1}}$ and

$$|M_a^l| \leq A_l^N := \frac{d}{2^\kappa - 1} (M-1)^{-1} |F_l(N)|\, 2^{(l+1)\kappa}, \quad l \in \mathbb{N}. \tag{2.63}$$

Proof. Applying [KPV15b, Lemma 2.1] with $\varphi(l) := 2^l$, which is a generalization of [Tem86, Lemma 1], yields the assertion. ■

Remark 2.33. In Lemma 2.32, the shells $F_l(N) := \mathcal{I}_{N2^l} \setminus \mathcal{I}_{N2^{l-1}}$, $l \in \mathbb{N}$, form a dyadic partition of the frequency set $\mathbb{Z}^d \setminus \mathcal{I}_N \subset \mathbb{Z}^d \setminus \mathcal{D}(I_N^{d,T,\mathbf{1}})$ and the sets M_a^l contain "non-trivial" frequencies from the dual lattice $\Lambda(\boldsymbol{z}, M)^\perp$ intersected with the shell $F_l(N)$, i.e., those frequencies from the dual lattice $\Lambda(\boldsymbol{z}, M)^\perp$ which are not multiples of the rank-1 lattice size M. The crucial property for improving the estimate of the sampling error is given in (2.63), which bounds the number of non-trivial dual lattice points in the shells $F_l(N)$. The Korobov form of the generating vector $\boldsymbol{z}$ is required by the proof of [KPV15b, Lemma 2.1] since Lagrange's Theorem from number theory is used therein, which states that the congruence $\boldsymbol{h} \cdot \boldsymbol{z} = h_1 + h_2\, a + \ldots + h_d\, a^{d-1} \equiv 0 \pmod{M}$ has at most $d-1$ many roots modulo M for fixed $\boldsymbol{h} \in \mathbb{Z}^d \setminus (M\mathbb{Z}^d)$. Upper bounds for the numbers of "trivial" frequencies from the dual lattice $\Lambda(\boldsymbol{z}, M)^\perp$ are given later in Lemma 2.35 and 2.38. □

The next theorem is a special case of [KPV15b, Theorem 3.4] and a generalization of [Tem86, Theorem 2]. The aliasing error $S_{I_N^{d,T,\mathbf{1}}} f - S^{\Lambda}_{I_N^{d,T,\mathbf{1}}} f$ is bounded from above for (continuous) functions f from periodic Sobolev spaces of generalized mixed smoothness $\mathcal{H}^{\alpha,\beta,\mathbf{1}}(\mathbb{T}^d)$ using the special reconstructing rank-1 lattices $\Lambda(\boldsymbol{z}, M, I_N^{d,T,\mathbf{1}})$.

Theorem 2.34. *Let the dimension $d \in \mathbb{N}$, $d \geq 2$, a parameter $\kappa > 0$, a function $f \in \mathcal{H}^{\alpha,\beta,\mathbf{1}}(\mathbb{T}^d) \cap \mathcal{C}(\mathbb{T}^d)$ with absolutely convergent Fourier series, smoothness parameters $\beta \geq 0$ and $\alpha > -\beta$ be given. Furthermore, let the frequency index sets*

$$\mathcal{I}_N^{d,T} := \begin{cases} I^{d,T,\mathbf{1}}_{2^{\frac{d-T}{1-T}} N^{1+\frac{d}{d-T}}} \supset \mathcal{D}\left(I_N^{d,T,\mathbf{1}}\right) & \text{for } -\infty \leq T \leq 0, \\ \mathcal{D}\left(I_N^{d,T,\mathbf{1}}\right) & \text{for } 0 < T < 1, \end{cases}$$

where the refinement $N \in \mathbb{R}$, $N \geq 1$, and the shape parameter $T := -\alpha/\beta \in [-\infty, 1)$. For each fixed refinement $N \in \mathbb{R}$, $N \geq 1$, let $\Lambda(\boldsymbol{z}, M, I_N^{d,T,\mathbf{1}})$ be a reconstructing rank-1 lattice with generating vector $\boldsymbol{z} := (1, a, \ldots, a^{d-1})^\top \in \mathbb{Z}^d$ of Korobov form and prime rank-1 lattice size $M > \frac{d|\mathcal{I}_N|}{1-2^{-\kappa}} + 1$ which fulfills property (2.63)*. Additionally, let the inequality*

$$\left|\mathcal{I}_{N2^l}^{d,T} \cap M\mathbb{Z}^d\right| \leq C \frac{|\mathcal{I}_{N2^l}^{d,T}|}{M} \psi(l) + 1 \quad \forall l \in \mathbb{N} \tag{2.64}$$

be valid, where $\psi : [0, \infty) \to [1, \infty)$,

$$\psi(l) := \begin{cases} 1 & \text{for } -\infty \leq T \leq 0 \\ l^{d-1} & \text{for } 0 < T < 1, \end{cases}$$

and $C > 0$ is a constant which does not depend on N or M. Then, the aliasing error is bounded by

$$\begin{aligned} \|S_{I_N^{d,T,\mathbf{1}}} f - S^{\Lambda}_{I_N^{d,T,\mathbf{1}}} f | L_2(\mathbb{T}^d)\| &\leq 2^{\alpha+\beta}\, N^{-(\alpha+\beta)}\, \|f | \mathcal{H}^{\alpha,\beta,\mathbf{1}}(\mathbb{T}^d)\| \\ &\quad \cdot \sum_{l=0}^{\infty} \sqrt{2\left(2 + (1-2^{-\kappa})\, C\, \psi(l+1)\right)}\, 2^{(l+1)(\frac{\kappa}{2}-\alpha-\beta)} \sqrt{\frac{|\mathcal{I}_{N2^{l+1}}^{d,T}|}{|\mathcal{I}_N^{d,T}|}}. \end{aligned} \tag{2.65}$$

Proof. We give the major steps of the proof. For more details, we refer to the proof of [KPV15b, Theorem 3.4]. First, one defines shells $U_l := I_{N2^{l+1}}^{d,T,\mathbf{1}} \setminus I_{N2^l}^{d,T,\mathbf{1}} \subset \mathbb{Z}^d$, $l \in \mathbb{N}_0$, which

fulfill the properties $U_{l'} \cap U_{l''} = \emptyset$ for $l' \neq l''$ and $\operatorname{supp}\hat{f} \setminus I \subset \bigcup_{l=0}^{\infty} U_l$, where $\operatorname{supp}\hat{f} := \{\boldsymbol{k} \in \mathbb{Z}^d \colon \hat{f}_{\boldsymbol{k}} \neq 0\}$. Due to [KPV15b, Lemma 3.2] the aliasing error can be estimated by

$$\|S_{I_N^{d,T,\mathbf{1}}} f - S^{\Lambda}_{I_N^{d,T,\mathbf{1}}} f | L_2(\mathbb{T}^d)\| \leq \sum_{l=0}^{\infty} \sigma_l, \qquad \sigma_l := \left(\frac{1}{M} \sum_{j=0}^{M-1} |S_{U_l} f(\boldsymbol{x}_j)|^2 \right)^{1/2}.$$

Using additional notation and the Cauchy Schwarz inequality twice yields

$$\begin{aligned} \sigma_l^2 &= \sum_{\boldsymbol{k},\boldsymbol{h} \in U_l} \hat{f}_{\boldsymbol{k}} \overline{\hat{f}_{\boldsymbol{h}}} \, \frac{1}{M} \sum_{j=0}^{M-1} \mathrm{e}^{2\pi \mathrm{i} j (\boldsymbol{k}-\boldsymbol{h}) \cdot \boldsymbol{z}/M} = \sum_{\boldsymbol{k} \in U_l} \hat{f}_{\boldsymbol{k}} \sum_{\boldsymbol{h} \in \theta_{l,\boldsymbol{k}}} \overline{\hat{f}_{\boldsymbol{h}}} \\ &\leq \left(\sum_{\boldsymbol{k} \in U_l} |\hat{f}_{\boldsymbol{k}}|^2 \right)^{1/2} \left(\sum_{\boldsymbol{k} \in U_l} |\theta_{l,\boldsymbol{k}}| \sum_{\boldsymbol{h} \in \theta_{l,\boldsymbol{k}}} |\hat{f}_{\boldsymbol{h}}|^2 \right)^{1/2}, \end{aligned}$$

where $\theta_{l,\boldsymbol{k}} := \left\{ \boldsymbol{h} \in U_l \colon \frac{1}{M} \sum_{j=0}^{M-1} \mathrm{e}^{2\pi \mathrm{i} j (\boldsymbol{k}-\boldsymbol{h}) \cdot \boldsymbol{z}/M} = 1 \right\} = \{\boldsymbol{h} \in U_l \colon (\boldsymbol{k}-\boldsymbol{h}) \cdot \boldsymbol{z} \equiv 0 \pmod{M}\}$ for $\boldsymbol{k} \in U_l$. Since $\boldsymbol{k} - \boldsymbol{h} \in \mathcal{D}(I^{d,T,\mathbf{1}}_{N2^{l+1}}) \subset \mathcal{I}^{d,T}_{N2^{l+1}}$ for $\boldsymbol{k}, \boldsymbol{h} \in U_l$ and using Lemma 2.32, the estimate

$$|\theta_{l,\boldsymbol{k}}| \leq |\{\boldsymbol{m} \in \mathcal{I}^{d,T}_{N2^{l+1}} \colon \boldsymbol{m} \cdot \boldsymbol{z} \equiv 0 \pmod{M}\}| \leq \sum_{j=1}^{l+1} A_j^N + C \frac{|\mathcal{I}^{d,T}_{N2^{l+1}}|}{M} \psi(l+1) + 1 =: B_l$$

follows from properties (2.63) and (2.64). Next, one obtains

$$\sum_{\boldsymbol{k} \in U_l} \sum_{\boldsymbol{h} \in \theta_{\ell,\boldsymbol{k}}} |\hat{f}_{\boldsymbol{h}}|^2 \leq \sum_{\boldsymbol{k} \in U_l} B_l |\hat{f}_{\boldsymbol{k}}|^2$$

and this yields

$$\begin{aligned} \sigma_l^2 &\leq \left(\sum_{\boldsymbol{k} \in U_l} |\hat{f}_{\boldsymbol{k}}|^2 \right)^{\frac{1}{2}} \left(B_l^2 \sum_{\boldsymbol{k} \in U_l} |\hat{f}_{\boldsymbol{k}}|^2 \right)^{\frac{1}{2}} \leq B_l \sum_{\boldsymbol{k} \in \mathbb{Z}^d \setminus I^{d,T,\mathbf{1}}_{N2^l}} |\hat{f}_{\boldsymbol{k}}|^2 \\ &\leq B_l \, (N2^l)^{-2(\alpha+\beta)} \, \|f | \mathcal{H}^{\alpha,\beta,\mathbf{1}}(\mathbb{T}^d)\|^2. \end{aligned}$$

For the first sum in B_l, the estimate

$$\sum_{j=1}^{l+1} A_j^N = \sum_{j=1}^{l+1} |\mathcal{I}^{d,T}_{N\,2^j} \setminus \mathcal{I}^{d,T}_{N\,2^{j-1}}| \frac{d 2^{(j+1)\kappa}}{(2^\kappa - 1)(M-1)} \leq d\, 2^{(l+1)\kappa} \frac{|\mathcal{I}^{d,T}_{N2^{l+1}}|}{M} \frac{2}{1-2^{-\kappa}}$$

holds. Due to lower bound on the rank-1 lattice size M in property (2.62), we continue $B_l \leq 2^{(l+1)\kappa+1} \frac{|\mathcal{I}^{d,T}_{N2^{l+1}}|}{|\mathcal{I}^{d,T}_N|} \left(2 + (1-2^{-\kappa}) \, C \, \psi(l+1)\right)$ and this means

$$\begin{aligned} \sigma_l &\leq (N2^l)^{-(\alpha+\beta)} \, \|f | \mathcal{H}^{\alpha,\beta,\mathbf{1}}(\mathbb{T}^d)\| \, \sqrt{B_l} \\ &\leq \sqrt{2\,(2 + (1-2^{-\kappa})\, C \, \psi(l+1))} \, 2^{\alpha+\beta} \, N^{-(\alpha+\beta)} \, \|f | \mathcal{H}^{\alpha,\beta,\mathbf{1}}(\mathbb{T}^d)\| \, 2^{(l+1)(\frac{\kappa}{2}-(\alpha+\beta))} \sqrt{\frac{|\mathcal{I}^{d,T}_{N2^{l+1}}|}{|\mathcal{I}^{d,T}_N|}}, \end{aligned}$$

which yields the assertion. ∎

Before we can use Theorem 2.34 to obtain an estimate for the sampling error, we need to show that condition (2.64) is fulfilled.

Lemma 2.35. *([KPV15b, Lemma 4.5]). Let the dimension $d \in \mathbb{N}$, $d \geq 2$, a shape parameter $T \in [-\infty, 0]$ and a number $M \in \mathbb{N}$, $M \geq 2$, be given. We set $\mathcal{I}_N^{d,T} := I^{d,T,\mathbf{1}}_{2^{\frac{d-T}{1-T}} N^{1+\frac{d}{d-T}}} \supset \mathcal{D}(I_N^{d,T,\mathbf{1}})$ and we have*

$$|\mathcal{I}_{N2^l}^{d,T} \cap M\mathbb{Z}^d| \leq C_{\mathrm{A}}(d,T)\, \frac{|\mathcal{I}_{N2^l}^{d,T}|}{M} + 1$$

for all refinements $N \in \mathbb{R}$, $N \geq 1$, and levels $l \in \mathbb{N}$, where $C_{\mathrm{A}}(d,T) \geq 1$ is a constant which only depends on d and T.

Proof. We denote $A_{N2^l}^{d,T} := \{\boldsymbol{m} \in \mathcal{I}_{N2^l}^{d,T} \colon \exists \boldsymbol{m'} \in \mathbb{Z}^d \text{ such that } \boldsymbol{m} = M\boldsymbol{m'}\}$ and we group the indices $\boldsymbol{m} \in A_{N2^l}^{d,T}$, where all components are zero, exactly one component is non-zero, …, $d-1$ components are non-zero, and all d components are non-zero. For $s = 0, \dots, d$, we denote $A_{N2^l,s}^{d,T} := \{\boldsymbol{m} \in A_{N2^l}^{d,T} \colon \text{exactly } s \text{ components of } \boldsymbol{m} \text{ are non-zero}\}$.

- Case $s = 0$. We have $A_{N2^l,0}^{d,T} = \{\mathbf{0}\}$.
- Case $1 \leq s \leq d$. If exactly the components $m_{i_1}, \dots, m_{i_s}$ of $\boldsymbol{m} \in A_{N2^l}^{d,T}$ are non-zero, $i_1, \dots, i_s \in \{1, \dots, d\}$, $i_j \neq i_{j'}$ for $j \neq j'$, we have

$$\begin{aligned}
\omega^{-\frac{T}{1-T},\frac{1}{1-T}}(\boldsymbol{m}) &= \max(1, \|M\boldsymbol{m'}\|_1)^{-\frac{T}{1-T}} \prod_{\tau=1}^{s} \max(1, M|m'_{i_\tau}|)^{\frac{1}{1-T}} \\
&= M^{-\frac{T}{1-T}} \max(1, \|\boldsymbol{m'}\|_1)^{-\frac{T}{1-T}}\, M^{\frac{s}{1-T}} \prod_{\tau=1}^{s} \max(1, |m'_{i_\tau}|)^{\frac{1}{1-T}} \\
&= M^{\frac{s-T}{1-T}} \omega^{-\frac{T}{1-T},\frac{1}{1-T}}(\boldsymbol{m'}) \leq 2^{\frac{d-T}{1-T}} N^{1+\frac{d}{d-T}}\, 2^{l(1+\frac{d}{d-T})} \\
\iff \omega^{-\frac{T}{1-T},\frac{1}{1-T}}(\boldsymbol{m'}) &\leq \frac{2^{\frac{d-T}{1-T}} N^{1+\frac{d}{d-T}}\, 2^{l(1+\frac{d}{d-T})}}{M^{\frac{s-T}{1-T}}}.
\end{aligned}$$

  Since there are $\binom{d}{s}$ choices for the non-zero components and due to the upper bounds in Lemma 2.5, we have

$$\left|A_{N2^l,s}^{d,T}\right| \leq \binom{d}{s} \cdot \begin{cases} C_1(d)\, \left(\frac{2\,N\,2^l}{M}\right)^s & \text{for } T = -\infty, \\ C_2(d,T)\, \frac{\left(2^{\frac{d-T}{1-T}} N^{1+\frac{d}{d-T}}\, 2^{l(1+\frac{d}{d-T})}\right)^{\frac{s(1-T)}{s-T}}}{M^s} & \text{for } -\infty < T < 0, \\ C_3(d)\, \left(\frac{2^d\, N^2\, 2^{2l}}{M^s}\right) \log^{s-1}\left(\frac{2^d\, N^2\, 2^{2l}}{M^s}\right) & \text{for } T = 0, \end{cases}$$

  for fixed $d \in \mathbb{N}$.

Summing up for $s \in \{0, \dots, d\}$ and using the lower bounds in Lemma 2.5, we obtain

- for $T = -\infty$

$$\begin{aligned}
|A_{N2^l}^{d,-\infty}| &\leq 1 + \sum_{s=1}^{d} \binom{d}{s} C_1(d) \left(\frac{2\,N\,2^l}{M}\right)^s \leq 1 + \frac{(2\,N\,2^l)^d}{M} C_1(d)\,(2^d - 1) \\
&\overset{L.\ 2.5}{\leq} 1 + \frac{|I^{d,-\infty}_{2\,N\,2^l}|}{M} \frac{C_1(d)}{c_1(d)}\,(2^d - 1) = (2^d - 1)\, \frac{C_1(d)}{c_1(d)}\, \frac{|\mathcal{I}_{N\,2^l}^{d,T}|}{M} + 1,
\end{aligned}$$

- for $-\infty < T < 0$

$$\begin{aligned}
\left|A^{d,T}_{N\,2^l}\right| &\leq 1 + \sum_{s=1}^{d} \binom{d}{s} C_2(d,T) \left(\frac{2^{\frac{d-T}{1-T}} N^{1+\frac{d}{d-T}}\, 2^{l(1+\frac{d}{d-T})}}{M^{\frac{s-T}{1-T}}} \right)^{\frac{s(1-T)}{s-T}} \\
&\leq 1 + C_2(d,T) \frac{\left(2^{\frac{d-T}{1-T}} N^{1+\frac{d}{d-T}}\, 2^{l(1+\frac{d}{d-T})}\right)^{\frac{d(1-T)}{d-T}}}{M} (2^d - 1) \\
&\overset{L.\ 2.5}{\leq} 1 + \frac{C_2(d,T)}{c_1(d)} \frac{\left|I^{d,T}_{2^{\frac{d-T}{1-T}} N^{1+\frac{d}{d-T}}\, 2^{l(1+\frac{d}{d-T})}}\right|}{M} (2^d - 1) \\
&= (2^d - 1)\, \frac{C_2(d,T)}{c_1(d)}\, \frac{|\mathcal{I}^{d,T}_{N\,2^l}|}{M} + 1,
\end{aligned}$$

- for $T = 0$

$$\begin{aligned}
\left|A^{d,0}_{2^d N^2\, 2^{2l}}\right| &\leq 1 + \sum_{s=1}^{d} \binom{d}{s} C_3(d) \left(\frac{2^d\, N^2\, 2^{2l}}{M^s} \right) \log^{s-1} \left(\frac{2^d\, N^2\, 2^{2l}}{M^s} \right) \\
&\leq 1 + C_3(d) \frac{2^d\, N^2\, 2^{2l}}{M} \log^{d-1} \left(2^d\, N^2\, 2^{2l}\right)\, (2^d - 1) \\
&\overset{L.\ 2.5}{\leq} 1 + \frac{\left|I^{d,0}_{2^d N^2\, 2^{2l}}\right|}{M} \frac{C_3(d)}{c_3(d)}\, (2^d - 1) = (2^d - 1)\, \frac{C_3(d)}{c_3(d)}\, \frac{|\mathcal{I}^{d,T}_{N\,2^l}|}{M} + 1.
\end{aligned}$$

We set

$$C_{\mathrm{A}}(d,T) := (2^d - 1) \cdot \begin{cases} C_1(d)/c_1(d) & \text{for } T = -\infty, \\ C_2(d,T)/c_1(d) & \text{for } -\infty < T < 0, \\ C_3(d)/c_3(d) & \text{for } T = 0, \end{cases}$$

and this yields the assertion. ∎

Collecting the previous statements, we estimate the sampling error for functions $f \in \mathcal{H}^{\alpha,\beta,\mathbf{1}}(\mathbb{T}^d) \cap \mathcal{C}(\mathbb{T}^d)$. As mentioned before, the previous results in Theorem 2.30 did not give improved statements for the case of isotropic smoothness $\alpha > 0$.

Theorem 2.36. *([KPV15a, Theorem 3.4] and [KPV15b, Theorem 4.7]).*
Let the dimension $d \in \mathbb{N}$, $d \geq 2$, a function $f \in \mathcal{H}^{\alpha,\beta,\mathbf{1}}(\mathbb{T}^d) \cap \mathcal{C}(\mathbb{T}^d)$ and a refinement $N \in \mathbb{R}$, $N \geq 2$, be given, where the dominating mixed smoothness $\beta \geq 0$ and the isotropic smoothness $\alpha \geq 0$ with

$$\alpha + \beta > \frac{d}{2} \frac{2d\beta + \alpha}{d\beta + \alpha} \frac{\beta + \alpha}{d\beta + \alpha} > 0. \tag{2.66}$$

We set the shape parameter $T := -\alpha/\beta \in [-\infty, 0]$. Additionally, let a prime number $M \in \mathbb{N}$,

$$M > \frac{d \left| I^{d,T,\mathbf{1}}_{2^{\frac{d-T}{1-T}} N^{1+\frac{d}{d-T}}} \right|}{1 - 2^{-\kappa}} + 1, \qquad \kappa := \alpha + \beta - \frac{d}{2} \frac{2d\beta + \alpha}{d\beta + \alpha} \frac{\beta + \alpha}{d\beta + \alpha},$$

be given. Then, there exists a generating vector $\boldsymbol{z} := (1, a, \ldots, a^{d-1})^\top \in \mathbb{Z}^d$ of Korobov form such that $\Lambda(\boldsymbol{z}, M, I^{d,T,\mathbf{1}}_N)$ is a reconstructing rank-1 lattice for the frequency index set $I^{d,T,\mathbf{1}}_N$,

which additionally fulfills property (2.63)*. Using this lattice, the sampling error is bounded by*

$$\|f - S^{\Lambda}_{I_N^{d,T,\mathbf{1}}} f | L_2(\mathbb{T}^d)\| \leq (1 + C(d,\alpha,\beta))\, N^{-(\alpha+\beta)}\, \|f|\mathcal{H}^{\alpha,\beta,\mathbf{1}}(\mathbb{T}^d)\|,$$

where $C(d,\alpha,\beta) > 0$ *is a constant which only depends on* d, α, β.

Proof. Due to Lemma 2.32, the claimed reconstructing rank-1 lattice $\Lambda(\boldsymbol{z}, M, I_N^{d,T,\mathbf{1}})$ exists. We use Theorem 2.20 for estimating the truncation error $f - S_{I_N^{d,T,\mathbf{1}}} f$ and we proceed with the aliasing error $S_{I_N^{d,T,\mathbf{1}}} f - S^{\Lambda}_{I_N^{d,T,\mathbf{1}}} f$. Due to Lemma 2.35, condition (2.64) is fulfilled and we can apply Theorem 2.34. This yields that there exists a reconstructing rank-1 lattice $\Lambda(\boldsymbol{z}, M, I_N^{d,T,\mathbf{1}})$ such that the aliasing error is bounded by

$$\begin{aligned}\|S_{I_N^{d,T,\mathbf{1}}} f - S^{\Lambda}_{I_N^{d,T,\mathbf{1}}} f | L_2(\mathbb{T}^d)\| \leq \sqrt{2\,(2 + (1-2^{-\kappa})\,C)}\; 2^{\alpha+\beta}\, N^{-(\alpha+\beta)}\, \|f|\mathcal{H}^{\alpha,\beta,\mathbf{1}}(\mathbb{T}^d)\| \\ \cdot \sum_{l=0}^{\infty} 2^{(l+1)(\frac{\kappa}{2}-\alpha-\beta)} \sqrt{\frac{|\mathcal{I}_{N2^{l+1}}|}{|\mathcal{I}_N|}}.\end{aligned}$$

Now, one can estimate $\sum_{l=0}^{\infty} 2^{(l+1)(\frac{\kappa}{2}-\alpha-\beta)} \sqrt{\frac{|\mathcal{I}_{N2^{l+1}}|}{|\mathcal{I}_N|}} \leq \tilde{C}(d,\alpha,\beta)$, where $\tilde{C}(d,\alpha,\beta) > 0$ is a constant which only depends on d, α, β, cf. the proof of [KPV15b, Theorem 4.7] for detailed estimates. Altogether, this yields the assertion. ■

Remark 2.37. In the case of functions from periodic Sobolev space of dominating mixed smoothness $\mathcal{H}^{0,\beta,\mathbf{1}}(\mathbb{T}^d)$, $\beta > 1$, and hyperbolic cross frequency index sets $I_N^{d,0,\mathbf{1}}$, the bound $M \gtrsim N^2 \log^{d-1} N$ in Theorem 2.36 is asymptotically larger by the logarithmic factor $(\log N)$ compared to Table 2.3. The reason for this is the choice $\mathcal{I}_N^{d,0} := I_{2^d N^2} \supset \mathcal{D}(I_N^{d,0,\mathbf{1}})$ in Lemma 2.32, which is due to the technical reason that we do not know an optimal lower bound for the difference set $\mathcal{D}(I_N^{d,0,\mathbf{1}})$ corresponding to the upper bound $|\mathcal{D}(I_N^{d,0,\mathbf{1}})| \lesssim N^2 \log^{d-2} N$. □

Additionally, one may consider the case of shape parameter $T := -\alpha/\beta \in (0,1)$. Here we obtain results where the order of approximation with respect to the refinement N is identical to Theorem 2.30. First we give an analog version of Lemma 2.35 which bounds the number of trivial aliases.

Lemma 2.38. *([KPV15b, Lemma 4.8]). Let the dimension* $d \in \mathbb{N}$, $d \geq 2$, *a shape parameter* $T \in (0,1)$, *a parameter* $\kappa > 0$, *and a number* $M \in \mathbb{N}$, $M > \frac{d\,|\mathcal{D}(I_N^{d,T})|}{1-2^{-\kappa}} + 1$ *be given. Then, we have*

$$|\mathcal{D}(I_{N2^l}^{d,T}) \cap M\mathbb{Z}^d| \leq C_{\mathrm{A}}(d,T)\, \frac{|\mathcal{D}(I_{N2^l}^{d,T})|}{M} l^{d-1} + 1$$

for all refinements $N \in \mathbb{R}$, $N \geq 1$, *and levels* $l \in \mathbb{N}$, *where* $C_{\mathrm{A}}(d,T) \geq 1$ *is a constant which only depends on* d *and* T.

Proof. We proceed analogously to the proof of Lemma 2.35. Especially, we use the properties $|\mathcal{D}(I_N^{d,T})| \geq (2N+1)^2 > N^2$ and the inclusions $I_N^{d,T} \subset I^{d,0}_{d^{\frac{T}{1-T}} N}$ due to Lemma 2.25 with $\widetilde{T} := 0$ for $N \in \mathbb{R}$, $N \geq 1$, and $0 < T < 1$. For more details, we refer to the proof of [KPV15b, Lemma 4.8]. ■

Theorem 2.39. *([KPV15a, Theorem 3.4] and [KPV15b, Theorem 4.10]). Let the dimension $d \in \mathbb{N}$, $d \geq 2$, a function $f \in \mathcal{H}^{\alpha,\beta,\mathbf{1}}(\mathbb{T}^d) \cap \mathcal{C}(\mathbb{T}^d)$ and a refinement $N \in \mathbb{R}$, $N \geq 2$, be given, where the isotropic smoothness $\alpha < 0$ and the dominating mixed smoothness $\beta > 1 - \alpha$. We set the shape parameter $T := -\alpha/\beta \in (0,1)$. Additionally, let a prime number $M \in \mathbb{N}$,*

$$M > \frac{d\left|\mathcal{D}\left(I_N^{d,T,\mathbf{1}}\right)\right|}{1 - 2^{1-\alpha-\beta}} + 1,$$

be given. Then, there exists a generating vector $\boldsymbol{z} := (1, a, \ldots, a^{d-1})^\top \in \mathbb{Z}^d$ of Korobov form such that $\Lambda(\boldsymbol{z}, M, I_N^{d,T,\mathbf{1}})$ is a reconstructing rank-1 lattice for the frequency index set $I_N^{d,T,\mathbf{1}}$, which additionally fulfills property (2.63)*. Using this lattice, the sampling error is bounded by*

$$\|f - S^{\Lambda}_{I_N^{d,T,\mathbf{1}}} f | L_2(\mathbb{T}^d)\| \leq (1 + C(d,\alpha,\beta))\, N^{-(\alpha+\beta)}\, \|f|\mathcal{H}^{\alpha,\beta,\mathbf{1}}(\mathbb{T}^d)\|,$$

where $C(d,\alpha,\beta) > 0$ is a constant which only depends on d, α, β.

Proof. The proof works analogously to the one of Theorem 2.36. Due to Lemma 2.32, the claimed reconstructing rank-1 lattice $\Lambda(\boldsymbol{z}, M, I_N^{d,T,\mathbf{1}})$ exists. We use Theorem 2.20 for estimating the truncation error $f - S_{I_N^{d,T,\mathbf{1}}} f$ and we proceed with the aliasing error $S_{I_N^{d,T,\mathbf{1}}} f - S^{\Lambda}_{I_N^{d,T,\mathbf{1}}} f$. Due to Lemma 2.38, condition (2.64) is fulfilled and we can apply Theorem 2.34. For the remaining technical details, we refer to the proof of [KPV15b, Theorem 4.10]. ∎

The upper bounds in Theorem 2.36 and 2.39 are optimal with respect to the refinement N up to constants which may depend on the dimension d and the smoothness parameters α, β, see estimate (2.45) in Theorem 2.20.

2.3.3.5 Sampling error with respect to number of samples

Until now, we have considered the sampling error with respect to the refinement N of the frequency index set $I_N^{d,T,\gamma}$. Another commonly used criterion is the number of samples M. Here again, we focus on the unweighted case with weight parameter $\boldsymbol{\gamma} := \mathbf{1}$ to simplify the notation and reduce the amount of technical details. We start with functions from the subspaces $\mathcal{A}^{\alpha,\beta,\mathbf{1}}(\mathbb{T}^d)$ of the Wiener algebra $\mathcal{A}(\mathbb{T}^d)$.

Corollary 2.40. *Let the smoothness parameters $\beta \geq 0$, $\alpha > -\beta$, the shape parameter $T := -\alpha/\beta$, the dimension $d \in \mathbb{N}$, $d \geq 2$, a function $f \in \mathcal{A}^{\alpha,\beta,\mathbf{1}}(\mathbb{T}^d) \cap \mathcal{C}(\mathbb{T}^d)$ and a frequency index set $I_N^{d,T,\mathbf{1}}$ with refinement $N \geq 1$ be given. Moreover, let $\Lambda(\boldsymbol{z}, M, I_N^{d,T,\mathbf{1}})$ be a reconstructing rank-1 lattice for $I_N^{d,T,\mathbf{1}}$ generated by [Käm14b, Table 3.1] or by Algorithm 2.2 with $M_{\text{start}} \lesssim |\mathcal{D}(I_N^{d,T,\mathbf{1}})|$. Then, the sampling error is bounded by*

$$\begin{aligned}\|f - S^{\Lambda}_{I_N^{d,T,\mathbf{1}}} f | L_\infty(\mathbb{T}^d)\| &\leq \|f - S^{\Lambda}_{I_N^{d,T,\mathbf{1}}} f | \mathcal{A}(\mathbb{T}^d)\| \\ &\lesssim \|f|\mathcal{A}^{\alpha,\beta,\mathbf{1}}(\mathbb{T}^d)\| \begin{cases} M^{-\left(\frac{\alpha}{d}+\beta\right)\left(1-\frac{\beta}{2\beta+\alpha/d}\right)} & \text{for } \alpha > \beta \geq 0, \\ M^{-\frac{\beta}{2}} (\log M)^{\frac{d-2}{2}\beta} & \text{for } \beta > \alpha = 0, \\ M^{-\frac{\alpha+\beta}{2}} & \text{for } -\beta < \alpha < 0, \end{cases}\end{aligned}$$

where the constants may depend on the dimension d and smoothness parameters α, β.

Proof. From Theorem 2.24, we obtain $\|f - S^{\Lambda}_{I_N^{d,T,\boldsymbol{\gamma}}} f|L_\infty(\mathbb{T}^d)\| \leq \|f - S^{\Lambda}_{I_N^{d,T,\boldsymbol{\gamma}}} f|\mathcal{A}(\mathbb{T}^d)\| \leq 2\, N^{-(\alpha+\beta)}\, \|f|\mathcal{A}^{\alpha,\beta,\boldsymbol{\gamma}}(\mathbb{T}^d)\|$ and we remark that the rank-1 lattice size $M \lesssim |\mathcal{D}(I_N^{d,T,\mathbf{1}})|$ due to the assumptions. For the first case, we use the inclusion (2.34) from Lemma 2.6 and obtain $M \lesssim N^{\frac{1-T}{1-T/d}\frac{2-T/d}{1-T/d}} = N^{\frac{\beta+\alpha}{\beta+\alpha/d}\frac{2\beta+\alpha/d}{\beta+\alpha/d}}$ due to (2.33), which gives the upper bound.
In the second case, we use the upper bound $M \lesssim |\mathcal{D}(I_N^{d,0,\mathbf{1}})| \lesssim N^2 \log^{d-2} N$, cf. [Käm13, Section 4] and [Käm14b, Section 3.8.2], which means $N^{-1} \lesssim M^{-1/2} \log^{(d-2)/2} N$, and this yields the upper bound due to $N \lesssim M$.
The third case follows analogously from $|\mathcal{D}(I_N^{d,T,\mathbf{1}})| \leq |I_N^{d,T,\mathbf{1}}|^2 \lesssim N^2$. ∎

We continue with functions from periodic Sobolev spaces of generalized mixed smoothness $\mathcal{H}^{\alpha,\beta,\mathbf{1}}(\mathbb{T}^d)$. First, we consider the case of frequency index sets $I_N^{d,T,\mathbf{1}}$ which are thicker than hyperbolic crosses, $T := -\alpha/\beta \in [-\infty, 0)$ and corresponding periodic Sobolev spaces of generalized mixed smoothness $\mathcal{H}^{\alpha,\beta,\mathbf{1}}(\mathbb{T}^d)$ for dominating mixed smoothness $\beta \geq 0$ and isotropic smoothness $\alpha > \max\big(d\,(\frac{1}{4} + \frac{1}{4}\sqrt{8\beta+1} - \beta), 0\big)$.

Corollary 2.41. *Let the dimension $d \in \mathbb{N}$, $d \geq 2$, the dominating mixed smoothness $\beta \geq 0$, the isotropic smoothness $\alpha > \max\big(d\,(\frac{1}{4} + \frac{1}{4}\sqrt{8\beta+1} - \beta), 0\big)$, the shape parameter $T := -\alpha/\beta \in [-\infty, 0)$, and a function $f \in \mathcal{H}^{\alpha,\beta,\mathbf{1}}(\mathbb{T}^d) \cap \mathcal{C}(\mathbb{T}^d)$ be given. For each fixed refinement $N \in \mathbb{R}$, $N \geq 2$, there exists a reconstructing rank-1 lattice $\Lambda(\boldsymbol{z}, M, I_N^{d,T,\mathbf{1}})$ with generating vector $\boldsymbol{z} := (1, a, \ldots, a^{d-1})^\top \in \mathbb{Z}^d$ of Korobov form and prime rank-1 lattice size $M \asymp N^{\frac{(2\beta+\alpha/d)(\alpha+\beta)}{(\beta+\alpha/d)^2}}$ which fulfills property* (2.63)*. Using these lattices, the sampling error is bounded from above by*

$$\|f - S^{\Lambda}_{I_N^{d,T,\mathbf{1}}} f|L_2(\mathbb{T}^d)\| \lesssim \|f|\mathcal{H}^{\alpha,\beta,\mathbf{1}}(\mathbb{T}^d)\|\, M^{-\left(\frac{\alpha}{d}+\beta\right)\left(1-\frac{\beta}{2\beta+\alpha/d}\right)},$$

where the constants may depend on the dimension d and smoothness parameters α, β.

Proof. Since $\beta \geq 0$ and $\alpha > \max\big(d\,(\frac{1}{4} + \frac{1}{4}\sqrt{8\beta+1} - \beta), 0\big)$, inequality (2.66) is fulfilled. From Theorem 2.36 and due to Bertrand's postulate, we obtain the existence of the reconstructing rank-1 lattices $\Lambda(\boldsymbol{z}, M, I_N^{d,T,\mathbf{1}})$ of size $M \asymp \left| I^{d,T,\mathbf{1}}_{2^{\frac{d-T}{1-T}} N^{1+\frac{d}{d-T}}} \right|$ fulfilling property (2.63) and that the sampling error is bounded from above by

$$\|f - S^{\Lambda}_{I_N^{d,T,\mathbf{1}}} f|L_2(\mathbb{T}^d)\| \lesssim N^{-(\alpha+\beta)}\, \|f|\mathcal{H}^{\alpha,\beta,\mathbf{1}}(\mathbb{T}^d)\|.$$

Due to the bounds on the cardinality of the frequency index set $I_N^{d,T,\mathbf{1}}$ in Table 2.3, we have $M \asymp N^{\frac{2d-T}{d-T}\frac{1-T}{1-T/d}} = N^{\frac{2d\beta+\alpha}{\alpha+d\beta}\frac{\alpha+\beta}{\beta+\alpha/d}} = N^{\frac{2\beta+\alpha/d}{\beta+\alpha/d}\frac{\alpha+\beta}{\beta+\alpha/d}}$ and this yields the assertion. ∎

Next, we deal with the case of hyperbolic cross index sets $I_N^{d,0,\mathbf{1}}$ and energy-norm based hyperbolic crosses $I_N^{d,T,\mathbf{1}}$, $T := -\alpha/\beta \in (0, 1)$. First, we give a lower bound of the error for rank-1 lattice sampling.

Theorem 2.42. *Let the dimension $d \in \mathbb{N}$, $d \geq 2$, the dominating mixed smoothness $\beta > \frac{1}{2}$ and $t \geq 0$ as well as the isotropic smoothness $\alpha \leq 0$ with $\alpha + \beta > \max\{t, \frac{1}{2}\}$ be given. Moreover, let $I \subset \mathbb{Z}^d$ be an arbitrary frequency index set of finite cardinality, $|I| < \infty$, and $\Lambda(\boldsymbol{z}, M) \subset \mathbb{T}^d$ be an arbitrary rank-1 lattice. Then, the operator norm of* $\mathrm{Id} - S_I^{\Lambda}$ *is bounded by*

$$\|\,\mathrm{Id} - S_I^{\Lambda}|\mathcal{H}^{\alpha,\beta,\mathbf{1}}(\mathbb{T}^d) \to \mathcal{H}^{0,t,\mathbf{1}}(\mathbb{T}^d)\| \geq 2^{-\left(\alpha+\beta-t+\frac{1}{2}\right)}\, M^{-\frac{\alpha+\beta-t}{2}},$$

where Id *denotes the embedding operator from $\mathcal{H}^{\alpha,\beta,\mathbf{1}}(\mathbb{T}^d)$ into $\mathcal{H}^{0,t,\mathbf{1}}(\mathbb{T}^d)$.*

Proof. We follow the proof of [BKUV16, Theorem 1] step-by-step. First define the two-dimensional axis cross $X^d_{\sqrt{M}} := \{\boldsymbol{h} \in \mathbb{Z}^2 \times \{0\}^{d-2} \colon \|\boldsymbol{h}\|_1 = \|\boldsymbol{h}\|_\infty \leq \sqrt{M}\}$ and fix an arbitrary rank-1 lattice $\Lambda(\boldsymbol{z}, M)$. Due to [BKUV16, Lemma 4], there exist two distinct frequencies $\boldsymbol{k'}, \boldsymbol{k''} \in X^d_{\sqrt{M}}$ which alias with respect to the rank-1 $\Lambda(\boldsymbol{z}, M)$, i.e. $\boldsymbol{k'} \cdot \boldsymbol{z} \equiv \boldsymbol{k''} \cdot \boldsymbol{z} \pmod{M}$. Using these indices, we construct the normalized fooling function

$$g(\boldsymbol{x}) := \frac{\mathrm{e}^{2\pi \mathrm{i} \boldsymbol{k'} \cdot \boldsymbol{x}} - \mathrm{e}^{2\pi \mathrm{i} \boldsymbol{k''} \cdot \boldsymbol{x}}}{\sqrt{\omega^{\alpha,\beta,\mathbf{1}}(\boldsymbol{k'})^2 + \omega^{\alpha,\beta,\mathbf{1}}(\boldsymbol{k''})^2}}, \qquad \|g|\mathcal{H}^{\alpha,\beta,\mathbf{1}}(\mathbb{T}^d)\| = 1,$$

which is zero at all rank-1 lattice nodes $\boldsymbol{x}_j := \frac{j}{M}\boldsymbol{z} \bmod 1$, i.e., we have $g(\boldsymbol{x}_j) = 0$ for all $j = 0, \ldots, M-1$. Consequently, $S^\Lambda_I g = 0$ and this means $\|g - S^\Lambda_I g|\mathcal{H}^{0,t,\mathbf{1}}(\mathbb{T}^d)\| = \|g|\mathcal{H}^{0,t,\mathbf{1}}(\mathbb{T}^d)\|$. W.l.o.g. we assume $\|\boldsymbol{k'}\|_1 \geq \|\boldsymbol{k''}\|_1$ and we infer

$$\omega^{\alpha,\beta,\mathbf{1}}(\boldsymbol{k'}) = \max(1, \|\boldsymbol{k'}\|_1)^\alpha \prod_{s=1}^d \max(1, |k'_s|)^\beta \geq \omega^{\alpha,\beta,\mathbf{1}}(\boldsymbol{k''}),$$

which yields

$$\|g|\mathcal{H}^{0,t,\mathbf{1}}(\mathbb{T}^d)\| = \frac{\sqrt{\omega^{0,t,\mathbf{1}}(\boldsymbol{k'})^2 + \omega^{0,t,\mathbf{1}}(\boldsymbol{k''})^2}}{\sqrt{\omega^{\alpha,\beta,\mathbf{1}}(\boldsymbol{k'})^2 + \omega^{\alpha,\beta,\mathbf{1}}(\boldsymbol{k''})^2}} \geq \frac{\sqrt{\omega^{0,t,\mathbf{1}}(\boldsymbol{k'})^2}}{\sqrt{2}\,\omega^{\alpha,\beta,\mathbf{1}}(\boldsymbol{k'})^2} = \frac{1}{\sqrt{2}\,\omega^{\alpha,\beta-t,\mathbf{1}}(\boldsymbol{k'})}.$$

For $\boldsymbol{k} \in X^d_{\sqrt{M}}$, we have $\|\boldsymbol{k}\|_\infty = \|\boldsymbol{k}\|_1 = |k_{s'}|$ and consequently

$$\omega^{\alpha,\beta-t,\mathbf{1}}(\boldsymbol{k'}) = \max(1, |k_{s'}|)^{\alpha+\beta-t} \leq \max(1, \sqrt{M})^{\alpha+\beta-t} \leq (2\sqrt{M})^{\alpha+\beta-t},$$

which yields the assertion. ∎

Remark 2.43. As discussed in [BKUV16, Remark 1], the lower bound for rank-1 lattice sampling in Theorem 2.42 is also valid for methods that use samples along so-called integration lattices, see e.g. [SJ94, Section 2.7] for definition. The corresponding proof works analogously by finding two distinct aliasing frequencies $\boldsymbol{k'}, \boldsymbol{k''}$ on the axis cross $X^d_{\sqrt{M}}$ and constructing a fooling function g. □

Now, we complement the obtained lower bounds for rank-1 lattice sampling by tight upper bounds, which are sharp up to logarithmic factors. The upper bounds are obtained for sampling along reconstructing rank-1 lattices $\Lambda(\boldsymbol{z}, M, I)$, which were generated by a constructive method.

Corollary 2.44. *Let the smoothness parameters $\beta > \frac{1}{2}$, $\alpha \leq 0$, $t \geq 0$ with $\alpha + \beta > \max\{t, \frac{1}{2}\}$, the dimension $d \in \mathbb{N}$, $d \geq 2$, a function $f \in \mathcal{H}^{\alpha,\beta,\mathbf{1}}(\mathbb{T}^d) \cap \mathcal{C}(\mathbb{T}^d)$ and a hyperbolic cross index set $I_N^{d,T,\mathbf{1}}$ with refinement $N \geq 2^{d+1}$ be given. Moreover, let $\Lambda(\boldsymbol{z}, M, I_N^{d,0,\mathbf{1}})$ be a reconstructing rank-1 lattice for $I_N^{d,0,\mathbf{1}}$ generated by [Käm14b, Table 3.1] or by Algorithm 2.2 with $M_{\text{start}} \lesssim |\mathcal{D}(I_N^{d,0,\mathbf{1}})|$. Then, the sampling error is bounded by*

$$\|f - S^\Lambda_{I_N^{d,0,\mathbf{1}}} f|\mathcal{H}^{0,t,\mathbf{1}}(\mathbb{T}^d)\| \lesssim \|f|\mathcal{H}^{\alpha,\beta,\mathbf{1}}(\mathbb{T}^d)\| \, \frac{(\log M)^{\frac{d-2}{2}(\alpha+\beta-t)}}{M^{\frac{\alpha+\beta-t}{2}}} \begin{cases} (\log M)^{(d-1)/2} & \text{for } \alpha = 0, \\ 1 & \text{for } \alpha < 0, \end{cases}$$

where the constants may depend on the dimension d and smoothness parameters α, β, t. Moreover, the operator norm of $\mathrm{Id} - S^\Lambda_{I_N^{d,0,\mathbf{1}}}$ is bounded from below by

$$\|\mathrm{Id} - S^\Lambda_{I_N^{d,0,\mathbf{1}}}|\mathcal{H}^{\alpha,\beta,\mathbf{1}}(\mathbb{T}^d) \to \mathcal{H}^{0,t,\mathbf{1}}(\mathbb{T}^d)\| \gtrsim M^{-\frac{\alpha+\beta-t}{2}}$$

for any rank-1 lattice $\Lambda(\boldsymbol{z}, M)$*, where* Id *denotes the embedding operator from* $\mathcal{H}^{\alpha,\beta,\mathbf{1}}(\mathbb{T}^d)$ *into* $\mathcal{H}^{0,t,\mathbf{1}}(\mathbb{T}^d)$ *and the constants may depend on* d, α, β, t*.*

Proof. From Theorem 2.30, we obtain

$$\|f - S^{\Lambda}_{I_N^{d,0,\mathbf{1}}} f | \mathcal{H}^{0,t,\mathbf{1}}(\mathbb{T}^d)\| \lesssim \|f|\mathcal{H}^{\alpha,\beta,\mathbf{1}}(\mathbb{T}^d)\| \, N^{-(\alpha+\beta-t)} \begin{cases} (\log N)^{(d-1)/2} & \text{for } \alpha = 0, \\ 1 & \text{for } \alpha < 0. \end{cases}$$

Since the rank-1 lattice size $M \lesssim |\mathcal{D}(I_N^{d,0,\mathbf{1}})| \lesssim N^2 \log^{d-2} N$, cf. [Käm13, Section 4] and [Käm14b, Section 3.8.2], we have $N^{-1} \lesssim M^{-1/2} \log^{(d-2)/2} N$ and this yields the upper bound due to $N \lesssim M$.
The lower bound follows directly from the general results of Theorem 2.42. ∎

In the next corollary, we reduce the logarithmic factors in the upper bound for certain cases using the special rank-1 lattices from Theorem 2.36 and 2.39.

Corollary 2.45. *Let the dimension* $d \in \mathbb{N}$*,* $d \geq 2$*, smoothness parameters* $\alpha \leq 0$ *and* $\beta > 1 - \alpha$*, the shape parameter* $T := -\alpha/\beta \in [0, 1)$*, and a function* $f \in \mathcal{H}^{\alpha,\beta,\mathbf{1}}(\mathbb{T}^d) \cap \mathcal{C}(\mathbb{T}^d)$ *be given. For each fixed refinement* $N \in \mathbb{R}$*,* $N \geq 2$*, there exists a reconstructing rank-1 lattice* $\Lambda(\boldsymbol{z}, M, I_N^{d,T,\mathbf{1}})$ *with generating vector* $\boldsymbol{z} := (1, a, \ldots, a^{d-1})^\top \in \mathbb{Z}^d$ *of Korobov form and prime rank-1 lattice size* $M \asymp N^2 \log^{d-1} N$ *for* $\alpha = 0$ *and* $M \asymp N^2$ *for* $\alpha < 0$ *which fulfills property* (2.63)*. Using these lattices, the sampling error is bounded by*

$$\|f - S^{\Lambda}_{I_N^{d,T,\mathbf{1}}} f | L_2(\mathbb{T}^d)\| \lesssim \|f|\mathcal{H}^{\alpha,\beta,\mathbf{1}}(\mathbb{T}^d)\| \, M^{-\frac{\alpha+\beta}{2}} \begin{cases} (\log M)^{(d-1)\frac{\alpha+\beta}{2}} & \text{for } \alpha = 0, \\ 1 & \text{for } \alpha < 0, \end{cases}$$

where the constants may depend on the dimension d *and smoothness parameters* α, β*. Moreover, the operator norm of* $\mathrm{Id} - S^{\Lambda}_{I_N^{d,T,\mathbf{1}}}$ *is bounded from below by*

$$\|\mathrm{Id} - S^{\Lambda}_{I_N^{d,T,\mathbf{1}}} | \mathcal{H}^{\alpha,\beta,\mathbf{1}}(\mathbb{T}^d) \to L_2(\mathbb{T}^d)\| \gtrsim M^{-\frac{\alpha+\beta}{2}}$$

for any rank-1 lattice $\Lambda(\boldsymbol{z}, M)$*, where* Id *denotes the embedding operator from* $\mathcal{H}^{\alpha,\beta,\mathbf{1}}(\mathbb{T}^d)$ *into* $L_2(\mathbb{T}^d)$ *and the constants may depend on* d, α, β*.*

Proof. For $\alpha = T = 0$, we obtain from Theorem 2.36 that there exists a reconstructing rank-1 lattice $\Lambda(\boldsymbol{z}, M, I_N^{d,0,\mathbf{1}})$ of size $M \asymp |I_{2^d N^2}^{d,0,\mathbf{1}}| \asymp N^2 \log^{d-1} N$ such that the sampling error is bounded by $\|f - S^{\Lambda}_{I_N^{d,T,\mathbf{1}}} f | L_2(\mathbb{T}^d)\| \lesssim N^{-(\alpha+\beta)} \, \|f|\mathcal{H}^{\alpha,\beta,\mathbf{1}}(\mathbb{T}^d)\| \lesssim M^{-\frac{\alpha+\beta}{2}} (\log N)^{(d-1)\frac{\alpha+\beta}{2}}$ and this yields the upper bound since $N \leq M$.
For $\alpha < 0$, we apply Theorem 2.39 and obtain that there exists a reconstructing rank-1 lattice $\Lambda(\boldsymbol{z}, M, I_N^{d,T,\mathbf{1}})$ of the claimed size which yields the upper bound.
The lower bound follows directly from the general results of Theorem 2.42. ∎

Compared to the upper bound from Corollary 2.44, we were able to decrease the logarithmic factor in the upper bound in the dominating mixed smoothness case $\alpha = 0$ when $\beta < d - 1$. Otherwise, the upper bound in Corollary 2.44 is asymptotically smaller. For $\alpha < 0$, the upper bounds in Corollary 2.45 correspond (asymptotically) to the upper bounds from Corollary 2.44. However, the results are based on Lemma 2.32 and are therefore based on a non-constructive proof.

2.3.4 Perturbed rank-1 lattice sampling

In Section 2.2.2, we have dealt with the fast and stable approximate reconstruction of multivariate trigonometric polynomials p_I by sampling at perturbed nodes $\boldsymbol{y}_j$, $j = 0, \ldots, M-1$, of a reconstructing rank-1 lattice $\Lambda(\boldsymbol{z}, M, I_N^{d,T,\gamma})$. Based on these results and the results from Section 2.3.3, we consider the approximation of functions $f \in \mathcal{A}^{\alpha,\beta,\gamma}(\mathbb{T}^d) \cap \mathcal{C}(\mathbb{T}^d)$ by sampling at perturbed rank-1 lattice nodes $\boldsymbol{y}_j$, $j = 0, \ldots, M-1$, see also [KPV15a]. We compute the approximated Fourier coefficients

$$\tilde{\hat{\boldsymbol{f}}} := \operatorname*{arg\,min}_{\hat{\boldsymbol{g}} \in \mathbb{C}^{|I_N^{d,T,\gamma}|}} \|\boldsymbol{A}_{m-1}\, \hat{\boldsymbol{g}} - \boldsymbol{f}\|_2 \tag{2.67}$$

by solving the normal equation $\boldsymbol{A}_{m-1}^{\mathrm{H}} \boldsymbol{A}_{m-1} \tilde{\hat{\boldsymbol{f}}} = \boldsymbol{A}_{m-1}^{\mathrm{H}} \boldsymbol{f}$, where $\tilde{\hat{\boldsymbol{f}}} := \left(\tilde{\hat{f}}_{\boldsymbol{k}}\right)_{\boldsymbol{k} \in I_N^{d,T,\gamma}}$ and $\boldsymbol{f} := f(\boldsymbol{y}_j)_{j=0}^{M-1}$. Using the LSQR algorithm [PS82] in combination with (2.18) and its adjoint version, we obtain an approximation $\tilde{\hat{\boldsymbol{h}}}$ of the approximated Fourier coefficients $\tilde{\hat{\boldsymbol{f}}}$ in $\mathcal{O}\left(K\, m^d (M \log M + d\,|I|)\right)$ arithmetic operations, where K is the maximal number of iterations of the LSQR algorithm. Choosing $K = \left\lceil \frac{\log(2\,\kappa(\boldsymbol{A}_{m-1})) - \log \delta}{\log(\kappa(\boldsymbol{A}_{m-1})+1) - \log(\kappa(\boldsymbol{A}_{m-1})-1)} \right\rceil$ guarantees a relative error $\|\tilde{\hat{\boldsymbol{f}}} - \tilde{\hat{\boldsymbol{h}}}\|_2 / \|\tilde{\hat{\boldsymbol{f}}}\|_2 \leq \delta$, cf. [Bjö96, Sec. 7.4.4], where $\kappa(\boldsymbol{A}_{m-1})$ denotes the condition number of the approximated Fourier matrix $\boldsymbol{A}_{m-1}$. If this condition number is unknown, we may use an upper bound of $\kappa(\boldsymbol{A}_{m-1})$, for instance the upper bound from Theorem 2.9. We stress the fact that the LSQR algorithm [PS82] in combination with (2.18) and its adjoint version indicates a fast reconstruction algorithm for moderate dimensionality d and moderate Taylor expansion parameter m.

The following theorem states that we obtain the same error bound as in Theorem 2.26 up to the additional constant $C(d,T,m)$ and the additional stability term $1/\left(2 - \exp\left(2\pi\left(d^{1+\max\left(0,\frac{T}{1-T}\right)}\right)N\varepsilon\right)\right)$ in the aliasing error.

Theorem 2.46. *([KPV15a, Theorem 5.1]). Let smoothness parameter $r, t, \alpha, \beta \geq 0$, $\beta \geq t \geq 0$, $\alpha + \beta > r + t$, be given and the shape parameter $T := -\frac{\alpha - r}{\beta - t} \in [-\frac{r}{t}, -\frac{\alpha}{\beta}]$ with $T := -\infty$ for $\beta = t$, $-\frac{r}{t} := -\infty$ for $t = 0$ and $-\frac{\alpha}{\beta} := -\infty$ for $\beta = 0$. Furthermore, let a Taylor expansion degree $m \in \mathbb{N}$ with $0 < \alpha + \beta \leq m$, a weighted frequency index set $I_N^{d,T,\gamma}$ and a reconstructing rank-1 lattice $\Lambda(\boldsymbol{z}, M, I_N^{d,T,\gamma})$ be given, where the refinement $N \geq 1$ and the weight parameter $\boldsymbol{\gamma} \in (0,1]^d$. Furthermore, let a set of sampling nodes $\mathcal{Y} = \{\boldsymbol{y}_j\}_{j=0}^{M-1}$ be given, where $\|\boldsymbol{y}_j - \boldsymbol{x}_j\|_\infty \leq \varepsilon$, $j = 0, \ldots, M-1$, for fixed perturbation parameter ε, $0 \leq \varepsilon < \left(2\pi\left(d^{1+\max\left(0,\frac{T}{1-T}\right)}\right)N\right)^{-1} \ln 2$. Then, the error of the approximation $S^{\mathcal{Y}}_{I_N^{d,T,\gamma}} f(\boldsymbol{x}) = \sum_{\boldsymbol{k} \in I_N^{d,T,\gamma}} \tilde{\hat{f}}_{\boldsymbol{k}}\, \mathrm{e}^{2\pi \mathrm{i} \boldsymbol{k} \cdot \boldsymbol{x}}$ of a function $f \in \mathcal{A}^{\alpha,\beta,\gamma}(\mathbb{T}^d) \cap \mathcal{C}(\mathbb{T}^d)$ with $\left(\tilde{\hat{f}}_{\boldsymbol{k}}\right)_{\boldsymbol{k} \in I_N^{d,T,\gamma}}$ from (2.67) is bounded by*

$$\begin{aligned}
&\|f - S^{\mathcal{Y}}_{I_N^{d,T,\gamma}} f | \mathcal{H}^{r,t,\gamma}(\mathbb{T}^d)\| \\
&\quad \leq N^{-(\alpha - r + \beta - t)} \left(\|f | \mathcal{H}^{\alpha,\beta,\gamma}(\mathbb{T}^d)\| + \frac{C(d,T,m)}{2 - \mathrm{e}^{2\pi\left(d^{1+\max\left(0,\frac{T}{1-T}\right)}\right)N\varepsilon}}\, \|f | \mathcal{A}^{\alpha,\beta,\gamma}(\mathbb{T}^d)\| \right), \qquad (2.68) \\
&\quad \leq \left(1 + \frac{C(d,T,m)}{2 - \mathrm{e}^{2\pi\left(d^{1+\max\left(0,\frac{T}{1-T}\right)}\right)N\varepsilon}}\right) N^{-(\alpha - r + \beta - t)}\, \|f | \mathcal{A}^{\alpha,\beta,\gamma}(\mathbb{T}^d)\|,
\end{aligned}$$

where $C(d,T,M) := 1 + \frac{\left(d^{\frac{T}{1-T}} \ln 2\right)^m}{m!}$.

Proof. We apply the triangle inequality (2.10) on $\|f - S^{\mathcal{Y}}_{I_N^{d,T,\boldsymbol{\gamma}}} f | \mathcal{H}^{r,t,\boldsymbol{\gamma}}(\mathbb{T}^d)\|$ and estimate the truncation error $\|f - S_{I_N^{d,T,\boldsymbol{\gamma}}} f | \mathcal{H}^{r,t,\boldsymbol{\gamma}}(\mathbb{T}^d)\|$ as in the proof of Theorem 2.26.
Next, we estimate the aliasing error $\|S_{I_N^{d,T,\boldsymbol{\gamma}}} f - S^{\mathcal{Y}}_{I_N^{d,T,\boldsymbol{\gamma}}} f | \mathcal{H}^{r,t,\boldsymbol{\gamma}}(\mathbb{T}^d)\|$. Based on the normal equation $\boldsymbol{A}_{m-1}^{\mathrm{H}} \boldsymbol{A}_{m-1} \tilde{\hat{\boldsymbol{f}}} = \boldsymbol{A}_{m-1}^{\mathrm{H}} \boldsymbol{f}$, we calculate

$$\boldsymbol{D}\left(\tilde{\hat{f}}_{\boldsymbol{k}} - \hat{f}_{\boldsymbol{k}}\right)_{\boldsymbol{k} \in I_N^{d,T,\boldsymbol{\gamma}}} = \boldsymbol{D}\left(\boldsymbol{A}_{m-1}^{\mathrm{H}} \boldsymbol{A}_{m-1}\right)^{-1} \boldsymbol{A}_{m-1}^{\mathrm{H}} \left(\boldsymbol{f} - \boldsymbol{A}_{m-1}\left(\hat{f}_{\boldsymbol{k}}\right)_{\boldsymbol{k} \in I_N^{d,T,\boldsymbol{\gamma}}}\right)$$

where $\boldsymbol{D} := \operatorname{diag}\left(\omega^{r,t,\boldsymbol{\gamma}}(\boldsymbol{k})\right)_{\boldsymbol{k} \in I_N^{d,T,\boldsymbol{\gamma}}}$, Consequently, we obtain

$$\begin{aligned} & \left\| S_{I_N^{d,T,\boldsymbol{\gamma}}} f - S^{\mathcal{Y}}_{I_N^{d,T,\boldsymbol{\gamma}}} f | \mathcal{H}^{r,t,\boldsymbol{\gamma}}(\mathbb{T}^d) \right\| = \left\| \boldsymbol{D}\left(\tilde{\hat{f}}_{\boldsymbol{k}} - \hat{f}_{\boldsymbol{k}}\right)_{\boldsymbol{k} \in I_N^{d,T,\boldsymbol{\gamma}}} \right\|_2 \\ \leq \; & \|\boldsymbol{D}\|_2 \left\| (\boldsymbol{A}_{m-1}^{\mathrm{H}} \boldsymbol{A}_{m-1})^{-1} \boldsymbol{A}_{m-1}^{\mathrm{H}} \right\|_2 \left\| \boldsymbol{f} - \boldsymbol{A}_{m-1}\left(\hat{f}_{\boldsymbol{k}}\right)_{\boldsymbol{k} \in I_N^{d,T,\boldsymbol{\gamma}}} \right\|_2 \end{aligned}$$

and we proceed as in the proof of Theorem 2.10 for $\left\|(\boldsymbol{A}_{m-1}^{\mathrm{H}} \boldsymbol{A}_{m-1})^{-1} \boldsymbol{A}_{m-1}^{\mathrm{H}}\right\|_2$. We infer

$$\begin{aligned} & \left\| \boldsymbol{f} - \boldsymbol{A}_{m-1}\left(\hat{f}_{\boldsymbol{k}}\right)_{\boldsymbol{k} \in I_N^{d,T,\boldsymbol{\gamma}}} \right\|_2 \leq \sqrt{M} \left\| \boldsymbol{f} - \boldsymbol{A}_{m-1}\left(\hat{f}_{\boldsymbol{k}}\right)_{\boldsymbol{k} \in I_N^{d,T,\boldsymbol{\gamma}}} \right\|_\infty \\ \leq \; & \sqrt{M} \left(\left\| \boldsymbol{f} - \boldsymbol{A}\left(\hat{f}_{\boldsymbol{k}}\right)_{\boldsymbol{k} \in I_N^{d,T,\boldsymbol{\gamma}}} \right\|_\infty + \left\| (\boldsymbol{A} - \boldsymbol{A}_{m-1})\left(\hat{f}_{\boldsymbol{k}}\right)_{\boldsymbol{k} \in I_N^{d,T,\boldsymbol{\gamma}}} \right\|_\infty \right) \\ = \; & \sqrt{M} \left(\left\| \left(\sum\nolimits_{\boldsymbol{k} \in \mathbb{Z}^d \setminus I_N^{d,T,\boldsymbol{\gamma}}} \hat{f}_{\boldsymbol{k}}\, \mathrm{e}^{2\pi \mathrm{i} \boldsymbol{k} \boldsymbol{y}_j} \right)_{j=0}^{M-1} \right\|_\infty + \left\| \left(R_m(\boldsymbol{y}_j)\right)_{j=0}^{M-1} \right\|_\infty \right), \end{aligned} \tag{2.69}$$

where $R_m(\boldsymbol{y}_j) = \sum_{\boldsymbol{k} \in I_N^{d,T,\boldsymbol{\gamma}}} \hat{f}_{\boldsymbol{k}}\, \mathrm{e}^{2\pi \mathrm{i} \boldsymbol{k} \cdot \boldsymbol{y}_j} - \sum_{|\boldsymbol{\nu}|=0}^{m-1} D^{\boldsymbol{\nu}} \Big(\sum_{\boldsymbol{k} \in I_N^{d,T,\boldsymbol{\gamma}}} \hat{f}_{\boldsymbol{k}}\, \mathrm{e}^{2\pi \mathrm{i} \boldsymbol{k} \cdot \boldsymbol{x}_j} \Big) \frac{(\boldsymbol{y}_j - \boldsymbol{x}_{j'})^{\boldsymbol{\nu}}}{\boldsymbol{\nu}!}$. Now, we apply inequality (2.44) from the proof of Theorem 2.24 on the first summand and Theorem 2.3 on the second summand in (2.69). Last, we obtain $\|\boldsymbol{D}\|_2 = \max_{\boldsymbol{k} \in I_N^{d,T,\boldsymbol{\gamma}}} \left\{\omega^{r,t,\boldsymbol{\gamma}}(\boldsymbol{k})\right\} \leq d^{(r+Tt)/(1-T)} N^{r+t}$ due to (2.59) in the proof of Theorem 2.26. Altogether, this yields the assertion. ∎

As in Theorem 2.26, we may use the inequality (2.41) in order to obtain the statement of Theorem 2.46 with the $\mathcal{H}^{\alpha,\beta+\lambda,\boldsymbol{\gamma}}(\mathbb{T}^d)$ norm on the right hand side for functions $f \in \mathcal{H}^{\alpha,\beta+\lambda,\boldsymbol{\gamma}}(\mathbb{T}^d) \cap \mathcal{C}(\mathbb{T}^d)$, $\lambda > 1/2$.

2.3.5 Numerical examples

All numerical tests of this section were performed in IEEE 754 double precision arithmetic using MATLAB R2015b on a computer with Intel Xeon E7-4880 2.50 GHz CPU. Parts of the results have already been published in [KPV15a] and [KPV15b].

We consider the test functions $G_{3,4}^d \colon \mathbb{T}^d \to \mathbb{C}$ from [KPV15a] and [KPV15b], $G_{3,4}^d(\boldsymbol{x}) := \prod_{s=1}^d g_{3,4}(x_s)$, where the one-dimensional function $g_{3,4} \colon \mathbb{T} \to \mathbb{C}$ is defined by

$$g_{3,4}(x) := 8\sqrt{\frac{6\pi}{6369\pi - 4096}} \left(4 + \operatorname{sgn}((x \bmod 1) - 1/2) \left[\sin(2\pi x)^3 + \sin(2\pi x)^4\right]\right)$$

and sgn denotes the signum function, $\operatorname{sgn}(x) := x/|x|$ for $x \neq 0$ and $\operatorname{sgn}(0) := 0$. The Fourier coefficients of $g_{3,4}$ are given by

$$(\widehat{g_{3,4}})_k = 8\sqrt{\frac{6\pi}{6369\pi - 4096}} \begin{cases} \frac{-12}{(k-3)(k-1)(k+1)(k+3)\pi} & \text{for } k \in 2\mathbb{Z} \setminus \{0\}, \\ \frac{48\mathrm{i}}{(k-4)(k-2)k(k+2)(k+4)\pi} & \text{for } k \text{ odd}, \\ 4 - \frac{4}{3\pi} & \text{for } k = 0, \end{cases}$$

and consequently, we have $G_{3,4}^d \in \mathcal{A}^{0,3-\epsilon,\mathbf{1}}(\mathbb{T}^d)$, $G_{3,4}^d \in \mathcal{H}^{0,\frac{7}{2}-\epsilon,\mathbf{1}}(\mathbb{T}^d)$, $\epsilon > 0$. Moreover, we remark that $\|G_{3,4}^d|L^2(\mathbb{T}^d)\| = 1$ and $\|G_{3,4}^d|\mathcal{A}(\mathbb{T}^d)\| = \left(8\sqrt{\frac{6\pi}{6369\pi-4096}}\left(4 + \frac{388}{105\pi}\right)\right)^d \approx (1.42522)^d$. As frequency index sets I, we use hyperbolic crosses $I_N^{d,0,\mathbf{1}}$ with various refinements $N \in \mathbb{N}$ in this section. For further considerations with different shape parameters T and weight parameters $\boldsymbol{\gamma}$, we refer to the detailed considerations in [KPV15a, Section 6] and [KPV15b, Section 5].

First, we investigate the truncation error $G_{3,4}^d - S_{I_N^{d,0,\mathbf{1}}} G_{3,4}^d$ with respect to the refinement N, which is an upper bound for the sampling error of our reconstruction method.

Example 2.47. For $d \in \{2,3,4,5,6\}$ and $N \in \{2^0, 2^1, 2^2, \ldots, 2^8\}$, the relative truncation error

$$\|G_{3,4}^d - S_{I_N^{d,0,\mathbf{1}}} G_{3,4}^d|\mathcal{A}(\mathbb{T}^d)\| / \|G_{3,4}^d|\mathcal{A}(\mathbb{T}^d)\|$$

is depicted in Figure 2.8a. From Theorem 2.17 with $\beta = 3 - \epsilon$ and $\alpha = 0$, we obtain the upper bound

$$\begin{aligned} \|G_{3,4}^d - S_{I_N^{d,0,\mathbf{1}}} G_{3,4}^d|L_\infty(\mathbb{T}^d)\| / \|f|\mathcal{A}(\mathbb{T}^d)\| &\leq \|G_{3,4}^d - S_{I_N^{d,0,\mathbf{1}}} G_{3,4}^d|\mathcal{A}(\mathbb{T}^d)\| / \|f|\mathcal{A}(\mathbb{T}^d)\| \\ &\leq N^{-3+\epsilon} \, \|G_{3,4}^d|\mathcal{A}^{0,3-\epsilon,\mathbf{1}}(\mathbb{T}^d)\| / \|G_{3,4}^d|\mathcal{A}(\mathbb{T}^d)\| \end{aligned}$$

and the observed decay rate corresponds roughly to the estimates. In this upper bound, the factor $\|G_{3,4}^d|\mathcal{A}^{0,3-\epsilon,\mathbf{1}}(\mathbb{T}^d)\| / \|G_{3,4}^d|\mathcal{A}(\mathbb{T}^d)\|$ may be large, for instance $> 13^d$ for $\epsilon = 0.05$. Additionally, the relative truncation error measured in the $L_2(\mathbb{T}^d)$ norm is shown in Figure 2.8b. From Theorem 2.20 with $\beta = 7/2 - \epsilon$ and $r = t = \alpha = 0$, the upper bound

$$\|G_{3,4}^d - S_{I_N^{d,0,\mathbf{1}}} f|L_2(\mathbb{T}^d)\| / \|G_{3,4}^d|L_2(\mathbb{T}^d)\| \leq N^{-7/2+\epsilon} \, \|G_{3,4}^d|\mathcal{H}^{0,7/2-\epsilon,\mathbf{1}}(\mathbb{T}^d)\| / \|G_{3,4}^d|L_2(\mathbb{T}^d)\|.$$

We observe that the rates of the measured errors approximately decay as the theoretical upper bounds suggest. Especially for higher dimensions d, the observed decay rate is slightly smaller, which most likely is caused by the relatively small values of the refinement N and the large constants (increasing with d). For instance, the factor $\|G_{3,4}^d|\mathcal{H}^{0,7/2-\epsilon,\mathbf{1}}(\mathbb{T}^d)\| / \|G_{3,4}^d|L_2(\mathbb{T}^d)\|$ is greater than 4.7^d for $\epsilon = 0.05$. □

Next, we consider rank-1 lattice sampling. In doing so, we use the reconstructing rank-1 lattices $\Lambda(\boldsymbol{z}, M, I_N^{d,0,\mathbf{1}})$ for hyperbolic cross frequency index sets $I_N^{d,0,\mathbf{1}}$ from Table 2.5, which were constructed by the implementation [Vol16b, `genlattice_cbc_incr_bisect`] of Algorithm 2.3 and parts of this table can be found as [KPV15a, Table 6.2b]. Moreover, we depict the oversampling factors $M/|I_N^{d,0,\mathbf{1}}|$ in Figure 2.12a. The observed oversampling factors are still moderate for the considered refinements N and approximately grow as the asymptotic upper bound $\mathcal{O}(N/\log N)$ on the existence of a reconstructing rank-1 lattice suggests, which can be derived from Table 2.3.

Now, we approximately reconstruct the Fourier coefficients $(\widehat{G_{3,4}^d})_{\boldsymbol{k}}$, $\boldsymbol{k} \in I_N^{d,0,\mathbf{1}}$, of the test functions $G_{3,4}^d$ using rank-1 lattice sampling, cf. Algorithm 2.4.

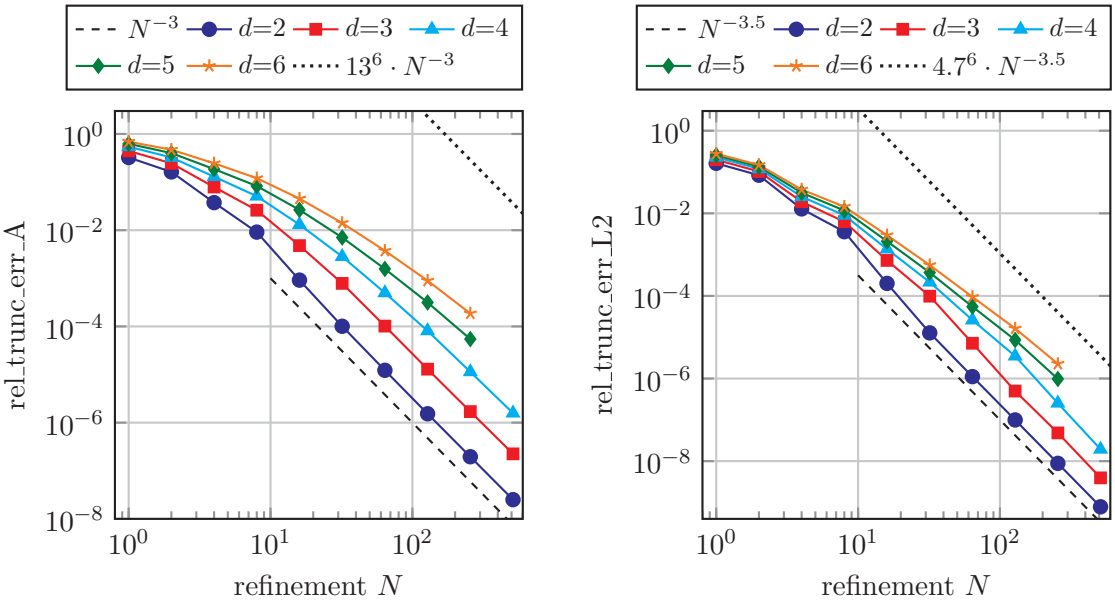

(a) relative $\mathcal{A}(\mathbb{T}^d)$ truncation errors

(b) relative $L_2(\mathbb{T}^d)$ truncation errors, see Figure 5.2 from [KPV15b]

Figure 2.8: Relative $\mathcal{A}(\mathbb{T}^d)$ truncation errors rel_trunc_err_A $:= \|G^d_{3,4} - S_I G^d_{3,4}|\mathcal{A}(\mathbb{T}^d)\| / \|G^d_{3,4}|\mathcal{A}(\mathbb{T}^d)\|$ and $L_2(\mathbb{T}^d)$ truncation errors rel_trunc_err_L2 $:= \|G^d_{3,4} - S_I G^d_{3,4}|L_2(\mathbb{T}^d)\| / \|G^d_{3,4}|L_2(\mathbb{T}^d)\|$ for $G^d_{3,4}$ with respect to the refinement N of hyperbolic cross frequency index sets $I := I_N^{d,0,\mathbf{1}}$.

Example 2.48. We employ the reconstructing rank-1 lattices $\Lambda(\boldsymbol{z}, M, I_N^{d,0,\mathbf{1}})$ from Table 2.5. The resulting sampling errors $G^d_{3,4} - S^{\Lambda}_{I_N^{d,0,\mathbf{1}}} G^d_{3,4}$ measured in the relative $\mathcal{A}(\mathbb{T}^d)$ and $L_2(\mathbb{T}^d)$ norm are only slightly larger than the corresponding truncation errors $G^d_{3,4} - S_{I_N^{d,0,\mathbf{1}}} G^d_{3,4}$. In Figure 2.9, we depict the relative sampling errors in the $\mathcal{A}(\mathbb{T}^d)$ norm with respect to the number of (approximately) computed Fourier coefficients $|I_N^{d,0,\mathbf{1}}|$ and lines $\asymp |I_N^{d,0,\mathbf{1}}|^{-3} \, (\log |I_N^{d,0,\mathbf{1}}|)^{3(d-1)}$ which decay (asymptotically) slightly faster than the theoretical upper bounds $|I_N^{d,0,\mathbf{1}}|^{-3+\epsilon} \, (\log |I_N^{d,0,\mathbf{1}}|)^{(3-\epsilon)(d-1)}$ from Theorem 2.24 and the proof of Corollary 2.21. The observed errors nearly decay as the upper bounds suggest.

Additionally, we consider the relative sampling errors in the $L_2(\mathbb{T}^d)$ norm. In Figure 2.10a, we show the relative sampling errors with respect to the number of (approximately) computed Fourier coefficients $|I_N^{d,0,\mathbf{1}}|$ and lines $\asymp |I_N^{d,0,\mathbf{1}}|^{-\frac{7}{2}} \, (\log |I_N^{d,0,\mathbf{1}}|)^{\frac{7}{2}(d-1)+\frac{d-1}{2}}$ (approximately) corresponding to the (asymptotic) upper bounds $|I_N^{d,0,\mathbf{1}}|^{-\frac{7}{2}+\epsilon} \, (\log |I_N^{d,0,\mathbf{1}}|)^{(\frac{7}{2}-\epsilon)(d-1)+\frac{d-1}{2}}$ which follow from Theorem 2.30 and the proof of Corollary 2.21. Again, the observed errors nearly decay as the upper bounds suggest. In Figure 2.17a, we depict the relative sampling errors for dimensions $d \in \{2, 3, \ldots, 10\}$. For higher dimensions $d \geq 7$, the decay is slower and we presumably observe pre-asymptotic behavior. For numerical results with weighted hyperbolic cross index sets $I_N^{d,0,\boldsymbol{\gamma}}$, we refer to [KPV15a], e.g. see [KPV15a, Fig. 6.1b] for $\boldsymbol{\gamma} := \mathbf{0.5}$.

Moreover, we consider the relative $L_2(\mathbb{T}^d)$ sampling error as a function of the rank-1 lattice size M in Figure 2.10b. Additionally, the reference lines $\asymp M^{-\frac{7}{4}} (\log M)^{\frac{7}{4}(d-2)+\frac{d-1}{2}}$ are depicted in Figure 2.10b, which are (asymptotically) slightly smaller than the upper bounds

$N\backslash s$	1	2	3	4	5	6	7
1	1	3	9	27	81	243	729
2	1	5	23	105	479	2 185	9 967
4	1	9	58	343	1 911	10 579	57 897
8	1	17	163	1 035	5 727	33 769	191 808
16	1	33	579	3 628	21 944	169 230	1 105 193
32	1	65	2 179	11 525	106 703	785 309	6 897 012
64	1	129	8 451	47 463	475 829	3 752 318	31 829 977
128	1	257	33 283	176 603	2 244 100	20 645 268	192 757 285
256	1	513	132 099	753 249	10 561 497	136 178 715	1 400 567 254
512	1	1 025	526 339	2 773 801	39 632 648	–	–

Table 2.5: Parameters z_s depending on the refinement N of reconstructing rank-1 lattices $\Lambda\left(\boldsymbol{z} = (z_1, \ldots, z_d)^\top, M = z_{d+1}, I_N^{d,0,\mathbf{1}}\right)$ for hyperbolic cross frequency index sets $I_N^{d,0,\mathbf{1}}$.

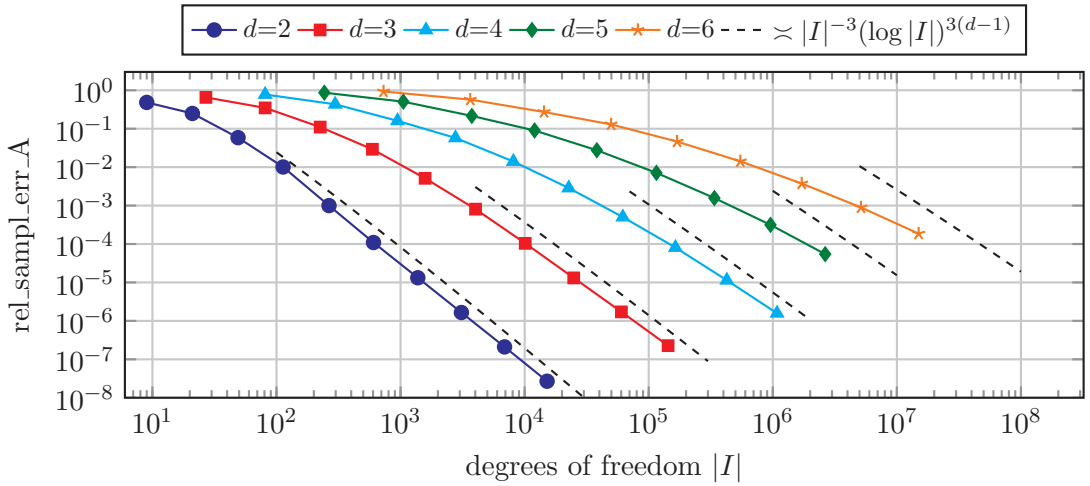

Figure 2.9: Relative $\mathcal{A}(\mathbb{T}^d)$ sampling errors rel_sampl_err_A $:= \|G_{3,4}^d - S_I^\Lambda G_{3,4}^d|\mathcal{A}(\mathbb{T}^d)\|/\|G_{3,4}^d|\mathcal{A}(\mathbb{T}^d)\|$ for $G_{3,4}^d$ with respect to the cardinality $|I|$ of hyperbolic cross frequency index sets $I := I_N^{d,0,\mathbf{1}}$ for increasing refinements N and fixed dimension d.

$\lesssim M^{-\frac{7}{4}+\frac{\epsilon}{2}}(\log M)^{(\frac{7}{4}-\frac{\epsilon}{2})(d-2)+\frac{d-1}{2}}$ from Corollary 2.44. The error plots decay similarly as the reference lines and they might decay slightly faster in the cases $d = 2, 3, 4$. We investigate the latter cases more closely in Figure 2.11, where we consider scaled relative $L_2(\mathbb{T}^d)$ sampling errors. We scale by the M dependent factors in the upper bound of Corollary 2.44 in Figure 2.11a and by the factor $M^{-\beta/2}$ from the lower bound of Corollary 2.44 in Figure 2.11b. Both bounds differ asymptotically by the factor $(\log M)^{\frac{d-2}{2}\beta+\frac{d-1}{2}}$. We remark that if the scaled error plots behave like a horizontal line, then the errors decrease (nearly) like the scaling factor. Here, we observe that the sampling errors seem to decay faster than the upper bound of Corollary 2.44 suggests in the cases $d = 2, 3, 4$. In the case $d = 2, 3$, the sampling errors should decay approximately like the lower bound of Corollary 2.44. In the case $d = 4$, the situation is not totally clear, but the error may also decay accordingly. □

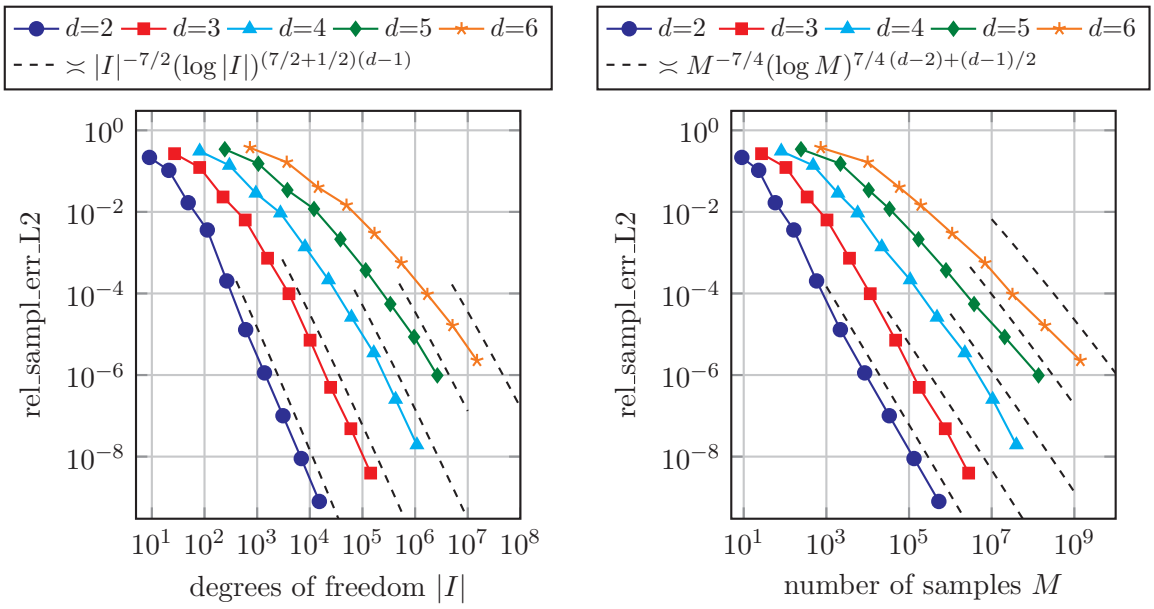

(a) with respect to $|I_N^{d,0,\mathbf{1}}|$

(b) with respect to M

Figure 2.10: Relative $L_2(\mathbb{T}^d)$ sampling errors rel_sampl_err_L2 $:= \|G_{3,4}^d - S_I^\Lambda G_{3,4}^d | L_2(\mathbb{T}^d)\| / \|G_{3,4}^d | L_2(\mathbb{T}^d)\|$ for $G_{3,4}^d$ with respect to the cardinality $|I|$ of hyperbolic cross frequency index sets $I := I_N^{d,0,\mathbf{1}}$ and the rank-1 lattice size M for increasing refinements N and fixed dimension d.

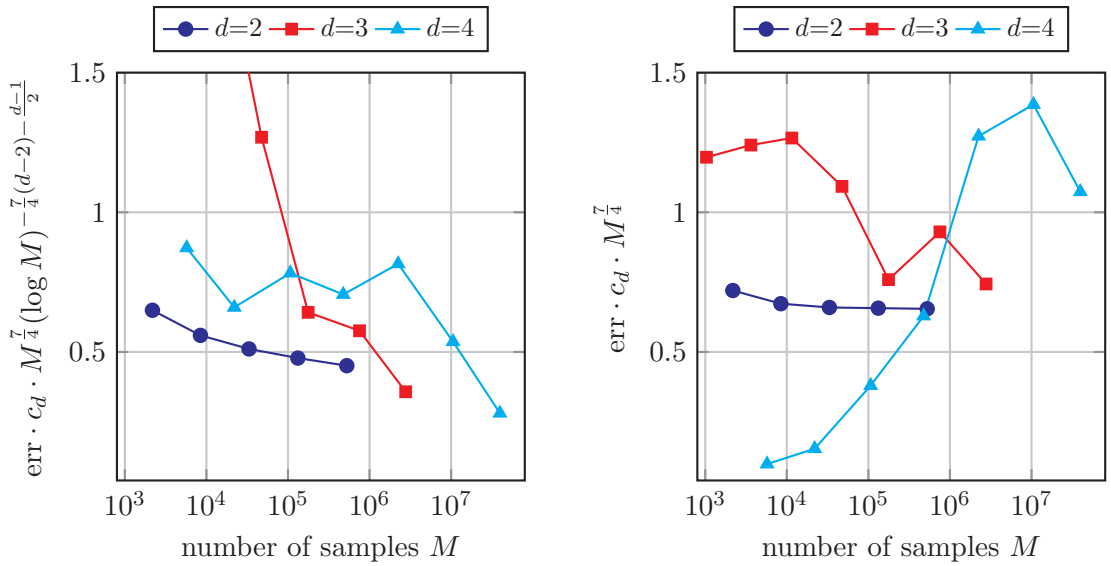

(a) scaled by upper bounds from Corollary 2.44 with $c_2 := 0.2$, $c_3 := 0.8$, $c_4 := 1.4$

(b) scaled by lower bound from Corollary 2.44 with $c_2 := 0.08$, $c_3 := 0.001$, $c_4 := 2.8\text{e-}6$

Figure 2.11: Relative $L_2(\mathbb{T}^d)$ sampling errors err $:= \|G_{3,4}^d - S_I^\Lambda G_{3,4}^d | L_2(\mathbb{T}^d)\| / \|G_{3,4}^d | L_2(\mathbb{T}^d)\|$ scaled by different factors for $G_{3,4}^d$ with respect to the rank-1 lattice size M, $I := I_N^{d,0,\mathbf{1}}$.

Next, we consider the test functions $G_3^d\colon \mathbb{T}^d \to \mathbb{C}$ from [KPV15a], $G_3^d(\boldsymbol{x}) := \prod_{s=1}^d g_3(x_s)$, where the one-dimensional function $g_3\colon \mathbb{T} \to \mathbb{C}$ is defined by

$$g_3(x) := 4\sqrt{\frac{3\pi}{207\pi - 256}}\left(2 + \operatorname{sgn}((x \bmod 1) - 1/2)\,\sin(2\pi x)^3\right)$$

and the Fourier coefficients of g_3 are given by

$$(\widehat{g_3})_k = 4\sqrt{\frac{3\pi}{207\pi - 256}}\begin{cases} \frac{-12}{(k-3)(k-1)(k+1)(k+3)\pi} & \text{for } k \in 2\mathbb{Z}\setminus\{0\}, \\ 0 & \text{for } k \text{ odd}, \\ 2 - \frac{4}{3\pi} & \text{for } k = 0, \end{cases}$$

which yields $G_3^d \in \mathcal{A}^{0,3-\epsilon,\mathbf{1}}(\mathbb{T}^d)$ and $G_3^d \in \mathcal{H}^{0,\frac{7}{2}-\epsilon,\mathbf{1}}(\mathbb{T}^d)$, $\epsilon > 0$. Moreover, we remark that $\|G_3^d|L^2(\mathbb{T}^d)\| = 1$ and $\|G_3^d|\mathcal{A}(\mathbb{T}^d)\| = \left(\frac{8(4+15\pi)}{5\sqrt{3\pi}(207\pi-256)}\right)^d \approx (1.34181)^d$. Since the Fourier coefficients $(\widehat{g_3})_k$ of g_3 are zero for odd frequencies $k \in (2\mathbb{Z}+1)$, we can use hyperbolic cross index sets "with holes" $I = I_{N,\text{even}}^{d,0,\mathbf{1}} := I_N^{d,0,\mathbf{1}} \cap (2\mathbb{Z})^d$. Correspondingly, we use the reconstructing rank-1 lattices $\Lambda(\boldsymbol{z}, M, I_{N,\text{even}}^{d,0,\mathbf{1}})$ from Table 2.6, which were constructed by the implementation [Vol16b, `genlattice_cbc_incr_bisect`] of Algorithm 2.3 and parts of this table can be found as [KPV15a, Table 6.3]. Moreover, we depict the oversampling factors $M/|I_{N,\text{even}}^{d,0,\mathbf{1}}|$ in Figure 2.12b. The observed oversampling factors are still moderate for the considered refinements N and approximately grow as the asymptotic upper bound $\mathcal{O}(N/\log N)$ on the existence of a reconstructing rank-1 lattice suggests, which can be derived from Table 2.3.

$N\backslash s$	1	2	3	4	5	6	7	8	9
1	1	1	1	1	1	1	1	1	1
2	1	3	5	7	9	11	13	15	17
4	1	5	13	29	49	81	137	183	255
8	1	9	41	97	257	543	983	1643	2895
16	1	17	145	395	1213	3079	6905	12543	23375
32	1	33	545	1721	5815	14253	34117	84845	184859
64	1	65	2113	5161	21535	78167	226951	574275	1248979
128	1	129	8321	21569	111015	404035	1373325	4068807	11051805
256	1	257	33025	85405	485913	2328905	8145033	27910471	84391053
512	1	513	131585	359213	2353599	12181705	50770301	179044805	600266399
1024	1	1025	525313	1383595	11148851	70968649	293168219	–	–
2048	1	2049	2099201	5416219	41601005	220147195	–	–	–

Table 2.6: Parameters z_s depending on the refinement N of reconstructing rank-1 lattices $\Lambda\left(\boldsymbol{z} = (z_1, \ldots, z_d)^\top, M = z_{d+1}, I_{N,\text{even}}^{d,0,\mathbf{1}}\right)$ for hyperbolic cross frequency index sets "with holes" $I_{N,\text{even}}^{d,0,\mathbf{1}}$.

Example 2.49. We apply rank-1 lattice sampling on the test functions G_3^d and use the reconstructing rank-1 lattices $\Lambda(\boldsymbol{z}, M, I_{N,\text{even}}^{d,0,\mathbf{1}})$ from Table 2.6. In Figure 2.13a, the relative sampling errors $\|G_3^d - S^{\Lambda}_{I_{N,\text{even}}^{d,0,\mathbf{1}}} G_3^d|\mathcal{A}(\mathbb{T}^d)\|/\|G_3^d|\mathcal{A}(\mathbb{T}^d)\|$ with respect to the refinement N are shown for $d \in \{2, 3, \ldots, 8\}$ and various refinements N. We remark that the corresponding relative truncation errors $\|G_3^d - S_{I_{N,\text{even}}^{d,0,\mathbf{1}}} G_3^d|\mathcal{A}(\mathbb{T}^d)\|/\|G_3^d|\mathcal{A}(\mathbb{T}^d)\|$ almost coincide. In the case $d = 2$ and $d = 3$, the obtained errors seem to decay approximately like N^{-3} in accordance

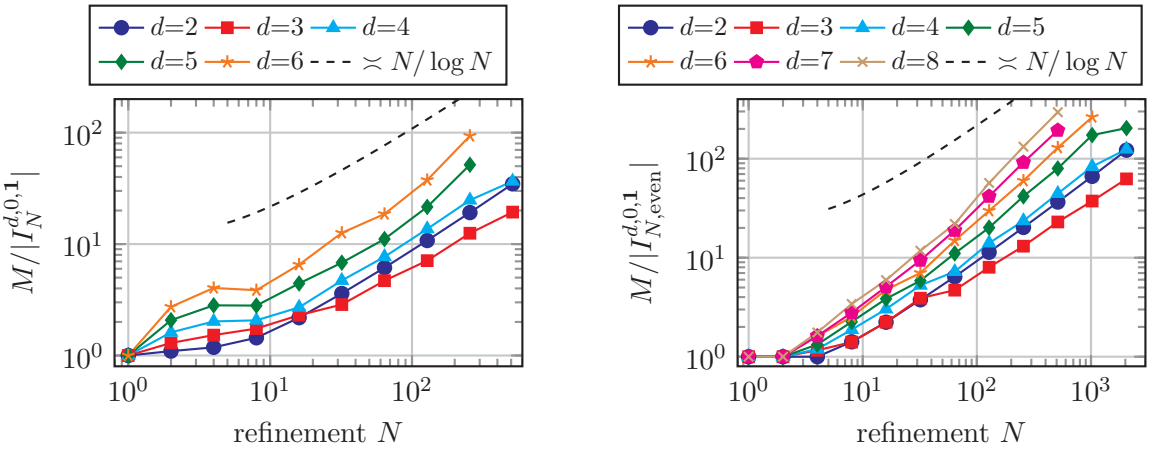

(a) $I := I_N^{d,0,\mathbf{1}}$ (b) $I := I_{N,\text{even}}^{d,0,\mathbf{1}}$

Figure 2.12: Oversampling factors $M/|I|$ for the reconstructing rank-1 lattice $\Lambda(\boldsymbol{z}, M, I)$ from Table 2.5 and 2.6.

with Theorem 2.17 as well as slightly slower for $d \geq 4$. In Figure 2.13b, the corresponding relative $L_2(\mathbb{T}^d)$ sampling errors are depicted, see also [KPV15a, Figure 6.4a]. These errors should approximately decay like $N^{-3.5}$ due to Theorem 2.20. Additionally, we consider the relative $\mathcal{A}(\mathbb{T}^d)$ and $L_2(\mathbb{T}^d)$ sampling errors with respect to the rank-1 lattice size M for $d \in \{2, 3, 4, 6\}$ in Figure 2.14a and 2.14b, respectively. We compare these results with the relative sampling errors when using standard hyperbolic crosses $I = I_N^{d,0,\mathbf{1}}$ and the reconstructing rank-1 lattices $\Lambda(\boldsymbol{z}, M, I_N^{d,0,\mathbf{1}})$ from Table 2.5. We observe that both plots for fixed dimension d behave similarly, they roughly look like shifted versions of each other. As expected, the errors for comparable numbers of samples are distinctly lower when using the hyperbolic cross index sets "with holes" $I_{N,\text{even}}^{d,0,\mathbf{1}} := I_N^{d,0,\mathbf{1}} \cap (2\mathbb{Z})^d$. Moreover, the shift clearly depends on the dimension d, most likely exponentially. Additionally, the theoretical upper bounds $\lesssim M^{-\frac{\beta}{2}} (\log M)^{\frac{d-2}{2}\beta}$ from Corollary 2.40 and $\lesssim M^{-\frac{\beta}{2}} (\log M)^{\frac{d-2}{2}\beta + \frac{d-1}{2}}$ from Corollary 2.44 are shown in Figure 2.14a and 2.14b, respectively. We observe that the obtained errors nearly decay as these bounds suggest. □

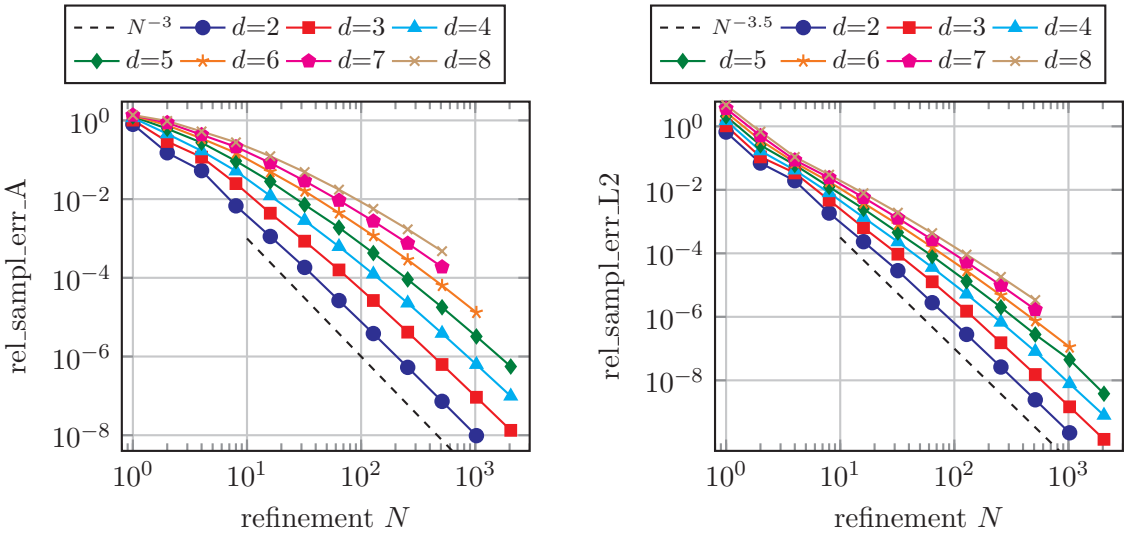

(a) relative $\mathcal{A}(\mathbb{T}^d)$ sampling error

(b) relative $L_2(\mathbb{T}^d)$ sampling error, see Figure 6.4a from [KPV15a]

Figure 2.13: Relative $\mathcal{A}(\mathbb{T}^d)$ sampling errors rel_sampl_err_A $:= \|G_3^d - S_I^\Lambda G_3^d|\mathcal{A}(\mathbb{T}^d)\|/\|G_3^d|\mathcal{A}(\mathbb{T}^d)\|$ and $L_2(\mathbb{T}^d)$ sampling errors rel_sampl_err_L2 $:= \|G_3^d - S_I^\Lambda G_3^d|L_2(\mathbb{T}^d)\|/\|G_3^d|L_2(\mathbb{T}^d)\|$ for G_3^d with respect to the refinement N, $I := I^{d,0,\mathbf{1}}_{N,\text{even}}$.

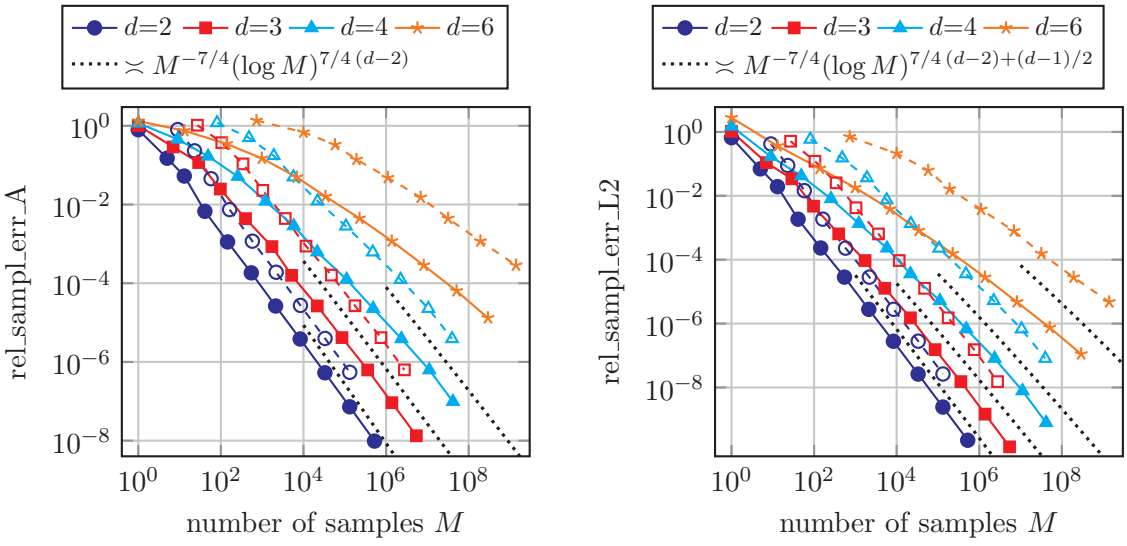

(a) relative $\mathcal{A}(\mathbb{T}^d)$ sampling error

(b) relative $L_2(\mathbb{T}^d)$ sampling error

Figure 2.14: Relative $\mathcal{A}(\mathbb{T}^d)$ sampling errors rel_sampl_err_A $:= \|G_3^d - S_I^\Lambda G_3^d|\mathcal{A}(\mathbb{T}^d)\|/\|G_3^d|\mathcal{A}(\mathbb{T}^d)\|$ and $L_2(\mathbb{T}^d)$ sampling errors rel_sampl_err_L2 $:= \|G_3^d - S_I^\Lambda G_3^d|L_2(\mathbb{T}^d)\|/\|G_3^d|L_2(\mathbb{T}^d)\|$ for G_3^d with respect to the rank-1 lattice size M, when using the frequency index sets $I := I^{d,0,\mathbf{1}}_{N,\text{even}}$ with corresponding reconstructing rank-1 lattices $\Lambda(\boldsymbol{z}, M, I^{d,0,\mathbf{1}}_{N,\text{even}})$ (denoted by solid lines) and $I := I_N^{d,0,\mathbf{1}}$ with corresponding reconstructing rank-1 lattices $\Lambda(\boldsymbol{z}, M, I_N^{d,0,\mathbf{1}})$ (denoted by dashed lines).

For the test functions G_3^d, we also consider higher dimensional cases up to 25 dimensions using frequency index sets "with holes" $I_{N,\text{even}}^{d,0,\mathbf{1}}$.

Example 2.50. We consider higher dimensional cases with dimension $d \in \{10, 15, 20, 25\}$ for the test functions G_3^d. In doing so, we use frequency index sets "with holes" $I := I_{N,\text{even}}^{d,0,\mathbf{1}}$ and we build reconstructing rank-1 lattices $\Lambda(\boldsymbol{z}, M, I_{N,\text{even}}^{d,0,\mathbf{1}})$ using implementation [Vol16b, `genlattice_cbc_incr_bisect`] of Algorithm 2.3. In Figure 2.13a, the relative $L_2(\mathbb{T}^d)$ sampling errors $\|G_3^d - S_I^\Lambda G_3^d | L_2(\mathbb{T}^d)\| / \|G_3^d | L_2(\mathbb{T}^d)\|$ with respect to the refinement N and cardinality $|I|$ are shown for various refinements N. We observe that the obtained errors decrease fast for increasing refinements N. The observed aliasing errors $S_I G_3^d - S_I^\Lambda G_3^d$ are larger than the corresponding truncation errors $G_3^d - S_I G_3^d$ for small refinements $N \leq 4$ and distinctly smaller for larger refinements $N \geq 8$. Moreover, we remark that some of the obtained relative $L_2(\mathbb{T}^d)$ sampling errors $\|G_3^d - S_I^\Lambda G_3^d | L_2(\mathbb{T}^d)\| / \|G_3^d | L_2(\mathbb{T}^d)\|$ belonging to smaller refinements N are greater than one, which is still below the asymptotic upper bounds in Theorem 2.30 stated relative to the $\|G_3^d | \mathcal{H}^{0,7/2-\epsilon,\mathbf{1}}(\mathbb{T}^d)\|$ norm, $\epsilon > 0$, and the factor $\|G_3^d | \mathcal{H}^{0,7/2-\epsilon,\mathbf{1}}(\mathbb{T}^d)\| / \|G_3^d | L_2(\mathbb{T}^d)\|$ is greater than 8^d for $\epsilon = 0.05$ for instance. □

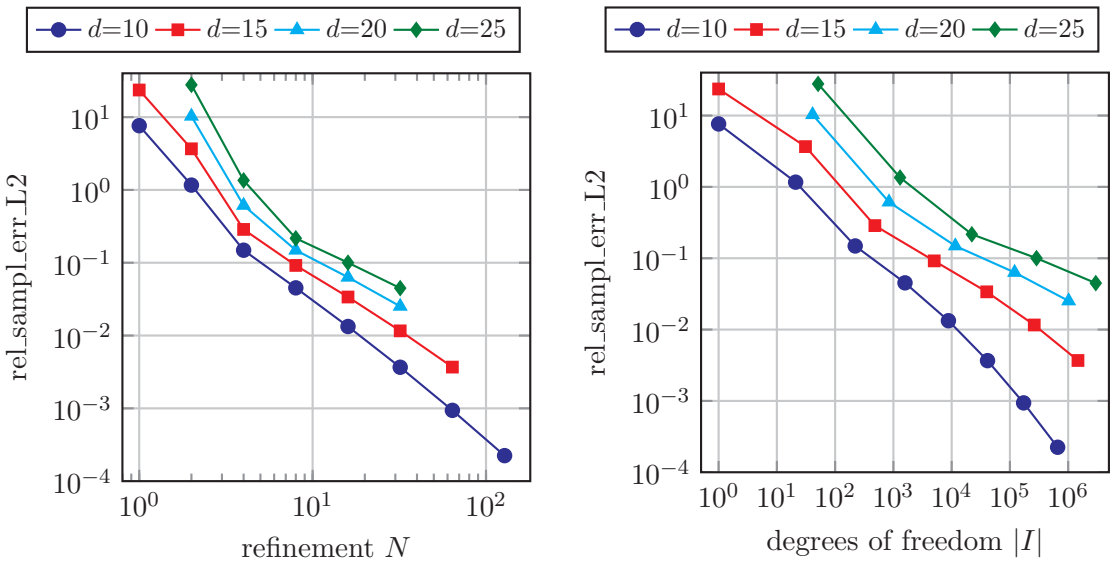

(a) with respect to the refinement N

(b) with respect to the cardinality $|I_{N,\text{even}}^{d,0,\mathbf{1}}|$

Figure 2.15: Relative $L_2(\mathbb{T}^d)$ sampling errors rel_sampl_err_L2 := $\|G_3^d - S_I^\Lambda G_3^d | L_2(\mathbb{T}^d)\| / \|G_3^d | L_2(\mathbb{T}^d)\|$ for test functions G_3^d, $d \in \{10, 15, 20, 25\}$, $I := I_{N,\text{even}}^{d,0,\mathbf{1}}$.

Next, we give a numerical example for sampling along perturbed rank-1 lattices as described in Section 2.3.4.

Example 2.51. We use the test functions $G_{3,4}^d$, hyperbolic cross frequency index sets $I_N^{d,0,\mathbf{1}}$ and the reconstructing rank-1 lattices $\Lambda(\boldsymbol{z}, M, I_N^{d,0,\mathbf{1}})$ from Table 2.5, see also [KPV15a, Example 6.4]. For each reconstructing rank-1 lattice $\Lambda(\boldsymbol{z}, M, I_N^{d,0,\mathbf{1}}) = \{\boldsymbol{x}_j\}_{j=0}^{M-1}$, we use sampling nodes $\boldsymbol{y}_j := \boldsymbol{x}_j + \boldsymbol{\eta}_j$, $j = 0, \ldots, M-1$, where $\boldsymbol{\eta}_j \in \{-\varepsilon, \varepsilon\}^d$ are drawn uniformly at random with $\varepsilon := \big(2\pi d N\big)^{-1} \ln 2$. We sample the function $G_{3,4}^d$ at the sampling nodes $\boldsymbol{y}_j$ and we compute the approximated Fourier coefficients $(\hat{\tilde{f}}_{\boldsymbol{k}})_{\boldsymbol{k} \in I_N^{d,T,\mathbf{1}}}$ by solving (2.67) using the LSQR

algorithm [PS82] in combination with (2.18) and its adjoint version. In doing so, we repeat the computation 10 times and determine the maximum of the obtained relative $L_2(\mathbb{T}^d)$ sampling errors. We consider the dimensions $d \in \{2,3,4,5\}$ for various refinements N and use Taylor expansion parameters $m \in \{1,2,3\}$. In Figure 2.16, we depict the results as well as the corresponding results of the unperturbed case from Figure 2.8b, which are denoted by "R1L". Since $G_{3,4}^d \in \mathcal{A}^{0,3-\epsilon,\mathbf{1}}(\mathbb{T}^d)$, $\epsilon > 0$, we expect the errors to decay at least like $\sim N^{-3+\epsilon}$ for $m = 3$ and slower for $m = 1,2$ due to Theorem 2.46. For dimension $d = 2$, we observe that the relative $L_2(\mathbb{T}^d)$ sampling error decays approximately like $\sim N^{-3.5}$ for the unperturbed case and the case $m = 3$, approximately like $\sim N^{-2}$ for $m = 2$ as well as $\sim N^{-1.5}$ for $m = 1$. In the higher dimensional cases $d = 3,4,5$, the plots for the unperturbed case and the case $m = 3$ again almost coincide but decay slower. Moreover, we approximately observe the decay $\sim N^{-2}$ in the cases $d = 3,4,5$ for Taylor expansion parameter $m = 2$ and $\sim N^{-1.5}$ for $m = 1$.
We also perform tests from [KPV15a, Example 6.4] for perturbations $\boldsymbol{\eta}_j$ drawn uniformly at random from $(-\varepsilon,\varepsilon)^d$ for dimensions $d \in \{2,3,\ldots,10\}$ and Taylor expansion parameter $m = 3$. The observed relative $L_2(\mathbb{T}^d)$ sampling errors are depicted in Figure 2.17b with respect to the cardinality $|I_N^{d,0,\mathbf{1}}|$. As expected, the errors decay for increasing cardinalities $|I_N^{d,0,\mathbf{1}}|$. We observe that the obtained errors almost coincide with those from the unperturbed case depicted in Figure 2.17a. For results with Taylor expansion parameter $m = 2$, we refer to [KPV15a, Fig. 6.9a]. These results are similar to the ones in Figure 2.16.
Additionally, we consider the test functions G_3^d in four and five dimensions. Here, we use hyperbolic cross frequency index sets "with holes" $I := I_{N,\text{even}}^{d,0,\mathbf{1}}$ and corresponding reconstructing rank-1 lattices $\Lambda(\boldsymbol{z}, M, I_{N,\text{even}}^{d,0,\mathbf{1}})$ from Table 2.6. Consequently, we can consider higher refinements N than for the test functions $G_{3,4}^d$. We sample at perturbed rank-1 lattice nodes $\boldsymbol{y}_j := \boldsymbol{x}_j + \boldsymbol{\eta}_j$, $j = 0,\ldots,M-1$, where $\boldsymbol{\eta}_j \in \{-\varepsilon,\varepsilon\}^d$ are drawn uniformly at random with $\varepsilon := \big(2\pi dN\big)^{-1} \ln 2$ and we use Taylor expansion parameters $m \in \{1,2,3\}$. The corresponding error plots are shown in Figure 2.18. The relative $L_2(\mathbb{T}^d)$ sampling errors for Taylor expansion parameter $m = 1$ and $m = 2$ behave similarly as before. For dimension $d = 4$, there is a significant difference in the obtained errors between the cases $m = 2$ and $m = 3$ for high refinements $N \geq 512$ or small error values. The obtained errors for $m = 3$ and the unperturbed case almost coincide. For dimension $d = 5$, the errors in the case $m = 1$ are again distinctly larger. The errors of the case $m = 3$ and the unperturbed case almost coincide. In the case $m = 2$, there is only a noticeable difference to the case $m = 3$ for refinement $N = 2048$. □

As we have seen in this chapter and in the numerical examples, the fast approximation of a sufficiently smooth high-dimensional function $f \in \mathcal{A}(\mathbb{T}^d) \cap \mathcal{C}(\mathbb{T}^d)$ from samples along reconstructing rank-1 lattices $\Lambda(\boldsymbol{z}, M, I)$ can be performed very easily and the obtained errors decay fast if the frequency index sets I are chosen correspondingly to the decay of the Fourier coefficients $\hat{f}_{\boldsymbol{k}}$ of the function or to the assumed decay given by a suitable function class. The computation of approximated Fourier coefficients $\hat{f}_{\boldsymbol{k}}^{\Lambda} \approx \hat{f}_{\boldsymbol{k}}$, $\boldsymbol{k} \in I$, can be performed very fast in $\mathcal{O}(M \log M + d\,|I|)$ arithmetic operations using Algorithm 2.4, which can be realized using two short lines of Octave / MATLAB code.

If the samples are not given at exact rank-1 lattice nodes $\boldsymbol{x}_j$, a method for the fast approximation of the function f using a rank-1 lattice based Taylor expansion can be applied. Then, we solve a linear system of equations using the LSQR algorithm with computational cost of $\mathcal{O}\big(K\, m^d (M \log M + d\,|I|)\big)$, where $m \in \mathbb{N}$ is the Taylor expansion parameter and K is the number of iterations, which depends on the targeted error and the condition number

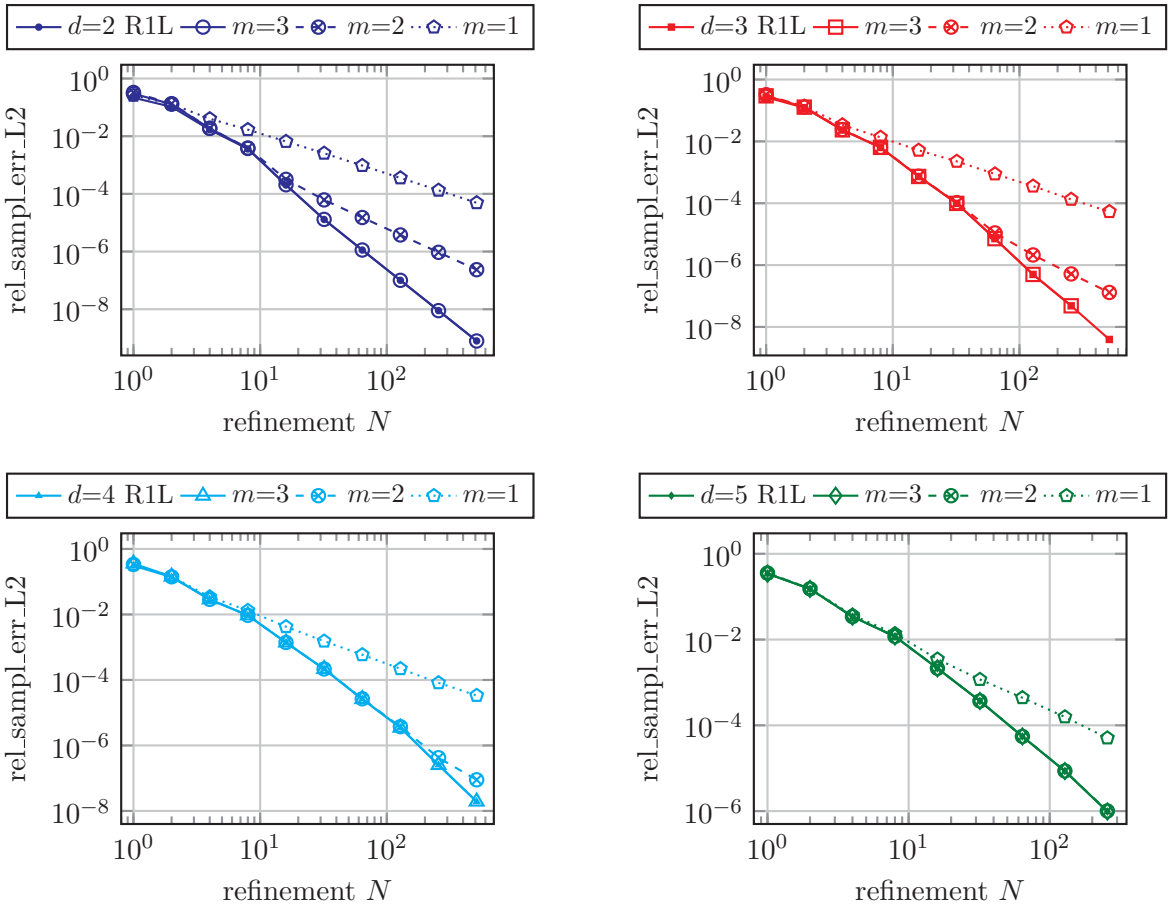

Figure 2.16: Relative $L_2(\mathbb{T}^d)$ errors rel_sampl_err_L2 $:= \|G^d_{3,4} - S^{\Lambda}_I G^d_{3,4}|L_2(\mathbb{T}^d)\|/\|G^d_{3,4}|L_2(\mathbb{T}^d)\|$ and $:= \|G^d_{3,4} - S^{\mathcal{Y}}_I G^d_{3,4}|L_2(\mathbb{T}^d)\|/\|G^d_{3,4}|L_2(\mathbb{T}^d)\|$ with hyperbolic cross frequency index sets $I := I^{d,0,\mathbf{1}}_N$ when sampling at rank-1 lattice nodes ("R1L") and perturbed rank-1 lattice nodes using (2.67) with Taylor expansion parameters $m = 1, 2, 3$.

of the system matrix, see Section 2.2.2 and 2.3.4.

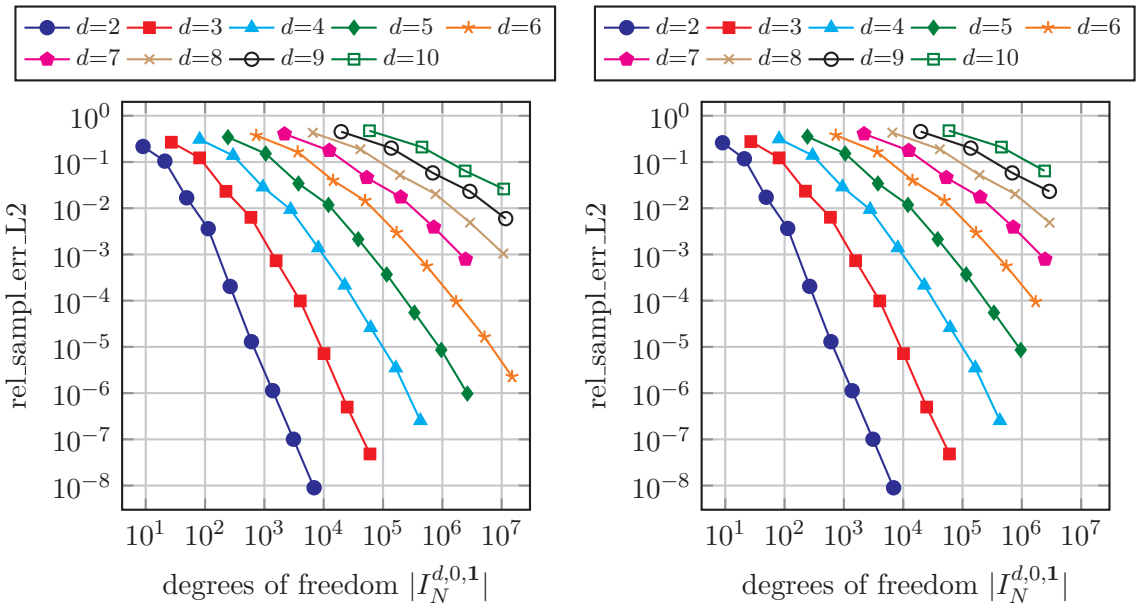

(a) ([KPV15a, Fig. 4.1a]), "R1L" (b) ([KPV15a, Fig. 6.9b]), $m = 3$

Figure 2.17: Relative $L_2(\mathbb{T}^d)$ errors rel_sampl_err_L2 $:= \|G_{3,4}^d - S_I^{\Lambda} G_{3,4}^d | L_2(\mathbb{T}^d)\| / \|G_{3,4}^d | L_2(\mathbb{T}^d)\|$ and $:= \|G_{3,4}^d - S_I^{\mathcal{Y}} G_{3,4}^d | L_2(\mathbb{T}^d)\| / \|G_{3,4}^d | L_2(\mathbb{T}^d)\|$ with hyperbolic cross frequency index sets $I := I_N^{d,0,\mathbf{1}}$ when sampling at rank-1 lattice nodes ("R1L") and perturbed rank-1 lattice nodes using (2.67) with Taylor expansion parameter $m = 3$.

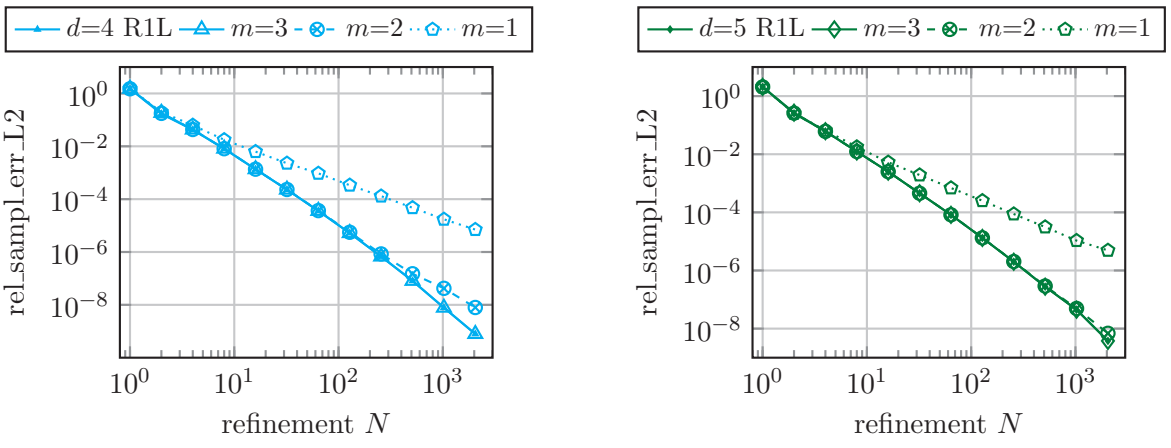

Figure 2.18: Relative $L_2(\mathbb{T}^d)$ errors rel_sampl_err_L2 $:= \|G_3^d - S_I^{\Lambda} G_3^d | L_2(\mathbb{T}^d)\| / \|G_3^d | L_2(\mathbb{T}^d)\|$ and $:= \|G_3^d - S_I^{\mathcal{Y}} G_3^d | L_2(\mathbb{T}^d)\| / \|G_3^d | L_2(\mathbb{T}^d)\|$ for G_3^d with hyperbolic cross index sets "with holes" $I := I_{N,\text{even}}^{d,0,\mathbf{1}}$ when sampling at rank-1 lattice nodes ("R1L") and perturbed rank-1 lattice nodes using (2.67) with Taylor expansion parameters $m = 1, 2, 3$.

Chapter 3

Multivariate Algebraic Polynomials in Chebyshev Form

We consider multivariate algebraic polynomials $a_I \colon [-1,1]^d \to \mathbb{R}$ in Chebyshev form,

$$a_I(\boldsymbol{x}) := \sum_{\boldsymbol{k}\in I} \hat{a}_{\boldsymbol{k}}\, T_{\boldsymbol{k}}(\boldsymbol{x}) = \sum_{\boldsymbol{k}\in I} \hat{a}_{\boldsymbol{k}} \prod_{t=1}^{d} T_{k_t}(x_t), \quad \hat{a}_{\boldsymbol{k}} \in \mathbb{R}, \tag{3.1}$$

where $I \subset \mathbb{N}_0^d$, $d \in \mathbb{N}$, is a non-negative index set of finite cardinality, $|I| < \infty$, and $T_{\boldsymbol{k}} \colon [-1,1]^d \to [-1,1]$, $T_{\boldsymbol{k}}(\boldsymbol{x}) := \prod_{t=1}^{d} T_{k_t}(x_t)$, $\boldsymbol{k} \in \mathbb{N}_0^d$, are multivariate Chebyshev polynomials defined on the closed box $[-1,1]^d$, built from Chebyshev polynomials of the first kind $T_l \colon [-1,1] \to [-1,1]$, $T_l(x) := \cos(l \arccos x)$, for frequencies $l \in \mathbb{N}_0$. For each $l \in \mathbb{N}_0$, the univariate Chebshev polynomial T_l is an algebraic polynomial of degree $\deg(T_l) = l$ restricted to the domain $[-1,1]$. Moreover, if the index set $I = I_{\mathrm{a},n}^{d,-\infty} := \{\boldsymbol{k} \in \mathbb{N}_0^d \colon \|\boldsymbol{k}\|_1 \le n\}$, $n \in \mathbb{N}_0$, is the ℓ_1-ball, then $\operatorname{span}\{T_{\boldsymbol{k}}(\circ) \colon \boldsymbol{k} \in I\}$ is the space of all algebraic polynomials of (total) degree $\le n$ in d variables restricted to the domain $[-1,1]^d$, see e.g. [CP11]. We remark that one may also consider other closed boxes $[a_1,b_1] \times \ldots \times [a_d,b_d] \subset \mathbb{R}^d$, $a_t < b_t$ for $t = 1,\ldots,d$, by a simple linear coordinate transform.

Let $L_{2,w}([-1,1])$ be the weighted Hilbert space of all square integrable functions $f \colon [-1,1] \to \mathbb{R}$ with respect to the Chebyshev weight $w(x) := 1/\sqrt{1-x^2}$,

$$\int_{-1}^{1} |f(x)|^2\, w(x)\, \mathrm{d}x < \infty,$$

equipped with the scalar product

$$(u,v)_{2,w} := \int_{-1}^{1} u(x)\, v(x)\, w(x)\, \mathrm{d}x = \int_{-1}^{1} \frac{u(x)\, v(x)}{\sqrt{1-x^2}}\, \mathrm{d}x,$$

see e.g. [Spr97b, Spr00]. The univariate Chebyshev polynomials T_l, $l \in \mathbb{N}_0$, form an orthogonal basis of the Hilbert space $L_{2,w}([-1,1])$,

$$(T_k, T_l)_{2,w} = \begin{cases} \pi & \text{for } k = l = 0, \\ \pi/2 & \text{for } k = l \neq 0, \\ 0 & \text{for } k \neq l, \end{cases} \tag{3.2}$$

see e.g. [Sze75, Boy00]. We remark that a Chebyshev series $g(x) := \sum_{k=0}^{\infty} \hat{a}_k T_k(x)$, $x \in [-1,1]$, corresponds to the Fourier-cosine series $G(\theta) = g(\cos\theta) = \sum_{k=0}^{\infty} \hat{a}_k \cos(k\theta)$, $\theta \in [0,\pi]$, using the coordinate transform $x := \cos\theta$ and the coefficients can be computed by $\hat{a}_k = \frac{2}{\pi} 2^{-\delta_{k,0}} \int_0^{\pi} g(\cos\theta) \cos(k\theta) \,\mathrm{d}\theta = \frac{2}{\pi} 2^{-\delta_{k,0}} \int_{-1}^{1} g(x)\, T_k(x)\, (1-x^2)^{-1/2} \,\mathrm{d}x$, see e.g. [GO77, Section 3]. Extending the setting to the multivariate case via tensorization, see e.g. [Wei80, Section 3.4], one obtains that the multivariate Chebyshev polynomials $T_{\boldsymbol{k}}$, $\boldsymbol{k} \in \mathbb{N}_0^d$, form an orthogonal basis of the weighted Hilbert space $L_{2,w}([-1,1]^d)$.

Analogously to the considerations in Chapter 2 for the periodic case, we are interested in methods for the *fast evaluation* of such a multivariate algebraic polynomial in Chebyshev form a_I from (3.1) at certain nodes as well as the *fast reconstruction* of the Chebyshev coefficients $\hat{a}_{\boldsymbol{k}}$, $\boldsymbol{k} \in I$, from samples. Additionally, we want to use these fast reconstruction methods for the *fast approximation* of multivariate non-periodic real-valued functions $f\colon [-1,1]^d \to \mathbb{R}$ by multivariate algebraic polynomials in Chebyshev form a_I from samples of f at certain nodes.

In one dimension, Chebyshev polynomials are frequently used in the non-periodic case for function interpolation at Chebyshev nodes or Chebyshev–Gauß–Lobatto nodes, which are the roots or extremal points of Chebyshev polynomials of the first kind T_l, see e.g. [AS72, p. 889]. This approach allows to mitigate Runge's phenomenon, see e.g. [Boy00, Section 4.2]. Moreover, there exist fast versions of the discrete cosine transform (DCT), which allow to compute Chebyshev coefficients from function samples and vice versa, see e.g. [CLW70, Ste92, BT97] and [VL92, p. 238]. Again, this approach may be transferred to dimensions $d \geq 2$ by tensorization, see e.g. [DL82].

In the multivariate case, if the frequency index set I of a multivariate algebraic polynomial in Chebyshev form a_I is a d-dimensional full grid, e.g. $I = \hat{G}_n^d := [0,n]^d \cap \mathbb{N}_0^d$ of refinement $n \in \mathbb{N}$, one may use the Chebyshev–Gauß–Lobatto nodes $\boldsymbol{y}_j \in \mathcal{Y} := \{\cos(l\pi/n)\colon l = 0,1,\ldots,n\}^d \subset [-1,1]^d$ in spatial domain. Then, a d-dimensional DCT of length $n+1$ in each coordinate direction can be applied to compute the function values $a_I(\boldsymbol{y}_j)$ from the Chebyshev coefficients $\hat{a}_{\boldsymbol{k}}$, $\boldsymbol{k} \in I$, and vice versa, see also Figure 3.1 for a two-dimensional example and the Chebfun toolbox [DHT14]. As in the periodic case, this approach suffers heavily from the curse of dimensionality.

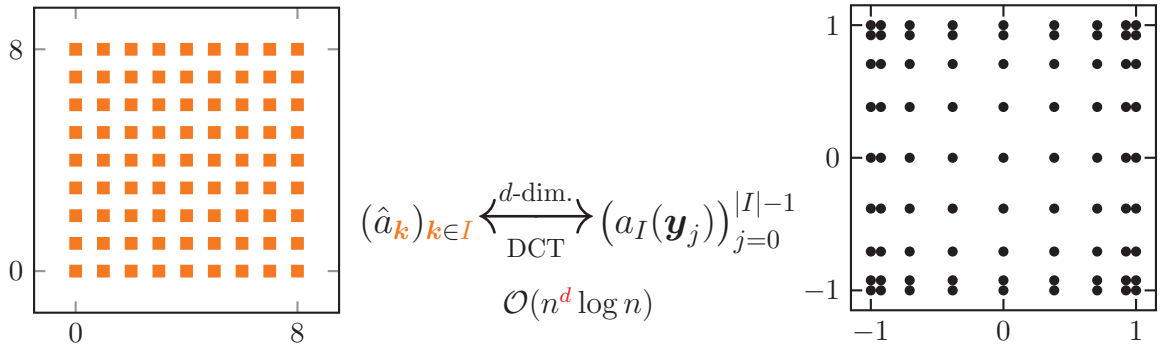

Figure 3.1: d-dimensional DCT between full grids.

Again, one may attenuate this problem by using nodes $\boldsymbol{y}_j$ on sparse grids as spatial discretization and hyperbolic cross frequency index sets I, cf. [BNR00, GH14]. Then, fast transforms for switching between the spatial and frequency domain exist, cf. [SY10], and software implementations are available, see e.g. the HCFFT [GH14], which allow for the computation of the transforms in $\mathcal{O}(n \log^d n)$ arithmetic operations. Still, this approach may

have the issues discussed in the introduction of Chapter 2. For instance, the frequency index set I may have several restrictions, e.g., it should be "without holes" or admissible, cf. [GG03].

In this chapter, we consider a rank-1 Chebyshev lattice $\mathrm{CL}(\boldsymbol{z}, M)$ as spatial discretization, which is defined by

$$\mathrm{CL}(\boldsymbol{z}, M) := \left\{ \boldsymbol{x}_j := \cos\left(\tfrac{j}{M}\pi\boldsymbol{z}\right) : j = 0, \ldots, M \right\} \subset [-1,1]^d, \tag{3.3}$$

with the generating vector $\boldsymbol{z} \in \mathbb{N}_0^d$ and the size parameter $M \in \mathbb{N}_0$, where the cosine is applied component-wise, cf. [CP11]. We remark that rank-1 Chebyshev lattices $\mathrm{CL}(\boldsymbol{z}, M)$ are nodes on so-called Lissajous curves, see e.g. [DE15] and the references therein. Examples for two-dimensional rank-1 Chebyshev lattices $\mathrm{CL}(\boldsymbol{z}, M)$ are shown in Fig. 3.2. Please note that not all $(M+1)$ nodes $\boldsymbol{x}_j$, $j = 0, \ldots, M$, have to be distinct, i.e., $|\mathrm{CL}(\boldsymbol{z}, M)| \in \{1, \ldots, M+1\}$, see e.g. Fig. 3.2a.

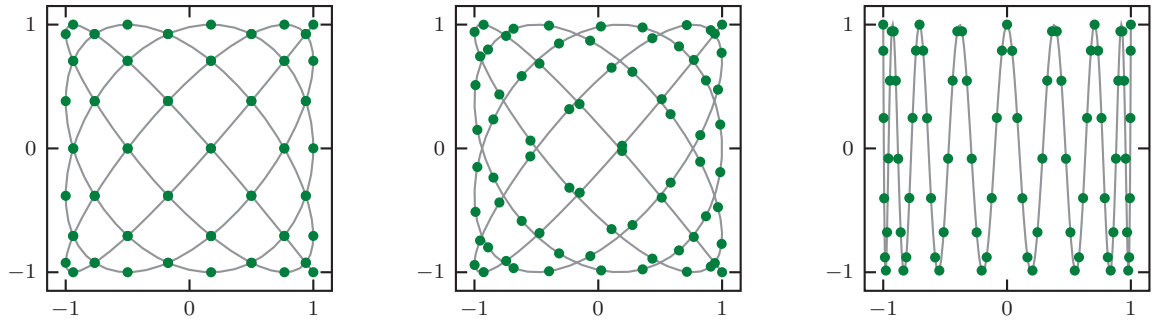

(a) $\boldsymbol{z} := (8,9)^\top$, $M := 72$, $|\mathrm{CL}(\boldsymbol{z}, M)| = 45$.

(b) $\boldsymbol{z} := (8,9)^\top$, $M := 73$, $|\mathrm{CL}(\boldsymbol{z}, M)| = 74$.

(c) $\boldsymbol{z} := (1,16)^\top$, $M := 76$, $|\mathrm{CL}(\boldsymbol{z}, M)| = 77$.

Figure 3.2: Examples of two-dimensional rank-1 Chebyshev lattices $\mathrm{CL}(\boldsymbol{z}, M)$.

When the frequency index set $I = I_{\mathrm{a},n}^{d,-\infty}$ is the ℓ_1-ball of refinement $n \in \mathbb{N}_0$, there exist various results. In the two-dimensional case, so-called Padua points [BCD+06, CDV08] may be used, which are specially chosen two-dimensional rank-1 Chebyshev lattices $\mathrm{CL}\left(\boldsymbol{z} := (n, n+1), M := n(n+1)\right)$, and there exists the Octave / MATLAB toolbox `Padua2DM` [CDMSV11] for the fast evaluation, reconstruction and interpolation. For dimension $d \geq 3$, further results have been developed. Choices for the generating vector $\boldsymbol{z}$ and the size parameter $M \in \mathbb{N}_0$ of a rank-1 Chebyshev lattice suitable for reconstruction are known for certain cases [CP11, BDMV16, BDMV15, DE15]. Moreover, there exists the Octave / MATLAB toolbox CHEBINT [PC13], which uses the Clenshaw algorithm [Cle55]. In general, we do not have an interpolation but so-called hyperinterpolation, see [Slo95].

In this work, we extend these considerations to multivariate algebraic polynomials in Chebyshev form a_I with arbitrarily chosen frequency index sets $I \subset \mathbb{N}_0^d$ of finite cardinality, $|I| < \infty$. Parts of the results were presented in [PV15]. We discuss a method for the fast evaluation of such an algebraic polynomial a_I at the nodes of an arbitrary rank-1 Chebyshev lattice $\mathrm{CL}(\boldsymbol{z}, M) \subset [-1,1]^d$, which only uses easy-to-compute index transforms and a single one-dimensional DCT. For the exact reconstruction of the Chebyshev coefficients $\hat{a}_{\boldsymbol{k}}$, $\boldsymbol{k} \in I$, from samples $a_I(\boldsymbol{x}_j)$ at rank-1 Chebyshev lattice nodes $\boldsymbol{x}_j := \cos(\frac{j}{M}\pi\boldsymbol{z})$, $j = 0, \ldots, M$, with the proposed method, the used rank-1 Chebyshev lattice $\mathrm{CL}(\boldsymbol{z}, M)$ needs to fulfill a *reconstruction property*, i.e., the equivalent conditions (3.22), (3.23) and (3.25). Then, $\mathrm{CL}(\boldsymbol{z}, M)$ will be called *reconstructing rank-1 Chebyshev lattice* for a given frequency index set I and will be denoted by $\mathrm{CL}(\boldsymbol{z}, M, I)$. It can be easily constructed using a component-by-component

(CBC) approach as discussed in this chapter. For general CBC constructions of integration lattices, we refer to the survey [DKS13] and the references therein. Using a reconstructing rank-1 Chebyshev lattice $\mathrm{CL}(\boldsymbol{z}, M, I)$, we are able to exactly reconstruct all the Chebyshev coefficients $\hat{a}_{\boldsymbol{k}}$, $\boldsymbol{k} \in I$, from the samples $a_I(\boldsymbol{x}_j)$ using a single one-dimensional DCT and easy-to-compute index transforms, see Figure 3.3 for illustration. The computational costs are $\lesssim M \log M + d\,|\mathcal{M}(I)| \lesssim M \log M + d\,2^d\,|I|$, where the extended symmetric index set $\mathcal{M}(I) := \{\boldsymbol{h} \in \mathbb{Z}^d \colon (|h_1|, \ldots, |h_d|)^\top \in I\}$.

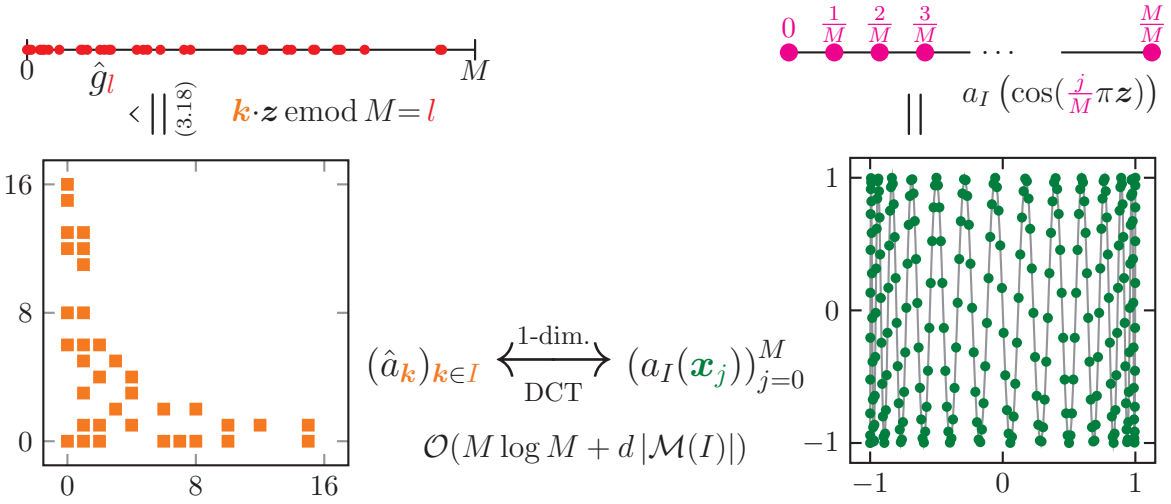

Figure 3.3: DCT between arbitrary index set I and reconstructing rank-1 Chebyshev lattice $\mathrm{CL}(\boldsymbol{z}, M, I)$.

Based on the reconstruction results, we are going to use multivariate algebraic polynomials in Chebyshev form a_I for the approximation of non-periodic functions from subspaces of the analogon of the Wiener algebra

$$\mathcal{A}([-1,1]^d) := \left\{ f \in L_{2,w}([-1,1]^d) \colon \|f|\mathcal{A}([-1,1]^d)\| := \sum_{\boldsymbol{k}\in\mathbb{N}_0^d} |\hat{f}_{\boldsymbol{k}}| < \infty \right\}, \tag{3.4}$$

cf. [Spr97b, Spr00], where the Chebyshev coefficients $\hat{f}_{\boldsymbol{k}}$, $\boldsymbol{k} \in \mathbb{N}_0^d$, of a function $f \in L_{2,w}([-1,1]^d)$ are formally given by

$$\hat{f}_{\boldsymbol{k}} := \frac{2^{|\boldsymbol{k}|_0}}{\pi^d} \int_{\boldsymbol{x}\in[-1,1]^d} \frac{f(\boldsymbol{x})\, T_{\boldsymbol{k}}(\boldsymbol{x})}{\prod_{s=1}^d \sqrt{1-x_s^2}}\, \mathrm{d}\boldsymbol{x}, \quad \boldsymbol{k} \in \mathbb{N}_0^d, \tag{3.5}$$

where $|\boldsymbol{k}|_0 := \sum_{s=1}^d \delta_{k_s,0}$ and the factor $2^{|\boldsymbol{k}|_0}/\pi^d$ is due to the orthogonality relation (3.2). In the following, we characterize a function $f \in \mathcal{A}([-1,1]^d)$ by the decay of its Chebyshev coefficients $\hat{f}_{\boldsymbol{k}}$. Analogously to the subspaces (2.13) of the Wiener algebra $\mathcal{A}(\mathbb{T}^d)$ in the periodic case in Chapter 2, we define the subspaces

$$\mathcal{A}^{\alpha,\beta}([-1,1]^d) := \left\{ f \in L_{2,w}([-1,1]^d) \colon \|f|\mathcal{A}^{\alpha,\beta}([-1,1]^d)\| := \sum_{\boldsymbol{k}\in\mathbb{N}_0^d} \omega^{\alpha,\beta,\mathbf{1}}(\boldsymbol{k})\, |\hat{f}_{\boldsymbol{k}}| < \infty \right\} \tag{3.6}$$

of $\mathcal{A}([-1,1]^d) = \mathcal{A}^{0,0}([-1,1]^d)$ with dominating mixed smoothness $\beta \geq 0$ and isotropic smoothness $\alpha \geq -\beta$, where the weights $\omega^{\alpha,\beta,\mathbf{1}}$ are defined as in (2.12). Moreover, we consider

the subspaces

$$\mathcal{H}^{\alpha,\beta}([-1,1]^d) := \left\{ f \in L_{2,w}([-1,1]^d) \colon \|f|\mathcal{H}^{\alpha,\beta}([-1,1]^d)\| := \sqrt{\sum_{\boldsymbol{k}\in\mathbb{N}_0^d} \omega^{\alpha,\beta,\mathbf{1}}(\boldsymbol{k})^2 \, |\hat{f}_{\boldsymbol{k}}|^2} < \infty \right\} \tag{3.7}$$

of the Hilbert space $L_{2,w}([-1,1]^d) = \mathcal{H}^{0,0}([-1,1]^d)$ analogously to the function spaces (2.11) from the periodic case. We remark that for the one-dimensional case, function spaces with norms equivalent to Sobolev-type spaces $\mathcal{H}^{\alpha,0}([-1,1])$, $\alpha \geq 0$, were considered in [BHS92] for Jacobi polynomials as well as their relation to spaces characterized by the derivatives $D^\nu f$, $\nu \in \mathbb{N}_0$. In the special case of Chebyshev polynomials of the first kind T_k, this means for $m \in \mathbb{N}_0$ the equivalence of the spaces $\mathcal{H}^{m,0}([-1,1])$ and

$$L^2_{\rho,\rho^{(m)}} := \left\{ f \in L_{2,w}([-1,1]) \colon \|f|L^2_{\rho,\rho^{(m)}}\|^2 := \sum_{\nu=0}^{m} \int_{-1}^{1} |D^\nu f(x)|^2 (1-x^2)^{-\frac{1}{2}+\nu} \,\mathrm{d}x < \infty \right\}$$

from [BHS92]. For the two-dimensional case, Sobolev-type spaces $H^\alpha_w([-1,1]^2)$ of order $\alpha \geq 0$ were characterized in [Spr97b], which are equivalent to $\mathcal{H}^{\alpha,0}([-1,1]^2)$, as well as Sobolev-type spaces with dominating mixed smoothness $S^{\beta,\beta}_w H([-1,1]^2)$ of order $\beta \geq 0$ denoted in [Spr97b], which are equivalent to $\mathcal{H}^{0,\beta}([-1,1]^2)$. This concept can be extended to higher dimensions using tensorization, cf. [Spr00, SW10].

Using the Chebyshev coefficients $\hat{f}_{\boldsymbol{k}}$, a function $f \in \mathcal{A}([-1,1]^d)$ can be approximated by the Chebyshev partial sum

$$S_I f := \sum_{\boldsymbol{k}\in I} \hat{f}_{\boldsymbol{k}} \, T_{\boldsymbol{k}}(\circ), \tag{3.8}$$

i.e., by a truncated Chebyshev series which is a multivariate algebraic polynomial in Chebyshev form a_I from (3.1). As in the periodic case, we call the error $f - S_I f$ of this approximation *truncation error*. In practice, we are going to compute approximated Chebyshev coefficients $\hat{f}^{\mathrm{CL}}_{\boldsymbol{k}} \approx \hat{f}_{\boldsymbol{k}}$, $\boldsymbol{k} \in I$, by applying a DCT on the samples $f(\boldsymbol{x}_j)$ taken at the nodes $\boldsymbol{x}_j := \cos(j\pi\boldsymbol{z}/M)$, $j = 0,\dots,M$, of a rank-1 Chebyshev lattice $\mathrm{CL}(\boldsymbol{z}, M)$ followed by computing index transforms, see (3.29). Then, we define an approximation of the function f by the approximated Chebyshev partial sum

$$S^{\mathrm{CL}}_I f := \sum_{\boldsymbol{k}\in I} \hat{f}^{\mathrm{CL}}_{\boldsymbol{k}} \, T_{\boldsymbol{k}}(\circ), \tag{3.9}$$

which itself is a multivariate algebraic polynomial in Chebyshev form a_I with frequencies supported on the index set I. In this work, we concentrate on using reconstructing rank-1 Chebyshev lattices $\mathrm{CL}(\boldsymbol{z}, M, I)$. Analogously to (2.9), we split the *sampling error* $f - S^{\mathrm{CL}}_I f$ into the truncation error $f - S_I f$ and *aliasing error* $S_I f - S^{\mathrm{CL}}_I f$. By the triangle inequality, we obtain

$$\|f - S^{\mathrm{CL}}_I f\| \leq \|f - S_I f\| + \|S_I f - S^{\mathrm{CL}}_I f\|, \tag{3.10}$$

where $\|\circ\|$ is a given norm.

We choose the frequency index set I in a suitable way corresponding to the used function spaces and norms in the error estimates. Correspondingly to the periodic case in (2.14), we define the frequency index sets $I = I^{d,T}_{\mathrm{a},n}$ of refinement $n \geq 1$ by

$$I^{d,T}_{\mathrm{a},n} := \left\{ \boldsymbol{k} \in \mathbb{N}_0^d \colon \omega^{-T,1,\mathbf{1}}(\boldsymbol{k}) = \max(1, \|\boldsymbol{k}\|_1)^{-T} \prod_{s=1}^{d} \max(1, |k_s|) \leq n^{1-T} \right\} \tag{3.11}$$

for shape parameter $-\infty < T < 1$ with the ℓ_1-ball extension

$$I_{\mathrm{a},n}^{d,-\infty} := \left\{ \boldsymbol{k} \in \mathbb{N}_0^d \colon \max(1, \|\boldsymbol{k}\|_1) \leq n \right\}$$

for shape parameter $T = -\infty$. We remark that multivariate algebraic polynomials with hyperbolic cross index sets $I = I_{\mathrm{a},n}^{d,0}$ have already been used for approximations in sparse high-dimensional spectral Galerkin methods, cf. [SW10] and [STW11, Section 8.5]. Please note that we do not use a weight parameter $\boldsymbol{\gamma}$ in our considerations for the non-periodic case to simplify the notation and reduce the amount of technical details, see also the discussion regarding the weight parameter $\boldsymbol{\gamma}$ of the weights (2.12) in the introduction of Chapter 2. Moreover, we have the relation $\mathcal{M}(I_{\mathrm{a},n}^{d,T}) = I_n^{d,T,\mathbf{1}}$ between the frequency index sets $I_{\mathrm{a},n}^{d,T}$ from the non-periodic case and the frequency index sets $I_n^{d,T,\mathbf{1}}$ from the periodic case.

The remaining parts of this chapter are structured as follows.

In Section 3.1, we develop a method for the fast evaluation of an arbitary multivariate algebraic polynomial in Chebyshev form a_I from (3.1) with frequencies supported on a given arbitrary index set $I \subset \mathbb{N}_0^d$ of finite cardinality, $|I| < \infty$, at the nodes $\boldsymbol{x}_j := \cos(\frac{j}{M}\pi\boldsymbol{z})$, $j = 0, \ldots, M$, of an arbitrary rank-1 Chebyshev lattice $\mathrm{CL}(\boldsymbol{z}, M) \subset [-1, 1]^d$, see also [PV15]. In doing so, we introduce additional notation and obtain Algorithm 3.1 for the fast and exact evaluation based on easy-to-compute index transforms and a single one-dimensional DCT, which requires $\mathcal{O}(M \log M + d\, 2^d\, |I|)$ arithmetic operations and these computational costs contain an additional factor 2^d compared to the periodic case in Section 2.1.1. We describe a modified version requiring only $\mathcal{O}(M \log M + d\, |\mathcal{M}(I)|)$ arithmetic operations, which may be a distinct reduction if only a small amount of components of the frequencies $\boldsymbol{k} \in I$ are non-zero, i.e., if only some dimensions are coupled.

In Section 3.2, we develop an approach for the fast and exact reconstruction of an arbitrary multivariate algebraic polynomial in Chebyshev form a_I with frequencies supported on an arbitrary known index set $I \subset \mathbb{N}_0^d$ of finite cardinality, $|I| < \infty$, from sampling values along a reconstructing rank-1 Chebyshev lattice $\mathrm{CL}(\boldsymbol{z}, M, I)$. In Section 3.2.1, we discuss conditions on a rank-1 Chebyshev lattice $\mathrm{CL}(\boldsymbol{z}, M)$ such that the reconstruction of all Chebyshev coefficients $\hat{a}_{\boldsymbol{k}}$, $\boldsymbol{k} \in I$, of such a multivariate algebraic polynomial in Chebyshev form a_I is possible. We describe a method for the fast and exact reconstruction in Algorithm 3.2, which only uses a single one-dimensional DCT and easy-to-compute index transforms. This approach has computational costs of $\mathcal{O}(M \log M + d\, 2^d\, |I|)$, which contain an additional factor of 2^d compared to Algorithm 2.1 in the periodic case. Again, we describe a modified version requiring only $\mathcal{O}(M \log M + d\, |\mathcal{M}(I)|)$ arithmetic operations. In Section 3.2.2, we discuss approaches for obtaining reconstructing rank-1 Chebyshev lattices $\mathrm{CL}(\boldsymbol{z}, M, I)$, see also [PV15]. We remark that for the special case of ℓ_1-ball frequency index sets $I = I_{\mathrm{a},n}^{d,-\infty}$, approaches for obtaining a reconstructing rank-1 Chebyshev lattice $\mathrm{CL}(\boldsymbol{z}, M, I)$ were already discussed in [CP11] and the references therein. In this work, we develop two general methods which allow for the handling of arbitrary frequency index sets $I \subset \mathbb{N}_0^d$ of finite cardinality, $|I| < \infty$. The first method is based on using a reconstructing rank-1 lattice $\Lambda(\boldsymbol{z}, M, \mathcal{M}(I))$ from the periodic case for the non-periodic case, see Theorem 3.4. The second method uses a direct CBC construction approach on the frequency index set I, cf. Algorithm 3.3, using ideas from [SR02, CN04, Käm14a].

In Section 3.3, we briefly discuss relations to other non-periodic approaches. In Section 3.3.1, we give more details for the reconstruction at Padua points and along Lissajous curves. In Section 3.3.2, we explain the relation to tent-transformed rank-1 lattices from [DNP14, SNC16, CKNS16].

In Section 3.4, we consider the approximation of functions f from subspaces $\mathcal{A}^{\alpha,\beta}([-1,1]^d)$ of the analogon of the Wiener algebra $\mathcal{A}([-1,1]^d)$ and of functions f from Sobolev-type spaces of generalized mixed smoothness $\mathcal{H}^{\alpha,\beta}([-1,1]^d)$ for suitable choices of the isotropic smoothness α and dominating mixed smoothness β using rank-1 Chebyshev lattice sampling. We discuss various embeddings between different function spaces in Lemma 3.9 which correspond to the periodic case from Section 2.3.1, see also Figure 2.6a. The allowed parameter choices of dominating mixed smoothness $\beta \geq 0$ and isotropic smoothness $\alpha > -\beta$ for functions $f \in \mathcal{A}^{\alpha,\beta}([-1,1]^d)$ and $f \in \mathcal{H}^{\alpha,\beta+\lambda}([-1,1]^d)$, $\lambda > 1/2$, guarantee the continuous embedding into the analogon of the Wiener algebra $\mathcal{A}([-1,1]^d)$ and consequently the existence of a continuous representative of the function f, cf. Lemma 3.9 and Remark 3.10. Moreover, we develop the general aliasing formula (3.31) in Lemma 3.11 for the approximated Chebyshev coefficients $\hat{f}^{\mathrm{CL}}_{\boldsymbol{k}}$ from (3.29) when using an arbitrary rank-1 Chebyshev lattice $\mathrm{CL}(\boldsymbol{z}, M) \subset [-1,1]^d$. Based on this aliasing formula (3.31), we obtain in Theorem 3.13 for sampling along reconstructing rank-1 Chebyshev lattices $\mathrm{CL}(\boldsymbol{z}, M, I)$ the general result

$$\|f - S^{\mathrm{CL}}_I f | L_\infty([-1,1]^d)\| \leq (1 + 2^{d-1}) \sum_{\boldsymbol{k} \in \mathbb{N}_0^d \setminus I} |\hat{f}_{\boldsymbol{k}}| = (1 + 2^{d-1}) \, \|f - S_I f | \mathcal{A}([-1,1]^d)\|$$

for the sampling error (of continuous representatives) of functions $f \in \mathcal{A}([-1,1]^d)$ and we also estimate the corresponding truncation error by

$$\|f - S_I f | L_\infty([-1,1]^d)\| \leq \sum_{\boldsymbol{k} \in \mathbb{N}_0^d \setminus I} |\hat{f}_{\boldsymbol{k}}| = \|f - S_I f | \mathcal{A}([-1,1]^d)\|.$$

The obtained upper bounds, especially the factor 2^{d-1}, are sharp in certain cases as we see in Example 3.14. For functions $f \in \mathcal{A}^{\alpha,\beta}([-1,1]^d)$ with dominating mixed smoothness $\beta \geq 0$ and isotropic smoothness $\alpha > -\beta$ using frequency index sets $I := I^{d,T}_{\mathrm{a},n}$ with shape parameter $T := -\alpha/\beta$, we obtain in Theorem 3.16 results which are analogous to the results from Theorem 2.17 and 2.24 for the periodic case. For the truncation error $f - S_I f$, we estimate

$$\|f - S_{I^{d,T}_{\mathrm{a},n}} f | L_\infty([-1,1]^d)\| \leq \|f - S_{I^{d,T}_{\mathrm{a},n}} f | \mathcal{A}([-1,1]^d)\| \leq n^{-(\alpha+\beta)} \, \|f | \mathcal{A}^{\alpha,\beta}([-1,1]^d)\|$$

and for sampling along reconstructing rank-1 Chebyshev lattices $\mathrm{CL}(\boldsymbol{z}, M, I^{d,T}_{\mathrm{a},n})$, we estimate the sampling error by

$$\|f - S^{\mathrm{CL}}_{I^{d,T}_{\mathrm{a},n}} f | L_\infty([-1,1]^d)\| \leq (1 + 2^{d-1}) \, n^{-(\alpha+\beta)} \, \|f | \mathcal{A}^{\alpha,\beta}([-1,1]^d)\|.$$

Additionally, we measure the errors with respect to Hilbert space norms. For functions $f \in \mathcal{H}^{\alpha,\beta}([-1,1]^d)$ with smoothness parameters $\beta \geq t \geq 0$ and $\alpha + \beta > r + t \geq 0$ using frequency index sets $I := I^{d,T}_{\mathrm{a},n}$ with shape parameter $T := -\frac{\alpha - r}{\beta - t} \in [-\infty, 1)$, we estimate the truncation error by

$$\|f - S_{I^{d,T}_{\mathrm{a},n}} f | \mathcal{H}^{r,t}([-1,1]^d)\| \leq n^{-(\alpha - r + \beta - t)} \, \|f | \mathcal{H}^{\alpha,\beta}([-1,1]^d)\|.$$

in Theorem 3.17 analogously to Theorem 2.20 from the periodic case. When we restrict the shape parameter $T := -\frac{\alpha - r}{\beta - t} \in [-\frac{r}{t}, -\frac{\alpha}{\beta}]$ and sample along reconstructing rank-1 Chebyshev lattices $\mathrm{CL}(\boldsymbol{z}, M, I^{d,T}_{\mathrm{a},n})$, then we obtain for the sampling error $f - S^{\mathrm{CL}}_{I^{d,T}_{\mathrm{a},n}} f$ (of continuous representatives) of functions $f \in \mathcal{H}^{\alpha,\beta+\lambda}([-1,1]^d)$, $\lambda > 1/2$, the upper bound

$$\|f - S^{\mathrm{CL}}_{I^{d,T}_{\mathrm{a},n}} f | \mathcal{H}^{r,t}([-1,1]^d)\| \leq \left(1 + 2^{d-1} \, (1 + 2\zeta(2\lambda))^{\frac{d}{2}}\right) n^{-(\alpha - r + \beta - t)} \|f | \mathcal{H}^{\alpha,\beta+\lambda}([-1,1]^d)\|$$

corresponding to Theorem 2.26 from the periodic case. We remark that for the case of sparse grid sampling with shape parameter $T := 0$ in the case of isotropic smoothness $r := 0, \alpha := 0$ and dominating mixed smoothness $t := 0$, $\beta > 1/2$, the error estimate

$$\|f - S^{\mathrm{SG}}_{I^{d,0}_{\mathrm{a},n}} f | L_{2,w}([-1,1]^d)\| \lesssim n^{-\beta} \log^{d-1} n \, \|f|\mathcal{H}^{0,\beta}([-1,1]^d)\|.$$

follows from [BNR00, inequality (14)] as a consequence of [Spr97b, Theorem 5], where $S^{\mathrm{SG}}_{I^{d,0}_{\mathrm{a},n}}$ denotes the sparse grid sampling operator, and the additive factor $\lambda > 1/2$ does not occur in this error estimate.

Finally, in Section 3.5, we give numerical examples for the methods and theoretical results of Section 3.2 and 3.4 in up to 25 dimensions.

3.1 Fast evaluation along rank-1 Chebyshev lattices

We consider the evaluation of a multivariate algebraic polynomial in Chebyshev form a_I from (3.1) with frequencies supported on an arbitrary index set $I \subset \mathbb{N}_0^d$, $|I| < \infty$, at the nodes $\boldsymbol{x}_j := \cos(\frac{j}{M}\boldsymbol{z})$, $j = 0, \ldots, M$, of an arbitrary rank-1 Chebyshev lattice $\mathrm{CL}(\boldsymbol{z}, M) \subset [-1,1]^d$,

$$a_I(\boldsymbol{x}_j) = \sum_{\boldsymbol{k} \in I} \hat{a}_{\boldsymbol{k}} \prod_{t=1}^{d} \cos\left(\frac{j}{M} \pi k_t z_t\right), \quad j = 0, \ldots, M. \tag{3.12}$$

Analogously to the approach in Chapter 2, we are going to use a one-dimensional discrete cosine transform of type I (DCT-I) for evaluating (3.12), see also [PV15]. A DCT-I of length $n+1$ applied to an input vector of coefficients $(b_j)_{j=0}^n \in \mathbb{R}^{n+1}$ computes $\hat{b}_k := \sum_{j=0}^n (\varepsilon_j^n)^2 \, b_j \cos(jk\pi/n)$ for $k = 0, \ldots, n$, where $\varepsilon_j^n := 1/\sqrt{2}$ for $j \in \{0, n\}$ and $\varepsilon_j^n := 1$ for $j \in \{1, \ldots, n-1\}$. In order to apply the DCT-I in the multivariate case, we transform the product of cosines $\prod_{t=1}^d \cos(\frac{j}{M}\pi k_t z_t)$ in (3.12) into a cosine of sums,

$$\cos\left(\frac{j}{M}\pi \left(k_1 z_1 + \ldots + k_d z_d\right)\right) = \cos\left(\frac{j}{M}\pi \, \boldsymbol{k} \cdot \boldsymbol{z}\right).$$

In doing so, we introduce additional notation following [PV15, Section II.B]. For a given arbitrary index set $I \subset N_0^d$ of finite cardinality, we define the extended symmetric index set

$$\mathcal{M}(I) := \{\boldsymbol{h} \in \mathbb{Z}^d \colon (|h_1|, \ldots, |h_d|)^\top \in I\},$$

which contains all frequencies $\boldsymbol{k} \in I$ and versions of these frequencies $\boldsymbol{k}$ (repeatedly) mirrored at all coordinate axes. We remark that we have the relation

$$\mathcal{M}(I^{d,T}_{\mathrm{a},n}) = I^{d,T,\mathbf{1}}_n \tag{3.13}$$

between the frequency index set $I^{d,T}_{\mathrm{a},n}$ from the non-periodic case as defined in (3.11) and the frequency index set $I^{d,T,\mathbf{1}}_n$ from the periodic case as defined in (2.14), and this relation will play an important role in this chapter. In addition to the extended symmetric index set $\mathcal{M}(I)$, we define the index sets

$$\mathcal{M}_\nu(I) := \{\boldsymbol{h} \in \mathcal{M}(I) \colon h_\nu \geq 0\}, \ \nu \in \{1, \ldots, d\},$$

which contain all frequencies $\boldsymbol{k} \in I$ and versions of these frequencies (repeatedly) mirrored at all coordinate axes except the ν-th. In Figure 3.4, we depict the ℓ_1-ball frequency index set

$I = I_{\mathrm{a},8}^{2,-\infty}$ as well as the corresponding extended symmetric index set $\mathcal{M}(I_{\mathrm{a},8}^{2,-\infty}) \subset \mathbb{Z}^2$ and mirrored index sets $\mathcal{M}_1(I_{\mathrm{a},8}^{2,-\infty}) \subset \mathbb{N}_0 \times \mathbb{Z}$, $\mathcal{M}_2(I_{\mathrm{a},8}^{2,-\infty}) \subset \mathbb{Z} \times \mathbb{N}_0$. Additionally, we give its cardinalities $|I|$. Here, the cardinalities of the index sets $\mathcal{M}_1(I_{\mathrm{a},8}^{2,-\infty})$ and $\mathcal{M}_2(I_{\mathrm{a},8}^{2,-\infty})$ coincide. Moreover, in Figure 3.5, we show an example for a sparser frequency index set $I \subset \mathbb{N}_0^2$ as well as the corresponding extended symmetric index set $\mathcal{M}(I) \subset \mathbb{Z}^2$ and mirrored index sets $\mathcal{M}_1(I) \subset \mathbb{N}_0 \times \mathbb{Z}$, $\mathcal{M}_2(I) \subset \mathbb{Z} \times \mathbb{N}_0$. We observe that the cardinalities of the index sets $\mathcal{M}_1(I)$ and $\mathcal{M}_2(I)$ differ for this example.

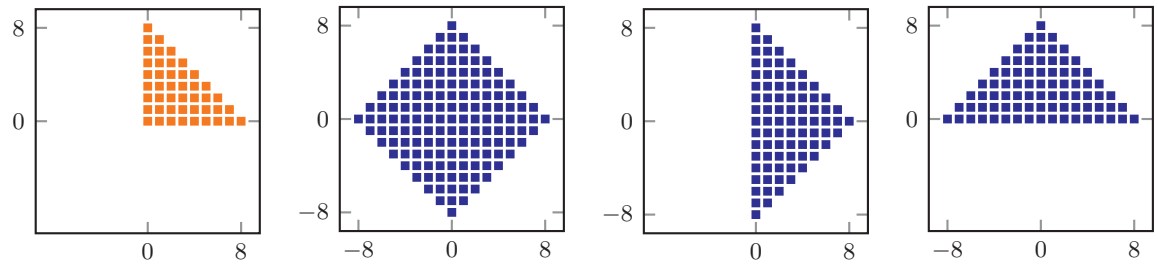

Figure 3.4: From left to right: frequency index sets $I_{\mathrm{a},8}^{2,-\infty}$, $\mathcal{M}(I_{\mathrm{a},8}^{2,-\infty}) = I_8^{2,-\infty,\mathbf{1}}$, $\mathcal{M}_1(I_{\mathrm{a},8}^{2,-\infty})$, $\mathcal{M}_2(I_{\mathrm{a},8}^{2,-\infty})$.

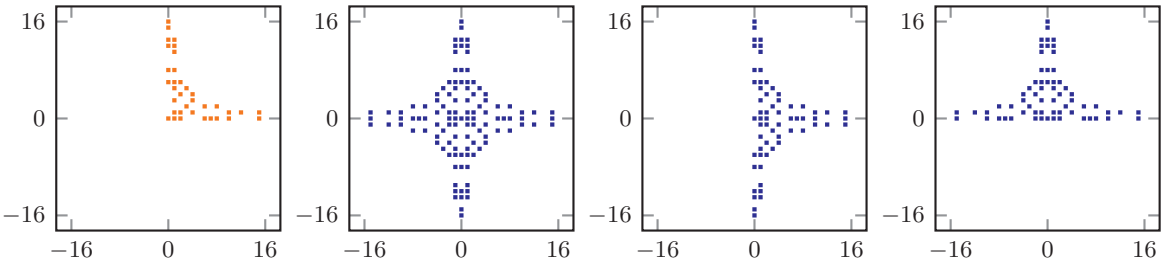

Figure 3.5: From left to right: frequency index sets $I \subset \mathbb{N}_0^2$, $\mathcal{M}(I) \subset \mathbb{Z}^2$, $\mathcal{M}_1(I)$, $\mathcal{M}_2(I)$.

Next, we remark that for $y_1, y_2 \in \mathbb{R}$, we have $\cos(y_1)\cos(y_2) = \frac{1}{2}(\cos(y_1+y_2)+\cos(y_1-y_2))$ and $\cos(y_1)\cos(y_2)\cos(y_3) = \frac{1}{4}(\cos(y_1+y_2+y_3)+\cos(y_1+y_2-y_3)+\cos(y_1-y_2+y_3)+\cos(y_1-y_2-y_3))$. Using induction on the dimension $d \in \mathbb{N}$ and due to the symmetry of the cosine $\cos(x) = \cos(-x)$ for all $x \in \mathbb{R}$, we obtain for $\boldsymbol{y} := (y_1, \ldots, y_d)^\top \in \mathbb{R}$

$$\prod_{t=1}^{d} \cos(y_t) = \sum_{\boldsymbol{m} \in \mathcal{M}_\nu(\{1\}^d)} \frac{1}{2^{d-1}} \cos(\boldsymbol{m} \cdot \boldsymbol{y}) \tag{3.14}$$

$$= \sum_{\boldsymbol{m} \in \{-1,1\}^d} \frac{1}{2^d} \cos(\boldsymbol{m} \cdot \boldsymbol{y}), \tag{3.15}$$

where $\boldsymbol{m} := (m_1, \dots, m_d)^\top$. Applying (3.14) and (3.15) on (3.12), we obtain

$$\begin{aligned} a_I(\boldsymbol{x}_j) &= \sum_{\boldsymbol{k}\in I} \frac{\hat{a}_{\boldsymbol{k}}}{2^{d-1}} \sum_{\boldsymbol{m}\in\mathcal{M}_\nu(\{1\}^d)} \cos\left(\frac{j}{M}\pi\,(\boldsymbol{m}\odot\boldsymbol{k})\cdot\boldsymbol{z}\right), \\ &= \sum_{\boldsymbol{k}\in I} \frac{\hat{a}_{\boldsymbol{k}}}{2^{d}} \sum_{\boldsymbol{m}\in\{-1,1\}^d} \cos\left(\frac{j}{M}\pi\,(\boldsymbol{m}\odot\boldsymbol{k})\cdot\boldsymbol{z}\right), \quad j = 0,\dots,M, \end{aligned}$$

for any $\nu \in \{1,\dots,d\}$ and for an arbitrary multivariate algebraic polynomial in Chebyshev form a_I from (3.1), where $\boldsymbol{m}\odot\boldsymbol{k} := (m_1k_1,\dots,m_dk_d)^\top$. For $M \in \mathbb{N}$ and $l \in \mathbb{Z}$, we define the even-mod relation

$$l \operatorname{emod} M := \begin{cases} l \bmod (2M), & l \bmod (2M) \le M, \\ 2M - (l \bmod (2M)) & \text{else}, \end{cases} \tag{3.16}$$

as well as in the special case $M = 0$, $l \operatorname{emod} 0 := 0$ for $l \in \mathbb{Z}$. For each $l \in \{0,\dots,M\}$, we consider the frequencies $\boldsymbol{k} \in I$ and $\boldsymbol{m} \in \mathcal{M}_\nu(\{1\}^d)$, such that $l = (\boldsymbol{m}\odot\boldsymbol{k})\cdot\boldsymbol{z} \operatorname{emod} M$. Then we obtain

$$a_I(\boldsymbol{x}_j) = \sum_{l=0}^{M} \left(\sum_{\boldsymbol{k}\in I} \sum_{\substack{\boldsymbol{m}\in\mathcal{M}_\nu(\{1\}^d) \\ (\boldsymbol{m}\odot\boldsymbol{k})\cdot\boldsymbol{z} \operatorname{emod} M = l}} \frac{\hat{a}_{\boldsymbol{k}}}{2^{d-1}} \right) \cos(jl\pi/M) \tag{3.17}$$

$$= \sum_{l=0}^{M} \underbrace{\left(\sum_{\boldsymbol{k}\in I} \sum_{\substack{\boldsymbol{m}\in\{-1,1\}^d \\ (\boldsymbol{m}\odot\boldsymbol{k})\cdot\boldsymbol{z} \operatorname{emod} M = l}} \frac{\hat{a}_{\boldsymbol{k}}}{2^{d}} \right)}_{\hat{g}_l} \cos(jl\pi/M), \quad j = 0,\dots,M, \tag{3.18}$$

for the nodes $\boldsymbol{x}_j := \cos(\frac{j}{M}\pi\boldsymbol{z})$ of a rank-1 Chebyshev lattice $\mathrm{CL}(\boldsymbol{z}, M)$, since $\cos(jl\pi/M) = \cos(\frac{j}{M}\pi\,(\boldsymbol{m}\odot\boldsymbol{k})\cdot\boldsymbol{z})$ for all $j = 0,\dots,M$. All inner double sums in (3.17) may have in total up to $2^{d-1}|I|$ many summands and in (3.18) up to $2^d|I|$ many. The outer sum is simply a one-dimensional DCT-I of length $M+1$, which can be computed fast using a fast version of the one-dimensional DCT-I or a one-dimensional FFT. In the end, we can evaluate an arbitrary multivariate algebraic polynomial in Chebyshev form a_I from (3.1) given by its Chebyshev coefficients $\hat{a}_{\boldsymbol{k}}$, $\boldsymbol{k} \in I$, at all nodes $\boldsymbol{x}_j := \cos(\frac{j}{M}\pi\boldsymbol{z})$, $j = 0,\dots,M$, of an arbitrary rank-1 Chebyshev lattice $\mathrm{CL}(\boldsymbol{z}, M) \subset [-1,1]^d$ in $\mathcal{O}(M\log M + d\,2^d|I|)$ arithmetic operations, cf. Algorithm 3.1. Alternatively, using ideas from [SNC16], we may rewrite the coefficient

$$\hat{g}_l := \sum_{\boldsymbol{k}\in I} \sum_{\substack{\boldsymbol{m}\in\{-1,1\}^d \\ (\boldsymbol{m}\odot\boldsymbol{k})\cdot\boldsymbol{z} \operatorname{emod} M = l}} \frac{\hat{a}_{\boldsymbol{k}}}{2^d} = \sum_{\boldsymbol{k}\in I} \sum_{\substack{\boldsymbol{h}\in\mathcal{M}(\{\boldsymbol{k}\}) \\ \boldsymbol{h}\cdot\boldsymbol{z} \operatorname{emod} M = l}} \frac{\hat{a}_{\boldsymbol{k}}}{2^{|\boldsymbol{h}|_0}}$$

in (3.18) and we obtain a modified version of Algorithm 3.1 with computational costs of $\mathcal{O}(M\log M + d\,|\mathcal{M}(I)|)$. If only a small amount of components of the frequencies $\boldsymbol{k} \in I$ are non-zero, i.e., only some dimensions are coupled, we have $|I| \le |\mathcal{M}(I)| \ll 2^d|I|$ and consequently the modified version may require distinctly less arithmetic operations.

Algorithm 3.1 Fast and exact evaluation of an arbitrary multivariate algebraic polynomial in Chebyshev form a_I, $I \subset \mathbb{N}_0^d$, $|I| < \infty$, at the nodes of an arbitrary rank-1 Chebyshev lattice $\mathrm{CL}(\boldsymbol{z}, M) \subset [-1,1]^d$.

Input:	$I \subset \mathbb{N}_0^d$	frequency index set of finite cardinality
	$(\hat{a}_{\boldsymbol{k}})_{\boldsymbol{k}\in I}$	Chebyshev coefficients of multivariate algebraic polynomial in Chebyshev form a_I
	$\mathrm{CL}(\boldsymbol{z}, M)$	arbitrary rank-1 Chebyshev lattice with size parameter $M \in \mathbb{N}$ and generating vector $\boldsymbol{z} \in \mathbb{N}_0^d$

Initialize $\hat{g}_l := 0$ for all $l = 0, \ldots, M$.
for each $\boldsymbol{k} \in I$ and **each** $\boldsymbol{m} \in \{-1,1\}^d$ **do**
  Compute $l := (\boldsymbol{m} \odot \boldsymbol{k}) \cdot \boldsymbol{z} \bmod M$.
  Set $\hat{g}_l := \hat{g}_l + \hat{a}_{\boldsymbol{k}} / 2^d / (\varepsilon_l^M)^2$.
end for
Compute $\boldsymbol{a} := \mathtt{DCT\_I}\left((\hat{g}_l)_{l=0}^M\right)$, i.e. $a_I(\boldsymbol{x}_j) = \sum_{l=0}^M (\varepsilon_j^M)^2\, \hat{g}_l \cos(jl\pi/M)$ for $j = 0, \ldots, M$.

Output:	$\boldsymbol{a} := (a_I(\boldsymbol{x}_j))_{j=0}^M$	function values of a_I at rank-1 Chebyshev lattice nodes $\boldsymbol{x}_j := \cos(j\pi\boldsymbol{z}/M)$, $j = 0, \ldots, M$
Complexity:	$\mathcal{O}(M \log M + d\, 2^d \lvert I\rvert)$	

3.2 Fast reconstruction for known frequency index sets

In this section, we consider the fast and exact reconstruction of a multivariate algebraic polynomial in Chebyshev form a_I from (3.1) with arbitrary frequency index set $I \subset \mathbb{N}_0^d$, $|I| < \infty$. In subsection 3.2.1, we describe a method for reconstructing the Chebyshev coefficients $\hat{a}_{\boldsymbol{k}}$, $\boldsymbol{k} \in I$, of the multivariate algebraic polynomial in Chebyshev form a_I from samples taken at the nodes $\boldsymbol{x}_j$ of a reconstructing rank-1 Chebyshev lattice $\mathrm{CL}(\boldsymbol{z}, M, I)$. In subsection 3.2.2, we discuss strategies for obtaining such a reconstructing rank-1 Chebyshev lattice $\mathrm{CL}(\boldsymbol{z}, M, I)$.

3.2.1 Reconstruction method based on rank-1 Chebyshev lattices

Similar to the fast evaluation, our approach for the fast reconstruction is based on applying a one-dimensional DCT-I on the sampling values $a_I(\boldsymbol{x}_j)$ at the nodes $\boldsymbol{x}_j := \cos(j\pi\boldsymbol{z}/M)$, $j = 0, \ldots, M$, of a rank-1 Chebyshev lattice $\mathrm{CL}(\boldsymbol{z}, M)$ fulfilling a certain property. The presented approach was first published in [PV15, Section III.B]. Formally, we compute the coefficients

$$\begin{aligned} \tilde{\hat{a}}_l &:= \sum_{j=0}^{M} (\varepsilon_j^M)^2\, a_I(\boldsymbol{x}_j) \cos\left(\frac{jl}{M}\pi\right) \\ &= \sum_{j=0}^{M} (\varepsilon_j^M)^2 \sum_{\boldsymbol{k}\in I} \hat{a}_{\boldsymbol{k}} \left(\prod_{t=1}^{d} \cos\left(\frac{j}{M}\pi\, k_t\, z_t\right)\right) \cos\left(\frac{jl}{M}\pi\right) \end{aligned} \tag{3.19}$$

for $l \in \{0, \ldots, M\}$ by a DCT-I of length $M+1$. Inserting formula (3.15), this yields

$$\tilde{\hat{a}}_l = \sum_{\boldsymbol{k}\in I} \frac{\hat{a}_{\boldsymbol{k}}}{2^d} \sum_{\boldsymbol{m}\in\{-1,1\}^d} \sum_{j=0}^{M} (\varepsilon_j^M)^2 \cos\left(\frac{j}{M}\pi\, (\boldsymbol{m}\odot\boldsymbol{k})\cdot\boldsymbol{z}\right) \cos\left(\frac{jl}{M}\pi\right)$$

for $l \in \{0, \ldots, M\}$. We remark that the orthogonality relation

$$\frac{2}{n}\varepsilon_k^n \varepsilon_{k'}^n \sum_{j=0}^{n} (\varepsilon_j^n)^2 \cos\left(\frac{jk\pi}{n}\right) \cos\left(\frac{jk'\pi}{n}\right) = \delta_{k,k'},\ k, k' \in \{0, \ldots, n\} \tag{3.20}$$

holds, where $\delta_{k,k'}$ is Kronecker's delta, see e.g. [RY90, Section 2.4], and that

$$\left\{\boldsymbol{m} \odot \boldsymbol{k} \colon \boldsymbol{m} \in \{-1, 1\}^d\right\} = \mathcal{M}(\{\boldsymbol{k}\}) \text{ for } \boldsymbol{k} \in I.$$

We consider the indices $l := \boldsymbol{k} \cdot \boldsymbol{z} \operatorname{emod} M$ for frequencies $\boldsymbol{k} \in I$ and consequently, we obtain

$$\tilde{\hat{a}}_l = \sum_{\boldsymbol{h} \in \mathcal{M}(I)} \frac{\hat{a}_{(|h_1|, \ldots, |h_d|)^\top}}{2^d} \left(\prod_{s=1}^{d} 2^{\delta_{h_s,0}}\right) \sum_{j=0}^{M} (\varepsilon_j^M)^2 \cos\left(\frac{j}{M}\pi\, \boldsymbol{h} \cdot \boldsymbol{z}\right) \cos\left(\frac{j}{M}\pi\, \boldsymbol{k} \cdot \boldsymbol{z}\right). \tag{3.21}$$

Using the orthogonality relation (3.20), we obtain that the summands of each coefficient $\tilde{\hat{a}}_l$, $l := \boldsymbol{k} \cdot \boldsymbol{z} \operatorname{emod} M$ for frequencies $\boldsymbol{k} \in I$, consist solely of the Chebyshev coefficient $\hat{a}_{\boldsymbol{k}}$ if and only if

$$\boldsymbol{k} \cdot \boldsymbol{z} \operatorname{emod} M \neq \boldsymbol{h} \cdot \boldsymbol{z} \operatorname{emod} M \text{ for all } \boldsymbol{k} \in I \text{ and } \boldsymbol{h} \in \mathcal{M}(I),\ \boldsymbol{k} \neq (|h_1|, \ldots, |h_d|)^\top. \tag{3.22}$$

For example, all the rank-1 Chebyshev lattices $\mathrm{CL}(\boldsymbol{z}, M)$ in Figure 3.2 fulfill property (3.22) for the ℓ_1-ball frequency index set $I = I_{\mathrm{a},8}^{2,-\infty}$ in Figure 3.4 and the rank-1 Chebyshev lattice $\mathrm{CL}(\boldsymbol{z}, M)$ in Figure 3.3 fulfills this property for the frequency index set I depicted therein.

Due to the symmetry of the emod operator, we can reduce the number of frequencies $\boldsymbol{h}$ in condition (3.22) by a factor of (about) two.

Lemma 3.1. *([PV15, Lemma III.1]). For $M \in \mathbb{N}_0$ and $l \in \mathbb{Z}$, we have $l \operatorname{emod} M = (-l) \operatorname{emod} M$.*

Proof. We consider the two different cases in the definition of the emod operator and additionally treat the case $l = 0$. For $0 < l \bmod (2M) < M$, we have $M < (-l) \bmod (2M) \leq 2M - 1$ and this means $(-l) \operatorname{emod} M = 2M - ((-l) \bmod (2M)) = 2M - (2M - (l \bmod (2M))) = l \operatorname{emod} M$. Otherwise, for $M < l \bmod (2M) < 2M$, we obtain $0 < (-l) \bmod (2M) < M$ and this yields $(-l) \operatorname{emod} M = (-l) \bmod (2M) = 2M - (l \bmod (2M)) = l \operatorname{emod} M$. For the remaining cases $l \bmod (2M) = 0$ and $l \bmod (2M) = M$, we also obtain $(-l) \operatorname{emod} M = l \operatorname{emod} M$. ∎

Lemma 3.2. *([PV15, Lemma III.2]). For a given arbitrary index set $I \subset \mathbb{N}_0^d$ of finite cardinality, $|I| < \infty$, let $\tilde{I} \subset \mathbb{Z}^d$ be an arbitrary index set with the property $\mathcal{M}(I) = \tilde{I} \cup \{-\boldsymbol{h} \colon \boldsymbol{h} \in \tilde{I}\}$. Then, condition (3.22) is equivalent to*

$$\boldsymbol{k} \cdot \boldsymbol{z} \operatorname{emod} M \neq \boldsymbol{h} \cdot \boldsymbol{z} \operatorname{emod} M \text{ for all } \boldsymbol{k} \in I \text{ and } \boldsymbol{h} \in \tilde{I},\ \boldsymbol{k} \neq (|h_1|, \ldots, |h_d|)^\top. \tag{3.23}$$

Proof. Due to $(-\boldsymbol{h}) \cdot \boldsymbol{z} = -(\boldsymbol{h} \cdot \boldsymbol{z})$ for $\boldsymbol{h} \in \mathbb{Z}^d$, we obtain

$$(-\boldsymbol{h}) \cdot \boldsymbol{z} \operatorname{emod} M = \boldsymbol{h} \cdot \boldsymbol{z} \operatorname{emod} M \text{ for } \boldsymbol{h} \in \mathbb{Z}^d \tag{3.24}$$

from Lemma 3.1 and the assertion follows. ∎

Corollary 3.3. *([PV15, Corollary III.3]). For any $\nu \in \{1,\ldots,d\}$, condition* (3.22) *is equivalent to*

$$\boldsymbol{k}\cdot\boldsymbol{z} \bmod M \neq \boldsymbol{h}\cdot\boldsymbol{z} \bmod M \text{ for all } \boldsymbol{k}\in I \text{ and } \boldsymbol{h}\in\mathcal{M}_\nu(I),\ \boldsymbol{k}\neq(|h_1|,\ldots,|h_d|)^\top. \quad (3.25)$$

If the equivalent conditions (3.22), (3.23) or (3.25) are fulfilled, we can reconstruct the Chebyshev coefficients $\hat{a}_{\boldsymbol{k}}$, $\boldsymbol{k}\in I$, in the following way. We apply a DCT-I to the sampling values $a_I(\boldsymbol{x}_j) = a_I(\cos(j\pi\boldsymbol{z}/M))$, $j=0,\ldots,M$, which yields the coefficients $\tilde{\hat{a}}_l$, $l\in\{0,\ldots,M\}$, in (3.19). Then, we obtain the Chebyshev coefficients $\hat{a}_{\boldsymbol{k}}$, $\boldsymbol{k}\in I$, of the multivariate algebraic polynomial in Chebyshev form a_I by

$$\hat{a}_{\boldsymbol{k}} = \frac{2^d(\varepsilon_l^M)^2}{M}\frac{\tilde{\hat{a}}_l}{|\{\boldsymbol{m}\in\mathcal{M}_\nu(\{1\}^d)\colon(\boldsymbol{m}\odot\boldsymbol{k})\cdot\boldsymbol{z}\bmod M = l\}|} \quad (3.26)$$

with $l := \boldsymbol{k}\cdot\boldsymbol{z} \bmod M$ for all frequencies $\boldsymbol{k}\in I$ and any $\nu\in\{1,\ldots,d\}$. Using a fast algorithm for the DCT-I, this computation can be performed in $\mathcal{O}(M\log M + d\,2^d|I|)$ arithmetic operations.

Analogously to the periodic case, we will name a rank-1 Chebyshev lattice $\mathrm{CL}(\boldsymbol{z},M)$ which fulfills the equivalent *reconstruction properties* (3.22), (3.23) and (3.25) for a given frequency index set $I\subset\mathbb{N}_0^d$ *reconstructing rank-1 Chebyshev lattice* for I and this will be denoted by $\mathrm{CL}(\boldsymbol{z},M,I)$. We stress the fact that throughout the discussions in this section, the frequency index set $I\subset\mathbb{N}_0^d$ was arbitrarily chosen of finite cardinality, $|I|<\infty$.

In Algorithm 3.2, we summarize the fast and exact reconstruction of the Chebyshev coefficients $\hat{a}_{\boldsymbol{k}}$, $\boldsymbol{k}\in I$, based on samples of the multivariate algebraic polynomial in Chebyshev form a_I at nodes $\boldsymbol{x}_j := \cos(j\pi\boldsymbol{z}/M)$ of a reconstructing rank-1 Chebyshev lattice $\mathrm{CL}(\boldsymbol{z},M,I)$. The realization requires only few lines of Octave / MATLAB code,

```
a_hat_tilde = dct_I( (a_I(x_j))_{j=0}^M );
a_hat_tilde(1) = a_hat_tilde(1) / 2;
if M > 0; a_hat_tilde(end) = a_hat_tilde(end) / 2; end;
for ik = 1:size(I,1)
  k_m = repmat(I(ik,:),2^(d-1),1) .* M_nu({1}^d);
  factor(ik) = length(find(emod(k_m*z',M)==emod(I(ik,:)*z',M)));
end
(a_hat_k)_{k in I} = 2^d / M ./ factor .* a_hat_tilde(emod(I*z',M)+1);
```

cf. [Vol16a], and has an arithmetic complexity of $\mathcal{O}(M\log M + d\,2^d\,|I|)$. We can rewrite the computation in (3.26) and in the for loop in Algorithm 3.2 as

$$\hat{a}_{\boldsymbol{k}}^{\mathrm{CL}} = \frac{2^{|\boldsymbol{k}|_0+1}\,(\varepsilon_l^M)^2}{M}\frac{\tilde{\hat{a}}_l}{|\{\boldsymbol{h}\in\mathcal{M}(\{\boldsymbol{k}\})\colon\boldsymbol{h}\cdot\boldsymbol{z}\bmod M = l\}|},\quad l := \boldsymbol{k}\cdot\boldsymbol{z}\bmod M,\quad \boldsymbol{k}\in I,$$

and we obtain an arithmetic complexity of $\mathcal{O}(M\log M + d\,|\mathcal{M}(I)|)$, which may be distinctly smaller if only a small amount of components of the frequencies $\boldsymbol{k}\in I$ are non-zero.

3.2.2 Building reconstructing rank-1 Chebyshev lattices

For an arbitrary frequency index set $I\subset\mathbb{N}_0^d$ of finite cardinality, $|I|<\infty$, we just discussed how to obtain the Chebyshev coefficients $\hat{a}_{\boldsymbol{k}}$, $\boldsymbol{k}\in I$, from samples of a multivariate algebraic polynomial in Chebyshev form a_I at nodes $\boldsymbol{x}_j$ of a reconstructing rank-1 Chebyshev

Algorithm 3.2 Fast and exact reconstruction of a multivariate algebraic polynomial in Chebyshev form a_I from sampling values on a reconstructing rank-1 Chebyshev lattice $\mathrm{CL}(\boldsymbol{z}, M, I)$.

Input:	$I \subset \mathbb{N}_0^d$	frequency index set of finite cardinality, $\lvert I\rvert < \infty$
	$\mathrm{CL}(\boldsymbol{z}, M, I)$	reconstructing rank-1 Chebyshev lattice for I with size parameter $M \in \mathbb{N}$ and generating vector $\boldsymbol{z} \in \mathbb{N}_0^d$
	$\boldsymbol{a} := (a_I(\boldsymbol{x}_j))_{j=0}^M$	sampling values of a_I at nodes $\boldsymbol{x}_j := \cos(j\pi\boldsymbol{z}/M)$ of $\mathrm{CL}(\boldsymbol{z}, M, I)$

Compute $\tilde{\hat{\boldsymbol{a}}} := \texttt{DCT\_I}(\boldsymbol{a})$, i.e. $\sum_{j=0}^M (\varepsilon_j^M)^2\, a_I\left(\cos(j\pi\boldsymbol{z}/M)\right)\cos(jl\pi/M)$ for $l = 0, \ldots, M$.
for each $\boldsymbol{k} \in I$ **do**
Compute $l := \boldsymbol{k}\cdot\boldsymbol{z} \bmod M$.

$$\hat{a}_{\boldsymbol{k}} = \hat{a}_{\boldsymbol{k}}^{\mathrm{CL}} := \frac{2^d (\varepsilon_l^M)^2}{M} \frac{\tilde{\hat{a}}_l}{\lvert\{\boldsymbol{m} \in \mathcal{M}_\nu(\{1\}^d) \colon (\boldsymbol{m}\odot\boldsymbol{k})\cdot\boldsymbol{z} \bmod M = l\}\rvert}.$$

end for

Output:	$\hat{\boldsymbol{a}} := \left(\hat{a}_{\boldsymbol{k}}^{\mathrm{CL}}\right)_{\boldsymbol{k}\in I}$	exact Chebyshev coefficients of a_I
Complexity:	$\mathcal{O}(M \log M + d\, 2^d \lvert I\rvert)$	

lattice $\mathrm{CL}(\boldsymbol{z}, M, I)$, which fulfills the reconstruction properties (3.22), (3.23) and (3.25) by definition. Next, we present two approaches for the easy construction.

The first construction method will be based on the search strategy from the periodic case in Section 2.2.1, cf. Algorithm 2.2 and 2.3. For this, we show the relation to reconstructing rank-1 lattices $\Lambda(\boldsymbol{z}, \hat{M}, \hat{I})$, $\lvert\hat{I}\rvert < \infty$, of multivariate trigonometric polynomials $p_{\hat{I}}$, where we denote the frequency index set $\subset \mathbb{Z}^d$ from the periodic case by $\hat{I}$ and the rank-1 lattice size by $\hat{M}$. This relation also leads to an upper bound in the non-periodic case on the size parameter M for the existence of a reconstructing rank-1 Chebyshev lattice $\mathrm{CL}(\boldsymbol{z}, M, I)$ in Corollary 3.6. We remark, that such a relation has already been considered for tent-transformed rank-1 lattices in [SNC16] in a different non-periodic setting, see also Section 3.3.2.

Theorem 3.4. *([PV15, Theorem IV.2]). Let $I \subset \mathbb{N}_0^d$ be an arbitrary index set of finite cardinality, $\lvert I\rvert < \infty$. Moreover, let $\Lambda(\boldsymbol{z}, \hat{M}, \hat{I}) := \{\frac{j}{\hat{M}}\boldsymbol{z} \bmod \mathbf{1} \colon j = 0, \ldots, \hat{M}-1\}$ be a reconstructing rank-1 lattice with generating vector $\boldsymbol{z} \in \mathbb{N}_0^d$ and even rank-1 lattice size $\hat{M} \in 2\mathbb{N}$ for the extended symmetric index set $\hat{I} := \mathcal{M}(I)$, i.e.,*

$$\boldsymbol{h}\cdot\boldsymbol{z} \not\equiv \boldsymbol{h'}\cdot\boldsymbol{z} \pmod{\hat{M}} \text{ for all } \boldsymbol{h}, \boldsymbol{h'} \in \mathcal{M}(I),\ \boldsymbol{h} \neq \boldsymbol{h'}. \tag{3.27}$$

Then, the rank-1 Chebyshev lattice $\mathrm{CL}(\boldsymbol{z}, M = \frac{\hat{M}}{2})$ fulfills the equivalent conditions (3.22), (3.23) and (3.25), i.e., we are able to exactly reconstruct all the Chebyshev coefficients $\hat{a}_{\boldsymbol{k}}$, $\boldsymbol{k} \in I$, of a multivariate algebraic polynomial in Chebyshev form a_I from (3.1) based on samples of a_I at the nodes $\boldsymbol{x}_j := \cos(j\pi\boldsymbol{z}/\frac{\hat{M}}{2})$, $j = 0, \ldots, \frac{\hat{M}}{2}$, of the reconstructing rank-1 Chebyshev lattice $\mathrm{CL}(\boldsymbol{z}, \frac{\hat{M}}{2}, I)$.

Proof. For $\boldsymbol{h} \in \mathcal{M}(I)$, we consider the values

$$\boldsymbol{h}\cdot\boldsymbol{z} \operatorname{emod} \frac{\hat{M}}{2} = \begin{cases} \boldsymbol{h}\cdot\boldsymbol{z} \bmod \hat{M}, & \boldsymbol{h}\cdot\boldsymbol{z} \bmod \hat{M} \leq \frac{\hat{M}}{2}, \\ \hat{M} - (\boldsymbol{h}\cdot\boldsymbol{z} \bmod \hat{M}) & \text{else.} \end{cases}$$

We remark that $\boldsymbol{h}\cdot\boldsymbol{z} \operatorname{emod} \frac{\hat{M}}{2} \in \{0, \ldots, \frac{\hat{M}}{2}\}$. Due to property (3.27), all values $\boldsymbol{h}\cdot\boldsymbol{z} \bmod \hat{M} \in$

$\{0,\dots,\hat{M}-1\}$ are distinct for $\boldsymbol{h}\in\mathcal{M}(I)$ and we obtain for each $l\in\{0,\dots,\hat{M}/2\}$ that one of the following three cases may occur: Either

1. exactly two distinct frequencies $\boldsymbol{h},\boldsymbol{h'}\in\mathcal{M}(I)$ exist such that $\boldsymbol{h}\cdot\boldsymbol{z}\bmod\frac{\hat{M}}{2}=\boldsymbol{h'}\cdot\boldsymbol{z}\bmod\frac{\hat{M}}{2}=l$, or
2. exactly one frequency $\boldsymbol{h}\in\mathcal{M}(I)$ exists such that $\boldsymbol{h}\cdot\boldsymbol{z}\bmod\frac{\hat{M}}{2}=l$, or
3. such a frequency does not exist for l.

In the first case, $\boldsymbol{h'}=-\boldsymbol{h}$ follows, since for each $\boldsymbol{h}\in\mathcal{M}(I)\setminus\{\boldsymbol{0}\}$, also the frequency $-\boldsymbol{h}\in\mathcal{M}(I)\setminus\{\boldsymbol{0}\}$ and we have (3.24) with $M:=\frac{\hat{M}}{2}$, i.e., $(-\boldsymbol{h})\cdot\boldsymbol{z}\bmod\frac{\hat{M}}{2}=\boldsymbol{h}\cdot\boldsymbol{z}\bmod\frac{\hat{M}}{2}=l$.
The second case can only occur for $\boldsymbol{h}=\boldsymbol{0}$, since otherwise the (non-zero) frequency $-\boldsymbol{h}\in\mathcal{M}(I)\setminus\{\boldsymbol{0}\}$, $-\boldsymbol{h}\neq\boldsymbol{h}$, and this would yield $(-\boldsymbol{h})\cdot\boldsymbol{z}\bmod\frac{\hat{M}}{2}=\boldsymbol{h}\cdot\boldsymbol{z}\bmod\frac{\hat{M}}{2}$ which would be in contradiction to the assumed uniqueness of case 2.
In total, we obtain $\boldsymbol{h}\cdot\boldsymbol{z}\bmod\frac{\hat{M}}{2}\neq\boldsymbol{h'}\cdot\boldsymbol{z}\bmod\frac{\hat{M}}{2}$ for all $\boldsymbol{h},\boldsymbol{h'}\in\mathcal{M}(I)$, $(|h_1|,\dots,|h_d|)^\top\neq(|h'_1|,\dots,|h'_d|)^\top$, implying condition (3.22) since $I\subset\mathcal{M}(I)$. ■

Remark 3.5. ([PV15, Remark IV.3]). Condition (3.22) and (3.27) with $\hat{M}=2M$ are not equivalent in general. For instance, the generating vector $\boldsymbol{z}:=(8,9)^\top$ and size parameter $M:=72$ from Fig. 3.2a fulfill condition (3.22) for $I=I_{\mathrm{a},8}^{2,-\infty}$ but not condition (3.27) with $\hat{M}=2M$. Clearly, there exist cases where both the conditions (3.22) and (3.27) are fulfilled, see e.g. the examples in Fig. 3.2b and 3.2c, which fulfill both conditions for $I=I_{\mathrm{a},8}^{2,-\infty}$. □

Corollary 3.6. *(see [PV15, Remark IV.4]). For a given frequency index set $I\subset\mathbb{N}_0^d$, $1\leq|I|<\infty$, and any prime size parameter*

$$M\geq\max\left\{\frac{|\mathcal{D}(\mathcal{M}(I))|+3}{2},\max_{\boldsymbol{k}\in I}2\|\boldsymbol{k}\|_\infty+1\right\},\tag{3.28}$$

there always exists a generating vector $\boldsymbol{z}\in\mathbb{N}_0^d$ such that the rank-1 Chebyshev lattice $\mathrm{CL}(\boldsymbol{z},M)$ is a reconstructing rank-1 Chebyshev lattice $\mathrm{CL}(\boldsymbol{z},M,I)$, which is suitable for the reconstruction of multivariate algebraic polynomials in Chebyshev form a_I from (3.1). Moreover, there always exists a reconstructing rank-1 Chebyshev lattice $\Lambda(\boldsymbol{z},M,I)$ for the frequency index set I with prime size parameter

$$M\leq\max\left\{\frac{2}{3}(|\mathcal{M}(I)|^2-|\mathcal{M}(I)|+8),\max_{\boldsymbol{k}\in I}3\|\boldsymbol{k}\|_\infty\right\}.$$

For such prime size parameter M, the generating vector $\boldsymbol{z}\in\mathbb{N}_0^d$ can be constructed using the component-by-component approach in Algorithm 2.2 with $I_{\mathrm{input}}:=\mathcal{M}(I)$ and $M_{\mathrm{start}}:=2M$.

Proof. We apply Theorem 2.4 on the index set $I:=\mathcal{M}(I)$. This yields that for any prime $\hat{M}\geq\max\left\{\frac{|\mathcal{D}(\mathcal{M}(I))|+3}{2},\max_{\boldsymbol{k}\in I}2\|\boldsymbol{k}\|_\infty+1\right\}$, there exists a reconstructing rank-1 lattice $\Lambda(\boldsymbol{z},\hat{M})$ for $\mathcal{M}(I)$ and the generating vector $\boldsymbol{z}$ can be constructed component-by-component. If $\Lambda(\boldsymbol{z},\hat{M})$ is a reconstructing rank-1 lattice for $\mathcal{M}(I)$, this is also true for $\Lambda(\boldsymbol{z},2\hat{M})$. Applying Theorem 3.4 yields that the rank-1 lattice fulfills condition (3.22) and we have the lower bound (3.28). The upper bound follows correspondingly. ■

Remark 3.7. If the reconstructing rank-1 Chebyshev lattice $\mathrm{CL}(\boldsymbol{z}, M, I)$ fulfills condition (3.27) with $\hat{M} = 2M$, then we may rewrite formula (3.26) as

$$\hat{a}_{\boldsymbol{k}} = \frac{\max(2, 2^{|\boldsymbol{k}|_0})\,(\varepsilon_l^M)^2}{M}\,\tilde{\hat{a}}_l, \quad l := \boldsymbol{k}\cdot\boldsymbol{z} \bmod M, \quad \boldsymbol{k} \in I,$$

i.e., we do not need to compute the cardinalities $|\{\boldsymbol{m} \in \mathcal{M}_\nu(\{1\}^d)\colon (\boldsymbol{m}\odot\boldsymbol{k})\cdot\boldsymbol{z} \bmod M = l\}|$ in the denominator of (3.26). □

Alternatively to building a reconstructing rank-1 Chebyshev lattice $\mathrm{CL}(\boldsymbol{z}, M, I)$ by applying Algorithm 2.2 in combination with Theorem 3.4, one may use a direct component-by-component approach which tests for condition (3.25) of the non-periodic case, see also [PV15, Fig. 5]. This means, we split the search for a reconstructing rank-1 Chebyshev lattice $\mathrm{CL}(\boldsymbol{z}, M, I)$ into two phases. First, given a size parameter M which is large enough, we perform a component-by-component search for a generating vector $\boldsymbol{z} \in \mathbb{N}_0^d$ which fulfills the equivalent conditions (3.22), (3.23) and (3.25). Second, we determine the smallest size parameter M for this generating vector $\boldsymbol{z}$. This approach is described as Algorithm 3.3.

Algorithm 3.3 ([PV15, Fig. 5]). Construction of reconstructing rank-1 Chebyshev lattice $\mathrm{CL}(\boldsymbol{z}, M, I_{\mathrm{input}})$ suitable for reconstruction of multivariate algebraic polynomials in Chebyshev form a_I from (3.1) supported on the index set $I := I_{\mathrm{input}}$.

Input: index set $I_{\mathrm{input}} \subset \mathbb{N}_0^d$, parameter $\nu \in \{1, \dots, d\}$.
1: Determine initial size parameter M_{start}, see e.g. Corollary 3.6.
2: **for** $t := 1, \dots, d$ **do**
3: **for** $z_t := 0, \dots, M_{\mathrm{start}}$ **do**
4: **if** condition (3.25) is valid for $I := \{(k_1, \dots, k_t)^\top \colon \boldsymbol{k} \in I_{\mathrm{input}}\}$, $\boldsymbol{z} := (z_1, \dots, z_t)^\top$, $M := M_{\mathrm{start}}$ **then**
5: **break**
6: **end if**
7: **end for**
8: **if** $z_t = M_{\mathrm{start}}$ **and** condition (3.25) is not valid for $I := \{(k_1, \dots, k_t)^\top \colon \boldsymbol{k} \in I_{\mathrm{input}}\}$, $\boldsymbol{z} := (z_1, \dots, z_t)^\top$, $M := M_{\mathrm{start}}$ **then**
9: increase M_{start} and **goto** line 2.
10: **end if**
11: **end for**
12: **for** $M := |I_{\mathrm{input}}| - 1, \dots, M_{\mathrm{start}}$ **do**
13: **if** condition (3.25) is valid for $I := I_{\mathrm{input}}$, $\boldsymbol{z} := (z_1, \dots, z_d)^\top$, M **then**
14: **break**
15: **end if**
16: **end for**
Output: generating vector $\boldsymbol{z} \in \mathbb{N}_0^d$ and size parameter $M \in \mathbb{N}_0$ fulfilling condition (3.22), (3.23), (3.25) for index set $I := I_{\mathrm{input}}$.

3.3 Relations to other non-periodic approaches

In this section, we shortly discuss relations of rank-1 Chebyshev lattices $\mathrm{CL}(\boldsymbol{z}, M)$ with Padua points and nodes on Lissajous curves as well as tent-transformed rank-1 lattices.

3.3.1 Nodes on Lissajous curves

As mentioned in the introduction of this chapter, the nodes $\boldsymbol{x}_j := (\cos(\frac{j}{M}\pi z_1), \dots, \cos(\frac{j}{M}\pi z_d))^\top$, $j = 0, \dots, M$, of a rank-1 Chebyshev lattice $\mathrm{CL}(\boldsymbol{z}, M)$ are equispaced points on a Lissajous curve $\mathrm{LC}_{\boldsymbol{z}}(t) := (\cos(z_1 t), \dots, \cos(z_d t))^\top \in [-1, 1]^d$, $t \in [0, \pi]$, having $t := j\pi/M$, see e.g. [BDMV16, DE15].

In two dimensions for a parameter $n \in \mathbb{N}$, choosing the generating vector $\boldsymbol{z} := (n, n+1)^\top$ and the size parameter $M := n(n+1)$ yields the so-called Padua points $\boldsymbol{x}_j := (\cos(j\pi/(n+1)), \cos(j\pi/n))^\top = \cos(j\pi \boldsymbol{z}/M)$, $j = 0, \dots, M$, of the rank-1 Chebyshev lattice $\mathrm{PP}(n) := \mathrm{CL}(\boldsymbol{z}, M)$, cf. [BCD+06]. As discussed in [BCD+06, Section 2], the Padua point set $\mathrm{PP}(n)$ only consists of $|I_{\mathrm{a},n}^{2,-\infty}| = \binom{n+2}{2} = \frac{n^2}{2} + \frac{3}{2}n + 1$ distinct points, whereas the size parameter $M = n^2 + n$, and $\mathrm{PP}(n)$ is a reconstructing rank-1 Chebyshev lattice for the ℓ_1-ball frequency index set $I_{\mathrm{a},n}^{2,-\infty}$ as the following lemma states.

Lemma 3.8. *([PV15, Lemma IV.1]). Let the frequency index set $I = I_{\mathrm{a},n}^{2,-\infty} := \{\boldsymbol{k} \in \mathbb{N}_0^2 \colon k_1 + k_2 \le n\}$ be the two-dimensional ℓ_1-ball of refinement $n \in \mathbb{N}$. Then, the Padua point set $\mathrm{PP}(n)$ is a reconstructing rank-1 Chebyshev lattice $\mathrm{CL}(\boldsymbol{z}, M, I_{\mathrm{a},n}^{2,-\infty})$ and we can exactly reconstruct any two-variate algebraic polynomial of total degree $\le n$ from sampling values at the nodes $\boldsymbol{x}_j$ of the Padua point set $\mathrm{PP}(n)$ using Algorithm 3.2.*

Proof. The assertion follows from the Lagrange interpolation formula [CDV08, (7c)]. Alternatively, condition (3.25) from Corollary 3.3 can be verified. ∎

Explicit choices of the generating vector $\boldsymbol{z}$ and size parameter M of a reconstructing rank-1 Chebyshev lattice $\mathrm{CL}(\boldsymbol{z}, M, I_{\mathrm{a},n}^{3,-\infty})$ for the three-dimensional ℓ_1-ball index set $I_{\mathrm{a},n}^{3,-\infty}$ are also known, see e.g. [CP11, BDMV16, BDMV15], or for certain subsets of d-dimensional ℓ_1-ball frequency index $I_{\mathrm{a},n}^{d,-\infty}$, cf. [DE15]. We remark that the obtained results yield a so-called hyperinterpolation for dimensions $d \ge 3$ and that any cubature formula which exactly integrates a multivariate algebraic polynomial of total degree $\le 2n$ may be used for the exact reconstruction of a polynomial of total degree $\le n$, cf. [Slo95, CP11].

3.3.2 Tent transformed rank-1 lattices

Point sets where the tent transform (or baker's transform)

$$\psi \colon [0,1] \to [0,1], \quad \psi(x) := 1 - |2x - 1|,$$

is applied component-wise to (shifted) lattices were introduced in [Hic02], and tent-transformed rank-1 lattices

$$\mathrm{P}_\psi(\boldsymbol{z}, M) := \{\psi(j\boldsymbol{z}/M \bmod \boldsymbol{1}) \colon j = 0, \dots, M-1\}$$

were considered in [DNP14] for the (approximate) integration of functions from smooth subspaces of $L_2([0,1]^d)$. Functions $g \in L_2([0,1]^d)$ are expanded into a cosine series $g(\boldsymbol{x}) := \sum_{\boldsymbol{k} \in \mathbb{N}_0^d} \hat{g}_{\boldsymbol{k}} \phi_{\boldsymbol{k}}(\boldsymbol{x})$, $\hat{g}_{\boldsymbol{k}} \in \mathbb{R}$, of half-periodic cosine functions

$$\phi_{\boldsymbol{k}}(\boldsymbol{x}) := \prod_{s=1}^{d} \sqrt{2}^{\,\delta_{0,k_s}} \cos(\pi k_s x_s), \quad \boldsymbol{k} \in \mathbb{N}_0^d,$$

where the latter form an orthonormal basis of $L_2([0,1]^d)$. In [SNC16], the reconstruction of truncated series expansions

$$g_I(\boldsymbol{x}) := \sum_{\boldsymbol{k} \in I} \hat{g}_{\boldsymbol{k}} \phi_{\boldsymbol{k}}(\boldsymbol{x})$$

was considered for weighted hyperbolic cross frequency index sets $I \subset \mathbb{N}_0^d$ using special tent-transformed rank-1 lattices $\mathrm{P}_\psi(\boldsymbol{z}, M)$. We remark that the functions g_I are not algebraic polynomials in general. It was discussed in [SNC16] that the reconstruction is possible if property (3.27) is fulfilled. This means, if the generating vector $\boldsymbol{z}$ and rank-1 lattice size M belong to a reconstructing rank-1 lattice $\Lambda(\boldsymbol{z}, M, \mathcal{M}(I))$ for the extended symmetric index set $\mathcal{M}(I)$, then the CBC construction method from [Käm13] can be used, cf. Figure 3.6 for a two-dimensional example. Moreover, the reconstruction can be performed by applying a single one-dimensional FFT on the function samples followed by index transforms and requires $\mathcal{O}(M \log M + d\,|\mathcal{M}(I)|)$ arithmetic operations, which corresponds to the arithmetic complexity of our method in Section 3.2.1. The method in [SNC16] is applied to the fast approximation of functions f from (non-periodic) weighted Korobov spaces $\subset L_2([0,1]^d)$. In [CKNS16], the utilization of fast CBC construction methods from [Nuy07] for tent-transformed rank-1 lattices $\mathrm{P}_\psi(\boldsymbol{z}, M)$ is considered for the integration and approximation of functions f using samples, where the generating vector $\boldsymbol{z}$ and rank-1 lattice size M do not necessarily belong to a reconstructing rank-1 lattice $\Lambda(\boldsymbol{z}, M, I)$. Moreover, an extensive theory is developed with error estimates for tent transformed rank-1 lattice sampling in non-periodic weighted Korobov spaces and very good tractability results are shown. The sampling rates are comparable to those obtained for the periodic case in Section 2.3.3.5.

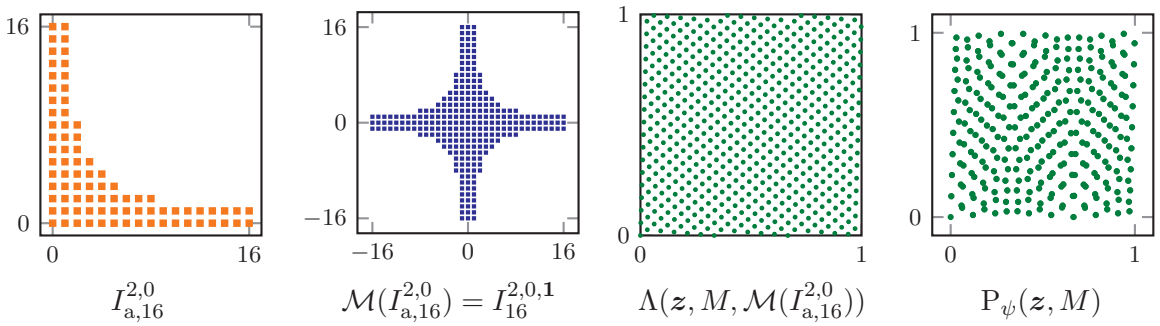

Figure 3.6: From left to right: hyperbolic cross index set $I^{2,0}_{\mathrm{a},16}$, extended symmetric index set $\mathcal{M}(I^{2,0}_{\mathrm{a},16}) = I^{2,0,\mathbf{1}}_{16}$, reconstructing rank-1 lattice $\Lambda(\boldsymbol{z}, M, \mathcal{M}(I^{2,0}_{\mathrm{a},16}))$ and tent-transformed rank-1 lattice $\mathrm{P}_\psi(\boldsymbol{z}, M)$ with generating vector $\boldsymbol{z} := (1, 33)$ and size $M := 579$.

3.4 Approximation of non-periodic signals by rank-1 Chebyshev lattice sampling

In this section, we consider the approximation of multivariate non-periodic signals $f\colon [-1,1]^d \to \mathbb{R}$ from certain function spaces by multivariate algebraic polynomials in Chebyshev form a_I from (3.1). The corresponding function spaces are characterized by the decay of the Chebyshev coefficients $\hat{f}_{\boldsymbol{k}}$, $\boldsymbol{k} \in \mathbb{N}_0^d$, of a function f as defined in (3.5). In this section, we assume that we (approximately) know the corresponding function spaces and we choose the frequency index set $I \subset \mathbb{N}_0^d$, $|I| < \infty$, accordingly. As mentioned in the introduction of this chapter, we consider subspaces $\mathcal{A}^{\alpha,\beta}([-1,1]^d)$ as defined in (3.6) of the analogon of the Wiener algebra $\mathcal{A}([-1,1]^d) = \mathcal{A}^{0,0}([-1,1]^d)$ and Sobolev-type spaces of generalized mixed smoothness $\mathcal{H}^{\alpha,\beta}([-1,1]^d)$ as defined in (3.7) for dominating mixed smoothness $\beta \geq 0$ and isotropic smoothness $\alpha > -\beta$.

Since the exact Chebyshev coefficients $\hat{f}_{\boldsymbol{k}}$, $\boldsymbol{k} \in \mathbb{N}_0^d$, are not known in general, we compute

the approximated Chebyshev coefficients $\hat{f}_{\boldsymbol{k}}^{\mathrm{CL}} \approx \hat{f}_{\boldsymbol{k}}$ of a function $f \in \mathcal{A}([-1,1]^d) \cap \mathcal{C}([-1,1]^d)$ by using the methods from Section 3.2. This means we apply a DCT-I on the samples $f(\boldsymbol{x}_j)$ taken at the nodes $\boldsymbol{x}_j := \cos(j\pi \boldsymbol{z}/M)$, $j = 0, \ldots, M$, of a rank-1 Chebyshev lattice $\mathrm{CL}(\boldsymbol{z}, M)$ and compute index transforms,

$$\tilde{\hat{a}}_l := \sum_{j=0}^{M} (\varepsilon_j^M)^2 \, f(\boldsymbol{x}_j) \, \cos\left(\frac{jl}{M}\pi\right), \quad l = 0, \ldots, M,$$

and for any $\nu \in \{1, \ldots, d\}$

$$\hat{f}_{\boldsymbol{k}}^{\mathrm{CL}} := \frac{2^d (\varepsilon_l^M)^2}{M} \frac{\tilde{\hat{a}}_l}{|\{\boldsymbol{m} \in \mathcal{M}_\nu(\{1\}^d) \colon (\boldsymbol{m} \odot \boldsymbol{k}) \cdot \boldsymbol{z} \bmod M = l\}|}, \; l := \boldsymbol{k} \cdot \boldsymbol{z} \bmod M, \; \boldsymbol{k} \in I. \tag{3.29}$$

This requires $\mathcal{O}(M \log M + d\, 2^d\, |I|)$ arithmetic operations. As in Section 3.2.1, we may rewrite formula (3.29) as

$$\hat{f}_{\boldsymbol{k}}^{\mathrm{CL}} = \frac{2^{|\boldsymbol{k}|_0+1} \, (\varepsilon_l^M)^2}{M} \frac{\tilde{\hat{a}}_l}{|\{\boldsymbol{h} \in \mathcal{M}(\{\boldsymbol{k}\}) \colon \boldsymbol{h} \cdot \boldsymbol{z} \bmod M = l\}|}, \quad l := \boldsymbol{k} \cdot \boldsymbol{z} \bmod M, \quad \boldsymbol{k} \in I,$$

and we obtain an arithmetic complexity of $\mathcal{O}(M \log M + d\, |\mathcal{M}(I)|)$. We define an approximation of the function f by the approximated Chebyshev partial sum $S_I^{\mathrm{CL}} f$ as defined in (3.9) which is a multivariate algebraic polynomial in Chebyshev form a_I with frequencies supported on the index set $I \subset \mathbb{N}_0^d$.

In the next lemma, we state embeddings between different function spaces which are analogous to Lemma 2.11 from the periodic case.

Lemma 3.9. *Let a function $f \in \mathcal{A}^{\alpha,\beta}([-1,1]^d)$ be given, where the dominating mixed smoothness $\beta \geq 0$ and the isotropic smoothness $\alpha > -\beta$. Then, we have $\|f|\mathcal{H}^{\alpha,\beta}([-1,1]^d)\| \leq \|f|\mathcal{A}^{\alpha,\beta}([-1,1]^d)\|$. For $f \in \mathcal{H}^{\alpha,\beta+\lambda}([-1,1]^d)$ with $\lambda > 1/2$, we have*

$$\|f|\mathcal{A}^{\alpha,\beta}([-1,1]^d)\| \leq (1 + 2\zeta(2\lambda))^{\frac{d}{2}} \, \|f|\mathcal{H}^{\alpha,\beta+\lambda}([-1,1]^d)\|, \tag{3.30}$$

where ζ denotes the Riemann zeta function. Therefore, we have the continuous embeddings

$$\mathcal{H}^{\alpha,\beta+\lambda}([-1,1]^d) \hookrightarrow \mathcal{A}^{\alpha,\beta}([-1,1]^d) \hookrightarrow \mathcal{A}([-1,1]^d) \hookrightarrow L_{2,w}([-1,1]^d).$$

Proof. Analogously to the proof of [KPV15a, Lemma 2.2], we infer

$$\|f|\mathcal{H}^{\alpha,\beta}([-1,1]^d)\|^2 = \sum_{\boldsymbol{k} \in \mathbb{N}_0^d} \omega^{\alpha,\beta,\mathbf{1}}(\boldsymbol{k})^2 \, |\hat{f}_{\boldsymbol{k}}|^2 \leq \left(\sum_{\boldsymbol{k} \in \mathbb{N}_0^d} \omega^{\alpha,\beta,\mathbf{1}}(\boldsymbol{k}) \, |\hat{f}_{\boldsymbol{k}}| \right)^2 = \|f|\mathcal{A}^{\alpha,\beta}([-1,1]^d)\|^2$$

and applying the Cauchy-Schwarz inequality for arbitrary $\lambda > 1/2$ yields

$$\begin{aligned}
\|f|\mathcal{A}^{\alpha,\beta}([-1,1]^d)\| &= \sum_{\boldsymbol{k} \in \mathbb{N}_0^d} \frac{\omega^{0,\lambda,\mathbf{1}}(\boldsymbol{k})}{\omega^{0,\lambda,\mathbf{1}}(\boldsymbol{k})} \quad \omega^{\alpha,\beta,\mathbf{1}}(\boldsymbol{k}) \left|\hat{f}_{\boldsymbol{k}}\right| \\
&\leq \left(\sum_{\boldsymbol{k} \in \mathbb{N}_0^d} \frac{1}{\omega^{0,\lambda,\mathbf{1}}(\boldsymbol{k})^2} \right)^{\frac{1}{2}} \left(\sum_{\boldsymbol{k} \in \mathbb{N}_0^d} \omega^{\alpha,\beta+\lambda,\mathbf{1}}(\boldsymbol{k})^2 \left|\hat{f}_{\boldsymbol{k}}\right|^2 \right)^{\frac{1}{2}} \\
&= (1 + 2\zeta(2\lambda))^{\frac{d}{2}} \, \|f|\mathcal{H}^{\alpha,\beta+\lambda}([-1,1]^d)\|.
\end{aligned}$$

The first embedding is due to (3.30) and the second one follows since the weights $\omega^{\alpha,\beta,\mathbf{1}}(\boldsymbol{k})$ are bounded from below for fixed dimension d. The third embedding follows from Parseval's identity, since we have

$$\|f|L_{2,w}([-1,1]^d)\| = \sqrt{\sum_{\boldsymbol{k}\in\mathbb{N}_0^d} \frac{\pi^d}{2^{|\boldsymbol{k}|_0}} |\hat{f}_{\boldsymbol{k}}|^2} \le \pi^{d/2} \sum_{\boldsymbol{k}\in\mathbb{N}_0^d} |\hat{f}_{\boldsymbol{k}}| = \pi^{d/2}\, \|f|\mathcal{A}([-1,1]^d)\|$$

for $f \in \mathcal{A}([-1,1]^d)$ due to (3.5). ■

As in Remark 2.15 of the periodic case, the considered parameter choices yield the existence of a continuous representative.

Remark 3.10. Since the Chebyshev coefficients $\hat{f}_{\boldsymbol{k}}$ of functions f from (subspaces $\mathcal{A}^{\alpha,\beta}([-1,1]^d)$, $\beta \ge 0$, $\alpha > -\beta$, of) the analogon of the Wiener algebra $\mathcal{A}([-1,1]^d)$ are absolutely summable, they have continuous representatives, $\mathcal{A}([-1,1]^d) \hookrightarrow \mathcal{C}([-1,1]^d)$. As we are going to construct the approximant $S_I^{\mathrm{CL}} f$ based on function values of the original function f, we usually identify a function $f \in \mathcal{A}([-1,1]^d)$ by its continuous representative given by its Chebyshev series $\sum_{\boldsymbol{k}\in\mathbb{N}_0^d} \hat{f}_{\boldsymbol{k}}\, T_{\boldsymbol{k}}(\circ)$ and denote this by $f \in \mathcal{A}([-1,1]^d) \cap \mathcal{C}([-1,1]^d)$. □

Next, we show an analogon of the aliasing formula from Lemma 2.23 in the non-periodic case for arbitrary rank-1 Chebyshev lattices $\mathrm{CL}(\boldsymbol{z}, M)$.

Lemma 3.11. *Let a function $f \in \mathcal{A}([-1,1]^d) \cap \mathcal{C}([-1,1]^d)$, an arbitrary frequency index set $I \subset \mathbb{N}_0^d$ of finite cardinality, $|I| < \infty$, and an arbitrary rank-1 Chebyshev lattice $\mathrm{CL}(\boldsymbol{z}, M) \subset [-1,1]^d$ be given. Then, for any $\nu \in \{1,\dots,d\}$, the aliasing formula of the approximated Chebyshev coefficients $\hat{f}_{\boldsymbol{k}}^{\mathrm{CL}}$ from (3.29) is given by*

$$\hat{f}_{\boldsymbol{k}}^{\mathrm{CL}} = \hat{f}_{\boldsymbol{k}} + \sum_{\boldsymbol{k}'\in\mathbb{N}_0^d\setminus\{\boldsymbol{k}\}} \hat{f}_{\boldsymbol{k}'}\, \frac{|\{\boldsymbol{m}\in\mathcal{M}_\nu(\{\mathbf{1}\})\colon (\boldsymbol{m}\odot\boldsymbol{k}')\cdot\boldsymbol{z} \bmod M = \boldsymbol{k}\cdot\boldsymbol{z} \bmod M\}|}{|\{\boldsymbol{m}\in\mathcal{M}_\nu(\{\mathbf{1}\})\colon (\boldsymbol{m}\odot\boldsymbol{k})\cdot\boldsymbol{z} \bmod M = \boldsymbol{k}\cdot\boldsymbol{z} \bmod M\}|} \tag{3.31}$$

for frequencies $\boldsymbol{k} \in I$, where $\mathbf{1} := (1,\dots,1)^\top \in \mathbb{N}^d$.

Proof. For the computation of the approximated Chebyshev coefficients $\hat{f}_{\boldsymbol{k}}^{\mathrm{CL}}$, $\boldsymbol{k} \in I$, we use formula (3.29),

$$\hat{f}_{\boldsymbol{k}}^{\mathrm{CL}} = \frac{2^d (\varepsilon^M_{\boldsymbol{k}\cdot\boldsymbol{z} \bmod M})^2}{M} \frac{\tilde{\hat{a}}_{\boldsymbol{k}\cdot\boldsymbol{z} \bmod M}}{|\{\boldsymbol{m}\in\mathcal{M}_\nu(\{\mathbf{1}\})\colon (\boldsymbol{m}\odot\boldsymbol{k})\cdot\boldsymbol{z} \bmod M = \boldsymbol{k}\cdot\boldsymbol{z} \bmod M\}|},$$

where

$$\begin{aligned}
\tilde{\hat{a}}_l &= \sum_{j=0}^{M} (\varepsilon_j^M)^2\, f(\boldsymbol{x}_j)\, \cos\left(\frac{jl}{M}\pi\right) \\
&= \sum_{j=0}^{M} (\varepsilon_j^M)^2 \left(\sum_{\boldsymbol{k}'\in\mathbb{N}_0^d} \hat{f}_{\boldsymbol{k}'} \prod_{t=1}^{d} \cos\left(\frac{j}{M}\pi\, k'_t\, z_t\right)\right) \cos\left(\frac{jl}{M}\pi\right) \\
&\overset{(3.14)}{=} \sum_{j=0}^{M} (\varepsilon_j^M)^2 \left(\sum_{\boldsymbol{k}'\in\mathbb{N}_0^d} \frac{\hat{f}_{\boldsymbol{k}'}}{2^{d-1}} \sum_{\boldsymbol{m}\in\mathcal{M}_\nu(\{\mathbf{1}\})} \cos\left(\frac{j}{M}\pi\,(\boldsymbol{m}\odot\boldsymbol{k}')\cdot\boldsymbol{z}\right)\right) \cos\left(\frac{jl}{M}\pi\right) \\
&= \sum_{\boldsymbol{k}'\in\mathbb{N}_0^d} \frac{\hat{f}_{\boldsymbol{k}'}}{2^{d-1}} \sum_{\boldsymbol{m}\in\mathcal{M}_\nu(\{\mathbf{1}\})} \sum_{j=0}^{M} (\varepsilon_j^M)^2 \cos\left(\frac{j}{M}\pi\,(\boldsymbol{m}\odot\boldsymbol{k}')\cdot\boldsymbol{z}\right) \cos\left(\frac{jl}{M}\pi\right)
\end{aligned}$$

for $l = 0, \ldots, M$. Due to orthogonality relation (3.20), we infer

$$\tilde{\hat{a}}_l \overset{(3.20)}{=} \sum_{\boldsymbol{k'} \in \mathbb{N}_0^d} \frac{\hat{f}_{\boldsymbol{k'}}}{2^{d-1}} \sum_{\substack{\boldsymbol{m} \in \mathcal{M}_\nu(\{\boldsymbol{1}\}) \\ (\boldsymbol{m} \odot \boldsymbol{k'}) \cdot \boldsymbol{z} \bmod M = l}} \frac{M}{2\,(\varepsilon_l^M)^2}$$

$$= \sum_{\boldsymbol{k'} \in \mathbb{N}_0^d} \hat{f}_{\boldsymbol{k'}} \frac{M\,|\{\boldsymbol{m} \in \mathcal{M}_\nu(\{\boldsymbol{1}\})\colon (\boldsymbol{m} \odot \boldsymbol{k'}) \cdot \boldsymbol{z} \bmod M = l\}|}{2^d\,(\varepsilon_l^M)^2}. \tag{3.32}$$

Due to the choice $l := \boldsymbol{k} \cdot \boldsymbol{z} \bmod M$ and together with (3.26), this yields the aliasing formula

$$\hat{f}_{\boldsymbol{k}}^{\mathrm{CL}} = \sum_{\boldsymbol{k'} \in \mathbb{N}_0^d} \hat{f}_{\boldsymbol{k'}} \frac{|\{\boldsymbol{m} \in \mathcal{M}_\nu(\{\boldsymbol{1}\})\colon (\boldsymbol{m} \odot \boldsymbol{k'}) \cdot \boldsymbol{z} \bmod M = \boldsymbol{k} \cdot \boldsymbol{z} \bmod M\}|}{|\{\boldsymbol{m} \in \mathcal{M}_\nu(\{\boldsymbol{1}\})\colon (\boldsymbol{m} \odot \boldsymbol{k}) \cdot \boldsymbol{z} \bmod M = \boldsymbol{k} \cdot \boldsymbol{z} \bmod M\}|}, \ \boldsymbol{k} \in I.$$

and the assertion follows. ∎

As we see in the aliasing formula (3.31), the approximated Chebyshev coefficients $\hat{f}_{\boldsymbol{k}}^{\mathrm{CL}}$ may contain original Chebyshev coefficients $\hat{f}_{\boldsymbol{k'}}^{\mathrm{CL}}$, $\boldsymbol{k'} \in \mathbb{N}_0^d \setminus \{\boldsymbol{k}\}$, of the function f, which are amplified or damped by factors $\theta(\boldsymbol{z}, M, \boldsymbol{k}, \boldsymbol{k'}) \in \{2^{1-d}, 2^{2-d}, \ldots, 2^{d-2}, 2^{d-1}\}$,

$$\theta(\boldsymbol{z}, M, \boldsymbol{k}, \boldsymbol{k'}) := \frac{|\{\boldsymbol{m} \in \mathcal{M}_\nu(\{\boldsymbol{1}\})\colon (\boldsymbol{m} \odot \boldsymbol{k'}) \cdot \boldsymbol{z} \bmod M = \boldsymbol{k} \cdot \boldsymbol{z} \bmod M\}|}{|\{\boldsymbol{m} \in \mathcal{M}_\nu(\{\boldsymbol{1}\})\colon (\boldsymbol{m} \odot \boldsymbol{k}) \cdot \boldsymbol{z} \bmod M = \boldsymbol{k} \cdot \boldsymbol{z} \bmod M\}|},$$

depending on the used rank-1 Chebyshev lattice $\mathrm{CL}(\boldsymbol{z}, M)$. Such a behavior can be observed in the following example.

Example 3.12. We consider the two-dimensional ℓ_1-ball frequency index set of refinement $n := 2$,

$$I = I_{\mathrm{a},2}^{2,-\infty} = \{(0,0)^\top, (0,1)^\top, (0,2)^\top, (1,0)^\top, (1,1)^\top, (2,0)^\top\}.$$

Then, the 2-dimensional rank-1 Chebyshev lattice $\mathrm{CL}(\boldsymbol{z}, M)$ with generating vector $\boldsymbol{z} := (1,4)^\top$ and size parameter $M := 7$ is a reconstructing rank-1 Chebyshev lattice $\mathrm{CL}(\boldsymbol{z}, M, I)$. For the test function $f\colon [-1,1]^2 \to \mathbb{R}$, $f(\boldsymbol{x}) := \hat{f}_{\boldsymbol{k'}}\, T_{\boldsymbol{k'}}(\boldsymbol{x})$, $\hat{f}_{\boldsymbol{k'}} \in \mathbb{R} \setminus \{0\}$, $\boldsymbol{k'} := (5,0)^\top$, we compute the approximated Chebyshev coefficients $\hat{f}_{\boldsymbol{k}}^{\mathrm{CL}}$, $\boldsymbol{k} \in I$, from sampling values of f at the nodes $\boldsymbol{x}_j$ of the reconstructing rank-1 Chebyshev lattice $\mathrm{CL}(\boldsymbol{z}, M, I)$ and we obtain one non-zero coefficient $\hat{f}_{(1,1)^\top}^{\mathrm{CL}} = 2\,\hat{f}_{(5,0)^\top}$. The reason for this is that we have with the frequency $\boldsymbol{k} := (1,1)^\top$ the relations

$$\frac{|\{\boldsymbol{m} \in \mathcal{M}_1(\boldsymbol{1})\colon (\boldsymbol{m} \odot \boldsymbol{k'}) \cdot \boldsymbol{z} \bmod M = \boldsymbol{k} \cdot \boldsymbol{z} \bmod M = 5\}|}{|\{\boldsymbol{m} \in \mathcal{M}_1(\boldsymbol{1})\colon (\boldsymbol{m} \odot \boldsymbol{k}) \cdot \boldsymbol{z} \bmod M = \boldsymbol{k} \cdot \boldsymbol{z} \bmod M = 5\}|} = \frac{\left|\{(1,1)^\top, (1,-1)^\top\}\right|}{|\{(1,1)^\top\}|} = \frac{2}{1}$$

for the case $\nu = 1$ and

$$\frac{|\{\boldsymbol{m} \in \mathcal{M}_2(\boldsymbol{1})\colon (\boldsymbol{m} \odot \boldsymbol{k'}) \cdot \boldsymbol{z} \bmod M = \boldsymbol{k} \cdot \boldsymbol{z} \bmod M = 5\}|}{|\{\boldsymbol{m} \in \mathcal{M}_2(\boldsymbol{1})\colon (\boldsymbol{m} \odot \boldsymbol{k}) \cdot \boldsymbol{z} \bmod M = \boldsymbol{k} \cdot \boldsymbol{z} \bmod M = 5\}|} = \frac{\left|\{(1,1)^\top, (-1,1)^\top\}\right|}{|\{(1,1)^\top\}|} = \frac{2}{1}$$

for the case $\nu = 2$ in the aliasing formula (3.31), but $\boldsymbol{k} \cdot \boldsymbol{z} \bmod M \neq 5$ for all remaining frequencies $\boldsymbol{k} \in I \setminus \{(1,1)^\top\}$.
If we consider the test function $f\colon [-1,1]^2 \to \mathbb{R}$, $f(\boldsymbol{x}) := \hat{f}_{\boldsymbol{k'}}\, T_{\boldsymbol{k'}}(\boldsymbol{x})$, $\hat{f}_{\boldsymbol{k'}} \in \mathbb{R} \setminus \{0\}$ with $\boldsymbol{k'} := (2,1)^\top$ instead, we obtain the two non-zero coefficients $\hat{f}_{(0,2)^\top}^{\mathrm{CL}} = \hat{f}_{(2,0)^\top}^{\mathrm{CL}} = \frac{1}{2}\,\hat{f}_{(2,1)^\top}$. Setting $\boldsymbol{k} := (0,2)^\top$ and $\boldsymbol{l} := (2,0)^\top$, this is due to

$$\frac{|\{\boldsymbol{m} \in \mathcal{M}_1(\boldsymbol{1})\colon (\boldsymbol{m} \odot \boldsymbol{k'}) \cdot \boldsymbol{z} \bmod M = \boldsymbol{k} \cdot \boldsymbol{z} \bmod M = 6\}|}{|\{\boldsymbol{m} \in \mathcal{M}_1(\boldsymbol{1})\colon (\boldsymbol{m} \odot \boldsymbol{k}) \cdot \boldsymbol{z} \bmod M = \boldsymbol{k} \cdot \boldsymbol{z} \bmod M = 6\}|} = \frac{\left|\{(1,1)^\top\}\right|}{|\{(1,1)^\top, (1,-1)^\top\}|} = \frac{1}{2}$$

and

$$\frac{|\{\boldsymbol{m} \in \mathcal{M}_1(\mathbf{1}) \colon (\boldsymbol{m} \odot \boldsymbol{k'}) \cdot \boldsymbol{z} \bmod M = \boldsymbol{l} \cdot \boldsymbol{z} \bmod M = 2\}|}{|\{\boldsymbol{m} \in \mathcal{M}_1(\mathbf{1}) \colon (\boldsymbol{m} \odot \boldsymbol{l}) \cdot \boldsymbol{z} \bmod M = \boldsymbol{l} \cdot \boldsymbol{z} \bmod M = 2\}|} = \frac{\left|\{(1,-1)^\top\}\right|}{|\{(1,1)^\top,(1,-1)^\top\}|} = \frac{1}{2}$$

for the case $\nu = 1$ as well as

$$\frac{|\{\boldsymbol{m} \in \mathcal{M}_2(\mathbf{1}) \colon (\boldsymbol{m} \odot \boldsymbol{k'}) \cdot \boldsymbol{z} \bmod M = \boldsymbol{k} \cdot \boldsymbol{z} \bmod M = 6\}|}{|\{\boldsymbol{m} \in \mathcal{M}_2(\mathbf{1}) \colon (\boldsymbol{m} \odot \boldsymbol{k}) \cdot \boldsymbol{z} \bmod M = \boldsymbol{k} \cdot \boldsymbol{z} \bmod M = 6\}|} = \frac{\left|\{(1,1)^\top\}\right|}{|\{(1,1)^\top,(-1,1)^\top\}|} = \frac{1}{2}$$

and

$$\frac{|\{\boldsymbol{m} \in \mathcal{M}_2(\mathbf{1}) \colon (\boldsymbol{m} \odot \boldsymbol{k'}) \cdot \boldsymbol{z} \bmod M = \boldsymbol{l} \cdot \boldsymbol{z} \bmod M = 2\}|}{|\{\boldsymbol{m} \in \mathcal{M}_2(\mathbf{1}) \colon (\boldsymbol{m} \odot \boldsymbol{l}) \cdot \boldsymbol{z} \bmod M = \boldsymbol{l} \cdot \boldsymbol{z} \bmod M = 2\}|} = \frac{\left|\{(-1,1)^\top\}\right|}{|\{(1,1)^\top,(-1,1)^\top\}|} = \frac{1}{2}$$

for the case $\nu = 2$ in the aliasing formula (3.31), but $\boldsymbol{k} \cdot \boldsymbol{z} \bmod M \notin \{2,6\}$ for all remaining frequencies $\boldsymbol{k} \in I \setminus \{(0,2)^\top,(2,0)^\top\}$. □

Since we do not want to have aliasing within the frequency index set $I \subset \mathbb{N}_0^d$, we use reconstructing rank-1 Chebyshev lattices $\mathrm{CL}(\boldsymbol{z}, M, I)$ as sampling sets. This yields Algorithm 3.4, which can be realized using few lines of Octave / MATLAB code,

```
a_hat_tilde = dct_I( (f(x_j))_{j=0}^M );
a_hat_tilde(1) = a_hat_tilde(1) / 2;
if M > 0; a_hat_tilde(end) = a_hat_tilde(end) / 2; end;
for ik = 1:size(I,1)
  k_m = repmat(I(ik,:),2^(d-1),1) .* M_nu({1}^d);
  factor(ik) = length(find(emod(k_m*z',M)==emod(I(ik,:)*z',M)));
end
(f_hat_k)_{k∈I} = 2^d / M ./ factor .* a_hat_tilde(emod(I*z',M)+1);
```

in $\mathcal{O}(M \log M + d\, 2^d |I|)$ arithmetic operations. As in Section 3.2.1, we can rewrite the computation in the for loop over $\boldsymbol{k} \in I$ in Algorithm 3.4 as

$$\hat{f}_{\boldsymbol{k}}^{\mathrm{CL}} := \frac{2^{|\boldsymbol{k}|_0+1}\,(\varepsilon_l^M)^2}{M} \frac{\tilde{\hat{a}}_l}{|\{\boldsymbol{h} \in \mathcal{M}(\{\boldsymbol{k}\}) \colon \boldsymbol{h} \cdot \boldsymbol{z} \bmod M = l\}|}, \quad l := \boldsymbol{k} \cdot \boldsymbol{z} \bmod M,$$

and we obtain an arithmetic complexity of $\mathcal{O}(M \log M + d\,|\mathcal{M}(I)|)$. Again, we may not need to compute the cardinalities in the denominator in certain cases, cf. Remark 3.7.

Using the aliasing formula (3.31) from Lemma 3.11, we obtain the following results for the truncation error $f - S_I f$ and sampling error $f - S_I^{\mathrm{CL}} f$ of a function f from the analogon of the Wiener algebra $\mathcal{A}([-1,1]^d)$ or its continuous representative, see Remark 3.10.

Theorem 3.13. *Let a function $f \in \mathcal{A}([-1,1]^d) \cap \mathcal{C}([-1,1]^d)$ and an arbitrary frequency index set $I \subset \mathbb{N}_0^d$ of finite cardinality, $|I| < \infty$, be given. Then, the truncation error $f - S_I f$ is bounded by*

$$\|f - S_I f | L_\infty([-1,1]^d)\| \leq \sum_{\boldsymbol{k} \in \mathbb{N}_0^d \setminus I} |\hat{f}_{\boldsymbol{k}}| = \|f - S_I f | \mathcal{A}([-1,1]^d)\|.$$

Additionally, let $\mathrm{CL}(\boldsymbol{z}, M, I)$ be a reconstructing rank-1 Chebyshev lattice for the frequency index set I. Then, the sampling error $f - S_I^{\mathrm{CL}} f$ is bounded by

$$\|f - S_I^{\mathrm{CL}} f | L_\infty([-1,1]^d)\| \leq (1 + 2^{d-1}) \sum_{\boldsymbol{k} \in \mathbb{N}_0^d \setminus I} |\hat{f}_{\boldsymbol{k}}| = (1 + 2^{d-1})\, \|f - S_I f | \mathcal{A}([-1,1]^d)\|. \quad (3.33)$$

Algorithm 3.4 Approximate reconstruction of a function $f \in \mathcal{A}([-1,1]^d) \cap \mathcal{C}([-1,1]^d)$ from sampling values on a reconstructing rank-1 Chebyshev lattice $\mathrm{CL}(\boldsymbol{z}, M, I)$ for frequency index set I, i.e., application of Algorithm 3.2 on a function $f \in \mathcal{A}([-1,1]^d) \cap \mathcal{C}([-1,1]^d)$.

Input:	$I \subset \mathbb{N}_0^d$	frequency index set of finite cardinality
	$\mathrm{CL}(\boldsymbol{z}, M, I)$	reconstructing rank-1 Chebyshev lattice for I with size parameter M and generating vector $\boldsymbol{z} \in \mathbb{N}_0^d$
	$\boldsymbol{f} = (f(\boldsymbol{x}_j))_{j=0}^M$	function values $f(\boldsymbol{x}_j)$, $\boldsymbol{x}_j := \cos\left(\frac{j}{M}\pi\boldsymbol{z}\right)$, of $f \in \mathcal{A}([-1,1]^d) \cap \mathcal{C}([-1,1]^d)$

Compute $\tilde{\hat{\boldsymbol{a}}} := \texttt{DCT\_I}(\boldsymbol{f})$, i.e. $\sum_{j=0}^M (\varepsilon_j^M)^2 \, f\left(\cos(j\pi\boldsymbol{z}/M)\right) \cos(jl\pi/M)$ for $l = 0, \ldots, M$.
for each $\boldsymbol{k} \in I$ **do**
Compute $l := \boldsymbol{k} \cdot \boldsymbol{z} \bmod M$.
$$\hat{f}_{\boldsymbol{k}}^{\mathrm{CL}} := \frac{2^d (\varepsilon_l^M)^2}{M} \frac{\tilde{\hat{a}}_l}{|\{\boldsymbol{m} \in \mathcal{M}_\nu(\{1\}^d) \colon (\boldsymbol{m} \odot \boldsymbol{k}) \cdot \boldsymbol{z} \bmod M = l\}|}.$$
end for

Output:	$\hat{\boldsymbol{f}}^{\mathrm{CL}} := \left(\hat{f}_{\boldsymbol{k}}^{\mathrm{CL}}\right)_{\boldsymbol{k} \in I}$	approximated Chebyshev coefficients of $f \in \mathcal{A}([-1,1]^d) \cap \mathcal{C}([-1,1]^d)$
Complexity:	$\mathcal{O}(M \log M + d\, 2^d\, \lvert I \rvert)$	

Proof. For the truncation error $f - S_I f$, we obtain

$$\|f - S_I f | L_\infty([-1,1]^d)\| = \operatorname{ess\,sup}_{\boldsymbol{x} \in [-1,1]^d} \left| \sum_{\boldsymbol{k} \in \mathbb{N}_0^d \setminus I} \hat{f}_{\boldsymbol{k}} T_{\boldsymbol{k}}(\boldsymbol{x}) \right| \leq \sum_{\boldsymbol{k} \in \mathbb{N}_0^d \setminus I} |\hat{f}_{\boldsymbol{k}}|. \tag{3.34}$$

We apply inequality (3.10) on the sampling error $f - S_I^{\mathrm{CL}} f$. For the aliasing error $S_I f - S_I^{\mathrm{CL}} f$, we use aliasing formula (3.31) and this yields

$$\begin{aligned}
& \|S_I f - S_I^{\mathrm{CL}} f | L_\infty([-1,1]^d)\| \\
= \;& \operatorname{ess\,sup}_{\boldsymbol{x} \in [-1,1]^d} \left| \sum_{\boldsymbol{k} \in I} \left(\hat{f}_{\boldsymbol{k}} - \hat{f}_{\boldsymbol{k}}^{\mathrm{CL}} \right) T_{\boldsymbol{k}}(\boldsymbol{x}) \right| \leq \sum_{\boldsymbol{k} \in I} \left| \hat{f}_{\boldsymbol{k}} - \hat{f}_{\boldsymbol{k}}^{\mathrm{CL}} \right| \\
\overset{(3.31)}{=} \;& \sum_{\boldsymbol{k} \in I} \left| \left(- \sum_{\boldsymbol{k}' \in \mathbb{N}_0^d \setminus \{\boldsymbol{k}\}} \hat{f}_{\boldsymbol{k}'} \frac{|\{\boldsymbol{m} \in \mathcal{M}_\nu(\{\boldsymbol{1}\}) \colon (\boldsymbol{m} \odot \boldsymbol{k}') \cdot \boldsymbol{z} \bmod M = \boldsymbol{k} \cdot \boldsymbol{z} \bmod M\}|}{|\{\boldsymbol{m} \in \mathcal{M}_\nu(\{\boldsymbol{1}\}) \colon (\boldsymbol{m} \odot \boldsymbol{k}) \cdot \boldsymbol{z} \bmod M = \boldsymbol{k} \cdot \boldsymbol{z} \bmod M\}|} \right) \right| \\
\leq \;& \sum_{\boldsymbol{k} \in I} \sum_{\boldsymbol{k}' \in \mathbb{N}_0^d \setminus \{\boldsymbol{k}\}} |\hat{f}_{\boldsymbol{k}'}| \frac{|\{\boldsymbol{m} \in \mathcal{M}_\nu(\{\boldsymbol{1}\}) \colon (\boldsymbol{m} \odot \boldsymbol{k}') \cdot \boldsymbol{z} \bmod M = \boldsymbol{k} \cdot \boldsymbol{z} \bmod M\}|}{|\{\boldsymbol{m} \in \mathcal{M}_\nu(\{\boldsymbol{1}\}) \colon (\boldsymbol{m} \odot \boldsymbol{k}) \cdot \boldsymbol{z} \bmod M = \boldsymbol{k} \cdot \boldsymbol{z} \bmod M\}|}.
\end{aligned}$$

For each $\boldsymbol{k} \in I$, there does not exist any frequency $\boldsymbol{k}' \in I \setminus \{\boldsymbol{k}\}$ such that the numerator is non-zero due to reconstruction property (3.22) and we continue by interchanging both sums

$$\overset{(3.22)}{=} \sum_{\boldsymbol{k}' \in \mathbb{N}_0^d \setminus I} \sum_{\boldsymbol{k} \in I} |\hat{f}_{\boldsymbol{k}'}| \frac{|\{\boldsymbol{m} \in \mathcal{M}_\nu(\{\boldsymbol{1}\}) \colon (\boldsymbol{m} \odot \boldsymbol{k}') \cdot \boldsymbol{z} \bmod M = \boldsymbol{k} \cdot \boldsymbol{z} \bmod M\}|}{|\{\boldsymbol{m} \in \mathcal{M}_\nu(\{\boldsymbol{1}\}) \colon (\boldsymbol{m} \odot \boldsymbol{k}) \cdot \boldsymbol{z} \bmod M = \boldsymbol{k} \cdot \boldsymbol{z} \bmod M\}|}.$$

Due to condition (3.22), we have $\boldsymbol{k} \cdot \boldsymbol{z} \bmod M \neq \tilde{\boldsymbol{k}} \cdot \boldsymbol{z} \bmod M$ for all frequencies $\boldsymbol{k}, \tilde{\boldsymbol{k}} \in I$, $\boldsymbol{k} \neq \tilde{\boldsymbol{k}}$. This means for fixed frequency $\boldsymbol{k}' \in \mathbb{N}_0^d \setminus I$ and for each $\boldsymbol{m} \in \mathcal{M}_\nu(\{\boldsymbol{1}\})$ that there

exists at most one frequency $\boldsymbol{k} \in I$ such that $(\boldsymbol{m} \odot \boldsymbol{k'}) \cdot \boldsymbol{z} \bmod M = \boldsymbol{k} \cdot \boldsymbol{z} \bmod M$. Since the cardinality $|\mathcal{M}_\nu(\{\mathbf{1}\})| = 2^{d-1}$, we obtain

$$\|S_I f - S_I^{\mathrm{CL}} f | L_\infty([-1,1]^d)\| \leq \sum_{\boldsymbol{k} \in I} \left| \hat{f}_{\boldsymbol{k}} - \hat{f}_{\boldsymbol{k}}^{\mathrm{CL}} \right| \leq 2^{d-1} \sum_{\boldsymbol{k'} \in \mathbb{N}_0^d \setminus I} |\hat{f}_{\boldsymbol{k'}}| \tag{3.35}$$

for the aliasing error and this yields the assertion. ■

The factor 2^{d-1} in the estimates (3.35) and (3.33) of Theorem 3.13 for the aliasing error $S_I f - S_I^{\mathrm{CL}} f$ and sampling error $f - S_I^{\mathrm{CL}} f$, respectively, may occur in practice as the following example illustrates.

Example 3.14. We consider the three-dimensional ℓ_1-ball index set $I := I_{\mathrm{a},4}^{3,-\infty}$ of refinement $n := 4$. Then, the 3-dimensional rank-1 Chebyshev lattice $\mathrm{CL}(\boldsymbol{z}, M)$ with generating vector $\boldsymbol{z} := (1, 8, 36)^\top$ and size parameter $M := 83$ is a reconstructing rank-1 Chebyshev lattice $\mathrm{CL}(\boldsymbol{z}, M, I)$. For the test function $f \colon [-1,1]^3 \to \mathbb{R}$, $f(\boldsymbol{x}) := \hat{f}_{\boldsymbol{k'}} T_{\boldsymbol{k'}}(\boldsymbol{x})$, $\hat{f}_{\boldsymbol{k'}} \in \mathbb{R}$, $\boldsymbol{k'} := (46, 0, 0)^\top$, we compute the approximated Chebyshev coefficients $\hat{f}_{\boldsymbol{k}}^{\mathrm{CL}}$, $\boldsymbol{k} \in I$, from sampling values of f at the nodes $\boldsymbol{x}_j$ of the reconstructing rank-1 Chebyshev lattice $\mathrm{CL}(\boldsymbol{z}, M, I)$ and we obtain one non-zero coefficient $\hat{f}_{(2,1,1)^\top}^{\mathrm{CL}} = 4\, \hat{f}_{(46,0,0)^\top}$. This means with the frequency $\boldsymbol{k} := (2, 1, 1)^\top$ and the node $\boldsymbol{y'} := (-1, 1, -1)^\top$, we have

$$\begin{aligned}
\|f - S_I^{\mathrm{CL}} f | L_\infty([-1,1]^d)\| &:= \operatorname{ess\,sup}_{\boldsymbol{x} \in [-1,1]^d} \left| \hat{f}_{\boldsymbol{k'}} T_{\boldsymbol{k'}}(\boldsymbol{x}) - \hat{f}_{\boldsymbol{k}}^{\mathrm{CL}} T_{\boldsymbol{k}}(\boldsymbol{x}) \right| \\
&= \left| \hat{f}_{\boldsymbol{k'}} T_{\boldsymbol{k'}}(\boldsymbol{y'}) - \hat{f}_{\boldsymbol{k}}^{\mathrm{CL}} T_{\boldsymbol{k}}(\boldsymbol{y'}) \right| = \left| \hat{f}_{\boldsymbol{k'}} T_{\boldsymbol{k'}}(\boldsymbol{y'}) - \hat{f}_{\boldsymbol{k}}^{\mathrm{CL}} T_{\boldsymbol{k}}(\boldsymbol{y'}) \right| \\
&= \left| \hat{f}_{\boldsymbol{k'}} + \hat{f}_{\boldsymbol{k}}^{\mathrm{CL}} \right| = 5\, |\hat{f}_{\boldsymbol{k'}}| = (1 + 2^2)\, |\hat{f}_{\boldsymbol{k'}}| = (1 + 2^{d-1})\, |\hat{f}_{\boldsymbol{k'}}|
\end{aligned}$$

which corresponds to the upper bound in Theorem 3.13 for the case $d = 3$. We remark that the considered rank-1 Chebyshev lattice $\mathrm{CL}(\boldsymbol{z}, M)$ is a reconstructing one fulfilling condition (3.22) according to Theorem 3.4, since the rank-1 lattice $\Lambda(\boldsymbol{z}, \hat{M})$ with generating vector $\boldsymbol{z} := (1, 8, 36)^\top$ and size $\hat{M} := 166$ is a reconstructing rank-1 lattice for the extended symmetric index set $\mathcal{M}(I_{\mathrm{a},4}^{3,-\infty}) = I_4^{3,-\infty,\mathbf{1}}$. □

Next, we consider functions f from general subspaces of the analogon of the Wiener algebra $\mathcal{A}([-1,1]^d)$, where these subspaces are defined similar to the weighted function spaces $\mathcal{A}_\omega(\mathbb{T}^d)$ in [Käm14b, Theorem 3.11]. Let $\tilde{\omega} \colon \mathbb{N}_0^d \to [c, \infty)$, $c > 0$, be a weight function, such that the frequency index set $I_{\mathrm{a},n}^{d,\tilde{\omega}} := \{\boldsymbol{k} \in \mathbb{N}_0^d \colon \tilde{\omega}(\boldsymbol{k}) \leq n\}$ is of finite cardinality, $|I_{\mathrm{a},n}^{d,\tilde{\omega}}| < \infty$, for each refinement $n \in \mathbb{R}$, $n \geq 1$. We define the function space

$$\mathcal{A}^{\tilde{\omega}}([-1,1]^d) := \left\{ f \in L_{2,w}([-1,1]^d) \colon \|f|\mathcal{A}^{\tilde{\omega}}([-1,1]^d)\| := \sum_{\boldsymbol{k} \in \mathbb{N}_0^d} \tilde{\omega}(\boldsymbol{k})\, |\hat{f}_{\boldsymbol{k}}| < \infty \right\}.$$

An upper bound for the sampling error $f - S_I^{\mathrm{CL}} f$ of functions f from $\mathcal{A}^{\tilde{\omega}}([-1,1]^d)$ is given in the next theorem.

Theorem 3.15. *Let $f \in \mathcal{A}^{\tilde{\omega}}([-1,1]^d) \cap \mathcal{C}([-1,1]^d)$ be a function and let a refinement parameter $n \in \mathbb{R}$, $n \geq 1$ be given. Moreover, let $\mathrm{CL}(\boldsymbol{z}, M, I)$ be a reconstructing rank-1 Chebyshev lattice for the frequency index set $I := I_{\mathrm{a},n}^{d,\tilde{\omega}}$. We approximate the function f by the approximated partial sum $S_I^{\mathrm{CL}} f$. Then, the sampling error is bounded by*

$$\|f - S_I^{\mathrm{CL}} f | L_\infty([-1,1]^d)\| \leq \frac{(1 + 2^{d-1})}{n} \sum_{\boldsymbol{k} \in \mathbb{N}_0^d \setminus I_{\mathrm{a},n}^{d,\tilde{\omega}}} \tilde{\omega}(\boldsymbol{k})\, |\hat{f}_{\boldsymbol{k}}| \leq \frac{(1 + 2^{d-1})}{n}\, \|f|\mathcal{A}^{\tilde{\omega}}([-1,1]^d)\|.$$

Proof. We apply Theorem 3.13 and use the weights $\tilde{\omega}(\boldsymbol{k})$. This yields

$$\begin{aligned}\|f - S_{I_{\mathrm{a},n}^{d,\tilde{\omega}}} f | L_\infty([-1,1]^d)\| &\overset{(3.33)}{\leq} (1+2^{d-1}) \sum_{\boldsymbol{k}\in\mathbb{N}_0^d \setminus I_{\mathrm{a},n}^{d,\tilde{\omega}}} |\hat{f}_{\boldsymbol{k}}| = (1+2^{d-1}) \sum_{\boldsymbol{k}\in\mathbb{N}_0^d \setminus I_{\mathrm{a},n}^{d,\tilde{\omega}}} \frac{\tilde{\omega}(\boldsymbol{k})}{\tilde{\omega}(\boldsymbol{k})} |\hat{f}_{\boldsymbol{k}}| \\ &\leq (1+2^{d-1}) \left(\max_{\boldsymbol{k}\in\mathbb{N}_0^d \setminus I_{\mathrm{a},n}^{d,\tilde{\omega}}} \frac{1}{\tilde{\omega}(\boldsymbol{k})} \right) \sum_{\boldsymbol{k}\in\mathbb{N}_0^d \setminus I_{\mathrm{a},n}^{d,\tilde{\omega}}} \tilde{\omega}(\boldsymbol{k}) |\hat{f}_{\boldsymbol{k}}|\end{aligned}$$

and the assertion follows. ∎

For functions $f \in \mathcal{A}^{\alpha,\beta}([-1,1]^d)$, we obtain analogous results as in Theorem 2.17 and 2.24. Correspondingly to the periodic case in (2.14), we use the frequency index sets $I_{\mathrm{a},n}^{d,T}$ as defined in (3.11). These frequency index sets are constructed differently compared to the frequency index sets $I_{\mathrm{a},n}^{d,\tilde{\omega}}$ from above, since we do not include the smoothness parameters α, β directly but only use their ratio via the shape parameter T.

Theorem 3.16. *Let a function $f \in \mathcal{A}^{\alpha,\beta}([-1,1]^d) \cap \mathcal{C}([-1,1]^d)$ and a frequency index set $I := I_{\mathrm{a},n}^{d,T}$ be given, where the refinement $n \geq 1$, the dominating mixed smoothness $\beta \geq 0$, the isotropic smoothness $\alpha > -\beta$ and the shape parameter $T := -\frac{\alpha}{\beta}$ with $T := -\infty$ for $\beta = 0$. Then, the truncation error $f - S_{I_{\mathrm{a},n}^{d,T}} f$ is bounded by*

$$\|f - S_{I_{\mathrm{a},n}^{d,T}} f | L_\infty([-1,1]^d)\| \leq \|f - S_{I_{\mathrm{a},n}^{d,T}} f | \mathcal{A}([-1,1]^d)\| \leq n^{-(\alpha+\beta)} \, \|f | \mathcal{A}^{\alpha,\beta}([-1,1]^d)\|$$

and the operator norm of $\mathrm{Id} - S_{I_{\mathrm{a},n}^{d,T}}$ *is bounded by*

$$(n+1)^{-(\alpha+\beta)} \leq \|\mathrm{Id} - S_{I_{\mathrm{a},n}^{d,T}} | \mathcal{A}^{\alpha,\beta}([-1,1]^d) \to L_\infty([-1,1]^d)\| \leq n^{-(\alpha+\beta)} \tag{3.36}$$

where Id *denotes the embedding operator from $\mathcal{A}^{\alpha,\beta}([-1,1]^d)$ into $L_\infty([-1,1]^d)$. Additionally, let $\mathrm{CL}(\boldsymbol{z}, M, I)$ be a reconstructing rank-1 Chebyshev lattice for the frequency index set $I := I_{\mathrm{a},n}^{d,T}$. Then, the sampling error is bounded by*

$$\|f - S_{I_{\mathrm{a},n}^{d,T}}^{\mathrm{CL}} f | L_\infty([-1,1]^d)\| \leq (1+2^{d-1}) \, n^{-(\alpha+\beta)} \, \|f | \mathcal{A}^{\alpha,\beta}([-1,1]^d)\|. \tag{3.37}$$

Proof. We apply Theorem 3.13 and we obtain for the truncation error

$$\begin{aligned}\|f - S_{I_{\mathrm{a},n}^{d,T}} f | L_\infty([-1,1]^d)\| &\leq \sum_{\boldsymbol{k}\in\mathbb{N}_0^d \setminus I_{\mathrm{a},n}^{d,T}} |\hat{f}_{\boldsymbol{k}}| = \|f - S_{I_{\mathrm{a},n}^{d,T}} f | \mathcal{A}([-1,1]^d)\| \\ &\leq \max_{\boldsymbol{k}\in\mathbb{N}_0^d \setminus I_{\mathrm{a},n}^{d,T}} \frac{1}{\omega^{\alpha,\beta,\mathbf{1}}(\boldsymbol{k})} \sum_{\boldsymbol{k}\in\mathbb{N}_0^d \setminus I_{\mathrm{a},n}^{d,T}} \omega^{\alpha,\beta,\mathbf{1}}(\boldsymbol{k}) \, |\hat{f}_{\boldsymbol{k}}| \\ &\leq n^{-(\alpha+\beta)} \, \|f | \mathcal{A}^{\alpha,\beta}([-1,1]^d)\|.\end{aligned}$$

For the lower bound in (3.36), we proceed analogously to the proof of Theorem 2.17. We define the d-variate algebraic polynomial $g(\boldsymbol{x}) := T_{\boldsymbol{k'}}(\boldsymbol{x})$ with $\boldsymbol{k'} := (n+1, 0, \ldots, 0)^\top \in \mathbb{N}_0^d$ and we conclude that the norm of $\mathrm{Id} - S_{I_{\mathrm{a},n}^{d,T}}$ is bounded from below by (3.36) since

$$\begin{aligned}&\|g - S_{I_{\mathrm{a},n}^{d,T}} g | L_\infty([-1,1]^d)\| = \|g | L_\infty([-1,1]^d)\| = \operatorname{ess\,sup}_{\boldsymbol{x}\in[-1,1]^d} |T_{\boldsymbol{k'}}(\boldsymbol{x})| = 1 \\ &= \|g | \mathcal{A}([-1,1]^d)\| = \omega^{-\alpha,-\beta,\mathbf{1}}(\boldsymbol{k'}) \, \omega^{\alpha,\beta,\mathbf{1}}(\boldsymbol{k'}) \, |\hat{f}_{\boldsymbol{k'}}| = (n+1)^{-(\alpha+\beta)} \, \|g | \mathcal{A}^{\alpha,\beta}([-1,1]^d)\|.\end{aligned}$$

Moreover, we estimate the sampling error by

$$\begin{aligned}\|f - S^{\mathrm{CL}}_{I^{d,T}_{\mathrm{a},n}} f | L_\infty([-1,1]^d)\| &\overset{(3.33)}{\leq} (1+2^{d-1}) \sum_{\boldsymbol{k}\in\mathbb{N}_0^d\setminus I^{d,T}_{\mathrm{a},n}} |\hat{f}_{\boldsymbol{k}}| \\ &\leq (1+2^{d-1})\, n^{-(\alpha+\beta)}\, \|f|\mathcal{A}^{\alpha,\beta}([-1,1]^d)\|,\end{aligned}$$

which completes the proof. ∎

As in Theorem 2.26 in the periodic case, we also show estimates for the sampling error $f - S^{\mathrm{CL}}_{I^{d,T}_{\mathrm{a},n}} f$ with respect to Hilbert space norms and we obtain analog results.

Theorem 3.17. *Let smoothness parameters $r,t,\alpha,\beta \in \mathbb{R}$ with $\beta \geq t \geq 0$ and $\alpha+\beta > r+t \geq 0$, a function $f \in \mathcal{H}^{\alpha,\beta}([-1,1]^d) \hookrightarrow \mathcal{A}^{\alpha,\beta}([-1,1]^d)$ and a frequency index set $I := I^{d,T}_{\mathrm{a},n}$ of refinement $n \geq 1$ with shape parameter $T := -\frac{\alpha-r}{\beta-t} \in [-\infty, 1)$ be given with $T := -\infty$ for $\beta = t$. Then, the truncation error is bounded by*

$$\|f - S_{I^{d,T}_{\mathrm{a},n}} f | \mathcal{H}^{r,t}([-1,1]^d)\| \leq n^{-(\alpha-r+\beta-t)}\, \|f|\mathcal{H}^{\alpha,\beta}([-1,1]^d)\|$$

and the operator norm of $\mathrm{Id} - S_{I^{d,T}_{\mathrm{a},n}}$ is bounded by

$$(n+1)^{-(\alpha-r+\beta-t)} \leq \|\,\mathrm{Id} - S_{I^{d,T}_{\mathrm{a},n}} | \mathcal{H}^{\alpha,\beta}([-1,1]^d) \to \mathcal{H}^{r,t}([-1,1]^d)\| \leq n^{-(\alpha-r+\beta-t)} \tag{3.38}$$

where Id *denotes the embedding operator from $\mathcal{H}^{\alpha,\beta}([-1,1]^d)$ into $\mathcal{H}^{r,t}([-1,1]^d)$.*
We restrict the shape parameter $T := -\frac{\alpha-r}{\beta-t} \in [-\frac{r}{t}, -\frac{\alpha}{\beta}]$ with $-\frac{r}{t} := -\infty$ for $t = 0$ and $-\frac{\alpha}{\beta} := -\infty$ for $\beta = 0$ as well as let the function $f \in \mathcal{A}^{\alpha,\beta}([-1,1]^d) \cap \mathcal{C}([-1,1]^d)$. Moreover, let $\mathrm{CL}(\boldsymbol{z}, M, I)$ be a reconstructing rank-1 Chebyshev lattice for the frequency index set $I := I^{d,T}_{\mathrm{a},n}$. Then, the sampling error is bounded by

$$\begin{aligned}&\|f - S^{\mathrm{CL}}_{I^{d,T}_{\mathrm{a},n}} f | \mathcal{H}^{r,t}([-1,1]^d)\| \\ &\leq n^{-(\alpha-r+\beta-t)} \left(\|f|\mathcal{H}^{\alpha,\beta}([-1,1]^d)\| + 2^{d-1}\, \|f|\mathcal{A}^{\alpha,\beta}([-1,1]^d)\| \right)\end{aligned} \tag{3.39}$$

and for functions $f \in \left(\mathcal{H}^{\alpha,\beta+\lambda}([-1,1]^d) \cap \mathcal{C}([-1,1]^d)\right) \subset \mathcal{A}^{\alpha,\beta}([-1,1]^d)$, $\lambda > 1/2$, this can be estimated by

$$\leq \left(1 + 2^{d-1}\,(1+2\zeta(2\lambda))^{\frac{d}{2}}\right) n^{-(\alpha-r+\beta-t)} \|f|\mathcal{H}^{\alpha,\beta+\lambda}([-1,1]^d)\|,\ \lambda > \tfrac{1}{2}. \tag{3.40}$$

Proof. We apply inequality (3.10) and proceed analogously to the proof of Theorem 2.26 from the periodic case. For the truncation error, we have $f - S_I f = \sum_{\boldsymbol{k}\in\mathbb{N}_0^d\setminus I} \hat{f}_{\boldsymbol{k}} T_{\boldsymbol{k}}(\circ)$ and thus,

$$\begin{aligned}\|f - S_{I^{d,T}_{\mathrm{a},n}} f | \mathcal{H}^{r,t}([-1,1]^d)\|^2 &= \sum_{\boldsymbol{k}\in\mathbb{N}_0^d\setminus I^{d,T}_{\mathrm{a},n}} \omega^{r,t,\mathbf{1}}(\boldsymbol{k})^2\, |\hat{f}_{\boldsymbol{k}}|^2 = \sum_{\boldsymbol{k}\in\mathbb{N}_0^d\setminus I^{d,T}_{\mathrm{a},n}} \frac{\omega^{r,t,\mathbf{1}}(\boldsymbol{k})^2}{\omega^{\alpha,\beta,\mathbf{1}}(\boldsymbol{k})^2}\, \omega^{\alpha,\beta,\mathbf{1}}(\boldsymbol{k})^2\, |\hat{f}_{\boldsymbol{k}}|^2 \\ &\leq \left(\max_{\boldsymbol{k}\in\mathbb{N}_0^d\setminus I^{d,T}_{\mathrm{a},n}} \frac{1}{\omega^{\alpha-r,\beta-t,\mathbf{1}}(\boldsymbol{k})^2} \right) \sum_{\boldsymbol{k}\in\mathbb{N}_0^d\setminus I^{d,T}_{\mathrm{a},n}} \omega^{\alpha,\beta,\mathbf{1}}(\boldsymbol{k})^2\, |\hat{f}_{\boldsymbol{k}}|^2 \\ &\leq n^{-2(\alpha-r+\beta-t)} \|f|\mathcal{H}^{\alpha,\beta}([-1,1]^d)\|^2.\end{aligned}$$

For the lower bound in (3.38), we use the example from the proof of Theorem 3.16. We define the algebraic polynomial $g(\boldsymbol{x}) := T_{\boldsymbol{k'}}(\boldsymbol{x})$ with $\boldsymbol{k'} := (n+1, 0, \ldots, 0)^\top \in \mathbb{N}_0^d$ and we conclude that the norm of $\mathrm{Id} - S_{I_{\mathrm{a},n}^{d,T}}$ is bounded from below by (3.38) since

$$\begin{aligned}\|g - S_{I_{\mathrm{a},n}^{d,T}} g | \mathcal{H}^{r,t}([-1,1]^d)\| &= \|g|\mathcal{H}^{r,t}([-1,1]^d)\| = \sqrt{\omega^{r-\alpha,t-\beta,\mathbf{1}}(\boldsymbol{k'})^2\ \omega^{\alpha,\beta,\mathbf{1}}(\boldsymbol{k'})^2\ |\hat{f}_{\boldsymbol{k'}}|^2} \\ &= (n+1)^{-(\alpha-r+\beta-t)}\ \|g|\mathcal{H}^{\alpha,\beta}([-1,1]^d)\|.\end{aligned}$$

For the aliasing error $S_{I_{\mathrm{a},n}^{d,T}} f - S^{\mathrm{CL}}_{I_{\mathrm{a},n}^{d,T}} f$ of a function $f \in \mathcal{A}^{\alpha,\beta}([-1,1]^d) \cap \mathcal{C}([-1,1]^d)$, we have the aliasing formula (3.31) and, in consequence of the concaveness of the square root function, we conclude

$$\begin{aligned}
\|S_{I_{\mathrm{a},n}^{d,T}} f - S^{\mathrm{CL}}_{I_{\mathrm{a},n}^{d,T}} f | \mathcal{H}^{r,t}([-1,1]^d)\| &= \left(\sum_{\boldsymbol{k} \in I_{\mathrm{a},n}^{d,T}} \omega^{r,t,\mathbf{1}}(\boldsymbol{k})^2 \left| \hat{f}_{\boldsymbol{k}} - \hat{f}^{\mathrm{CL}}_{\boldsymbol{k}} \right|^2 \right)^{\frac{1}{2}} && (3.41) \\
&\leq \sum_{\boldsymbol{k} \in I_{\mathrm{a},n}^{d,T}} \omega^{r,t,\mathbf{1}}(\boldsymbol{k}) \left| \hat{f}_{\boldsymbol{k}} - \hat{f}^{\mathrm{CL}}_{\boldsymbol{k}} \right| && (3.42) \\
&\leq \max_{\boldsymbol{k} \in I_{\mathrm{a},n}^{d,T}} \omega^{r,t,\mathbf{1}}(\boldsymbol{k}) \sum_{\boldsymbol{k} \in I_{\mathrm{a},n}^{d,T}} \left| \hat{f}_{\boldsymbol{k}} - \hat{f}^{\mathrm{CL}}_{\boldsymbol{k}} \right| \\
&\overset{(2.59)}{\underset{(3.35)}{\leq}} d^{(Tt+r)/(1-T)} n^{r+t} \quad 2^{d-1} \sum_{\boldsymbol{k} \in \mathbb{N}_0^d \setminus I_{\mathrm{a},n}^{d,T}} \frac{\omega^{\alpha,\beta,\mathbf{1}}(\boldsymbol{k})}{\omega^{\alpha,\beta,\mathbf{1}}(\boldsymbol{k})} |\hat{f}_{\boldsymbol{k}}| \\
&\leq d^{\frac{Tt+r}{1-T}} n^{r+t}\ 2^{d-1} \max_{\boldsymbol{k} \in \mathbb{N}_0^d \setminus I_{\mathrm{a},n}^{d,T}} \frac{1}{\omega^{\alpha,\beta,\mathbf{1}}(\boldsymbol{k})}\ \|f|\mathcal{A}^{\alpha,\beta}([-1,1]^d)\| \\
&\overset{L.\ 2.16}{\leq} 2^{d-1}\ n^{-(\alpha-r+\beta-t)}\ \|f|\mathcal{A}^{\alpha,\beta}([-1,1]^d)\|
\end{aligned}$$

and we obtain (3.39). For functions $f \in \mathcal{H}^{\alpha,\beta+\lambda}([-1,1]^d) \cap \mathcal{C}([-1,1]^d)$, $\lambda > 1/2$, we use inequality (3.30) and the inequality $\|f|\mathcal{H}^{\alpha,\beta}([-1,1]^d)\| \leq \|f|\mathcal{H}^{\alpha,\beta+\lambda}([-1,1]^d)\|$, which yield the estimate (3.40). ∎

Since we have relation (3.13), we obtain the asymptotic bounds (2.33) from Lemma 2.5 on the cardinalities $|I_{\mathrm{a},n}^{d,T}|$ of the frequency index sets $I_{\mathrm{a},n}^{d,T}$ from the non-periodic case. This yields upper bounds on the sampling errors $f - S^{\mathrm{CL}}_{I_{\mathrm{a},n}^{d,T}} f$ with respect to the degrees of freedom $|I_{\mathrm{a},n}^{d,T}|$.

Corollary 3.18. *Let a function $f \in \mathcal{A}^{\alpha,\beta}([-1,1]^d) \cap \mathcal{C}([-1,1]^d)$, a frequency index set $I := I_{\mathrm{a},n}^{d,T}$ and a reconstructing rank-1 Chebyshev lattice $\mathrm{CL}(\boldsymbol{z}, M, I)$ be given, where the refinement $n \geq 1$, the dominating mixed smoothness $\beta \geq 0$, the isotropic smoothness $\alpha > -\beta$ and the shape parameter $T := -\frac{\alpha}{\beta}$ with $T := -\infty$ for $\beta = 0$. Then, for fixed dimension d, the sampling error is bounded by*

$$\|f - S^{\mathrm{CL}}_{I_{\mathrm{a},n}^{d,T}} f | L_\infty([-1,1]^d)\| \lesssim \|f|\mathcal{A}^{\alpha,\beta}([-1,1]^d)\| \begin{cases} |I_{\mathrm{a},n}^{d,T}|^{-(\beta+\alpha/d)} & \text{for } T \in [-\infty, 0), \\ |I_{\mathrm{a},n}^{d,0}|^{-\beta} (\log |I_{\mathrm{a},n}^{d,0}|)^{(d-1)\beta} & \text{for } T = 0, \\ |I_{\mathrm{a},n}^{d,T}|^{-(\alpha+\beta)} & \text{for } T \in (0,1). \end{cases}$$

Proof. Using estimate (3.37) from Theorem 3.16 and proceeding similar to the proof of Corollary 2.21 together with relation (3.13), we obtain the assertion. ∎

Corollary 3.19. *Let smoothness parameters $r, t, \alpha, \beta \in \mathbb{R}$ with $\beta \geq t \geq 0$ and $\alpha+\beta > r+t \geq 0$, a function $f \in \mathcal{H}^{\alpha,\beta+\lambda}([-1,1]^d) \cap \mathcal{C}([-1,1]^d)$, $\lambda > 1/2$, a frequency index set $I := I_{\mathrm{a},n}^{d,T}$ of refinement $n \geq 1$ and a reconstructing rank-1 Chebyshev lattice $\mathrm{CL}(\boldsymbol{z}, M, I)$ be given, where the shape parameter $T := -\frac{\alpha-r}{\beta-t} \in [-\frac{r}{t}, -\frac{\alpha}{\beta}]$ with $-\frac{r}{t} := -\infty$ for $t = 0$ and $-\frac{\alpha}{\beta} := -\infty$ for $\beta = 0$. Then, for fixed dimension d, the sampling error is bounded by*

$$\|f - S^{\mathrm{CL}}_{I_{\mathrm{a},n}^{d,T}} f | \mathcal{H}^{r,t}([-1,1]^d)\| \lesssim \|f|\mathcal{H}^{\alpha,\beta+\lambda}([-1,1]^d)\| \cdot \begin{cases} |I_{\mathrm{a},n}^{d,T}|^{-(\beta-t+\frac{\alpha-r}{d})} & \text{for } T \in [-\infty, 0), \\ |I_{\mathrm{a},n}^{d,0}|^{-(\beta-t)} (\log |I_{\mathrm{a},n}^{d,0}|)^{(d-1)(\beta-t)} & \text{for } T = 0, \\ |I_{\mathrm{a},n}^{d,T}|^{-(\alpha-r+\beta-t)} & \text{for } T \in (0, 1). \end{cases}$$

Proof. Using estimate (3.40) from Theorem 3.17 and proceeding similar to the proof of Corollary 2.21 together with relation (3.13), we obtain the assertion. ∎

3.5 Numerical examples

In this section, we present numerical results for the considerations in Section 3.2 and 3.4. All numerical tests were performed in IEEE 754 double precision arithmetic using MATLAB R2015b on a computer with Intel Xeon E7-4880 2.50 GHz CPU.

We start with the reconstruction of random multivariate algebraic polynomials in Chebyshev form a_I from samples along reconstructing rank-1 Chebyshev lattices $\mathrm{CL}(\boldsymbol{z}, M, I)$.

Example 3.20. For each dimension $d \in \{2, \ldots, 5\}$, we randomly generate 100 multivariate algebraic polynomials in Chebyshev form a_I with 1000 frequencies $\boldsymbol{k} \in I$, $|I| = 1000$, chosen uniformly at random from $\hat{G}_{128}^d := \{0, 1, \ldots, 128\}^d$, and with corresponding Chebyshev coefficients $\hat{a}_{\boldsymbol{k}}$, $\boldsymbol{k} \in I$, chosen uniformly at random from $[-1, 1]$. For these polynomials a_I, we build reconstructing rank-1 Chebyshev lattices $\mathrm{CL}(\boldsymbol{z}, M, I)$ using the two approaches discussed in Section 3.2.2. The first approach for obtaining reconstructing rank-1 Chebyshev lattices is based on Theorem 3.4, i.e., we construct a reconstructing rank-1 lattice $\Lambda(\boldsymbol{z}, \hat{M}, \mathcal{M}(I))$ from the periodic case for the extended symmetric index set $\mathcal{M}(I)$ with even rank-1 lattice size $\hat{M} \in 2\mathbb{N}$ and we obtain the reconstructing rank-1 Chebyshev lattice $\mathrm{CL}(\boldsymbol{z}, M = \frac{\hat{M}}{2}, I)$ for I. In doing so, we first apply Algorithm 2.2 on the extended symmetric index set $\mathcal{M}(I)$ and obtain reconstructing rank-1 lattices $\Lambda(\boldsymbol{z}, \hat{M}, \mathcal{M}(I))$. If the corresponding rank-1 lattice size $\hat{M}$ is not even, we search for a larger (even) one. This yields a reconstructing rank-1 Chebyshev lattice $\mathrm{CL}(\boldsymbol{z}, M = \frac{\hat{M}}{2}, I)$ for each frequency index set I. The second approach directly builds a reconstructing rank-1 Chebyshev lattice $\mathrm{CL}(\boldsymbol{z}, M, I)$ using Algorithm 3.3. Having a reconstructing rank-1 Chebyshev lattice $\mathrm{CL}(\boldsymbol{z}, M, I)$, we sample the multivariate algebraic polynomials in Chebyshev form a_I at the corresponding nodes $\boldsymbol{x}_j := \cos(\frac{j}{M}\pi\boldsymbol{z})$, $j = 0, \ldots, M$, and reconstruct the Chebyshev coefficients $\hat{a}_{\boldsymbol{k}}$, $\boldsymbol{k} \in I$, using Algorithm 3.2. We determine the relative ℓ_1 error $\sum_{\boldsymbol{k}\in I} |\tilde{\hat{a}}_{\boldsymbol{k}} - \hat{a}_{\boldsymbol{k}}| / \sum_{\boldsymbol{k}\in I} |a_{\boldsymbol{k}}|$, where $\tilde{\hat{a}}_{\boldsymbol{k}}$ denote the numerically reconstructed Chebyshev coefficients from Algorithm 3.2. The obtained relative ℓ_1 errors are up to 4.8e-11 in IEEE 754 double precision arithmetic if the sampling values $a_I(\boldsymbol{x}_j)$ are generated by a direct computation of formula (3.12). When we use Algorithm 3.1 with a fast version of the DCT instead for generating sampling values $a_I(\boldsymbol{x}_j)$, we obtain a maximal relative ℓ_1 error of 1.1e-15. In Table 3.1, we present the numerical results. In the columns 3–5, we show the results for reconstructing rank-1 Chebyshev lattices $\mathrm{CL}(\boldsymbol{z}, M, I)$ generated by Algorithm 2.2 in combination with Theorem 3.4 and in columns 6–8 the results when generated by Algorithm 3.3. In both cases, we give the minimal and maximal size parameter M

and the maximal relative ℓ_1 error, where the maximum is computed over the 100 multivariate algebraic polynomials in Chebyshev form a_I for each dimension d. We observe that the errors for both construction methods behave similarly and are at most 1.1e-15. The reconstruction using Algorithm 3.2 succeeded in all considered cases. For dimensions $d \geq 3$, the direct construction approach of Algorithm 3.3 yields distinctly smaller size parameters M compared the method based on Theorem 3.4 which first builds a reconstructing rank-1 lattice $\Lambda(\boldsymbol{z}, \hat{M}, \mathcal{M}(I))$ for the extended symmetric index set $\mathcal{M}(I)$. Moreover, we observe that the maximal size parameters M are roughly the same for dimension $d = 4$ and $d = 5$ when using the direct construction approach of Algorithm 3.3. For the construction approach via a reconstructing rank-1 lattice $\Lambda(\boldsymbol{z}, \hat{M}, \mathcal{M}(I))$ based on Theorem 3.4, the maximal size parameters M grow for increasing dimension d by a factor of about 3.5 starting from $d \geq 3$. For the considered test cases, already the first three or four components of the generating vector $\boldsymbol{z} \in \mathbb{N}_0^d$ of a reconstructing rank-1 Chebyshev lattice $\mathrm{CL}(\boldsymbol{z}, M, I)$ often suffice to have the reconstruction property (3.22) fulfilled and the remaining components of $\boldsymbol{z}$ (except the t-th) may be set to zero due to the large numbers of possible frequencies $|\hat{G}_{128}^d| = 129^d$ and the small cardinality $|I| = 1\,000$ of the used frequency index sets I. However, if we use the construction approach via a reconstructing rank-1 lattice $\Lambda(\boldsymbol{z}, \hat{M}, \mathcal{M}(I))$ based on Theorem 3.4, the cardinalities $|\mathcal{M}(I)| \leq 2^d |I|$ of the extended symmetric index sets $\mathcal{M}(I)$ grow for increasing dimension d and the rank-1 lattice sizes $\hat{M}$ grow since we have necessarily $\hat{M} \geq |\mathcal{M}(I)|$ due to reconstruction property (2.27) compared to $M \geq |I|$ caused by reconstruction property (3.22) of the direct construction approach of Algorithm 3.3. □

parameters		$\mathrm{CL}(\boldsymbol{z}, M = \frac{\hat{M}}{2}, I)$ Algorithm 2.2, Theorem 3.4			$\mathrm{CL}(\boldsymbol{z}, M, I)$ Algorithm 3.3		
d	$\lvert I\rvert$	min M	max M	max_err	min M	max M	max_err
2	1 000	15 239	18 076	7.5e-16	15 982	17 781	6.2e-16
3	1 000	336 475	508 623	7.8e-16	151 998	238 070	9.6e-16
4	1 000	1 253 573	1 793 631	1.1e-15	145 074	473 323	9.7e-16
5	1 000	4 559 243	6 371 833	1.1e-15	156 237	452 740	9.6e-16

Table 3.1: Minimal and maximal size parameters M of reconstructing rank-1 Chebyshev lattices $\mathrm{CL}(\boldsymbol{z}, M, I)$ for 100 random frequency index sets $I \subset \hat{G}_{128}^d := \{0, 1, \ldots, 128\}^d$ as well as maximal relative ℓ_1 errors when using Algorithm 3.2 for the reconstruction of multivariate algebraic polynomials in Chebyshev form a_I with random Chebyshev coefficients $\hat{a}_{\boldsymbol{k}} \in [-1, 1]$.

Next, we determine reconstructing rank-1 Chebyshev lattices $\mathrm{CL}(\boldsymbol{z}, M, I_{\mathrm{a},n}^{d,0})$ for hyperbolic cross frequency index sets $I := I_{\mathrm{a},n}^{d,0}$ using the methods from Section 3.2.2. These will be used in later examples.

Example 3.21. We build reconstructing rank-1 Chebyshev lattices $\mathrm{CL}(\boldsymbol{z}, M, I_{\mathrm{a},n}^{d,0})$ for hyperbolic cross frequency index sets $I := I_{\mathrm{a},n}^{d,0}$ of dimensions $d = 2, 3, 4, 5, 6$ and various refinements $n \in \mathbb{N}$ using the two approaches discussed in Section 3.2.2. In Table 3.2, we give the cardinalities $|I|$ of the considered hyperbolic crosses as well as the cardinalities of the mirrored frequency index sets $\mathcal{M}_1(I)$ and extended symmetric index sets $\mathcal{M}(I)$. We observe almost a constant ratio $|\mathcal{M}(I)|/|I|$ for increasing refinement n and fixed dimension $d \in \{3, 4, 5, 6\}$ as well as approximately $|\mathcal{M}(I)|/|I| \asymp 1.6^d$ for increasing dimension d and fixed refinement $n \in \{32, 64, 128\}$. In the 6th and 7th column of Table 3.2, the size

parameters $M = \hat{M}/2$ and oversampling factors $(\hat{M}/2+1)/|I_{\mathrm{a},n}^{d,0}|$ of reconstructing rank-1 Chebyshev lattices $\mathrm{CL}(\boldsymbol{z}, M = \hat{M}/2, I) = \Lambda(\boldsymbol{z}, \hat{M}, \mathcal{M}(I))$ constructed by Algorithm 2.2 in combination with Theorem 3.4 are given. Additionally, we directly build the reconstructing rank-1 Chebyshev lattices $\mathrm{CL}(\boldsymbol{z}, M, I)$ using Algorithm 3.3. The corresponding size parameters M and oversampling factors $(M+1)/|I_{\mathrm{a},n}^{d,0}|$ are shown in the 8th and 9th column of Table 3.2. We observe that the obtained size parameters M for both construction approaches coincide in the considered cases for dimension $d = 2$ and almost coincide for dimension $d = 3$. However, for dimension $d = 4, 5, 6$, the obtained values differ distinctly in several cases, the resulting size parameters M may be considerably lower when using Algorithm 3.3. For instance for refinement $n = 128$ and dimension $d = 6$, there is a factor of about 1.6 between both approaches.
In Figure 3.7, we compare the oversampling factors $M/|I_n^{d,0,\mathbf{1}}|$ of the reconstructing rank-1 lattices $\Lambda(\boldsymbol{z}, M, I_n^{d,0,\mathbf{1}})$ for hyperbolic cross frequency index sets $I_n^{d,0,\mathbf{1}}$ from Table 2.5 and $(M+1)/|I_{\mathrm{a},n}^{d,0}|$ of the reconstructing rank-1 Chebyshev lattices $\mathrm{CL}(\boldsymbol{z}, M, I_{\mathrm{a},n}^{d,0})$ for hyperbolic cross frequency index sets $I_{\mathrm{a},n}^{d,0}$ from Table 3.2. In Figure 3.7a, we visualize the oversampling factors for fixed dimension $d \in \{3, 4, 6\}$. Due to the theoretical results for hyperbolic cross frequency index sets $I_n^{d,0,\mathbf{1}}$ in Table 2.3, the oversampling factors should behave approximately like $\asymp n/\log n$ and this behavior should transfer to the non-periodic case, since we have Corollary 3.6 and since we numerically observe approximately $1.6^d \asymp |\mathcal{M}(I_{\mathrm{a},n}^{d,0})|/|I_{\mathrm{a},n}^{d,0}| = |I_n^{d,0}|/|I_{\mathrm{a},n}^{d,0}|$. We obtain that the oversampling factors grow approximately like this upper bound for the considered refinements $n \in \mathbb{N}$, or slightly larger which may be because of the relatively small values of the refinement n. Moreover, the constants for the reconstructing rank-1 Chebyshev lattices $\mathrm{CL}(\boldsymbol{z}, M, I_{\mathrm{a},n}^{d,0})$ are higher than the ones for the reconstructing rank-1 lattices $\Lambda(\boldsymbol{z}, M, I_n^{d,0,\mathbf{1}})$. In Figure 3.7b, we consider the growth of the oversampling factors with respect to the dimension d for fixed refinement $n \in \{32, 64, 128\}$. We observe that the oversampling factors $M/|I_n^{d,0,\mathbf{1}}|$ of the reconstructing rank-1 lattices $\Lambda(\boldsymbol{z}, M, I_n^{d,0,\mathbf{1}})$ grow approximately like $\asymp 1.62^d$. Moreover, the oversampling factors $(M+1)/|I_{\mathrm{a},n}^{d,0}|$ of the reconstructing rank-1 Chebyshev lattices $\mathrm{CL}(\boldsymbol{z}, M, I_{\mathrm{a},n}^{d,0})$ increase approximately between $\asymp 2.05^d$ and $\asymp 2.2^d$. □

Based on the reconstructing rank-1 Chebyshev lattices $\mathrm{CL}(\boldsymbol{z}, M, I_{\mathrm{a},n}^{d,0})$ for hyperbolic cross frequency index sets $I := I_{\mathrm{a},n}^{d,0}$ from Table 3.2, we generate random Chebyshev coefficients $\hat{a}_{\boldsymbol{k}}$, $\boldsymbol{k} \in I$, which yield multivariate algebraic polynomials in Chebyshev form a_I, and we reconstruct a_I from samples using Algorithm 3.2.

Example 3.22. We perform reconstruction tests similar to the ones in Example 3.20 for multivariate algebraic polynomials in Chebyshev form a_I for hyperbolic cross frequency index sets $I := I_{\mathrm{a},n}^{d,0}$ of refinements $n \in \{16, 32, 64, 128, 256\}$ and dimensions $d \in \{3, 4, 5\}$ with Chebyshev coefficients $\hat{a}_{\boldsymbol{k}}$ chosen uniformly at random from $[-1, 1]$. We use the reconstructing rank-1 Chebyshev lattices $\mathrm{CL}(\boldsymbol{z}, M, I)$ from Table 3.2. We sample at the corresponding nodes $\boldsymbol{x}_j$, $j = 0, \ldots, M$, and apply Algorithm 3.2 for the reconstruction of the Chebyshev coefficients $\hat{a}_{\boldsymbol{k}}$, $\boldsymbol{k} \in I$. For each hyperbolic cross frequency index set $I := I_{\mathrm{a},n}^{d,0}$, we repeat the tests 10 times with different random Chebyshev coefficients $\hat{a}_{\boldsymbol{k}}$ and determine the maximal relative ℓ_1 error of the Chebyshev coefficients $\hat{a}_{\boldsymbol{k}}$. We observe that the reconstruction succeeded in all considered cases. The observed maximal relative ℓ_1 error was $7.4 \cdot 10^{-16}$. In Table 3.3, we show the obtained results. □

Next, we approximately reconstruct Chebyshev coefficients $\hat{f}_{\boldsymbol{k}}$ of test functions f using the results from Section 3.4. We define the shifted, scaled and dilated B-Spline $B_2 \colon \mathbb{R} \to \mathbb{R}$

parameters		cardinalities for hyperbolic cross index set $I := I^{d,0}_{\mathrm{a},n}$			$\mathrm{CL}(\boldsymbol{z}, M = \frac{\hat{M}}{2}, I)$ Algorithm 2.2, Theorem 3.4		$\mathrm{CL}(\boldsymbol{z}, M, I)$ Algorithm 3.3	
d	n	$\lvert I^{d,0}_{\mathrm{a},n}\rvert$	$\lvert\mathcal{M}_1(I^{d,0}_{\mathrm{a},n})\rvert$	$\lvert\mathcal{M}(I^{d,0}_{\mathrm{a},n})\rvert = \lvert I^{d,0,\mathbf{1}}_{n}\rvert$	$M = \frac{\hat{M}}{2}$	$\frac{\frac{\hat{M}}{2}+1}{\lvert I^{d,0}_{\mathrm{a},n}\rvert}$	M	$\frac{M+1}{\lvert I^{d,0}_{\mathrm{a},n}\rvert}$
2	8	37	65	113	82	2.24	82	2.24
2	16	83	149	265	290	3.51	290	3.51
2	32	184	335	605	1 090	5.93	1 090	5.93
2	64	409	753	1 377	4 226	10.33	4 226	10.33
2	128	902	1 675	3 093	16 642	18.45	16 642	18.45
2	256	1 979	3 701	6 889	66 050	33.38	66 050	33.38
2	512	4 305	8 097	15 169	263 170	61.13	263 170	61.13
3	8	123	353	593	518	4.22	518	4.22
3	16	309	921	1 577	1 814	5.87	1 814	5.87
3	32	754	2 313	4 021	6 222	8.25	5 859	7.77
3	64	1 829	5 745	10 113	26 501	14.49	18 473	10.10
3	128	4 365	13 981	24 869	94 755	21.71	89 198	20.44
3	256	10 303	33 553	60 217	359 075	34.85	302 883	29.40
3	512	23 976	79 197	143 225	1 424 662	59.42	1 424 613	59.42
4	8	368	1 681	2 769	2 864	7.79	2 181	5.93
4	16	1 009	4 845	8 113	13 656	13.54	8 492	8.42
4	32	2 665	13 343	22 665	52 079	19.54	44 000	16.51
4	64	6 945	36 001	61 889	249 837	35.97	176 948	25.48
4	128	17 700	94 503	164 137	1 083 747	61.23	860 284	48.60
4	256	44 403	243 205	426 193	4 355 469	98.09	3 136 383	70.63
4	512	109 395	612 765	1 082 305	19 550 612	178.72	14 659 035	134.00
5	8	1 032	7 401	12 033	18 245	17.68	12 691	12.30
5	16	3 042	23 153	38 193	89 911	29.56	57 985	19.06
5	32	8 603	69 025	115 385	376 606	43.78	288 785	33.57
5	64	23 853	200 097	338 305	1 703 741	71.43	1 382 832	57.97
5	128	64 373	561 241	958 345	9 138 634	141.96	6 843 471	106.31
5	256	170 299	1 535 585	2 644 977	41 255 293	242.25	31 997 990	187.89
6	8	2 768	30 897	49 761	95 904	34.65	65 849	23.79
6	16	8 684	103 701	169 209	557 773	64.23	303 396	34.94
6	32	26 088	331 423	547 461	2 867 903	109.93	1 751 513	67.14
6	64	76 433	1 024 081	1 709 857	13 603 339	177.98	8 979 932	117.49
6	128	217 113	3 048 067	5 137 789	83 435 553	384.30	51 662 221	237.95

Table 3.2: Cardinalities of hyperbolic cross frequency index sets $I := I^{d,0}_{\mathrm{a},n}$, mirrored index sets $\mathcal{M}_1(I^{d,0}_{\mathrm{a},n})$ and extended symmetric index sets $\mathcal{M}(I^{d,0}_{\mathrm{a},n}) = I^{d,0,\mathbf{1}}_{n}$ as well as size parameters M and oversampling factors $(M+1)/|I|$ of reconstructing rank-1 Chebyshev lattices $\mathrm{CL}(\boldsymbol{z}, M, I)$, when using Algorithm 2.2 in combination with Theorem 3.4 as well as Algorithm 3.3.

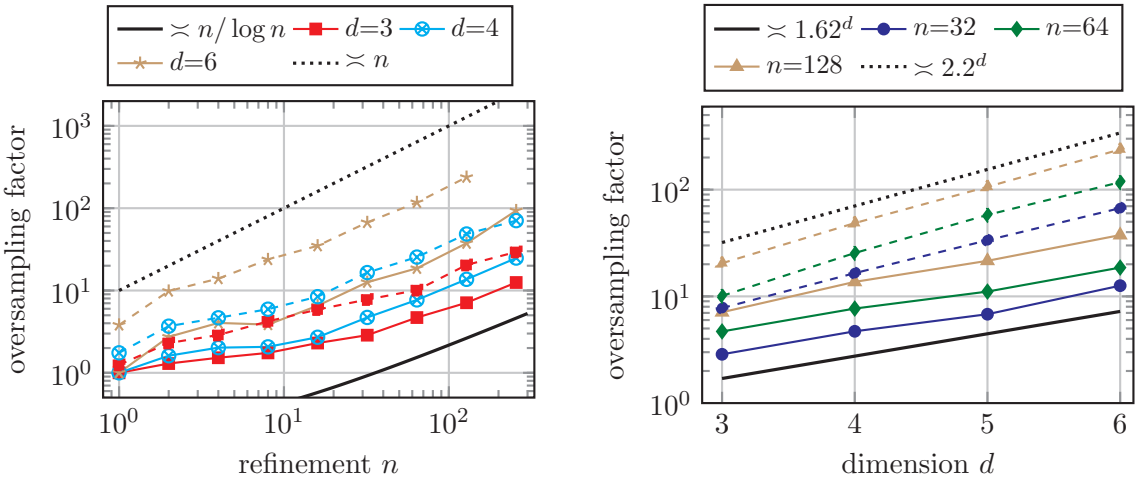

(a) with respect to the refinement $n \in \mathbb{N}$ for fixed dimensions $d \in \{3, 4, 6\}$

(b) with respect to the dimension d for fixed refinement $n \in \{32, 64, 128\}$

Figure 3.7: Illustration of oversampling factors $M/|I_n^{d,0,\mathbf{1}}|$ of reconstructing rank-1 lattices $\Lambda(\boldsymbol{z}, M, I_n^{d,0,\mathbf{1}})$ from Table 2.5 (solid lines with marks) and $(M+1)/|I_{\mathrm{a},n}^{d,0}|$ of reconstructing rank-1 Chebyshev lattices $\mathrm{CL}(\boldsymbol{z}, M, I_{\mathrm{a},n}^{d,0})$ from Table 3.2 (dashed lines with marks).

parameters			$\mathrm{CL}(\boldsymbol{z}, M = \frac{\hat{M}}{2}, I)$ Algorithm 2.2, Theorem 3.4		$\mathrm{CL}(\boldsymbol{z}, M, I)$ Algorithm 3.3	
d	n	$\lvert I\rvert$	M	max_err	M	max_err
3	16	309	1 814	3.7e-16	1 814	3.7e-16
3	32	754	6 222	3.0e-16	5 859	2.4e-16
3	64	1 829	26 501	5.0e-16	18 473	2.1e-16
3	128	4 365	94 755	3.4e-16	89 189	7.4e-16
3	256	10 303	359 075	6.7e-16	302 883	6.0e-16
4	16	1 009	13 656	4.4e-16	8 492	3.8e-16
4	32	2 665	52 079	3.1e-16	44 000	2.1e-16
4	64	6 945	249 837	2.9e-16	176 948	3.6e-16
4	128	17 700	1 083 747	3.1e-16	860 284	3.4e-16
4	256	44 403	4 355 469	3.7e-16	3 136 383	4.1e-16
5	16	3 042	89 911	3.9e-16	57 985	6.4e-16
5	32	8 603	376 606	3.1e-16	288 785	6.9e-16
5	64	23 853	1 703 741	2.9e-16	1 382 832	3.7e-16
5	128	64 373	9 138 634	2.4e-16	6 843 471	4.8e-16
5	256	170 299	41 255 293	3.0e-16	31 997 990	3.5e-16

Table 3.3: Size parameters M of reconstructing rank-1 Chebyshev lattices $\mathrm{CL}(\boldsymbol{z}, M, I)$ for symmetric hyperbolic cross frequency index sets $I := I_{\mathrm{a},n}^{d,0}$ as well as maximal relative ℓ_1 errors of the Chebyshev coefficients $\hat{a}_{\boldsymbol{k}}$ when using Algorithm 3.2 for the reconstruction of 10 multivariate algebraic polynomials in Chebyshev form a_I with random Chebyshev coefficients $\hat{a}_{\boldsymbol{k}} \in [-1, 1]$, $\boldsymbol{k} \in I_{\mathrm{a},n}^{d,0}$.

of order 2 by

$$B_2(x) := \begin{cases} x^2/8 + 9x/8 + 81/32 & \text{for } -9/2 \le x < -5/2, \\ -x^2/4 - 3x/4 + 3/16 & \text{for } -5/2 \le x < -1/2, \\ x^2/8 - 3x/8 + 9/32 & \text{for } -1/2 \le x < 3/2, \\ 0 & \text{otherwise.} \end{cases} \tag{3.43}$$

Using tensorization, we define the d-variate version $B_2^d(\boldsymbol{x}) := \prod_{t=1}^d B_2(x_t)$. We restrict our consideration on the function B_2^d to the box $[-1,1]^d$ and we are going to approximate $f := B_2^d \in L_{2,\mathrm{w}}([-1,1]^d)$ by the truncated Chebyshev series $S_I B_2^d(\boldsymbol{x}) := \sum_{\boldsymbol{k}\in I} \hat{f}_{\boldsymbol{k}} T_{\boldsymbol{k}}(\boldsymbol{x})$. Due to the tensor product structure, we use hyperbolic cross frequency index sets $I := I_{\mathrm{a},n}^{d,0}$. In Figure 3.8, we visualize the one-dimensional function B_2 as well as the two-dimensional hyperbolic cross frequency index set $I_{\mathrm{a},16}^{2,0}$ and a reconstructing rank-1 Chebyshev lattice $\mathrm{CL}(\boldsymbol{z}, M, I_{\mathrm{a},16}^{2,0})$.

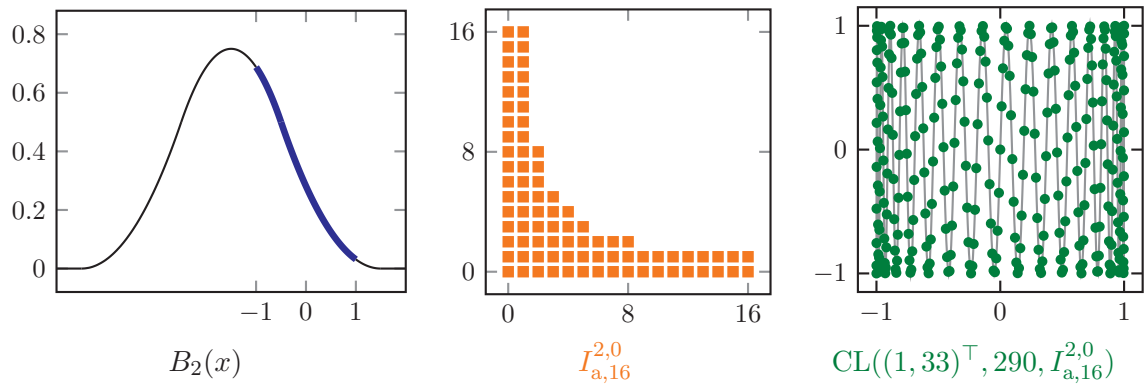

Figure 3.8: Visualization of shifted, scaled and dilated B-Spline B_2 of order 2 as well as hyperbolic cross frequency index set $I_{\mathrm{a},16}^{2,0}$ and corresponding reconstructing rank-1 Chebyshev lattice $\mathrm{CL}(\boldsymbol{z}, M, I_{\mathrm{a},16}^{2,0})$ with generating vector $\boldsymbol{z} := (1,33)^\top$ and size parameter $M := 290$.

The Chebyshev coefficients $\hat{f}_k$, $k \in \mathbb{N}_0$, of B_2 are given by

$$\hat{f}_k = \begin{cases} \dfrac{9\sqrt{3}k\cos(2k\pi/3) - 9(-2+k^2)\sin(2k\pi/3)}{8k(4-5k^2+k^4)\pi} & \text{for } k \ge 3, \\ 9\sqrt{3}/(128\pi) & \text{for } k = 2, \\ -1/2 + 9\sqrt{3}/(32\pi) & \text{for } k = 1, \\ 1/4 + 9\sqrt{3}/(64\pi) & \text{for } k = 0, \end{cases} \tag{3.44}$$

which yields $|\hat{f}_k| \lesssim k^{-3}$. Consequently, we have $B_2^d \in \mathcal{A}^{0,2-\epsilon}([-1,1]^d)$ and $B_2^d \in \mathcal{H}^{0,5/2-\epsilon}([-1,1]^d)$ for any $\epsilon > 0$.

First, we investigate the truncation errors $B_2^d - S_{I_{\mathrm{a},n}^{d,0}} B_2^d$ with respect to the refinement $n \in \mathbb{N}$.

Example 3.23. For $d \in \{2,3,4,5,6\}$ and refinements $n \in \{1, 2^1, 2^2, \ldots, 2^9\}$, the relative truncation errors

$$\|B_2^d - S_{I_{\mathrm{a},n}^{d,0}} B_2^d | \mathcal{A}([-1,1]^d)\| / \|B_2^d | \mathcal{A}([-1,1]^d)\|$$

are depicted in Figure 3.9a. From Theorem 3.16 with dominating mixed smoothness $\beta = 2-\epsilon$,

$\epsilon > 0$, and isotropic smoothness $\alpha = 0$, we obtain the upper bound

$$\frac{\|B_2^d - S_{I_{\mathrm{a},n}^{d,0}} B_2^d | L_\infty([-1,1]^d)\|}{\|B_2^d | \mathcal{A}([-1,1]^d)\|} \leq \frac{\|B_2^d - S_{I_{\mathrm{a},n}^{d,0}} B_2^d | \mathcal{A}([-1,1]^d)\|}{\|B_2 | \mathcal{A}([-1,1]^d)\|} \leq n^{-2+\epsilon} \frac{\|B_2^d | \mathcal{A}^{0,2-\epsilon}([-1,1]^d)\|}{\|B_2^d | \mathcal{A}([-1,1]^d)\|}$$

and the observed decay rates correspond roughly to the estimates. In this upper bound, the factor $\|B_2^d | \mathcal{A}^{0,2-\epsilon}([-1,1]^d)\| / \|B_2^d | \mathcal{A}([-1,1]^d)\|$ may be large, for instance $> 4.19^d$ for $\epsilon = 0.05$. Additionally, the relative truncation error measured in the $L_{2,w}([-1,1]^d)$ norm is shown in Figure 3.9b. Theorem 3.17 with $\beta = 5/2 - \epsilon$ and $r = t = \alpha = 0$ yields the upper bound

$$\frac{\|B_2^d - S_{I_{\mathrm{a},n}^{d,0}} B_2^d | L_{2,w}([-1,1]^d)\|}{\|B_2^d | L_{2,w}([-1,1]^d)\|} \leq \pi^{\frac{d}{2}} n^{-5/2+\epsilon} \frac{\|B_2^d | \mathcal{H}^{0,5/2-\epsilon}([-1,1]^d)\|}{\|B_2^d | L_{2,w}([-1,1]^d)\|}.$$

We observe that the rates of the measured errors approximately decay as the theoretical upper bounds suggest. Especially for higher dimensions d, the observed decay rate is slightly smaller, which most likely is caused by the relatively small values of the refinement n and the large constants (increasing with d). For instance, the factor $\|B_2^d | \mathcal{H}^{0,5/2-\epsilon}([-1,1]^d) / \|B_2^d | L_{2,w}([-1,1]^d)\|$ is greater than 1.65^d for $\epsilon = 0.05$. □

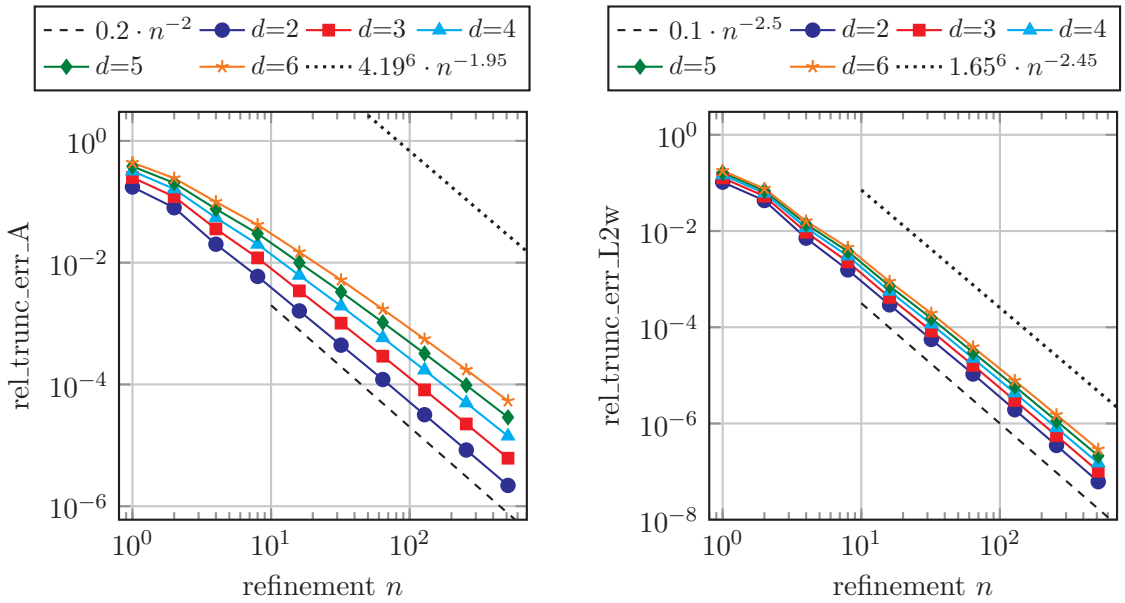

(a) relative $\mathcal{A}([-1,1]^d)$ truncation errors

(b) relative $L_{2,w}([-1,1]^d)$ truncation errors

Figure 3.9: Relative $\mathcal{A}([-1,1]^d)$ truncation errors rel_trunc_err_A $:= \|B_2^d - S_I B_2^d | \mathcal{A}([-1,1]^d)\| / \|B_2^d | \mathcal{A}([-1,1]^d)\|$ and $L_{2,w}([-1,1]^d)$ truncation errors rel_trunc_err_L2w $:= \|B_2^d - S_I B_2^d | L_{2,w}([-1,1]^d)\| / \|B_2^d | L_{2,w}([-1,1]^d)\|$ for B_2^d with respect to the refinement n of the hyperbolic cross $I := I_{\mathrm{a},n}^{d,0}$.

Next, we consider the approximation of the test function B_2^d based on samples along reconstructing rank-1 Chebyshev lattices $\mathrm{CL}(\boldsymbol{z}, M, I)$.

Example 3.24. We use the reconstructing rank-1 Chebyshev lattices $\mathrm{CL}(\boldsymbol{z}, M, I)$ built by Algorithm 3.3 in Example 3.21 for hyperbolic cross frequency index sets $I := I^{d,0}_{\mathrm{a},n}$, where the obtained size parameters M are shown in the 8th column of Table 3.2, and we additionally build reconstructing rank-1 Chebyshev lattices $\mathrm{CL}(\boldsymbol{z}, M, I)$ for dimensions $d \in \{7, 8, \dots, 11\}$. Then, we sample the test functions $f := B^d_2$ at the corresponding nodes and apply Algorithm 3.4. The resulting sampling errors $B^d_2 - S^{\mathrm{CL}}_I B^d_2$ measured in the relative $\mathcal{A}([-1,1]^d)$ and $L_{2,w}([-1,1]^d)$ norm are only slightly larger than the corresponding truncation errors $B^d_2 - S_I B^d_2$, the obtained results are visualized in Figure 3.10a and 3.10b, respectively. For the considered test function B^d_2, we do not see the factor $(1 + 2^{d-1})$ from the estimates in Theorem 3.16 and 3.17. However, as we have seen in Example 3.14 of Section 3.4, this factor may occur in principle. For the relative $\mathcal{A}([-1,1]^d)$ sampling errors $B^d_2 - S^{\mathrm{CL}}_I B^d_2$, we obtain that the error decays like $\lesssim n^{-2+\epsilon}$ from Theorem 3.16 and this corresponds approximately to the observed behavior. For the relative $L_{2,w}([-1,1]^d)$ sampling error $B^d_2 - S^{\mathrm{CL}}_I B^d_2$, we obtain an error decay like $\lesssim n^{-2+\epsilon}$ from Theorem 3.17 due to the factor $\lambda > 1/2$. However, we do not observe this factor here and the obtained errors nearly decay approximately like $\asymp n^{-2.5+\epsilon}$.

In addition to the error plots with respect to the refinement n, we also depict the relative sampling errors with respect to the number $|I^{d,0}_{\mathrm{a},n}|$ of approximated Chebyshev coefficients in Figure 3.11 for dimensions $d \in \{2, 3, \dots, 6\}$. These plots behave like in the periodic case since the cardinalities $|I^{d,0}_{\mathrm{a},n}| \asymp n \log^{d-1} n$ for fixed dimension d. In Figure 3.11a, we depict the relative $\mathcal{A}([-1,1]^d)$ sampling errors and lines $\asymp |I^{d,0}_{\mathrm{a},n}|^{-2} \, (\log |I^{d,0}_{\mathrm{a},n}|)^{2(d-1)}$ which decay (asymptotically) slightly faster than the theoretical upper bounds $|I^{d,0}_{\mathrm{a},n}|^{-2+\epsilon} \, (\log |I^{d,0}_{\mathrm{a},n}|)^{(2-\epsilon)(d-1)}$. The observed errors nearly decay as the upper bounds suggest. For the relative sampling errors in the $L_{2,w}([-1,1]^d)$ norm, we show the corresponding errors in Figure 3.11b as well as lines $\asymp |I^{d,0}_{\mathrm{a},n}|^{-\frac{5}{2}} \, (\log |I^{d,0}_{\mathrm{a},n}|)^{\frac{5}{2}(d-1)}$ (approximately) corresponding to the suspected (asymptotic) upper bounds without the factor $\lambda > 1/2$. Again, the observed errors nearly decay as the lines suggest. □

Example 3.25. Additionally, we use the test functions $f^d_4 \colon \mathbb{R} \to \mathbb{R}$, $f^d_4(\boldsymbol{x}) := \prod_{t=1}^d f_4(x_t)$, consisting of univariate dilated B-Splines of order 4,

$$f_4(x) := \begin{cases} \frac{115}{192} - \frac{125}{288}x^2 + \frac{625}{5184}x^4 & \text{for } |x| < \frac{3}{5}, \\ \frac{55}{96} + \frac{25}{144}|x| - \frac{125}{144}x^2 + \frac{625}{1296}|x|^3 - \frac{625}{7776}x^4 & \text{for } \frac{3}{5} \le |x| < \frac{9}{5}, \\ \frac{625}{31104}(|x| - 3)^4 & \text{for } \frac{9}{5} \le |x| < 3, \\ 0 & \text{otherwise.} \end{cases}$$

We only consider the functions f^d_4 within the box $[-1,1]^d$ and obtain that the corresponding Chebyshev coefficients $\hat{f}_k$, $k \in \mathbb{N}_0$, of the univariate function $f_4(x)$ restricted to the interval $[-1,1]$ behave like $|\hat{f}_k| \lesssim k^{-5}$. Consequently, we have $f^d_4 \in \mathcal{H}^{0,9/2-\epsilon}([-1,1]^d)$ for any $\epsilon > 0$. Moreover, all Chebyshev coefficients $\hat{f}_k$ belonging to odd frequencies $k \in (2\mathbb{N}_0 + 1)$ are zero. This means, we can use frequency index sets "with holes" $I = I^{d,0}_{\mathrm{a},n,\mathrm{even}} := I^{d,0}_{\mathrm{a},n} \cap (2\mathbb{N}_0)^d$ analogously to Example 2.50 in the periodic case. We sample the functions f^d_4 along reconstructing rank-1 Chebyshev lattices $\mathrm{CL}(\boldsymbol{z}, M, I^{d,0}_{\mathrm{a},n,\mathrm{even}})$, which are constructed based on Theorem 3.4 via the reconstructing rank-1 lattices $\Lambda(\boldsymbol{z}, M, I^{d,0,\mathbf{1}}_{n,\mathrm{even}})$ used in Example 2.50. We visualize the obtained relative $L_{2,w}([-1,1]^d)$ sampling errors $f^d_4 - S^{\mathrm{CL}}_I f^d_4$ for dimensions $d \in \{5, 10, 15, 20, 25\}$ in Figure 3.12 and we observe that the errors decrease fast for increasing refinements n. We remark that the obtained relative $L_{2,w}([-1,1]^d)$ sampling errors

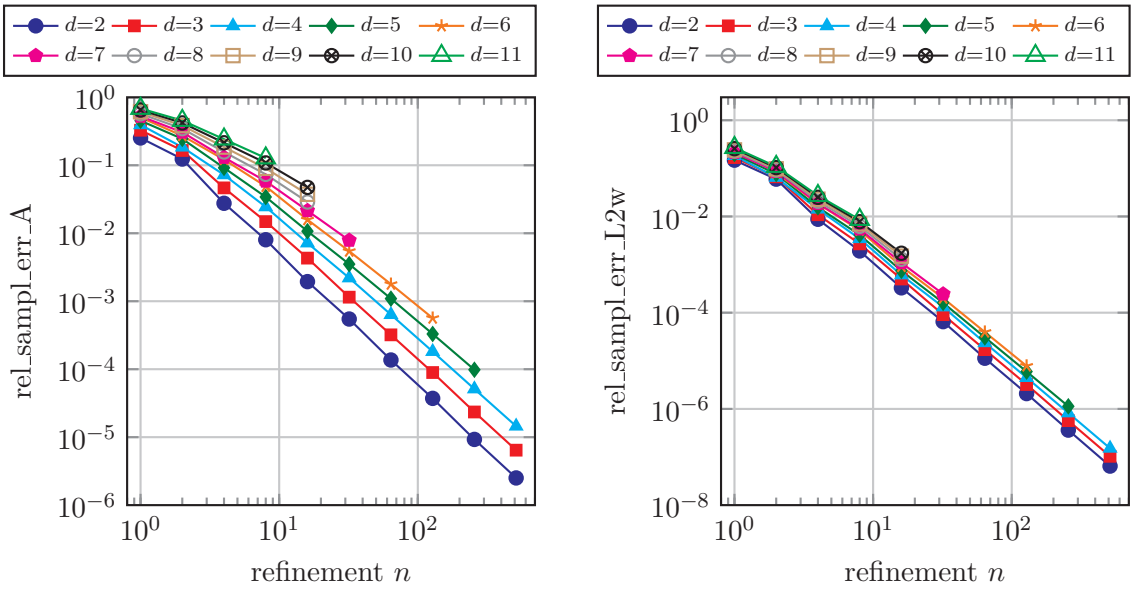

(a) relative $\mathcal{A}([-1,1]^d)$ sampling errors

(b) relative $L_{2,w}([-1,1]^d)$ sampling errors

Figure 3.10: Relative $\mathcal{A}([-1,1]^d)$ sampling errors rel_sampl_err_A $:= \|B_2^d - S_I^{\mathrm{CL}} B_2^d | \mathcal{A}([-1,1]^d)\| / \|B_2^d | \mathcal{A}([-1,1]^d)\|$ and $L_{2,w}([-1,1]^d)$ sampling errors rel_sampl_err_L2w $:= \|B_2^d - S_I^{\mathrm{CL}} B_2^d | L_{2,w}([-1,1]^d)\| / \|B_2^d | L_{2,w}([-1,1]^d)\|$ for B_2^d with respect to the refinement n of the hyperbolic cross $I := I_{\mathrm{a},n}^{d,0}$.

$f_4^d - S_I^{\mathrm{CL}} f_4^d$ are only slightly larger than the corresponding truncation errors $f_4^d - S_I f_4^d$ and we may still observe pre-asymptotic behavior since the observed error decay rate is lower than $n^{-9/2+\epsilon+\lambda}$, $\lambda > 1/2$, for the considered refinements n and dimensions d. □

As we have seen in this chapter and in the numerical examples, we were able to transfer methods and results from the periodic case of Chapter 2 to the non-periodic case. We can reconstruct multivariate algebraic polynomials in Chebyshev form a_I in a fast and exact way from samples along reconstructing rank-1 Chebyshev lattices $\mathrm{CL}(\boldsymbol{z}, M, I)$. These methods can be applied in approximately reconstructing a sufficiently smooth high-dimensional non-periodic function $f \in \mathcal{A}([-1,1]^d) \cap \mathcal{C}([-1,1]^d)$ and the obtained errors decay fast if the frequency index sets I are chosen correspondingly to the decay of the Chebyshev coefficients $\hat{f}_{\boldsymbol{k}}$ of the function f or to the assumed decay given by a suitable function class. The computation of approximated Chebyshev coefficients $\hat{f}_{\boldsymbol{k}}^{\mathrm{CL}} \approx \hat{f}_{\boldsymbol{k}}$, $\boldsymbol{k} \in I$, can be performed fast in $\mathcal{O}(M \log M + d\, 2^d |I|)$ arithmetic operations using Algorithm 3.4, which can be realized using few lines of Octave / MATLAB code. Using a modified version of Algorithm 3.4 as discussed in Section 3.4, we require $\mathcal{O}(M \log M + d\, |\mathcal{M}(I)|)$ arithmetic operations.

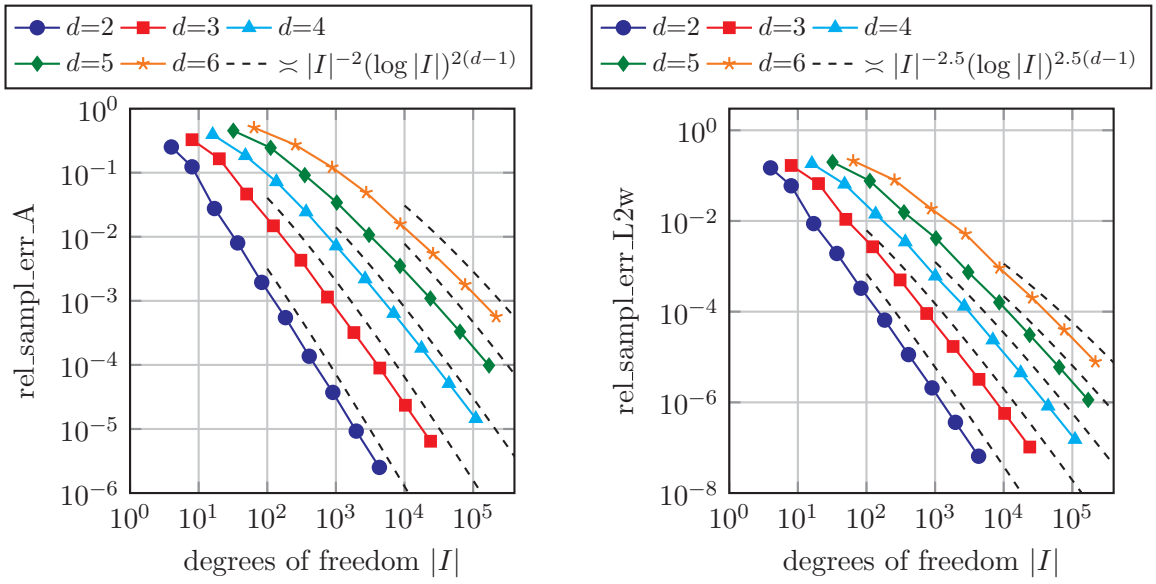

(a) relative $\mathcal{A}([-1,1]^d)$ sampling errors

(b) relative $L_{2,w}([-1,1]^d)$ sampling errors

Figure 3.11: Relative $\mathcal{A}([-1,1]^d)$ sampling errors rel_sampl_err_A $:= \|B_2^d - S_I^{\mathrm{CL}} B_2^d|\mathcal{A}([-1,1]^d)\|/\|B_2^d|\mathcal{A}([-1,1]^d)\|$ and $L_{2,w}([-1,1]^d)$ sampling errors rel_sampl_err_L2w $:= \|B_2^d - S_I^{\mathrm{CL}} B_2^d|L_{2,w}([-1,1]^d)\|/\|B_2^d|L_{2,w}([-1,1]^d)\|$ for B_2^d with respect to the cardinality $|I|$ of hyperbolic cross frequency index sets $I := I_{\mathrm{a},n}^{d,0}$ for increasing refinements n and fixed dimension d.

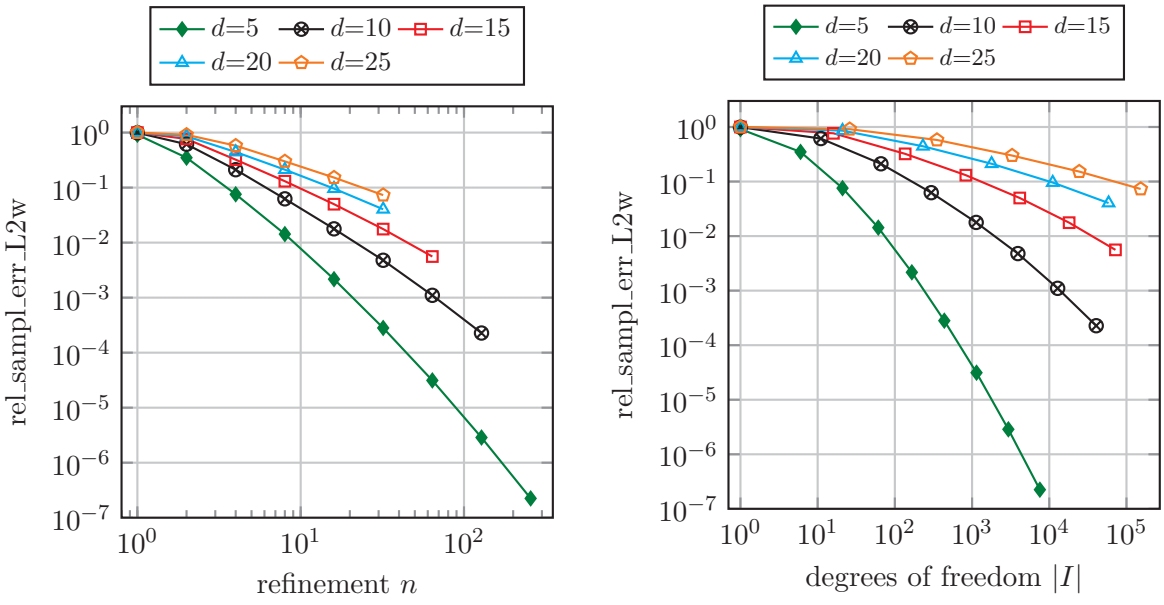

Figure 3.12: Relative $L_{2,w}([-1,1]^d)$ sampling errors rel_sampl_err_L2w $:= \|f_4^d - S_I^{\mathrm{CL}} f_4^d|L_{2,w}([-1,1]^d)\|/\|f_4^d|L_{2,w}([-1,1]^d)\|$ for f_4^d with respect to the refinement n and the cardinality $|I|$ of hyperbolic cross frequency index sets "with holes" $I := I_{\mathrm{a},n,\mathrm{even}}^{d,0}$ for increasing refinements n and fixed dimension d.

Chapter 4

High-Dimensional Sparse FFT

In the previous chapters, we discussed the fast evaluation and reconstruction of multivariate trigonometric and algebraic polynomials as well as the fast approximation of high-dimensional functions. In Chapter 2, we considered the fast reconstruction of arbitrary high-dimensional trigonometric polynomials p_I as defined in (2.2) with frequencies supported on arbitrary known index sets $I \subset \mathbb{Z}^d$ of finite cardinality, $|I| < \infty$. As sampling sets we used reconstructing rank-1 lattices $\Lambda(\boldsymbol{z}, M, I)$ and we were able to exactly reconstruct all Fourier coefficients $\hat{p}_{\boldsymbol{k}}$, $\boldsymbol{k} \in I$, from samples $p_I(\boldsymbol{x}_j)$ at rank-1 lattice nodes $\boldsymbol{x}_j$, $j = 0, \ldots, M-1$, using a single one-dimensional FFT and a simple index transform. We successfully applied this approach for the approximate reconstruction of Fourier coefficients $\hat{f}_{\boldsymbol{k}}$ of high-dimensional periodic functions $f \in \mathcal{A}(\mathbb{T}^d)$ based on function samples $f(\boldsymbol{x}_j)$. In Chapter 3, we transferred these results to the non-periodic case, where we considered the reconstruction of arbitrary multivariate algebraic polynomials in Chebyshev form a_I as defined in (3.1) with frequencies supported on arbitrary known index sets $I \subset \mathbb{N}_0^d$, $|I| < \infty$, from samples $a_I(\boldsymbol{x}_j)$ taken at the nodes $\boldsymbol{x}_j$, $j = 0, \ldots, M$, of a reconstructing rank-1 Chebyshev lattice $\mathrm{CL}(\boldsymbol{z}, M, I)$. The reconstruction can be performed using a single one-dimensional DCT and easy-to-compute index transforms. We applied this method for the approximation of high-dimensional non-periodic functions $f \in \mathcal{A}([-1,1]^d)$.

We stress the fact that we assumed for both the periodic and non-periodic case that we know the corresponding frequency index sets I of the Fourier coefficients $\hat{p}_{\boldsymbol{k}}$ or Chebyshev coefficients $\hat{a}_{\boldsymbol{k}}$, $\boldsymbol{k} \in I$, for the reconstruction of a multivariate trigonometric polynomial p_I or multivariate algebraic polynomial in Chebyshev form a_I, respectively. Similarly, in case of approximation of a multivariate function f, we assumed that we know the frequencies $\boldsymbol{k} \in I$ belonging to the (approximately) largest Fourier or Chebyshev coefficients $\hat{f}_{\boldsymbol{k}}$. For instance, one may know a suitable function class for such a function f and corresponding frequency index sets I.

In this chapter, we assume that we do not have this knowledge and that the frequency index set I is unknown. This means, we need strategies to additionally search for the locations $\operatorname{supp} \hat{p} := \{\boldsymbol{k} \in I \colon \hat{p}_{\boldsymbol{k}} \neq 0\} \subset \mathbb{Z}^d$ of the non-zero Fourier coefficients $\hat{p}_{\boldsymbol{k}} \neq 0$ of a multivariate trigonometric polynomial p_I or the locations $\operatorname{supp} \hat{a} := \{\boldsymbol{k} \in I \colon \hat{a}_{\boldsymbol{k}} \neq 0\}$ of the non-zero Chebyshev coefficients $\hat{a}_{\boldsymbol{k}} \neq 0$ of a multivariate algebraic polynomial in Chebyshev form a_I. Similarly, we want to search for the locations of the (approximately) largest Fourier or Chebyshev coefficients $\hat{f}_{\boldsymbol{k}}$ of a multivariate function f. The parts of this chapter dealing with the periodic case have already been presented in [PV16].

In practice, it may not be feasible to consider all possible integer frequencies $\boldsymbol{k} \in \mathbb{Z}^d$ or $\boldsymbol{k} \in \mathbb{N}_0^d$ in a numerical algorithm. Instead, we restrict the consideration to a (possibly very large) search domain $\Gamma \subset \mathbb{Z}^d$ or $\Gamma \subset \mathbb{N}_0^d$, for example a full grid $\hat{G}_N^d$ in d dimensions of refinement $N \in \mathbb{N}$ with integer frequencies $\|\boldsymbol{k}\|_\infty \leq N$. A method which allows for the efficient determination of a suitable frequency index set $I \subset \Gamma$ and the corresponding Fourier coefficients $\hat{p}_{\boldsymbol{k}}$ or Chebyshev coefficients $\hat{a}_{\boldsymbol{k}}$, $\boldsymbol{k} \in I$, from samples will be denoted by *sparse FFT* in this chapter.

We start our considerations with the periodic case. When the search domain $\Gamma \subset \mathbb{Z}^d$ is the full grid $\hat{G}_N^d := \{\boldsymbol{k} \in \mathbb{Z}^d \colon \|\boldsymbol{k}\|_\infty \leq N\}$, one may use the simple approach of computing a d-dimensional FFT of length $(2N+1, \dots, 2N+1)^\top$ to obtain Fourier coefficients $\tilde{\hat{p}}_{\boldsymbol{k}}$, $\boldsymbol{k} \in \Gamma$, and determine the non-zero ones. Clearly, we have $\tilde{\hat{p}}_{\boldsymbol{k}} = \hat{p}_{\boldsymbol{k}}$, $\boldsymbol{k} \in \operatorname{supp} \hat{p}$, if $\operatorname{supp} \hat{p} \subset \Gamma := \hat{G}_N^d$. However, as discussed in the introduction of Chapter 2, this approach suffers heavily from the curse of dimensionality and an alternative approach is required for practical computations.

Various methods for multivariate sparse FFT exist which are based on different concepts and approaches, like e.g. compressed sensing [Don06, Can06, FR13], randomized subsampling and filters [IK14], Chinese Remainder Theorem [Iwe13], randomized Kronecker substitution [AR14, AGR16], Zippel's algorithm [Zip79], Ben-Or/Tiwari algorithm [KL03, CsL08, JM10], or Prony's method [PT13, PPS15, KPRv16, PTV16], see also [PV16]. However, many of the mentioned methods may have one or several of the following issues. Some of the algorithms use randomized sampling and the obtained results are only "with high probability". Moreover, the constants in the number of samples or arithmetic complexity may be unknown due to missing implementations or severely grow with the dimension d. Some of the methods may not be numerically stable if used on problems with large sparsity, e.g. thousands or more of non-zero Fourier coefficients $\hat{p}_{\boldsymbol{k}} \neq 0$, arbitrary (e.g. clustered) locations $\operatorname{supp} \hat{p}$, very large search domain Γ or if the samples are perturbed by noise. In the following, we give an overview for some of the mentioned methods.

One approach, which requires a relatively small amount of samples, is applying random sampling in compressed sensing [Don06, Can06, FR13]. If a so-called restricted isometry condition is fulfilled, ℓ_1 minimization can be applied, cf. [CT05, Rau07, Rau08a, Rau08b, NV09, KR08]. The restricted isometry condition is fulfilled with probability at least $1 - \eta$ if the number of samples $L \geq C\, |\operatorname{supp} \hat{p}|\, \log^4(|\Gamma|)\, \log^2(1/\eta)$, where C is an absolute constant independent of the dimension d, see also [KR08] and the references therein. However, the number of required arithmetic operations contains the cardinality $|\Gamma|$ of the search domain Γ, see e.g. [FR13, KKM$^+$14], and therefore typically suffers heavily from the curse of dimensionality.

In [IK14], a multivariate sparse FFT method was discussed which uses randomized subsampling and filters. The method is based on the one-dimensional versions from [HIKP12b, HIKP12a, IKP14]. As search domain Γ, a full grid $\hat{G}_N^d$ is used and the number of required samples is $\mathcal{O}(|\operatorname{supp} \hat{p}| \log N)$ for constant dimension d and the arithmetic complexity is $\mathcal{O}(N^d \log^{\mathcal{O}(1)} N)$. We remark that the sample complexity $\mathcal{O}(|\operatorname{supp} \hat{p}| \log N)$ contains a factor of $d^{\mathcal{O}(d)}$, cf. [IK14, Section IV].

In [Iwe13], a deterministic multivariate sparse FFT algorithm was presented, which uses the Chinese Remainder Theorem and which requires $\mathcal{O}(d^4\, |\operatorname{supp} \hat{p}|^2 \log^4(dN))$ samples and arithmetic operations. This means there is neither exponential/super-exponential dependency on the dimension $d \in \mathbb{N}$ nor a dependency on a failure probability in the asymptotics of the number of samples and arithmetic operations for this method. Besides this deterministic algorithm, there also exists a randomized version which only requires $\mathcal{O}(d^4\, |\operatorname{supp} \hat{p}| \log^4(dN))$ samples and arithmetic operations.

Alternatively, one may combine sub-sampling on a reconstructing rank-1 lattice $\Lambda(\boldsymbol{z}, M, \Gamma)$ and a one-dimensional sparse FFT method. If we consider the evaluation of a multivariate trigonometric polynomial $p_I(\boldsymbol{x}) := \sum_{\boldsymbol{k}\in I} \hat{p}_{\boldsymbol{k}}\, \mathrm{e}^{2\pi\mathrm{i}\boldsymbol{k}\cdot\boldsymbol{x}} = \sum_{l=1}^{|I|} \hat{p}_l\, \mathrm{e}^{2\pi\mathrm{i}\boldsymbol{k}_l\cdot\boldsymbol{x}}$ at the nodes $\boldsymbol{x}_j := \frac{j}{M}\boldsymbol{z} \bmod \boldsymbol{1}$ of a reconstructing rank-1 lattice $\Lambda(\boldsymbol{z}, M, \Gamma)$ for the search domain $\Gamma \supset I$, we obtain

$$p_I\left(\frac{j}{M}\boldsymbol{z} \bmod \boldsymbol{1}\right) = \sum_{l=1}^{|I|} \hat{p}_l\, \mathrm{e}^{2\pi\mathrm{i}(\boldsymbol{k}_l\cdot\boldsymbol{z})\, j/M} = \sum_{l=1}^{|I|} \hat{p}_l\, \mathrm{e}^{2\pi\mathrm{i} f_l\, j/M} = \tilde{p}_{\tilde{I}}\left(\frac{j}{M}\right),\ j = 0, \dots, M-1,$$

where the one-dimensional frequencies $f_l := \boldsymbol{k}_l \cdot \boldsymbol{z} \bmod M \in \tilde{I} = \{0, 1, \dots, M-1\}$. This means we may regard the evaluation of a multivariate trigonometric polynomial $p_I \colon \mathbb{T}^d \to \mathbb{C}$ at the nodes $\boldsymbol{x}_j$, $j = 0, \dots, M-1$, of a reconstructing rank-1 lattice $\Lambda(\boldsymbol{z}, M, \Gamma)$ as the evaluation of a one-dimensional trigonometric polynomial $\tilde{p}_{\tilde{I}} \colon \mathbb{T} \to \mathbb{C}$ at the nodes j/M and we have an injective mapping of multi-dimensional frequencies $\boldsymbol{k}_l \in I$ to one-dimensional frequencies $f_l \in \tilde{I}$ given by

$$\Gamma \to \tilde{I} := \{0, 1, \dots, M-1\},\ \boldsymbol{k}_l \mapsto \boldsymbol{k}_l \cdot \boldsymbol{z} \bmod M =: f_l,\ l = 1, \dots, |I|,$$

see also [PTV16]. Consequently, we may apply a one-dimensional sparse FFT method on (parts of the) samples $\tilde{p}_{\tilde{I}}(j/M)$ to determine the unknown one-dimensional frequencies $f_l \in \tilde{I}$ belonging to non-zero Fourier coefficients $\hat{p}_l \neq 0$ and compute its d-dimensional counterparts $\boldsymbol{k}_l \in I$ using the relation $f_l = \boldsymbol{k}_l \cdot \boldsymbol{z} \bmod M$. For one-dimensional sparse FFTs, very efficient methods are available, for instance randomized algorithms based on filters [HIKP12b, HIKP12a, IKP14] or shifted sampling [CLW16] as well as deterministic methods based on Chinese Remainder Theorem [Iwe10], splitting approaches [PW16a, PW16b] or Prony's method [PP13, PTV16]. However, many methods have certain restrictions for the unknown one-dimensional frequencies f_l. For instance, approaches based on filters may require the one-dimensional frequencies f_l to be well-distributed or the approach [PW16a] requires all one-dimensional frequencies f_l to be within a certain small interval. Another approach presented in [PTV16] is based on shifted sampling, see e.g. [CLW16], reconstructing rank-1 lattices $\Lambda(\boldsymbol{z}, M, \Gamma)$ as well as a version of Prony's method and the approach requires for numerical stability that there is a certain minimum distance between the one-dimensional frequencies f_l, which also depends on the rank-1 lattice size M and the numbers of samples. In general, such properties may be hard to guarantee for the one-dimensional frequencies f_l, which are the combination of unknown d-dimensional frequencies $\boldsymbol{k}_l \in I \subset \Gamma \subset \mathbb{Z}^d$ and a reconstructing rank-1 lattice $\Lambda(\boldsymbol{z}, M, \Gamma)$ of (potentially) very large size $M \geq |\Gamma|$.

In this work, we are interested in developing a sparse FFT method based on rank-1 lattice sampling which works well for the reconstruction of high-dimensional trigonometric polynomials p_I with thousands and more non-zero Fourier coefficients $\hat{p}_{\boldsymbol{k}} \neq 0$ at unknown frequency locations $\operatorname{supp}\hat{p}$ within a certain (possibly) very large search domain $\Gamma \subset \mathbb{Z}^d$ without additional restrictions on the frequencies $\boldsymbol{k}$. The method should also work when samples are perturbed by noise and be applicable for the approximation of multivariate periodic functions f having infinitely many non-zero Fourier coefficients $\hat{f}_{\boldsymbol{k}}$. Moreover, the approach is transferred to the non-periodic case obtaining a method based on rank-1 Chebyshev lattice sampling for the reconstruction of high-dimensional algebraic polynomials in Chebyshev form a_I and for the approximation of multivariate non-periodic functions f.

This chapter is structured as follows.

In Section 4.1, we discuss an approach for the dimension-incremental reconstruction of multivariate trigonometric polynomials p_I from samples, see also [PV16]. Similar to the

component-by-component search for reconstructing rank-1 lattices $\Lambda(\boldsymbol{z}, M, I)$, we adaptively construct the index set of frequencies belonging to the non-zero Fourier coefficients $\hat{p}_{\boldsymbol{k}} \neq 0$ in a dimension-incremental way. We remark that a similar idea was used in [PT13], where a dimension-incremental method for anharmonic trigonometric polynomials based on Prony's method was presented, and similar concepts already occurred in [Zip79]. In Section 4.1.1, we describe the general approach of dimension-incremental reconstruction based on projections parallel to the coordinate axes and we present the general approach as Algorithm 4.1. Moreover, we explain each step of Algorithm 4.1 for the reconstruction of a three-dimensional trigonometric polynomial p_I using rank-1 lattice sampling and we illustrate the computation steps in Figure 4.1. In Section 4.1.2, we describe two realizations of Algorithm 4.1 indicated in Algorithm 4.2 and 4.3, which partially use random values for the sampling nodes. Both algorithms are based on sampling along reconstructing rank-1 lattices $\Lambda(\boldsymbol{z}, M, \tilde{I})$ and only differ in the way how these lattices are constructed. Algorithm 4.2 performs a search as in Algorithm 2.2 for a relatively large index set of frequency candidates in step 2b, whereas Algorithm 4.3 uses the explicit construction from Theorem 2.7. This yields possible improvements in the runtime for Algorithm 4.3 at the price of possibly more samples. In Section 4.1.3, we discuss when the detection of all non-zero Fourier coefficients $\hat{p}_{\boldsymbol{k}} \neq 0$ succeeds and possible cases where the detection may fail. In Section 4.1.4, we discuss the sampling and arithmetic complexity of Algorithm 4.2 and 4.3, which depend on the sparsity parameter s. This sparsity parameter s is an input parameter of both algorithms and is used to truncate the number of detected frequencies in the dimension-incremental steps. Assuming that the search domain Γ is the d-dimensional full grid $\hat{G}_N^d$ of refinement $N \in \mathbb{N}$ and $\sqrt{N} \lesssim s \lesssim N^d$ for sparsity parameter $s \in \mathbb{N}$, we require $\mathcal{O}(d\, s^2 N)$ many samples for both algorithms as well as $\mathcal{O}(d\, s^3 N^2)$ arithmetic operations for Algorithm 4.2 and $\mathcal{O}(d\, s^3 + d\, s^2 N \log(s\, N))$ arithmetic operations for Algorithm 4.3. In the case $s \lesssim \sqrt{N}$, we require $\mathcal{O}(d\, N^2)$ many samples for both algorithms as well as $\mathcal{O}(d\, s\, N^3)$ and $\mathcal{O}(d\, N^2 \log N)$ arithmetic operations for Algorithm 4.2 and 4.3, respectively. If the detection steps of Algorithm 4.2 or 4.3 succeed, we can replace the sparsity parameter s in the stated sampling and arithmetic complexities by the number $|\operatorname{supp} \hat{p}|$ of non-zero Fourier coefficients $\hat{p}_{\boldsymbol{k}} \neq 0$. In Section 4.1.5, we describe a deterministic version of Algorithm 4.2 and 4.3, which can be used when the Fourier coefficients $\hat{p}_{\boldsymbol{k}}$ fulfill certain properties, e.g. if all Fourier coefficients $\hat{p}_{\boldsymbol{k}}$ are non-negative or non-positive. In Section 4.1.6, we present results of numerical tests for Algorithm 4.2 and 4.3 in up to 30 dimensions. We successfully apply both methods on random sparse trigonometric polynomials p_I and compare the required numbers of samples and the runtime. We observe that Algorithm 4.3 requires slightly more samples for the considered test cases but has distinctly less runtime. Moreover, we consider the case of noisy samples and also successfully reconstruct the considered multivariate trigonometric polynomials p_I in this case. Afterwards, we numerically compute the (approximately) largest Fourier coefficients $\hat{f}_{\boldsymbol{k}}$ and the corresponding frequency locations I of a 10-dimensional test function f.

In Section 4.2, we transfer the method for the dimension-incremental reconstruction from the periodic case with rank-1 lattice sampling to the non-periodic case using rank-1 Chebyshev lattice sampling. In Section 4.2.1, we discuss the modifications to the approach from Section 4.1 for the reconstruction of multivariate algebraic polynomials in Chebyshev form a_I from samples taken at the nodes of reconstructing rank-1 Chebyshev lattices $\mathrm{CL}(\boldsymbol{z}, M, \tilde{I})$. We give two algorithms which are adapted versions of Algorithm 4.2. In Algorithm 4.4, the reconstructing rank-1 Chebyshev lattices $\mathrm{CL}(\boldsymbol{z}, M, \tilde{I})$ are built via reconstructing rank-1 lattices $\mathrm{CL}(\boldsymbol{z}, M, \mathcal{M}(\tilde{I}))$ from the periodic case, cf. Theorem 3.4 and Corollary 3.6. In Algorithm 4.5, the reconstructing rank-1 Chebyshev lattices $\mathrm{CL}(\boldsymbol{z}, M, \tilde{I})$ are directly built using a

CBC approach with reconstruction property (3.22) fulfilled. In Section 4.2.2, we evaluate the proposed methods in numerical tests in up to 15 dimensions. We successfully reconstruct all non-zero Chebyshev coefficients $\hat{a}_{\boldsymbol{k}} \neq 0$ and the corresponding frequency locations $\operatorname{supp} \hat{a}$ of random sparse algebraic polynomials in Chebyshev form a_I. We observe that Algorithm 4.5 requires distinctly less samples compared to Algorithm 4.4 in several cases. Moreover, we successfully reconstruct approximate Chebyshev coefficients $\hat{\tilde{f}}_{\boldsymbol{k}}$ and the corresponding frequency locations I of a 9-dimensional test function f.

4.1 Periodic case — rank-1 lattice sampling

This section has already been presented in [PV16]. In Section 4.1.1, we discuss the general approach of a high-dimensional sparse FFT based on dimension-incremental projection. We explain the method on the example of the reconstruction of a three-dimensional trigonometric polynomial p_I based on rank-1 lattice sampling and visualize the involved computation steps in detail. In Section 4.1.2, we describe two specific realizations of the approach which use reconstructing rank-1 lattices $\Lambda(\boldsymbol{z}, M, \tilde{I})$ for the lower components and randomly chosen values for the higher components of the sampling nodes. In Section 4.1.3, we describe cases where the proposed method may fail to detect all the frequencies $\boldsymbol{k}$ belonging to non-zero Fourier coefficients $\hat{p}_{\boldsymbol{k}} \neq 0$. In Section 4.1.4, we discuss the sampling and arithmetic complexity of the proposed methods. In Section 4.1.5, we describe a completely deterministic version, which can be applied if the Fourier coefficients $\hat{p}_{\boldsymbol{k}}$ of the multivariate trigonometric polynomials p_I fulfill certain properties. In Section 4.1.6, we present numerical examples in up to 30 dimensions. Especially, we deal with the case where we determine the frequency locations I of the approximately largest Fourier coefficients $\hat{f}_{\boldsymbol{k}}$ of a 10-dimensional test function $f\colon \mathbb{T}^{10} \to \mathbb{R}$ with infinitely many non-zero Fourier coefficients $\hat{f}_{\boldsymbol{k}} \neq 0$.

4.1.1 Dimension-incremental projection

The proposed method is based on reconstructing rank-1 lattices $\Lambda(\boldsymbol{z}, M, \tilde{I})$ and the computation of projected Fourier coefficients. For the explanations, we introduce some additional notation from [PV16]. As mentioned in the introduction of this chapter, we assume that the unknown support of the trigonometric polynomial p_I in frequency domain, $\operatorname{supp} \hat{p} := \{\boldsymbol{k} \in I\colon \hat{p}_{\boldsymbol{k}} \neq 0\} \subset \mathbb{Z}^d$, lies within a certain superset $\Gamma \subset \mathbb{Z}^d$ of finite cardinality, $|\Gamma| < \infty$. This superset Γ may be very large, for instance a d-dimensional full grid $\hat{G}_N^d$ of refinement $N \in \mathbb{N}$. The elements of the set $\operatorname{supp} \hat{p}$ are those frequencies $\boldsymbol{k} \in \mathbb{Z}^d$ which belong to the non-zero Fourier coefficients $\hat{p}_{\boldsymbol{k}} \neq 0$ of the multivariate trigonometric polynomial p_I. In this context, Γ will also be denoted as the *search domain* of frequencies $\boldsymbol{k}$. Examples for those search domains Γ are a d-dimensional full grid $\hat{G}_N^d$ or (generalized) hyperbolic crosses $I_N^{d,T,\gamma}$. Moreover, we denote the projection of a frequency $\boldsymbol{k} := (k_1, \ldots, k_d)^\top \in \mathbb{Z}^d$ to the components $\boldsymbol{i} := (i_1, \ldots, i_m) \in \{1, \ldots, d\}^m$ by $\mathcal{P}_{\boldsymbol{i}}(\boldsymbol{k}) := (k_{i_1}, \ldots, k_{i_m})^\top \in \mathbb{Z}^m$. Correspondingly, we define the projection of a frequency index set $I \subset \mathbb{Z}^d$ to the components $\boldsymbol{i}$ by $\mathcal{P}_{\boldsymbol{i}}(I) := \{(k_{i_1}, \ldots, k_{i_m})\colon \boldsymbol{k} \in I\}$.

Using this notation, we present the general strategy of the proposed method in Algorithm 4.1. Since the description in Algorithm 4.1 is rather general, we illustrate the approach in more detail on a three-dimensional trigonometric polynomial p_I with 10 non-zero Fourier coefficients $\hat{p}_{\boldsymbol{k}}$ with frequencies $\boldsymbol{k}$ within the search domain $\Gamma = \hat{G}_8^3$ when using rank-1 lattice sampling, cf. Figure 4.1. The frequency locations $\operatorname{supp} \hat{p}$ of the three-dimensional trigonometric polynomial p_I are shown in Figure 4.1a.

Algorithm 4.1 ([PV16, Section 2.2.1]). General approach for dimension-incremental reconstruction of multivariate trigonometric polynomial p_I from samples for unknown frequency index set $I \subset \Gamma \subset \mathbb{Z}^d$ and known (possibly very large) search domain $\Gamma \supset I$.

1. Determine a frequency index set $I^{(1)} \subseteq \mathcal{P}_{(1)}(\Gamma)$ which should be identical to the projection $\mathcal{P}_{(1)}(\operatorname{supp}\hat{p})$ or contain this projection, $I^{(1)} \supseteq \mathcal{P}_{(1)}(\operatorname{supp}\hat{p})$. This means we try to detect the first component of the locations $\operatorname{supp}\hat{p}$ of those frequencies $\boldsymbol{k}$ which belong to the non-zero Fourier coefficients $\hat{p}_{\boldsymbol{k}} \neq 0$ of the multivariate trigonometric polynomial p_I.

2. For dimension increment step $t = 2, \ldots, d$

   (a) Determine a frequency index set $I^{(t)} \subseteq \mathcal{P}_{(t)}(\Gamma)$ which should be identical to the projection $\mathcal{P}_{(t)}(\operatorname{supp}\hat{p})$ or contain this projection, $I^{(t)} \supseteq \mathcal{P}_{(t)}(\operatorname{supp}\hat{p})$. In other words, we try to detect the t-th component of the frequency locations $\operatorname{supp}\hat{p}$ belonging to the non-zero Fourier coefficients $\hat{p}_{\boldsymbol{k}} \neq 0$.

   (b) Determine a suitable sampling set $\mathcal{X}^{(1,\ldots,t)} \subset \mathbb{T}^d$, $|\mathcal{X}^{(1,\ldots,t)}| \ll |\Gamma|$, which allows to determine the first t components from the index set $(I^{(1,\ldots,t-1)} \times I^{(t)}) \cap \mathcal{P}_{(1,\ldots,t)}(\Gamma)$ of those frequencies $\boldsymbol{k}$ belonging to non-zero Fourier coefficients $\hat{p}_{\boldsymbol{k}} \neq 0$.

   (c) Sample the multivariate trigonometric polynomial p_I at the nodes of the sampling set $\mathcal{X}^{(1,\ldots,t)}$.

   (d) Compute the (projected) Fourier coefficients $\tilde{\hat{p}}_{(1,\ldots,t),\boldsymbol{k}}$, $\boldsymbol{k} \in (I^{(1,\ldots,t-1)} \times I^{(t)}) \cap \mathcal{P}_{(1,\ldots,t)}(\Gamma)$.

   (e) Determine the non-zero (projected) Fourier coefficients from $\tilde{\hat{p}}_{(1,\ldots,t),\boldsymbol{k}}$, $\boldsymbol{k} \in (I^{(1,\ldots,t-1)} \times I^{(t)}) \cap \mathcal{P}_{(1,\ldots,t)}(\Gamma)$, and obtain the index set $I^{(1,\ldots,t)}$ of the first t components of the frequency locations. The frequency index set $I^{(1,\ldots,t)}$ should be equal to the projection $\mathcal{P}_{(1,\ldots,t)}(\operatorname{supp}\hat{p})$. In simplified terms, we should have detected the first t components of the frequency locations $\operatorname{supp}\hat{p}$ belonging to the non-zero Fourier coefficients $\hat{p}_{\boldsymbol{k}} \neq 0$ of the multivariate trigonometric polynomial p_I.

3. Use the frequency index set $I^{(1,\ldots,d)}$ and the computed Fourier coefficients $\tilde{\hat{p}}_{(1,\ldots,d),\boldsymbol{k}}$, $\boldsymbol{k} \in (I^{(1,\ldots,d)}$, as an approximation for the support in frequency domain $\operatorname{supp}\hat{p}$ and the corresponding Fourier coefficients $\hat{p}_{\boldsymbol{k}}$, $\boldsymbol{k} \in \operatorname{supp}\hat{p}$, of the multivariate trigonometric polynomial p_I.

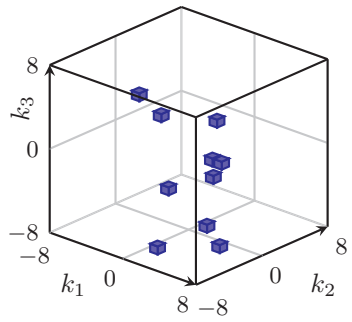

(a) Frequencies $\boldsymbol{k} \in \operatorname{supp} \hat{p} \subset \Gamma$ belonging to non-zero Fourier coefficients $\hat{p}_{\boldsymbol{k}} \neq 0$ of multivariate trigonometric polynomial p_I, p_I is only given as black-box.

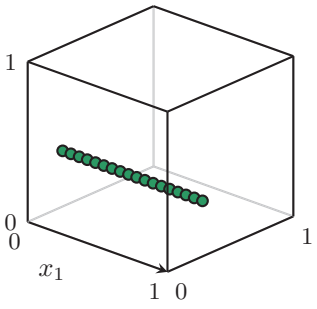

(b) Sample in first direction at $\mathcal{X}^{(1)}$, $|\mathcal{X}^{(1)}| = 17$.
(step 1)

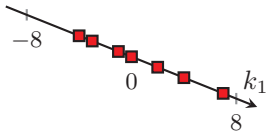

(c) 1d-FFT along first direction, determine $I^{(1)} \subset \mathcal{P}_{(1)}(\Gamma)$.
(step 1)

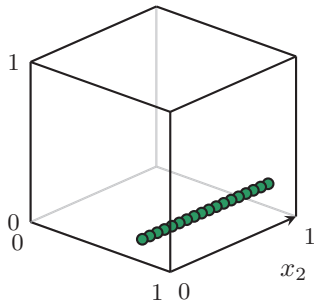

(d) Sample in second direction at $\mathcal{X}^{(2)}$, $|\mathcal{X}^{(2)}| = 17$.
($t = 2$, step 2a)

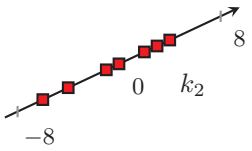

(e) 1d-FFT along 2nd direction, determine $I^{(2)} \subset \mathcal{P}_{(2)}(\Gamma)$.
($t = 2$, step 2a)

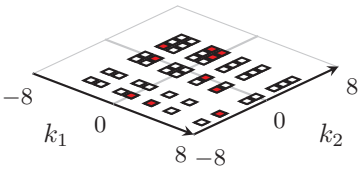

(f) Build index set $I^{(1)} \times I^{(2)}$, $|I^{(1)} \times I^{(2)}| = 49$.
($t = 2$, step 2b)

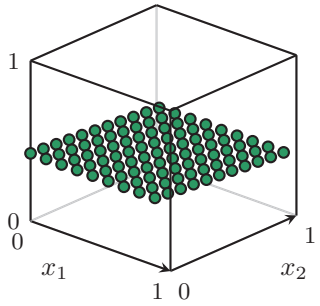

(g) Build reconstructing rank-1 lattice $\Lambda(\boldsymbol{z}, M, I^{(1)} \times I^{(2)}) \in \mathbb{T}^2$ in first two directions, $\boldsymbol{z} = (1, 9)^\top$, $M = 99$.
Choose $x_3' \in \mathbb{T}$ and set $\mathcal{X}^{(1,2)} := \Lambda(\boldsymbol{z}, M) \times \{x_3'\}$.
($t = 2$, step 2b)
Sample along first two directions at $\mathcal{X}^{(1,2)}$.
($t = 2$, step 2c)

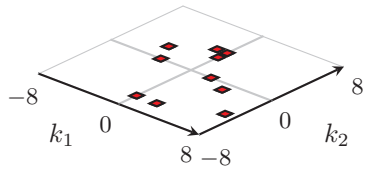

(h) Compute 1d-FFT and a simple index transform (Algorithm 2.1 along first two directions).
($t = 2$, step 2d)
Determine $I^{(1,2)} \subset \mathcal{P}_{(1,2)}(\Gamma)$.
($t = 2$, step 2e)

Figure 4.1: ([PV16, Figure 2.1]). Reconstruction of a 3-dimensional trigonometric polynomial p_I based on Algorithm 4.1.

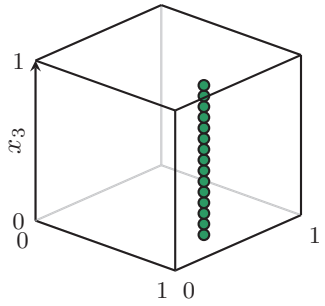

(i) Sample in third direction at $\mathcal{X}^{(3)}$, $|\mathcal{X}^{(3)}| = 17$.
($t = 3$, step 2a).

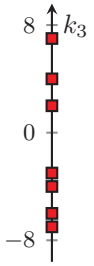

(j) 1d-FFT along 3rd direction, determine $I^{(3)} \subset \mathcal{P}_{(3)}(\Gamma)$.
($t = 3$, step 2a).

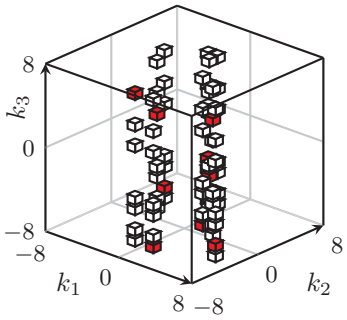

(k) Build index set $I^{(1,2)} \times I^{(3)}$, $|I^{(1,2)} \times I^{(3)}| = 70$.
($t = 3$, step 2b).

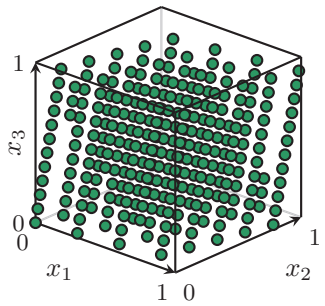

(l) Build reconstructing rank-1 lattice $\mathcal{X}^{(1,2,3)} := \Lambda(\boldsymbol{z}, M, I^{(1,2)} \times I^{(3)})$, $\boldsymbol{z} = (1, 4, 23)^\top$, $M = 276$.
($t = 2$, step 2b)
Sample at $\mathcal{X}^{(1,2,3)}$.
($t = 3$, step 2c)

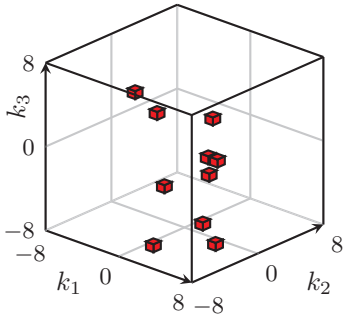

(m) Compute 1d-FFT and a simple index transform (Algorithm 2.1).
($t = 2$, step 2d)
Determine $I^{(1,2,3)} \subset \Gamma$.
($t = 3$, step 2e)
We have $I^{(1,2,3)} = \operatorname{supp} \hat{p}$.

Figure 4.1: (continued) ([PV16, Figure 2.1]). Reconstruction of a 3-dimensional trigonometric polynomial p_I based on Algorithm 4.1.

In the first step, we choose a suitable sampling set to determine the first components of the frequency locations $\operatorname{supp} \hat{p}$. Since the search domain Γ has 17 successive frequencies in the first coordinate direction, $\mathcal{P}_{(1)}(\Gamma) = \{-8, -7, \ldots, 8\}$, we use a set $\mathcal{X}^{(1)} \in \mathbb{T}^3$ of 17 equispaced sampling nodes along the first coordinate direction, see Figure 4.1b, where we fix the second and third component of the sampling nodes. We sample p_I at the nodes from the sampling set $\mathcal{X}^{(1)}$ and apply a one-dimensional FFT on these sampling values. From the resulting Fourier coefficients, we search for the non-zero ones (or the ones above a certain threshold) and put the corresponding frequencies into the index set $I^{(1)}$. This index set $I^{(1)} \subset \mathcal{P}_{(1)}(\Gamma) \subset \mathbb{Z}$ contains (possibly a subset of) the first components of the frequency locations of those frequencies $\boldsymbol{k}$ which belong to the non-zero Fourier coefficients $\hat{p}_{\boldsymbol{k}}$ of the multivariate trigonometric polynomial p_I under consideration. In our example, all seven frequency components are successfully detected, see Figure 4.1c,

At the beginning of the second step ($t = 2$), we proceed analogously for the second coordinate direction. This means we use a set $\mathcal{X}^{(2)}$ of 17 equispaced sampling nodes along the second coordinate direction where we fix the first and third component of the sampling nodes, cf. Figure 4.1d. We sample the multivariate trigonometric polynomial p_I at the nodes

from the sampling set $\mathcal{X}^{(2)} \in \mathbb{T}^3$ and apply a one-dimensional FFT on these sampling values. From the resulting Fourier coefficients, we search for the non-zero ones (or the ones above a certain threshold) and put the corresponding frequencies into the index set $I^{(2)}$. This index set $I^{(2)} \subset \mathcal{P}_{(2)}(\Gamma) \subset \mathbb{Z}$ contains (possibly a subset of) the second components of the frequency locations of those frequencies $\boldsymbol{k}$ which belong to the non-zero Fourier coefficients $\hat{p}_{\boldsymbol{k}} \neq 0$ of the multivariate trigonometric polynomial p_I and all seven frequency components are successfully detected in our example as depicted in Figure 4.1e. Next, we build the frequency index set $I^{(1)} \times I^{(2)} \subset \mathbb{Z}^2$, which acts as a (reduced) search domain for the first two components of the frequency locations in $\operatorname{supp} \hat{p}$ and which contains 49 elements in our example, see Figure 4.1f. We build a reconstructing rank-1 lattice $\Lambda(\boldsymbol{z}, M, I^{(1)} \times I^{(2)}) \subset \mathbb{T}^2$, choose a fixed third component $x'_3 \in \mathbb{T}$, obtain the set $\mathcal{X}^{(1,2)} := \Lambda(\boldsymbol{z}, M) \times \{x'_3\} \in \mathbb{T}^3$ of sampling nodes, see Figure 4.1g, and we sample the multivariate trigonometric polynomial p_I at these nodes. Then, we apply a rank-1 lattice FFT, i.e., a one-dimensional FFT followed by a simple index transform, cf. Algorithm 2.1. Now, we obtain (projected) Fourier coefficients and we search for the non-zero ones (or the ones above a certain threshold) and put the corresponding frequencies into the index set $I^{(1,2)} \subset I^{(1)} \times I^{(2)} \subset \mathcal{P}_{(1,2)}(\Gamma) \subset \mathbb{Z}^2$, which contains (possibly a subset of) the first two components of the frequency locations of those frequencies $\boldsymbol{k}$ which belong to the non-zero Fourier coefficients $\hat{p}_{\boldsymbol{k}} \neq 0$ of the multivariate trigonometric polynomial p_I, cf. Figure 4.1h.

Afterwards, we deal with the third component ($t = 3$). We use a set $\mathcal{X}^{(3)}$ of 17 equispaced sampling nodes along the third coordinate direction where we fix the first and second component of the sampling nodes, cf. Figure 4.1i. We sample the multivariate trigonometric polynomial p_I at the nodes from the sampling set $\mathcal{X}^{(3)} \in \mathbb{T}^3$ and apply a one-dimensional FFT on these sampling values. From the resulting (projected) Fourier coefficients, we search for the non-zero ones (or the ones above a certain threshold) and put the corresponding frequencies into the index set $I^{(3)}$. This frequency index set $I^{(3)} \subset \mathcal{P}_{(3)}(\Gamma)$ contains (possibly a subset of) the third components of the frequency locations of those frequencies $\boldsymbol{k}$ which belong to the non-zero Fourier coefficients $\hat{p}_{\boldsymbol{k}} \neq 0$ of the multivariate trigonometric polynomial p_I and all seven frequency components are successfully detected in our example as depicted in Figure 4.1j. Next, we build the index set $I^{(1,2)} \times I^{(3)} \subset \Gamma \subset \mathbb{Z}^3$, which now acts as a (reduced) search domain for the frequency locations in $\operatorname{supp} \hat{p}$ and which contains 70 elements in our example, see Figure 4.1k. We build a reconstructing rank-1 lattice $\Lambda(\boldsymbol{z}, M, I^{(1,2)} \times I^{(3)}) \subset \mathbb{T}^3$ and use this as the set $\mathcal{X}^{(1,2,3)}$ of sampling nodes, see Figure 4.1l. Again, we apply a rank-1 lattice FFT, i.e., a one-dimensional FFT followed by a simple index transform, cf. Algorithm 2.1. Now, we obtain Fourier coefficients and we search for the non-zero ones (or the ones above a certain threshold) and put the corresponding frequencies into the index set $I^{(1,2,3)} \subset I^{(1,2)} \times I^{(3)} \subset \Gamma \subset \mathbb{Z}^3$, which contains (possibly a subset of) the frequency locations of those frequencies $\boldsymbol{k}$ which belong to the non-zero Fourier coefficients $\hat{p}_{\boldsymbol{k}} \neq 0$ of the multivariate trigonometric polynomial p_I, cf. Figure 4.1m. Finally, this frequency index set $I^{(1,2,3)} \subset \Gamma \subset \mathbb{Z}^3$ and the corresponding Fourier coefficients $\tilde{\hat{p}}_{(1,2,3),\boldsymbol{k}}$, $\boldsymbol{k} \in I^{(1,2,3)}$, are used as an approximation for the frequency locations $\operatorname{supp} \hat{p}$ and for the corresponding Fourier coefficients $\hat{p}_{\boldsymbol{k}}$ of the multivariate trigonometric polynomial p_I, respectively. If all prior steps succeeded, we have successfully detected all frequencies $\boldsymbol{k}$, $I^{(1,2,3)} = \operatorname{supp} \hat{p}$, and the corresponding Fourier coefficients $\tilde{\hat{p}}_{(1,2,3),\boldsymbol{k}} = \hat{p}_{\boldsymbol{k}}$, $\boldsymbol{k} \in \operatorname{supp} \hat{p}$, of the multivariate trigonometric polynomial p_I.

4.1.2 Randomized version

4.1.2.1 Dimension-incremental reconstruction algorithm

Here, we present Algorithm 4.2 ([PV16, Algorithm 1]) as a realization of the general approach in Algorithm 4.1, which uses reconstructing rank-1 lattices as sampling sets and rank-1 lattice FFTs (Algorithm 2.1) for the computation of (projected) Fourier coefficients. Besides the search domain $\Gamma \supset \operatorname{supp} \hat{p}$ and the multivariate trigonometric polynomial p_I (as black box), Algorithm 4.2 has three additional input parameters, which are the relative threshold $\theta \in (0,1)$, the sparsity parameter $s \in \mathbb{N}$ and the number of detection iterations $r \in \mathbb{N}$. The relative threshold parameter $\theta \in (0,1)$ is used to determine the "non-zero" Fourier coefficients from $\tilde{\hat{p}}_{1,k_1}$ for $k_1 \in \mathcal{P}_1(\Gamma)$ in step 1, $\tilde{\hat{p}}_{t,k_t}$ for $k_t \in \mathcal{P}_t(\Gamma)$ in step 2a, $t \in \{2,\dots,d\}$, as well as $\tilde{\hat{p}}_{(1,\dots,t),\boldsymbol{k}}$ for $\boldsymbol{k} \in (I^{(1,\dots,t-1)} \times I^{(t)}) \cap \mathcal{P}_{(1,\dots,t)}(\Gamma)$ in step 2e. Since numerical algorithms are used to compute the Fourier coefficients $\tilde{\hat{p}}_{(1,\dots,t),\boldsymbol{k}}$, the actual computed values of "zero" Fourier coefficients may be larger than zero but are smaller than a certain (relative) threshold. The sparsity parameter $s \in \mathbb{N}$ may be used to truncate the number of detected frequencies and corresponding Fourier coefficients. Last, the input parameter $r \in \mathbb{N}$ for the number of detection iterations controls how many times the sampling and frequency detection in the step 2 is performed for each dimension increment step $t \in \{2,\dots,d\}$. Repetitions in these computations r times may be necessary to ensure a successful exact reconstruction of the multivariate trigonometric polynomial p_I, as we describe in this section and in Section 4.1.3.

First in step 1, we determine the index set of detected frequency locations for the first component $I^{(1)} \subset \mathcal{P}_1(\operatorname{supp} \hat{p})$. For this, we set the last $d-1$ components in $\boldsymbol{x} := (x_1,\dots,x_d)^\top$ to fixed randomly chosen values $x'_2,\dots,x'_d \in \mathbb{T}$. We sample the multivariate trigonometric polynomial p_I at the nodes of the sampling set $\mathcal{X}^{(1)} := \left\{ (\frac{l}{L_1}, x'_2,\dots,x'_d)^\top : l = 0,\dots,L_1-1 \right\}$, where $L_1 := \max(\mathcal{P}_1(\Gamma)) - \min(\mathcal{P}_1(\Gamma)) + 1$, and we compute one-dimensional projected Fourier coefficients for the first component

$$\tilde{\hat{p}}_{1,k_1} := \frac{1}{L_1} \sum_{l=0}^{L_1-1} p_I \left(\left(\frac{l}{L_1}, x'_2,\dots,x'_d \right)^\top \right) \mathrm{e}^{-2\pi \mathrm{i} l k_1 / L_1}, \quad k_1 \in \mathcal{P}_1(\Gamma),$$

using a one-dimensional FFT of length L_1. Due to the definition of the multivariate trigonometric polynomial p_I, we obtain

$$\begin{aligned}
\tilde{\hat{p}}_{1,k_1} &= \frac{1}{L_1} \sum_{l=0}^{L_1-1} \sum_{\boldsymbol{h}:=(h_1,\dots,h_d)^\top \in \operatorname{supp} \hat{p}} \hat{p}_{\boldsymbol{h}} \, \mathrm{e}^{2\pi \mathrm{i}(h_2 x'_2 + \dots + h_d x'_d)} \, \mathrm{e}^{2\pi \mathrm{i}(h_1 - k_1) l / L_1} \\
&= \sum_{\boldsymbol{h} \in \operatorname{supp} \hat{p}} \hat{p}_{\boldsymbol{h}} \, \mathrm{e}^{2\pi \mathrm{i}(h_2 x'_2 + \dots + h_d x'_d)} \, \frac{1}{L_1} \sum_{l=0}^{L_1-1} \mathrm{e}^{2\pi \mathrm{i}(h_1 - k_1) l / L_1} \\
&= \sum_{\substack{\boldsymbol{h} \in \operatorname{supp} \hat{p} \\ h_1 \equiv k_1 \pmod{L_1}}} \hat{p}_{\boldsymbol{h}} \, \mathrm{e}^{2\pi \mathrm{i}(h_2 x'_2 + \dots + h_d x'_d)}
\end{aligned}$$

for $k_1 \in \mathcal{P}_1(\Gamma)$. We define the index set of detected frequency locations for the first component $I^{(1)} := \{k_1 \in \mathcal{P}_1(\Gamma) \colon \tilde{\hat{p}}_{1,k_1} \neq 0\}$. In practice, we do not test if the Fourier coefficients $\tilde{\hat{p}}_{1,k_1} \neq 0$, but use a threshold $\theta \in (0,1)$ relative to the largest absolute value of the computed Fourier coefficients $\tilde{\hat{p}}_{1,k_1}$ in numerical computations and we restrict the number of detected frequencies to the sparsity parameter s, i.e.,

$$I^{(1)} := I^{(1)} \cup \left\{ k_1 \in \mathcal{P}_1(\Gamma) \colon \text{(up to) } s\text{-largest values } |\tilde{\hat{p}}_{1,k_1}| \geq \theta \cdot \max_{\tilde{k}_1 \in \mathcal{P}_1(\Gamma)} |\tilde{\hat{p}}_{1,\tilde{k}_1}| \right\}. \tag{4.1}$$

Algorithm 4.2 ([PV16, Algorithm 1]). Dimension-incremental reconstruction of a multivariate trigonometric polynomial p_I from samples for unknown frequency index set $\mathrm{I} \subset \Gamma \subset \mathbb{Z}^d$.

Input:	$\Gamma \subset \mathbb{Z}^d$	search domain for frequencies $\boldsymbol{k}$, superset for $\operatorname{supp} \hat{p}$
	$p_I(\circ)$	multivariate trigonometric polynomial p_I as black box (function handle)
	$\theta \in (0,1)$	relative threshold
	$s \in \mathbb{N}$	sparsity parameter
	$r \in \mathbb{N}$	number of detection iterations

(step 1)
Set $L_1 := \max(\mathcal{P}_1(\Gamma)) - \min(\mathcal{P}_1(\Gamma)) + 1$, $I^{(1)} := \emptyset$.
for $i := 1, \ldots, r$ **do**
Choose $x'_2, \ldots, x'_d \in \mathbb{T}$ uniformly at random.
Compute $\tilde{\hat{p}}_{1,k_1} := \frac{1}{L_1} \sum_{l=0}^{L_1-1} p_I(\frac{l}{L_1}, x'_2, \ldots, x'_d)\, \mathrm{e}^{-2\pi \mathrm{i} l k_1 / L_1}$, $k_1 \in \mathcal{P}_1(\Gamma)$, with 1-dim. FFT.
$I^{(1)} := I^{(1)} \cup \{k_1 \in \mathcal{P}_1(\Gamma)\colon$ (up to) s-largest values $|\tilde{\hat{p}}_{1,k_1}| \geq \theta \cdot \max_{\tilde{k}_1 \in \mathcal{P}_1(\Gamma)} |\tilde{\hat{p}}_{1,\tilde{k}_1}|\}$
end for i
Determine $S_1 := \min\big\{m \in \mathbb{N}\colon |\{k_1 \bmod m\colon k_1 \in I^{(1)}\}| = |I^{(1)}|\big\}$. Set $M_1 := S_1$, $z_1 := 1$.
(step 2) **for** $t := 2, \ldots, d$ **do**
(step 2a) Set $L_t := \max(\mathcal{P}_t(\Gamma)) - \min(\mathcal{P}_t(\Gamma)) + 1$, $I^{(t)} := \emptyset$.
for $i := 1, \ldots, r$ **do**
Choose $x'_1, \ldots, x'_{t-1}, x'_{t+1}, \ldots, x'_d \in \mathbb{T}$ uniformly at random.
$\tilde{\hat{p}}_{t,k_t} := \sum_{l=0}^{L_t-1} p_I(x'_1, \ldots, x'_{t-1}, \frac{l}{L_t}, x'_{t+1}, \ldots, x'_d)\, \mathrm{e}^{-2\pi \mathrm{i} l k_t / L_t}$, $k_t \in \mathcal{P}_t(\Gamma)$, using 1-dim. FFT.
Set $I^{(t)} := I^{(t)} \cup \{k_t \in \mathcal{P}_t(\Gamma)\colon$ (up to) s-largest values $|\tilde{\hat{p}}_{t,k_t}| \geq \theta \cdot \max_{\tilde{k}_t \in \mathcal{P}_t(\Gamma)} |\tilde{\hat{p}}_{t,\tilde{k}_t}|\}$.
end for i
(step 2b) Set $\tilde{r} := \begin{cases} r & \text{for } t < d, \\ 1 & \text{for } t = d. \end{cases}$
Determine $S_t := \min\big\{m \in \mathbb{N}\colon |\{k_t \bmod m\colon k_t \in I^{(t)}\}| = |I^{(t)}|\big\}$. Set $I^{(1,\ldots,t)} := \emptyset$.
Build reconstructing rank-1 lattice $\Lambda(\boldsymbol{z}, M_t, \tilde{I})$ for $\tilde{I} := (I^{(1,\ldots,t-1)} \times I^{(t)}) \cap \mathcal{P}_{(1,\ldots,t)}(\Gamma)$, $\boldsymbol{z} \in \mathbb{Z}^t$:
Set initial $M_t := M_{t-1} \cdot S_t$, cf. Theorem 2.7.
Search for $z_t \in \{0, \ldots, M_t - 1\}$ such that reconstruction property (2.27) is fulfilled.
Reduce rank-1 lattice size M_t with reconstruction property (2.27) fulfilled.
for $i := 1, \ldots, \tilde{r}$ **do**
Choose $x'_{t+1}, \ldots, x'_d \in \mathbb{T}$ uniformly at random.
Set $\mathcal{X}^{(1,\ldots,t)} := \{\boldsymbol{x}_j := (\frac{j}{M_t} z_1, \ldots, \frac{j}{M_t} z_t, x'_{t+1}, \ldots, x'_d)^\top \bmod \mathbf{1}\colon j = 0, \ldots, M_t - 1\}$.
(step 2c) Sample p_I at the nodes of the sampling set $\mathcal{X}^{(1,\ldots,t)}$.
(step 2d)
Compute $\tilde{\hat{p}}_{(1,\ldots,t),\boldsymbol{k}} := \frac{1}{M_t} \sum_{j=0}^{M_t-1} p_I(\boldsymbol{x}_j)\, \mathrm{e}^{-2\pi \mathrm{i} \boldsymbol{k} \cdot \boldsymbol{x}_j}$ for $\boldsymbol{k} \in (I^{(1,\ldots,t-1)} \times I^{(t)}) \cap \mathcal{P}_{(1,\ldots,t)}(\Gamma)$ with inverse rank-1 lattice FFT based on a single 1-dim. FFT, see Algorithm 2.1.
(step 2e)
absolute_threshold $:= \theta \cdot \max_{\tilde{\boldsymbol{k}} \in (I^{(1,\ldots,t-1)} \times I^{(t)}) \cap \mathcal{P}_{(1,\ldots,t)}(\Gamma)} |\tilde{\hat{p}}_{(1,\ldots,t),\tilde{\boldsymbol{k}}}|$.
Set $I^{(1,\ldots,t)} := I^{(1,\ldots,t)} \cup \{\boldsymbol{k} \in (I^{(1,\ldots,t-1)} \times I^{(t)}) \cap \mathcal{P}_{(1,\ldots,t)}(\Gamma)\colon$
(up to) s-largest values $|\tilde{\hat{p}}_{(1,\ldots,t),\boldsymbol{k}}| \geq$ absolute_threshold$\}$.
end for i

Algorithm 4.2 continued.

(additional step 2f)

If $t < d$, build (possibly) smaller reconstructing rank-1 lattice $\Lambda(\boldsymbol{z}, M_t, \tilde{I})$ for $\tilde{I} := I^{(1,\ldots,t)}$:
Search for new $z_t \in \{0, \ldots, M_t - 1\}$ where reconstruction property (2.27) is fulfilled.
Reduce rank-1 lattice size M_t with reconstruction property (2.27) fulfilled.

end for t

Output:	$I^{(1,\ldots,d)} \subset \mathbb{Z}^d$	index set of detected frequencies
	$\tilde{\hat{\boldsymbol{p}}} := \left(\tilde{\hat{p}}_{(1,\ldots,d),\boldsymbol{k}}\right)_{\boldsymbol{k} \in I^{(1,\ldots,d)}} \in \mathbb{C}^{\lvert I^{(1,\ldots,d)}\rvert}$	corresponding Fourier coefficients

Since this frequency detection may fail, see Section 4.1.3 for details, we repeatedly perform the sampling, the computation of the projected Fourier coefficients $\tilde{\hat{p}}_{1,k_1}$, $k_1 \in \mathcal{P}_1(\Gamma)$, and the determination of the index set $I^{(1)}$ in totally $r \in \mathbb{N}$ detection iterations with different randomly chosen values $x'_2, \ldots, x'_d \in \mathbb{T}$. Then, we use the union of the obtained index sets $I^{(1)}$. We determine $S_1 := \min\left\{m \in \mathbb{N} \colon \lvert\{k_1 \bmod m \colon k_1 \in I^{(1)}\}\rvert = \lvert I^{(1)}\rvert\right\}$ and obtain a reconstructing rank-1 lattice $\Lambda(z_1, M_1, I^{(1)})$ for the index set of detected frequency locations for the first component $I^{(1)}$ by setting $z_1 := 1$ and $M_1 := S_1$.

Then, we continue with step 2 in Algorithm 4.2 for $t = 2, \ldots, d$. In step 2a, we randomly choose values $x'_1, \ldots, x'_{t-1}, x'_{t+1}, \ldots, x'_d \in \mathbb{T}$, we determine $L_t := \max(\mathcal{P}_t(\Gamma)) - \min(\mathcal{P}_t(\Gamma)) + 1$ and we compute the one-dimensional projected Fourier coefficients for the t-th component

$$\tilde{\hat{p}}_{t,k_t} := \frac{1}{L_t} \sum_{l=0}^{L_t-1} p_I\left(\left(x'_1, x'_{t-1}, \frac{l}{L_t}, x'_{t+1}, \ldots, x'_d\right)^\top\right) \mathrm{e}^{-2\pi \mathrm{i} l k_t / L_t} \tag{4.2}$$

$$= \sum_{\substack{\boldsymbol{h} \in \operatorname{supp} \hat{p} \\ h_t \equiv k_t \pmod{L_t}}} \hat{p}_{\boldsymbol{h}} \, \mathrm{e}^{2\pi \mathrm{i}(h_1 x'_1 + \ldots + h_{t-1} x'_{t-1} + h_{t+1} x'_{t+1} + \ldots + h_d x'_d)} \tag{4.3}$$

for $k_t \in \mathcal{P}_t(\Gamma)$, using a one-dimensional FFT of length L_t. Similarly as in step 1, we obtain $r \in \mathbb{N}$ many index sets of detected frequency locations for the t-th component $\{k_t \in \mathcal{P}_t(\Gamma) \colon$ (up to) s-largest values $\lvert\tilde{\hat{p}}_{t,k_t}\rvert \geq \theta \cdot \max_{\tilde{k}_t \in \mathcal{P}_t(\Gamma)} \lvert\tilde{\hat{p}}_{t,\tilde{k}_t}\rvert\}$ in $r \in \mathbb{N}$ detection iterations with different randomly chosen values $x'_1, \ldots, x'_{t-1}, \ldots, x'_{t+1}, \ldots, x'_d \in \mathbb{T}$ and we set the union of these sets as the index set $I^{(t)}$.

Afterwards in step 2b, we determine $S_t := \min\left\{m \in \mathbb{N} \colon \lvert\{k_t \bmod m \colon k_t \in I^{(t)}\}\rvert = \lvert I^{(t)}\rvert\right\}$ and we search for a reconstructing rank-1 lattice $\Lambda(\boldsymbol{z}, M_t, \tilde{I})$ for the index set $\tilde{I} := (I^{(1,\ldots,t-1)} \times I^{(t)}) \cap \mathcal{P}_{(1,\ldots,t)}(\Gamma)$. For this, the initial rank-1 lattice size M_t is set to $M_{t-1} \cdot S_t$, cf. Theorem 2.7. The components $z_1, \ldots, z_{t-1}$ of the generating vector $\boldsymbol{z}$ from the previous dimension increment steps $1, \ldots, t-1$ are re-used and only one component $z_t \in \{0, \ldots, M_t - 1\}$ is searched for, such that reconstruction property (2.27) is fulfilled. Next, the rank-1 lattice size M_t is reduced with reconstruction property (2.27) fulfilled. We set the sampling set $\mathcal{X}^{(1,\ldots,t)} := \{\boldsymbol{x}_j := (\frac{j}{M_t} z_1, \ldots, \frac{j}{M_t} z_t, x'_{t+1}, \ldots, x'_d)^\top \bmod \mathbf{1} \colon j = 0, \ldots, M_t - 1\}$ containing the sampling nodes $\boldsymbol{x}_j$ with fixed randomly chosen values $x'_{t+1}, \ldots, x'_d \in \mathbb{T}$. Then, we sample the multivariate trigonometric polynomial p_I at these nodes $\boldsymbol{x}_j$ in step 2c. Next, we compute t-dimensional projected Fourier coefficients for the first t components

$$\tilde{\hat{p}}_{(1,\ldots,t),\boldsymbol{k}} := \frac{1}{M_t} \sum_{j=0}^{M_t-1} p_I(\boldsymbol{x}_j) \, \mathrm{e}^{-2\pi \mathrm{i} j \boldsymbol{k} \cdot \boldsymbol{z} / M_t} \tag{4.4}$$

$$= \hat{g}_{\boldsymbol{k} \cdot (z_1,\ldots,z_t)^\top \bmod M_t} \quad \text{for } \boldsymbol{k} \in (I^{(1,\ldots,t-1)} \times I^{(t)}) \cap \mathcal{P}_{(1,\ldots,t)}(\Gamma)$$

in step 2d using a rank-1 lattice FFT, see Algorithm 2.1, where

$$\hat{g}_l := \frac{1}{M_t} \sum_{j=0}^{M_t-1} p_I \left(\left(\frac{j}{M_t}(z_1, \ldots, z_t) \bmod \mathbf{1}, x'_{t+1}, \ldots, x'_d \right)^\top \right) \mathrm{e}^{-2\pi \mathrm{i} j l / M_t}. \tag{4.5}$$

This means, we use only a single one-dimensional FFT and a simple index transform. Note that we have

$$\begin{aligned} \tilde{\hat{p}}_{(1,\ldots,t),\boldsymbol{k}} &= \sum_{\boldsymbol{h} \in \operatorname{supp} \hat{p}} \left(\hat{p}_{\boldsymbol{h}} \, \mathrm{e}^{2\pi \mathrm{i} (h_{t+1}, \ldots, h_d)^\top \cdot (x'_{t+1}, \ldots, x'_d)^\top} \right) \left(\frac{1}{M_t} \sum_{j=0}^{M_t-1} \mathrm{e}^{2\pi \mathrm{i} j (\boldsymbol{h}-\boldsymbol{k}) \cdot \boldsymbol{z} / M_t} \right) \\ &= \sum_{\substack{\boldsymbol{h} \in \operatorname{supp} \hat{p} \\ \left((h_1, \ldots, h_t)^\top - \boldsymbol{k}\right) \cdot \boldsymbol{z} \equiv 0 \pmod{M_t}}} \hat{p}_{\boldsymbol{h}} \, \mathrm{e}^{2\pi \mathrm{i} (h_{t+1}, \ldots, h_d)^\top \cdot (x'_{t+1}, \ldots, x'_d)^\top}. \end{aligned} \tag{4.6}$$

If the conditions $I^{(1,\ldots,t-1)} = \mathcal{P}_{(1,\ldots,t-1)}(\operatorname{supp} \hat{p})$ and $I^{(t)} = \mathcal{P}_t(\operatorname{supp} \hat{p})$ are fulfilled, then

$$\tilde{\hat{p}}_{(1,\ldots,t),\boldsymbol{k}} = \begin{cases} \displaystyle\sum_{\substack{(h_{t+1}, \ldots, h_d)^\top \in \mathcal{P}_{(t+1,\ldots,d)}(\operatorname{supp} \hat{p}) \\ (k_1, \ldots, k_t, h_{t+1}, \ldots, h_d)^\top \in \operatorname{supp} \hat{p}}} \hat{p}_{(k_1, \ldots, k_t, h_{t+1}, \ldots, h_d)^\top} \, \mathrm{e}^{2\pi \mathrm{i} (h_{t+1} x'_{t+1} + \ldots + h_d x'_d)}, & t < d, \\ \hat{p}_{\boldsymbol{k}}, & t = d, \end{cases}$$

for $\boldsymbol{k} \in (I^{(1,\ldots,t-1)} \times I^{(t)}) \cap \mathcal{P}_{(1,\ldots,t)}(\operatorname{supp} \hat{p})$ and $\tilde{\hat{p}}_{(1,\ldots,t),\boldsymbol{k}} = 0$ for $\boldsymbol{k} \in (I^{(1,\ldots,t-1)} \times I^{(t)}) \cap \big(\mathcal{P}_{(1,\ldots,t)}(\Gamma) \setminus \mathcal{P}_{(1,\ldots,t)}(\operatorname{supp} \hat{p})\big)$.
In step 2e, we determine the index set of detected frequency locations for the first t components $\tilde{I}^{(1,\ldots,t)} := \{\boldsymbol{k} \in (I^{(1,\ldots,t-1)} \times I^{(t)}) \cap \mathcal{P}_{(1,\ldots,t)}(\Gamma) \colon |\tilde{\hat{p}}_{(1,\ldots,t),\boldsymbol{k}}| \geq \theta \cdot \max_{\tilde{\boldsymbol{k}} \in (I^{(1,\ldots,t-1)} \times I^{(t)}) \cap \mathcal{P}_{(1,\ldots,t)}(\Gamma)} |\tilde{\hat{p}}_{(1,\ldots,t),\tilde{\boldsymbol{k}}}|\}$. If the cardinality $|\tilde{I}^{(1,\ldots,t)}|$ is larger than the sparsity parameter s, $s \geq |\operatorname{supp} \hat{p}|$, we restrict the index set in $\tilde{I}^{(1,\ldots,t)}$ to frequencies $\boldsymbol{k}$ belonging to the s-largest values $|\tilde{\hat{p}}_{(1,\ldots,t),\boldsymbol{k}}|$. We repeatedly perform the sampling, the computation of the projected Fourier coefficients $\tilde{\hat{p}}_{(1,\ldots,t),\boldsymbol{k}}$ and the determination of the frequency index sets $\tilde{I}^{(1,\ldots,t)}$ in total for $r \in \mathbb{N}$ detection iterations if $t < d$ and $r = 1$ detection iteration if $t = d$. Afterwards, we use the union of the obtained index sets $\tilde{I}^{(1,\ldots,t)}$ as $I^{(1,\ldots,t)}$.
In the additional step 2f if $t < d$, we build a reconstructing rank-1 lattice $\Lambda(\boldsymbol{z}, M_t, I^{(1,\ldots,t)})$ for the index set $I^{(1,\ldots,t)}$. As initial rank-1 lattice size, we use the value M_t from step 2b. We only search for the component z_t of the generating vector $\boldsymbol{z}$ as in step 2b and then reduce the rank-1 lattice size M_t with reconstruction property (2.27) fulfilled.

Finally, we obtain the frequency index set $I^{(1,\ldots,d)} \subset \Gamma \subset \mathbb{Z}^d$. If all frequency detections were successful, i.e.,

$$\begin{aligned} I^{(t)} &= \mathcal{P}_t(\operatorname{supp} \hat{p}) && \text{for } t = 1, \ldots, d && \text{and} \\ I^{(1,\ldots,t)} &= \mathcal{P}_{(1,\ldots,t)}(\operatorname{supp} \hat{p}) && \text{for } t = 1, \ldots, d-1, \end{aligned}$$

then we have

$$\begin{aligned} I^{(1,\ldots,d)} &= \operatorname{supp} \hat{p}, \\ \tilde{\hat{p}}_{(1,\ldots,d),\boldsymbol{k}} &= \hat{p}_{\boldsymbol{k}} \neq 0 && \text{for all } \boldsymbol{k} \in I^{(1,\ldots,d)} && \text{and} \\ p_I = \sum_{\boldsymbol{k} \in \operatorname{supp} \hat{p}} \hat{p}_{\boldsymbol{k}} \, \mathrm{e}^{2\pi \mathrm{i} \boldsymbol{k} \cdot \circ} &= \sum_{\boldsymbol{k} \in I^{(1,\ldots,d)}} \tilde{\hat{p}}_{(1,\ldots,d),\boldsymbol{k}} \, \mathrm{e}^{2\pi \mathrm{i} \boldsymbol{k} \cdot \circ}. \end{aligned}$$

Note that we do not necessarily have $I^{(1,\dots,d)} \subset \operatorname{supp} \hat{p}$, i.e., the algorithm may wrongly yield frequencies $\boldsymbol{k} \in \Gamma$ where the true Fourier coefficients $\hat{p}_{\boldsymbol{k}}$ are zero, see case iv in Section 4.1.3 and the discussion concerning this case. However, this only happens if a previous detection step fails.

Note that the illustrated example in Figure 4.1 corresponds to one run of Algorithm 4.2 with $r = 1$ detection iteration.

4.1.2.2 Modified Algorithm with less rank-1 lattice searches

Algorithm 4.3 ([PV16, Algorithm 2]). Dimension-incremental reconstruction of a multivariate trigonometric polynomial p_I from samples for unknown frequency index set $I \subset \Gamma \subset \mathbb{Z}^d$ with less rank-1 lattice searches.

Modifications of Algorithm 4.2:

$\vdots$

(step 2b) Set $\tilde{r} := \begin{cases} r & \text{for } t < d, \\ 1 & \text{for } t = d. \end{cases}$

Determine $S_t := \min\left\{m \in \mathbb{N} \colon |\{k_t \bmod m \colon k_t \in I^{(t)}\}| = |I^{(t)}|\right\}$. Set $I^{(1,\dots,t)} := \emptyset$.

Build reconstructing rank-1 lattice $\Lambda(\boldsymbol{z}, M_t, (I^{(1,\dots,t-1)} \cap \mathcal{P}_{(1,\dots,t-1)}(\Gamma)) \times (I^{(t)} \cap \mathcal{P}_{(t)}(\Gamma)))$:

Set $M_t := M_{t-1} \cdot S_t$ and $z_t := M_{t-1}$, i.e., $\boldsymbol{z} = (z_1, \dots, z_{t-1}, M_{t-1})^\top$, cf. Theorem 2.7.

for $i := 1, \dots, \tilde{r}$ **do**

$\vdots$

Algorithm 4.3 is another realization for the dimension-incremental method. The approach is based on Algorithm 4.2. However, in step 2b, we do not search for a reconstructing rank-1 lattice for the frequency index set $I^{(1,\dots,t-1)} \times I^{(t)}$ but we explicitly build one using the construction from Theorem 2.7 in Section 2.2.1. The other steps of Algorithm 4.2 remain unchanged in Algorithm 4.3.

The arithmetic complexity for Algorithm 4.3 is distinctly lower than for Algorithm 4.2, see Section 4.1.4, and the upper bound for the number of samples is asymptotically the same for both algorithms. However, in practice, the number of samples when using Algorithm 4.3 may be larger because we do not search for a preferably small rank-1 lattice size M_t. Especially, if the search domain Γ is distinctly smaller than the full grid $\hat{G}_N^d$ and Γ is not a tensor product grid, then Algorithm 4.2 should be better suited with respect to the number of samples. We observe this behavior in the numerical results in Section 4.1.6. For our small example from Figure 4.1, Algorithm 4.3 yields the identical index sets and reconstructing rank-1 lattices $\Lambda\big(\boldsymbol{z}, M_t, (I^{(1,\dots,t-1)} \cap \mathcal{P}_{(1,\dots,t-1)}(\Gamma)) \times (I^{(t)} \cap \mathcal{P}_{(t)}(\Gamma))\big)$ as Algorithm 4.2.

4.1.3 Successful and failed detection

As mentioned in the previous sections, the successful detection of all non-zero Fourier coefficients $\hat{p}_{\boldsymbol{k}} \neq 0$ of a multivariate trigonometric polynomial p_I and the corresponding frequencies $\boldsymbol{k}$, i.e., obtaining $I^{(1,\dots,d)} = \operatorname{supp} \hat{p}$, is not guaranteed. In the following, we discuss conditions for the successful detection and we address the question if it is possible to notice that not all frequencies were detected successfully during the incremental detection process in Section 4.1. We remark that the computations in (4.2) are responsible for the correct frequency detection, which belong to the computation steps 1 and 2a of Algorithm 4.2 and 4.3, as well as the computations in (4.4), which belong to the computation step 2d.

In [PV16, Theorem 5.2], the probability that the detection fails for a frequency location in step 1, 2a and 2d is estimated by the upper bound

$$C(p,\theta) := \exp\left(-2\frac{(\min_{\boldsymbol{h}\in\operatorname{supp}\hat{p}}|\hat{p}_{\boldsymbol{h}}| - \theta\cdot\sum_{\boldsymbol{h}\in\operatorname{supp}\hat{p}}|\hat{p}_{\boldsymbol{h}}|)^2}{(\sum_{\boldsymbol{h}\in\operatorname{supp}\hat{p}}|\hat{p}_{\boldsymbol{h}}|)^2}\right) < 1 \quad \text{for} \quad \theta < \frac{\min_{\boldsymbol{h}\in\operatorname{supp}\hat{p}}|\hat{p}_{\boldsymbol{h}}|}{\sum_{\boldsymbol{h}\in\operatorname{supp}\hat{p}}|\hat{p}_{\boldsymbol{h}}|}.$$

Since we use $r \in \mathbb{N}$ many detection iterations with new values $x'_1,\dots,x'_{t-1},x'_{t+1},\dots,x'_d \in \mathbb{T}$ independently chosen uniformly at random, the frequency detection succeeds if we find the frequency locations in at least one detection iteration $i \in \{1,\dots,r\}$, and we obtain the probability $\mathbb{P}(k_t \in I^{(t)}) \geq 1-(C(p))^r$ for each $k_t \in \mathcal{P}_t(\operatorname{supp}\hat{p})$ in step 1 and 2a of Algorithm 4.2 and 4.3 for the index set $I^{(t)}$, assuming that the sparsity parameter $s \geq |\operatorname{supp}\hat{p}|$ and the search domain $\Gamma \supset \operatorname{supp}\hat{p}$. Note that this probability can be arbitrarily close to 1 if the number r of detection iterations is sufficiently large. Similarly, the frequency detection for $\boldsymbol{k} \in (I^{(1,\dots,t-1)}\times I^{(t)})\cap\mathcal{P}_{(1,\dots,t)}(\operatorname{supp}\hat{p})$ succeeds with probability $\mathbb{P}(\boldsymbol{k}\in I^{(1,\dots,t)}) \geq 1-(C(p))^r$ for each $\boldsymbol{k} \in (I^{(1,\dots,t-1)}\times I^{(t)})\cap\mathcal{P}_{(1,\dots,t)}(\operatorname{supp}\hat{p})$, assuming that the sparsity parameter $s \geq |\operatorname{supp}\hat{p}|$, the search domain $\Gamma \supset \operatorname{supp}\hat{p}$, $I^{(\tau)} = \mathcal{P}_\tau(\operatorname{supp}\hat{p})$ for $\tau \in \{1,\dots,t\}$ and $I^{(1,\dots,\tau)} = \mathcal{P}_{(1,\dots,\tau)}(\operatorname{supp}\hat{p})$ for $\tau \in \{2,\dots,t-1\}$.

Finally, all non-zero Fourier coefficients $\hat{p}_{\boldsymbol{k}} \neq 0$ of the multivariate trigonometric polynomial p_I and the corresponding frequencies $\boldsymbol{k}$ are successfully detected if the frequency detections in the dimension increment steps $t \in \{1,\dots,d\}$ succeed. During the computations in step 2 of Algorithm 4.2 and 4.3, the following cases may occur.

i. For a frequency $\boldsymbol{k} \in (I^{(1,\dots,t-1)}\times I^{(t)})\cap\mathcal{P}_{(1,\dots,t)}(\Gamma)$, we have $\tilde{\hat{p}}_{(1,\dots,t),\boldsymbol{k}} \neq 0$ and $\boldsymbol{k} \in \mathcal{P}_{(1,\dots,t)}(\operatorname{supp}\hat{p})$, i.e., the detection of the frequency $\boldsymbol{k}$ was successful.

ii. For a frequency $\boldsymbol{k} \in (I^{(1,\dots,t-1)}\times I^{(t)})\cap\mathcal{P}_{(1,\dots,t)}(\Gamma)$, we have $\tilde{\hat{p}}_{(1,\dots,t),\boldsymbol{k}} = 0$ but $\boldsymbol{k} \in \mathcal{P}_{(1,\dots,t)}(\operatorname{supp}\hat{p})$, i.e., the frequency $\boldsymbol{k}$ was considered but not recognized, and the detection of the frequency $\boldsymbol{k}$ failed.

iii. For a frequency $\boldsymbol{k} \in \mathcal{P}_{(1,\dots,t)}(\operatorname{supp}\hat{p})$, we have $\boldsymbol{k} \notin (I^{(1,\dots,t-1)}\times I^{(t)})\cap\mathcal{P}_{(1,\dots,t)}(\Gamma)$, i.e., the frequency $\boldsymbol{k}$ was not considered. This means the detection of the frequency $\boldsymbol{k}$ failed.

   (a) For a frequency $l \in \{0,\dots,M_t-1\}$, we have $\hat{g}_l \neq 0$ in (4.5) but $\nexists\,\boldsymbol{k} \in I^{(1,\dots,t-1)}\times I^{(t)}$ such that $\boldsymbol{k}\cdot(z_1,\dots,z_t)^\top \equiv l \pmod{M_t}$.

iv. For a frequency $\boldsymbol{k} \in (I^{(1,\dots,t-1)}\times I^{(t)})\cap\mathcal{P}_{(1,\dots,t)}(\Gamma)$, we have $\tilde{\hat{p}}_{(1,\dots,t),\boldsymbol{k}} \neq 0$ but $\boldsymbol{k} \notin \mathcal{P}_{(1,\dots,t)}(\operatorname{supp}\hat{p})$, i.e., the frequency $\boldsymbol{k}$ was falsely detected.

As discussed before, we do not test the Fourier coefficients for zero/non-zero but if their absolute values are below or above a certain threshold. Correspondingly, $\tilde{\hat{p}}_{(1,\dots,t),\boldsymbol{k}} \neq 0$ means $|\tilde{\hat{p}}_{(1,\dots,t),\boldsymbol{k}}| \geq$ threshold_value and $\tilde{\hat{p}}_{(1,\dots,t),\boldsymbol{k}} = 0$ means $|\tilde{\hat{p}}_{(1,\dots,t),\boldsymbol{k}}| <$ threshold_value.

Case i is the optimal case where the frequency $\boldsymbol{k}$ was in the candidate list $(I^{(1,\dots,t-1)}\times I^{(t)})\cap\mathcal{P}_{(1,\dots,t)}(\Gamma)$ and detected correctly.

In contrast, case ii means that the frequency also was in the candidate list but was wrongly not included in the index set $I^{(1,\dots,t)}$ of detected frequency locations. Similar to the discussion for the computation (4.2), the fixed values $x'_{t+1},\dots,x'_d \in \mathbb{T}$ influence the successful frequency detection, see the aliasing formula (4.6). Again, we suggest to repeatedly evaluate (4.4) with different randomly chosen values $x'_{t+1},\dots,x'_d \in \mathbb{T}$ and compare the obtained index sets $I^{(1,\dots,t)}$ of detected frequency locations. If all of them coincide, it is very likely that the case ii did

not occur. Otherwise, we suggest to use the union of the obtained index sets $I^{(1,\dots,t)}$ for the computations that follow.

In case iii, at least one frequency $\boldsymbol{k} \in \mathcal{P}_{(1,\dots,t)}(\operatorname{supp}\hat{p})$ is already missing in the candidate list $(I^{(1,\dots,t-1)} \times I^{(t)}) \cap \mathcal{P}_{(1,\dots,t)}(\Gamma)$. Possibly, we will not be able to even notice this. If we encounter case iiia, which is a special variant of case iii, we know that there exists at least one frequency $\boldsymbol{k} := \binom{\boldsymbol{k}'}{k''} \in \mathcal{P}_{(1,\dots,t)}(\operatorname{supp}\hat{p})$ for which $\boldsymbol{k} \notin (I^{(1,\dots,t-1)} \times I^{(t)}) \cap \mathcal{P}_{(1,\dots,t)}(\Gamma)$, but we do not exactly know which and how many frequencies are affected by this. However, we know that these frequencies are from the set $\{\boldsymbol{h} \in \mathcal{P}_{(1,\dots,t)}(\Gamma) \colon \boldsymbol{h} \cdot (z_1,\dots,z_t)^\top \equiv l \pmod{M_t}\}$ for Algorithm 4.2.

Furthermore, case iv may occur and is a consequence of having $I^{(t)} \not\supset \mathcal{P}_t(\operatorname{supp}\hat{p})$ in the current (t-th) dimension increment step or case iii in one of the preceding dimension increment steps $1,\dots,t-1$. This means, in the current or one of the previous dimension increment steps, at least one frequency was not detected. Moreover, we have $I^{(1,\dots,t)} \not\subset \mathcal{P}_{(1,\dots,t)}(\operatorname{supp}\hat{p})$. However, we may not be able to notice that this case has occurred.

4.1.4 Number of samples and arithmetic complexity

In this section, we give upper bounds for the number of samples and for the arithmetic complexity of Algorithm 4.2 and 4.3 in the case where the search domain Γ is the full grid $\hat{G}_N^d$, see also [PV16, Section 2.2.3]. For computing the index set of detected frequencies for the t-th component $I^{(t)}$, $t = 1,\dots,d$, in the steps 1 and 2a of Algorithm 4.3, $(2N+1)$ function samples are taken and the one-dimensional FFT requires at most $C_1\, N \log N$ arithmetic operations in each detection iteration $i \in \{1,\dots,r\}$ for each $t \in \{1,\dots,d\}$, where the constant $C_1 \geq 1$ does not depend on N. This yields $r\,d\,|\hat{G}_N^1| = r\,d\,(2N+1)$ function samples and at most $\tilde{C}\, r\, d\, N \log N$ arithmetic operations for determining the frequency index sets $I^{(1)},\dots,I^{(d)}$, where $\tilde{C} \geq 1$ is an absolute constant.

In step 2 of Algorithm 4.2 and 4.3 for dimension increment step t, the index sets $I^{(1,\dots,t-1)}$ and $I^{(t)}$ consist of at most rs many frequencies. This yields that the index set $I^{(1,\dots,t-1)} \times I^{(t)}$ consists of $|I^{(1,\dots,t-1)} \times I^{(t)}| \leq r\,s\,|\hat{G}_N^1|$ frequency candidates. The sampling set $\mathcal{X}^{(1,\dots,t)}$ constructed in step 2b of Algorithm 4.2 and 4.3 has the size $|\mathcal{X}^{(1,\dots,t)}| = M_t$, where the rank-1 lattice size $M_t \leq \max\{2r^2s^2, 3N\}\,(2N+1)$ due to Corollary 2.8. Calling Algorithm 2.1 in step 2d requires no more than $C_1 M_t \log M_t + 2t|I^{(1,\dots,t-1)} \times I^{(t)}|$ arithmetic operations for each detection iteration $i \in \{1,\dots,r\}$ and each dimension increment step $t \in \{2,\dots,d\}$.
For each detection iteration $i \in \{1,\dots,r\}$ and each dimension increment step $t \in \{2,\dots,d\}$ when searching for the next component z_t of the generating vector $\boldsymbol{z}$ in step 2b in Algorithm 4.2, the number of arithmetic operations is bounded by $3\,|I^{(1,\dots,t-1)} \times I^{(t)}|\,M_t \leq 3\,r\,s\,(2N+1)\max\{2r^2s^2, 3N\}(2N+1)$, see the proof of Theorem 2.4. Moreover, reducing the rank-1 lattice size M_t, e.g. by using [Käm14b, Algorithm 3.5], requires no more arithmetic operations.
At the end of step 2e, the index set $I^{(1,\dots,t)}$ consists of no more than $|I^{(1,\dots,t)}| \leq r\,s$ frequencies. Consequently, when searching for the new reconstructing rank-1 lattice $\Lambda((z_1,\dots,z_t)^\top, M_t, I^{(1,\dots,t)})$ in the additional step 2f of Algorithm 4.2 and 4.3 for each $t \in \{2,\dots,d-1\}$, the new rank-1 lattice size M_t is bounded by $\max\{2r^2s^2, 3N\}$ due to Theorem 2.4. The number of arithmetic operations for the search of the next component z_t of the generating vector $\boldsymbol{z}$ is bounded by $3\,|I^{(1,\dots,t)}|\,M_t \leq 3\,r\,s\,\max\{2r^2s^2, 3N\}$, see the proof of Theorem 2.4. Reducing the rank-1 lattice size M_t requires no more than $3\,r\,s\,\max\{2r^2s^2, 3N\}$ arithmetic operations.

In total, this yields no more than

$$r\,(d-1)\max\{2r^2s^2,3N\}\,2(N+1)+r\,d\,(2N+1)$$

many samples for Algorithm 4.2 and 4.3 as well as

$$C\,d\cdot\big(\max\{r^3s^3N^2,r\,s\,N^3\}+\max\{r^3s^2N,r\,N^2\}\log(\max\{r^2s^2N,N^2\})\big)$$

arithmetic operations for Algorithm 4.2 and

$$C\,d\cdot\big(\max\{r^3s^3,r\,s\,N\}+\max\{r^3s^2N,r\,N^2\}\log(\max\{r^2s^2N,N^2\})\big)$$

arithmetic operations for Algorithm 4.3, where $C>1$ is an absolute constant. We remark that a large contribution to the arithmetic complexity comes from the rank-1 lattice search, in particular for Algorithm 4.2 in step 2b. Moreover, we have no exponential dependence in the dimension d, neither for the number of samples nor the arithmetic complexity. Assuming $\sqrt{N}\lesssim s\lesssim N^d$, we require $\mathcal{O}(d\,s^2N)$ many samples for both algorithms as well as $\mathcal{O}(d\,s^3N^2)$ and $\mathcal{O}(d\,s^3+d\,s^2N\log(s\,N))$ arithmetic operations for Algorithm 4.2 and 4.3, respectively. In the case $s\lesssim\sqrt{N}$, we need $\mathcal{O}(d\,N^2)$ many samples for both algorithms as well as $\mathcal{O}(d\,s\,N^3)$ and $\mathcal{O}(d\,N^2\log N)$ arithmetic operations for Algorithm 4.2 and 4.3, respectively.

Remark 4.1. If all detection steps in Algorithm 4.2 or 4.3 succeed, see also Section 4.1.3, we can replace the sparsity parameter s in the sampling and arithmetic complexities by the number $|\operatorname{supp}\hat{p}|$ of non-zero Fourier coefficients $\hat{p}_{\boldsymbol{k}}\neq 0$ of a multivariate trigonometric polynomial p_I. Assuming $\sqrt{N}\lesssim|\operatorname{supp}\hat{p}|\lesssim N^d$, we require $\mathcal{O}(d\,|\operatorname{supp}\hat{p}|^2N)$ many samples for both algorithms as well as $\mathcal{O}(d\,|\operatorname{supp}\hat{p}|^3N^2)$ and $\mathcal{O}(d\,|\operatorname{supp}\hat{p}|^3+d\,|\operatorname{supp}|^2N\log(|\operatorname{supp}\hat{p}|\,N))$ arithmetic operations for Algorithm 4.2 and 4.3, respectively. □

4.1.5 Deterministic version

As described in [PV16], we do not need to use random sampling if the Fourier coefficients $\hat{p}_{\boldsymbol{k}}$, $\boldsymbol{k}\in\operatorname{supp}\hat{p}$, of the multivariate trigonometric polynomial p_I fulfill the property that the signs of the real part $\operatorname{Re}(\hat{p}_{\boldsymbol{k}})$ of all Fourier coefficients $\hat{p}_{\boldsymbol{k}}$ are identical $\neq 0$ or that the signs of the imaginary part $\operatorname{Im}(\hat{p}_{\boldsymbol{k}})$ are identical $\neq 0$. Then, we may set the number of detection iterations $r:=1$, the sparsity parameter $s:=\operatorname{supp}\hat{p}$ as well as the (random) components $x'_1,\dots,x'_d$ of the sampling nodes always to zero in Algorithm 4.2 and 4.3, by which both algorithms become deterministic.

Because of the above choice of the components $x'_1,\dots,x'_d:=0$, the aliasing formula in (4.3) simplifies to

$$\tilde{\hat{p}}_{t,k_t}=\sum_{\substack{\boldsymbol{h}\in\operatorname{supp}\hat{p}\\ h_t\equiv k_t\pmod{L_t}}}\hat{p}_{(h_1,\dots,h_{t-1},k_t,h_{t+1},\dots,h_d)^\top},$$

which means the one-dimensional projected Fourier coefficients for the t-th component are simply sums of the corresponding Fourier coefficients $\hat{p}_{\boldsymbol{k}}$ of the multivariate trigonometric polynomial p_I, as well as the aliasing formula in (4.6) simplifies to

$$\tilde{\hat{p}}_{(1,\dots,t),\boldsymbol{k}}=\sum_{\substack{\boldsymbol{h}\in\operatorname{supp}\hat{p}\\ \left((h_1,\dots,h_t)^\top-\boldsymbol{k}\right)\cdot\boldsymbol{z}\equiv 0\pmod{M_t}}}\hat{p}_{\boldsymbol{h}}.$$

Consequently, if the Fourier coefficients $\hat{p}_{\boldsymbol{k}}$ fulfill the above assumptions, then aliasing Fourier coefficients $\hat{p}_{(h_1,\dots,h_{t-1},k_t,h_{t+1},\dots,h_d)^\top}$ or $\hat{p}_{\boldsymbol{h}}$ do not sum up to zero or very small values below a certain threshold and the detection succeeds. However, for arbitrary Fourier coefficients $\hat{p}_{\boldsymbol{k}}\in\mathbb{C}$, we rely on random sampling in both algorithms.

4.1.6 Numerical results

The numerical results of this section were published in [PV16, Section 3]. An implementation of Algorithm 4.2 and 4.3 as well as MATLAB code for performing tests are available online [Vol15]. Most of the numerical tests of this section were run on a computer with Intel Xeon CPU E5-4640 CPU in MATLAB R2015b using IEEE 754 double precision arithmetic. Time measurements were taken on a computer with Intel i7-970 CPU (3.2 GHz) using only one thread.

4.1.6.1 Random sparse trigonometric polynomial in the noiseless case

We set the refinement $N := 32$ and construct random multivariate trigonometric polynomials p_I with frequencies supported within the full grid $\hat{G}_{32}^d$. This means, we choose $|\operatorname{supp}\hat{p}|$ many frequencies uniformly at random from $\hat{G}_{32}^d \subset \mathbb{Z}^d$ and corresponding Fourier coefficients $\hat{p}_{\boldsymbol{k}} \in [-1,1) + [-1,1)\mathrm{i}$, $|\hat{p}_{\boldsymbol{k}}| \geq 10^{-6}$, $\boldsymbol{k} \in I = \operatorname{supp}\hat{p}$. For the reconstruction of the multivariate trigonometric polynomials p_I, we choose the search domain $\Gamma := \hat{G}_{32}^d$. We do not truncate the frequency index sets of detected frequencies $I^{(1,\ldots,t)}$, $t \in \{2,\ldots,d\}$ here, i.e., we set the sparsity parameter $s := |\Gamma|$ for Algorithm 4.2 and 4.3. The truncation of detected frequencies may only be required if the samples are perturbed by noise, see Section 4.1.6.2, or if we have infinitely many non-zero Fourier coefficients, see the 10-dimensional test function in Section 4.1.6.4. Alternatively, choosing the sparsity parameter $s := |\operatorname{supp}\hat{p}|$ gives the same results in the examples of this section. Moreover, we set the number of detection iterations $r := 1$. All tests are repeated 10 times with newly chosen frequencies $\boldsymbol{k}$ and Fourier coefficients $\hat{p}_{\boldsymbol{k}}$. We start with tests for Algorithm 4.2.

Example 4.2. ([PV16, Example 3.1], *reconstruction of random sparse trigonometric polynomials using Algorithm 4.2*). We set the threshold parameter $\theta := 10^{-12}$. For the sparsities $|\operatorname{supp}\hat{p}| \in \{1\,000, 10\,000\}$, we applied Algorithm 4.2. In the cases $|\operatorname{supp}\hat{p}| = 1\,000$ and $|\operatorname{supp}\hat{p}| = 10\,000$, we ran the tests for dimensions $d \in \{3,4,\ldots,10,15,20,25,30\}$ and $d \in \{3,4,5,6,7\}$, respectively. In each test, all frequencies were successfully detected, $I^{(1,\ldots,d)} = \operatorname{supp}\hat{p}$. The used parameters and results are presented in Table 4.1. The column "max cand." shows the maximal number $\max_{t=2,\ldots,d} |I^{(1,\ldots,t-1)} \times I^{(t)}|$ of frequency candidates of all 10 repetitions and "max M" the overall maximal rank-1 lattice size used. Furthermore, the total number of samples for each repetition was computed and the maximum of these numbers for the 10 repetitions can be found in the column "#samples". The relative ℓ_2-error $\|(\tilde{\hat{p}}_{\boldsymbol{k}})_{\boldsymbol{k}\in I} - (\hat{p}_{\boldsymbol{k}})_{\boldsymbol{k}\in I}\|_2 / \|(\hat{p}_{\boldsymbol{k}})_{\boldsymbol{k}\in I}\|_2$ of the computed Fourier coefficients $(\tilde{\hat{p}}_{\boldsymbol{k}})_{\boldsymbol{k}\in I^{(1,\ldots,d)}}$ was determined for each repetition, where $I := \operatorname{supp}\hat{p} \cup I^{(1,\ldots,d)}$ and $\tilde{\hat{p}}_{\boldsymbol{k}} := 0$ for $\boldsymbol{k} \in I \setminus I^{(1,\ldots,d)}$, and the column "rel. ℓ_2-error" contains the maximal value of the 10 repetitions. In all tests, the relative ℓ_2-error is smaller than $1.4 \cdot 10^{-15}$ and is caused by the utilized IEEE 754 double precision arithmetic. The numbers of used samples "#samples" increase for increasing dimensions d and sparsities $|\operatorname{supp}\hat{p}|$ of the trigonometric polynomials p_I. Compared to the cardinality of the full grids $|\Gamma| = |\hat{G}_N^d|$, the observed numbers of samples are still moderate. For sparsity $|\operatorname{supp}\hat{p}| = 1\,000$, the largest increase of the maximal rank-1 lattice size "max M" is from dimension $d = 3$ to $d = 4$. For dimensions $d \geq 5$, the maximal number of frequency candidates "max cand." is 65 000 and the maximal rank-1 lattice size "max M" is between about 2.6 and 3.0 million. This is caused by the relatively large numbers of possible frequencies $|\Gamma| = |\hat{G}_{32}^d| = 65^d$ and the small sparsity $|\operatorname{supp}\hat{p}| = 1\,000$, which cause that all 1 000 non-zero Fourier coefficients $\hat{p}_{\boldsymbol{k}} \neq 0$ are already detected in dimension-incremental step $t = 4$ or $t = 5$ and that higher components z_τ, $5 \leq \tau < t$, (except the highest component z_t)

of the generating vector $\boldsymbol{z} := (z_1, \ldots, z_t)^\top$ of the reconstructing rank-1 lattices $\Lambda(\boldsymbol{z}, M, \tilde{I})$ are zero in most cases. Consequently, the numbers of used samples "#samples" increase by about 2.6 to 3.0 million per additional dimension. Moreover, we have a similar behavior for sparsity $|\operatorname{supp} \hat{p}| = 10\,000$ at dimensions $d \geq 6$, where the maximal rank-1 lattice size "max M" is about 160 million and the numbers of used samples "#samples" increase correspondingly per additional dimension. We remark that we may have found all non-zero Fourier coefficients $\hat{p}_{\boldsymbol{k}} \neq 0$ in a dimension-incremental step $t \leq 5$, but we still need to continue with remaining dimension-incremental steps $t \geq 6$ in order to determine the higher components k_t, $t \in \{6, \ldots, d\}$, of the frequencies $\boldsymbol{k}$. □

d	$\lvert\operatorname{supp} \hat{p}\rvert$	$\lvert\Gamma\rvert = \lvert\hat{G}_N^d\rvert$	max cand.	max M	#samples	rel. ℓ_2-error
3	1 000	274 625	53 365	142 870	145 275	4.5e-16
4	1 000	17 850 625	64 870	2 331 030	2 472 145	8.3e-16
5	1 000	1.16e+09	65 000	2 935 419	4 979 314	8.9e-16
6	1 000	7.54e+10	65 000	2 655 816	7 479 265	7.0e-16
7	1 000	4.90e+12	65 000	2 685 234	9 905 378	6.2e-16
8	1 000	3.19e+14	65 000	2 665 578	11 820 279	7.8e-16
9	1 000	2.07e+16	65 000	2 690 118	14 531 442	6.1e-16
10	1 000	1.35e+18	65 000	2 714 623	16 986 369	1.3e-15
15	1 000	1.56e+27	65 000	2 827 045	30 461 941	5.0e-16
20	1 000	1.81e+36	65 000	2 836 998	42 580 486	7.6e-16
25	1 000	2.10e+45	65 000	2 978 356	56 432 050	5.5e-16
30	1 000	2.44e+54	65 000	2 920 928	68 237 645	4.3e-16
3	10 000	274 625	143 585	147 810	150 280	5.0e-16
4	10 000	17 850 625	629 200	9 023 625	9 165 390	6.7e-16
5	10 000	1.16e+09	649 740	137 285 053	146 360 548	1.3e-15
6	10 000	7.54e+10	650 000	162 562 853	309 453 235	1.1e-15
7	10 000	4.90e+12	650 000	159 449 641	453 175 172	9.7e-16

Table 4.1: ([PV16, Table 3.1]). Results for random sparse multivariate trigonometric polynomials p_I, $I \subset \hat{G}_{32}^d$, using reconstructing rank-1 lattices $\Lambda(\boldsymbol{z}, M, \tilde{I})$ and Algorithm 4.2 when considering frequencies within the search domain $\Gamma = \hat{G}_{32}^d$.

Next, we run tests for Algorithm 4.3, which internally performs less searches for reconstructing rank-1 lattices $\Lambda(\boldsymbol{z}, M, \tilde{I})$.

Example 4.3. ([PV16, Example 3.2], *reconstruction of random sparse trigonometric polynomials using Algorithm 4.3*). We set the threshold parameter $\theta := 10^{-12}$. For the sparsities $|\operatorname{supp} \hat{p}| \in \{1\,000, 10\,000\}$ and dimensions $d \in \{3, 4, \ldots, 10, 15, 20, 25, 30\}$, we applied Algorithm 4.3. In each test, all frequencies were successfully detected, $I^{(1,\ldots,d)} = \operatorname{supp} \hat{p}$. The numerical results are presented in Table 4.2, where the column names have the same meaning as described in Example 4.2. The relative ℓ_2 errors are similar to the ones for Algorithm 4.2 in Table 4.1. In this example, the maximal rank-1 lattice sizes M are larger compared to the results for Algorithm 4.2 in Table 4.1, since the reconstructing rank-1 lattices $\Lambda(\boldsymbol{z}, M, \tilde{I})$ are reduced by an additional search in step 2b of Algorithm 4.2 whereas they are explicitly constructed in Algorithm 4.3 without the reduction step, cf. Theorem 2.7. Correspondingly, the total numbers of samples are slightly higher in this example compared to the results when using Algorithm 4.2 for identical refinement N, dimension d and sparsity $|\operatorname{supp} \hat{p}|$. However, the runtime of the algorithms can differ significantly due to the additional search in

Algorithm 4.2, see Example 4.4. As in Example 4.2, the maximal number of frequency candidates "max cand." is 65 000 for sparsity $|\operatorname{supp}\hat{p}| = 1\,000$ and the maximal rank-1 lattice size "max M" is now between about 2.7 and 3.1 million. Again, this is caused by the relatively large numbers of possible frequencies $|\Gamma| = |\hat{G}_{32}^d| = 65^d$ and the small sparsity $|\operatorname{supp}\hat{p}| = 1\,000$, which cause that all 1 000 non-zero Fourier coefficients $\hat{p}_{\boldsymbol{k}} \neq 0$ are already detected in a dimension-incremental step $t \leq 5$ and higher components z_τ, $6 \leq \tau < t$, (except the highest component z_t) of the generating vector $\boldsymbol{z}$ of the reconstructing rank-1 lattices $\Lambda(\boldsymbol{z}, M, \tilde{I})$ to be zero in most cases. Consequently, the numbers of used samples "#samples" increase by about 2.7 to 3.1 million per additional dimension. For sparsity $|\operatorname{supp}\hat{p}| = 10\,000$, we have analogously 650 000 maximal frequency candidates "max cand." and the maximal rank-1 lattice size "max M" is now between about 192 and 204 million. Correspondly, the numbers of samples increase by this for each additional dimension. □

d	$\lvert\operatorname{supp}\hat{p}\rvert$	max cand.	max M	#samples	rel. ℓ_2-error
6	1 000	65 000	2 761 655	8 139 560	6.4e-16
7	1 000	65 000	2 795 390	10 953 150	4.8e-16
8	1 000	65 000	3 052 335	13 145 275	9.1e-16
9	1 000	65 000	2 932 085	16 339 115	8.0e-16
10	1 000	65 000	3 056 560	18 674 565	4.5e-16
20	1 000	65 000	3 056 560	46 572 500	4.4e-16
30	1 000	65 000	3 068 000	73 665 475	6.2e-16
6	10 000	650 000	192 287 810	392 345 005	8.9e-16
7	10 000	650 000	194 595 570	572 814 190	6.8e-16
8	10 000	650 000	197 127 645	745 706 455	8.9e-16
9	10 000	650 000	203 536 385	967 031 390	5.8e-16
10	10 000	650 000	200 068 050	1 132 939 795	9.0e-16
20	10 000	650 000	200 385 055	2 959 435 895	7.4e-16
30	10 000	650 000	203 592 740	4 924 539 100	6.9e-16

Table 4.2: ([PV16, Table 3.2]). Results for random sparse trigonometric polynomials using reconstructing rank-1 lattices $\Lambda(\boldsymbol{z}, M, \tilde{I})$ and Algorithm 4.3 when considering frequencies within the search domain $\Gamma = \hat{G}_{32}^d$.

Next, we compare the runtimes of both algorithms for certain parameter choices.

Example 4.4. ([PV16, Example 3.6], *runtimes of Algorithm 4.2 and 4.3*). In Table 4.3, we compare the runtimes for Algorithm 4.2 and 4.3. For both algorithms, we consider the runtimes for the reconstruction of multivariate trigonometric polynomials p_I with sparsity $|\operatorname{supp}\hat{p}| = 1\,000\}$ and frequencies $\boldsymbol{k}$ supported within the d-dimensional full grid $\hat{G}_N^d$ of refinement $N = 32$ and dimensions $d \in \{6, 10\}$. For Algorithm 4.3, we additionally consider the sparsity $|\operatorname{supp}\hat{p}| = 10\,000$. The tests for each method and set of parameters were repeated 10 times. We present the results in Table 4.3. The "total runtime" was measured without the time required for sampling the multivariate trigonometric polynomials p_I. We observe that the total runtimes when using Algorithm 4.3 are dramatically smaller by about two orders of magnitude compared to Algorithm 4.2. The reason for this behavior is that in Algorithm 4.3 only one reconstructing rank-1 lattice $\Lambda(\boldsymbol{z}, M, \tilde{I})$ for the index set of detected frequencies $\tilde{I} := I^{(1,\ldots,t)}$, $|I^{(1,\ldots,t)}| \leq s$, is searched for in the additional step 2f in each dimension increment step $t \in \{2, \ldots, d\}$, whereas an additional reconstructing rank-1 lattice for the index set of

frequency candidates $I^{(1,\dots,t-1)} \times I^{(t)}$ is searched for in step 2b of Algorithm 4.2. This is apparent from the runtimes required for the rank-1 lattice constructions in column "time lattice search" in Table 4.3. □

			time lattice search (in s)			total runtime (in s)		
method	d	$\lvert\operatorname{supp}\hat{p}\rvert$	min	max	avg	min	max	avg
Algorithm 4.2	6	1 000	191	247	215	193	249	217
Algorithm 4.3	6	1 000	0.3	0.4	0.4	2.0	2.6	2.2
Algorithm 4.2	10	1 000	608	746	662	612	751	667
Algorithm 4.3	10	1 000	0.6	0.8	0.7	3.8	4.9	4.4
Algorithm 4.3	6	10 000	63	215	133	168	324	231
Algorithm 4.3	10	10 000	137	359	263	430	652	566

Table 4.3: Runtimes for random sparse multivariate trigonometric polynomial p_I using Algorithm 4.2 and 4.3.

In all our examples, the frequency detections succeeded and the Fourier coefficients $\hat{p}_{\boldsymbol{k}}$ were reconstructed exactly up to a small error caused by the used IEEE 754 double precision arithmetic. Algorithm 4.2 and 4.3 worked very well for the reconstruction of sparse high-dimensional trigonometric polynomials p_I.

4.1.6.2 Random sparse trigonometric polynomial with complex Gaussian noise

Next, we test the robustness of our method from Section 4.1.2 to noisy samples. We construct random multivariate trigonometric polynomials p_I with frequencies supported within the d-dimensional full grids $\hat{G}_N^d \subset \mathbb{Z}^d$ of refinement $N \in \mathbb{N}$ and dimension $d \in \mathbb{N}$. In doing so, we randomly choose $|\operatorname{supp}\hat{p}|$ many frequencies $\boldsymbol{k} \in \hat{G}_N^d$ and we set the corresponding Fourier coefficients $\hat{p}_{\boldsymbol{k}} := \mathrm{e}^{2\pi\mathrm{i}\varphi_{\boldsymbol{k}}} \in \mathbb{C}$, $|\hat{p}_{\boldsymbol{k}}| = 1$, $\boldsymbol{k} \in I = \operatorname{supp}\hat{p}$, where the angles $\varphi_{\boldsymbol{k}} \in [0,1)$ are chosen uniformly at random. For the reconstruction of multivariate trigonometric polynomials p_I, we only assume $\operatorname{supp}\hat{p} \subset \Gamma := \hat{G}_N^d$. We perturb the samples $p_I(\boldsymbol{x}_j)$ taken at nodes $\boldsymbol{x}_j \in \mathbb{T}^d$, $j = 0,\dots,M-1$, of the multivariate trigonometric polynomial p_I by additive complex white Gaussian noise $\eta_j \in \mathbb{C}$ with zero mean and standard deviation σ, i.e., we have measurements $f(\boldsymbol{x}_j) = p_I(\boldsymbol{x}_j) + \eta_j$. Then, we may approximately compute the signal-to-noise ratio (SNR) in our case by

$$\mathrm{SNR} \approx \frac{\sum_{j=0}^{M-1} |p_I(\boldsymbol{x}_j)|^2/M}{\sum_{j=0}^{M-1} |\eta_j|^2/M} \approx \frac{\sum_{\boldsymbol{k}\in\operatorname{supp}\hat{p}} |\hat{p}_{\boldsymbol{k}}|^2}{\sigma^2} = \frac{|\operatorname{supp}\hat{p}|}{\sigma^2}.$$

Correspondingly, we choose $\sigma := \sqrt{|\operatorname{supp}\hat{p}|}/\sqrt{\mathrm{SNR}}$ for a targeted SNR value. For our numerical tests in MATLAB, we generate the noise by $\eta_j := \sigma/\sqrt{2}$ `* (randn + 1i*randn)`, $j = 0,\dots,M-1$. The SNR is often measured using the logarithmic decibel scale (dB), where $\mathrm{SNR}_{\mathrm{dB}} = 10\log_{10}\mathrm{SNR}$ and $\mathrm{SNR} = 10^{\mathrm{SNR}_{\mathrm{dB}}/10}$, i.e., a linear $\mathrm{SNR} = 10^8$ corresponds to a logarithmic $\mathrm{SNR}_{\mathrm{dB}} = 80\mathrm{dB}$ and $\mathrm{SNR} = 1$ corresponds to $\mathrm{SNR}_{\mathrm{dB}} = 0\mathrm{dB}$.

Example 4.5. ([PV16, Example 3.15], *reconstruction of random sparse trigonometric polynomials using Algorithm 4.3, where the samples are perturbed by additive complex Gaussian noise*). We choose the dimension $d := 10$, the refinement $N := 32$ and the sparsity

$\mathrm{SNR}_{\mathrm{dB}}$	noise σ	#detect. iter. r	#samples	min #freq. correct	success rate (all freq. correct)	rel. ℓ_2-error
80	3.2e-03	1	22 216 155	998	0.995	4.5e-02
70	1.0e-02	1	23 004 475	998	0.986	4.5e-02
60	3.2e-02	1	22 381 905	998	0.974	5.5e-02
50	1.0e-01	1	22 533 615	996	0.893	7.1e-02
40	3.2e-01	1	22 434 295	994	0.722	8.4e-02
30	1.0e+00	1	22 662 055	988	0.319	1.2e-01
20	3.2e+00	1	22 646 975	979	0.032	1.5e-01
50	1.0e-01	2	49 597 275	1 000	1.000	7.5e-05
40	3.2e-01	2	55 243 565	998	0.998	4.5e-02
30	1.0e+00	2	41 881 645	998	0.994	5.5e-02
20	3.2e+00	2	42 064 815	996	0.933	7.7e-02
10	1.0e+01	2	41 512 185	990	0.465	1.1e-01
0	3.2e+01	2	43 322 695	942	0.000	2.5e-01
40	3.2e-01	3	61 300 655	1 000	1.000	2.3e-04
30	1.0e+00	3	61 847 825	1 000	1.000	7.1e-04
20	3.2e+00	3	61 477 195	998	0.998	4.5e-02
10	1.0e+01	3	60 542 365	996	0.936	6.4e-02
0	3.2e+01	3	61 832 225	984	0.015	1.4e-01
20	3.2e+00	4	82 104 165	1 000	1.000	2.4e-03
10	1.0e+01	4	80 312 115	998	0.997	4.5e-02
0	3.2e+01	4	81 618 355	994	0.442	9.1e-02
20	3.2e+00	5	101 459 605	1 000	1.000	2.3e-03
10	1.0e+01	5	99 610 745	1 000	1.000	7.3e-03
0	3.2e+01	5	98 090 005	997	0.869	7.4e-02

Table 4.4: ([PV16, Table 3.18]). Results for random sparse multivariate trigonometric polynomials p_I with sparsity $|\operatorname{supp}\hat{p}| = 1\,000$ perturbed by additive white Gaussian noise, when using reconstructing rank-1 lattices $\Lambda(\boldsymbol{z}, M, \tilde{I})$ and Algorithm 4.3.

$|\operatorname{supp}\hat{p}| = 1\,000$. We apply Algorithm 4.3 and we set the search domain $\Gamma := \hat{G}_{32}^{10}$, the sparsity parameter $s := 1\,000$ as well as the threshold parameter $\theta := 10^{-12}$. The algorithm is run setting the number of detection iterations to $r := 1, 2, 3, 4, 5$ and using the SNR values $\mathrm{SNR}_{\mathrm{dB}} := 80, 70, \ldots, 10, 0$ (which corresponds to $\mathrm{SNR} = 10^8, 10^7, \ldots, 10, 1$). For each of these 45 test settings, Algorithm 4.3 is repeatedly run 1 000 times. In each of the total 45 000 test runs, new random frequencies $\boldsymbol{k}$ and Fourier coefficients $\hat{p}_{\boldsymbol{k}}$ are drawn. A selection of the test results is presented in Table 4.4. The total number of samples for each of the 1 000 repetitions was computed and the maximum of these numbers for each test setting can be found in the column "#samples". In the column "min #freq. correct", the minimal number of correctly detected frequencies $|I^{(1,\ldots,10)} \cap \operatorname{supp}\hat{p}|$ for the 1 000 repetitions is shown, where $\operatorname{supp}\hat{p}$ denotes the set of true (input) frequencies of a trigonometric polynomial p_I and $I^{(1,\ldots,10)}$ the frequencies returned by the detection algorithm. The column "success rate (all freq. correct)" represents the relative number of the 1 000 repetitions where all frequencies were successfully detected, $I^{(1,\ldots,10)} = \operatorname{supp}\hat{p}$. Moreover, the relative ℓ_2-error $\|(\tilde{\hat{p}}_{\boldsymbol{k}})_{\boldsymbol{k}\in I} - (\hat{p}_{\boldsymbol{k}})_{\boldsymbol{k}\in I}\|_2 / \|(\hat{p}_{\boldsymbol{k}})_{\boldsymbol{k}\in I}\|_2$ of the computed Fourier coefficients $(\tilde{\hat{p}}_{\boldsymbol{k}})_{\boldsymbol{k}\in I^{(1,\ldots,10)}}$ was determined for each repetition, where

$I := \operatorname{supp} \hat{p} \cup I^{(1,\dots,10)}$ and $\tilde{\hat{p}}_{\boldsymbol{k}} := 0$ for $\boldsymbol{k} \in I \setminus I^{(1,\dots,10)}$, and the column "rel. ℓ_2-error" contains the maximal value of the 1 000 repetitions. For test settings with larger SNR values, which are not shown in Table 4.4, all frequencies in all 1 000 repetitions where correctly detected, i.e., the column "min #freq. correct"=1 000 and "success rate"=1.000. In general, we observe that for decreasing SNR values, the minimal numbers of correctly detected frequencies and the success rates decrease. When using $r = 1$ test iterations, there were always some (of the 1 000 test runs), where one or two frequencies were incorrect. However, in all test runs of all test settings, more than 77 percent of the frequencies were correctly detected, even for the case $\mathrm{SNR}_{\mathrm{dB}} = 0$ ($\mathrm{SNR} = 1$) where the signal level may approximately correspond to the noise level. When we increased the number of detection iterations r, the SNR level at which all frequencies in all of the 1 000 test runs were correctly detected also decreased. For instance for $r = 5$ detection iterations, the success rate was at 100 percent including the case $\mathrm{SNR}_{\mathrm{dB}} = \mathrm{SNR} = 10$. However, we require about 5 times of the samples for $r = 5$ detection iterations compared to the test settings with $r = 1$ detection iteration. □

4.1.6.3 Symmetric weighted hyperbolic cross

Next, we reconstruct multivariate trigonometric polynomials p_I with frequencies supported on weighted hyperbolic crosses $I = I_N^{d,0,\boldsymbol{\gamma}}$, where we only assume that the search domain Γ is the d-dimensional full grid $\hat{G}_N^d$ of refinement N.

Example 4.6. ([PV16, Example 3.7], *reconstruction of hyperbolic cross trigonometric polynomials using Algorithm 4.2 and 4.3*). All tests are repeated 10 times with different randomly chosen Fourier coefficients $\hat{p}_{\boldsymbol{k}} \in [-1,1) + [-1,1)\mathrm{i}$, $|\hat{p}_{\boldsymbol{k}}| \geq 10^{-6}$, $\boldsymbol{k} \in I$, for weighted hyperbolic cross frequency index sets $I = I_N^{d,0,\boldsymbol{\gamma}}$. We set the number of detection iterations $r := 1$ and the threshold parameter $\theta := 10^{-12}$. Moreover, we set the sparsity parameter $s := |\Gamma|$, i.e., we do not truncate the frequency index sets of detected frequencies $I^{(1,\dots,t)}$, $t \in \{2,\dots,d\}$. The considered refinements N, dimensions d and weight parameters $\boldsymbol{\gamma}$ are shown in Table 4.5. We apply Algorithm 4.2 and 4.3 on these test cases. In all tests, all the frequencies were successfully detected, $I^{(1,\dots,d)} = I_N^{d,0,\boldsymbol{\gamma}}$, and the Fourier coefficients $(\hat{p}_{\boldsymbol{k}})_{\boldsymbol{k} \in I_N^{d,0,\boldsymbol{\gamma}}}$ were computed correctly up to small numerical errors caused by the used IEEE 754 double precision arithmetic. We depict the results for Algorithm 4.3 in Table 4.5, where the columns have the same meaning as in Example 4.2. When using Algorithm 4.2, we obtain almost identical results with about 5 to 10 percent smaller maximal rank-1 lattice sizes "max M" and total number of samples "#samples". □

4.1.6.4 Tensor-product function

Next, we apply our method from Section 4.1.2 to a multivariate periodic function $f\colon \mathbb{T}^d \to \mathbb{C}$, which is not sparse in frequency domain. In doing so, we consider the function $f\colon \mathbb{T}^{10} \to \mathbb{R}$,

$$f((x_1,\dots,x_{10})^\top) := \prod_{t\in\{1,3,8\}} N_2(x_t) + \prod_{t\in\{2,5,6,10\}} N_4(x_t) + \prod_{t\in\{4,7,9\}} N_6(x_t), \tag{4.7}$$

where $N_m : \mathbb{T} \to \mathbb{R}$ is the B-Spline of order $m \in \mathbb{N}$,

$$N_m(x) := C_m \sum_{k\in\mathbb{Z}} \cos(\pi k)\ \operatorname{sinc}\left(\frac{\pi}{m}k\right)^m \mathrm{e}^{2\pi \mathrm{i} k x},$$

$$\operatorname{sinc}(y) := \begin{cases} \sin(y)/y & \text{for } y \neq 0, \\ 1 & \text{for } y = 0, \end{cases}$$

N	d	γ_2	$\lvert I_N^{d,0,\boldsymbol{\gamma}}\rvert$	max cand.	max M	#samples	rel. ℓ_2-error
32	6	0.80	11 593	173 397	990 990	1745 779	2.1e-16
32	8	0.80	15 477	197 081	1 338 974	4 360 512	5.0e-16
32	10	0.80	16 871	197 081	1 430 231	6 961 062	5.5e-16
16	10	0.87	22 953	200 541	1 358 148	5 032 864	6.3e-16
16	15	0.87	25 963	200 541	1 358 148	10 175 387	7.3e-16
16	20	0.87	26 185	200 541	1 358 148	12 687 242	7.6e-16
32	10	0.84	40 387	531 145	5 337 879	23 712 165	3.4e-16
32	15	0.84	44 201	531 145	5 337 879	41 732 585	2.6e-16
32	20	0.84	44 433	531 145	5 337 879	49 777 589	2.7e-16

Table 4.5: ([PV16, Table 3.8]). Results for trigonometric polynomials with frequencies supported on symmetric weighted hyperbolic cross $I_N^{d,0,\boldsymbol{\gamma}}$ with weights $\boldsymbol{\gamma} = (1, \gamma_2, \gamma_2^2, \ldots, \gamma_2^{d-1})^\top$ using reconstructing rank-1 lattices $\Lambda(\boldsymbol{z}, M, \tilde{I})$ and Algorithm 4.3 with search domain $\Gamma = \hat{G}_N^d$.

and $C_m > 0$ is a constant such that $\|N_m|L_2(\mathbb{T})\| = 1$. We remark that the factor $\cos(\pi k)$ simply causes a shift by $1/2$ and consequently N_m has its maximum at $x = 1/2$. We approximate the function f by multivariate trigonometric polynomials p_I.

First, we compute reference results with Algorithm 2.4 using rank-1 lattice sampling.

Example 4.7. ([PV16, Example 3.12], *s-sparse approximation using Algorithm 2.4*). In this example, we compute reference results which we compare with the dimension-incremental method from this chapter in a later example. For this, we have to choose frequency index sets I which contain the (approximately) largest Fourier coefficients $\hat{f}_{\boldsymbol{k}}$ of the test function f. Due to the tensor product structure of our test function f as defined in (4.7), we use hyperbolic cross index sets $I = I_N^{10,0,\mathbf{1}} := \{\boldsymbol{k} \in \mathbb{Z}^d \colon \prod_{t=1}^{10} \max(1, |k_t|) \leq N\}$, of refinement $N = 4, 8, 16$, and the corresponding reconstructing rank-1 lattices $\Lambda(\boldsymbol{z}, M, I_N^{10,0,\mathbf{1}})$ from Table 2.5. We sample the function f at the rank-1 lattice nodes $\boldsymbol{x}_j$ and compute all approximated Fourier coefficients $\hat{f}_{\boldsymbol{k}}^{\Lambda}$, $\boldsymbol{k} \in I_N^{10,0,\mathbf{1}}$. Then, we use sparsity $s = 1000, 2000, 3000, 4000$ many of the largest of these approximated Fourier coefficients $\hat{f}_{\boldsymbol{k}}^{\Lambda}$ and obtain the approximated Fourier partial sums $S_I^{\Lambda} f$ of the function f. We compute the relative $L_2(\mathbb{T}^{10})$ sampling errors $\|f - S_I^{\Lambda} f|L_2(\mathbb{T}^{10})\| / \|f|L_2(\mathbb{T}^{10})\|$ and the results are shown in Table 4.6. We observe that the relative $L_2(\mathbb{T}^{10})$ sampling errors do not decrease further when we use sparsity $s = 3000$ instead of $s = 2000$ for the considered refinement $N = 4, 8, 16$. The reason for this is that the number of non-zero Fourier coefficients $\hat{f}_{\boldsymbol{k}} \neq 0$ is small and the sampling error $f - S_I^{\Lambda} f$ is limited by the truncation error $f - S_I f$. Moreover, the number of used samples is already larger than 2 billion for refinement $N = 16$. □

Next, we determine a frequency index set $I = I^{(1,\ldots,10)} \subset \Gamma$ and compute approximated Fourier coefficients $\tilde{\hat{p}}_{\boldsymbol{k}}$, $\boldsymbol{k} \in I$, from sampling values of f using Algorithm 4.2, where the search space Γ is chosen as the 10-dimensional full grid $\hat{G}_N^{10}$ of refinement N. For numerical results with Algorithm 4.3, we refer to [PV16, Section 3.3]. We expect the frequency index set I to "consist of" three manifolds, a three-dimensional hyperbolic cross like structure in the dimensions $1, 3, 8$, a four-dimensional hyperbolic cross like structure in the dimensions $2, 5, 6, 10$ and a three-dimensional hyperbolic cross like structure in the dimensions $4, 7, 9$. Furthermore, the cardinality $|I|$ should be $\mathcal{O}(N \log^3 N)$ and the largest rank-1 lattice of size $M = \mathcal{O}(N^3 \log^2 N)$.

N	sparsity	$\lvert I_N^{10,0,\mathbf{1}}\rvert$	M = #samples	rel. L_2-error
4	1 000	2 421 009	30 780 958	3.8e-02
4	2 000	2 421 009	30 780 958	3.8e-02
8	1 000	10 819 089	194 144 634	1.4e-02
8	2 000	10 819 089	194 144 634	1.1e-02
8	3 000	10 819 089	194 144 634	1.1e-02
16	1 000	45 548 649	2 040 484 044	1.2e-02
16	2 000	45 548 649	2 040 484 044	4.3e-03
16	3 000	45 548 649	2 040 484 044	3.6e-03
16	4 000	45 548 649	2 040 484 044	3.6e-03

Table 4.6: ([PV16, Table 3.14]). Relative $L_2(\mathbb{T}^{10})$ sampling errors for function $f\colon \mathbb{T}^{10} \to \mathbb{R}$ from (4.7) for Algorithm 2.4 when only considering frequencies $\boldsymbol{k}$ within the hyperbolic cross $\Gamma = I_N^{10,0,\mathbf{1}}$.

All tests were run 10 times and the relative $L_2(\mathbb{T}^{10})$ approximation error

$$\|f - \tilde{S}_I f | L_2(\mathbb{T}^{10})\| / \|f | L_2(\mathbb{T}^{10})\| = \sqrt{\|f | L_2(\mathbb{T}^{10})\|^2 - \sum_{\boldsymbol{k}\in I} |\hat{f}_{\boldsymbol{k}}|^2 + \sum_{\boldsymbol{k}\in I} |\tilde{\hat{p}}_{\boldsymbol{k}} - \hat{f}_{\boldsymbol{k}}|^2} / \|f | L_2(\mathbb{T}^{10})\|$$

is computed, where the approximated Fourier partial sum $\tilde{S}_I f := \sum_{\boldsymbol{k}\in I} \tilde{\hat{p}}_{\boldsymbol{k}}\, \mathrm{e}^{2\pi \mathrm{i} \boldsymbol{k}\cdot \circ}$.

Example 4.8. (See also [PV16, Example 3.13], *approximation of a function using Algorithm 4.2 and 4.3 with minor modifications*). We describe minor modifications to Algorithm 4.2 and 4.3 to handle functions with infinitely many non-zero Fourier coefficients $\hat{f}_{\boldsymbol{k}} \neq 0$ better. For the truncation of the one-dimensional index sets $I^{(t)}$ of frequency candidates for component t, $t \in \{1, \ldots, d\}$, the relative threshold parameter $\theta :=$"threshold"/10 is used, whereas $\theta :=$"threshold" is used for all other truncations. We apply this modified version of Algorithm 4.2 on our test function f from (4.7). We choose the search domain $\Gamma = \hat{G}_{64}^{10}$ as the full 10-dimensional grid of refinement $N = 64$, which consists of $|\Gamma| = |\hat{G}_{64}^{10}| \approx 1.276 \cdot 10^{21}$ frequency candidates. We set the number of detection iterations $r := 10$. Moreover, the sparsity parameter $s \in \mathbb{N}$ is set to $|\Gamma|$, i.e., we do not additionally truncate the frequency index sets $I^{(1,\ldots,t)}$ in Algorithm 4.2. The results for "threshold" values $\in \{10^{-2}, 10^{-3}, \ldots, 10^{-6}\}$ are shown in Table 4.7. We observe that the numbers of used frequencies $|I|$ and the numbers of used samples "#samples" are distinctly lower for similar $L_2(\mathbb{T}^{10})$ approximation errors compared with the results of rank-1 lattice sampling in Table 4.6. We successfully determined about 7 400 approximated Fourier coefficients $\tilde{\hat{f}}_{\boldsymbol{k}}$ of out about $1.276 \cdot 10^{21}$ possible ones using about 132 million samples of the function f and we achieve a relative $L_2(\mathbb{T}^{10})$ approximation error which is about one order of magnitude lower than using rank-1 lattice sampling as in Example 4.7 with about 2 billion samples. Additionally, we apply the modified version of Algorithm 4.3 and the results are shown in Table 4.8. We observe that the obtained $L_2(\mathbb{T}^{10})$ approximation errors and total numbers of samples are similar. □

Until now, we have only assumed that the search domain Γ is a large 10-dimensional full grid $\hat{G}_N^{10}$. If we restrict the search domain Γ to a hyperbolic cross $I_N^{10,0,\mathbf{1}}$, we can reduce the numbers of required samples distinctly.

N	threshold	$\lvert I\rvert$	max cand.	max M	#samples	rel. L_2-error
64	1.0e-02	493	3 885	19 201	327 689	1.3e-01
64	1.0e-03	1 109	25 039	191 307	2 551 143	1.1e-02
64	1.0e-04	3 009	135 321	966 241	17 198 228	2.0e-03
64	1.0e-05	7 435	285 735	10 633 082	132 285 922	4.8e-04
64	1.0e-06	20 721	1 187 379	104 739 006	949 519 196	4.1e-04

Table 4.7: Results for approximation of function $f\colon \mathbb{T}^{10} \to \mathbb{R}$ from (4.7) using Algorithm 4.2 when considering frequencies $\boldsymbol{k}$ within $\Gamma = \hat{G}_N^{10}$. "#samples" means worst case number of function evaluations for 1 test run (out of the 10 runs).

N	threshold	$\lvert I\rvert$	max cand.	max M	#samples	rel. L^2-error
64	1.0e-02	493	3 885	21 047	338 630	6.8e-02
64	1.0e-03	1 113	24 893	224 589	3 079 656	1.1e-02
64	1.0e-04	3 013	127 839	1 119 994	17 437 584	2.0e-03
64	1.0e-05	7 405	290 895	10 409 782	155 282 274	4.8e-04
64	1.0e-06	20 637	1 178 955	98 868 166	980 232 256	4.1e-04

Table 4.8: Results for approximation of function $f\colon \mathbb{T}^{10} \to \mathbb{R}$ from (4.7) using Algorithm 4.3 when considering frequencies $\boldsymbol{k}$ within $\Gamma = \hat{G}_N^{10}$. "#samples" means worst case number of function evaluations for 1 test run (out of the 10 runs).

Example 4.9. (See also [PV16, Example 3.14], *approximation of a function using Algorithm 4.2 with minor modifications and restricting the search domain* $\Gamma = I_N^{d,0,\mathbf{1}}$). We apply Algorithm 4.2 with the minor modifications described in Example 4.8 on the test function f from (4.7). As search domain Γ, we use the symmetric hyperbolic cross frequency index set $I_N^{10,0,\mathbf{1}}$ of refinement $N := 64$. The used parameters and obtained results are presented in Table 4.9. We observe that the number of used samples is distinctly lower for comparable numbers $|I|$ of used approximated Fourier coefficients $\hat{\tilde{f}}_{\boldsymbol{k}}$ and comparable relative $L_2(\mathbb{T}^d)$ approximation errors compared to the results in Table 4.7. For instance for "threshold"$= 10^{-5}$, we only require about 22 million samples to obtain about 6 900 approximated Fourier coefficients $\hat{\tilde{f}}_{\boldsymbol{k}}$ yielding a relative $L_2(\mathbb{T}^d)$ approximation error of $5.1 \cdot 10^{-4}$ compared to about 132 million samples to obtain about 7 400 approximated Fourier coefficients $\hat{\tilde{f}}_{\boldsymbol{k}}$ yielding a relative $L_2(\mathbb{T}^d)$ approximation error of $4.8 \cdot 10^{-4}$. □

N	threshold	$\lvert I_N^{10,0,\mathbf{1}}\rvert$	$\lvert I\rvert$	max cand.	max M	#samples	rel. L_2-error
64	1.0e-02	696 036 321	493	3 613	17 222	316 144	6.5e-02
64	1.0e-03	696 036 321	1 111	10 407	99 815	1 653 252	1.1e-02
64	1.0e-04	696 036 321	3 009	27 567	598 638	7 794 193	1.7e-03
64	1.0e-05	696 036 321	6 925	46 435	2 465 161	22 479 540	5.1e-04
64	1.0e-06	696 036 321	14 179	67 497	5 062 313	49 241 549	4.2e-04

Table 4.9: Results for function $f\colon \mathbb{T}^{10} \to \mathbb{R}$ from (4.7) for Algorithm 4.2 when only considering frequencies $\boldsymbol{k}$ within $\Gamma = I_N^{10,0,\mathbf{1}}$. "#samples" means worst case number of function evaluations for 1 test run (out of the 10 runs).

As we have seen in the numerical examples of Section 4.1.6, we can easily apply the methods from Section 4.1.2 for the exact reconstruction of multivariate trigonometric polynomials p_I from samples along reconstructing rank-1 lattices $\Lambda(\boldsymbol{z}, M, \tilde{I})$ when the frequency index set $I \subset \mathbb{Z}^d$ is unknown and only a (possibly very large) superset $\Gamma \supset I$ is known. These methods were also applied to the approximation of a 10-dimensional periodic function f by an approximated Fourier partial sum with its largest approximated Fourier coefficients $\tilde{\hat{f}}_{\boldsymbol{k}}$.

In the next section, we transfer these results from the periodic case to the non-periodic case using the approach from Chapter 3.

4.2 Non-periodic case — rank-1 Chebyshev lattice sampling

Next, we adapt our dimension-incremental reconstruction method from Section 4.1 for the reconstruction of multivariate algebraic polynomials in Chebyshev form a_I from samples along rank-1 Chebyshev lattices $\mathrm{CL}(\boldsymbol{z}, M)$. In the non-periodic case, we proceed analogously to the periodic case. In principle, we replace one-dimensional FFTs by DCTs, rank-1 lattice sampling by rank-1 Chebyshev lattice sampling and Algorithm 2.1 by Algorithm 3.2. In Section 4.2.1, we describe the changes in detail and obtain Algorithms 4.4 and 4.5 as non-periodic versions of the periodic dimension-incremental reconstruction methods from Section 4.1. In Section 4.2.2, we present numerical results which demonstrate the effectiveness and possibilities of the proposed non-periodic dimension-incremental reconstruction method for the exact reconstruction of sparse multivariate algebraic polynomials in Chebyshev form a_I and the approximation of a 9-dimensional test function $f\colon [-1,1]^9 \to \mathbb{R}$.

4.2.1 Method

As mentioned above, we are going to adapt the dimension-incremental projection method from Algorithm 4.1 in Section 4.1.1 for the non-periodic case. In detail, we modify the steps of the dimension-incremental reconstruction Algorithm 4.2 to be able to reconstruct multivariate algebraic polynomials in Chebyshev form a_I from samples along reconstructing rank-1 Chebyshev lattices $\mathrm{CL}(\boldsymbol{z}, M, \tilde{I})$. This yields Algorithm 4.4. In the following, we describe the adaption step-by-step.

Analogously to applying a one-dimensional FFT for the computation of one-dimensional projected Fourier coefficients for the t-th component (4.2) in step 1 and 2a in Algorithm 4.2, we apply a one-dimensional DCT-I in Algorithm 4.4. In detail, we choose values $x'_1, \ldots, x'_{t-1}, x'_{t+1}, \ldots, x'_d \in [-1,1]$ uniformly at random and compute the one-dimensional projected Chebyshev coefficients for the t-th component

$$\begin{aligned}\tilde{\hat{a}}_{t,k_t} &:= \frac{2(\varepsilon_{k_t}^{L_t})^2}{L_t} \sum_{l=0}^{L_t} (\varepsilon_l^{L_t})^2 \, a_I\left(\left(x'_1, \ldots, x'_{t-1}, \cos(\tfrac{l}{L_t}\pi), x'_{t+1}, \ldots, x'_d\right)^\top\right) \cos\left(\frac{lk_t}{L_t}\pi\right) \qquad (4.8)\\ &= \frac{2(\varepsilon_{k_t}^{L_t})^2}{L_t} \sum_{l=0}^{L_t} (\varepsilon_l^{L_t})^2 \sum_{\boldsymbol{h} \in \operatorname{supp} \hat{a}} \hat{a}_{\boldsymbol{h}} \left(\prod_{\substack{\tau=1\\ \tau\neq t}}^{d} \cos(h_\tau \arccos(x'_\tau))\right)\\ &\qquad \cdot \cos\left(h_t \arccos(\cos(\tfrac{l}{L_t}\pi))\right) \cos\left(\frac{lk_t}{L_t}\pi\right), \; k_t \in \mathcal{P}_t(\Gamma).\end{aligned}$$

Algorithm 4.4 Dimension-incremental reconstruction of a multivariate algebraic polynomial in Chebyshev form a_I from samples for unknown frequency index set $I \subset \Gamma \subset \mathbb{N}_0^d$.

Input:	$\Gamma \subset \mathbb{N}_0^d$	search domain for frequencies $\boldsymbol{k}$, superset for $\operatorname{supp} \hat{a}$
	$a_I(\circ)$	multivariate algebraic polynomial in Chebyshev form a_I as black box (function handle)
	$\theta \in (0,1)$	relative threshold
	$s \in \mathbb{N}$	sparsity parameter
	$r \in \mathbb{N}$	number of detection iterations

(step 1)
Set $L_1 := \max(\mathcal{P}_1(\Gamma))$, $I^{(1)} := \emptyset$, $z_1 := 1$.
for $i := 1, \dots, r$ **do**
Choose $x'_\tau \in [-1,1]$ uniformly at random for $\tau = 2, \dots, d$.
Compute $\tilde{\hat{a}}_{1,k_1} := \frac{2(\varepsilon_{k_1}^{L_1})^2}{L_1} \sum_{l=0}^{L_1} (\varepsilon_l^{L_1})^2 \, a_I\left(\cos(\frac{l}{L_1}\pi), x'_2, \dots, x'_d\right) \cos\left(\frac{lk_1}{L_1}\pi\right)$, $k_1 \in \mathcal{P}_1(\Gamma)$, with 1d DCT-I.
$I^{(1)} := I^{(1)} \cup \{k_1 \in \mathcal{P}_1(\Gamma)\colon$ (up to) s-largest values $|\tilde{\hat{a}}_{1,k_1}| \geq \theta \cdot \max_{\tilde{k}_1 \in \mathcal{P}_1(\Gamma)} |\tilde{\hat{a}}_{1,\tilde{k}_1}|\}$
end for i
Determine $S_1 := \min\left\{m \in \mathbb{N}\colon |\{k_1 \bmod m\colon k_1 \in \mathcal{M}(I^{(1)})\}| = |\mathcal{M}(I^{(1)})|\right\}$.
Set $M_1 := S_1$.

(step 2) **for** $t := 2, \dots, d$ **do**
(step 2a) Set $L_t := \max(\mathcal{P}_t(\Gamma))$, $I^{(t)} := \emptyset$.
for $i := 1, \dots, r$ **do**
Choose $x'_\tau \in [-1,1]$ uniformly at random for $\tau = 1, \dots, t-1, t+1, \dots, d$.
Compute $\tilde{\hat{a}}_{t,k_t} := \frac{2(\varepsilon_{k_t}^{L_t})^2}{L_t} \sum_{l=0}^{L_t} (\varepsilon_l^{L_t})^2 \, a_I\left(x'_1, \dots, x'_{t-1}, \cos(\frac{l}{L_t}\pi), x'_{t+1}, \dots, x'_d\right) \cos\left(\frac{lk_t}{L_t}\pi\right)$, $k_t \in \mathcal{P}_t(\Gamma)$, using 1d DCT-I.
Set $I^{(t)} := I^{(t)} \cup \{k_t \in \mathcal{P}_t(\Gamma)\colon$ (up to) s-largest values $|\tilde{\hat{a}}_{t,k_t}| \geq \theta \cdot \max_{\tilde{k}_t \in \mathcal{P}_t(\Gamma)} |\tilde{\hat{a}}_{t,\tilde{k}_t}|\}$.
end for i
(step 2b) Set $\tilde{r} := \begin{cases} r & \text{for } t < d, \\ 1 & \text{for } t = d. \end{cases}$
Determine $S_t := \min\left\{m \in \mathbb{N}\colon |\{k_t \bmod m\colon k_t \in \mathcal{M}(I^{(t)})\}| = |\mathcal{M}(I^{(t)})|\right\}$.
Build reconstructing rank-1 Chebyshev lattice $\mathrm{CL}(\boldsymbol{z}, M_t, \tilde{I})$ for $\tilde{I} := (I^{(1,\dots,t-1)} \times I^{(t)}) \cap \mathcal{P}_{(1,\dots,t)}(\Gamma)$ via reconstructing rank-1 lattice $\Lambda(\boldsymbol{z}, 2M_t, \mathcal{M}(\tilde{I}))$, cf. Theorem 3.4 and Corollary 3.6:
Set initial $\hat{M}_t := 2 \cdot M_{t-1} \cdot S_t$, cf. Theorem 2.7.
Search for $z_t \in \{0, \dots, \hat{M}_t - 1\}$ such that property (2.27) is fulfilled for $\mathcal{M}(\tilde{I})$.
Reduce rank-1 lattice size $\hat{M}_t \in 2\mathbb{N}$ with reconstruction property (2.27) fulfilled.
Set size parameter $M_t := \hat{M}_t / 2$.
for $i := 1, \dots, \tilde{r}$ **do**
Choose $x'_\tau \in [-1,1]$ uniformly at random for $\tau = t+1, \dots, d$.
Set $\mathcal{X}^{(1,\dots,t)} := \{\boldsymbol{x}_j := (\cos(\frac{j}{M_t}\pi z_1), \dots, \cos(\frac{j}{M_t}\pi z_t), x'_{t+1}, \dots, x'_d)^\top\colon j = 0, \dots, M_t\}$.
(step 2c) Sample multivariate algebraic polynomial in Chebyshev form a_I at the nodes of the sampling set $\mathcal{X}^{(1,\dots,t)}$.

Algorithm 4.4 continued.

(step 2d)

Compute $\tilde{\hat{a}}_l := \sum_{j=0}^{M_t} (\varepsilon_j^{M_t})^2 \, a_I(\boldsymbol{x}_j) \cos\left(\frac{jl}{M_t}\pi\right)$, $l = 0, \ldots, M_t$, with 1d DCT-I.

Compute $\tilde{\hat{a}}_{(1,\ldots,t),\boldsymbol{k}} := \dfrac{2^d (\varepsilon_l^{M_t})^2}{M_t} \dfrac{\tilde{\hat{a}}_l}{|\{\boldsymbol{m} \in \mathcal{M}_\nu(\{1\}^t) \colon (\boldsymbol{m} \odot \boldsymbol{k}) \cdot \boldsymbol{z} \bmod M_t = l\}|}$, for $\boldsymbol{k} \in (I^{(1,\ldots,t-1)} \times I^{(t)}) \cap \mathcal{P}_{(1,\ldots,t)}(\Gamma)$ with $l := \boldsymbol{k} \cdot \boldsymbol{z} \bmod M_t$.

(step 2e)

absolute_threshold $:= \theta \cdot \max_{\tilde{\boldsymbol{k}} \in (I^{(1,\ldots,t-1)} \times I^{(t)}) \cap \mathcal{P}_{(1,\ldots,t)}(\Gamma)} |\tilde{\hat{a}}_{(1,\ldots,t),\tilde{\boldsymbol{k}}}|$.

Set $I^{(1,\ldots,t)} := I^{(1,\ldots,t)} \cup \{\boldsymbol{k} \in (I^{(1,\ldots,t-1)} \times I^{(t)}) \cap \mathcal{P}_{(1,\ldots,t)}(\Gamma) \colon$ (up to) s-largest values $|\tilde{\hat{a}}_{(1,\ldots,t),\boldsymbol{k}}| \geq$ absolute_threshold$\}$.

end for i

(additional step 2f)

If $t < d$, build (possibly) smaller reconstructing rank-1 Chebyshev lattice $\mathrm{CL}(\boldsymbol{z}, M_t, I^{(1,\ldots,t)})$ via reconstructing rank-1 lattice $\Lambda(\boldsymbol{z}, 2M_t, \mathcal{M}(I^{(1,\ldots,t)}))$ for $I^{(1,\ldots,t)}$:

Search for new $z_t \in \{0, \ldots, \hat{M}_t - 1\}$ where property (2.27) is fulfilled for $\mathcal{M}(I^{(1,\ldots,t)})$.

Reduce rank-1 lattice size $\hat{M}_t \in 2\mathbb{N}$ with reconstruction property (2.27) fulfilled.

Set size parameter $M_t := \hat{M}_t / 2$.

end for t

Output: $I^{(1,\ldots,d)} \subset \mathbb{N}_0^d$ — index set of detected frequencies

$\tilde{\hat{\boldsymbol{a}}} := \left(\tilde{\hat{a}}_{(1,\ldots,d),\boldsymbol{k}}\right)_{\boldsymbol{k} \in I^{(1,\ldots,d)}} \in \mathbb{R}^{|I^{(1,\ldots,d)}|}$ — corresponding Chebyshev coefficients

Using orthogonality relation (3.20), we continue

$$\begin{aligned}
\tilde{\hat{a}}_{t,k_t} &= \sum_{\boldsymbol{h} \in \operatorname{supp} \hat{a}} \hat{a}_{\boldsymbol{h}} \left(\prod_{\substack{\tau=1 \\ \tau \neq t}}^{d} T_{h_\tau}(x'_\tau) \right) \underbrace{\frac{2(\varepsilon_{k_t}^{L_t})^2}{L_t} \sum_{l=0}^{L_t} (\varepsilon_l^{L_t})^2 \cos\left(\frac{l h_t}{L_t}\pi\right) \cos\left(\frac{l k_t}{L_t}\pi\right)}_{\delta_{(h_t \bmod L_t), k_t}} \\
&= \sum_{\substack{\boldsymbol{h} \in \operatorname{supp} \hat{a} \\ h_t \bmod L_t = k_t}} \hat{a}_{\boldsymbol{h}} \, T_{(h_1,\ldots,h_{t-1},h_{t+1},\ldots,h_d)^\top}\left(\left(x'_1, \ldots, x'_{t-1}, x'_{t+1}, \ldots, x'_d\right)^\top\right) \text{ for } k_t \in \mathcal{P}_t(\Gamma).
\end{aligned} \tag{4.9}$$

Similar to the aliasing formula (4.6) from the periodic case, we may regard each coefficient $\tilde{\hat{a}}_{t,k_t}$ as the evaluation of a $(d-1)$-dimensional algebraic polynomial in Chebyshev form $\tilde{\hat{a}}_{t,k_t} := \tilde{\hat{a}}_{t,k_t}(\tilde{\boldsymbol{x}})$ at the node $\tilde{\boldsymbol{x}} := (x'_1, \ldots, x'_{t-1}, x'_{t+1}, \ldots, x'_d)^\top \in [-1,1]^{d-1}$.

Analogously to applying Algorithm 2.1 in step 2d of Algorithm 4.2 for the computation of t-dimensional projected Fourier coefficients for the first t components (4.4), we apply Algorithm 3.2 in step 2d of Algorithm 4.4 and compute t-dimensional projected Chebyshev coefficients for the first t components

$$\tilde{\hat{a}}_{(1,\ldots,t),\boldsymbol{k}} := \frac{2^d (\varepsilon_l^{M_t})^2}{M_t} \frac{\tilde{\hat{a}}_{\boldsymbol{k} \cdot \boldsymbol{z} \bmod M_t}}{|\{\boldsymbol{m} \in \mathcal{M}_\nu(\{1\}^t) \colon (\boldsymbol{m} \odot \boldsymbol{k}) \cdot \boldsymbol{z} \bmod M_t = \boldsymbol{k} \cdot \boldsymbol{z} \bmod M_t\}|}, \ \boldsymbol{k} \in \tilde{I}.$$

Here, the coefficients $\tilde{\hat{a}}_l := \sum_{j=0}^{M_t} (\varepsilon_j^{M_t})^2 \, a_I(\boldsymbol{x}_j) \cos\left(\frac{jl}{M_t}\pi\right)$, $l = 0, \ldots, M_t$, result from a one-dimensional DCT-I applied to samples of the multivariate algebraic polynomial a_I at the

nodes $\boldsymbol{x}_j := (x_{j,1}, \dots, x_{j,t}, x'_{t+1}, \dots, x'_d)^\top$, where $(x_{j,1}, \dots, x_{j,t})^\top$ are the nodes of a reconstructing rank-1 Chebyshev lattice $\mathrm{CL}(\boldsymbol{z}, M_t, \tilde{I})$ for $\tilde{I} := (I^{(1,\dots,t-1)} \times I^{(t)}) \cap \mathcal{P}_{(1,\dots,t)}(\Gamma)$ and $\nu \in \{1, \dots, d\}$.

Since we have

$$\begin{aligned}
\tilde{\hat{a}}_l &:= \sum_{j=0}^{M_t} (\varepsilon_j^{M_t})^2 \, a_I(\boldsymbol{x}_j) \cos\left(\frac{jl}{M_t}\pi\right) \\
&= \sum_{j=0}^{M_t} (\varepsilon_j^{M_t})^2 \sum_{\boldsymbol{h} \in \operatorname{supp} \hat{a}} \hat{a}_{\boldsymbol{h}} \left(\prod_{\tau=1}^{t} \cos(h_\tau \tfrac{j}{M_t} \pi z_\tau)\right) \left(\prod_{\tau=t+1}^{d} T_{h_\tau}(x'_\tau)\right) \cos\left(\frac{jl}{M_t}\pi\right) \\
&= \sum_{\boldsymbol{h} \in \operatorname{supp} \hat{a}} \hat{a}_{\boldsymbol{h}} \left(\prod_{\tau=t+1}^{d} T_{h_\tau}(x'_\tau)\right) \sum_{j=0}^{M_t} (\varepsilon_j^{M_t})^2 \left(\prod_{\tau=1}^{t} \cos(h_\tau \tfrac{j}{M_t} \pi z_\tau)\right) \cos\left(\frac{jl}{M_t}\pi\right) \\
&\overset{(3.32)}{=} \sum_{\boldsymbol{h} \in \operatorname{supp} \hat{a}} \hat{a}_{\boldsymbol{h}} \left(\prod_{\tau=t+1}^{d} T_{h_\tau}(x'_\tau)\right) \\
&\qquad \cdot \frac{M_t \, \left|\left\{\boldsymbol{m} \in \mathcal{M}_\nu(\{1\}^t) \colon \left(\boldsymbol{m} \odot (h_1, \dots, h_t)^\top\right) \cdot \boldsymbol{z} \bmod M_t = l\right\}\right|}{2^d \, (\varepsilon_l^{M_t})^2}
\end{aligned}$$

for $l = 0, \dots, M_t$, the aliasing formula

$$\begin{aligned}
\tilde{\hat{a}}_{(1,\dots,t),\boldsymbol{k}} &= \sum_{\boldsymbol{h} \in \operatorname{supp} \hat{a}} \hat{a}_{\boldsymbol{h}} \, T_{(h_{t+1},\dots,h_d)^\top}\left(\left(x'_{t+1}, \dots, x'_d\right)^\top\right) \\
&\qquad \cdot \frac{\left|\left\{\boldsymbol{m} \in \mathcal{M}_\nu(\{\mathbf{1}\}) \colon \left(\boldsymbol{m} \odot (h_1, \dots, h_t)^\top\right) \cdot \boldsymbol{z} \bmod M_t = \boldsymbol{k} \cdot \boldsymbol{z} \bmod M_t\right\}\right|}{\left|\left\{\boldsymbol{m} \in \mathcal{M}_\nu(\{\mathbf{1}\}) \colon (\boldsymbol{m} \odot \boldsymbol{k}) \cdot \boldsymbol{z} \bmod M_t = \boldsymbol{k} \cdot \boldsymbol{z} \bmod M_t\right\}\right|}
\end{aligned}$$

follows for $\boldsymbol{k} \in (I^{(1,\dots,t-1)} \times I^{(t)}) \cap \mathcal{P}_{(1,\dots,t)}(\Gamma)$, which corresponds to aliasing formula (3.31) with the additional term $T_{(h_{t+1},\dots,h_d)^\top}\left(\left(x'_{t+1}, \dots, x'_d\right)^\top\right)$ when setting $\boldsymbol{k'} := (h_1, \dots, h_t)^\top$. If the conditions $I^{(1,\dots,t-1)} = \mathcal{P}_{(1,\dots,t-1)}(\operatorname{supp} \hat{a})$ and $I^{(t)} = \mathcal{P}_t(\operatorname{supp} \hat{a})$ are fulfilled, this simplifies to

$$\tilde{\hat{a}}_{(1,\dots,t),\boldsymbol{k}} = \sum_{\substack{\boldsymbol{h} \in \operatorname{supp} \hat{a} \\ (h_1,\dots,h_t)^\top = \boldsymbol{k}}} \hat{a}_{\boldsymbol{h}} \, T_{(h_{t+1},\dots,h_d)^\top}\left(\left(x'_{t+1}, \dots, x'_d\right)^\top\right).$$

For building the reconstructing rank-1 Chebyshev lattices $\mathrm{CL}(\boldsymbol{z}, M, \tilde{I})$ in Algorithm 4.4, we use Theorem 3.4 and Algorithm 2.2, i.e., we build a reconstructing rank-1 lattice $\Lambda(\boldsymbol{z}, 2M, \mathcal{M}(\tilde{I}))$ for the extended symmetric index set $\mathcal{M}(\tilde{I})$. Alternatively, one may use the direct CBC construction method from Algorithm 3.3 for building a reconstructing rank-1 Chebyshev lattices $\mathrm{CL}(\boldsymbol{z}, M, \tilde{I})$. This approach is described as Algorithm 4.5.

Remark 4.10. As discussed in Section 4.1.5 for the periodic case, we may use a deterministic version of Algorithm 4.4 or 4.5, when all Chebyshev coefficients $\hat{a}_{\boldsymbol{k}}$, $\boldsymbol{k} \in I$, of a multivariate algebraic polynomial in Chebyshev form a_I are either non-negative or non-positive. We obtain this deterministic dimension-incremental reconstruction method by setting the number of detection iterations $r := 1$ and choosing the nodes $x'_\tau := 1$ in the steps 1, 2a and 2b. □

Algorithm 4.5 Dimension-incremental reconstruction of a multivariate algebraic polynomial in Chebyshev form a_I from samples for unknown frequency index set $I \subset \Gamma \subset \mathbb{N}_0^d$ with direct search for reconstructing rank-1 Chebyshev lattices $\mathrm{CL}(\boldsymbol{z}, M_t, \tilde{I})$.

Modifications of Algorithm 4.4:

$\vdots$

Set $S_1 := \min\big\{m \in \mathbb{N}\colon |\{k_1 \bmod (2m)\colon k_1 \in \mathcal{M}(I^{(1)})\}| = |\mathcal{M}(I^{(1)})|\big\}$. Set $M_1 := S_1$.

(step 2) **for** $t := 2, \ldots, d$ **do**

$\vdots$

(step 2b) Set $\tilde{r} := \begin{cases} r & \text{for } t < d, \\ 1 & \text{for } t = d. \end{cases}$

Set $S_t := \min\big\{m \in \mathbb{N}\colon |\{k_t \bmod (2m)\colon k_t \in \mathcal{M}(I^{(t)})\}| = |\mathcal{M}(I^{(t)})|\big\}$. Set $I^{(1,\ldots,t)} := \emptyset$.

Build reconstructing rank-1 Chebyshev lattice $\mathrm{CL}(\boldsymbol{z}, M_t, \tilde{I})$

for $\tilde{I} := (I^{(1,\ldots,t-1)} \times I^{(t)}) \cap \mathcal{P}_{(1,\ldots,t)}(\Gamma)$, $\boldsymbol{z} \in \mathbb{N}_0^t$:

Set initial $M_t := 4 \cdot M_{t-1} \cdot S_t$.

Search for $z_t \in \{0, \ldots, M_t\}$ such that reconstruction property (3.22) is fulfilled, increase size parameter M_t if necessary.

Reduce size parameter M_t with reconstruction property (3.22) fulfilled.

for $i := 1, \ldots, \tilde{r}$ **do**

$\vdots$

(additional step 2f)

If $t < d$, build (possibly) smaller reconstructing rank-1 Chebyshev lattice $\mathrm{CL}(\boldsymbol{z}, M_t, I^{(1,\ldots,t)})$ for $I^{(1,\ldots,t)}$:

Search for new $z_t \in \{0, \ldots, M_t - 1\}$ where reconstruction property (3.23) is fulfilled.

Reduce size parameter M_t with reconstruction property (3.23) fulfilled.

end for t

$\vdots$

4.2.2 Numerical results

An implementation of Algorithm 4.4 and 4.5 as well as MATLAB code for performing tests are available online [Vol16a]. The numerical tests of this section were run on a computer with Intel Xeon E7-4880 CPU in MATLAB R2015b using IEEE 754 double precision arithmetic.

We set the refinement $n := 32$ and construct random multivariate algebraic polynomials in Chebyshev form a_I with frequencies supported within the d-dimensional full grid $\hat{G}_{32}^d$. This means, we choose $|\operatorname{supp} \hat{a}|$ many frequencies uniformly at random from $\hat{G}_{32}^d \subset \mathbb{N}_0^d$ and corresponding Chebyshev coefficients $\hat{a}_{\boldsymbol{k}} \in [-1, 1]$, $|\hat{a}_{\boldsymbol{k}}| \geq 10^{-6}$, $\boldsymbol{k} \in I = \operatorname{supp} \hat{a}$. For the reconstruction of the multivariate algebraic polynomials in Chebyshev form a_I, we choose the search domain $\Gamma := \hat{G}_{32}^d$. We do not truncate the frequency index sets of detected frequencies $I^{(1,\dots,t)}$, $t \in \{2, \dots, d\}$, i.e., we set the sparsity parameter $s := |\Gamma|$ in Algorithm 4.4 and 4.5. As discussed in Section 4.1.6.1, we may alternatively set the sparsity parameter $s := |\operatorname{supp} \hat{a}|$ and obtain the same results. Moreover, we set the number of detection iterations $r := 1$. All tests are repeated 10 times with newly chosen frequencies $\boldsymbol{k}$ and Chebyshev coefficients $\hat{a}_{\boldsymbol{k}}$. First, we test Algorithm 4.4.

Example 4.11. (*Sampling along reconstructing rank-1 Chebyshev lattices constructed via reconstructing rank-1 lattices using Algorithm 4.4*). We set the threshold parameter $\theta := 10^{-12}$. For dimensions $d \in \{3, 4, \dots, 8\}$ and sparsity $|\operatorname{supp} \hat{a}| = 100$, we apply Algorithm 4.4. In each test, all frequencies were successfully detected, $I^{(1,\dots,d)} = \operatorname{supp} \hat{a}$. The used parameters and results are presented in Table 4.10. The column "max cand." shows the maximal number $\max_{t=2,\dots,d} |I^{(1,\dots,t-1)} \times I^{(t)}|$ of frequency candidates of all 10 repetitions and "max M" the overall maximal size parameter used. Furthermore, the total number of samples for each repetition was computed and the maximum of these numbers for the 10 repetitions can be found in the column "#samples". The relative ℓ_2-error $\|(\tilde{\hat{a}}_{\boldsymbol{k}})_{\boldsymbol{k} \in I} - (\hat{a}_{\boldsymbol{k}})_{\boldsymbol{k} \in I}\|_2 / \|(\hat{a}_{\boldsymbol{k}})_{\boldsymbol{k} \in I}\|_2$ of the computed Chebyshev coefficients $(\tilde{\hat{a}}_{\boldsymbol{k}})_{\boldsymbol{k} \in I^{(1,\dots,d)}}$ was determined for each repetition, where $I := \operatorname{supp} \hat{a} \cup I^{(1,\dots,d)}$ and $\tilde{\hat{a}}_{\boldsymbol{k}} := 0$ for $\boldsymbol{k} \in I \setminus I^{(1,\dots,d)}$, and the column "rel. ℓ_2-error" contains the maximal value of the 10 repetitions. In all tests, the relative ℓ_2-error is smaller than $7.2 \cdot 10^{-16}$ and is caused by the utilized IEEE 754 double precision arithmetic. The numbers of used samples "#samples" increase for increasing dimensions d. For dimensions $d \geq 4$, Algorithm 4.4 required less samples than there are possible frequencies in the search domain $\Gamma = \hat{G}_{32}^d$. In the case $d = 8$, only about 1/19 000 of the samples are required compared to the utilization of a tensor Chebyshev grid and a d-dimensional DCT. □

n	d	$\lvert\operatorname{supp} \hat{a}\rvert$	$\lvert\Gamma\rvert = \lvert\hat{G}_n^d\rvert$	max cand.	max M	#samples	rel. ℓ_2-error
32	3	100	35 937	3 168	115 119	117 336	6.76e-16
32	4	100	1 185 921	3 300	452 247	540 429	4.72e-16
32	5	100	39 135 393	3 300	1 502 107	2 002 277	6.64e-16
32	6	100	1 291 467 969	3 300	4 619 745	6 409 969	4.73e-16
32	7	100	42 618 442 977	3 300	15 620 108	21 770 762	6.80e-16
32	8	100	1.406e+12	3 300	54 705 235	74 598 246	7.16e-16

Table 4.10: Results for random sparse multivariate algebraic polynomials in Chebyshev form a_I, $I \subset \hat{G}_{32}^d$, using reconstructing rank-1 Chebyshev lattices $\mathrm{CL}(\boldsymbol{z}, M, \tilde{I})$ built via reconstructing rank-1 lattices $\Lambda(\boldsymbol{z}, 2M, \mathcal{M}(\tilde{I}))$ and Algorithm 4.4 when considering frequencies within the search domain $\Gamma = \hat{G}_{32}^d$.

We can reduce the numbers of required samples distinctly if we directly search for re-

constructing rank-1 Chebyshev lattices $\mathrm{CL}(\boldsymbol{z}, M, \tilde{I})$ via a CBC construction method as the following example demonstrates.

Example 4.12. (*Sampling along reconstructing rank-1 Chebyshev lattices using Algorithm 4.5*). Again, we set the threshold parameter $\theta := 10^{-12}$. For dimensions $d \in \{3, 4, \ldots, 9, 10, 15\}$ and sparsity $|\operatorname{supp} \hat{a}| = 100$, we apply Algorithm 4.5. In each test, all frequencies were successfully detected, $I^{(1,\ldots,d)} = \operatorname{supp} \hat{a}$. The used parameters and results are presented in Table 4.11 and the columns have the same meaning as in Example 4.11. In all tests, the relative ℓ_2-error is smaller than $1.2 \cdot 10^{-15}$ and is caused by the utilized IEEE 754 double precision arithmetic. The numbers of used samples "#samples" increase for increasing dimensions d. For dimensions $d \geq 4$, Algorithm 4.5 required less samples than there are possible frequencies in the search domain $\Gamma = \hat{G}_{32}^d$. The numbers of used samples "#samples" are dramatically lower than for the results of Algorithm 4.4 in Table 4.10. We remark that we observed a similar behavior in Example 3.20. For instance, in the case $d = 6$, only about $1/1600$ of the samples are required compared to the usage of a full-tensor Chebyshev grid and $1/8$ of the samples compared to Algorithm 4.4. Similar to Example 4.2, the maximal number of frequency candidates "max cand." is 3 300 and the maximal size parameter "max M" is between about about 220 000 and 460 000 in Table 4.11 for dimensions $d \geq 4$. This is caused by the relatively large numbers of possible frequencies $|\Gamma| = |\hat{G}_{32}^d| = 33^d$ and the small sparsity $|\operatorname{supp} \hat{a}| = 100$, which cause that all 100 non-zero Chebyshev coefficients $\hat{a}_{\boldsymbol{k}} \neq 0$ are already detected in dimension-incremental steps $t \leq 4$ and higher components z_τ, $5 \leq \tau < t$, (except the highest component z_t) of the generating vector $\boldsymbol{z} := (z_1, \ldots, z_t)^\top$ of the reconstructing rank-1 Chebyshev lattices $\Lambda(\boldsymbol{z}, M, \tilde{I})$ to be zero in most cases. Consequently, the numbers of used samples "#samples" increase by about 220 000 to 460 000 per additional dimension. We remark that we may have found all non-zero Chebyshev coefficients $\hat{a}_{\boldsymbol{k}} \neq 0$ in a dimension-incremental step $t \leq 4$, but we still need to continue with remaining dimension-incremental steps $t \geq 5$ in order to determine the higher components k_t, $t \in \{5, \ldots, d\}$, of the frequencies $\boldsymbol{k} \in \operatorname{supp} \hat{a}$.
Additionally, we apply Algorithm 4.5 for dimensions $d \in \{3, 4, \ldots, 8\}$ and higher sparsity $|\operatorname{supp} \hat{a}| = 1\,000$. In each test, all frequencies were successfully detected, $I^{(1,\ldots,d)} = \operatorname{supp} \hat{a}$. We observe for dimensions $d = 3, 4$ that we require more samples than we have possible frequencies in the search domain $\Gamma = \hat{G}_n^d$. For dimension $d = 5$, Algorithm 4.5 yields less samples and for dimensions $d \geq 6$ distinctly less samples than there are frequencies in the search domain $\Gamma = \hat{G}_n^d$. For dimension $d = 6$, we have seven test runs where all 1 000 non-zero Chebyshev coefficients $\hat{a}_{\boldsymbol{k}} \neq 0$ are already found in dimension increment step $t = 5$ yielding size parameters M of about 21 million and numbers of used samples of about 50 million. However, we still have three test runs, where all 1 000 non-zero Chebyshev coefficients $\hat{a}_{\boldsymbol{k}} \neq 0$ are found not until the last dimension increment step $t = 6$ yielding the maximal size parameter "max M" of about 45 million and the numbers of used samples "#samples" of about 74 million in Table 4.11. In dimensions $d \geq 7$, all 1 000 non-zero Chebyshev coefficients $\hat{a}_{\boldsymbol{k}} \neq 0$ are already found in dimension increment steps $t \leq 6$ for all ten test runs. Analogously to the behavior for sparsity $|\operatorname{supp} \hat{a}| = 100$, we expect the numbers of used samples "#samples" to increase by about 20 to 45 million per additional dimension for dimensions $d \geq 6$. □

Remark 4.13. The large difference in the maximal size parameters "max M" and the numbers of used samples when utilizing Algorithm 4.4 and 4.5 is caused by the following issue, which corresponds to the one observed and discussed in Example 3.20. In the additional step 2f of Algorithm 4.4, the reconstructing rank-1 Chebyshev lattice $\mathrm{CL}(\boldsymbol{z}, M_t, I^{(1,\ldots,t)})$ for the frequency index set $I^{(1,\ldots,t)}$ is built via a reconstructing rank-1

n	d	$\lvert\operatorname{supp}\hat{a}\rvert$	$\lvert\Gamma\rvert = \lvert\hat{G}_n^d\rvert$	max cand.	max M	#samples	rel. ℓ_2-error
32	3	100	35 937	3 168	81 642	83 826	4.92e-16
32	4	100	1 185 921	3 300	221 260	295 118	7.17e-16
32	5	100	39 135 393	3 300	234 655	537 964	5.45e-16
32	6	100	1 291 467 969	3 300	241 391	785 671	1.17e-15
32	7	100	42 618 442 977	3 300	456 119	1 614 677	9.37e-16
32	8	100	1.406e+12	3 300	392 251	1 828 842	6.43e-16
32	9	100	4.641e+13	3 300	386 490	2 195 804	7.30e-16
32	10	100	1.532e+15	3 300	414 611	2 710 158	1.78e-15
32	15	100	5.994e+22	3 300	380 502	4 439 451	4.20e-14
32	3	1 000	35 937	15 873	73 856	75 080	5.53e-16
32	4	1 000	1 185 921	32 604	6 490 663	6 630 162	6.74e-16
32	5	1 000	39 135 393	33 000	27 021 660	34 116 319	7.44e-16
32	6	1 000	1 291 467 969	33 000	44 791 174	74 215 472	1.48e-15
32	7	1 000	42 618 442 977	33 000	42 401 071	113 804 504	8.03e-16
32	8	1 000	1.406e+12	33 000	43 799 177	161 481 230	1.49e-15

Table 4.11: Results for random sparse multivariate algebraic polynomials in Chebyshev form a_I, $I \subset \hat{G}_{32}^d$, using reconstructing rank-1 Chebyshev lattices $\mathrm{CL}(\boldsymbol{z}, M, \tilde{I})$ and Algorithm 4.5 when considering frequencies within the search domain $\Gamma = \hat{G}_{32}^d$.

lattice $\Lambda(\boldsymbol{z}, 2M_t, \mathcal{M}(I^{(1,\dots,t)}))$ for the extended symmetric index set $\mathcal{M}(I^{(1,\dots,t)})$ for each $t = 2, \dots, d-1$, and we have for the size parameter $M_t \geq |\mathcal{M}(I^{(1,\dots,t)})|/2$ since reconstruction property (2.27) needs to be fulfilled with $I := \mathcal{M}(I^{(1,\dots,t)})$. Even if the cardinality $|I^{(1,\dots,t)}|$ of the frequency index sets $|I^{(1,\dots,t)}|$ does not increase for dimension increment steps $t \geq t'$, the extended symmetric index sets $\mathcal{M}(I^{(1,\dots,t)})$ still grow in general and may contain up to $2^t \,|\operatorname{supp}\hat{a}|$ many frequencies. On the contrary, the reconstructing rank-1 Chebyshev lattice $\mathrm{CL}(\boldsymbol{z}, M_t, I^{(1,\dots,t)})$ built in the additional step 2f of Algorithm 4.5 is obtained by testing the reconstruction property (3.22) with $I := I^{(1,\dots,t)}$, which requires for the size parameter $M_t \geq |I^{(1,\dots,t)}|$ and consequently has a possibly much lower bound. □

Next, we apply our method for the non-periodic dimension-incremental reconstruction to a multivariate function $f\colon [-1,1]^d \to \mathbb{C}$, which is not sparse in frequency domain. In doing so, we consider the 9-dimensional test function $f\colon [-1,1]^9 \to \mathbb{R}$,

$$f\left((x_1,\dots,x_9)^\top\right) := \prod_{t\in\{1,3,4,7\}} B_2(x_t) + \prod_{t\in\{2,5,6,8,9\}} B_4(x_t), \tag{4.10}$$

where B_2 is the shifted, scaled and dilated B-Spline of order 2 as defined in (3.43) with Chebyshev coefficients as given in (3.44) and $B_4\colon \mathbb{R} \to \mathbb{R}$ is the shifted, scaled and dilated B-Spline of order 4,

$$B_4(x) := \begin{cases} (2x+15)^4/6144 & \text{for } -15/2 \leq x < -11/2, \\ -\frac{5645}{1536} - \frac{205}{48}x - \frac{95}{64}x^2 - \frac{5}{24}x^3 - \frac{1}{96}x^4 & \text{for } -11/2 \leq x < -7/2, \\ \frac{715}{3072} + \frac{25}{128}x + \frac{55}{128}x^2 + \frac{5}{32}x^3 + \frac{1}{64}x^4 & \text{for } -7/2 \leq x < -3/2, \\ \frac{155}{1536} - \frac{5}{32}x + \frac{5}{64}x^2 - \frac{1}{96}x^4 & \text{for } -3/2 \leq x < 1/2, \\ (2x-5)^4/6144 & \text{for } 1/2 \leq x < 5/2, \\ 0 & \text{otherwise,} \end{cases}$$

with Chebyshev coefficients $\hat{B}_{4,k}$, $k \in \mathbb{N}_0$, given by

$$\hat{B}_{4,k} = \begin{cases} \dfrac{(900\sqrt{3}k(-9+k^2)(-1)^k/3) + 90(152-75k^2+3k^4)\sin(k\pi/3)}{768k(-16+k^2)(-9+k^2)(-4+k^2)(-1+k^2)\pi} & \text{for } k \geq 5, \\ -7/9216 - 93\sqrt{3}/(114688\pi) & \text{for } k = 4, \\ 5(-70+(27\sqrt{3})/\pi)/32256 & \text{for } k = 3, \\ 181/4608 - 39\sqrt{3}/(4096\pi) & \text{for } k = 2, \\ -(95/576) + 33\sqrt{3}/(2048\pi) & \text{for } k = 1, \\ 2603/18432 - 75\sqrt{3}/(8192\pi) & \text{for } k = 0. \end{cases}$$

We approximate the test function f from (4.10) by multivariate algebraic polynomials in Chebyshev form a_I. For this, we determine a frequency index set $I = I^{(1,\ldots,9)} \subset \Gamma := \hat{G}_n^9 \subset \mathbb{N}_0^d$ and compute approximated Chebyshev coefficients $\tilde{\hat{a}}_{\boldsymbol{k}}$, $\boldsymbol{k} \in I$, from sampling values of f using Algorithm 4.4 and 4.5. We expect the frequency index set I to "consist of" two manifolds, a four-dimensional hyperbolic cross like structure in the dimensions $1, 3, 4, 7$, and a five-dimensional hyperbolic cross like structure in the dimensions $2, 5, 6, 8, 9$. All tests were run 10 times and the relative $L_{2,w}([-1,1]^9)$ approximation errors

$$\frac{\|f - \tilde{S}_I f | L_{2,w}([-1,1]^9)\|}{\|f|L_{2,w}([-1,1]^9)\|} = \frac{\sqrt{\|f|L_{2,w}([-1,1]^9)\|^2 - \sum_{\boldsymbol{k}\in I} |\hat{f}_{\boldsymbol{k}}|^2 \frac{\pi^9}{2^{|\boldsymbol{k}|_0}} + \sum_{\boldsymbol{k}\in I} |\tilde{\hat{a}}_{\boldsymbol{k}} - \hat{f}_{\boldsymbol{k}}|^2 \frac{\pi^9}{2^{|\boldsymbol{k}|_0}}}}{\|f|L_{2,w}([-1,1]^9)\|}$$

are computed, where the approximated Chebyshev partial sum $\tilde{S}_I f := \sum_{\boldsymbol{k}\in I} \tilde{\hat{a}}_{\boldsymbol{k}} T_{\boldsymbol{k}}(\circ)$.

Example 4.14. (*Approximation of a function using Algorithm 4.4 and 4.5 with minor modifications*). We describe minor modifications to Algorithm 4.4 and 4.5 to handle functions with infinitely many non-zero Chebyshev coefficients $\hat{f}_{\boldsymbol{k}} \neq 0$ better. For the truncation of the one-dimensional index sets $I^{(t)}$ of frequency candidates for component t, $t \in \{1, \ldots, d\}$, the relative threshold parameter $\theta :=$"threshold"/100 is used. Otherwise, the relative threshold parameter $\theta :=$"threshold" is used. We apply this modified version of Algorithm 4.4 and 4.5 on our test function f from (4.10). We choose the search domain $\Gamma = \hat{G}_{32}^9 \subset \mathbb{N}_0^d$ as the full 9-dimensional grid of refinement $n = 32$, which consists of $|\Gamma| = |\hat{G}_{32}^9| \approx 4.641 \cdot 10^{13}$ frequency candidates. We set the number of detection iterations $r := 5$. Moreover, the sparsity parameter $s \in \mathbb{N}$ is set to $|\Gamma|$, i.e., we do not additionally truncate the frequency index sets $I^{(1,\ldots,t)}$. The results for "threshold" values $\in \{10^{-2}, 10^{-3}, 10^{-4}, 10^{-5}\}$ are shown in Table 4.12 for Algorithm 4.4. For instance for "threshold"$=10^{-4}$, we obtain a maximal relative $L_{2,w}([-1,1]^9)$ approximation error of $4.0 \cdot 10^{-4}$ using 1 434 Chebyshev coefficients $\tilde{\hat{a}}_{\boldsymbol{k}}$ and about 8 million samples were taken. We require lower numbers of samples when using Algorithm 4.5, between about 10 and 50 percent less in the considered cases, and we obtain similar errors. The corresponding results are given in Table 4.13. We may reduce the numbers of samples further by restricting the search domain Γ, e.g. to a hyperbolic cross $I_{\mathrm{a},32}^{10,0}$, and still obtain comparable maximal relative $L_{2,w}([-1,1]^9)$ approximation errors, see Table 4.14 for Algorithm 4.5. For instance for "threshold"$=10^{-4}$, we only required about half the number of samples. □

As we have seen in the numerical examples of this section, we can easily apply the methods from Section 4.2.1 for the exact reconstruction of multivariate algebraic polynomials in Chebyshev form a_I from samples along reconstructing rank-1 Chebyshev lattices $\Lambda(\boldsymbol{z}, M, \tilde{I})$ when the frequency index set $I \subset \mathbb{Z}^d$ is unknown and only a (possibly very large) superset $\Gamma \supset I$ is known. These methods were also successfully applied to the approximation of a 9-dimensional non-periodic test function f.

n	threshold	$\lvert I\rvert$	max cand.	max M	#samples	rel. $L_{2,w}$-error
32	1.0e-02	145	1 080	12 896	145 331	1.5e-02
32	1.0e-03	493	4 920	176 604	1 439 846	6.1e-03
32	1.0e-04	1 434	16 497	1 852 309	7 957 720	4.0e-04
32	1.0e-05	3 483	65 780	14 307 770	53 735 836	1.0e-04

Table 4.12: Results for approximation of function $f\colon [-1,1]^9 \to \mathbb{R}$ from (4.10) using Algorithm 4.4 when considering frequencies $\boldsymbol{k}$ within $\Gamma = \hat{G}_n^9$. "#samples" means worst case number of function evaluations for 1 test run (out of the 10 runs).

n	threshold	$\lvert I\rvert$	max cand.	max M	#samples	rel. $L_{2,w}$-error
32	1.0e-02	149	1 116	14 391	135 216	1.7e-02
32	1.0e-03	485	4 710	95 522	898 310	6.7e-03
32	1.0e-04	1 431	18 200	753 373	5 662 360	4.7e-04
32	1.0e-05	3 465	63 800	5 629 313	27 009 528	9.4e-05

Table 4.13: Results for approximation of function $f\colon [-1,1]^9 \to \mathbb{R}$ from (4.10) using Algorithm 4.5 when considering frequencies $\boldsymbol{k}$ within $\Gamma = \hat{G}_n^9$. "#samples" means worst case number of function evaluations for 1 test run (out of the 10 runs).

n	threshold	$\lvert I\rvert$	max cand.	max M	#samples	rel. $L_{2,w}$-error
32	1.0e-02	147	851	9 080	99 181	1.7e-02
32	1.0e-03	486	2 979	101 449	586 317	5.6e-03
32	1.0e-04	1 438	6 038	506 963	2 802 539	4.1e-04
32	1.0e-05	2 784	9 656	2 368 670	8 340 927	1.3e-04

Table 4.14: Results for approximation of function $f\colon [-1,1]^9 \to \mathbb{R}$ from (4.10) using Algorithm 4.5 when only considering frequencies $\boldsymbol{k}$ within $\Gamma = I_{\mathrm{a},n}^{9,0}$. "#samples" means worst case number of function evaluations for 1 test run (out of the 10 runs).

Chapter 5

Conclusion

In this work, the approximation of multivariate smooth periodic functions $f\colon \mathbb{T}^d \to \mathbb{C}$ by multivariate trigonometric polynomials was considered. The smoothness of functions f was characterized via the decay of their Fourier coefficients $\hat{f}_{\boldsymbol{k}} := \int_{\mathbb{T}^d} f(\boldsymbol{x})\, \mathrm{e}^{-2\pi \mathrm{i} \boldsymbol{k}\cdot\boldsymbol{x}}\, \mathrm{d}\boldsymbol{x}$, $\boldsymbol{k} \in \mathbb{Z}^d$.

A fast method for the evaluation of multivariate trigonometric polynomials p_I with frequencies supported on arbitrary index sets $I \subset \mathbb{Z}^d$, $|I| < \infty$, at all nodes $\boldsymbol{x}_j$ of an arbitrary rank-1 lattice $\Lambda(\boldsymbol{z}, M)$ was recapitulated, which only uses a simple index transform and a single one-dimensional FFT. Moreover, reconstruction properties were repeated, which allow for the exact reconstruction from samples $p_I(\boldsymbol{x}_j)$ using only a single one-dimensional FFT and a simple index transform. Additionally, simple component-by-component (CBC) construction methods for obtaining such reconstructing rank-1 lattices $\Lambda(\boldsymbol{z}, M, I)$ were given.

The reconstruction method was successfully applied to multivariate smooth periodic functions f from subspaces of the Wiener algebra $\mathcal{A}(\mathbb{T}^d)$ and approximated Fourier coefficients $\hat{f}^{\Lambda}_{\boldsymbol{k}} := \frac{1}{M} \sum_{j=0}^{M-1} f(\boldsymbol{x}_j)\, \mathrm{e}^{-2\pi \mathrm{i} \boldsymbol{k}\cdot\boldsymbol{x}_j}$, $\boldsymbol{k} \in I$, were computed from samples $f(\boldsymbol{x}_j)$, yielding approximants $p_I = S^{\Lambda}_I f := \sum_{\boldsymbol{k}\in I} \hat{f}^{\Lambda}_{\boldsymbol{k}}\, \mathrm{e}^{2\pi \mathrm{i} \boldsymbol{k}\cdot\circ}$. The computations can be performed using only a single one-dimensional FFT and a simple index transform, which require $\mathcal{O}(M \log M + d\,|I|)$ arithmetic operations in total. For specific function classes and suitable frequency index sets I, an extensive theory for estimating the sampling errors $f - S^{\Lambda}_I f$ was developed. To this end, the sampling error $f - S^{\Lambda}_I f$ was split into the truncation error $f - S_I f$ and aliasing error $S_I f - S^{\Lambda}_I f$, where $S_I f := \sum_{\boldsymbol{k}\in I} \hat{f}_{\boldsymbol{k}}\, \mathrm{e}^{2\pi \mathrm{i} \boldsymbol{k}\cdot\circ}$ is the truncated Fourier series. With the help of suitable proof techniques, estimates for aliasing errors $S_I f - S^{\Lambda}_I f$ were shown and error rates were obtained which are comparable to the ones of corresponding truncation errors $f - S_I f$. Numerical tests for up to 25 dimensions confirmed the effectiveness and high performance of the proposed method.

Moreover, an approximate method for the fast evaluation of multivariate trigonometric polynomials p_I at perturbed rank-1 lattice nodes $\boldsymbol{y}_j$ was introduced, which is based on Taylor expansion and one-dimensional FFTs. When the nodes $\boldsymbol{y}_j$ are perturbed versions of the nodes $\boldsymbol{x}_j$ of a reconstructing rank-1 lattice $\Lambda(\boldsymbol{z}, M, I)$ and the perturbations are not too large, multivariate trigonometric polynomials p_I with frequencies supported on arbitrary known index sets $I \subset \mathbb{Z}^d$, $|I| < \infty$, can be approximately reconstructed in a fast way using an iterative method. This approach was also applied to the fast approximation of multivariate periodic functions $f \in \mathcal{A}(\mathbb{T}^d)$. The corresponding sampling errors are estimated by terms similar to those from the unperturbed case.

The method for the fast evaluation and reconstruction of multivariate trigonometric polynomials p_I as well as fast approximation of functions $f \in \mathcal{A}(\mathbb{T}^d)$ from samples along a re-

constructing rank-1 lattice $\Lambda(\boldsymbol{z}, M, I)$ was transferred to the non-periodic case. For many of the concepts and results from the periodic case, a non-periodic counterpart was developed. Multivariate algebraic polynomials in Chebyshev form $a_I(\boldsymbol{x}) := \sum_{\boldsymbol{k}\in I} \hat{a}_{\boldsymbol{k}}\, T_{\boldsymbol{k}}(\boldsymbol{x})$ were used as ansatz functions for the approximation of multivariate smooth non-periodic functions $f\colon [-1,1]^d \to \mathbb{R}$. Rank-1 Chebyshev lattices $\mathrm{CL}(\boldsymbol{z}, M)$, characterized by a generating vector $\boldsymbol{z} \in \mathbb{N}_0^d$ and size parameter $M \in \mathbb{N}_0$, were used as corresponding spatial discretizations. Multivariate algebraic polynomials in Chebyshev form a_I with frequencies supported on arbitrary index sets $I \subset \mathbb{N}_0^d$, $|I| < \infty$, can be evaluated in a fast and exact way at the corresponding nodes $\boldsymbol{x}_j := \cos(\frac{j}{M}\pi\boldsymbol{z})$, $j = 0, \ldots, M$, in $\mathcal{O}(M \log M + d\,|\mathcal{M}(I)|)$ arithmetic operations by using easy-to-compute index transforms and a single one-dimensional discrete cosine transform (DCT). Analogously to the reconstruction properties of reconstructing rank-1 lattices $\Lambda(\boldsymbol{z}, M, I)$ in the periodic case, similar reconstruction properties were derived in this work for the non-periodic case and the term reconstructing rank-1 Chebyshev lattice $\mathrm{CL}(\boldsymbol{z}, M, I)$ was introduced. The fast and exact reconstruction of all Chebyshev coefficients $\hat{a}_{\boldsymbol{k}}$, $\boldsymbol{k} \in I$, can be performed by applying a single one-dimensional DCT to the samples $a_I(\boldsymbol{x}_j)$ along a reconstructing rank-1 Chebyshev lattice $\mathrm{CL}(\boldsymbol{z}, M, I)$ followed by easy-to-compute index transforms. This reconstruction requires $\mathcal{O}(M \log M + d\,|\mathcal{M}(I)|)$ arithmetic operations in total. For determining reconstructing rank-1 Chebyshev lattices $\mathrm{CL}(\boldsymbol{z}, M, I)$, simple CBC construction approaches were presented.

The reconstruction method was successfully applied to the approximation of multivariate smooth non-periodic functions f from subspaces of the analogon of the Wiener algebra $\mathcal{A}([-1,1]^d)$ and an error theory analogously to the periodic case was developed, where functions f are characterized by the decay of their Chebyshev coefficients $\hat{f}_{\boldsymbol{k}} := 2^{|\boldsymbol{k}|_0}/\pi^d \int_{[-1,1]^d} f(\boldsymbol{x})\; T_{\boldsymbol{k}}(\boldsymbol{x})/(\prod_{s=1}^d \sqrt{1-x_s^2})\,\mathrm{d}\boldsymbol{x}$, $\boldsymbol{k} \in \mathbb{N}_0^d$. Numerical tests for up to 25 dimensions were successfully performed.

An additional important contribution of this work is the development of methods for the exact reconstruction of high-dimensional sparse trigonometric polynomials p_I and high-dimensional sparse algebraic polynomials in Chebyshev form a_I with unknown frequency index sets I from samples. The proposed methods can also be applied in determining unknown frequency locations I of the approximately largest Fourier or Chebyshev coefficients $\hat{f}_{\boldsymbol{k}}$ of a function f, which may be non-sparse in frequency domain. A suitable frequency index set I is searched for in a dimension-incremental way with the help of projections parallel to the coordinate axes and samples along reconstructing rank-1 (Chebyshev) lattices. Components of frequency locations belonging to non-zero or the approximately largest Fourier or Chebyshev coefficients $\hat{f}_{\boldsymbol{k}}$ are efficiently determined within a search domain Γ, which may be extremely large, for instance a d-dimensional full grid. In each dimension increment step $t = 1, \ldots, d$, the t-th component of the unknown frequency locations is detected, i.e., one component at a time starting with the first one. For high-dimensional sparse polynomials and functions with arbitrary Fourier or Chebyshev coefficients $\hat{f}_{\boldsymbol{k}}$, a randomized approach was proposed, which performs repeated sampling in each dimension increment step t with different randomly chosen higher components $x_{j,t+1}, \ldots, x_{j,d}$ of the sampling nodes $\boldsymbol{x}_j$. Numerical tests performed for up to 30 dimensions confirmed high reliability for the exact reconstruction of high-dimensional sparse polynomials. For a 10-dimensional periodic and 9-dimensional non-periodic test function, the frequency locations I belonging to the approximately largest Fourier and Chebyshev coefficients $\hat{f}_{\boldsymbol{k}}$ were successfully determined, respectively. Moreover, the method was successfully applied to 10-dimensional sparse trigonometric polynomials p_I, where the samples were perturbed by noise. Additional requirements on the Fourier or Chebyshev coefficients $\hat{f}_{\boldsymbol{k}}$ even allow for a deterministic version of the dimension-incremental approach.

Bibliography

[AD96] C. Anderson and M. Dahleh. Rapid computation of the discrete Fourier transform. *SIAM J. Sci. Comput.*, 17:913–919, 1996. (Cited on page 29.)

[AGR16] A. Arnold, M. Giesbrecht, and D. S. Roche. Faster sparse multivariate polynomial interpolation of straight-line programs. *J. Symbolic Comput.*, 75:4–24, 2016. Special issue on the conference ISSAC 2014: Symbolic computation and computer algebra. (Cited on page 122.)

[AR14] A. Arnold and D. S. Roche. Multivariate sparse interpolation using randomized Kronecker substitutions. In *Proceedings of the 39th International Symposium on Symbolic and Algebraic Computation*, ISSAC '14, pages 35–42, New York, NY, USA, 2014. ACM. (Cited on page 122.)

[AS72] M. Abramowitz and I. A. Stegun, editors. *Handbook of Mathematical Functions*. National Bureau of Standards, Washington, DC, USA, 1972. (Cited on page 84.)

[BCD+06] L. Bos, M. Caliari, S. De Marchi, M. Vianello, and Y. Xu. Bivariate Lagrange interpolation at the Padua points: The generating curve approach. *J. Approx. Theory*, 143:15–25, 2006. Special Issue on Foundations of Computational Mathematics. (Cited on pages 85 and 99.)

[BD89] G. Baszenski and F.-J. Delvos. A discrete Fourier transform scheme for Boolean sums of trigonometric operators. In C. K. Chui, W. Schempp, and K. Zeller, editors, *Multivariate Approximation Theory IV*, ISNM 90, pages 15–24. Birkhäuser, Basel, 1989. (Cited on pages 10 and 18.)

[BDMV15] L. Bos, S. De Marchi, and M. Vianello. Polynomial approximation on Lissajous curves in the d-cube. preprint on webpage at `www.math.unipd.it/~demarchi/papers/TenProdLissa1`, 2015. (Cited on pages 11, 85, and 99.)

[BDMV16] L. Bos, S. De Marchi, and M. Vianello. Trivariate polynomial approximation on Lissajous curves. *IMA J. Numer. Anal.*, 2016. (Cited on pages 11, 85, and 99.)

[BDuSU16] G. Byrenheid, D. Dũng, W. Sickel, and T. Ullrich. Sampling on energy-norm based sparse grids for the optimal recovery of Sobolev type functions in H^γ. *J. Approx. Theory*, 207:207–231, 2016. (Cited on pages 22, 23, 27, and 28.)

[Bel61] R. E. Bellman. *Adaptive control processes — A guided tour*. Princeton University Press, Princeton, New Jersey, U.S.A., 1961. (Cited on pages 9 and 17.)

[BG99] H.-J. Bungartz and M. Griebel. A note on the complexity of solving Poisson's equation for spaces of bounded mixed derivatives. *J. Complexity*, 15:167–199, 1999. (Cited on page 18.)

[BG04] H.-J. Bungartz and M. Griebel. Sparse grids. *Acta Numer.*, 13:147–269, 2004. (Cited on page 18.)

[BHS92] D. Berthold, W. Hoppe, and B. Silbermann. A fast algorithm for solving the generalized airfoil equation. *J. Comput. Appl. Math.*, 43:185–219, 1992. (Cited on page 87.)

[Bjö96] Å. Björck. *Numerical Methods for Least Squares Problems.* SIAM, Philadelphia, PA, USA, 1996. (Cited on pages 41, 43, and 70.)

[BKUV16] G. Byrenheid, L. Kämmerer, T. Ullrich, and T. Volkmer. Tight error bounds for rank-1 lattice sampling in spaces of hybrid mixed smoothness. *Numer. Math.*, 2016. accepted, preprint arXiv:1510.08336 [math.NA]. (Cited on pages 11, 12, 22, 23, 28, 38, 44, 46, 51, 54, 57, 58, 59, and 68.)

[BNR00] V. Barthelmann, E. Novak, and K. Ritter. High dimensional polynomial interpolation on sparse grids. *Adv. Comput. Math.*, 12:273–288, 2000. (Cited on pages 84 and 90.)

[Boy00] J. P. Boyd. *Chebyshev and Fourier Spectral Methods.* Dover Press, New York, NY, USA, second edition, 2000. (Cited on page 84.)

[BT97] G. Baszenski and M. Tasche. Fast polynomial multiplication and convolution related to the discrete cosine transform. *Linear Algebra Appl.*, 252:1–25, 1997. (Cited on page 84.)

[Can06] E. J. Candès. Compressive sampling. In *International Congress of Mathematicians. Vol. III*, pages 1433–1452. Eur. Math. Soc., Zürich, 2006. (Cited on page 122.)

[CDMSV11] M. Caliari, S. De Marchi, A. Sommariva, and M. Vianello. Padua2DM: fast interpolation and cubature at the Padua points in Matlab/Octave. *Numer. Alg.*, 56:45–60, 2011. (Cited on page 85.)

[CDV08] M. Caliari, S. De Marchi, and M. Vianello. Bivariate Lagrange interpolation at the Padua points: Computational aspects. *J. Comput. Appl. Math.*, 221:284–292, 2008. Special Issue: Recent Progress in Spline and Wavelet Approximation. (Cited on pages 85 and 99.)

[CKN10] R. Cools, F. Y. Kuo, and D. Nuyens. Constructing lattice rules based on weighted degree of exactness and worst case error. *Computing*, 87:63–89, 2010. (Cited on pages 10, 11, and 21.)

[CKNS16] R. Cools, F. Y. Kuo, D. Nuyens, and G. Suryanarayana. Tent-transformed lattice rules for integration and approximation of multivariate non-periodic functions. *J. Complexity*, 36:166–181, 2016. (Cited on pages 88 and 100.)

[Cle55] C. W. Clenshaw. A note on the summation of Chebyshev series. *Math. Comput.*, 9:118–120, 1955. (Cited on page 85.)

[CLW70] J. Cooley, P. Lewis, and P. Welch. The fast Fourier transform algorithm: Programming considerations in the calculation of sine, cosine and Laplace transforms. *J. Sound Vibration*, 12:315–337, 1970. (Cited on page 84.)

[CLW16] A. Christlieb, D. Lawlor, and Y. Wang. A multiscale sub-linear time Fourier algorithm for noisy data. *Appl. Comput. Harmon. Anal.*, 40:553–574, 2016. (Cited on page 123.)

[CN04] R. Cools and D. Nuyens. Fast algorithms for component-by-component construction of rank-1 lattice rules in shift-invariant reproducing kernel Hilbert spaces. *Math. Comp.*, 75:903–920, 2004. (Cited on page 88.)

[CN08] R. Cools and D. Nuyens. A Belgian view on lattice rules. In A. Keller, S. Heinrich, and H. Niederreiter, editors, *Monte Carlo and Quasi-Monte Carlo Methods 2006*, pages 3–21. Springer Berlin Heidelberg, 2008. (Cited on pages 10, 19, and 21.)

[CP11] R. Cools and K. Poppe. Chebyshev lattices, a unifying framework for cubature with Chebyshev weight function. *BIT Numerical Mathematics*, 51:275–288, 2011. (Cited on pages 11, 83, 85, 88, and 99.)

[CsL08] A. Cuyt and W. shin Lee. A new algorithm for sparse interpolation of multivariate polynomials. *Theor. Comput. Sci.*, 409(2):180–185, 2008. (Cited on page 122.)

[CT05] E. J. Candès and T. Tao. Decoding by linear programming. *IEEE Trans. Inform. Theory*, 51:4203–4215, 2005. (Cited on page 122.)

[DE15] P. Dencker and W. Erb. Multivariate polynomial interpolation on Lissajous-Chebyshev nodes. *ArXiv e-prints*, 2015. arXiv:1511.04564 [math.NA]. (Cited on pages 85 and 99.)

[DHT14] T. A. Driscoll, N. Hale, and L. N. Trefethen. *Chebfun Guide*. Pafnuty Publications, 2014. `http://www.chebfun.org/docs/guide/`. (Cited on page 84.)

[DKS13] J. Dick, F. Y. Kuo, and I. H. Sloan. High-dimensional integration: The quasi-Monte Carlo way. *Acta Numer.*, 22:133–288, 2013. (Cited on pages 10, 11, 19, 33, and 86.)

[DL82] M. Deville and G. Labrosse. An algorithm for the evaluation of multidimensional (direct and inverse) discrete Chebyshev transforms. *J. Comput. Appl. Math.*, 8:293–304, 1982. (Cited on page 84.)

[DNP14] J. Dick, D. Nuyens, and F. Pillichshammer. Lattice rules for nonperiodic smooth integrands. *Numer. Math.*, 126:259–291, 2014. (Cited on pages 88 and 99.)

[Don06] D. L. Donoho. Compressed sensing. *IEEE Trans. Inform. Theory*, 52:1289–1306, 2006. (Cited on page 122.)

[DTU16] D. Dũng, V. N. Temlyakov, and T. Ullrich. Hyperbolic cross approximation. *ArXiv e-prints*, December 2016. arXiv:1601.03978 [math.NA]. (Cited on pages 9, 10, 17, 20, 21, 22, 23, 27, 28, and 57.)

[DuU13] D. Dũng and T. Ullrich. N-widths and ε-dimensions for high-dimensional approximations. *Found. Comput. Math.*, 13:965–1003, 2013. (Cited on pages 9 and 20.)

[FG93] H. G. Feichtinger and K. Gröchenig. Theory and practice of irregular sampling. In J. Benedetto and M. Frazier, editors, *Wavelets: Mathematics and Applications*, pages 305–363, CRC Press, 1993. (Cited on page 42.)

[FR13] S. Foucart and H. Rauhut. *A Mathematical Introduction to Compressive Sensing*. Applied and Numerical Harmonic Analysis. Birkhäuser/Springer, New York, 2013. (Cited on page 122.)

[GG03] T. Gerstner and M. Griebel. Dimension–adaptive tensor–product quadrature. *Computing*, 71:65–87, 2003. (Cited on pages 19 and 85.)

[GH07] M. Griebel and J. Hamaekers. Sparse grids for the Schrödinger equation. *M2AN Math. Model. Numer. Anal.*, 41:215–247, 2007. (Cited on page 22.)

[GH14] M. Griebel and J. Hamaekers. Fast discrete Fourier transform on generalized sparse grids. In J. Garcke and D. Pflüger, editors, *Sparse Grids and Applications - Munich 2012*, volume 97 of *Lect. Notes Comput. Sci. Eng.*, pages 75–107. Springer International Publishing, 2014. (Cited on pages 10, 18, 22, and 84.)

[GK00] M. Griebel and S. Knapek. Optimized tensor-product approximation spaces. *Constructive Approximation*, 16:525–540, 2000. (Cited on pages 22 and 37.)

[GK09] M. Griebel and S. Knapek. Optimized general sparse grid approximation spaces for operator equations. *Math. Comp.*, 78:2223–2257, 2009. (Cited on page 37.)

[GO77] D. Gottlieb and S. A. Orszag. *Numerical Analysis of Spectral Methods*. SIAM, Philadelphia, PA, USA, 1977. 200 pp. (Cited on page 84.)

[Gra07] V. Gradinaru. Fourier transform on sparse grids: Code design and the time dependent Schrödinger equation. *Computing*, 80:1–22, 2007. (Cited on pages 10 and 18.)

[Grö92] K. Gröchenig. Reconstruction algorithms in irregular sampling. *Math. Comput.*, 59:181–194, 1992. (Cited on page 42.)

[Hal92] K. Hallatschek. Fouriertransformation auf dünnen Gittern mit hierarchischen Basen. *Numer. Math.*, 63:83–97, 1992. (Cited on pages 10, 18, and 37.)

[Hic02] F. J. Hickernell. Obtaining $O(N^{-2+\epsilon})$ convergence for lattice quadrature rules. In *Monte Carlo and Quasi-Monte Carlo Methods 2000: Proceedings of a Conference held at Hong Kong Baptist University, Hong Kong SAR, China, November 27 – December 1, 2000*, pages 274–289. Springer Berlin Heidelberg, 2002. (Cited on page 99.)

[HIKP12a] H. Hassanieh, P. Indyk, D. Katabi, and E. Price. Nearly optimal sparse Fourier transform. In *Proceedings of the Forty-fourth Annual ACM Symposium on Theory of Computing*, pages 563–578. ACM, 2012. (Cited on pages 122 and 123.)

[HIKP12b] H. Hassanieh, P. Indyk, D. Katabi, and E. Price. Simple and practical algorithm for sparse Fourier transform. In *Proceedings of the Twenty-third Annual ACM-SIAM Symposium on Discrete Algorithms*, pages 1183–1194. SIAM, 2012. (Cited on pages 122 and 123.)

[HJ91] R. A. Horn and C. R. Johnson. *Topics in Matrix Analysis*. Cambridge University Press, Cambridge, UK, 1991. (Cited on page 42.)

[Hla62] E. Hlawka. Zur angenäherten Berechnung mehrfacher Integrale. *Monatshefte für Mathematik*, 66:325–333, 1962. (Cited on page 10.)

[Hör90] L. Hörmander. *The analysis of linear partial differential operators: Distribution theory and Fourier analysis*. Springer-Verlag, 1990. (Cited on page 30.)

[IK14] P. Indyk and M. Kapralov. Sample-Optimal Fourier Sampling in Any Constant Dimension. In *Foundations of Computer Science (FOCS), 2014 IEEE 55th Annual Symposium on*, pages 514–523, Oct 2014. (Cited on page 122.)

[IKP14] P. Indyk, M. Kapralov, and E. Price. (Nearly) sample-optimal sparse Fourier transform. In *Proceedings of the Forty-fourth Annual ACM Symposium on Theory of Computing*, pages 563–578. ACM, 2014. (Cited on pages 122 and 123.)

[Iwe10] M. A. Iwen. Combinatorial sublinear-time Fourier algorithms. *Found. Comput. Math.*, 10:303–338, 2010. (Cited on page 123.)

[Iwe13] M. A. Iwen. Improved approximation guarantees for sublinear-time Fourier algorithms. *Appl. Comput. Harmon. Anal.*, 34:57–82, 2013. (Cited on page 122.)

[JM10] S. M. M. Javadi and M. Monagan. Parallel sparse polynomial interpolation over finite fields. In *Proceedings of the 4th International Workshop on Parallel and Symbolic Computation*, PASCO '10, pages 160–168, New York, NY, USA, 2010. ACM. (Cited on page 122.)

[Käm13] L. Kämmerer. Reconstructing hyperbolic cross trigonometric polynomials by sampling along rank-1 lattices. *SIAM J. Numer. Anal.*, 51:2773–2796, 2013. (Cited on pages 11, 19, 24, 33, 38, 39, 67, 69, and 100.)

[Käm14a] L. Kämmerer. Reconstructing multivariate trigonometric polynomials from samples along rank-1 lattices. In G. E. Fasshauer and L. L. Schumaker, editors, *Approximation Theory XIV: San Antonio 2013*, pages 255–271. Springer International Publishing, 2014. (Cited on pages 11, 19, 21, 24, 33, 34, 35, 36, 38, and 88.)

[Käm14b] L. Kämmerer. *High Dimensional Fast Fourier Transform Based on Rank-1 Lattice Sampling*. Dissertation. Universitätsverlag Chemnitz, 2014. (Cited on pages 11, 24, 33, 35, 36, 40, 45, 47, 49, 66, 67, 68, 69, 106, and 136.)

[Käm14c] L. Kämmerer. LFFT, MATLAB® toolbox for the lattice and generated set based FFT. `http://www.tu-chemnitz.de/~lkae/lfft`, 2014. (Cited on pages 28, 34, and 52.)

[KK11] L. Kämmerer and S. Kunis. On the stability of the hyperbolic cross discrete Fourier transform. *Numer. Math.*, 117:581–600, 2011. (Cited on pages 10 and 18.)

[KKM+14] L. Kämmerer, S. Kunis, I. Melzer, D. Potts, and T. Volkmer. Computational Methods for the Fourier Analysis of Sparse High-Dimensional Functions. In S. Dahlke, W. Dahmen, M. Griebel, W. Hackbusch, K. Ritter, R. Schneider, C. Schwab, and H. Yserentant, editors, *Extraction of Quantifiable Information from Complex Systems*, 2014. (Cited on pages 12 and 122.)

[KKP12] L. Kämmerer, S. Kunis, and D. Potts. Interpolation lattices for hyperbolic cross trigonometric polynomials. *J. Complexity*, 28:76–92, 2012. (Cited on pages 11, 19, 23, 24, 28, and 37.)

[KL03] E. Kaltofen and W. Lee. Early termination in sparse interpolation algorithms. *J. Symbolic Comput.*, 36:365–400, 2003. ISSAC 2002. (Cited on page 122.)

[Kna00] S. Knapek. Approximation und Kompression mit Tensorprodukt-Multiskalenräumen. Dissertation, Universität Bonn, 2000. (Cited on pages 18 and 57.)

[Knu76] D. E. Knuth. Big omicron and big omega and big theta. *ACM SIGACT News*, 8(2):18–24, 1976. (Cited on pages 170, 171, and 172.)

[Kor59] N. Korobov. On the approximate computation of multiple integrals. *Dokl. Akad. Nauk*, 124:1207–1210, 1959. In Russian. (Cited on pages 10 and 21.)

[Kor60] N. Korobov. Properties and calculation of optimal coefficients. *Dokl. Akad. Nauk*, 132:1009–1012, 1960. In Russian. (Cited on page 27.)

[Kor63] N. Korobov. *Number-Theoretic Methods in Approximate Analysis*. Fizmatgiz, Moscow, 1963. In Russian. (Cited on pages 10 and 21.)

[KPRv16] S. Kunis, T. Peter, T. Roemer, and U. von der Ohe. A multivariate generalization of Prony's method. *Linear Algebra Appl.*, 490:31–47, 2016. (Cited on page 122.)

[KPV15a] L. Kämmerer, D. Potts, and T. Volkmer. Approximation of multivariate periodic functions by trigonometric polynomials based on rank-1 lattice sampling. *J. Complexity*, 31:543–576, 2015. (Cited on pages 11, 12, 21, 24, 25, 28, 29, 31, 32, 33, 40, 41, 42, 44, 45, 47, 48, 49, 50, 52, 53, 54, 55, 64, 66, 70, 71, 72, 73, 76, 77, 78, 79, 80, 82, and 101.)

[KPV15b] L. Kämmerer, D. Potts, and T. Volkmer. Approximation of multivariate periodic functions by trigonometric polynomials based on sampling along rank-1 lattice with generating vector of Korobov form. *J. Complexity*, 31:424–456, 2015. (Cited on pages 11, 12, 21, 23, 24, 25, 27, 33, 36, 37, 46, 48, 49, 50, 60, 61, 62, 63, 64, 65, 66, 71, 72, and 73.)

[KR08] S. Kunis and H. Rauhut. Random sampling of sparse trigonometric polynomials II, Orthogonal matching pursuit versus basis pursuit. *Found. Comput. Math.*, 8:737–763, 2008. (Cited on page 122.)

[KSU14] T. Kühn, W. Sickel, and T. Ullrich. Approximation numbers of Sobolev embeddings — sharp constants and tractability. *J. Complexity*, 30:95–116, 2014. (Cited on pages 9, 20, and 22.)

[KSU15] T. Kühn, W. Sickel, and T. Ullrich. Approximation of mixed order Sobolev functions on the d-torus — asymptotics, preasymptotics and d-dependence. *Constr. Approx.*, 42:353–398, 2015. (Cited on pages 9, 20, and 22.)

[KSW06] F. Y. Kuo, I. H. Sloan, and H. Woźniakowski. Lattice rules for multivariate approximation in the worst case setting. In H. Niederreiter and D. Talay, editors, *Monte Carlo and Quasi-Monte Carlo Methods 2004*, pages 289–330. Springer Berlin Heidelberg, Berlin, 2006. (Cited on pages 10, 21, and 22.)

[KSW08] F. Y. Kuo, I. H. Sloan, and H. Woźniakowski. Lattice rule algorithms for multivariate approximation in the average case setting. *J. Complexity*, 24:283–323, 2008. (Cited on pages 10 and 21.)

[Kun08] S. Kunis. Nonequispaced fast Fourier transforms without oversampling. *Proc. Appl. Math. Mech.*, 8:10977–10978, 2008. (Cited on page 29.)

[Kuo03] F. Y. Kuo. Component-by-component constructions achieve the optimal rate of convergence for multivariate integration in weighted Korobov and Sobolev spaces. *J. Complexity*, 19:301–320, 2003. Oberwolfach Special Issue. (Cited on page 10.)

[KWW09] F. Y. Kuo, G. W. Wasilkowski, and H. Woźniakowski. Lattice algorithms for multivariate L_∞ approximation in the worst-case setting. *Constr. Approx.*, 30:475–493, 2009. (Cited on pages 10 and 21.)

[LH03] D. Li and F. J. Hickernell. Trigonometric spectral collocation methods on lattices. In S. Y. Cheng, C.-W. Shu, and T. Tang, editors, *Recent Advances in Scientific Computing and Partial Differential Equations*, volume 330 of *Contemp. Math.*, pages 121–132. AMS, 2003. (Cited on pages 10, 11, 21, 23, and 28.)

[Nie78] H. Niederreiter. Quasi-Monte Carlo methods and pseudo-random numbers. *B. Am. Math. Soc.*, 84:957–1041, 1978. (Cited on pages 10 and 33.)

[NSW04] E. Novak, I. H. Sloan, and H. Woźniakowski. Tractability of approximation for weighted Korobov spaces on classical and quantum computers. *Found. Comput. Math.*, 4:121–156, 2004. (Cited on page 22.)

[Nuy07] D. Nuyens. *Fast construction of good lattice rules.* Dissertation. Numerical Analysis and Applied Mathematics Section, Department of Computer Science, KU Leuven, 2007. (Cited on pages 10, 21, and 100.)

[NV09] D. Needell and R. Vershynin. Uniform uncertainty principle and signal recovery via regularized orthogonal matching pursuit. *Found. Comput. Math.*, 9:317–334, 2009. (Cited on page 122.)

[PC13] K. Poppe and R. Cools. CHEBINT: A MATLAB/Octave toolbox for fast multivariate integration and interpolation based on Chebyshev approximations over hypercubes. *ACM Trans. Math. Softw.*, 40(1):2:1–2:13, October 2013. (Cited on page 85.)

[Pfl10] D. Pflüger. *Spatially Adaptive Sparse Grids for High-Dimensional Problems.* Dissertation, Institut für Informatik, Technische Universität München, 2010. (Cited on page 10.)

[PP13] T. Peter and G. Plonka. A generalized Prony method for reconstruction of sparse sums of eigenfunctions of linear operators. *Inverse Problems*, 29:025001, 2013. (Cited on page 123.)

[PPS15] T. Peter, G. Plonka, and R. Schaback. Prony's method for multivariate signals. *PAMM*, 15:665–666, 2015. (Cited on page 122.)

[PS82] C. C. Paige and M. A. Saunders. LSQR: An algorithm for sparse linear equations and sparse least squares. *ACM Trans. Math. Software*, 8:43–71, 1982. (Cited on pages 40, 70, and 80.)

[PT08] D. Potts and M. Tasche. Numerical stability of nonequispaced fast Fourier transforms. *J. Comput. Appl. Math.*, 222:655–674, 2008. (Cited on page 42.)

[PT13] D. Potts and M. Tasche. Parameter estimation for multivariate exponential sums. *Electron. Trans. Numer. Anal.*, 40:204–224, 2013. (Cited on pages 122 and 124.)

[PTV16] D. Potts, M. Tasche, and T. Volkmer. Efficient spectral estimation by MUSIC and ESPRIT with application to sparse FFT. *Front. Appl. Math. Stat.*, 2, 2016. (Cited on pages 12, 122, and 123.)

[PV15] D. Potts and T. Volkmer. Fast and exact reconstruction of arbitrary multivariate algebraic polynomials in Chebyshev form. In *11th international conference on Sampling Theory and Applications (SampTA 2015)*, pages 392–396, 2015. (Cited on pages 11, 12, 85, 88, 90, 93, 94, 95, 96, 97, 98, and 99.)

[PV16] D. Potts and T. Volkmer. Sparse high-dimensional FFT based on rank-1 lattice sampling. *Appl. Comput. Harmon. Anal.*, 41:713–748, 2016. (Cited on pages 12, 33, 35, 38, 39, 121, 122, 123, 125, 126, 127, 128, 130, 131, 134, 135, 136, 137, 138, 139, 140, 141, 142, 143, 144, 145, and 146.)

[PW16a] G. Plonka and K. Wannenwetsch. A deterministic sparse FFT algorithm for vectors with small support. *Numerical Algorithms*, 71:889–905, 2016. (Cited on page 123.)

[PW16b] G. Plonka and K. Wannenwetsch. A sparse fast Fourier algorithm for real nonnegative vectors. *ArXiv e-prints*, 2016. arXiv:1602.05444 [math.NA]. (Cited on page 123.)

[Rau07] H. Rauhut. Random sampling of sparse trigonometric polynomials. *Appl. Comput. Harmon. Anal.*, 22:16–42, 2007. (Cited on page 122.)

[Rau08a] H. Rauhut. On the impossibility of uniform sparse reconstruction using greedy methods. *Sampl. Theory Signal Image Process.*, 7:197–215, 2008. (Cited on page 122.)

[Rau08b] H. Rauhut. Stability results for random sampling of sparse trigonometric polynomials. *IEEE Trans. Inform. Theory*, 54:5661–5670, 2008. (Cited on page 122.)

[RY90] K. R. Rao and P. Yip. *Discrete Cosine Transform: Algorithms, Advantages, Applications.* Academic Press, Boston, 1990. (Cited on page 94.)

[SJ94] I. H. Sloan and S. Joe. *Lattice methods for multiple integration.* Oxford Science Publications. The Clarendon Press Oxford University Press, New York, 1994. (Cited on pages 10, 19, and 68.)

[SK87] I. H. Sloan and P. J. Kachoyan. Lattice methods for multiple integration: Theory, error analysis and examples. *SIAM J. Numer. Anal.*, 24:116–128, 1987. (Cited on page 10.)

[SKJ02a] I. H. Sloan, F. Y. Kuo, and S. Joe. Constructing randomly shifted lattice rules in weighted Sobolev spaces. *SIAM J. Numer. Anal.*, 40:1650–1665, 2002. (Cited on page 10.)

[SKJ02b] I. H. Sloan, F. Y. Kuo, and S. Joe. On the step-by-step construction of quasi–Monte Carlo integration rules that achieve strong tractability error bounds in weighted Sobolev spaces. *Math. Comput.*, 71:1609–1640, 2002. (Cited on page 10.)

[Slo95] I. H. Sloan. Polynomial interpolation and hyperinterpolation over general regions. *J. Approx. Theory*, 83:238–254, 1995. (Cited on pages 24, 85, and 99.)

[Smo63] S. Smolyak. Quadrature and interpolation formulas for tensor products of certain classes of functions. *Dokl. Akad. Nauk*, 148:1042–1045, 1963. (Cited on pages 9 and 17.)

[SNC16] G. Suryanarayana, D. Nuyens, and R. Cools. Reconstruction and collocation of a class of non-periodic functions by sampling along tent-transformed rank-1 lattices. *J. Fourier Anal. Appl.*, 22:187–214, 2016. (Cited on pages 11, 88, 92, 96, 99, and 100.)

[Spr97a] F. Sprengel. Interpolation und Waveletzerlegung multivariater periodischer Funktionen. Dissertation, Universität Rostock, 1997. (Cited on pages 21 and 22.)

[Spr97b] F. Sprengel. A unified approach to error estimates for interpolation on full and sparse Gauß-Chebyshev grids. *Rostock. Math. Kolloq.*, 51:51–64, 1997. (Cited on pages 83, 86, 87, and 90.)

[Spr00] F. Sprengel. Interpolation of functions from Besov-type spaces on Gauß-Chebyshev grids. *J. Complexity*, 16(2):507–523, 2000. (Cited on pages 83, 86, and 87.)

[SR02] I. H. Sloan and A. V. Reztsov. Component-by-component construction of good lattice rules. *Math. Comp.*, 71:263–273, 2002. (Cited on pages 10 and 88.)

[ST87] H.-J. Schmeisser and H. Triebel. *Topics in Fourier analysis and function spaces*, volume 42 of *Mathematik und ihre Anwendungen in Physik und Technik*. Akademische Verlagsgesellschaft Geest & Portig K.-G., Leipzig, 1987. (Cited on page 22.)

[Ste92] G. Steidl. Fast radix–p discrete cosine transform. *Appl. Algebra Eng. Commun. Comput.*, 3:39–46, 1992. (Cited on page 84.)

[STW11] J. Shen, T. Tang, and L.-L. Wang. *Spectral Methods*, volume 41 of *Springer Ser. Comput. Math.* Springer-Verlag Berlin Heidelberg, Berlin, 2011. (Cited on page 88.)

[SU07] W. Sickel and T. Ullrich. The Smolyak algorithm, sampling on sparse grids and function spaces of dominating mixed smoothness. *East J. Approx.*, 13:387–425, 2007. (Cited on pages 23 and 27.)

[SW98] I. H. Sloan and H. Woźniakowski. When are quasi-Monte Carlo algorithms efficient for high dimensional integrals? *J. Complexity*, 14:1–33, 1998. (Cited on page 22.)

[SW01] I. H. Sloan and H. Woźniakowski. Tractability of multivariate integration for weighted Korobov classes. *J. Complexity*, 17:697–721, 2001. (Cited on page 10.)

[SW10] J. Shen and L.-L. Wang. Sparse spectral approximations of high-dimensional problems based on hyperbolic cross. *SIAM J. Numer. Anal.*, 48:1087–1109, 2010. (Cited on pages 87 and 88.)

[SY10] J. Shen and H. Yu. Efficient spectral sparse grid methods and applications to high-dimensional elliptic problems. *SIAM J. Sci. Comput.*, 32:3228–3250, 2010. (Cited on page 84.)

[Sze75] G. Szegő. *Orthogonal Polynomials*. Amer. Math. Soc., Providence, RI, USA, 4th edition, 1975. (Cited on page 84.)

[Tem85] V. N. Temlyakov. Approximate recovery of periodic functions of several variables. *Mat. Sbornik.*, 128:256–268, 1985. English translation in Math. USSR Sbornik., 56, 249–261 (1987). (Cited on pages 9, 17, and 20.)

[Tem86] V. N. Temlyakov. Reconstruction of periodic functions of several variables from the values at the nodes of number-theoretic nets. *Anal. Math.*, 12:287–305, 1986. In Russian. (Cited on pages 10, 19, 21, 27, 60, and 61.)

[Tem89] V. N. Temlyakov. Approximation of functions with bounded mixed derivative. *Proc. Steklov Inst. Math.*, 1989. A translation of Trudy Mat. Inst. Steklov 178 (1986). (Cited on pages 9, 10, 20, and 22.)

[Tem93] V. N. Temlyakov. *Approximation of periodic functions*. Computational Mathematics and Analysis Series. Nova Science Publishers Inc., Commack, NY, 1993. (Cited on pages 9, 10, 17, 20, and 21.)

[Ull08] T. Ullrich. Smolyak's algorithm, sampling on sparse grids and Sobolev spaces of dominating mixed smoothness. *East J. Approx.*, 14:1–38, 2008. (Cited on pages 9 and 17.)

[VL92] C. F. Van Loan. *Computational Frameworks for the Fast Fourier Transform*. SIAM, Philadelphia, PA, USA, 1992. (Cited on page 84.)

[Vol13] T. Volkmer. Taylor and rank-1 lattice based nonequispaced fast Fourier transform. In *10th international conference on Sampling Theory and Applications (SampTA 2013)*, pages 576–579, Bremen, Germany, 2013. (Cited on pages 11, 12, 23, 28, 29, and 30.)

[Vol15] T. Volkmer. sparseFFTr1l, MATLAB® toolbox for computing the sparse fast Fourier transform based on reconstructing rank-1 lattices in a dimension incremental way. `http://www.tu-chemnitz.de/~tovo/software`, 2015. (Cited on page 138.)

[Vol16a] T. Volkmer. nonperiodicR1L, MATLAB® toolbox for computing the rank-1 Chebyshev lattice based FFT. `http://www.tu-chemnitz.de/~tovo/software`, 2016. (Cited on pages 95 and 152.)

[Vol16b] T. Volkmer. taylorR1Lnfft, MATLAB® toolbox for computing the Taylor expansion and rank-1 lattice based non-equispaced FFT. `http://www.tu-chemnitz.de/~tovo/software`, 2016. (Cited on pages 72, 76, and 79.)

[Wei80] J. Weidmann. *Linear Operators in Hilbert Spaces*, volume 68 of *Graduate Texts in Mathematics*. Springer-Verlag New York, 1980. (Cited on page 84.)

[Zip79] R. Zippel. Probabilistic algorithms for sparse polynomials. In *Proceedings of the International Symposiumon on Symbolic and Algebraic Computation*, EUROSAM '79, pages 216–226, London, UK, UK, 1979. Springer-Verlag. (Cited on pages 122 and 124.)

[ZLH06] X. Zeng, K.-T. Leung, and F. J. Hickernell. Error analysis of splines for periodic problems using lattice designs. In H. Niederreiter and D. Talay, editors, *Monte Carlo and Quasi-Monte Carlo Methods 2004*, pages 501–514. Springer Berlin Heidelberg, 2006. (Cited on pages 10 and 21.)

Notations

$\cdot$	Usual Euclidian scalar product.
$\odot$	Component-wise product of two vectors.
$\mathbf{1}$	Vector $\mathbf{1} := (1, \ldots, 1) \in \mathbb{N}^s$, where $s \in \mathbb{N}$ depends on the context.
$\| \circ \|_p$	Usual p norm of a vector, $\|\boldsymbol{x}\|_p := (\sum_{t=1}^{d} \|x_t\|^p)^{1/p}$ for $\boldsymbol{x} := (x_1, \ldots, x_d)^\top \in \mathbb{C}^d$ and $1 \leq p < \infty$, $\|\boldsymbol{x}\|_p := \max_{t=1,\ldots,d} \|x_t\|$.
$\|\boldsymbol{k}\|_0$	Number of nonzero components of a vector $\boldsymbol{k} \in \mathbb{R}^d$, $\|\boldsymbol{k}\|_0 := \sum_{t=1}^{d} \delta_{k_t,0}$.
$\|x\|X\|$	Norm of an element x of a normed vector space X.
$\|A\|X \to Y\|$	Operator norm of linear operator $A\colon X \to Y$ between normed vector spaces X and Y, $\|A\|X \to Y\| := \sup_{f \in X \setminus \{0\}} \frac{\|Af\|Y\|}{\|f\|X\|} = \sup_{\|f\|X\|=1} \|Af\|Y\|$ for $X \neq \{0\}$.
a_I	Algebraic polynomial in Chebyshev basis with Chebyshev coefficients $a_{\boldsymbol{k}} \in \mathbb{R}$, $\boldsymbol{k} \in I$, cf. (3.1).
$\mathcal{A}^{\alpha,\beta,\boldsymbol{\gamma}}(\mathbb{T}^d)$	Subspaces of the Wiener algebra $\mathcal{A}(\mathbb{T}^d) = \mathcal{A}^{0,0,\mathbf{1}}(\mathbb{T}^d)$ for $\beta \geq 0$ and $\alpha \geq -\beta$, cf. (2.13).
$\mathcal{A}^{\alpha,\beta}([-1,1]^d)$	Subspaces of the non-periodic analogon of the Wiener algebra $\mathcal{A}([-1,1]^d) = \mathcal{A}^{0,0}([-1,1]^d)$ for $\beta \geq 0$ and $\alpha \geq -\beta$, cf. (3.6).
$\mathcal{A}(\mathbb{T}^d)$	Wiener algebra, cf. (2.4).
$\mathcal{A}([-1,1]^d)$	Analogon of the Wiener algebra $\mathcal{A}(\mathbb{T}^d)$, cf. (3.4).
$\mathrm{CL}(\boldsymbol{z}, M)$	Rank-1 Chebyshev lattice of size M with generating vector $\boldsymbol{z} \in \mathbb{N}_0^d$, cf. (3.3).
$\mathrm{CL}(\boldsymbol{z}, M, I)$	Reconstructing rank-1 Chebyshev lattice, which is a rank-1 Chebyshev lattice $\mathrm{CL}(\boldsymbol{z}, M)$ fulfilling the equivalent reconstruction properties (3.22), (3.23) and (3.25) for a given frequency index set $I \in \mathbb{N}_0^d$.
$\mathbb{C}$	Complex numbers.
$\hookrightarrow$	Continuous embedding between normed vector spaces. $X \hookrightarrow Y :\Leftrightarrow X \subseteq Y$ and $\exists$ constant $C \geq 0\colon \|x\|Y\| \leq C \, \|x\|X\|$ for all $x \in X$.
$\cos(\boldsymbol{x})$	Component-wise cosine of a vector $\boldsymbol{x} \in \mathbb{R}^d$, i.e. $\cos((x_1, \ldots, x_d)) := (\cos(x_1), \ldots, \cos(x_d))$.

$\delta_{\boldsymbol{k},\boldsymbol{k'}}$	Kronecker's delta, $\delta_{\boldsymbol{k},\boldsymbol{k'}} = 1$ for $\boldsymbol{k} = \boldsymbol{k'}$ and $\delta_{\boldsymbol{k},\boldsymbol{k'}} = 0$ for $\boldsymbol{k} \neq \boldsymbol{k'}$.
$\mathcal{D}(I)$	Difference set of frequency index set $I \subset \mathbb{Z}^d$, $\mathcal{D}(I) := \{\boldsymbol{h} := \boldsymbol{k} - \boldsymbol{k'} \colon \boldsymbol{k}, \boldsymbol{k'} \in I\}$.
d	Spatial dimension.
$D^{\boldsymbol{\nu}} f$	$\boldsymbol{\nu}$-th derivative of a function f, $D^{\boldsymbol{\nu}} f(\boldsymbol{x}) := \frac{\partial^{\nu_1}}{\partial {x_1}^{\nu_1}} \ldots \frac{\partial^{\nu_d}}{\partial {x_d}^{\nu_d}} f(\boldsymbol{x})$, $\boldsymbol{\nu} \in \mathbb{N}_0^d$.
emod	$l \operatorname{emod} M := \begin{cases} l \bmod (2M), & l \bmod (2M) \leq M, \\ 2M - (l \bmod (2M)) & \text{else,} \end{cases}$ for $M \in \mathbb{N}$ and $l \operatorname{emod} 0 := 0$.
ε_j^n	$\varepsilon_j^n := 1/\sqrt{2}$ for $j \in \{0, n\}$ and $\varepsilon_j^n := 1$ for $j \in \{1, \ldots, n-1\}$, $n \in \mathbb{N}_0$.
ess sup	Essential supremum.
$\hat{f}_{\boldsymbol{k}}$	Fourier coefficient of a function $f \in L_1(\mathbb{T}^d)$, cf. (2.5), or Chebyshev coefficient of a function $f \in L_{2,w}(\mathbb{T}^d)$, cf. (3.5).
$\hat{f}_{\boldsymbol{k}}^{\mathrm{CL}}$	Approximated Chebyshev coefficient $\approx \hat{f}_{\boldsymbol{k}}$ computed by using the rank-1 Chebyshev lattice $\mathrm{CL}(\boldsymbol{z}, M)$, cf. (3.29).
$\hat{f}_{\boldsymbol{k}}^{\Lambda}$	Approximated Fourier coefficient $\approx \hat{f}_{\boldsymbol{k}}$ computed by using the rank-1 lattice $\Lambda(\boldsymbol{z}, M)$, cf. (2.7).
Γ	Search domain $\subset \mathbb{Z}^d$ or $\subset \mathbb{N}_0^d$ for frequency locations.
$\hat{G}_N^d$	d-dimensional full grid of refinement $N \in \mathbb{N}_0$, $\hat{G}_N^d := \{\boldsymbol{k} \in \mathbb{Z}^d \colon \|\boldsymbol{k}\|_\infty \leq N\}$ or $\hat{G}_N^d := \{\boldsymbol{k} \in \mathbb{N}_0^d \colon \|\boldsymbol{k}\|_\infty \leq N\}$.
$\mathcal{H}^{\alpha,\beta,\boldsymbol{\gamma}}(\mathbb{T}^d)$	Periodic Sobolev spaces of generalized mixed smoothness, cf. (2.11).
$\mathcal{H}^{\alpha,\beta}([-1,1]^d)$	Sobolev-type spaces of generalized mixed smoothness, cf. (3.7).
$\boldsymbol{I}$	Identity matrix.
I	Frequency index set, $I \subset \mathbb{Z}^d$ in the periodic case and $I \subset \mathbb{N}_0^d$ in the non-periodic case.
$I_{\mathrm{a},n}^{d,T}$	Frequency index set $\subset \mathbb{N}_0^d$ as defined in (3.11).
$I_N^{d,T,\boldsymbol{\gamma}}$	Weighted frequency index set $\subset \mathbb{Z}^d$ as defined in (2.14).
$\Lambda(\boldsymbol{z}, M)$	Rank-1 lattice of size M with generating vector $\boldsymbol{z} \in \mathbb{Z}^d$, cf. (2.3).
$\Lambda(\boldsymbol{z}, M)^\perp$	Integer dual lattice of rank-1 lattice $\Lambda(\boldsymbol{z}, M)$, cf. (2.29).
$\Lambda(\boldsymbol{z}, M, I)$	Reconstructing rank-1 lattice, which is a rank-1 lattice $\Lambda(\boldsymbol{z}, M)$ fulfilling the equivalent reconstruction properties (2.25), (2.26), (2.27), (2.28) and (2.30) for a given frequency index set $I \in \mathbb{Z}^d$.
$\lesssim, \asymp$	$g(\boldsymbol{x}) \lesssim h(\boldsymbol{x}) \Leftrightarrow g(\boldsymbol{x}) \in \mathcal{O}(h(\boldsymbol{x}))$, $g(\boldsymbol{x}) \asymp h(\boldsymbol{x}) \Leftrightarrow g(\boldsymbol{x}) \in \Theta(h(\boldsymbol{x}))$, cf. [Knu76].
$L_p(\mathbb{T}^d)$	Space of all measurable functions $f \colon \mathbb{T}^d \to \mathbb{C}$ with norm $\|f \mid L_p(\mathbb{T}^d)\| := (\int_{\mathbb{T}^d} \lvert f(\boldsymbol{x})\rvert^p \, \mathrm{d}\boldsymbol{x})^{1/p} < \infty$ for $1 \leq p < \infty$ and $\|f \mid L_\infty(\mathbb{T}^d)\| := \operatorname{ess\,sup}_{\boldsymbol{x} \in \mathbb{T}^d} \lvert f(\boldsymbol{x})\rvert < \infty$ for $p = \infty$.

$L_p([-1,1]^d)$	Space of all measurable functions $f\colon [-1,1]^d \to \mathbb{R}$ with norm $\|f\|L_p([-1,1]^d)\| := (\int_{[-1,1]^d} \lvert f(\boldsymbol{x})\rvert^p \,\mathrm{d}\boldsymbol{x})^{1/p} < \infty$ for $1 \le p < \infty$ and $\|f\|L_\infty([-1,1]^d)\| := \operatorname{ess\,sup}_{\boldsymbol{x}\in[-1,1]^d} \lvert f(\boldsymbol{x})\rvert < \infty$ for $p = \infty$.
$L_{2,w}([-1,1]^d)$	Weighted Hilbert space of all square integrable functions $f\colon [-1,1]^d \to \mathbb{R}$ with respect to the (product) Chebyshev weight $w(\boldsymbol{x}) := \prod_{t=1}^d 1/\sqrt{1-x_t^2}$ with norm $\|f\|L_{2,w}([-1,1]^d)\| := \sqrt{\int_{[-1,1]^d} \lvert f(\boldsymbol{x})\rvert^2 \, w(\boldsymbol{x}) \,\mathrm{d}\boldsymbol{x}}$.
M	Size $\in \mathbb{N}$ of rank-1 lattice $\Lambda(\boldsymbol{z}, M)$ or size parameter $\in \mathbb{N}_0$ of rank-1 Chebyshev lattice $\mathrm{CL}(\boldsymbol{z}, M)$.
$\mathcal{M}(I)$	Extended symmetric index set $\mathcal{M}(I) := \{\boldsymbol{h} \in \mathbb{Z}^d\colon (\lvert h_1\rvert, \dots, \lvert h_d\rvert)^\top \in I\} \subset \mathbb{Z}^d$ of frequency index set $I \subset \mathbb{Z}^d$.
$\mathcal{M}_\nu(I)$	Frequency index set $\mathcal{M}_\nu(I) := \{\boldsymbol{h} \in \mathcal{M}(I)\colon h_\nu \ge 0\} \subset \mathbb{Z}^d$, $\nu \in \{1, \dots, d\}$.
mod	Component-wise modulo of a vector $\boldsymbol{x} \in \mathbb{R}^d$, $\boldsymbol{x} \bmod \mathbf{1} = (x_t - \lfloor x_t \rfloor)_{t=1}^d$, $\boldsymbol{x} \bmod M = (x_t - \lfloor x_t/M \rfloor M)_{t=1}^d$ for $M \in \mathbb{N}$.
N, n	Refinement of frequency index set $I_N^{d,T,\boldsymbol{\gamma}}$ or $I_{\mathrm{a},n}^{d,T}$.
$\mathbb{N}$	Positive integers.
$\mathbb{N}_0$	Non-negative integers.
$\mathcal{O}(h(\boldsymbol{x}))$	Denotes the set of all functions $g\colon \mathbb{R}^d \mapsto \mathbb{R}$ such that there exist positive constants $C_{g,\boldsymbol{p}} \in \mathbb{R}^+$ and $\boldsymbol{n}_0 \in \mathbb{N}^d$ with $\lvert g(\boldsymbol{x})\rvert \le C_{g,\boldsymbol{p}}\, h(\boldsymbol{x})$ for all $\boldsymbol{x} \ge \boldsymbol{n}_0$, where the constant $C_{g,\boldsymbol{p}}$ may depend on the function g and additional parameters $\boldsymbol{p} \in \mathbb{R}^d$ but does not depend on the variables $\boldsymbol{x}$, cf. [Knu76]. Especially, we may have $h(\boldsymbol{x}) = h(\boldsymbol{x}, \boldsymbol{p})$. Whether a symbol belongs to the parameters $\boldsymbol{p}$ or variables $\boldsymbol{x}$ depends on the context.
$\Omega(h(\boldsymbol{x}))$	$g \in \Omega(h(\boldsymbol{x})) \Leftrightarrow h \in \mathcal{O}(g(\boldsymbol{x}))$, cf. [Knu76].
$\omega^{\alpha,\beta,\boldsymbol{\gamma}}(\boldsymbol{k})$	Weights $\omega^{\alpha,\beta,\boldsymbol{\gamma}}(\boldsymbol{k}) := \max(1, \|\boldsymbol{k}\|_1)^\alpha \prod_{t=1}^d \max(1, \gamma_t^{-1}\lvert k_t\rvert)^\beta$ for frequency $\boldsymbol{k} := (k_1, \dots, k_d)^\top \in \mathbb{Z}^d$, cf. (2.12).
p_I	Trigonometric polynomial with Fourier coefficients $\hat{p}_{\boldsymbol{k}} \in \mathbb{C}$, $\boldsymbol{k} \in I$, cf. (2.2).
Π_I	Space of trigonometric polynomials with frequencies supported on I, cf. (2.1).
$\mathcal{P}_{\boldsymbol{i}}$	Projection of a frequency $\boldsymbol{k} \in \mathbb{Z}^d$ to the components $\boldsymbol{i} := (i_1, \dots, i_m) \in \{1, \dots, d\}^m$, $\mathcal{P}_{\boldsymbol{i}}(\boldsymbol{k}) := (k_{i_1}, \dots, k_{i_m})^\top \in \mathbb{Z}^m$, or of a frequency index set $I \subset \mathbb{Z}^d$, $\mathcal{P}_{\boldsymbol{i}}(I) := \{(k_{i_1}, \dots, k_{i_m})\colon \boldsymbol{k} \in I\}$.
$\mathbb{R}$	Real numbers.
s	Sparsity parameter $s \in \mathbb{N}$ of Algorithm 4.2, 4.3, 4.4 and 4.5 in Chapter 4.
$S_I f$	Fourier partial sum $S_I f := \sum_{\boldsymbol{k}\in I} \hat{f}_{\boldsymbol{k}}\, \mathrm{e}^{2\pi \mathrm{i} \boldsymbol{k}\cdot\circ}$ or Chebyshev partial sum $S_I f := \sum_{\boldsymbol{k}\in I} \hat{f}_{\boldsymbol{k}}\, T_{\boldsymbol{k}}(\circ)$.

$S_I^{\mathrm{CL}} f$	Approximated Chebyshev partial sum $S_I^{\mathrm{CL}} f := \sum_{\boldsymbol{k} \in I} \hat{f}_{\boldsymbol{k}}^{\mathrm{CL}} T_{\boldsymbol{k}}(\circ)$ using approximated Chebyshev coefficients $\hat{f}_{\boldsymbol{k}}^{\mathrm{CL}}$, $\boldsymbol{k} \in I \subset \mathbb{N}_0^d$, from (3.29).
$S_I^{\Lambda} f$	Approximated Fourier partial sum $S_I^{\Lambda} f := \sum_{\boldsymbol{k} \in I} \hat{f}_{\boldsymbol{k}}^{\Lambda} \mathrm{e}^{2\pi \mathrm{i} \boldsymbol{k} \cdot \circ}$ using approximated Fourier coefficients $\hat{f}_{\boldsymbol{k}}^{\Lambda}$, $\boldsymbol{k} \in I \subset \mathbb{Z}^d$, from (2.7).
s_m	Taylor expansion of total degree m (excluding m-th derivatives), cf. (2.17).
$\operatorname{supp} \hat{a}$	Location $\operatorname{supp} \hat{a} := \{\boldsymbol{k} \in I \colon \hat{a}_{\boldsymbol{k}} \neq 0\} \subset \mathbb{N}_0^d$ of non-zero Chebyshev coefficients $\hat{a}_{\boldsymbol{k}} \neq 0$ of a multivariate algebraic polynomial in Chebyshev form a_I.
$\operatorname{supp} \hat{p}$	Location $\operatorname{supp} \hat{p} := \{\boldsymbol{k} \in I \colon \hat{p}_{\boldsymbol{k}} \neq 0\} \subset \mathbb{Z}^d$ of non-zero Fourier coefficients $\hat{p}_{\boldsymbol{k}} \neq 0$ of a multivariate trigonometric polynomial p_I.
$\mathbb{T}$	One-dimensional torus $\simeq [0, 1)$.
$\Theta(h(\boldsymbol{x}))$	$= \Omega(h(\boldsymbol{x})) \cap \mathcal{O}(h(\boldsymbol{x}))$, cf. [Knu76].
$T_{\boldsymbol{k}}$	Tensor product of Chebyshev polynomials of the first kind, $T_{\boldsymbol{k}} \colon [-1, 1]^d \to [-1, 1]$, $T_{\boldsymbol{k}}(\boldsymbol{x}) := \prod_{t=1}^d T_{k_t}(x_t)$ for frequency $\boldsymbol{k} \in \mathbb{N}_0^d$, $T_{k_t}(x_t) := \cos(k_t \arccos x_t)$.
$\mathcal{Y}$	Sampling scheme on the d-dimensional torus $\mathbb{T}^d$ or box $[-1, 1]^d$.
$\mathbb{Z}$	Integers.
ζ	Riemann zeta function $\zeta(\xi) = \sum_{n=1}^{\infty} n^{-\xi}$, $\xi \in \mathbb{C}$, $\operatorname{Re}(\xi) > 1$.
$\boldsymbol{z}$	Generating vector $\in \mathbb{Z}^d$ of rank-1 lattice $\Lambda(\boldsymbol{z}, M)$ or $\in \mathbb{N}_0^d$ of rank-1 Chebyshev lattice $\mathrm{CL}(\boldsymbol{z}, M)$.

The most frequently used notations are listed above. However, the table is not comprehensive. Several necessary additional notations appear locally throughout the whole work.

Theses

1. The utilization of multivariate trigonometric polynomials $p_I(\boldsymbol{x}) := \sum_{\boldsymbol{k}\in I} \hat{p}_{\boldsymbol{k}}\, \mathrm{e}^{2\pi \mathrm{i}\boldsymbol{k}\cdot\boldsymbol{x}}$, $\hat{p}_{\boldsymbol{k}} \in \mathbb{C}$, is a suitable approach for the approximation of multivariate smooth periodic functions $f\colon \mathbb{T}^d \to \mathbb{C}$, where the frequency index set $I \subset \mathbb{Z}^d$, $|I| < \infty$, is chosen appropriately. The characterization of the smoothness of functions f via the decay of their Fourier coefficients $\hat{f}_{\boldsymbol{k}} := \int_{\mathbb{T}^d} f(\boldsymbol{x})\, \mathrm{e}^{-2\pi \mathrm{i}\boldsymbol{k}\cdot\boldsymbol{x}}\, \mathrm{d}\boldsymbol{x}$, $\boldsymbol{k} \in \mathbb{Z}^d$, provides a good starting point for error considerations in weighted norms. Relatively thin frequency index sets I, like hyperbolic crosses, may be used without distinctly deteriorating the approximation error compared to full grid frequency index sets, when the considered functions f are sufficiently smooth, for instance, if they have bounded mixed derivatives. A truncated Fourier series $S_I f := \sum_{\boldsymbol{k}\in I} \hat{f}_{\boldsymbol{k}}\, \mathrm{e}^{2\pi \mathrm{i}\boldsymbol{k}\cdot\circ}$, i.e., the Fourier partial sum consisting of the Fourier coefficients $\hat{f}_{\boldsymbol{k}}$, $\boldsymbol{k} \in I$, of a function f, may be used as an approximant in practice if the Fourier coefficients $\hat{f}_{\boldsymbol{k}}$ are explicitly known. In general, this approximation causes an error, the truncation error $f - S_I f$, and asymptotically best possible truncation errors $f - S_I f$ are shown in this work for functions f from periodic Sobolev spaces of generalized mixed smoothness

$$\mathcal{H}^{\alpha,\beta,\boldsymbol{\gamma}}(\mathbb{T}^d) := \left\{ f \in L_1(\mathbb{T}^d)\colon \|f|\mathcal{H}^{\alpha,\beta,\boldsymbol{\gamma}}(\mathbb{T}^d)\| := \sqrt{\sum_{\boldsymbol{k}\in\mathbb{Z}^d} \omega^{\alpha,\beta,\boldsymbol{\gamma}}(\boldsymbol{k})^2 |\hat{f}_{\boldsymbol{k}}|^2} < \infty \right\},$$

where the weights $\omega^{\alpha,\beta,\boldsymbol{\gamma}}(\boldsymbol{k}) := \max(1, \|\boldsymbol{k}\|_1)^\alpha \prod_{s=1}^d \max(1, \gamma_s^{-1}|k_s|)^\beta$ with dominating mixed smoothness $\beta \geq 0$, isotropic smoothness $\alpha > -\beta$ and weight parameter $\boldsymbol{\gamma} \in (0,1]^d$. Moreover, asymptotically best possible truncation errors $f - S_I f$ are shown for functions f from weighted subspaces

$$\mathcal{A}^{\alpha,\beta,\boldsymbol{\gamma}}(\mathbb{T}^d) := \left\{ f \in L_1(\mathbb{T}^d)\colon \|f|\mathcal{A}^{\alpha,\beta,\boldsymbol{\gamma}}(\mathbb{T}^d)\| := \sum_{\boldsymbol{k}\in\mathbb{Z}^d} \omega^{\alpha,\beta,\boldsymbol{\gamma}}(\boldsymbol{k}) |\hat{f}_{\boldsymbol{k}}| < \infty \right\}$$

of the Wiener algebra $\mathcal{A}(\mathbb{T}^d) = \mathcal{A}^{0,0,\mathbf{1}}(\mathbb{T}^d)$.

2. Approximated Fourier partial sums of smooth periodic functions $f\colon \mathbb{T}^d \to \mathbb{C}$, where approximated Fourier coefficients are numerically computed from sampling values of f, are considered in this work. In particular, we use the nodes $\boldsymbol{x}_j := \frac{j}{M}\boldsymbol{z} \bmod 1$, $j = 0, \ldots, M-1$, of a rank-1 lattice $\Lambda(\boldsymbol{z}, M)$ as sampling nodes, where $\boldsymbol{z} \in \mathbb{Z}^d$ is the generating vector and $M \in \mathbb{N}$ is the rank-1 lattice size. Rank-1 lattices $\Lambda(\boldsymbol{z}, M)$ are well suited due to their good constructibility as a consequence of their simple structure and due to the existence of a fast Fourier transform (FFT) for the computation of approximated Fourier coefficients $\hat{f}_{\boldsymbol{k}}^{\Lambda} := \frac{1}{M}\sum_{j=0}^{M-1} f(\boldsymbol{x}_j)\, \mathrm{e}^{-2\pi \mathrm{i}\boldsymbol{k}\cdot\boldsymbol{x}_j}$, $\boldsymbol{k} \in I$, from samples $f(\boldsymbol{x}_j)$, $j = 0, \ldots, M-1$. The computation of these approximated Fourier coefficients $\hat{f}_{\boldsymbol{k}}^{\Lambda}$,

$\boldsymbol{k} \in I$, can be performed using only a single one-dimensional FFT and a simple index transform, which require $\mathcal{O}(M \log M + d\,|I|)$ arithmetic operations in total. Special rank-1 lattices fulfilling a certain reconstruction property, so-called reconstructing rank-1 lattices $\Lambda(\boldsymbol{z}, M, I)$, allow for the fast and exact reconstruction of arbitrary multivariate trigonometric polynomials p_I with frequencies supported on arbitrary known index sets $I \subset \mathbb{Z}^d$, $|I| < \infty$, from samples $p_I(\boldsymbol{x}_j)$, $j = 0, \ldots, M-1$. The approximation of smooth periodic functions $f\colon \mathbb{T}^d \to \mathbb{C}$ by partial sums $S_I^\Lambda f := \sum_{\boldsymbol{k} \in I} \hat{f}_{\boldsymbol{k}}^\Lambda \, \mathrm{e}^{2\pi \mathrm{i} \boldsymbol{k} \cdot \circ}$ is considered, where the approximated Fourier coefficients $\hat{f}_{\boldsymbol{k}}^\Lambda$ are computed from samples along a reconstructing rank-1 lattice $\Lambda(\boldsymbol{z}, M, I)$, and an extensive error theory is developed for suitable frequency index sets I. Splitting the sampling error $f - S_I^\Lambda f$ into the truncation error $f - S_I f$ and aliasing error $S_I f - S_I^\Lambda f$ yields a practical approach for obtaining error estimates. With the help of suitable proof techniques, estimates for aliasing errors $S_I f - S_I^\Lambda f$ are shown and error rates are obtained which are comparable to the ones of corresponding truncation errors $f - S_I f$. Numerical tests for up to 25 dimensions confirm the effectiveness and high performance of the proposed method.

3. Perturbed rank-1 lattice nodes $\boldsymbol{y}_j$ can be used instead of exact rank-1 lattice nodes $\boldsymbol{x}_j$ if the perturbations are sufficiently small. Then, multivariate trigonometric polynomials p_I can be fast evaluated by an approximate method based on Taylor expansion and one-dimensional FFTs. When the nodes $\boldsymbol{y}_j$ are perturbed versions of the nodes $\boldsymbol{x}_j$ of a reconstructing rank-1 lattice $\Lambda(\boldsymbol{z}, M, I)$, multivariate trigonometric polynomials p_I with frequencies supported on arbitrary known index sets $I \subset \mathbb{Z}^d$, $|I| < \infty$, can be approximately reconstructed in a fast way using an iterative method. This approach can be applied to the fast approximation of multivariate smooth periodic functions $f\colon \mathbb{T}^d \to \mathbb{C}$ yielding similar error estimates as in the unperturbed case for reconstructing rank-1 lattices $\Lambda(\boldsymbol{z}, M, I)$.

4. The method for the fast reconstruction of multivariate trigonometric polynomials p_I and fast approximation of multivariate smooth periodic functions $f\colon \mathbb{T}^d \to \mathbb{C}$ from samples along reconstructing rank-1 lattices $\Lambda(\boldsymbol{z}, M, I)$ can be transferred to the non-periodic case. For many of the concepts and results from the periodic case, a non-periodic counterpart can be used or established. Multivariate algebraic polynomials in Chebyshev form $a_I(\boldsymbol{x}) := \sum_{\boldsymbol{k} \in I} \hat{a}_{\boldsymbol{k}} \, T_{\boldsymbol{k}}(\boldsymbol{x})$ represent adequate ansatz functions for the approximation of multivariate smooth non-periodic functions $f\colon [-1,1]^d \to \mathbb{R}$. Rank-1 Chebyshev lattices $\mathrm{CL}(\boldsymbol{z}, M)$, characterized by generating vector $\boldsymbol{z} \in \mathbb{N}_0^d$ and size parameter $M \in \mathbb{N}_0$, are used as corresponding spatial discretizations. Multivariate algebraic polynomials in Chebyshev form a_I with frequencies supported on arbitrary index sets $I \subset \mathbb{N}_0^d$, $|I| < \infty$, can be evaluated in a fast and exact way at the corresponding nodes $\boldsymbol{x}_j := \cos(\frac{j}{M}\pi \boldsymbol{z})$, $j = 0, \ldots, M$, in $\mathcal{O}(M \log M + d\,|\mathcal{M}(I)|)$ arithmetic operations by using easy-to-compute index transforms and a single one-dimensional discrete cosine transform (DCT). Analogously to the reconstruction properties of reconstructing rank-1 lattices $\Lambda(\boldsymbol{z}, M, I)$ in the periodic case, similar reconstruction properties are derived in this work for the non-periodic case and the term reconstructing rank-1 Chebyshev lattice $\mathrm{CL}(\boldsymbol{z}, M, I)$ is introduced. The fast and exact reconstruction of arbitrary multivariate algebraic polynomials in Chebyshev form a_I with frequencies supported on arbitrary known index sets $I \subset \mathbb{N}_0^d$, $|I| < \infty$, can be performed by applying a single one-dimensional DCT to the samples $a_I(\boldsymbol{x}_j)$, $j = 0, \ldots, M$, along a reconstructing rank-1 Chebyshev lattice $\mathrm{CL}(\boldsymbol{z}, M, I)$ followed by easy-to-compute index transforms. This reconstruction requires $\mathcal{O}(M \log M + d\,|\mathcal{M}(I)|)$

arithmetic operations in total. The construction of reconstructing rank-1 Chebyshev lattices $\mathrm{CL}(\boldsymbol{z}, M, I)$ can be performed using a simple component-by-component (CBC) approach. Reconstructing rank-1 Chebyshev lattices $\mathrm{CL}(\boldsymbol{z}, M, I)$ are well-suited as sampling sets for the approximation of multivariate smooth non-periodic functions $f\colon [-1,1]^d \to \mathbb{R}$ and an error theory analogously to the periodic case is developed in this work, where functions f are characterized by the decay of their Chebyshev coefficients $\hat{f}_{\boldsymbol{k}} := 2^{|\boldsymbol{k}|_0}/\pi^d \int_{\boldsymbol{x}\in[-1,1]^d} f(\boldsymbol{x})\ T_{\boldsymbol{k}}(\boldsymbol{x})/(\prod_{s=1}^d \sqrt{1-x_s^2})\,\mathrm{d}\boldsymbol{x}$, $\boldsymbol{k} \in \mathbb{N}_0^d$. Analogously to the periodic case, we consider subspaces $\mathcal{H}^{\alpha,\beta}([-1,1]^d)$ of the Hilbert space $L_{2,w}([-1,1]^d)$ with Chebyshev product weight $w(\boldsymbol{x}) := 1/(\prod_{s=1}^d \sqrt{1-x_s^2})$ and subspaces $\mathcal{A}^{\alpha,\beta}([-1,1]^d)$ of the analogon of the Wiener algebra $\mathcal{A}([-1,1]^d) = \mathcal{A}^{0,0}([-1,1]^d)$. Numerical tests for up to 25 dimensions confirm the effectiveness and high performance of the proposed method.

5. The exact reconstruction of high-dimensional sparse trigonometric polynomials p_I and high-dimensional sparse algebraic polynomials in Chebyshev form a_I as well as the approximation of multivariate periodic and non-periodic functions f can be realized based on samples without exact knowledge of the frequency index sets I containing the non-zero or largest coefficients. Methods performing a dimension-incremental determination of frequency index sets $\tilde{I}$ with the help of projections parallel to the coordinate axes are suggested as reconstruction approaches. Components of frequency locations belonging to non-zero or the approximately largest Fourier or Chebyshev coefficients can be efficiently determined within a search domain Γ, which may be very large, for instance a d-dimensional full grid. In each dimension increment step $t = 1, \ldots, d$, the t-th component of the unknown frequency locations is considered, i.e., one component at a time starting with the first one. The utilization of reconstructing rank-1 lattices $\Lambda(\boldsymbol{z}, M, \tilde{I})$ in the periodic case and reconstructing rank-1 Chebyshev lattices $\mathrm{CL}(\boldsymbol{z}, M, \tilde{I})$ in the non-periodic case enables the easy, fast and robust computation of projected Fourier or Chebyshev coefficients and, based on these, the determination of relevant components of a frequency index set I. For the case where high-dimensional sparse polynomials and functions have arbitrary Fourier or Chebyshev coefficients, a randomized approach is proposed, which performs repeated sampling in each dimension increment step t with different randomly chosen higher components $x_{j,t+1}, \ldots, x_{j,d}$ of the sampling nodes $\boldsymbol{x}_j$. Numerical tests performed for up to 30 dimensions in this work confirm high reliability for the exact reconstruction of high-dimensional sparse polynomials. For a 10-dimensional periodic and 9-dimensional non-periodic test function, the frequency locations I belonging to the approximately largest Fourier and Chebyshev coefficients $\hat{f}_{\boldsymbol{k}}$ were successfully determined, respectively. The case where the samples are perturbed by noise is considered for 10-dimensional sparse trigonometric polynomials p_I and the frequency locations belonging to the non-zero Fourier coefficients are successfully reconstructed. A deterministic version of the dimension-incremental approach is proposed, which may be applied when the Fourier coefficients fulfill certain properties. Correspondingly, this result is transferred to the non-periodic case and a deterministic version is described.